SAFETY IN MINES RESEARCH ADVISORY COMMITTEE

SIMRAC

Final Project Report

Title: REDUCE THE METHANE HAZARDS IN COLLIERIES

VOLUME I I - APPENDICES A to F

Author/s: F J van Zyl, P Linzer

Research Agency: CSIR, Division of Materials Science and Technology

Project No: COL 030

Date: October 1996

INFRARED METHANE MONITORING

Dr V A Kononov, CSIR Division of Mining Technology

1.Introduction

Localized ventilation inadequacies coupled with the natural liberation of methane gas from coal seams may produce local explosive methane/air mixtures in underground coal workings if the methane concentration in air is in the range from 5 to 15% by volume. The presence of airborne fine coal particles aggravates this hazard by decreasing the lower explosive limit (LEL).

Methane liberation rates depend to a large extent on mining rates, so that areas where coal is being broken will have a higher methane concentration. Newer, mechanised mining methods release methane faster than traditional (hand got) methods due to their higher extraction rates. Moreover, higher gas concentrations are found in the vicinity of a continuous miner (CM) cutting drum. Sparks may be generated by a pick impacting a hard inclusion in the coal or harder overlying or underlying strata. If an explosive mixture of methane is present and a spark of greater than 0.3mJ energy is generated within this mixture, methane ignition will occur [1], normally with disastrous consequences.

Environmental conditions, such as airborne coal dust levels and ventilation, can make the difference between ignitions affecting only the immediate cutting area and those developing throughout an entire section or even larger areas by escalating to a coal dust explosion. Such explosions are the greatest hazards faced by coal miners, and cost an average of 150 to 200 lives annually worldwide besides the material damage wreaked. The disaster at Uzulmez Colliery in the Zonguldak coal field in Turkey took ± 260 lives. The recent methane/coal dust at Sukhodolskaya-Vostochnaya Colliery in the Ukraine killed eight miners instantly, but CO and smoke suffocated another 43 workers [2]. The last example indicates a further hazard associated with methane explosions - suffocation.

It is difficult to overestimate the importance of monitoring methane and coal dust as well as air flow around the CM in a cutting area. Research [3] has clearly shown how intricate this problem is, even in laboratory simulations. Underground conditions, being even less ideal, confound the issue of comprehensive gas/dust monitoring at a coal face further.

For over thirty years the most common flammable gas monitoring technique in use has been the catalytic sensor. Electrocatalytic sensors are unsuited to the underground environment due to the high dust levels and the presence of water sprays affecting the reading obtained from the sensor [3]. A further technical draw-back is the inability of the sensor to operate without oxygen and "poisoning" of the catalyst by silicones, hydrocarbons etc. A new generation of poison resistant sensors has been developed [4], but catalytic sensors are not failsafe and hence require extensive maintenance and attention.

Different methods of methane monitoring were investigated to alleviate these problems and one of these methods was the use of optical rather than chemical or electrochemical apparatus.

2. Physical Aspects and Techniques for Optical Gas Detection

Infrared gas analyzers have been used for many years as laboratory tools. The optical method of measuring CH_4 concentration is based on the gas molecules absorbing radiation in the Infrared (IR)

bands of wavelength 1.33, 1.665, 3.3, 3.53 and 3.84μm and 115 absorption lines between 7.21 and 8.29μm [8,11]. Technically, it is possible to use 1.33 and 1.665μm absorption peaks (Fig.1) for CH_4 identification. Since the 1.665μm absorption band is of greater spectral width, this wavelength is normally used in methane monitoring (MM) experiments [4,7,9].

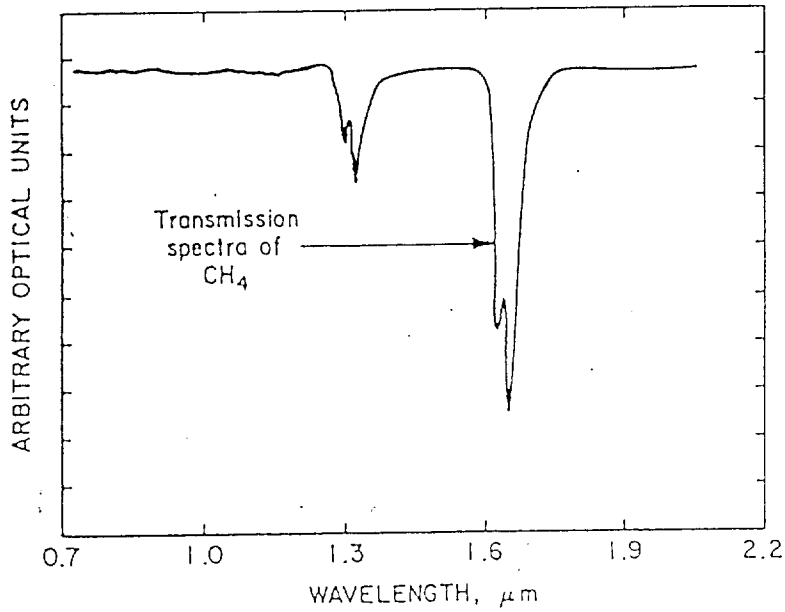

Figure 1 - CH_4 absorption peaks.

The two main measuring systems are the dual path/single wavelength and the single path/dual wavelength arrangements (Fig.2). The dual path instruments are commonly used in laboratory work. The single path instrument uses one wavelength for reference, while absorption of the other yields information about the gas concentration. Two different optical filters and wide band sources or two monochromatic sources can be used for this instrument.

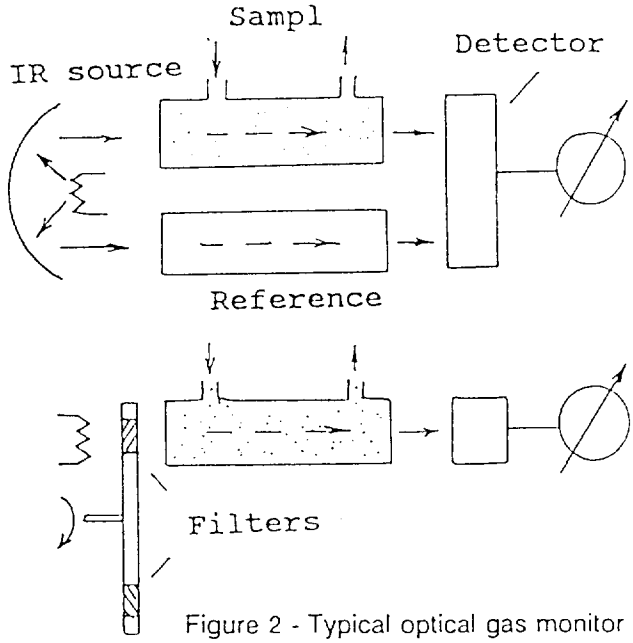

Figure 2 - Typical optical gas monitor arrangements.

An example of an early attempt to adapt the optical method for industrial application is the German UNOR 1 which was used for methane detection in German mines from 1962 [4]. This unit was based on the Luft cell which he proposed in 1943 (Fig.3).

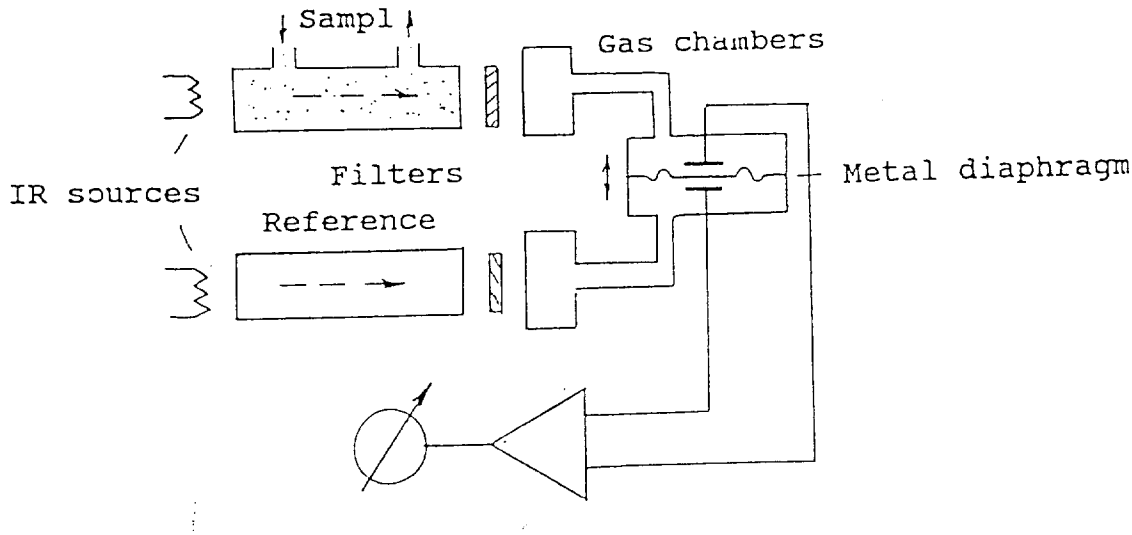

Figure 3 - Luft cell.

The simplicity of this obsolete design clearly shows its method of operation. The Luft detector consists of two hermetic gas filled chambers separated by a metal diaphragm. The heating effect of dissipated IR radiation causes the gas in these chambers to expand. The presence of an IR absorbing gas in the sample cell causes a reduction in the IR power reaching one gas chamber, causing this gas to heat more slowly. The resulting pressure difference causes the diaphragm to move, which can be measured as a change in capacitance [4].

The Astro Resources instrument is housed in a flameproof case. The IR beam passes through a window and gas gap, reflects back off a mirror, through the window, chopper and two narrow band filters into a detector. Over 5000 units have been sold. The same principle was used in the Norwegian Simrad Unit [4]. Neither of these units has a window cleaning facility and no reference to their use at a coal face was found.

The Sieger Model 5050 is based on a more complex single path/single wavelength technique. Pressure and temperature sensors are used for drift compensation. The reference signal is generated via calcium fluoride and the instrument alternatively sees the sample atmosphere and the zero reference with the same source, light path and detector. This instrument was satisfactorily tested for coal and rock mining applications [4].

A relatively recent and promising development is the so called "Open Path" method of gas detection [4,11]. This type of instrument does not take spot samples, but measures the average gas concentration over a long path (100 - 10 000m) by detecting either reflected or backscattered radiation from the projected IR beam. A few models such as the "Lidar", the Swedish "Opsis", the American "Wright & Wright" and the British "Sieger Search-line" were or are in commercial production [4]. The last model needs a multi-corner cube reflector to return the beam to the instrument. Field trials have shown atmospheric conditions such as snow, rain, fog, smoke etc. to have little influence on readings.

Research efforts in Japan, UK, Norway, Australia and USA over the last decade have concentrated on using fibre-optics in gas monitoring [4...10] which could enable remote detection of methane

concentrations. One of the few fibre-optic systems commercially available is the Norwegian ASEA. Each monitoring unit can accommodate up to 16 sensors with separate IR sources.

3. Experiments and Results

There is no information available on the use of any commercial or developed IR gas detectors in coal face conditions. Even where some underground tests were done, environmental conditions were not specified.

It should be noted that the term "remote methane monitor" does not mean that the sensor itself is positioned away from a measuring point. All references [5...10] emphasize the need to develop an intrinsically safe (IS) remote MM system which incorporates a fibre-optic (FO) network (10-20km) as a link between the sensor and the monitoring equipment or between hazardous and non-hazardous areas (Fig.4). The reason for this is optical fibre's intrinsic immunity to electromagnetic interference, its flexibility and material (chemical) stability.

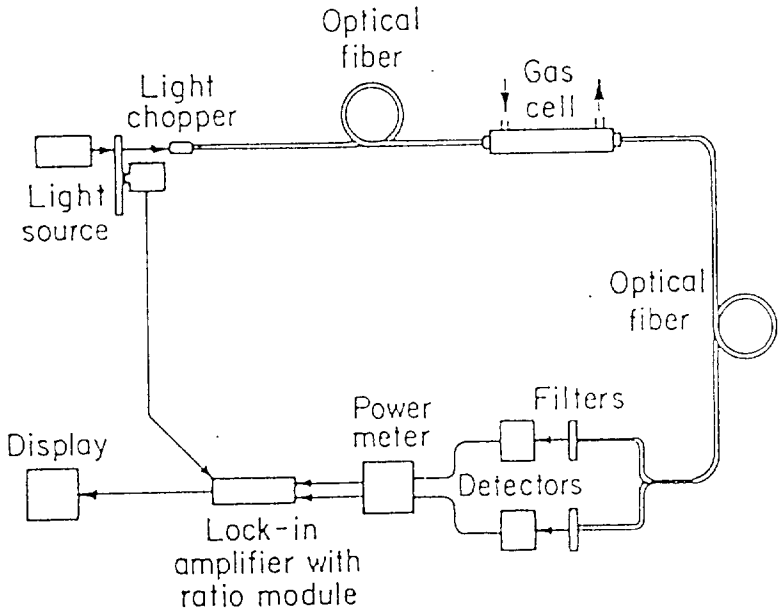

Figure 4 - Fiber-optic CH_4 monitor.

Application of a FO link consequently leads to the use of an optical gas sensor to provide a fully IS loop, and reduces the amount of signal conversion. For this purpose an absorption gas cell with a 50cm air gap between emitting and receiving (input/ output) fibres has to be installed at a measuring point. For

the proper coupling of light between the input and output FO, two lenses are used.

Several different IR sources could be used in such system: laser diodes (LD), light-emitting diodes (LED) [8] or tungsten halogen lamps [9], for example are all suitable. LDs or LEDs are more suitable for electrical modulation and can easily be synchronized with an amplifier, while a lamp requires the use of a mechanical light chopper.

Modulated 1.33 or 1.665μm IR radiation from a source is transmitted via FO to a remote gas cell, and the signal (less the portion absorbed) returned to the monitoring station (Fig.4). The monitoring setup is a relatively standard installation. Absorption cells are used as the gas sensors in which the partial pressure of methane is changed while the total pressure of the methane/air mixture is kept at 1 atm. (It is assumed that dry air and pure gas was used). Fig.5 shows the percentage absorbtion for different CH_4 concentrations obtained during the test [9]. The minimum detectable concentration was estimated as 0.2%. To increase the sensitivity, one can increase the path length of the cell or use a narrower filter.

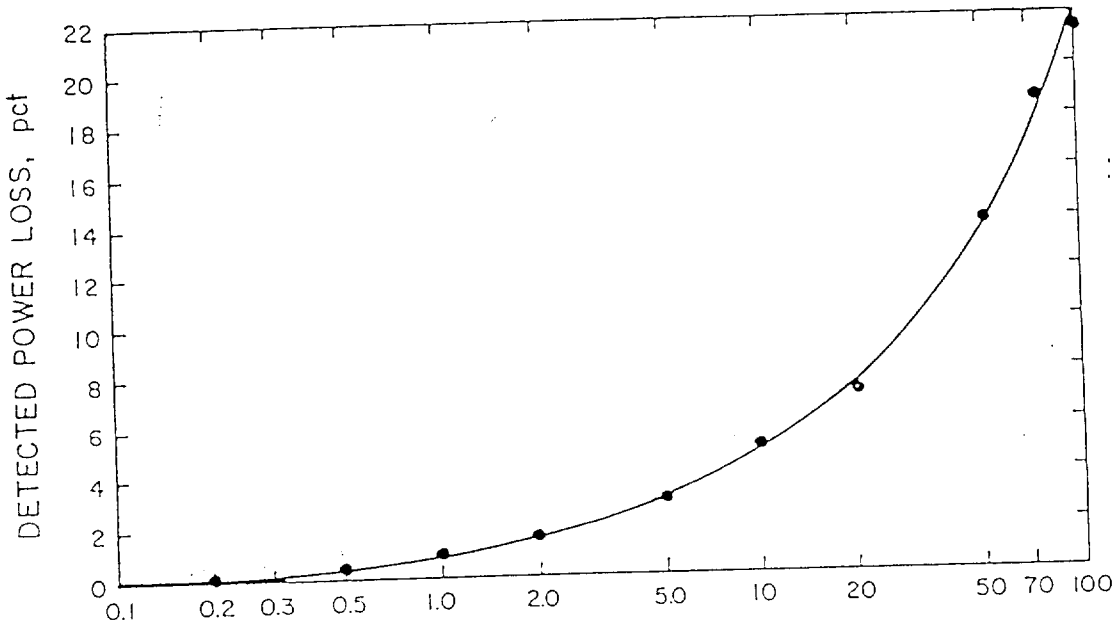

Figure 5 - Percent power loss for various concentration of methane.

These authors [9] have reported that a series of in-mine tests were done, but unfortunately underground environmental conditions such as dust and humidity at the test site are not given. Despite this, this research is closest to coal mining requirements [9].

Some factors that affect methane readings were noted [9]. An 8°C change in ambient temperature, for example, led to the output drifting by 3% CH_4. Other researches also noted this effect [10] and attributed it to a temperature-sensitive optical filter in the monitor. A few other gases similar in molecular structure to methane such as ethane (C_2H_6), propane (C_3H_8) and butane (C_4H_{10}) were introduced into the gas cell. Ethane gave one-third of the response of methane in the same concentration, while propane and butane gave unexpected negative readings. Thus, equal quantities of methane and butane would provide a zero reading. The different refractive indices of the gases are the cause of such errors.

Whenever light passes from glass (refractive index of 1.53) to air (1.000292), a portion of the light is reflected back and the remainder transmitted through. For a single glass-air interface, the increment of transmitted light, δI, is

$$\delta I = 0.20\ I_0\ \delta(n\text{-}1) \quad [9]$$

where I_0 = initial light intensity;
n = refractive index.

This expression shows that transmitted light increases in direct proportion to the increase in gas refractive index. A summary of refractive indices for different gases (Fig.6) indicates the severity of mutual interference in monitoring methane in the presence of heavier hydrocarbons. This effect was also noted in [4].

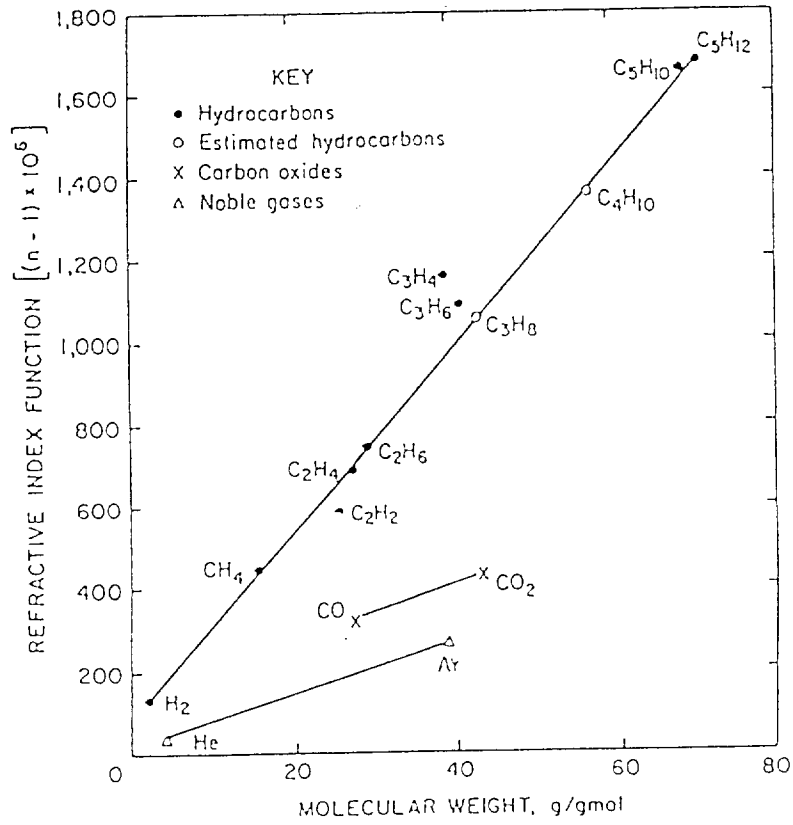

Figure 6 - Refractive index as a function of molecular weight.

A differential detection technique with a reference wavelength very close to that absorbed may compensate for lamp dimming, dust, humidity and other wavelength-independent fluctuations [9]. No information about the reference wavelength used is given, but the refractive index effect is noted. Also, it was shown that even dual wavelength devices have a problem with oil mist and hydrocarbon film contamination [4].

4. Summary of Technical Aspects

4.1 Although some commercial IR gas detectors are available and researchers reported on working models, no units are currently suitable for coal face application.

4.2 IR gas detectors are used and tested mainly in industrial and laboratory settings; in-mine tests were rarely done and no results about the effects of (rock or coal) dust, humidity or atmospheric pressure were specified.

4.3 Optical gas detectors require optical window cleaning and calibration before every start-up.

4.4 Changing the methane concentration from 0.2% to 1.0% increments the measured signal by only 0.9%.

4.5 Temperature effects are easily reducible, but minimization of refractive index effects is very difficult.

4.6 The influence of mine atmosphere pressure variations on gas refractive index [13] has not been considered.

4.7 With reference to 4.5, the systems [4,9] did not eliminate errors due to the presence of ethane, propane and butane.

4.8 The refractive index values for visible light were used [9,13]; the correct value for 1.66μm would be lower.

4.9 To achieve good resolution, an optical power meter with a cooled germanium detector was used, which is not well-suited to underground use.

4.10 Such systems are (still) bulky (15-30kg).

4.11 The system requires much more refinement before it will be amenable to coal face use.

5. Feasibility Study concerning the use of Optical Methane Monitoring in a Coal Cutting Area

5.1 Description of the system

Three possible ways of using optical MM are identified in terms of the positioning of the sensor and the corresponding optical effect used in the measurement:

1. Emitter and receiver are positioned outside the cutting area (open path).
   Attenuation of IR radiation reflected and scattered from cutting area vicinity is used.

2. Emitter and receiver are in the cutting area with an acceptable air gap between them.
   Attenuation of direct IR beam is used.
3. Two lenses to couple light through an air gap between transmitting and receiving fibre-optic lines in the cutting area; monitoring unit is outside of a cutting or even hazardous area.
   Attenuation of direct IR beam is used.

It is evident that in addition to temperature and gas refractive index effects, significant interference by water sprays and rock/ coal dust must be taken into account. Water spray must be considered the most important factor, because apart from directly reducing IR radiation, it changes dust optical and physical parameters as well as refractive indices of optical systems.

It was noted only that the refractive index of gases depend on wavelength [9], but the fact that IR reflection and attenuation by water vapour and coal/rock dust are wavelength-dependent as well [4,14] is important, and this makes coal face application of the optical MM method more problematic.

5.2. Recommendations

-All three options require a device for cleaning the optics.

-The second option should provide better accuracy as wave-length-dependent IR reflection and scattering off the mining atmosphere would be excluded from effects which contribute to methane reading errors. Presumably, the "Sieger Searchline" utilizes a special reflector to return the IR beam for these purposes.

-In order to achieve good compensation of deleterious effects, the same broad-band light source must be used for both the absorption and reference measuring channels.

-For the second option, a halogen lamp in a flameproof enclosure is the recommended light source.

-The third option is an application of the standard fibre-optic system [8,9], but requires a special power trailing cable for the CM and at least two extra optical connectors.

6. Commercial Aspects

6.1 It has to be taken into account that the optical IR methane sensor was proposed mainly for remote IS fibre-optic gas monitoring systems. This means that only one electro-optical measuring apparatus and multiple fibre-optic links with gas cells are required for quasi-real-time gas monitoring around an industrial or mining area. This approach reduces the cost per monitoring point. The mining industry must be prepared to pay a high price for every separately installed methanometer. For example, the "Sieger 5050" model costs ±$5000.

6.2 Undoubtedly, the cost of further research and development of IR MM at the coal face (with uncertain results) will be high.

7. Conclusions

7.1 An IR methanometer installed on a CM defeats the essential optical monitoring system advantage of being totally passive and, hence, intrinsically safe.

7.2 At the present level of technology, the likelihood of measuring methane concentrations at a coal face in the range 0.2 to 2% with acceptable accuracy is questionable.

7.3 The optical method for MM at a coal face needs further investigation.

7.4 Catalytic gas detectors will probably be widely used in the mining industry for at least 10 years hence, before optical units are developed to acceptable accuracies, weight and cost.

8. Proposal

Considering sections 6 and 7, it appears more promising to finance R&D work in the following areas:

-CM cutting area ventilation, possibly via the hollow boom, as is used in shearers, as well as section ventilation improvement;

-Devising a unit that samples continuously from various points, which is capable of removing dust and moisture from the samples and providing airflow data using existing methanometer. This could be extended to include dust level monitoring.

9. References

1. Environmental Engineering in South African mines. The Mine Ventilation Society of South Africa. 1982

2. Ukrainian explosion kills at least 55. Engineering and Mining Journal, July 1992, p.16E.

3. R.Bhaskar, K.Yang and S.Page. Development of a system for analyses of airflow patterns in full-scale laboratory investigations of dust control systems. Mining Engineering, October 1991, pp. 1249-1254.

4. J.I.Markley. Infra-red gas detection comes of age. ISA Calgary 89 Symposium, pp.227-239.

5. K.Chan, H.Ito and H.Inaba. Absorption measurement of v_2+2v_3 band of CH_4 at 1.33μm using an InGaAsP light emitting diode. Appl. Opt., vol.22, pp.3802-3804, 1983.

6. K.Chan, H.Ito and H.Inaba. Optical remote monitoring of CH_4 gas using low-loss optical fiber link and InGaAsP light emitting diode in 1.33μm region. Appl.Phys.Lett., vol.43, pp.634-636, 1983.

7. K.Chan, H.Ito and H.Inaba. Optical-fiber remote sensing system of low-level propane gas using a 1.68μm InGaAs light emitting diode. Opt.Lasers Eng., vol.6, pp.119-123, 1985.

8. K.Chan, H.Ito and H.Inaba. All-Optical-Fiber-Based Remote Sensing System for Near Infrared Absorption of Low-Level CH_4 Gas. J. Lightwave Technol., vol.LT-5, No.12, Dec.1987, pp.1706-1711.

9. T.H.Dubaniewicz and J.E.Chilton. Remote Fiber-Optic Methane Monitor. Report of investigations, 1992, Bureau of Mines USA.

10. J.P.Dakin, C.A.Wade, D.Pinchbeck and J.S.Wykes. A Novel Optical Fiber Methane Sensor. Proc.Photo-Opt.Instrum.Eng., vol.734, 1987, pp.254-260.

11. R.M.Measures. Laser Remote Sensing Fundamentals and Applications. New York, Wiley, 1984.

12. R.A.Smith, F.E.Jones and R.P.Chasmar. The detection and measurement of infra-red radiation. Oxford, 1957.

13. M.Born and E.Wolf. Principles of Optics. Pergamon Press, 1959.

14. A.M.Onishenko, I.B.Krichko and A.V.Ivashev. To the problem of control of mining industry processes by infrared methods. Fiziko-Tekhnicheskie Problemy Razrabotki Poleznykh Iskopaemych. Jan-Feb 1991, pp.84-87. Inst. Gornogo Dela im.A.A.Skochinskogo, Moscow.

APPENDIX A1

Assessment 1: 1995-03-08

SENSOR POSITION	MAX. LEVEL RECORDED (%)	LEVELS RELATIVE TO CAB SENSOR (%)	
		MEAN	SSD
RIGHT REAR(CABIN)	0.09	REF	REF
RIGHT FRONT	0.98	391.7	381.6
LEFT FRONT	2.61	2036.4	2305.0
LEFT MIDDLE FRONT	0.73	153.8	215.5
LEFT MIDDLE	0.44	229.0	196.6
LEFT REAR	0.31	260.6	81.0

ASSESMENT 1 : 1995-03-08

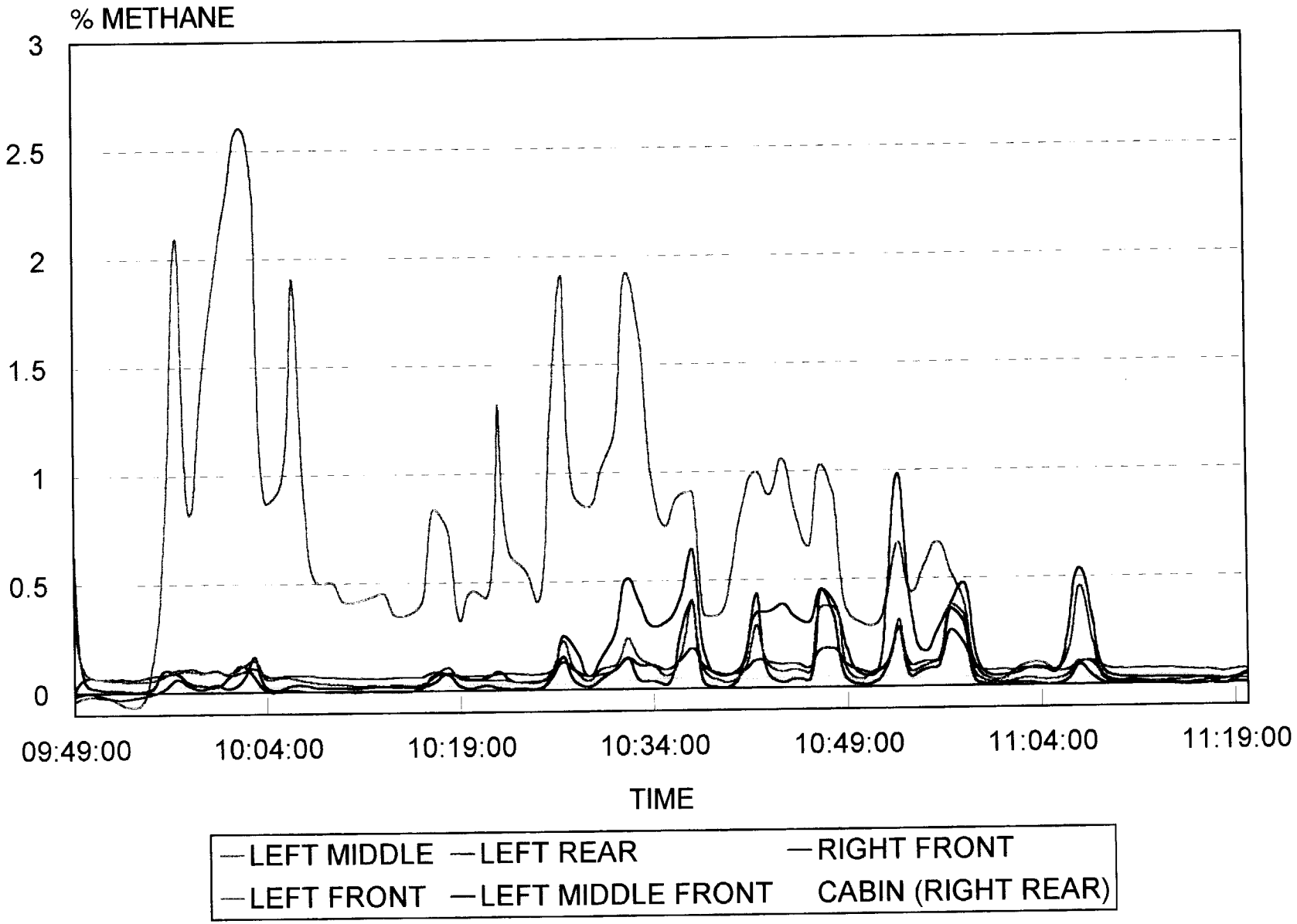

Assessment 2 : 1995-03-16

SENSOR POSITION	MAX. LEVEL RECORDED (%)	LEVELS RELATIVE TO CAB SENSOR (%)	
		MEAN	SSD
RIGHT REAR(CABIN)	0.26	REF	REF
RIGHT FRONT	-	-	-
LEFT FRONT	2.10	293.87	190.10
LEFT MIDDLE FRONT	0.84	107.13	92.61
LEFT MIDDLE	0.70	91.28	85.85
LEFT REAR	0.42	156.69	43.28

ASSESMENT 2 : 1995-03-16

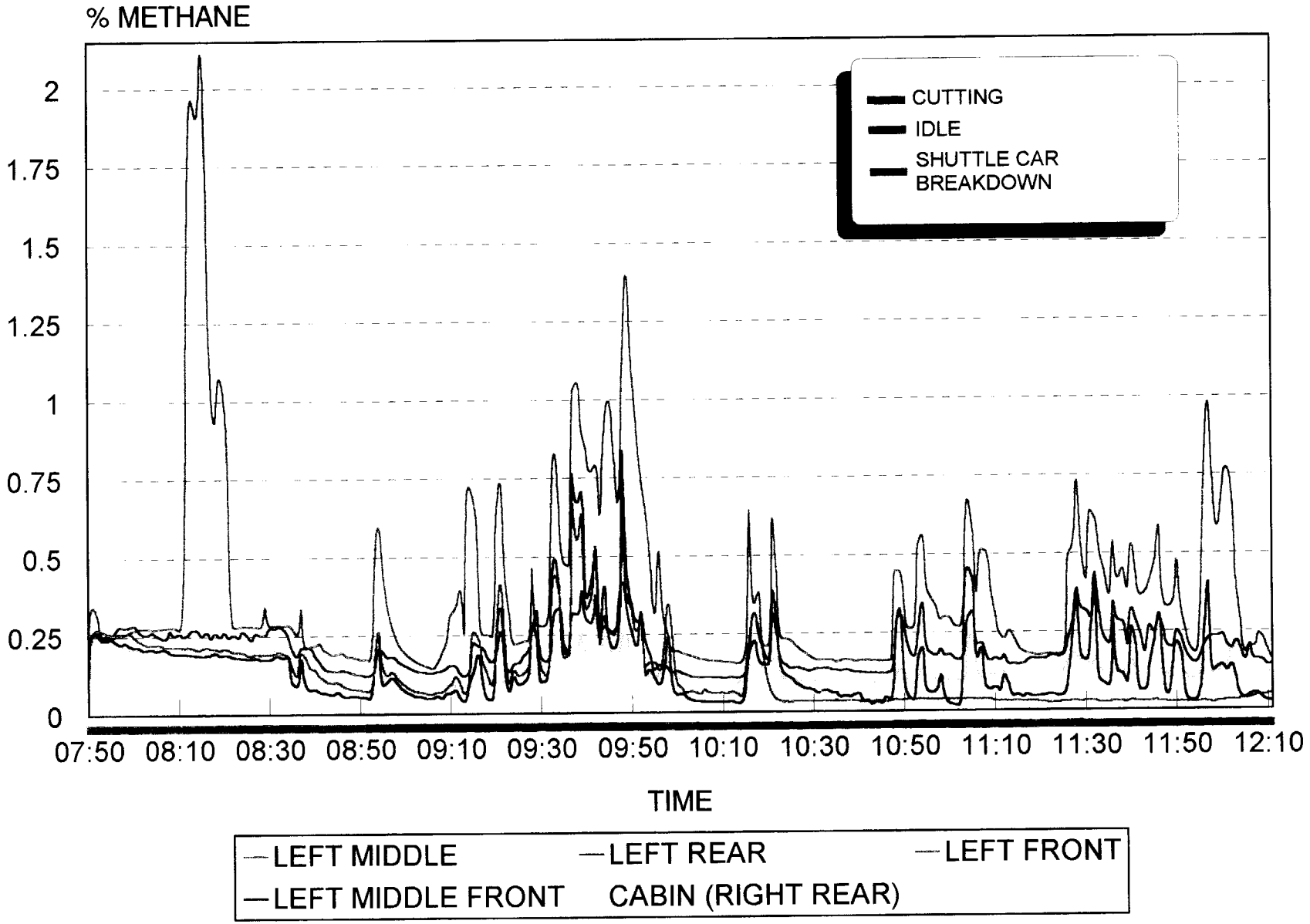

APPENDIX A2

Assessment 1 : 1995-07-31

SENSOR POSITION	MAX. LEVEL RECORDED (%)	LEVEL RELATIVE TO CAB SENSOR (%)	
		MEAN	SSD.
RIGHT REAR (CABIN)	0.1	REF	REF
RIGHT MIDDLE	1.63	267.42	75.45
RIGHT FRONT	4.00	1327.08	278.32
LEFT FRONT	0.21	3396.01	7392.02
LEFT MIDDLE	1.03	752.01	357.28
LEFT REAR	0.32	278.32	78.67

ASSESMENT 1 : 1995-07-31

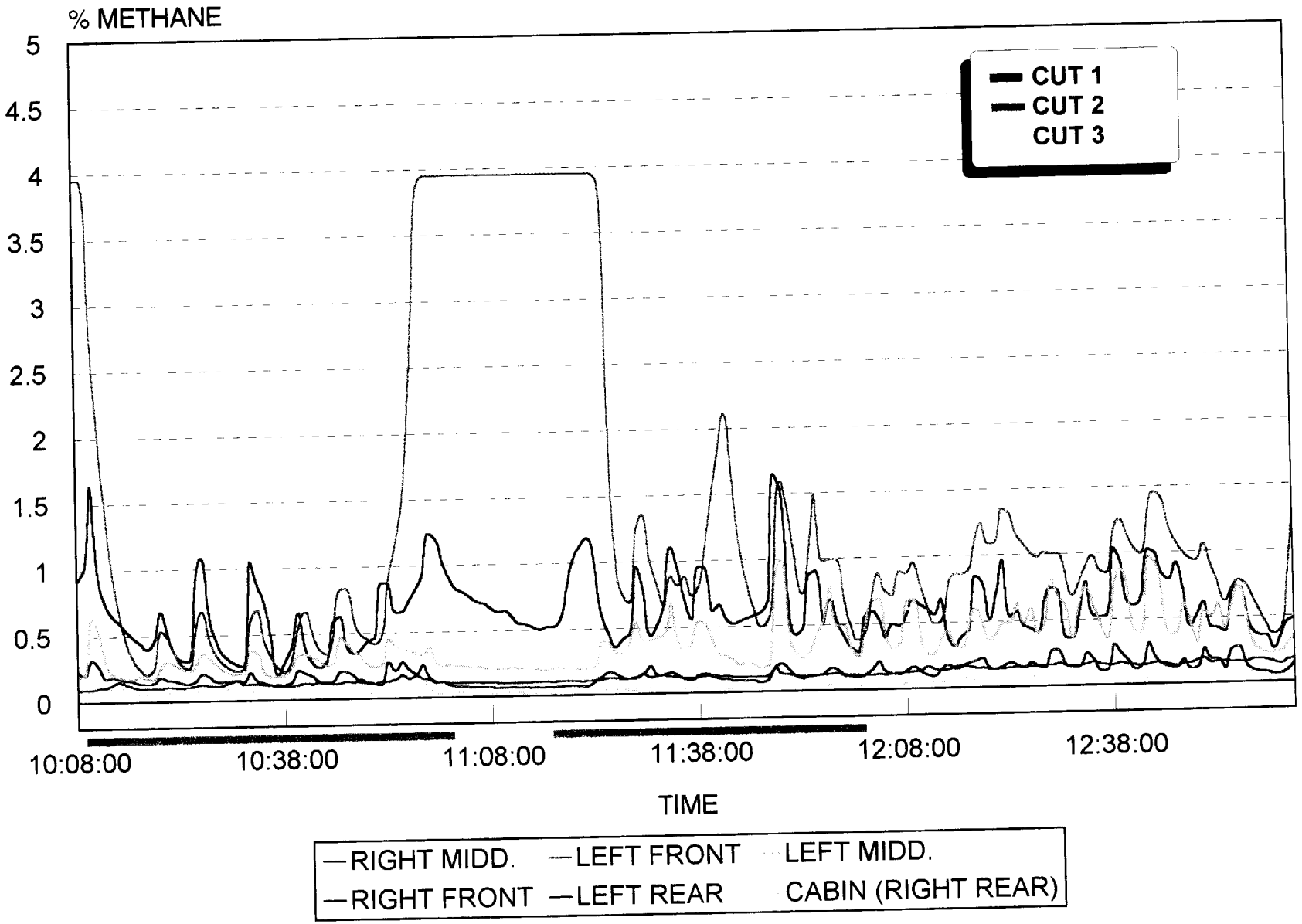

CUT REFERS TO THE PROGRESSION IN THE DIFFERENT CUTS FOR THE SHIFT.

Assessment 2 : 1995-08-02

SENSOR POSITION	MAX. LEVEL RECORDED (%)	LEVEL RELATIVE TO CAB SENSOR (%)	
		MEAN	SSD
RIGHT REAR (CABIN)	0.40	REF	REF
RIGHT MIDDLE	2.65	257.69	66.62
RIGHT FRONT	2.12	750.98	535.87
LEFT FRONT	0.95	902.14	528.04
LEFT MIDDLE	1.08	465.15	263.88
LEFT REAR	0.30	133.83	90.03

ASSESMENT 2 : 1995-08-02

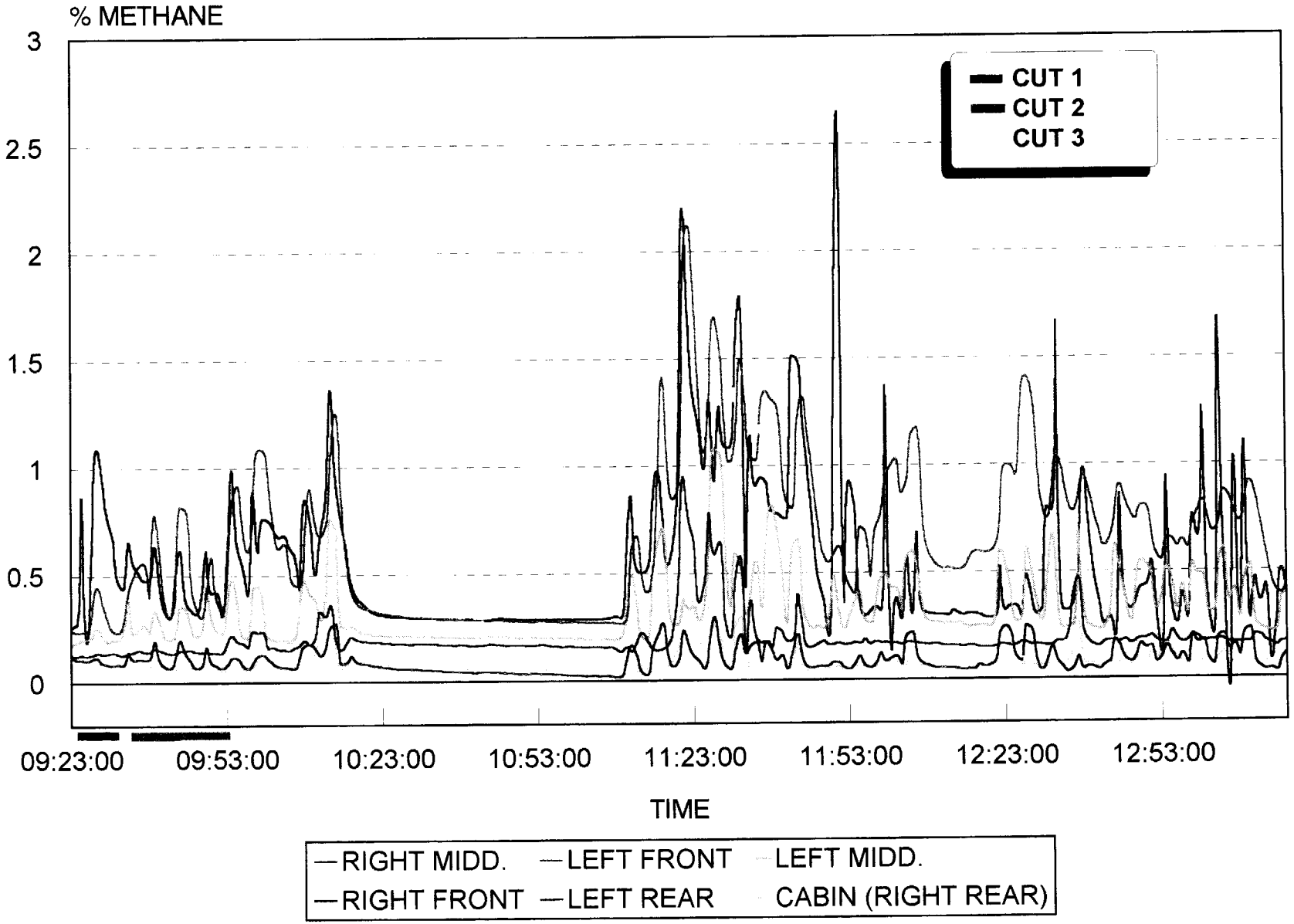

CUT REFERS TO THE PROGRESSION IN THE DIFFERENT CUTS FOR THE SHIFT.

Assessment 3 : 1995-08-02

SENSOR POSITION	MAX. LEVEL RECORDED (%)	LEVEL RELATIVE TO CAB SENSOR (%)	
		MEAN	SSD
RIGHT REAR (CABIN)	0.40	REF	REF
RIGHT MIDDLE	0.81	397.18	870.85
RIGHT FRONT	-	-	-
LEFT FRONT	1.43	1125.72	2036.76
LEFT MIDDLE	0.87	725.49	1420.78
LEFT REAR	0.34	133.23	136.72

ASSESMENT 3 : 1995-08-02

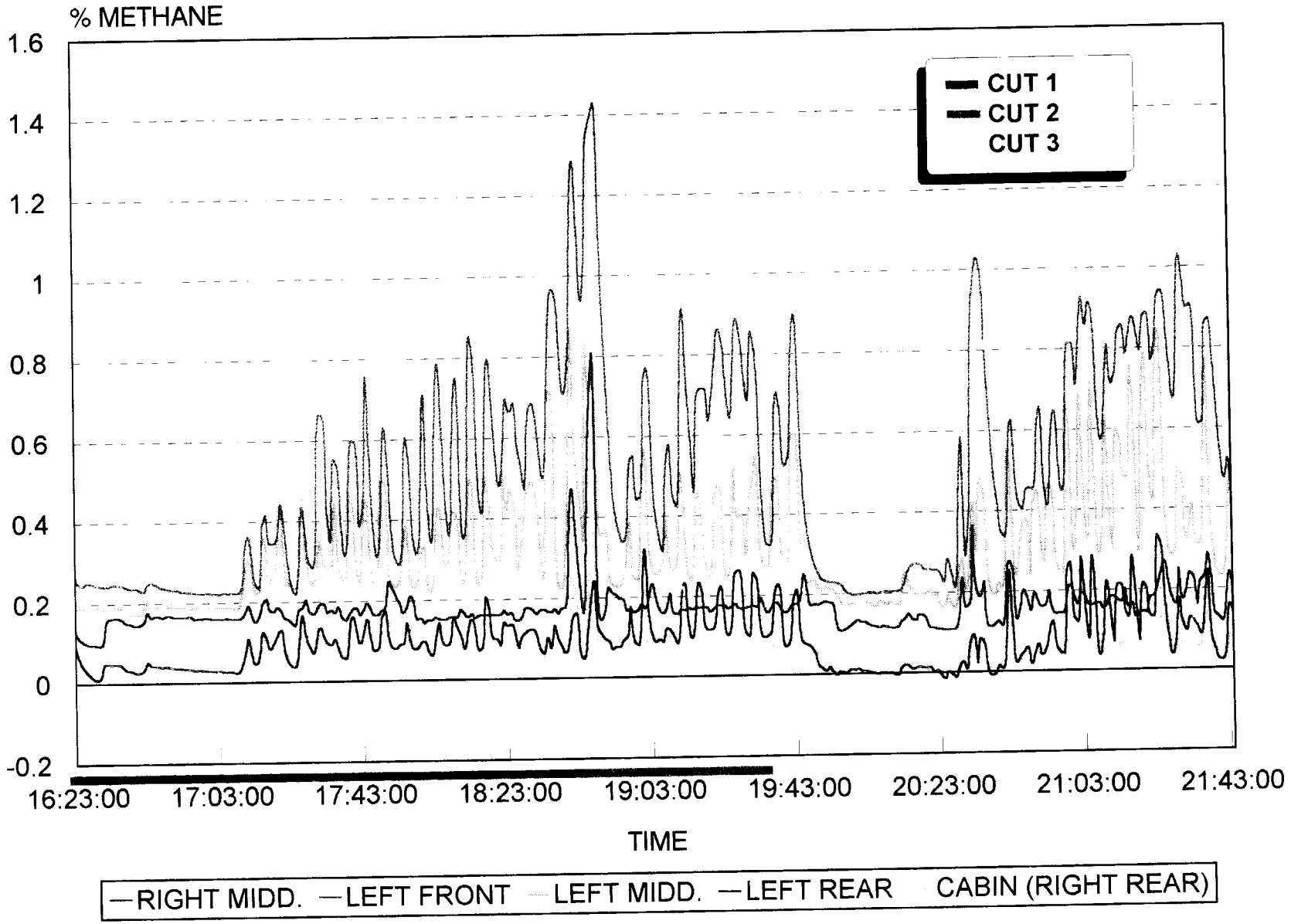

CUT REFERS TO THE PROGRESSION IN THE DIFFERENT CUTS FOR THE SHIFT.

Assessment 4 : 1995-08-04

SENSOR POSITION	MAX. LEVEL RECORDED (%)	% VARIATION FROM FRONT LEFT SENSOR	
		MEAN	SSD
RIGHT REAR (CABIN)	0.12	REF	REF
RIGHT MIDDLE	0.23	247.85	64.89
RIGHT FRONT	-	-	-
LEFT FRONT	1.02	644.16	391.71
LEFT MIDDLE	0.37	323.43	101.20
LEFT REAR	0.13	88.87	21.32

ASSESMENT 4 : 1995-08-04

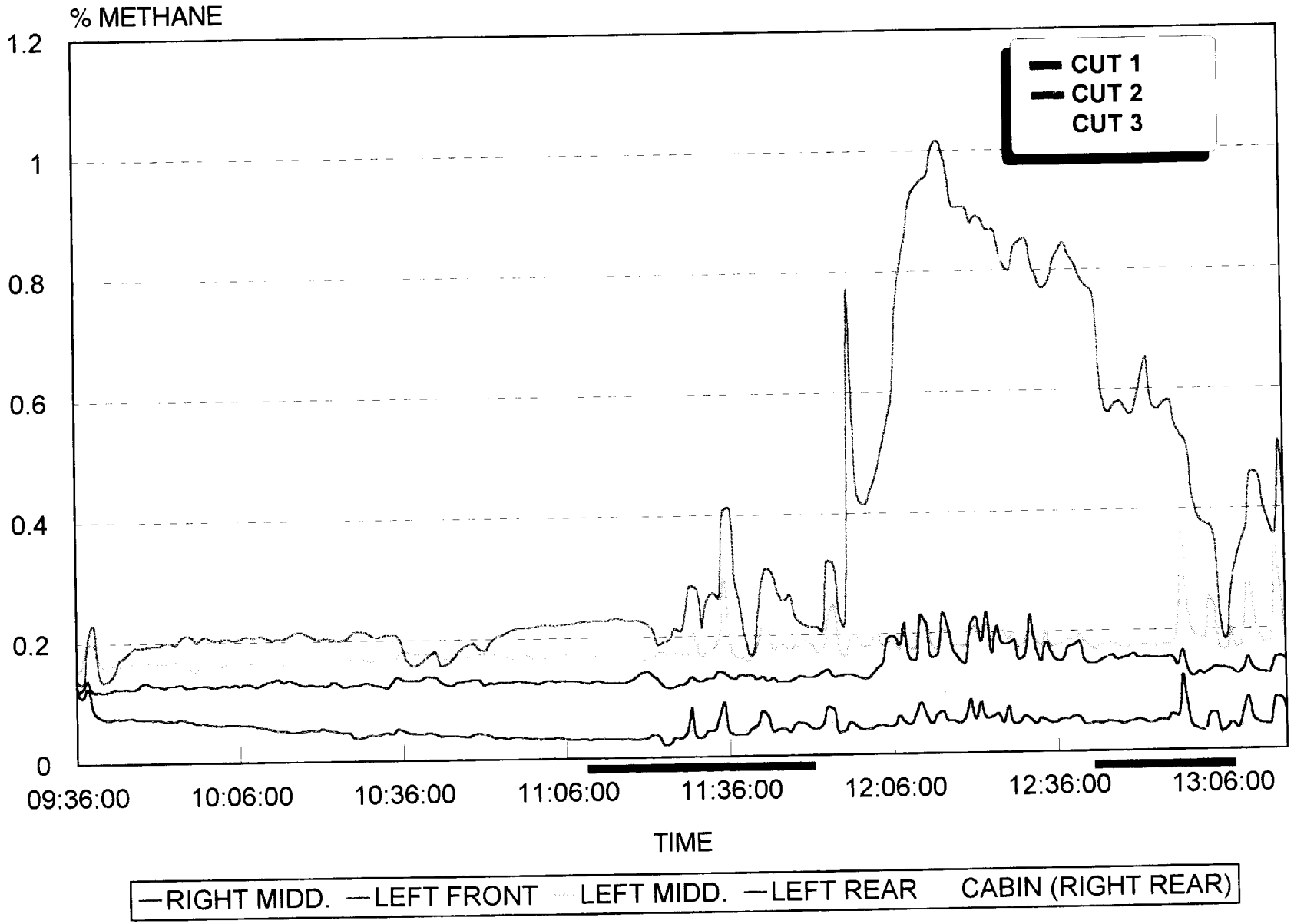

CUT REFERS TO THE PROGRESSION IN THE DIFFERENT CUTS FOR THE SHIFT.

Assessment 5 : 1995-08-10

SENSOR POSITION	MAX. LEVEL RECORDED (%)	% VARIATION FROM FRONT LEFT SENSOR	
		MEAN	SSD
RIGHT REAR (CABIN)	0.25	REF	REF
RIGHT MIDDLE	0.30	171.88	28.18
RIGHT FRONT	-	-	-
LEFT FRONT	2.18	561.46	351.98
LEFT MIDDLE	. 1.40	309.66	133.77
LEFT REAR	0.39	95.71	44.64

ASSESMENT 5 : 1995-08-10

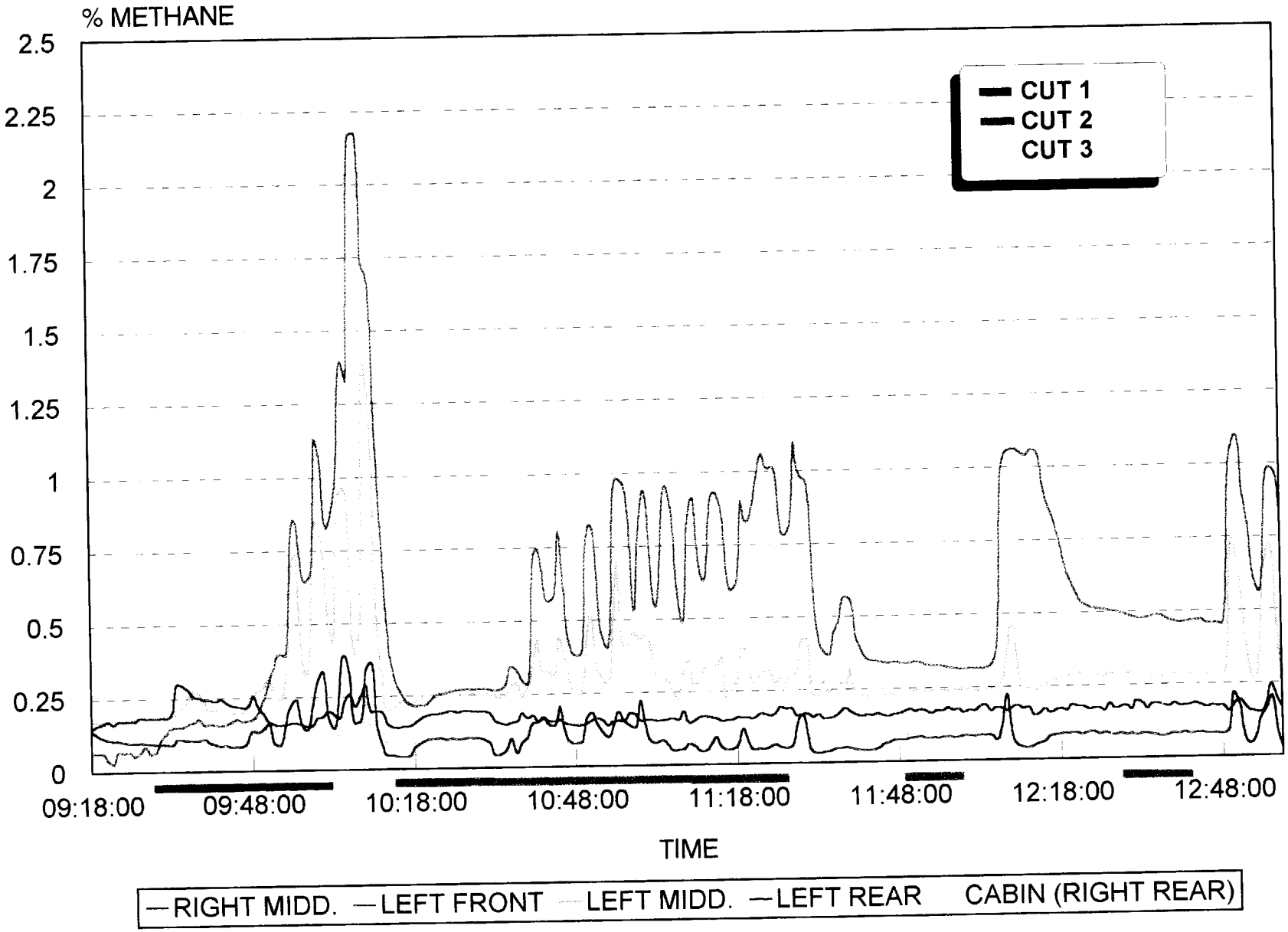

CUT REFERS TO THE PROGRESSION IN THE DIFFERENT CUTS FOR THE SHIFT.

METHANE MONITORING USING A MULTIPURPOSE DATA LOGGING STATION

AP Cook

CSIR MININGTEK, Johannesburg, South Africa

ABSTRACT: Methane levels have been continuously monitored and recorded, at several positions, on and around continuous miners and roadheaders during mining operations. This has been achieved using a data logger system recording input from six methanometers every 10 seconds over a full shift. The logger is fully self contained, comprising a battery, recording station, data logger and methanometers.
Methane levels around continuous miners and roadheaders are generally less than 1 %, but can be higher, particularly on the return side of the machine, and around the cutting drum if ventilation flow to the face is restricted.
A smaller two-channel version is being used to monitor methane levels and atmospheric pressure. Methane in a return affected by a sealed off section shows two distinct periods of increased levels during each 24 hour period, coinciding with reductions in atmospheric pressure.
The data logger system has potential for further development, with the addition of other suitable types of sensor. Present work is to add two dust sensors for evaluation of hybrid mixtures at the face.

1. INTRODUCTION

The Mining Technology Division of the CSIR (Miningtek) is carrying out a wide ranging research programme aimed at reducing the hazards of methane gas in South African mines. The work covers methane emission rates, drainage, effects of atmospheric pressure, effective ventilation, and improved methane monitoring. The main focus is mechanised mining sections using continuous miners (CM's) and roadheaders (RH's.) and ensuring adequate ventilation and methane monitoring requirements. This involves accurate monitoring of methane in working sections and around mining machines while they are operating. The positions are not manually accessible so remote means was required to measure and record data. A system was being developed for longer term recording of atmospheric pressure and methane levels, so this was adapted for multi-input recording over a shift. The main application of the system therefore became monitoring methane

levels on and around mechanical mining machines.
This paper briefly describes the data logger system and its application for methane monitoring as well as giving some example results from CM's, RH's and atmospheric pressure monitoring.

2. DATA LOGGER SYSTEM

A detailed description is given by Kononov and Cook, 1995.

2.1 Multi-channel methane monitor

The system is fully self contained, independent of an outside power source or outside inputs, and is built inside a carry case of dimensions 300*300*100 mm, see Figure 1. It comprises a data logger with eight analogue and two digital input channels, and an input station to house the logger. The initial version has six methanometers, powered by a 12v battery. The methanometers are connected by 12 m armoured cables to square sockets on the outside of the case, allowing the case to be disconnected and removed without removing the methanometers from their installed positions. The cables and sockets are colour coded for ease of repeat installation.

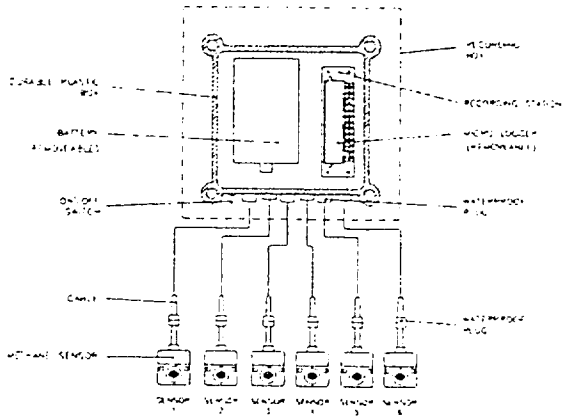

Figure 1. 6-Channel data logger unit

2.2 Two-channel pressure and methane monitor

This unit is also fully self contained, and is in a smaller case as only two sensors are required, see Figure 2. The pressure sensor is inside the case, to offer it protection, and the methanometer is attached to the outside.

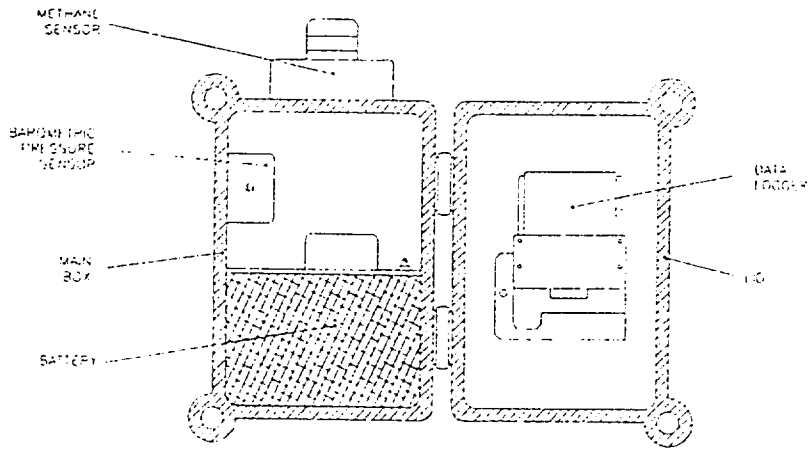

Figure 2. Atmospheric pressure and methane monitoring unit

2.3 Operation

The data logger is programmed and downloaded using a PC. Each of the channels can be programmed independently for sampling intervals, gain and offset, and output units. After being programmed recording begins when it is installed in the recording station and stops again when it is removed. Data can be retained for up to 30 days by the logger before downloading, but in normal use the logger is downloaded immediately after a test, and then stored on trickle charge.

3. CONTINUOUS MINER INSTALLATION

An installation configuration for a continuous miner is shown in Figure 3. The six methanometers are positioned on the CM as close to the cutting drum as possible; on the return side of the boom; at the drivers cab; and at the mid point and rear return side. These positions give comparisons of levels around the CM, and also indicate the effectiveness of common ,or possible, positions for production methanometer applications. The methanometers and cables are fastened using cable ties, and plastic hoods protect the sensors most exposed to sprays, dust and coal. The simple plastic hoods extend the operating life of these sensors from 15 minutes to 10 days.
Methanometer positions vary from these depending on the CM and the ventilation system used. This particular example has been used to illustrate a low seam application with no on-board scrubber.

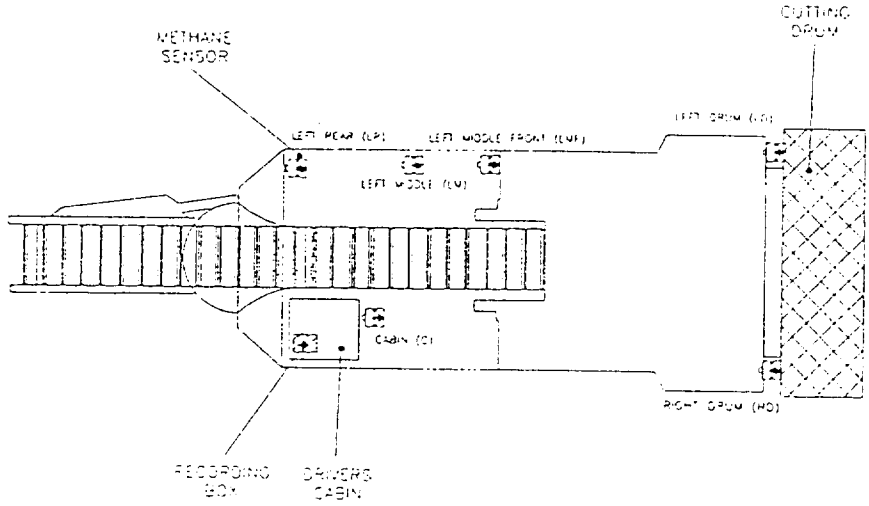

Figure 3. Typical methane montoring positions on a continuous miner.

3.1 Continuous miner results

Methane levels recorded on a CM working a 2 m seam height are given in Figure 4, which shows a plot of methane levels against time. Only a short period from a full shift is presented for clarity. Ventilation was by force and exhaust columns.
The highest levels were recorded at the front left boom position in the early part of the shift, when the methane peaked at over 2 % and remained at levels above 1% for more than 1 hour. During this period the CM was sliping to the left, so the left front boom was confined and the ventilation flow to this area obviously restricted. These high levels do show a general downward trend as the CM advances and the restriction to the front left becomes less. This CM was not equipped with directional sprays, which would have assisted in getting air to the front.
In general around the CM, the methane levels were below 1%, so the ventilation over the CM is sufficient to dilute the methane.

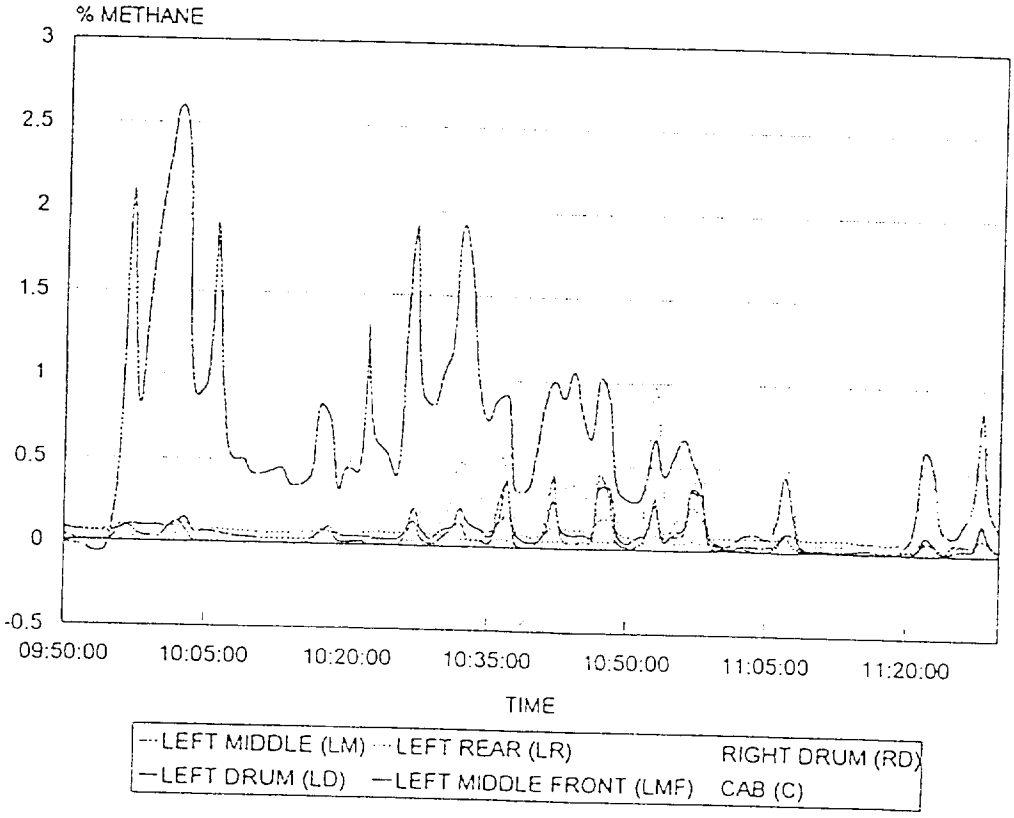

Figure 4. Methane levels recorded around an active continuous miner.

4. ROAD HEADER INSTALLATION

Roadheader installation is similar to that for CMs with the only significant difference being on the boom, see Figure 5. Two methanometers are positioned on the boom, left and right, but there is not the same distance between them as on the CM. Also they are not as close to the cutting head as there is no practical place to fasten them. A more permanent installation would require welding on supporting brackets.
This example is of a RH equipped with an on-board scrubber, and working in a 4 m seam height. Force ventilation was from an air jet fan.

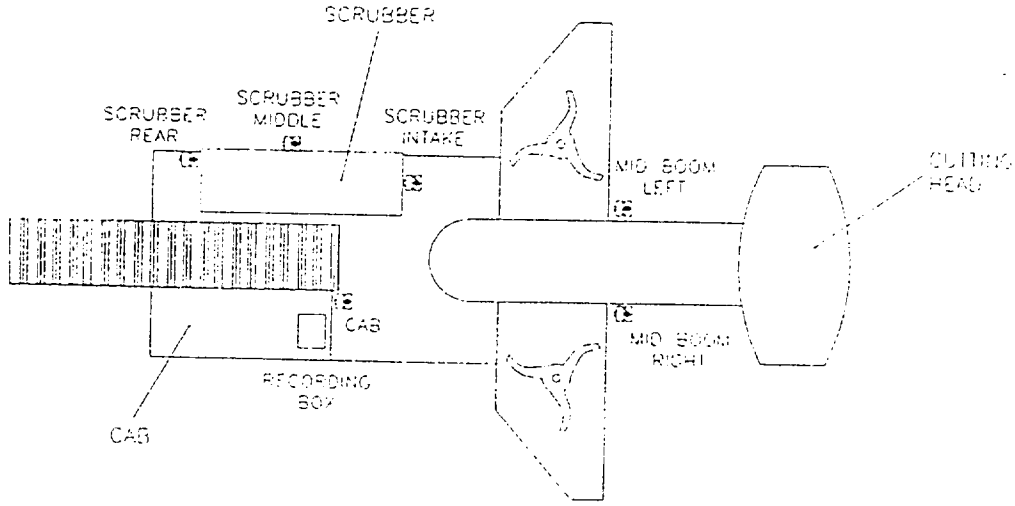

Figure 5. Typical methane monitoring positions on a roadheader

4.1 Roadheader results

Methane levels recorded on a RH are given in Figures 6 and 7, showing plots of methane levels against time. Again only short periods are given from each shift.

Figure 6 shows advance in a straight, from initially being in through ventilation, to being a fully developed heading. The two boom sensors generally recorded the highest methane levels, with the rear scrubber position being lowest. The scrubber intake position began at high readings but these declined as the RH advanced, from a peak of around 0.5 % to a constant 0.2 %. So this position was certainly influenced by the through ventilation, before being affected only by the high volume of the scrubber flow. So the scrubber intake is not a very effective position for a methanometer as the response time is inadequate for the high volume flow.

As the RH advanced the two mid position sensors, scrubber middle and the cabin, show increasing levels, and also increasing with respect to the boom. So the effectiveness of the ventilation to dilute the methane form the face back over the RH is reduced.

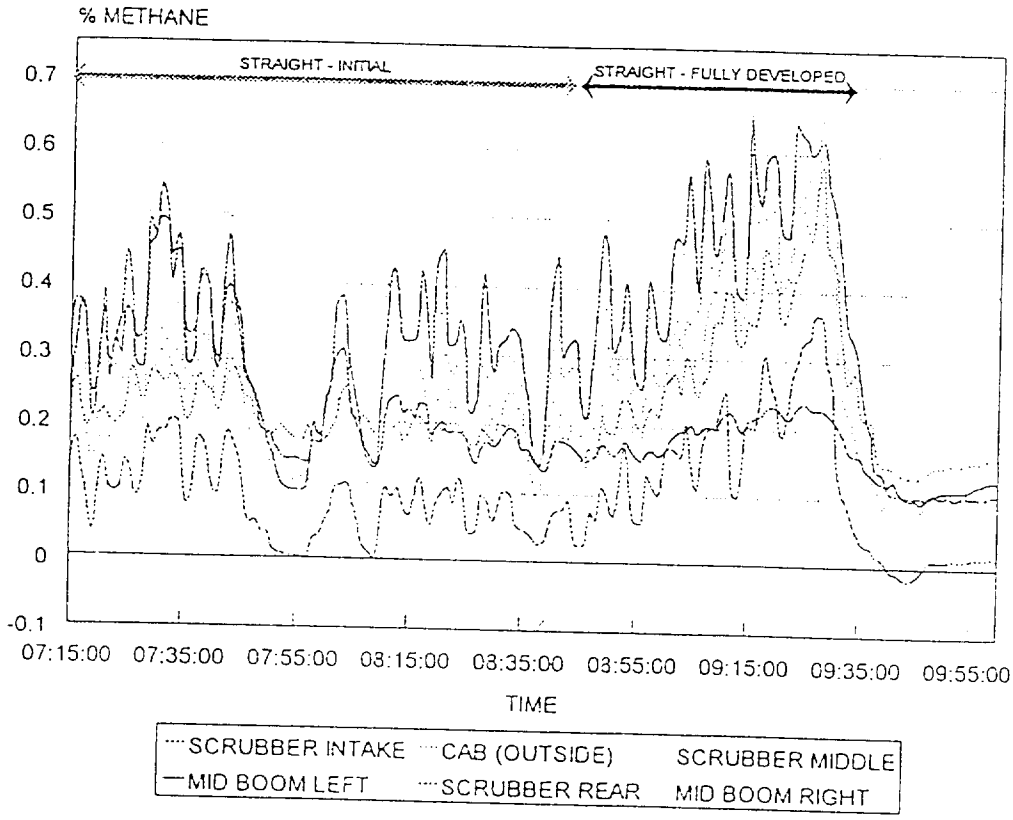

Figure 6. Methane levels recorded around an active roadheader.

Figure 7 shows results for mining in a split to the left. At the beginning of the shift the two boom sensors recorded the highest levels., but as the RH advanced the mid positions became more significant, eventually replacing the boom right as the second highest readings. Again the ratio between the boom sensors and mid sensor readings decreased with advance, so the ventilation effectiveness dropped.
The rear return sensor recorded the lowest levels, with the scrubber intake being constant throughout the shift, where the volume flow is too great for suitable response.

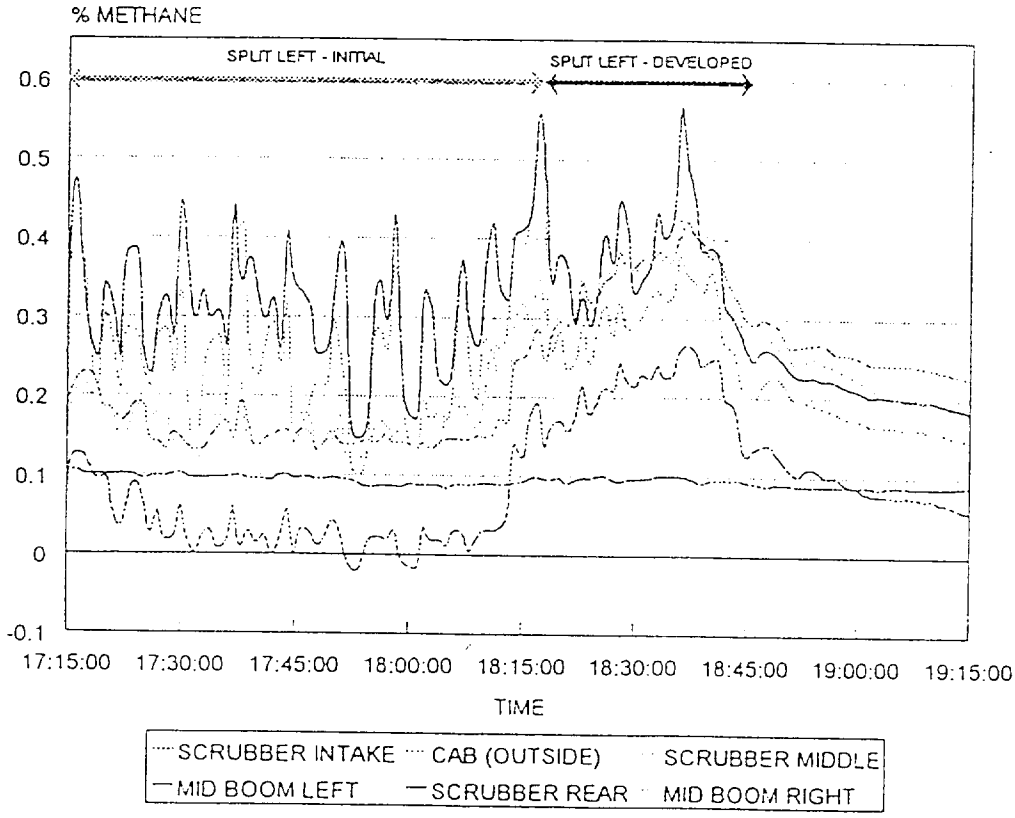

Figure 7. Methane levels recorded around an active roadheader.

5. ATMOSPHERIC PRESSURE

The smaller atmospheric unit is carried underground, and installed in the required monitoring position. It operates unattended for about ten days, recording from the two sensors every five minutes.

5.1 Atmospheric pressure results

Methane levels compared to atmospheric pressure are shown in Figures 8 and 9, plotted against time over a 24 hour period.

Figure 8 shows results from the return of a conventional drill and blast section. There is no obvious correlation between the methane and the pressure, with a fairly constant pressure plot comparing with variable methane levels showing peaks and drops. The recording period was 24 hours, with pressure remaining around 84 kPa and methane levels remaining below 1 %.

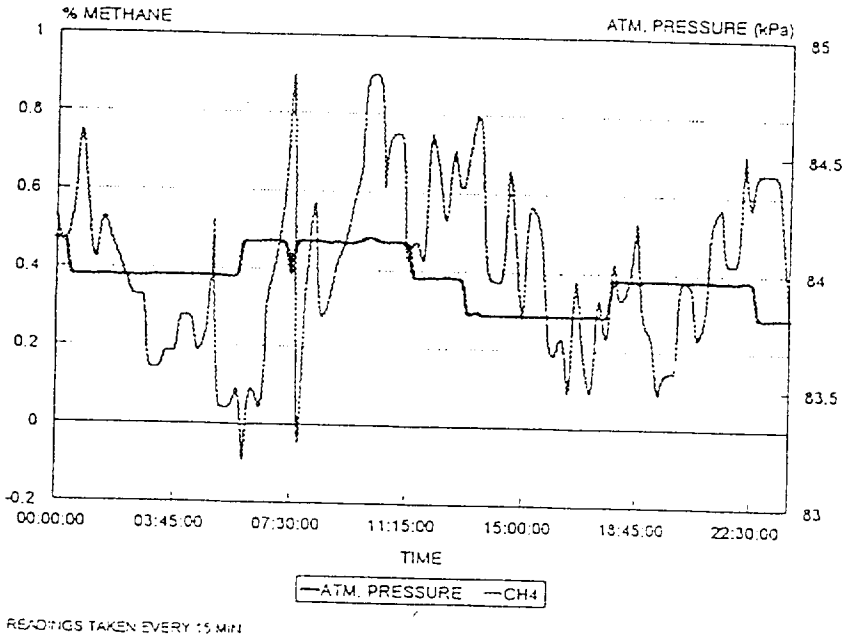

Figure 8. Methane levels and atmospheric pressure recorded over a 24 hour period.

Figure 9 shows results from a return influenced by a sealed off area. Methane levels behind the seal were 34 % at the time of the monitoring, and some of the gas was definitely being emitted through the seals into the return. In this case there are obvious patterns to the methane levels, with two distinct periods when methane occurred. These coincide with the diurnal changes in pressure.

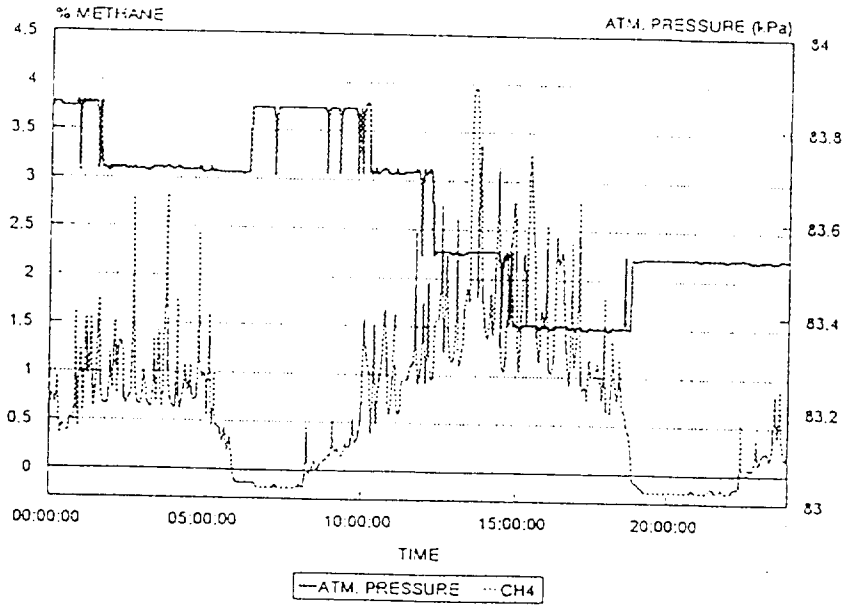

Figure 9. Methane levels and atmospheric pressure recorded over a 24 hour period.

Figure 10 shows these results over a three day period, and the pattern is obvious over the full monitoring time. There are two periods of increased methane levels within every 24 hours.

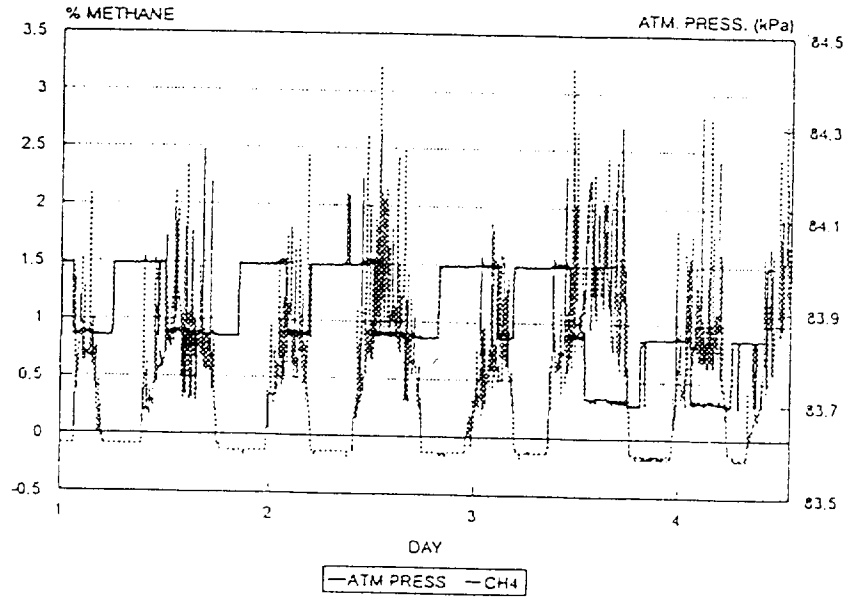

Figure 10. Methane levels and atmospheric pressure recorded over a period of three and a half days.

6. CONCLUSIONS

Methane monitoring over extended time periods has been possible using the data logger system developed by Miningtek. It has enabled real time monitoring both in positions that cannot be manually recorded, as well as over long term periods.

Methane levels around continuous miners are generally less than 1 % but with regular peaks higher than this close to the cutting drum, and extended periods higher where the ventilation flow is restricted.

For roadheaders the methane pattern is similar to that for continuous miners, although to date, sensors could not be positioned as close to the cutting drum.

Ventilation effectiveness for methane dilution reduces as the machines advance, with all sensors recording increased methane levels, and the mid position sensors showing increased levels compared to those at the cutting drums.

The scrubber intake is not a very effective position for methanometers, with the response being too slow for the high volume flow, and a damped effect generally being recorded.

This position does show better results when the machine is still in through ventilation

Atmospheric results are as yet inconclusive, as this is intended as a longer term monitoring programme, however for the return influenced by the sealed off section there were two definite periods of increased methane levels during each 24 hour period, coinciding with lower atmospheric pressure.

7. FURTHER DEVELOPMENT

The basic system has potential for further development and a range of applications, both as a research tool and for the production environment. Initial research developments are the addition of further sensors. Two optical type dust sensors are being added to quantify the hybrid dust and methane mixtures present around the cutting drum, and other suitable environmental sensors are being sourced.
There is also intended development as a full environmental monitoring station, for application as a short term alternative or support to a mine wide system.

8. ACKNOWLEDGEMENT

This work forms part of the coal mining safety research programme approved and supported by the Safety in Mines Research Advisory Committee (SIMRAC). The author acknowledges the contribution and input of the members of SIMRAC, SIMCOL, COLLEAG and the SIGEH and SIGDS interest groups.

9. REFERENCE

Kononov, V.A. and Cook, A.P., "Multi Purpose Data Logging Stations for Underground Experimental Monitoring" 26th International Conference of Safety in Mines Research Institutes, Katowice, Poland, September 1995.

APPENDIX B

B1. P. Linzer, A 3-Dimensional Dual-Porosity Single-Phase Unsteady-State Mathematical Model of Gas Transport in Coal Structures, 26th International Conferences of Safety in Mines Research Institutes, September 1995, CSIR Division of Mining Technology.

B2. P. Linzer and A.P. Cook, Quantifying Methane Emissions from Coal, SIMRAC Symposium, July 1995, CSIR Division of Mining Technology.

B3. P. Linzer, A Numerical Simulator for 3-D Unsteady-State Dual-Porosity Modelling of Gas Flow Within a Coal Structure, 7th US Mine Ventilation Symposium, June 1995, CSIR Division of Mining Technology.

B4. P. Linzer , A General State Model of Methane Transport in Coal Structures, Draft Report, May 1994, CSIR Division of Mining Technology.

B5. P. Linzer, Report Back of European Visits to Determine the Position of Miningtek's Methane Emission Model, Internal note, September 1995, CSIR Division of Mining Technology.

B6. A.P. Cook, Evaluating the Methane Gas Conditions in Underground South African Coal Mines, 25th International Conference of Safety in Mines Research Institutes, September 1993, CSIR Division of Mining Technology.

B7. CSIR Miningtek, Typical Values for South African Coal Properties as Methane Emission Prediction Model Inputs, January 1993 to November 1995, CSIR Division of Mining Technology.

APPENDIX B1

A 3-DIMENSIONAL DUAL-POROSITY SINGLE-PHASE UNSTEADY-STATE MATHEMATICAL MODEL OF GAS TRANSPORT IN COAL STRUCTURES

Patrick Linzer

CSIR Division of Mining Technology
PO Box 91230, Auckland Park, 2006
Republic of South Africa

ABSTRACT: The liberation of combustible gas from coal seams into underground workings is a well-recognised hazard and modelling of the phenomenon generally inefficient. In accordance with the theoretical bases of most of the more complex extant models describing gas migration in, and liberation from, coal formations, the one presented herein proceeds from the assumption that two principal gas flow modes, namely diffusive and Darcy permeable, coexist in an idealised matrix. Diffusive flow within individual coal/carbonaceous grains is approximated to a high degree of accuracy. Darcy flow considerations include *inter alia* corrections for laminar-inertial turbulence, induced strains and the presence of water, although water transport is neglected. The model does not treat the large-scale structure as a continuum, nor does it assume isotropy or homogeneity in geometric or physical properties. Elemental random fluctuations in these properties are catered for, as are the effects of mining activity, goafing (where applicable) and the contributions made by the surrounding geology on total gas make. Some suggestions for PC adaption of the model are made.

1. INTRODUCTION

The single greatest hazard associated with coal exploitation from underground workings is the almost continuous and ubiquitous liberation of combustible gases, chiefly composed of methane and hydrogen, into the working environment. These gases mix with the ventilating air and may result in (localised) regions of flammable or even explosible gas mixtures which require very little energy for their ignition. Such an ignition usually has disastrous consequences.

Much effort has been invested worldwide in gaining an understanding of the mechanisms involved in gas formation, its retention and its release in order that effective countermeasures can be implemented. A key element to the success of this endeavour rests on the availability of efficient and reasonably accurate quantitative prediction models. Such models do exist but their predictions do not generally correlate well with observations made in the South African context. This may be as a result of various factors that include oversimplifications, input data deficiencies, inadequate approximations and/or computational instabilities.

In addition, the availability of such models in South Africa is poor, with collieries having to resort

to expensive overseas facilities for this service.

This paper outlines the derivation of such a prediction model for South African conditions. The model is currently in a process of computerisation for PC use, and once this is complete, its predictive value will be assessed.

2. MODEL OUTLINE

Existing models of this nature range from the relatively simple to the very complex. Most of the complex models rest on the assumption that two dominant flow regimes control the gas flow in an idealised coal structure (Figure 1).

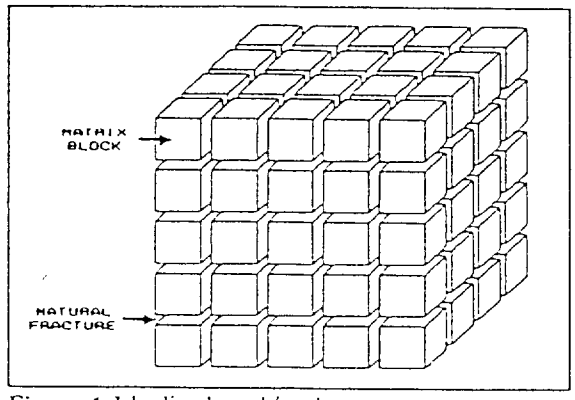

Figure 1 Idealised coal/rock structure

Diffusive flow (carbonaceous material only) is limited to grains or particles (areas labelled 'MATRIX BLOCK'), while Darcy permeable flow is confined to void spaces such as cleats and natural fractures. The two gas transport mechanisms are interlinked in that the gas diffusing from the particle affects the pressure gradient in the matrix, which controls the macroscopic permeable flow rate, while the local pressure in the void space affects the adsorbed gas concentration on the free surfaces of the particle, which in turn affects the microscopic diffusion rate. The flow modes are linked via the Langmuir isotherm describing monolayer (ad)sorption.

This idealisation reflects the dual-porosity and fundamentally discrete nature of coal formations. All carbonaceous material is treated similarly due to the affinity carbon has for compounds with protruding hydrogen groups (eg. CH_4, H_2O). Non-carbonaceous material is similarly idealised, but it is assumed that no diffusive gas transport occurs in the particles. The idealisation is rationalised in the case of carbonaceous material by the presence therein of a great number of cleats, fractures and other planar discontinuities, and in the case of other mineral matter by its granular composition.

Diffusive flow in a particle is treated as a continuum process and is analyzed separately. A suitably accurate approximation describing this phenomenon replaces the 'exact' numerical technique(s) normally employed in generating solutions to a given diffusion problem, reducing the required computational effort. Sorptive processes on free surfaces are assumed to occur sufficiently fast for equilibrium conditions to exist on these surfaces.

Unlike other models, the analysis of Darcy flow is not taken to the limiting case where elements are assumed to be infinitesimally small, so that the resulting equations contain finite difference terms rather than differentials. Material permeability is quantified from first principles in terms of the idealised structure geometry to facilitate appraisal of the effect induced strains and free moisture have on the permeability and thus on flow rates. The contribution made by dissolved gas in moving groundwater is neglected since very few South African collieries have significant quantities of moving groundwater.

To varying degrees, all of the factors governing methane transport in coal are subject to spatial and temporal variabilities of a (seemingly) random nature. For example, cleat widths can vary from a few μm to a few mm, and it is highly improbable that diffusion coefficients and intrinsic permeabilities are

uniformly distributed. It is commonly held that these variations are adequately catered for by averages, but secure knowledge of these averages is rare and often meaningless as a result of ignorance surrounding the type and dispersion of the distribution of values they represent. Most existing models are in this sense completely deterministic.

To cater for the above, the model includes a device which allows normally and lognormally distributed random factors (within definable limits) to be applied to any or all governing parameters. The author believes that this will enhance the model's predictive merit.

Since coal structures have remained relatively undisturbed for long periods, it is reasonable to assume that initially, the amount of adsorbed gas held in the particles is in equilibrium with the (pressurised) free gas present in the void space, and remains so until this balance is disturbed. Thus, both the initial pressure gradient and the initial concentration gradient in the case of carbonaceous material are zero in an undisturbed region within a coal formation. Other mineral matter initially has only a zero pressure gradient.

Mining or drilling of a seam disturbs the equilibrium by allowing free gas to escape, thus altering the in-seam pressure distribution profile. Consequently, gas molecules desorb from free surfaces within zones of diminished pressure and appear as free gas. Gas desorption in turn changes the adsorbed gas concentration. The planar discontinuity network (macropore network) provides the conduits in which free gas migrates under the influence of local pressure gradients.

Changes in the adsorbed gas concentration on surfaces adjoining or delimiting the macropore network introduce non-zero concentration gradients within the particle's pores (micropore system), which, in accordance with Fick's first law, preferentially drive gas molecules from areas of higher to areas of lower concentration -ie. internally adsorbed gas diffuses in the micropore regions, prevalently migrating towards surfaces where the free gas pressure is at a minimum.

From the preceding discussion, it is clear that in-seam gas transport occurs as long as adsorbed gas is present and either pressure or concentration differences, or both, exist, and consequently that gas will be emitted from any free coal surface as long as these conditions hold. It has been estimated that as much as 90% of the total seam gas content is retained by adsorption [Stripp,1989], and since diffusion is a comparatively slow process, gas is constantly being emitted in any underground coal working.

3. MATHEMATICAL DERIVATIONS

Diffusion: From the preceding description of adsorbed gas behaviour in a particle, it is clear that the following set of similar constraints always applies: (1) a uniformly distributed initial concentration, and (2) an outer surface concentration quantifiable in terms of the surrounding gas pressure.

General state diffusion without sources or sinks is described by

$$\frac{\partial C}{\partial t} = \nabla(D \cdot \nabla C) \qquad (1)$$

[A glossary of the mathematical symbols used is appended to this article]

The initial and boundary conditions that the solution to Equation (1) must satisfy disallow analytical

methods. Traditionally, the solution is generated numerically, but the methods employed are generally time consuming, particularly when accuracy is a prime concern. This problem is overcome by assuming the following (refer also to Figure 2):

(1) The coal particle is a homogeneous isotropic cube with a side length of 2λ, $\lambda > 0$ -ie. $\delta x = \delta y = \delta z = 2\lambda$ so that D is constant and the directional dependence of permeability is catered for by allowing the width of the void space at various faces of the cube to vary -ie. $\Delta x \neq \Delta y \neq \Delta z$ generally;

(2) Diffusive flow is symmetric along any symmetry axis of the particle. Thus the cube can be divided into six equal right pyramids with their apexes at the geometric centre of the cube and within each pyramid gas flow is unidirectional along the line joining the centre of the base and the apex;

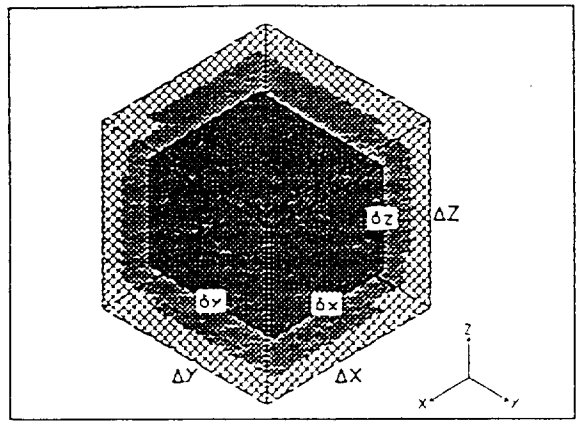

Figure 2 Idealised coal/rock element

(3) The instantaneous surface concentration C_s changes (decreases) smoothly and relatively slowly so that it may be approximated by a constant over a short time period, and the initial concentration C_0 is uniform throughout the cube. This assumption is warranted on the basis of in-seam gas generally not being subject to pressure or temperature extremes or abrupt changes in these.

Using these assumptions and Equation (1), diffusive flow in any pyramid is described by

$$\frac{\partial C}{\partial t} = D \cdot \frac{\partial^2 C}{\partial x^2} \tag{2}$$

where x increases from the apex perpendicularly towards the centre of the pyramid's base. Both x and t can now be normalized by letting $x = \lambda \xi$ and $Dt = \lambda^2 \tau$. Since any linear function of a solution to Equation (2) is also a solution, letting $C = C_s + (C_0 - C_s) \cdot C^*$ reduces the problem to solving

$$\frac{\partial C^*}{\partial \tau} = \frac{\partial^2 C^*}{\partial \xi^2} \tag{3}$$

subject to $0 \leq \xi < 1$, $\tau \geq 0$, $C^*(\xi,0) = 1$ and $C^*(1,\tau) = 0$.

For the model, the particle's internal concentration distribution is not important, merely the total gas content therein as a function of time, the initial concentration and the instantaneous surface concentration. For convenience, concentrations are measured in units of mass of gas per unit mass of coal, so that the total gas mass in the cube at time t is given by Equation (4).

$$Q(t) = 8\lambda^3 \rho_c \left(C_s + 3 \cdot (C_0 - C_s) \cdot \int_0^1 C^* \xi^2 \, \partial \xi \right) \tag{4}$$

Solutions to Equation (3) were generated numerically and the corresponding value of the integral term in Equation (4) determined at 52 different times, the largest of which corresponds to $\tau = 1.6$, where the integral term is less than 10^{-8}. This was done with the pyramid divided into 25, 50, 100, 200, 400 and 1000 slices. A graph of the results is shown in Figure 3.

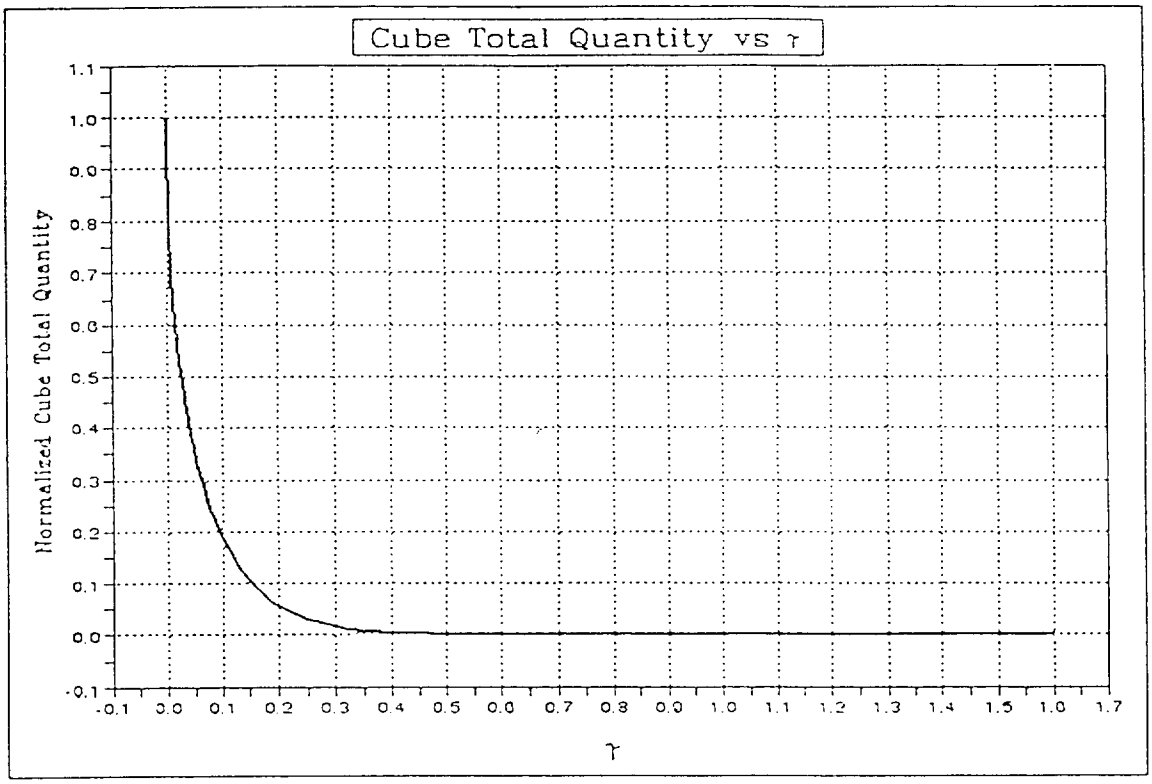

Figure 3 Graph of $Q(\tau)$ normalized vs τ

The following regression equation was fitted to the results:

$$Q(t) = 8\lambda^3 \rho_c \left(C_S + (C_0 - C_S)\cdot e^{T}\right)$$

$$T = k_0\tau + k_1\left((1+k_2\tau)^{\alpha} - \frac{k_3}{k_3 + (k_4\tau)^{\beta}}\right)^{\frac{1}{\alpha}}$$

$$\tau = \frac{D}{\lambda^2}t$$

$$k_0 = 7.264 \quad k_1 = -0.513 \quad k_2 = 37.168 \quad k_3 = 0.692$$

$$k_4 = 15.831 \quad \alpha = 1.876 \quad \beta = 1.593 \qquad (5)$$

The regression coefficient for this relationship is $r^2 = 0.999999831$, indicating an excellent fit. The largest absolute error is +0.00013 at $\tau = 0$, and the largest relative error is +0.89% at $\tau = 0.24$.

Sorption and Gaseous Behaviour: In order to quantify the surface concentration C_S and the initial concentration C_0 of the particle, use is made of the Langmuir isotherm (Equation (6)) and the Real Gas Law (Equation (7)).

$$V_{eq} = m_c \cdot \left(\frac{L_1 L_2 p}{1 + L_2 p} \right) \tag{6}$$

$$pV = \kappa n R T = \kappa \frac{m_G}{M_G} R T \tag{7}$$

The Langmuir isotherm relates the total adsorbed gas volume (at stp) at a fixed temperature to the ambient gas pressure. On the assumption that sorption rates on the outer surfaces of the particle are sufficiently rapid, a suitable rearrangement of Equations (6) and (7) yields

$$C_s = \left(\frac{p_{std} M_G}{\kappa R T_{std}} \right) \cdot \left(\frac{L_1 L_2 p}{1 + L_2 p} \right) \tag{8}$$

and

$$C_0 = \left(\frac{p_{std} M_G}{\kappa R T_{std}} \right) \cdot \left(\frac{L_1 L_2 p_-}{1 + L_2 p_-} \right) \tag{9}$$

It should be noted that pressures are absolute, not gauge pressures. In addition, the mass of free gas held in the void space of an element in terms of the surrounding gas pressure and the element dimensions can be related by substituting the relevant expressions into Equation (7) and rearranging. This results in

$$m_G = \left(\frac{M_G (\Delta x \Delta y \Delta z - 8\lambda^3)}{\kappa R T} \right) \cdot p \tag{10}$$

Permeability and Darcy Flow: The fundamental steady state Darcy permeable flow equation for anisotropic permeability in a three-dimensional rectangular co-ordinate system is

$$\vec{q} = -\frac{1}{\eta} \cdot \left(K_x \frac{\partial p}{\partial x} \vec{i} + K_y \frac{\partial p}{\partial y} \vec{j} + K_z \frac{\partial p}{\partial z} \vec{k} \right) \tag{11}$$

For a particular direction $\vec{\zeta}$, Equation (11) reduces to

$$q_\zeta = -\frac{K_\zeta}{\eta} \cdot \frac{\partial p}{\partial \zeta} \tag{12}$$

Analytically, it has been shown [De Wiest, 1969] that Darcy's law is the empirical equivalent of the general Navier-Stokes equations statistically averaged in a steady flow regime with negligible inertia, but the demonstration requires assumptions of invariance in certain quantities known not to behave thus. The permeability of a material is proportional to its porosity and the square of the average pore size, but the constant of proportionality is indeterminate without knowledge of the permeability. A

different approach to quantifying the permeability is via the steady state laminar flow law for circular ducts proposed by Poiseuille

$$\dot{V}_\zeta = -\frac{\pi a^4}{8\eta}\cdot\frac{\partial p}{\partial \zeta} \tag{13}$$

From the preceding discussion it is clear that permeability is affected by the void cross-sectional area available to flow per unit cross-sectional area of medium, and the internal surface area with which the fluid is in contact per unit volume of medium. For a short cylindrical duct of radius a and length $\Delta\zeta$ through a 'solid' medium of uniform cross-sectional area A_s, Equation (13) translates to

$$q_\zeta = \frac{\dot{V}_\zeta}{A_s} = -\frac{\pi a^4}{8\eta A_s}\cdot\frac{\partial p}{\partial \zeta} = -\frac{K_o}{\eta}\cdot\left(\frac{2\pi a\Delta\zeta}{A_s\Delta\zeta}\right)^{\alpha_0}\cdot\left(\frac{\pi a^2}{A_s}\right)^{\alpha_1}\cdot\frac{\partial p}{\partial \zeta}$$

$$= -\frac{K_o}{\eta}\cdot\left(\frac{A_c}{V_s}\right)^{\alpha_0}\cdot\left(\frac{A_f}{A_s}\right)^{\alpha_1}\cdot\frac{\partial p}{\partial \zeta} \tag{13.a}$$

Analysis of the exponents of a and A_f in the above relationship yields $\alpha_0 = -2$, $\alpha_1 = 3$ and $K_o = 1/2$. It can be shown that the specific discharge of a rectangular duct is in the ratio 8:9 with that of a circular duct for the same fluid velocity, so that the permeability of a medium with rectangular ducts is given by

$$K_{\zeta\square} = \frac{4}{9}\cdot\left(\frac{A_f}{A_c}\right)^3\cdot\left(\frac{V_s}{A_c}\right)^2 \tag{14}$$

The four quantities on the right hand side of Equation (14) are readily expressed in terms of the element dimensions. By letting X stand for any one of x, y or z and Y and Z for the remaining two dimensions, the three equations relating the permeabilities in the three principal directions are summarized by

$$K_X = \frac{\Delta X^2\lambda^2}{9\,\Delta Y\,\Delta Z}\cdot\left(\frac{\Delta Y\,\Delta Z}{4\lambda^2} - 1\right)^3 \tag{15}$$

Given the permeabilities and λ, Δx, Δy and Δz can be solved for, but for the solution to be physically meaningful, $\Delta x \geq 2\lambda$, $\Delta y \geq 2\lambda$ and $\Delta z \geq 2\lambda$ must be satisfied. To facilitate this, the following scheme proves useful:

$$T_x = \sqrt[3]{\frac{9K_x}{\lambda^2}} \qquad T_y = \sqrt[3]{\frac{9K_y}{\lambda^2}} \qquad T_z = \sqrt[3]{\frac{9K_z}{\lambda^2}}$$

$$\Delta x = 2\lambda\sqrt{v}\,(v - T_x) \qquad \Delta y = 2\lambda\sqrt{v}\,(v - T_y) \qquad \Delta z = 2\lambda\sqrt{v}\,(v - T_z)$$

where v is the solution to $(v - T_x)(v - T_y)(v - T_z) = 1$. (15.a)

The *in situ* gas permeability is affected by the following three factors: the fluid pressure, the presence of water and the state of stress in the medium. The fluid pressure dependence is known as the 'Klinkenberg Effect/Slippage' and is quantified by Equation (16).

$$K_\zeta = K_{-\zeta} \cdot \left(1 + \frac{b_\zeta}{p}\right) \tag{16}$$

The presence of (free) water has the effect of reducing the medium's permeability by diminishing the duct area available to flow. It is assumed that water is held as a thin uniform film on the outer surfaces of the particle. The free moisture content of South African coals rarely exceeds 0.05 (viz. 5% of total) by mass, and water, being a polar molecule with protruding hydrogen atoms, will tend to adhere to free coal (carbon) surfaces, so that the assumption about its mode of retention is reasonable. If λ_0 is the particle half-length of a dry particle, then the half-length of a moist particle is given by

$$\lambda = \lambda_0 \cdot \sqrt[3]{1 + \frac{\mu_w \rho_c}{(1 + \mu_w)\rho_w}} \tag{17}$$

The effect of stresses is to alter the void space sizes in accordance with Hooke's Law. Adopting the same symbolic conventions used in Equations (15) and (17), stress effects are described by

$$\Delta X = \Delta X_0 \cdot (1 - \varepsilon_X) \quad \text{where} \quad E\varepsilon_X = \sigma_X - \nu\sigma_Y - \nu\sigma_Z - (1 - 2\nu)\cdot p. \tag{18}$$

The Darcy equation as used so far is valid only where flow is laminar. However, as the gas migrates through the medium, it encounters corners, edges and other irregularities and its flow will hence be (locally) turbulent. The one-dimensional laminar-inertial turbulence corrected flow relationship is derived from the following equations

$$q_\zeta = -C_\Lambda \frac{K_\zeta}{\eta} \cdot \frac{\partial p}{\partial \zeta} \qquad C_\Lambda = 1 + \tfrac{1}{2} \cdot \left(\sqrt{1 + 4Re_\zeta} - 1\right) \qquad Re_\zeta = \frac{\rho_G \sqrt{K_\zeta}\, q_\zeta}{\eta} \qquad \rho_G = \frac{M_G p}{\kappa R T} \tag{19}$$

and is

$$q_\zeta = -\frac{K_\zeta}{\eta} \cdot \left(1 - \frac{M_G \sqrt{K_\zeta^3}\, p}{\kappa R T \eta^2} \cdot \frac{\partial p}{\partial \zeta}\right) \cdot \frac{\partial p}{\partial \zeta} \tag{20}$$

With reference to Figure 4, the mass of gas that diffuses from the particle in element i from time t to t + Δt is given by the relationship $\Delta m_D = Q(t) - Q(t + \Delta t)$ where Q(t) is the function given by Equations (5), (8) and (9). By considering the Darcy flow from element i-1 to i and from i to i+1 as given by Equation (20), the mass of free gas in the void space of element i is readily quantified. The introduction of subscripted ordinal numbers ijk (i ↦ x, j ↦ y and k ↦ z) to distinguish individual elements from one another allows the derivation to be extended to three dimensions, resulting in the set of equations (22).

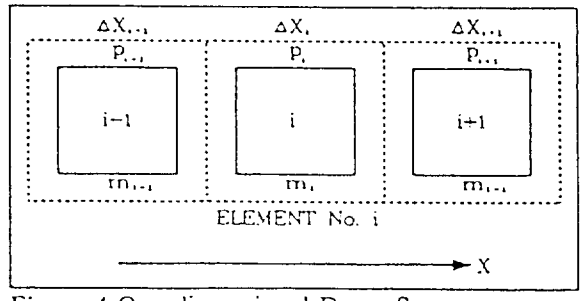

Figure 4 One-dimensional Darcy flow geometry

$$m_{ijk}|_{t+\Delta t} = m_{ijk}|_t + \Delta m_{D\,ijk} + \Delta m_{K\,ijk}$$

$$\Delta m_{K\,ijk} = c_{ijk} \cdot \Delta t \cdot \sum_{\Omega = x,y,z} \left(\Gamma_{\Omega\,ijk} \cdot \left(1 + \frac{c_{ijk}}{\eta_{ijk}} \cdot \Gamma^{*}_{\Omega\,ijk} \right) \right)$$

$$c_{ijk} = -\frac{2M_G}{\kappa R T_{ijk} \eta_{ijk}} \cdot p_{ijk}$$

$$\Gamma_{x\,ijk} = K_{x\,ijk} \cdot \Delta y_{ijk} \cdot \Delta z_{ijk} \cdot \left(\frac{p_{ijk} - p_{i-1jk}}{\Delta x_{ijk} + \Delta x_{i-1jk}} - \frac{p_{i-1jk} - p_{ijk}}{\Delta x_{ijk} + \Delta x_{i-1jk}} \right)$$

$$\Gamma^{*}_{x\,ijk} = \sqrt{K^3_{x\,ijk}} \cdot \left(\frac{p_{ijk} - p_{i-1jk}}{\Delta x_{ijk} + \Delta x_{i-1jk}} + \frac{p_{i-1jk} - p_{ijk}}{\Delta x_{ijk} + \Delta x_{i-1jk}} \right)$$

$$\Gamma_{y\,ijk} = K_{y\,ijk} \cdot \Delta x_{ijk} \cdot \Delta z_{ijk} \cdot \left(\frac{p_{ijk} - p_{ij-1k}}{\Delta y_{ijk} + \Delta y_{ij-1k}} - \frac{p_{ij-1k} - p_{ijk}}{\Delta y_{ijk} + \Delta y_{ij-1k}} \right)$$

$$\Gamma^{*}_{y\,ijk} = \sqrt{K^3_{y\,ijk}} \cdot \left(\frac{p_{ijk} - p_{ij-1k}}{\Delta y_{ijk} + \Delta y_{ij-1k}} + \frac{p_{ij-1k} - p_{ijk}}{\Delta y_{ijk} + \Delta y_{ij-1k}} \right)$$

$$\Gamma_{z\,ijk} = K_{z\,ijk} \cdot \Delta x_{ijk} \cdot \Delta y_{ijk} \cdot \left(\frac{p_{ijk} - p_{ijk-1}}{\Delta z_{ijk} + \Delta z_{ijk-1}} - \frac{p_{ijk-1} - p_{ijk}}{\Delta z_{ijk} + \Delta z_{ijk-1}} \right)$$

$$\Gamma^{*}_{z\,ijk} = \sqrt{K^3_{z\,ijk}} \cdot \left(\frac{p_{ijk} - p_{ijk-1}}{\Delta z_{ijk} + \Delta z_{ijk-1}} + \frac{p_{ijk-1} - p_{ijk}}{\Delta z_{ijk} + \Delta z_{ijk-1}} \right) \qquad (22)$$

The viscosity η of a fluid is a measure of its resistance to deformation by external forces and usually depends predominantly on the fluid temperature. Methane dynamic viscosity (in Pa·s) is closely related to its absolute temperature by $\eta = (4.1596 \cdot T^{0.624} - 35) \cdot 10^{-7}$ in the range $100K \leq T \leq 800K$.

Random Variations: In order to 'reproduce' naturally occurring random fluctuations, a (pseudo)random number generator that produces uniformly distributed random numbers n_ϱ, $0 \leq n_\varrho < 1$, is used, which can then be mapped onto the required distribution via a suitable transformation. In the case of a lognormally distributed quantity, the logarithms of the population values are normally distributed, so that it is necessary only to relate a uniform to a normal distribution. This is done on the basis of equal cumulative probabilities and leads to the relationship

$$n_\varrho = \int_{-\infty}^{\vartheta} \frac{1}{\sqrt{2\pi}} \cdot e^{-\frac{1}{2}\psi^2} d\psi = F(\vartheta) \qquad (23)$$

$F(\vartheta)$ in Equation (23) is the cumulative normal distribution function, which cannot be evaluated analytically. In theory, ϑ must satisfy $-\infty < \vartheta < +\infty$ to encompass all possible values, but since $-4 \leq \vartheta \leq +4$ includes at least 99.99% of same, these limits are chosen for simplicity to represent the full range. A reasonably accurate approximation (maximum relative errors of -1.28% at $\vartheta = 0.01$ and +2.14% at $\vartheta = 0.60$) is given by

$$\Phi(\vartheta) = \tfrac{1}{2} \cdot \left(1 + \sqrt{1 - e^{-0.6093 \cdot |\vartheta|^{1.9401}}} \right)$$

with $F(\vartheta) = \Phi(\vartheta)$ if $\vartheta \geq 0$ and $F(\vartheta) = 1 - \Phi(\vartheta)$ if $\vartheta < 0$. (24)

Rearranging Equations (23) and (24),

$$|\hat{v}| = 1.2843 \cdot \left[-\mathrm{Ln}\left(4\, n_\varrho\, (1 - n_\varrho)\right)\right]^{0.505} \qquad (25)$$

where $\hat{v}$ is positive if $n_\varrho \geq ½$ and negative otherwise.

In order to satisfy $|\hat{v}| \leq 4$, $0.000019 \leq n_\varrho \leq 0.999981$ must be satisfied. This is achieved by replacing every occurrence of n_ϱ in Equation (26) by n_ϱ', where $n_\varrho' = 0.000019 + 0.999962 \cdot n_\varrho$.

If v_M is the maximum allowable variation around the mean (as a fraction thereof) of a normally distributed quantity, then random fluctuations are introduced by applying $f_N = 1 + ¼ \cdot \hat{v} \cdot v_M$ as a factor to the mean value. In the case of a lognormally varying quantity, the factor is given by $\log_{10}(f_{LN}) = ⅛ \cdot \hat{v} \cdot N_{OM}$, where N_{OM} is the number of orders of magnitude (powers of 10) the allowable variation covers.

Boundary Conditions: Two types of boundary are identified: (a) free faces -ie. areas exposed to the atmosphere, and (b) modelled region boundaries -ie. the peripheries of the modelled region. In the case of any region boundary, one of three ideal states is assumed:

(1) At *impermeable* boundaries, gas release is purely diffusive into the modelled region. Mathematically, $\Delta m_{K\,ijk} = 0$. (26.a)

(2) At *constant pressure* boundaries, depending on their location and orientation, one or more of the following conditions hold: $p_{i\pm1jk} = p_{ijk}$ or $p_{ij\pm1k} = p_{ijk}$ or $p_{ijk\pm1} = p_{ijk}$. (26.b)

(3) At *constant pressure gradient* boundaries, depending on their location and orientation, one or more of the following hold: $p_{i\pm1jk} - p_{ijk} = c$ or $p_{ij\pm1k} - p_{ijk} = c$ or $p_{ijk\pm1} - p_{ijk} = c$ where c is a constant. (26.c)

The conditions at free faces are more complex since these are destressed and usually fractured. An empirical relationship [Ozan, 1992] for the depth of pillar fracturing (in m) from a free face is

$$d_f = 0.615 \cdot \mathrm{Ln}\left[\frac{H}{44.174 + 25.92 \cdot h}\right] \qquad (27)$$

It is assumed that at all vertical free (coal) faces the vertical stress increases from zero linearly with depth into the face up to the limit of fracturing, where it equals the peak abutment stress σ_P, and beyond this limit it decays exponentially, tending to its virgin value σ_-. Empirically,

$$\sigma_P = 1.2 \cdot e^{3.56 \cdot h^{-0.44} \cdot d_f} \qquad (28)$$

The vertical stress behind a vertical free face is then

$$\xi > d_f \quad - \quad \sigma_z = \sigma_- + (\sigma_P - \sigma_-) \cdot e^{-k_c \cdot (\xi - d_f)}$$

$$\xi \leq d_f \quad - \quad \sigma_z = \frac{\sigma_P}{d_f} \cdot \xi$$

$$k_c = \frac{\sigma_P - \sigma_-}{\sigma_-(d_f + h) - \frac{1}{2} \cdot d_f \cdot \sigma_P} \qquad (29)$$

Equations (29) apply also in the case of total extraction methods involving goafing, with the slight modification that σ_P is replaced by UCS, since the horizontal confining stresses acting in the plane of the seam will disappear as there is no solid roof to transmit them. In all cases, the two horizontal stresses are assumed to obey $\sigma_x = \sigma_y = c_o \cdot \sigma_z$, where c_o is a constant (usually between ½ and 2).

Horizontal free faces (eg. roof and floor) of the excavation are generally subject to tensile horizontal stresses where no goafing occurs. For present purposes, it may be assumed that where such a face is comprised of carbonaceous material, the degree of 'stretching' is sufficient for gas transport to be governed only by diffusive processes, while where it is non-carbonaceous, the degree of 'stretching' is insufficient to significantly alter the permeability due to the generally high Young's moduli exhibited by these materials. Work aimed at devising a simple and relatively accurate representation of this is still in progress.

The gas pressure at any free face is equal to the prevailing atmospheric pressure, so that, depending on the face's location and orientation, one or more of the following holds: $p_{ijk} = p_{atm}$ and $p_{i\pm1,j\pm1,k\pm1} = p_{atm}$ (30)

Further Considerations:

(1) Initial conditions: Ideally, a complete specification of the spatial and temporal of the relevant physical properties in the region to be modelled at some instant is required. Practically, these properties can only be known at a few isolated points. This may be used as a basis for assigning values to other points via suitable inter- and extrapolation schemes.

Such a scheme is provided by an inverse-distance weighting, but this notion may be extended to the more general case where the weighting factors are the inverse distances raised to some power ϵ. Thus, if q_i represents the values of a quantity at points with co-ordinates (x_i, y_i, z_i), then q_{ijk} is the value of that quantity at a point with co-ordinates $(x_{ijk}, y_{ijk}, z_{ijk})$ and is given by

$$q_{ijk} = \left(\sum_{i=1}^{N_K} q_i \cdot s_{i\,ijk}^{-\epsilon} \right) \cdot \left(\sum_{i=1}^{N_K} s_{i\,ijk}^{-\epsilon} \right)^{-1} \qquad (31)$$

$$s_{i\,ijk} = \sqrt{(x_i - x_{ijk})^2 + (y_i - y_{ijk})^2 + (z_i - z_{ijk})^2}$$

It should be noted that different quantities may be known at different numbers of points N_K, that ϵ may differ among different quantities and that this procedure is valid only within (sub)regions of similar composition.

(2) Dynamic mining activity: The assumption that coal releases the entirety of its free gas upon being broken leads to the following relationship:

$$\Delta m_{DMA} = \sum_i \sum_j \sum_k \left(\frac{M_G \left(\Delta x_{ijk} \Delta y_{ijk} \Delta z_{ijk} - 8 \lambda_{ijk}^3 \right)}{\kappa R T_{ijk}} \right) \cdot \left(p_{ijk} - p_{atm} \right) \qquad (32)$$

The element parameters are taken to be those at the time step just prior to being broken, and the

summations extend only over those elements separated from the mined region. This contribution is calculated *before* any other in order to cater for possible substantial pressure gradient increases. The newly exposed area becomes a new boundary.

It is assumed that the residence time of broken (carbonaceous) material in the excavation is sufficiently short for subsequent sorptive and diffusive gas release therefrom to be insignificant, which is reasonable, given today's production methods.

(3) Transport in non-carbonaceous regions: Since gas migration in such regions is purely Darcy permeable, the diffusion term in Equation (22) is zero. Thus, $\Delta m_{D\,ijk} = 0$ (33)

(4) Goafing and caving: Where coal exploitation involves this, the effect thereof depends on the type of material broken. Non-carbonaceous material releases all the gas held in the void space, whereafter no further gas is contributed. This is quantified by Equation (32). Carbonaceous material behaves the same way upon breaking, but further gas release is purely diffusive. In terms of the surface concentration C_s of caved elements, this means

$$C_s = \left(\frac{p_{std} M_G}{\kappa R T_{std}}\right) \cdot \left(\frac{L_1 L_2 p_{atm}}{1 + L_2 p_{atm}}\right) \tag{34}$$

4. MODIFICATIONS FOR COMPUTERISATION

In order to apply the preceding mathematical considerations to practical instances, an indication of the element sizes is required. It has been noted that sorption rates of crushed coal samples are apparently independent of average particle size in the range from about 20mm to about 3mm. Smaller particles show a dramatic increase in this rate, while that of larger particles gradually decreases. The size at which the increase appears is termed the 'Fracture Network Size', or FNS.

One possible explanation for this phenomenon is that particles larger than the FNS are effectively composed of blocks this size and provided that the particles are not too large, free gas diffused from individual blocks can flow relatively unhindered through cleats and fractures. The larger the particles, the more such blocks they contain, which increases the gas's migration distance and retards the sorption rate as a result of pressure build-up. Conversely, particles smaller than the FNS have a greater free surface area for sorptive processes, a reduced diffusing distance and uninhibited free gas flow, so that release rates are substantially higher.

South African coals analyzed in this respect thus far uniformly show FNSs very close to 3mm. From the preceding discussion, it is reasonably deduced that $\lambda \approx 1.5$mm for SA coals. It is immediately apparent that an immense number of elements would be required to model gas transport, even in small regions. By way of illustration, a coal cube with a side length of 1m contains roughly 37 million elements. Consequently, it is totally impractical to model a region on the basis of individual elements.

This problem may be substantially reduced by considering an elemental region ('c-element') composed of a collection of elements that all behave in a similar manner. The validity of this approach hinges on (1) the size of the c-element in relation to that of an element, (2) the shape of the c-element and (3) the prevalent physical conditions in adjacent c-elements.

The c-element size is to a large extent determined by the computational ability of the system it is targeted for in conjunction with the size of the region that is to be modelled. The data segment

restrictions on most PC installations will result in relatively high disk read/write time sacrifices.

The recommended shape of the c-element is a rectangular paralleliped, since the coal structure is defined within a Cartesian co-ordinate system and the elements themselves are of this shape. This arrangement makes for reasonably simple discretisation.

Physical conditions in adjacent c-elements should not differ dramatically since the more pronounced these differences are, the less accurate the results are. It is recommended that the free gas pressure differences between adjacent c-elements be kept relatively constant for each of the three principal directions. This indicates that the region's discretisation should be periodically reassessed. From a computational point of view, it is not especially difficult to merge or split c-elements.

5. CONCLUSIONS

The derivations presented herein form part of a project aimed at providing the local coal mining industry with guidelines for the improvement of underground environmental conditions with a view to enhanced safety of personnel. It is envisioned that this work will be successfully translated into a PC based application for the industry.

In its present form, the model is not restricted in any way by such factors as the geological setting and the mining layout, and can be applied to virtually any imaginable situation, including gas drainage. Provided that the required input data are adequately well known, the model is expected to provide reasonably accurate and reliable information about gas emission and in-seam behaviour for underground collieries.

The model neglects ground water flow as a result of this not being a significant factor locally. It may become necessary to include this at a subsequent stage if sites suffering therefrom come to light. Presently, the only restrictions on the model are placed by the speed and maximum data capacity of the computer system on which it is processed.

Upon completion of the coding, model verification/evaluation and any further required modifications will be done. If it is found to be a valid and practicable model, a complete methane emission prediction software package will be produced which will fill a large gap in the local coal mining industry's tool box.

NOMENCLATURE (only symbols not defined in the text)

C : adsorbed gas concentration, [mass ratio];
t : time, [s];
∇ : Laplacian grad operator;
D : diffusion coefficient, [$m^2 \cdot s^{-1}$];
Δx, Δy, Δz : element dimensions, [m];
C_s : particle surface concentration, [mass ratio];
C_0 : particle initial concentration, [mass ratio];
ξ : distance into a free face, [m];
C^* : normalized gas concentration, [-];
ρ_c : particle density, [$kg \cdot m^{-3}$];
V_{eq} : Langmuir stp volume of adsorbed gas, [m^3];
m_c : coal mass, [kg];
L_1, L_2 : Langmuir constants, [$m^3 \cdot kg^{-1}$] and [Pa^{-1}], respectively;
p : gas pressure, [Pa];
κ : gas supercompressibility fraction, [-];
n : number of moles of gas, [-];
R : universal gas constant, [8.31432 $J \cdot mol^{-1} \cdot {}^\circ K^{-1}$];

T : free gas temperature, [°K];
m_G : mass of gas, [kg];
M_G : Molecular mass of the gas, [CH_4: 0.016043 kg·mol^{-1}];
p_{std} : standard pressure, [101325 Pa];
T_{std} : standard temperature, [273.15 °K];
p_- : virgin (seam) gas pressure, [Pa];
$\bar{q}$: specific discharge, [m^3·s^{-1} per m^2 = m·s^{-1}];
η : gas dynamic viscosity, [Pa·s];
K_x, K_y, K_z : principal intrinsic permeabilities, [m^2];
$\bar{i}$, $\bar{j}$, $\bar{k}$: unit vectors in the x, y and z direction, respectively, [-];
$\dot{V}_\zeta$: volumetric flow rate in the $\bar{\zeta}$ direction, [m^3·s^{-1}];
a : circular duct radius, [m];
A_s : cross-sectional area of the permeable medium, [m^2];
A_c : area of contact between fluid and medium, [m^2];
A_f : cross-sectional area available to fluid flow, [m^2];
V_s : total volume of medium (including voids), [m^3];
b_ζ : Klinkenberg slippage factor in the $\bar{\zeta}$ direction, [Pa];
μ_w : moisture content (of coal), [mass ratio];
ρ_w : moisture density, [kg·m^{-3}];
ε_x, ε_y, ε_z : normal strains, [-];
σ_x, σ_y, σ_z : normal stresses, [MPa];
E : Young's modulus, [MPa];
ν : Poisson's ratio, [-];
C_A : laminar-inertial turbulence correction factor, [-];
Re_ζ : porous flow Reynold's number in the $\bar{\zeta}$ direction, [-];
Δm_K : Darcy flow gas mass change in time Δt, [kg];
ϑ : normalised Gaussian random variable, [-];
H : mining depth below surface, [m];
h : excavation height, [m];
k_ζ : stress decay constant, [m^{-1}];
UCS : unconfined compressive strength, [MPa];
Δm_{DMA} : gas mass contributed by mining activity, [kg];
p_{atm} : prevailing atmospheric pressure, [Pa];
N_K : number of points at which a quantity is known, [-];

REFERENCES

Cook, A.P. and Erwee, E.C. Methane Properties of South African Coals, Part 1 : Sorption Characteristics. Coal Mining, Chamber of Mines Research Organisation, Johannesburg. Reference report No. 16/91. 1991.

De Wiest, R.J.M. (Editor). Flow Through Porous Media. Academic Press, New York. 1969.

King, G.R. and Ertekin, T. State-of-the-Art Modelling of Unconventional Gas Recovery. SPE Joint Rocky Mountain Regional/Low Permeability Reservoirs Symposium and Exhibition. Society of Petroleum Engineers, Inc., Denver, Colorado. 1989.

Ozan T.T. The Determination of the Depth of Fractured Zones around Coal Pillars. MASSMIN '92 Symposium. The South African Institute of Mining and Metallurgy Symposium Series S12, Johannesburg. 1992.

Stripp, G.P. Methane Emission Characteristics of South African Coal Seam Strata. PhD Thesis, University of the Witwatersrand. 1989.

Weast R.C. (Editor). CRC Handbook of Chemistry and Physics, 63rd Edition, 1982-1983. CRC Press, Inc., Boca Raton, Florida. 1982.

APPENDIX B2

Quantifying Methane Emissions from Coal

P Linzer[†] and AP Cook[‡]

7 July 1995

[†]Research Engineer - Mining Operations and Environment, CSIR Division of Mining Technology, PO Box 91230, Auckland Park, 2006, South Africa. ☎ 358-0115 FAX 726-2638

[‡]Project Manager - Mining Operations and Environment, CSIR Division of Mining Technology

SYNOPSIS

It is often mistakenly believed that the amount of methane a coal seam contains is adequate information to quantify and predict methane emissions. However, in reality, the quantity and the surrounding geometry change as mining operations progress, inducing a time-dependence in the required emissive parameters. This time-dependence is essential for a meaningful quantification of methane emission into underground workings and can be established by either measurement or by prediction using empirical models or numerical simulators.

Measurements only provide information on specific instances and are hence solely relevant to those instances. Empirical models are generalisations derived from numerous measurements, usually without any reference to underlying physical processes and interrelationships, and hence can only be applied with confidence in a narrow set of conditions. Numerical simulators, on the other hand, require an understanding of the underlying mechanisms of methane migration, and, although the effort required for this is much greater, the result has a much wider range of application.

Worldwide, interested parties have opted either for empirical models or simulators, preferring the latter where these are available. The CSIR's Division of Mining Technology has devised such a simulator for South African conditions, and only the computerisation and verification thereof needs completion this urgently required tool is available to the local coal mining industry.

INTRODUCTION

The Safety in Mines Research Advisory Committee (SIMRAC) is supporting a project, currently in its third year, aimed at quantifying and addressing the hazards related to a continual flammable gas presence in underground coal workings. A substantial portion of this project focuses on the development of techniques by which methane emissions can be measured or quantified and to this end, a large volume of work was completed prior to SIMRAC's involvement[1..10].

A common misconception about gas emission is that it is sufficient to know the *amount* of gas that is contained by a geologic formation. This is probably as a result of the often asked, but poorly phrased question, 'how much methane is there?' The nature of the phenomenon also requires consideration of the *rate* at which the gas appears in the underground environment, its *point(s) of origin* and the *time-dependence* each of these manifests in terms of changing conditions[5,6,9..22]. Thus, the questions, 'what do we wish to establish and why?' and subsequently, 'how can we achieve this?' need to be answered.

To meet the objectives of the project, it is necessary to establish reliable and straightforward tools or techniques to assess rates of methane ingress at various locations, and in varying conditions, into coal workings. The project and the development of such tools and techniques have a number of greater goals: firstly, the reduction or elimination of the fire and explosion hazard[1,7,12,15,16,23..30] associated with the presence of the gas, particularly as the means (viz. ventilation) to deal with the hazard[23..27] exist. Secondly, they would enable a proactive approach to alleviating the hazard, with the development of hazardous conditions being anticipated more effectively[5..7,9..12,15..21]. Thirdly, by using such a tool interactively with ventilation design and fluid flow analysis facilities, improvements to and optimisations of existing ventilation methods are possible[5,7,9,12,15,16,23..27]. Fourthly, the tools would assist in identifying where and when methane drainage is viable and/or necessary, and how such drainage might best be implemented[10,11,13..15,17..21,31]. Lastly, each of the preceding has a potentially beneficial effect on the overall cost of mining in terms of human lives, resource utilisation and ultimately money[15].

There are two forms such a tool might assume, namely measurement and prediction. Measurement entails devising a procedure whereby the required emission information is acquired by making certain measurements at the location(s) of interest and possibly subjecting this data to a suitable analysis[2..4,7,8,10,13..33]. It answers the question, 'what is happening here and now?' in a particular instance. Prediction entails devising a procedure whereby a more general principle is applied to (possibly a reduced set of) measured data to extract useful information therefrom[5..7,9..12,15..21]. It has the ability of answering the questions, 'what has happened, is happening or will happen?' in a range of instances.

Prediction in its practicable form usually takes the form of either empirical models or simulators. Empirical models are general principles extracted from a number of observations without reference to any underlying causal framework. Simulators are general principles derived either solely from some pre-existent theoretical considerations or from such considerations in conjunction with empirical principles.

The CSIR's Division of Mining Technology (Miningtek) is currently able to measure gas emissions, although this is a time-consuming and expensive process[2..4,34..37], and so has extended the utility of the measurements by constructing a methane emission simulator. The theoretical basis thereof[5..7,12,15,38,39] has been completed and is in the process of being coded into a computer program. The simulation algorithm's complexity renders such coding the only practicable way of applying the model[12,15].

MEASUREMENT AND PREDICTION

Measurement

The measurement of methane characteristics can be divided into coal/seam properties and liberated gas properties. Each of these holds some value in terms of quantifying the (potential) hazard of a specific situation, but they apply only to the position and time at which they were taken. The taking of such measurements is well documented[2..4,7,8,10,13,14,16,23..26,28..30,32,34..37,40..44], and practised

worldwide. Methods developed for South Africa[2..4,8,16,23..30,34..37,40..42] are very similar to foreign methods. Proximate and sorption analyses and the use of boreholes and packers yield coal and seam data, while methanometers are used to assess methane concentrations and ventilation strategies. Innovations by Miningtek include the use of SF_6 tracer gas to measure in-seam flow velocities[10], and a multi-channel data logger[34..36] to record methane concentrations from several methanometers continuously, the latter being used mostly on and around continuous miners. Thus, measuring various methane parameters is well founded, but what value do such readings have and which are relevant?

Measurement has the advantage of delivering information relatively quickly, with standard procedures requiring from a few seconds to a few weeks[2..4,8,10,13,14,16,22..30,32,34..37,40..44]. During such lengthier periods, the configuration of the measurement location is very likely to change, and, with it, the emission parameters. Thus, seen in isolation, the value of such a measurement is questionable. A number of such measurements at various times and places can give an indication of general emissive trends, and in this sense measurement exhibits a further advantage. Finally, an extensive body of measurements can be useful in deducing empirical principles and/or verifying simulator principles.

Generally, coal and seam measurements are disadvantaged by being relatively costly in terms of labour and effort[2..4,8,10,13,14,16,22,23,28,32,34..37,40..44] and, since a single measurement is of dubious worth, great expense is required before any firm conclusions can be reached. Furthermore, there is a learning process involved in distinguishing significant and conclusive measurements from those that are insignificant and inconclusive since there exist no rigorous guidelines for the data analyses.

Another disadvantage of measurement is that, unless it is practised either over a lengthy time period (six to 12 months) or at periodic intervals in the same circumstances, it reveals nothing about the time-dependence of the required emissive aspects. Imprecision is also inherent in the methods in terms of both changing configurations and the point of gas origin, as only averages are reflected. Such averages alone are quite meritless without at least a reasonable idea of the range and dispersion of values they

are deemed to represent, which again raises the spectre of multiple measurements. Thus, measurements without further analyses reveal only a small portion of what we require. Extensive literature reviews of US, Eurasian and Australian coal mining publications have not revealed a single case where measurement alone is used to determine emission quantities[7,11,16..21,31,33,43].

Prediction

Methane prediction goes beyond simple measurement, and is a means of analysing and reviewing (usually measured) data with a view to making valid assertions about methane behaviour at certain times and places. This can be achieved either by taking measurements of a particular situation and assuming them to apply to similar situations, or by developing a logical understanding of the processes involved and imitating them. The former is the empirical approach and the latter is simulation.

Empirical models

An empirical model is derived from a sizeable body of measurements. This derivation entails identifying germane and/or critical quantities as well as general trends and correlations between or among these quantities. Once identified, such trends and correlations are translated into general, usually mathematical, relations. In this process, possible underlying causal connections are rarely, if ever, identified or referenced. The resultant model thus abstracts and encapsulates the observations used in its derivation, normally in an approximate way, since deviant measurements are either discarded or diluted. The model is then applied to similar circumstances from which the measurements were taken in order to generate relevant information about those circumstances.

In Europe, some empirical models have been developed and are applied to predict methane emissions from longwall mining configurations[43]. European coal deposits differ significantly from South African deposits in respect of geological setting, depth, composition, magnitude and gassiness, and in South

Africa coal is mined predominantly by bord and pillar methods. It is thus questionable to apply these models uncritically and without an extensive confirmatory body of measurements to local coal deposits. The same caution applies to Australian empirical models. In China, methane emission is dealt with by a set of guidelines which describe the conditions under which pre-mining drainage becomes mandatory, and the drainage procedure[45]. Largely empirical, these guidelines are of questionable validity for South African conditions due once again to significant differences in the respective coal formations.

Empirical models are sometimes applied in the USA, but almost exclusively in the coalbed methane reservoir industry, which uses such models to predict gas yields from boreholes and viable lifetimes of these. Owing to the vast logistical differences between coal mining and gas production, most existing empirical models from the USA fail to provide answers relevant to coal exploitation. Limited empirical modelling, based essentially on seam gas content[44], has been applied to bord and pillar workings. This gives a very approximate long term emission prediction[43], but cannot be applied to short term or immediate face predictions. The USBM therefore measures only the seam gas content ahead of mining via the direct or modified direct method[46,47].

The major advantage of an empirical model over measurement is that it reduces the amount and/or complexity of the data it requires in order to deliver answers. By summarising the data used in its derivation, it embodies the data in a more compact form. The question, 'what if...?' can now be asked, and a definite and unambiguous answer obtained (albeit of debatable accuracy), without actually implementing the 'what if' circumstances and measuring the consequences thereof. A successful empirical model can also, over a period of time, be evolved to encompass an increasing range of applicability without a commensurate increase in complexity.

There are also disadvantages to empirical models. The criteria used to decide what constitutes 'a sizeable body of measurement' are subjective. To statistically analyse a model as a hypothesis to decide whether or not to accept it, a decision must first be made regarding the required confidence. This in

itself is subjective, and can lead to erroneous acceptance or rejection. The identification of relevant quantities is rarely as clear-cut as it might sound and often requires further subjective judgment. Once correlations are established, the manner in which these correlations are formulated is entirely at the discretion of the persons deriving the model. Moreover, correlations that are not immediately obvious can be missed or disregarded, resulting in an inferior or even useless description of the observations.

The set of observations from which the model is derived is necessarily incomplete, since it is practically impossible to measure every instance of the phenomena the model is meant to describe. For this reason, the model can only be applied with confidence where the input data lie within the scope of the data that was used to make the model. This is well illustrated by applying various European empirical models to the same situation and observing the appreciable variations in their answers[43]. A further disadvantage of empirical models is that periodic measurements in different circumstances should be undertaken in order to reassess the reliability and range of applicability. An observation that refutes the model has much more severe consequences than one that confirms it, since, rightfully, the model and the aberrant observation should be analysed in order to pinpoint where the deficiency crept in.

Simulators

Simulation is the ability to imitate the process(es) underpinning the measurements and observations. It relies on an ability to build a rigorous and testable hypothesis (based on pre-existent facts and secure theories) which incorporates the causal links and quantitative dependencies among various facets of the observations, and to translate this into a logically consistent description of those observations. If, in addition, every factor that has an impact on the observations is successfully identified and quantitatively related to all such factors within the framework of the hypothesis, then a thorough understanding of the phenomena as well as the ability to imitate the processes accurately in virtually any conceivable arrangement wherein these processes can occur can be claimed. This constitutes the ultimate utility and strength of simulation.

Almost every pitfall that encumbers the empirical approach is avoided. The rules of logic are not subjective and hence much of the empirical model's subjectivity is avoided. A certain measure of subjectivity resides only in the initial hypothesis, but analysis of a given hypothesis is completely objective since assumed causal links necessarily imply unique and definite logical consequences. If the hypothesis is valid and complete, no influences or interrelationships can be missed or disregarded without damaging the logic. The line of reasoning followed in building a simulator from a valid hypothesis is purely deductive, and therefore erring by equating correlation with causality is avoided.

A valid simulator is applicable in the entire scope of possible arrangements the initial hypothesis embraces, and a good hypothesis will be as general as possible. Thus, a simulator can be applied with confidence to a much broader spectrum of circumstances than an empirical model. A valid simulator is also a great deal easier to verify confidently, since it is necessary only to test whether its principles have been implemented correctly, which requires only a few measurements. Once operational, a good simulator, much like an empirical model, reduces the necessary effort of providing input data.

On the negative side, the construction of a simulator requires the formulation of a valid hypothesis from which to proceed. For methane emission, this is an iterative process since each aspect of the hypothesis must be justified in causal terms. Intuitive guesses must be tested and often adjusted or even rejected in the light of their implications or the failure of their consequences to conform with observations, and counter-intuitive observations must be explained. As with empirical models, a simulator's reliability should be periodically reassessed. In the case where a measurement differs significantly from the prediction, only the measurement need initially be suspected. If the measurement is found to be valid, the hypothesis and subsequently the simulator must be extended, thus enhancing its validity. In contrast, an empirical model usually requires complete revision to incorporate deviant observations.

In the USA, simulators are widely used in the gas reservoir industry. Most of these are, however, limited to describing gas well performances and are unable to model emissions into underground

mines[11,15..21,31,48,49]. Those that have this ability are mainframe computer-based applications and are not commercially available. Simulator consultancies are almost exclusively geared towards supplying methane drainage information, which is not suited to South African purposes. Simulators in Eurasia and Australia are not only rare, but also solely available on a consultancy basis. Those simulators that have come to the authors' attention[33] are limited in application to longwall mining and thus have little appeal for South Africa.

METHANE SIMULATION BY MININGTEK

With the distinct advantages of simulation over empirical prediction and measurement, it was decided within Mining Operations and Environment (MOE - a programme of Miningtek), with the support of SIMRAC, that developing a gas emission simulator suited to the South African coal industry conditions is the best option for accurate methane emission prediction as a ventilation tool. However, in order to simulate the emission of gas effectively, the mechanisms that produce this effect must be fully understood.

The MOE methane project team has developed a high level of such understanding, but this has been a long and arduous process. When the organisation (then COMRO) undertook an investigation into the practicalities of quantifying methane emission, initial anticipation of an easy answer was overly optimistic. Several years of literature and technical research were required to bring local knowledge up to the international level, and this research is continued to maintain the level.

The Development Process

Three basic stages characterise the development of MOE's simulator. Firstly, an understanding of the mechanisms and processes that cause methane emissions was obtained. Secondly, a suitable gas transport model was derived. The final stage, currently underway, comprises the computerisation of

the model. The majority of time and effort was invested in the first stage, where several man years were required of the entire project team before an adequate understanding of the mechanisms was gained. Specific team members then concentrated on the second and final stages.

Flow mechanisms

Defining and understanding these mechanisms relied heavily on previous work and literature from similar efforts in other countries. Critical parameters and the means of quantifying them were thus identified. A large data base of coal properties was also prepared, and this assisted in determining the operating ranges of these parameters. Early misunderstandings of the gas transport mechanisms led to both over-optimistic attempts at modelling[5..7], and time and effort lost subcontracting the implementation of these models to qualified mathematicians.

Further study of the principles embodied in a wide variety of more or less successful gas well and drainage simulators[11,16..21] revealed that a number of further influences needed to be incorporated into the existing description. Thus, the ideas of unsteady state dual flow modes, stress and moisture dependent permeabilities and corrections for laminar/turbulent transitions were adopted and analysed. This analysis, however, avoided two common features of other simulators. Firstly, the medium (ie. coal) was not assumed to be a continuum; rather, its fundamentally discrete nature was taken into account. Secondly, a facility was derived which allows naturally occurring variations in certain quantities (eg. fracture widths) to be imitated by the simulator.

Model derivation and computerisation

In binding the various factors together into a consistent whole, it became immediately obvious that processing the resultant equations in even the simplest case would be a mammoth task. The basic reason for this is that it is necessary to simulate the totality of processes occurring inside the coal at each and every particle, including the mutual influences of neighbouring particles on one another. In this way, methane emission prediction is actually a by-product of simulating interior processes, much

like the marking of time by a clock is a by-product of the operation of its interior mechanism.

Consequently, the mathematical descriptions needed streamlining and/or condensation without compromising their effectiveness. This was accomplished on a trial-and-error basis by approximating one of the gas flow modes to a high degree of accuracy, thus significantly reducing the effort required to generate answers. At this stage the translation of the mathematical model into a computer application commenced and is currently progressing. Streamlining of permeability calculations was achieved by applying suitable mathematical transformations. The model was also enhanced later on by removing the assumption that one of the flow governing parameters was constant in a particular situation, although further research into this parameter's relationship to others is required.

Output and Results

The simulator will have the ability to simulate any practical mining situation. The accuracy and reliability of the answers it will generate will depend mostly on the degree of detail and accuracy of the input data that it receives. The answers it generates will provide overviews and details of methane behaviour in terms of emission rates, gas content and pressure contours and flow vector fields at selected times and locations. The simulator treats the problem in three space dimensions and incorporates the effects of gas contributions from mining activity as well as from goafing where the mining method involves this. It must also be mentioned that the required processing time will depend on the computer system and the degree of geological and geometrical complexity of the simulated situation, and can potentially be excessive[15].

CURRENT WORLDWIDE STATUS OF SIMULATORS

In other countries, attempts at simulating methane emission had either floundered completely or had met with (often severely) limited success. In addition, the overwhelming majority of these attempts were focused on describing drainage of gas as an energy source, rather than on its emission into underground coal workings[11,17..21], and this is still the case. Recent simulators such as ROOFGAS, FLOORGAS, CBMVENT and COMET2 are not so much extensions and enhancements of older algorithms as adaptations of their respective principles to suit recent advances in computer hardware technology, thus improving their efficiencies[33,50,51].

The FLOORGAS and ROOFGAS simulators, besides being limited to longwall configurations, do not provide methane emission rates, except as averages over lengthy time periods, and are used mainly to assess stress distributions and to assist in identifying potential high release areas[33]. COMET2 is aimed at the gas well industry[48..50], while CBMVENT is an ambitious attempt at consolidating methane emission prediction with mine ventilation and suffers from the drawback of being a two-dimensional model that does not permit irregular boundaries and complex geologies[51]. MOE's simulator compares very favourably[15,39] with all of the most complex models on which information was found[11].

CONCLUSIONS

Quantifying methane emissions from coal into underground workings has no simple solution. Measurement of the phenomenon is both difficult and costly, besides having little relevance beyond the time and location at which the measurement was made. Valid empirical models rest on a large body of measurements, and, since some of the measurements in South African conditions are scarce, it would be naïve and potentially dangerous to accept unequivocally foreign models of this type. The flexibility, relatively easy maintenance and sound foundations of a valid simulator marked this as the best way to determine methane emissions. This approach is also favoured in other countries.

Most of the overseas simulators do not cater for mining applications, and are hence of little value to local collieries. Where mining is catered for, they are mostly limited in application to longwall mining, besides being not commercially available. MOE's simulator caters for methane emission in all practical mining situations, quantifying methane flow into workings, in-seam gas and drainage behaviour.

The simulator was long in construction, due mostly to an initial lack of understanding of the underlying complexities, and hence is behind schedule in terms of computerisation. Nevertheless, its principles of operation are in line with the current thinking of other parties similarly engaged, and in some respects go beyond this.

Owing to the simulator's relatively easy maintainability, its completion will not necessarily mark the end of work in this field. The simulator will require testing for deficiencies and possible enhancements or extensions.

REFERENCES

1. Pardoe, D.R. and Baker, R.H. (1985). An Analysis of Six Colliery Fires and Explosions with Reference to the Lifesaving Potential of Self-rescuers. Coal Mining Laboratory, COMRO, Johannesburg. Reference Report No. 7/86.

2. Cook, A.P. and Erwee, E.C. (1991). Methane Properties of South African Coals Part 1: Sorption Characteristics. Coal Mining, COMRO, Johannesburg. Reference Report No. 16/91.

3. Cook, A.P. (1992). Methane Characteristics of the Coal Seams at Ermelo Mines. Coal Mining, COMRO, Johannesburg. Consultancy Report No. 27/92.

4. Cook, A.P. (1992). The Methane Emission Characteristics of South African Coals. MASSMIN '92 Symposium. SAIMM Symposium Series S12, Johannesburg.

5. Leibowitz, A.G. (1991). Derivation of a Pseudo-steady-state Mathematical Model to Describe the Transient Flow of Methane Through Coal. Coal Mining, COMRO, Johannesburg. Tech. Note 91/16.

6. Leibowitz, A.G. (1991). Understanding the Dynamics of Methane Flow Through Coal. Coal Mining, COMRO, Johannesburg. Presentation to CRAC-CE Committee.

7. Cook, A.P. (1989). Towards a Method of Methane Prediction for South African Collieries. 23rd International Conference of Safety in Mines Research Institutes, Washington DC, USA.

8. Erwee, E.C. and Cook, A.P. (1991). Methane Sorption Properties of SA Coals, and their Determination by Means of a Gravimetric Sorption Laboratory. 24th International Conference of Safety in Mines Research Institutes, USSR.

9. Leibowitz, A.G. and Cook, A.P. (1992). The Dynamics of Methane Flow through Coal. MASSMIN '92 Symposium. SAIMM Symposium Series S12, Johannesburg.

10. Leibowitz, A.G. and Cook, A.P. (1992). The Directional Dependence of Coalbed Permeability and its Implications for Methane Emission into Workings. 5th International Mine Ventilation Congress, Johannesburg.

11. King, G.R. and Ertekin, T. (1989). State-of-the-art Modeling of Unconventional Gas Recovery. SPE joint Rocky Mountains Regional\Low Permeability Reservoirs Symposium and Exhibition. SPE, Inc., Denver, Colorado. No. 18947.

12. Linzer, P. (1993). An Outline of the Adopted Strategy towards an Approximated Solution for a General State Methane Flow Model within a Coal Structure. Coal Mining, COMRO, Johannesburg.

13. Rocha, M. and Franciss, F. (1978). Determination of Permeability in Anisotropic Rock-masses from Integral Samples. Laboratório Nacional De Engenhara Civil, Lisboa. Memória No. 495.

14. Taber, J.J. et al (1974). Development of Techniques and Measurement of Relative Permeability and Capillary Pressure Relationships in Coal. USBM, Washington DC. BuMines OFR 22-74.

15. Linzer, P. (1994). A General State Model of Methane Transport in Coal Structures. Mining Operations and Environment, CSIR, Johannesburg. SIMRAC Draft Report.

16. Stripp, G.P. (1989). Methane Emission Characteristics of South African Coal Seam Strata. PhD Thesis, University of the Witwatersrand, Johannesburg.

17. Spencer, S.J. et al (1987). Numerical Simulation of Gas Drainage from Coal Seams. 62nd Annual Technical Conference and Exhibition of the SPE, Inc., Dallas, Texas. No. 16857.

18. Kelso, B.S. and Kelafant, J.A. (1989). A Strategy for Coalbed Methane Production Development Part 1: Geologic Characterisation. Proceedings of the 1989 Coalbed Methane Symposium, Tuscaloosa.

19. Wicks, D.E. et al (1989). A Strategy for Coalbed Methane Production Development Part 2: Reservoir Characterisation. Proceedings of the 1989 Coalbed Methane Symposium Tuscaloosa.

20. King, G.R. et al (1983). Numerical Simulation of the Transient Behavior of Coal Seam Degasification Wells. Reservoir Simulation Symposium, SPE, Inc., Dallas, Texas. No. 12258.

21. Zuber, M.D. et al (1987). The Use of Simulation and History Matching to Determine Critical Coalbed Methane Reservoir Properties. SPE/DOE Low Permeability Reservoirs Symposium, Denver, Colorado. No. 16420.

22. Hanson, D.R. and Holub, R.F. (1991). Methane Release from Actively Yielding Coal and its Implications for Yield Zone Determination. Int. J. R. M., Min. Sc. & GeoMech, Vol. 27 No. 3.

23. Cook , A.P. (1993). Evaluating the Methane Gas Conditions in Underground South African Coal Mines. 25th International Conference of Safety in Mines Research Institutes, Pretoria.

24. Burrows, J. (Ed) (1982). Environmental Engineering in South African Mines. MVSA, Johannesburg.

25. Le Roux, W.L. (1990). Le Roux's Notes on Mine Environmental Control, 4th Edition. MVSA, Johannesburg.

26. Marais, D. (1989). Practical Aspects of Methane Measurements. Symposium on Methane Detection and Explosion Prevention. MVSA, Johannesburg.

27. Viljoen, P.L.J. (1989). Case Histories and Preventative Measures with Relevance to Methane Ignitions/Explosions. Symposium on Methane Detection and Explosion Prevention. MVSA, Johannesburg.

28. Phillips, H.R. and Landman, G.v.R. (1992). The Explosion Potential of Methane/Dust Mixtures at the Coal Face. Fifth International Mine Ventilation Congress. MVSA, Johannesburg.

29. Gardiner, L.R. (1989). Methanometry in Mining - A South African Case Study. Symposium on Methane Detection and Explosion Prevention. MVSA, Johannesburg.

30. Kononov, V.A. (1993). Infrared Methane Monitoring. Mining Operations and Environment, CSIR, Johannesburg. SIMRAC Report.

31. Cook, A.P. (1993). Methane Drainage Systems and Future Requirements in South African Coal Mines. 6th US Mine Ventilation Symposium, Salt Lake City, Utah.

32. Mavor, M.J. (1992). Western Cretaceous Coal Seam Project Monthly Report - March 1992. Resource Enterprises, Inc., Salt Lake City, Utah.

33. Kidybinski, A. and Lunarzewski, L. (1994). Floorgas and Roofgas Simulation Programs. Lunagas Pty Ltd, Newcastle.

34. Cook, A.P. (1995). Methane Safety Research for Continuous Miners in South Africa. Proceedings of the 7th US Mine Ventilation Symposium, AIME, Lexington, Kentucky.

35. Cook, A.P. (1995). Methane Monitoring using a Multi-channel Data Logger. 26th International Conference of Safety in Mines Research Institutes, Katowice, Poland.

36. Kononov, V.A. and Cook, A.P. (1995). Multi-purpose Data Logging Station for Underground Environmental Monitoring. 26th International Conference of Safety in Mines Research Institutes, Katowice, Poland.

37. Cook, A.P. (1993). Determining the Methane Content of a Coal Seam by means of the Direct Method - A Review of the Procedures. Mining Operations and Environment, CSIR, Johannesburg.

38. Linzer, P. (1995). A Numerical Simulator for 3-D Unsteady-state Dual-porosity Modelling of Gas Flow within a Coal Structure. Proceedings of the 7th US Mine Ventilation Symposium, AIME, Lexington, Kentucky.

39. Linzer, P. (1995). A 3-D Dual-porosity Single-phase Unsteady-state Mathematical Model of Gas Transport in Coal Structures. 26th International Conference of Safety in Mines Research Institutes, Katowice, Poland.

40. Linzer, P. (1994). Report on the Initial CH_4 Build-up and Depletion Test, Twistdraai Colliery. Mining Operations and Environment, CSIR, Johannesburg. Consultancy Report.

41. Linzer, P. (1994). Report on the Second CH_4 Build-up and Depletion Test, Twistdraai Colliery. Mining Operations and Environment, CSIR, Johannesburg. Consultancy Report.

42. Linzer, P. (1994). Report on the Third CH_4 Build-up and Depletion Test, Twistdraai Colliery. Mining Operations and Environment, CSIR, Johannesburg. Consultancy Report.

43. Curl, S.J. (1978). Methane Prediction in Coal Mines. Report No. ICTIS/04, IEA Coal Research, London.

44. Kissel, F.N. et al (1973). The Direct Method of Determining Methane Content of Coalbeds for Ventilation Designs. USBM Report of Investigation, RI7767, Washington DC.

45. Yongyan, W. and Edwards, J.S. (1993). Coal Mine Methane Drainage in China. The Mining Engineer, November 1993, pp. 141-143.

46. Schatzel, S.J. (1995). Personal communication, USBM, Pittsburgh.

47. Garcia, F. (1995). Personal communication, USBM, Pittsburgh.

48. Kelafant, J.R. (1995). Personal communication, ARI, Arlington.

49. Reeves, S.R. (1995). Personal communication, ARI, Arlington.

50. ARI advertising brochure (1995). COMET2 - The Preferred Fractured Reservoir Simulator.

51. Patton, S.B. et al (1994). Simulator for Degasification, Methane Emission Prediction and Mine Ventilation. Mining Engineering, April 1994, pp. 341-345.

APPENDIX B3

Chapter 44

A NUMERICAL SIMULATOR FOR 3-D UNSTEADY-STATE DUAL-POROSITY MODELLING OF GAS FLOW WITHIN A COAL STRUCTURE

Patrick Linzer

CSIR Division of Mining Technology
PO Box 91230, Auckland Park, 2006
Republic of South Africa

The majority of existing models describing (methane) gas transport within, and liberation from, coal structures treat these as continua wherein two main gas flow modes (diffusive and Darcy permeable) prevail, and use finite difference techniques to generate solutions to the resulting multivariate parabolic partial differential equation(s). Isotropy and homogeneity in the physical and geometric coal structure properties are often assumed, and the existence of fundamental random fluctuations in these properties is not catered for. The model proposed herein does not suffer these inadequacies, and its efficiency is enhanced by the replacement of the diffusion equation by an accurate approximation. Dynamic mining activity, gas contributions made by the geology surrounding the mining seam, goafing of overlying strata and the effects of induced strain are all taken into account.

INTRODUCTION

The more or less ubiquitous presence of combustible gases, principally composed of methane and hydrogen, in coal formations constitutes the single greatest hazard associated with coal exploitation from underground workings. Gas release into the confines of such workings may lead to explosible mixtures, which, when ignited, often have disastrous consequences.

A great deal of effort has been expended worldwide by coal mining industries on the establishment of accurate and efficient quantitative models that would allow this hazard to be reduced or even eliminated. Existing models range from the relatively simple to the very complex and generally their predictions do not correlate well with observed data as a result of a variety of factors that include oversimplifications, input data deficiencies, inadequate approximations and computational instabilities.

Occasionally, European or American empirical models are applied to local ventilation designs, but their relevance to South African conditions has not been thoroughly examined. The geological settings of overseas coal deposits are generally different to those of their South African counterparts, which are also mostly shallower, greater in magnitude, less undulatory and lower in gas content. These differences may well be sufficiently pronounced to place local coals outside the ranges of applicability of these models.

MODEL OUTLINE

In accordance with the theoretical bases of most of the more complex extant models, the one presented herein proceeds from the assumption that two principal gas flow regimes, namely diffusive and Darcy permeable, coexist in an idealised coal structure (illustrated in Figure 1), which consists of distinct elements comprised of homogeneous particles inside a geometrically regular void space.

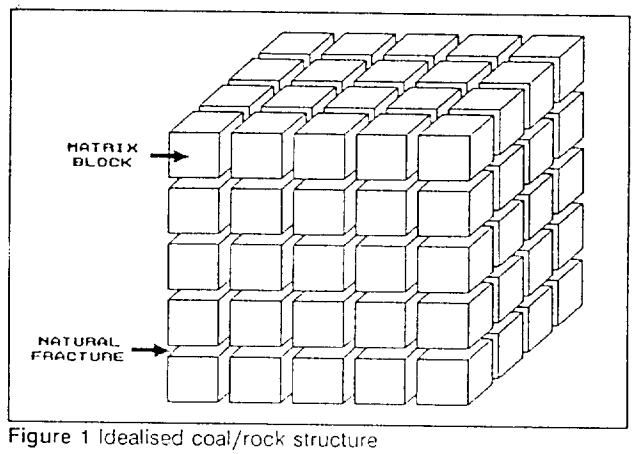

Figure 1 Idealised coal/rock structure

Diffusive flow (carbonaceous material only) is confined to the particle, while Darcy permeable flow is confined to the void space. The two modes of gas transport are interdependent in that the gas diffusing from the particle affects the pressure in the void space, which influences the macroscopic permeable flow rate, while the pressure in the void space controls the amount of gas adsorbed on the free surfaces of the particle, which in turn affects the microscopic diffusion rate. The flow modes are linked via the Langmuir isotherm describing monolayer (ad)sorption.

This idealisation thus reflects the dual-porosity and fundamentally discrete nature of coal formations. Non-carbonaceous material is similarly idealised, except that no diffusive gas transport occurs. The congruence between the idealisation and the reality is supported in the case of coal by the presence of a great number of cleats, fractures and other planar discontinuities of apparently random orientation, and in the case of other mineral matter by its granular composition.

Diffusive flow in a particle is treated as a continuum process and is analyzed separately. A suitably accurate approximation describing this phenomenon replaces the 'exact' numerical technique normally used in generating solutions to a given diffusion problem, reducing the required computational effort. Sorptive processes on free surfaces are assumed to occur very rapidly.

Unlike other models, the analysis of Darcy flow is not taken to the limiting case where elements are assumed to be of infinitesimal size. The resulting equations thus contain finite difference terms rather than differentials, rendering them more amenable to

coding into a computer program. Material permeability is quantified from first principles in terms of the idealised structure geometry to facilitate appraisal of the effect induced strains have on flow rates.

Since very few South African collieries have a significant ingress water problem, the effect of moving groundwater carrying dissolved gas with it is neglected. Free moisture in the structure is accounted for on the assumption that it obstructs voids, thus reducing the effective permeability to gas.

Virtually all of the parameters that play a rôle in the methane-in-coal process exhibit spatial and temporal variabilities of a random nature. For example, cleat widths can vary from a few Å to a few mm, and it is highly improbable that diffusion coefficients and intrinsic permeabilities are uniform, even within very small regions. It is commonly held that these variations are adequately catered for by averages, but secure knowledge of these averages is rare and often meaningless as a result of ignorance surrounding the type and dispersion of the distribution of values they represent.

Consequently, the model includes a device which allows normally and lognormally distributed random factors within definable limits to be applied to any or all model parameters.

Coal structures have remained relatively undisturbed for a long period, so that it is reasonable to assume the amount of adsorbed gas held in the micropore network (particles) to be in equilibrium with the (pressurised) free gas held in the macropore network (void space), and remains so until this balance is disturbed.

Mining or drilling of the seam does this by allowing free gas to escape, altering the in-seam pressure distribution profile. This causes gas molecules to desorb from free surfaces within zones of diminished pressure and to appear as free gas, which in turn changes the adsorbed gas concentration. The macropore network provides the conduits in which free gas migrates under the influence of pressure gradients, and this behaviour is (within limits) described by the Darcy flow relationship.

Changes in the concentration of adsorbed gas on surfaces adjoining or delimiting the macropore network introduce non-zero concentration gradients within the micropore system, which, in accordance with Fick's first law, drive gas molecules from areas of higher to areas of lower concentration -ie. internally adsorbed gas diffuses in the micropore regions, prevalently migrating towards surfaces where the free gas pressure is at a minimum.

From the preceding discussion, it is clear that in-seam gas transport occurs as long as either pressure or concentration differences, or both, exist, and that gas will be emitted from any free coal surface as long as these conditions hold.

MATHEMATICAL DERIVATIONS

Diffusion

The diffusive behaviour of adsorbed gas in a particle is always subject to similar constraints. These constraints are a uniformly distributed initial concentration and an outer surface concentration quantifiable in terms of the surrounding pressure.

General state diffusion without sources or sinks is described by

$$\frac{\partial C}{\partial t} = \nabla(D\cdot\nabla C) \qquad (1)$$

[An explanation of the mathematical symbols used is appended to this article]

The required initial and boundary conditions disallow a useful analytical solution to this equation. Traditionally, the solution is generated numerically, but the methods employed are generally time consuming, particularly when accuracy is a prime concern. This problem is overcome by assuming the following (refer also to Figure 2):

(1) The coal particle is a homogeneous isotropic cube with a side length of 2λ, $\lambda > 0$ -ie. $\delta x = \delta y = \delta z = 2\lambda$ and D is constant;

(2) The directional dependence of permeability is catered for by allowing the width of the void space at various faces of the cube to vary -ie. $\Delta x \neq \Delta y \neq \Delta z$ generally;

(3) Diffusive flow is symmetric with respect to any symmetry axis of the particle, allowing the cube to be divided into six equal right pyramids with their apexes at the geometric centre of the cube and within each of which gas flow is unidirectional from the apex to the base;

(4) The instantaneous surface concentration C_s changes (decreases) smoothly and relatively slowly so that it may be approximated by a constant over a short time period, and the initial concentration C_0 is uniform throughout the cube.

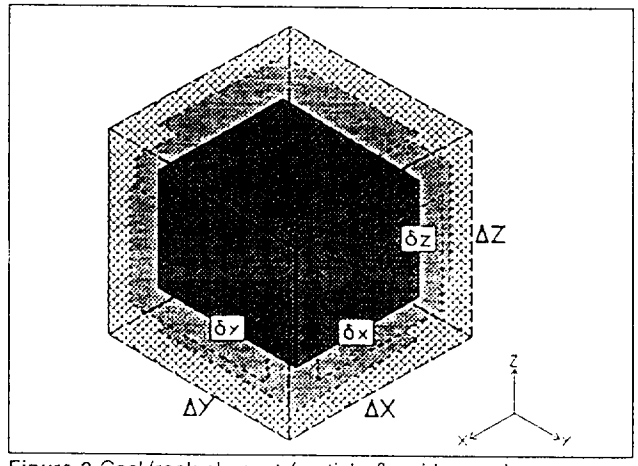

Figure 2 Coal/rock element (particle & void space)

With the foregoing assumptions, diffusive flow in any pyramid is described by

$$\frac{\partial C}{\partial t} = D\cdot\frac{\partial^2 C}{\partial x^2} \qquad (2)$$

where x increases from the apex perpendicularly to the base of the pyramid. Both x and t can be normalized by letting $x = \lambda\xi$ and $Dt = \lambda^2\tau$. If $C = C_S + (C_0 - C_S)\cdot C^*$, the problem is reduced to solving

$$\frac{\partial C^*}{\partial \tau} = \frac{\partial^2 C^*}{\partial \xi^2} \qquad (3)$$

subject to $0 \leq \xi < 1$, $\tau \geq 0$, $C^*(\xi,0) = 1$ and $C^*(1,\tau) = 0$.

For the purpose of the model, the concentration distribution inside the cube is not important, merely its total gas content as a function of time. For convenience, the concentration is measured in mass of gas per unit mass of coal, so that the total gas mass in the cube at time t is given by

$$Q(t) = 8\lambda^3\rho_c\left(C_S + 3\cdot(C_0 - C_S)\cdot\int_0^1 C^*\,\xi^2\,\partial\xi\right) \qquad (4)$$

Solutions to Equation 3 were generated numerically and the corresponding value of the integral term in Equation 4 determined at 52 different times, the largest of which corresponds to

τ = 1.6, where the integral term is less than 10^{-8}. This was done with the pyramid divided into 25, 50, 100, 200, 400 and 1000 slices. A graph of the results is shown in Figure 3.

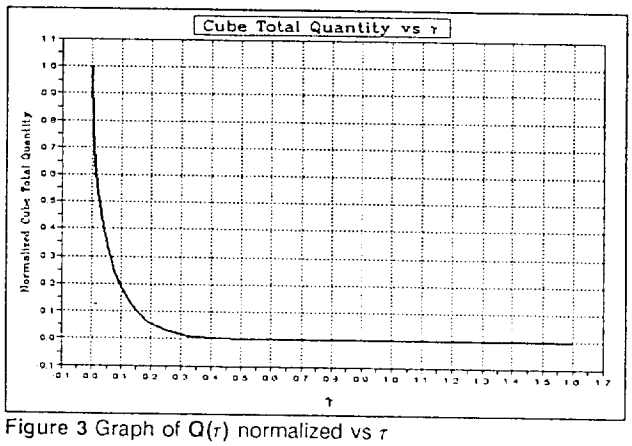

Figure 3 Graph of $Q(\tau)$ normalized vs τ

The following regression equation was fitted to the results:

$$Q(t) = 8\lambda^3 \rho_c (C_S + (C_0 - C_S)\cdot\theta^T)$$

$$T = k_0\tau + k_1\left((1+k_2\tau)^{\alpha} - \frac{k_3}{k_3 + (k_4\tau)^{\beta}}\right)^{\frac{1}{\alpha}}$$

$$\tau = \frac{D}{\lambda^2}t \qquad (5)$$

k_0 = 7.084 k_1 = -0.513 k_2 = 37.169 k_3 = 0.932

k_4 = 15.831 α = 1.876 β = 1.593

The regression coefficient (squared) for this relationship is r^2 = 0.999999831, indicating an excellent fit. The largest absolute error is +0.00013 at τ = 0, and the largest relative error is +0.89% at τ = 0.24.

Sorption and Gaseous Behaviour

In order to quantify the surface concentration C_S and the initial concentration C_0 of the particle, use is made of the Langmuir isotherm (Equation 6) and the Real Gas Law (Equation 7).

$$V_{eq} = m_c\cdot\left(\frac{L_1 L_2 p}{1 + L_2 p}\right) \qquad (6)$$

$$pV = \kappa nRT = \kappa\frac{m_G}{M_G}RT \qquad (7)$$

The concentrations are measured in mass of gas per unit mass of coal. The Langmuir isotherm relates the total adsorbed gas volume (at stp) at a fixed temperature to the ambient gas pressure. On the assumption that sorption rates on the outer surfaces of the particle are sufficiently rapid, the initial and surface concentrations are described in terms of the (absolute) void space and virgin seam gas pressures by

$$C_S = \left(\frac{p_{std} M_G}{\kappa R T_{std}}\right)\cdot\left(\frac{L_1 L_2 p}{1 + L_2 p}\right) \qquad (8)$$

and

$$C_0 = \left(\frac{p_{std} M_G}{\kappa R T_{std}}\right)\cdot\left(\frac{L_1 L_2 p_-}{1 + L_2 p_-}\right) \qquad (9)$$

In addition, the mass of free gas held in the void space of an element is given by

$$m_G = \left(\frac{M_G(\Delta x\Delta y\Delta z - 8\lambda^3)}{\kappa RT}\right)\cdot p \qquad (10)$$

Permeability and Darcy Flow

The fundamental steady state Darcy permeable flow equation for anisotropic permeability in a three-dimensional rectangular co-ordinate system is

$$q = -\frac{1}{\eta}\cdot\left(K_x\frac{\partial p}{\partial x}\vec{i} + K_y\frac{\partial p}{\partial y}\vec{j} + K_z\frac{\partial p}{\partial z}\vec{k}\right) \qquad (11)$$

For a particular direction $\vec{\zeta}$, Equation 11 reduces to

$$q_\zeta = -\frac{K_\zeta}{\eta}\cdot\frac{\partial p}{\partial \zeta} \qquad (12)$$

The above relationship is valid only in a laminar flow regime, which affords an opportunity of expressing the permeability of the medium in terms of the element geometry via the steady state laminar flow law for circular ducts proposed by Poiseuille. This is

$$\dot{V}_\zeta = -\frac{\pi a^4}{8\eta}\cdot\frac{\partial p}{\partial \zeta} \qquad (13)$$

Permeability is affected by (1) the void cross-sectional area available to flow per unit cross-sectional area of the medium, and (2) the internal surface area with which the fluid is in contact per unit volume of the medium. For a short cylindrical duct of radius a and length $\Delta\zeta$ through a 'solid' medium of uniform cross-sectional area A_s, Equation 13 translates to

$$q_\zeta = \frac{\dot{V}_\zeta}{A_s} = -\frac{\pi a^4}{8\eta A_s}\cdot\frac{\partial p}{\partial \zeta} = -\frac{K_o}{\eta}\cdot\left(\frac{2\pi a\Delta\zeta}{A_s\Delta\zeta}\right)^{\alpha_0}\cdot\left(\frac{\pi a^2}{A_s}\right)^{\alpha_1}\cdot\frac{\partial p}{\partial \zeta}$$

$$= -\frac{K_o}{\eta}\cdot\left(\frac{A_c}{V_s}\right)^{\alpha_0}\cdot\left(\frac{A_f}{A_s}\right)^{\alpha_1}\cdot\frac{\partial p}{\partial \zeta}$$

Analysis of the exponents of a and A_s in the above relationship yields α_0 = -2, α_1 = 3 and K_o = 1/2. It can be shown that the specific discharge of a rectangular duct is in the ratio 8:9 with that of a circular duct, so that the permeability of a medium with rectangular ducts is given by

$$K_{\zeta\square} = \frac{4}{9}\cdot\left(\frac{A_f}{A_s}\right)^3\cdot\left(\frac{V_s}{A_c}\right)^2 \qquad (14)$$

The four quantities on the right hand side of Equation 14 are readily expressed in terms of the element dimensions. By letting X stand for any one of x, y or z and Y and Z for the remaining two dimensions, the three equations relating the permeabilities in the three principal directions are summarized by

$$K_X = \frac{\Delta X^2\lambda^2}{9\,\Delta Y\,\Delta Z}\cdot\left(\frac{\Delta Y\,\Delta Z}{4\lambda^2} - 1\right)^3 \qquad (15)$$

Given the permeabilities and λ, Δx, Δy and Δz can be solved for (suitable substitutions reduce this to finding the roots of a cubic), but for the solution to be physically meaningful, $\Delta x \geq 2\lambda$, $\Delta y \geq 2\lambda$ and $\Delta z \geq 2\lambda$ must be satisfied.

The *in situ* gas permeability is affected by the following three factors: (1) the fluid pressure, (2) the presence of water and (3) the state of stress in the medium. The fluid pressure dependence is known as the 'Klinkenberg Effect' and is quantified by

$$K_\zeta = K_{-\zeta}\cdot\left(1 + \frac{b_\zeta}{p}\right) \qquad (16)$$

The presence of (free) water reduces the permeability of the medium by diminishing the effective duct size. It is assumed that such water is held as a thin uniform film on the outer surfaces of the particle. The free moisture content of South African coals rarely exceeds 0.05 (viz. 5%) by mass, and water, being a polar molecule with protruding hydrogen atoms, will tend to adhere to free coal (carbon) surfaces, so that the assumption about its mode of retention is reasonable. If λ_0 is the particle half-length of a dry particle, then the half-length of a moist particle is given by

$$\lambda = \lambda_0\cdot\sqrt[3]{1 + \frac{\mu_w \rho_c}{(1+\mu_w)\rho_w}} \qquad (17)$$

The effect of stresses is to alter the void space sizes in accord-

ance with Hooke's Law. Adopting the same symbolic conventions used in Equations 15 and 17, stress effects are described by

$$\Delta X = \Delta X_0 \cdot (1 - \varepsilon_X)$$
$$E\varepsilon_X = \sigma_X - \nu\sigma_Y - \nu\sigma_Z - (1 - 2\nu)\cdot p \qquad (18)$$

The Darcy equation as used so far is valid only where flow is laminar. However, as the gas migrates through the medium, it encounters corners, edges and other irregularities and its flow will hence be (locally) turbulent. The one-dimensional laminar-inertial turbulence corrected flow relationship is derived from the following equations

$$q_\zeta = -C_\Lambda \frac{K_\zeta}{\eta}\cdot\frac{\partial p}{\partial \zeta} \qquad C_\Lambda = 1 + \tfrac{1}{2}\cdot\left(\sqrt{1 + 4Re_\zeta} - 1\right)$$
$$Re_\zeta = \frac{\rho_G\sqrt{K_\zeta}\,q_\zeta}{\eta} \qquad \rho_G = \frac{M_G\,p}{\kappa RT} \qquad (19)$$

and is

$$q_\zeta = -\frac{K_\zeta}{\eta}\cdot\left(1 - \frac{M_G\sqrt{K_\zeta^3}\,p}{\kappa RT\eta^2}\cdot\frac{\partial p}{\partial \zeta}\right)\cdot\frac{\partial p}{\partial \zeta} \qquad (20)$$

With reference to Figure 4, the mass of gas that diffuses from the particle in element i from time t to t + Δt is given by

$$\Delta m_D = Q(t) - Q(t + \Delta t) \qquad (21)$$

where Q(t) is the function given by Equations 5, 8 and 9. By considering the Darcy flow from element i-1 to i and from i to i+1 as given by Equation 20, the mass of free gas in the void space of element i is readily quantified. The introduction of subscripted ordinal numbers ijk (i ↦ x, j ↦ y and k ↦ z) to distinguish individual elements from one another allows the derivation to be extended to three dimensions.

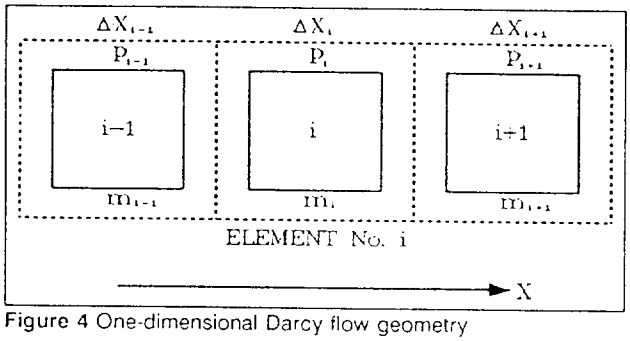

Figure 4 One-dimensional Darcy flow geometry

Thus,

$$m_{ijk}|_{t+\Delta t} = m_{ijk}|_t + \Delta m_{D\,ijk} + \Delta m_{K\,ijk}$$
$$\Delta m_{K\,ijk} = c_{ijk}\cdot\Delta t\cdot\sum_{\Omega = x,y,z}\left(\Gamma_{\Omega\,ijk}\cdot\left(1 + \frac{c_{ijk}}{\eta_{ijk}}\cdot\Gamma^*_{\Omega\,ijk}\right)\right)$$
$$c_{ijk} = -\frac{2M_G}{\kappa RT_{ijk}\eta_{ijk}}\cdot p_{ijk}$$
$$\Gamma_{x\,ijk} = K_{x\,ijk}\cdot\Delta y_{ijk}\cdot\Delta z_{ijk}\cdot\left(\frac{p_{ijk} - p_{i-1jk}}{\Delta x_{ijk} + \Delta x_{i-1jk}} - \frac{p_{i+1jk} - p_{ijk}}{\Delta x_{ijk} + \Delta x_{i+1jk}}\right)$$
$$\Gamma^*_{x\,ijk} = \sqrt{K^3_{x\,ijk}}\cdot\left(\frac{p_{ijk} - p_{i-1jk}}{\Delta x_{ijk} + \Delta x_{i-1jk}} + \frac{p_{i+1jk} - p_{ijk}}{\Delta x_{ijk} + \Delta x_{i+1jk}}\right) \qquad (22)$$
$$\Gamma_{y\,ijk} = K_{y\,ijk}\cdot\Delta x_{ijk}\cdot\Delta z_{ijk}\cdot\left(\frac{p_{ijk} - p_{ij-1k}}{\Delta y_{ijk} + \Delta y_{ij-1k}} - \frac{p_{ij+1k} - p_{ijk}}{\Delta y_{ijk} + \Delta y_{ij+1k}}\right)$$
$$\Gamma^*_{y\,ijk} = \sqrt{K^3_{y\,ijk}}\cdot\left(\frac{p_{ijk} - p_{ij-1k}}{\Delta y_{ijk} + \Delta y_{ij-1k}} + \frac{p_{ij+1k} - p_{ijk}}{\Delta y_{ijk} + \Delta y_{ij+1k}}\right)$$
$$\Gamma_{z\,ijk} = K_{z\,ijk}\cdot\Delta x_{ijk}\cdot\Delta y_{ijk}\cdot\left(\frac{p_{ijk} - p_{ijk-1}}{\Delta z_{ijk} + \Delta z_{ijk-1}} - \frac{p_{ijk+1} - p_{ijk}}{\Delta z_{ijk} + \Delta z_{ijk+1}}\right)$$
$$\Gamma^*_{z\,ijk} = \sqrt{K^3_{z\,ijk}}\cdot\left(\frac{p_{ijk} - p_{ijk-1}}{\Delta z_{ijk} + \Delta z_{ijk-1}} + \frac{p_{ijk+1} - p_{ijk}}{\Delta z_{ijk} + \Delta z_{ijk+1}}\right)$$

The viscosity η of a fluid is a measure of its resistance to deformation by external forces and usually depends predominantly on the fluid temperature. Methane dynamic viscosity (in Pa·s) is closely related to its absolute temperature by

$$\eta = (4.1596\cdot T^{0.624} - 35)\cdot 10^{-7} \qquad (23)$$

in the range 100K ≤ T ≤ 800K.

Random Variations

In order to 'reproduce' naturally occurring random fluctuations, a (pseudo)random number generator that produces uniformly distributed random numbers n_ϱ in the range $0 \le n_\varrho < 1$ is used, which can then be mapped onto the required distribution via a suitable transformation. In the case of a lognormally distributed quantity, the logarithms of the population values are normally distributed, so that it is necessary only to relate a uniform to a normal distribution. This is done on the basis of equal cumulative probabilities and leads to the relationship

$$n_\varrho = \int_{-\infty}^{\vartheta}\frac{1}{\sqrt{2\pi}}\cdot e^{-\frac{1}{2}\psi^2}\,d\psi = F(\vartheta) \qquad (24)$$

$F(\vartheta)$ in Equation 24 is the cumulative normal distribution function, which cannot be evaluated analytically. In theory, ϑ must satisfy $-\infty < \vartheta < +\infty$ to encompass all possible values, but since $-4 \le \vartheta \le +4$ includes at least 99.99% of same, these limits are chosen for simplicity to represent the full range. A reasonably accurate approximation (maximum relative errors of -1.28% at $\vartheta = 0.01$ and +2.14% at $\vartheta = 0.60$) is given by

$$\Phi(\vartheta) = \tfrac{1}{2}\cdot\left(1 + \sqrt{1 - e^{-0.6093\cdot|\vartheta|^{1.8601}}}\right) \qquad (25)$$

with $F(\vartheta) = \Phi(\vartheta)$ if $\vartheta \ge 0$ and $F(\vartheta) = 1 - \Phi(\vartheta)$ if $\vartheta < 0$. Rearranging Equations 24 and 25,

$$|\vartheta| = 1.2843\cdot\left[-\mathrm{Ln}\left(4\,n_\varrho\,(1 - n_\varrho)\right)\right]^{0.505} \qquad (26)$$

where ϑ is positive if $n_\varrho \ge \tfrac{1}{2}$ and negative otherwise. In order to satisfy $|\vartheta| \le 4$, $0.000019 \le n_\varrho \le 0.999981$ must be satisfied. This is achieved by replacing every occurrence of n_ϱ in Equation 26 by n'_ϱ, where $n'_\varrho = 0.000019 + 0.999962\cdot n_\varrho$.

If υ_M (as a fraction of the mean) is the maximum allowable variation around the mean of a normally distributed quantity, then random fluctuations are introduced by applying $f_N = 1 + \tfrac{1}{4}\cdot\vartheta\cdot\upsilon_M$ as a factor to the mean value. In the case of a lognormally varying quantity, the factor is $f_{LN} = 10^{\frac{1}{4}\cdot\vartheta\cdot N_{OM}}$, where N_{OM} is the number of orders of magnitude (powers of 10) the allowable variation covers.

Boundary Conditions

Two types of boundary are identified: (1) free faces -ie. areas exposed to the atmosphere, and (2) modelled region boundaries -ie. the peripheries of the modelled region. In the case of any region boundary, one of three ideal states is assumed:

(1) At *impermeable* boundaries, gas release is purely diffusive. Mathematically,

$$\Delta m_{K\,ijk} = 0 \qquad (27)$$

(2) At *constant pressure* boundaries, depending on their location and orientation, one or more of the following hold:

$$p_{i+1jk} = p_{ijk} \text{ or } p_{ij+1k} = p_{ijk} \text{ or } p_{ijk+1} = p_{ijk} \qquad (28)$$

(3) At *constant pressure gradient* boundaries one or more of the following hold:

$$p_{i+1jk} - p_{ijk} = c \text{ or } p_{ij+1k} - p_{ijk} = c \text{ or } p_{ijk+1} - p_{ijk} = c \qquad (29)$$

where c is a constant.

The conditions at free faces are more complex since these are

destressed and usually fractured. An empirical relationship for the depth of pillar fracturing (in m) from a free face is

$$d_f = 0.615 \cdot \mathrm{Ln}\left[\frac{H}{44.174 + 25.92 \cdot h}\right] \quad (30)$$

It is assumed that at all vertical free (coal) faces the vertical stress increases from zero linearly with depth into the face up to the limit of fracturing, where it equals the peak abutment stress σ_P, and beyond this limit it decays exponentially, tending to its virgin value σ_-. An empirical relationship quantifying σ_P is

$$\sigma_P = 1.2 \cdot e^{3.56 \cdot h^{-0.86} \cdot d_f} \quad (31)$$

The vertical stress behind a vertical free face is then

$$\begin{aligned} \xi > d_f \quad &- \quad \sigma_z = \sigma_- + (\sigma_P - \sigma_-) \cdot e^{-k_c \cdot (\xi - d_f)} \\ \xi \le d_f \quad &- \quad \sigma_z = \frac{\sigma_P}{d_f} \cdot \xi \\ k_c &= \frac{\sigma_P - \sigma_-}{\sigma_-(d_f + h) - \tfrac{1}{2} \cdot d_f \cdot \sigma_P} \end{aligned} \quad (32)$$

Equations 32 apply also in the case of total extraction methods involving goafing, with the slight modification that σ_P is replaced by UCS, since the horizontal confining stresses acting in the plane of the seam will disappear as there is no solid roof to transmit them. In all cases, the two horizontal stresses are assumed to obey $\sigma_x = \sigma_y = c_o \cdot \sigma_z$, where c_o is a constant (usually between ½ and 2).

Horizontal free faces (eg. roof and floor) of the excavation are generally subject to tensile horizontal stresses where no goafing occurs. For present purposes, it may be assumed that where such a face is comprised of carbonaceous material, the degree of 'stretching' is sufficient for gas transport to be governed only by diffusive processes, while where it is non-carbonaceous, the degree of 'stretching' is insufficient to significantly alter the permeability due to the generally high Young's moduli exhibited by these materials. Work aimed at devising a simple and relatively accurate representation of this is still in progress.

The gas pressure at any free face is equal to the prevailing atmospheric pressure, so that, depending on the face's location and orientation, one or more of the following hold:

$$p_{ijk} = p_{atm} \quad (= p_{i+1|,1k,1}) \quad (33)$$

Further Considerations

(1) Transport in non-carbonaceous regions: Since gas migration in such regions is purely Darcy permeable, the diffusion term in Equation 22 is zero. Thus,

$$\Delta m_{D\,ijk} = 0 \quad (34)$$

(2) Dynamic mining activity: The assumption that coal releases the entirety of its free gas upon being broken leads to the following relationship:

$$\Delta m_{DMA} = \sum_i \sum_j \sum_k \left(\frac{M_G\left(\Delta x_{ijk} \Delta y_{ijk} \Delta z_{ijk} - 8\lambda_{ijk}^3\right)}{\kappa R T_{ijk}} \right) \cdot (p_{ijk} - p_{atm}) \quad (35)$$

The element parameters are taken to be those at the time step just prior to being broken, and the summations extend only over those elements separated from the mined region. This contribution is calculated *before* any other in order to cater for possible substantial pressure gradient increases. The newly exposed area becomes a new boundary.

It is assumed that the residence time of broken (carbonaceous) material in the excavation is sufficiently short for subsequent sorptive and diffusive gas release therefrom to be insignificant, which is reasonable, given today's production methods.

(3) Goafing and caving: Where coal exploitation involves this, the effect thereof depends on the type of material broken. Non-carbonaceous material releases all the gas held in the void space, whereafter no further gas is contributed. This is quantified by Equation 35. Carbonaceous material behaves the same way upon breaking, but further gas release is purely diffusive. In terms of the surface concentration C_S of caved elements, this means

$$C_S = \left(\frac{p_{std} M_G}{\kappa R T_{std}}\right) \cdot \left(\frac{L_1 L_2 p_{atm}}{1 + L_2 p_{atm}}\right) \quad (36)$$

(4) Initial conditions: Ideally, a complete specification of the spatial distribution of the relevant physical properties in the region to be modelled at some instant is required. Practically, these properties can only be known at a few isolated points. This may be used as a basis for assigning values to other points via suitable inter- and extrapolation schemes.

Such a scheme is provided by an inverse-distance weighting, but this notion may be extended to the more general case where the weighting factors are the inverse distances raised to some power ϵ. Thus, if q_i represents the values of a quantity at points with co-ordinates (x_i, y_i, z_i), then q_{ijk} is the value of that quantity at a point with co-ordinates $(x_{ijk}, y_{ijk}, z_{ijk})$ and is given by

$$\begin{aligned} q_{ijk} &= \left(\sum_{i=1}^{N_K} q_i \cdot s_{i\,ijk}^{-\epsilon}\right) \cdot \left(\sum_{i=1}^{N_K} s_{i\,ijk}^{-\epsilon}\right)^{-1} \\ s_{i\,ijk} &= \sqrt{(x_i - x_{ijk})^2 + (y_i - y_{ijk})^2 + (z_i - z_{ijk})^2} \end{aligned} \quad (37)$$

It should be noted that different quantities may be known at different numbers of points N_K, that ϵ may differ among different quantities and that this procedure is valid only within (sub)regions of similar composition.

Modifications for Computerisation

In order to apply the preceding mathematical considerations to practical instances, an indication of the element sizes is required. It has been noted that sorption rates of crushed coal samples are apparently independent of average particle size in the range from about 20mm to about 3mm. Smaller particles show a dramatic increase in this rate, while that of larger particles gradually decreases. The size at which the increase appears is termed the 'Fracture Network Size', or FNS.

One possible explanation for this phenomenon is that particles larger than the FNS are effectively composed of blocks this size and provided that the particles are not too large, free gas diffused from individual blocks can flow relatively unhindered through cleats and fractures. The larger the particles, the more such blocks they contain, which increases the gas's migration distance and retards the sorption rate as a result of pressure build-up. Conversely, particles smaller than the FNS have a greater free surface area for sorptive processes, a reduced diffusing distance and uninhibited free gas flow, so that release rates are substantially higher.

South African coals analyzed in this respect thus far uniformly show FNSs very close to 3mm. From the preceding discussion, it is reasonably deduced that $\lambda \approx 1.5$mm for SA coals. It is immediately apparent that an immense number of elements would be required to model gas transport, even in small regions. By way of illustration, a coal cube with a side length of 1m contains roughly 37 million elements. Consequently, it is totally impractical to model a region on the basis of individual elements.

This problem may be substantially reduced by considering an elemental region ('c-element') composed of a collection of elements that all behave in a similar manner. The validity of this approach hinges on (1) the size of the c-element in relation to

that of an element, (2) the shape of the c-element and (3) the prevalent physical conditions in adjacent c-elements.

The c-element size is to a large extent determined by the computational ability of the system it is targeted for in conjunction with the size of the region that is to be modelled. The data segment restrictions on most PC installations will result in relatively high disk read/write time sacrifices.

The recommended shape of the c-element is a rectangular paralleliped, since the coal structure is defined within a Cartesian co-ordinate system and the elements themselves are of this shape. This arrangement makes for reasonably simple discretisation.

Physical conditions in adjacent c-elements should not differ dramatically since the more pronounced these differences are, the less accurate the results are. It is recommended that the free gas pressure differences between adjacent c-elements be kept relatively constant for each of the three principal directions. This indicates that the region's discretisation should be periodically reassessed. From a computational point of view, it is not especially difficult to merge or split c-elements.

Conclusions

The derivations presented herein form part of a project aimed at providing the local coal mining industry with guidelines for the improvement of underground environmental conditions with a view to enhanced safety of personnel. It is envisioned that this work will be successfully translated into a PC based application for the industry.

In its present form, the model is not restricted in any way by such factors as the geological setting and the mining layout, and can be applied to virtually any imaginable situation, including gas drainage. Provided that the required input data are adequately well known, the model is expected to provide reasonably accurate and reliable information about gas emission and in-seam behaviour for underground collieries.

The model neglects ground water flow as a result of this not being a significant factor locally. It may become necessary to include this at a subsequent stage if sites suffering therefrom come to light. Presently, the only restrictions on the model are placed by the speed and maximum data capacity of the computer system on which it is processed.

Upon completion of the coding, model verification/evaluation and any further required modifications will be done. If it is found to be a valid and practicable model, a complete methane emission prediction software package will be produced which will fill a large gap in the local coal mining industry's tool box.

Nomenclature (only symbols not defined in the text)

C : adsorbed gas concentration, [mass ratio];
t : time, [s];
∇ : Laplacian **grad** operator;
D : diffusion coefficient, [$m^2 \cdot s^{-1}$];
Δx, Δy, Δz : element dimensions, [m];
C_S : particle surface concentration, [mass ratio];
C_0 : particle initial concentration, [mass ratio];
ξ : distance into a free face, [m];
C^* : normalized gas concentration, [-];
ρ_c : particle density, [$kg \cdot m^{-3}$];
V_{eq} : Langmuir stp volume of adsorbed gas, [m^3];
m_c : coal mass, [kg];
L_1, L_2 : Langmuir constants, [$m^3 \cdot kg^{-1}$] and [Pa^{-1}], respectively;
p : gas pressure, [Pa];
κ : gas supercompressibility fraction, [-];
n : number of moles of gas, [-];
R : universal gas constant, [8.31432 $J \cdot mol^{-1} \cdot °K^{-1}$];
T : free gas temperature, [°K];
m_G : mass of gas, [kg];
M_G : Molecular mass of the gas, [CH_4: 0.016043 $kg \cdot mol^{-1}$];
p_{std} : standard pressure, [101325 Pa];
T_{std} : standard temperature, [273.15 °K];
p_∞ : virgin (seam) gas pressure, [Pa];
q : specific discharge, [$m^3 \cdot s^{-1}$ per m^2 = $m \cdot s^{-1}$];
η : gas dynamic viscosity,[Pa•s];
K_x, K_y, K_z : principal intrinsic permeabilities, [m^2];
$\vec{i}$, $\vec{j}$, $\vec{k}$: unit vectors in the **x**, **y** and **z** direction, respectively, [-];
$\dot{V}_\zeta$: volumetric flow rate in the $\vec{\zeta}$ direction, [$m^3 \cdot s^{-1}$];
a : circular duct radius, [m];
A_s : cross-sectional area of the permeable medium, [m^2];
A_c : area of contact between fluid and medium, [m^2];
A_f : cross-sectional area available to fluid flow, [m^2];
V_s : total volume of medium (including voids), [m^3];
b_ζ : Klinkenberg slippage factor in the $\vec{\zeta}$ direction, [Pa];
μ_w : moisture content (of coal), [mass ratio];
ρ_w : moisture density, [$kg \cdot m^{-3}$];
ε_x, ε_y, ε_z : normal strains, [-];
σ_x, σ_y, σ_z : normal stresses, [MPa];
E : Young's modulus, [MPa];
ν : Poisson's ratio, [-];
C_A : laminar-inertial turbulence correction factor, [-];
Re_ζ : porous flow Reynold's number in the $\vec{\zeta}$ direction, [-];
Δm_K : Darcy gas mass change in time Δt, [kg];
ϑ : normalised Gaussian random variable, [-];
H : mining depth below surface, [m];
h : excavation height, [m];
k_ζ : stress decay constant, [m^{-1}];
UCS : unconfined compressive strength, [MPa];
Δm_{DMA} : gas mass contributed by mining activity, [kg];
p_{atm} : prevailing atmospheric pressure, [Pa];
N_K : number of points at which a quantity is known, [-];

References

Cook, A.P. and Erwee, E.C. Methane Properties of South African Coals, Part 1 : Sorption Characteristics. Coal Mining, Chamber of Mines Research Organisation, Johannesburg. Reference report No. 16/91. 1991.

De Wiest, R.J.M. (Editor). Flow Through Porous Media. Academic Press, New York. 1969.

King, G.R. and Ertekin, T. State-of-the-Art Modelling of Unconventional Gas Recovery. SPE Joint Rocky Mountain Regional/Low Permeability Reservoirs Symposium and Exhibition. Society of Petroleum Engineers, Inc., Denver, Colorado. 1989.

Ozan T.T. The Determination of the Depth of Fractured Zones around Coal Pillars. MASSMIN '92 Symposium. The South African Institute of Mining and Metallurgy Symposium Series S12, Johannesburg. 1992.

Stripp, G.P. Methane Emission Characteristics of South African Coal Seam Strata. PhD Thesis, University of the Witwatersrand. 1989.

Weast R.C. (Editor). CRC Handbook of Chemistry and Physics, 63rd Edition, 1982-1983. CRC Press, Inc., Boca Raton, Florida. 1982.

APPENDIX B4

A GENERAL STATE MODEL OF METHANE TRANSPORT IN COAL STRUCTURES

P LINZER

DRAFT REPORT
PROJECT NO. COL 030
MAY 1994

SIMRAC REPORT NUMBER: COL 030
MININGTEK TASK NUMBER: Y3201
FIRST AUTHOR: P LINZER
DATE: 94-05-17

TITLE: A General State Model of Methane Transport in Coal Structures

TYPE OF REPORT: Draft Report

AUTHOR: P Linzer

ABSTRACT: A great deal of effort has been expended by coal mining industries worldwide on the derivation of efficient algorithms that describe the transport and liberation of CH_4 gas from coal structures. The majority of these models treat the structures as continua wherein two main gas flow modes (diffusive and Darcy permeable) prevail, and use finite element or finite difference techniques in processing the two resulting parabolic partial differential equations. Many of the algorithms assume isotropy in geometric and physical coal structure properties and do not recognize the existence of fundamental random fluctuations in these. The model proposed herein does not suffer from these shortcomings, and its efficiency is enhanced by the complete elimination of one of the differential equations. Further work will comprise the evaluation of its predictive merit against observed data

KEYWORDS: Coalbed structure, Computer model, Darcy permeable flow, Diffusive flow, Gas emission, Gas transport, Mathematical model

DISTRIBUTION: J W Oberholzer, A Cook, SIMRAC June 1994

Mining Technology

CSIR

CSIR Division of Mining Technology
Mining Environment Draft Report

PREFACE

The single greatest hazard facing most underground coal mining operations is the continuous liberation of combustible gas, principally methane, from both the seam being mined and the surrounding geological structures into the working environment. The laws and mechanisms describing this process give rise to complex quantitative interrelationships that complicate endeavours to model the phenomenon within acceptable limits of accuracy. Such modelling would be of great benefit to the coal mining fraternity as it would allow predictions to be made about environmental conditions in varying mining geometries, methods, rates and coal structure properties, thus facilitating the design and implementation of preventive or hazard reducing measures

Colliery ventilation strategies are primarily designed around maintaining flammable gas concentrations below statutory limits. These designs rarely proceed from more than cursory knowledge of actual gas release rates, which often renders them inappropriate to the realities. A reasonably accurate and efficient method of estimating such release rates would alleviate this deficiency appreciably.

This report describes the derivation of such a method and the resulting model. The quantitative relationships among the various parameters are presented as equations of a form requiring little or no further development to improve their amenability to coding into a computer program. An outline of the features of the necessary data structures and processing functions and procedures is presented in order to expedite such coding

Evaluation of this model awaits the completion of coding in the Turbo Pascal language. This report therefore, details only the theoretical basis and development of the model without reference to actual observations. This is reserved for future work, and in all likelihood will necessitate modifications to that which is presented here.

Patrick Linzer

May 1994
Johannesburg, South Africa

SUMMARY

The Mining Environment Programme in the CSIR's Division of Mining Technology (formerly the Chamber of Mines Research Organisation) has been tasked by SIMRAC with providing the South African coal mining industry with suitable guidelines for the planning of ventilation layouts for underground workings in order to reduce or even eliminate methane related accidents. This requires a relatively accurate indication of the amount of this gas that can be expected in a given situation - ie. a methane prediction model.

Existing computerised models range from the relatively simple to the very complex and generally the results do not correlate well with observed data as a result of a variety of factors that include oversimplifications, input data deficiencies, inadequate approximations and computational instabilities.

In accordance with the theoretical bases of most of the more complex extant models, the one presented here proceeds from the assumption that two principal gas flow regimes, namely diffusive and Darcy permeable, govern the bulk of the gas migration within coal. It then presumes an idealised coal microstructure, consisting of distinct elements comprised of homogeneous (coal) particles surrounded by a geometrically regular void space. Diffusive flow is confined to the particle, while Darcy permeable flow is confined to the void space.

The two modes of flow are interdependent in that the gas diffusing from the particle affects the pressure in the void space, which influences the macroscopic permeable flow rate, while the pressure in the void space determines the amount of gas adsorbed on the free surfaces of the particle, which in turn affects the microscopic diffusion rate. The model links the flow modes via the Langmuir isotherm on the basis of a mass balance.

As a result of the assumed coal particle homogeneity, the diffusive phase is treated as a continuum process. This has been analysed separately, and a suitable approximation fitted to the results, thus eliminating the need to solve one parabolic partial differential equation and consequently reducing the required computational effort.

Unlike other models, the analysis of Darcy permeable flow is not taken to the limiting case where elements are assumed to be of infinitesimal size, so that the resulting equations are left in a form containing finite differences rather than differentials. Furthermore, in an attempt to cater for statistically random variations, an approximate relationship has been derived which allows normally and lognormally distributed factors within definable limits to be applied to any or all model parameters. This permits definition of the degree to which the model is deterministic.

Regions in the coal structure consisting of rock are similarly described, except that gas migration is limited to Darcy permeable flow only.

An attempt is made to quantify from first principles the effects of both stress distributions and dynamic mining activity on gas transport and emission rates within the modelled region. The model is then compared to some existing ones, and details of modifications and data structures for computerisation are provided.

The model's predictive value is presently believed to depend on two main divergent constraints: firstly, there is the limit set by the available computing power and the coding language, which together determine both the maximum size of the region that can be modelled and the required processing time, and secondly, there is the limit set by the accuracy of the required input parameters, which determine the representativeness of the modelled region. Possible techniques for alleviating these limitations are presented.

All of the preceding considerations are then consolidated in a coherent mathematical description of the methane in-coal phenomenon.

CONTENTS

LIST OF FIGURES

LIST OF TABLES

NOMENCLATURE (Listed in order of appearance in the text)

SYMBOL(S)	MEANING	UNITS
xyz	Rectangular co-ordinate system within which the mining geometry is defined. The xy plane is coplanar with the coal seam. z is a normalised random variable in Section E.6.	m
C	Mass concentration of diffusing substance in the medium	-
t	Time elapsed from a given reference	s
D	Diffusion coefficient of the coal particle	$m^2 s^{-1}$
∇	Laplacian Grad operator	
$\Delta x\ \Delta y\ \Delta z$	Element dimensions	m
λ	Particle (cube) half side length	m
ξ	Normalised diffusive flow direction axis	-
τ	Normalised diffusive flow time	-
C_0	Initial particle gas mass concentration	-
C_S	Particle surface gas mass concentration	-
C^*	Normalised gas concentration	-
ρ_c	Particle density	$kg\ m^{-3}$
N	Number of slabs for numerical diffusion model	-
Q	Total gas mass in the particle	kg
C^*_{ij}	Normalised gas concentration in slab i at time step j	-
Q_j	Total gas mass in the particle at time step j	kg
V_{eq}	Langmuir STP volume of adsorbed gas	m^3
m_c	Coal mass in an element	kg
k_1	Coal Langmuir constant 1	$m^3\ kg^{-1}$
k_2	Coal Langmuir constant 2	Pa^{-1}
p	Gas pressure (absolute)	Pa
κ	Gas supercompressibility fraction	-
n	Number of moles of gas	-
R	Universal gas constant	$J\ mol^{-1}\ °K^{-1}$

NOMENCLATURE CONTINUED

SYMBOL(S)	MEANING	UNITS
T	Free gas temperature in the void space of the element	°K
M_G	Molecular mass of the gas	Kg mol^{-1}
p_{STD}	Standard pressure	Pa
T_{STD}	Standard temperature	°K
p_∞	Virgin seam gas pressure	Pa
m	Gas mass	kg
q_s	Specific discharge	m s^{-1}
η	Gas dynamic viscosity	Pa s
$K_x\ K_y\ K_z$	Principal intrinsic material permeabilities	m^2
$\bar{i}\ \bar{j}\ \bar{k}$	Unit vectors in the x, y and z directions	-
$\bar{\zeta}$	Unit vector of arbitrary direction	-
q_ζ	Specific discharge in the direction of $\bar{\zeta}$	m s^{-1}
U	Fluid velocity	m s^{-1}
a	Duct radius	m
r	Distance from duct central axis	m
$\dot{V}_\zeta$	Volumetric flow rate in the direction of $\bar{\zeta}$	m^3 s^{-1}
A_s	Cross-sectional area of permeable medium	m^2
A_c	Internal contact area between fluid and medium	m^2
V_s	Total medium volume, including voids	m^3
A_f	Cross-sectional area available to flow	m^2
$\phi_x\ \phi_y\ \phi_z$	Ratio of obstructive cross-sectional area to total cross-sectional area of the permeable medium	-
b_ζ	Klinkenberg slippage factor in the $\bar{\zeta}$ direction	Pa
$K_{\infty\zeta}$	Infinite pressure permeability in the $\bar{\zeta}$ direction	m^2
$\bar{p}$	Mean fluid pressure	Pa
μ_w	Moisture content (mass ratio)	-
ρ_w	Moisture density	kg m^{-3}

NOMENCLATURE CONTINUED

SYMBOL(S)	MEANING	UNITS
$\varepsilon_x\ \varepsilon_y\ \varepsilon_z$	Normal strains	-
E	Young's modulus	MPa
$\sigma_x\ \sigma_y\ \sigma_z$	Normal stresses	MPa
ν	Poisson's ratio	-
$\Delta x_0\ \Delta y_0\ \Delta z_0$	Initial (unstressed) element dimensions	m
λ_0	Dry particle size (cube side half length)	m
C_{LIT}	Correction factor for laminar-inertial turbulence	-
Re_ζ	Reynold's number for porous flow in the $\vec{\zeta}$ direction	-
ρ_G	Gas density	kg m^{-3}
$\dot{m}_X$	Gas mass flow rate in the X direction	kg s^{-1}
Δm_D	Gas mass diffused in time Δt	kg
$i\ j\ k$	Ordinal element numbers in the x, y and z directions	-
Δm_K	Gas mass change due to permeable flow in time Δt	kg
Π_ϱ	Probability density function of random numbers	
Π_N	Probability density function of the normal distribution	
$F(z)$	Cumulative normal distribution function	
ϱ	Random number within specified limits (Section E 6)	-
υ	Maximum allowable variation about mean for normally distributed quantities	-
$f_{\upsilon N}$	Factor for normally distributed random variations	-
f_{LN}	Factor for lognormally distributed random variations	-
N_{OM}	Maximum number of orders of magnitude lognormally distributed quantities may vary	-
$RN_{\|RN\| < 1}$	Random number between 0 and 1	-
Q'	Varied quantity	
$\overline{Q}$	Mean value of varied quantity	
d_f	Depth of fractured zone	m

NOMENCLATURE CONTINUED

SYMBOL(S)	MEANING	UNITS
h	Mining (seam) height	m
H	Mining depth	m
σ_P	Peak abutment stress	MPa
σ_z	Vertical stress	MPa
σ_∞	Vertical virgin stress	MPa
w_x w_y	Pillar dimensions in the plane of the seam	m
k_ς	Stress decay constant	m^{-1} or m^{-2}
r_x r_y	Roadway widths in the plane of the seam	m
UCS	Unconfined uniaxial compressive strength (coal)	MPa
c_o	Ratio of horizontal to vertical stress	-
Δm_M	Gas mass released by broken/mined material	kg
p_{atm}	Prevailing atmospheric pressure	Pa
N_K	Number of points at which the value of a quantity is known	-
ι	Subscript indicating a known value	-
ε	Exponent for distance weighting/interpolating	-

VALUE OF CONSTANTS

SYMBOL	VALUE
p_{STD}	101 325 Pa
R	8 314 32 J mol^{-1} $°K^{-1}$
T_{STD}	273 15 °K
M_G (Methane)	0 016 043 03 kg mol^{-1}

A. INTRODUCTION

Efforts by the Mining Environment Programme in the CSIR's Division of Mining Technology to quantify and address the hazards related to the continual presence of flammable gas mixtures in underground coal workings focus on four main objectives. These are:-

- the improvement of flammable gas detection equipment;
- the development of flammable gas drainage methods;
- the relationship between flammable gas emissions and barometric pressure variations; and
- the development of a quantitative flammable gas emission prediction technique

The second and third of these are largely contingent on attaining the fourth objective, as this would allow the assessment of various drainage configurations and of emission rates against barometric pressure fluctuations

The paucity of reasonably accurate techniques for the prediction of flammable gas emissions from coal structures into underground workings often detrimentally affects the design and implementation of efficient and effective strategies aimed at reducing or eliminating the hazards associated with such emissions The need for a prediction technique capable of providing reliable output is generally recognised, and evidenced by the high incidence of flammable gas ignitions and deflagrations, which frequently escalate to extensive and catastrophic coal dust explosions, costly in terms of lives lost, property damage and production losses

The aim of this report is to provide a detailed description of the derivation and construction of one such technique It commences with an in-depth elucidation of the need for such a model and the desirable features thereof, followed by a detailed qualitative account of the model s theoretical foundations and the interrelationships among these Thereafter, the salient attributes are sequentially quantified in isolation, their logical consequences analysed and presented in a step-by-step manner, and their logical connection to preceding attributes explained The effects of external factors, such as dynamic mining activity and mining induced stress distributions, on the model behaviour are then assessed and the model consolidated A qualitative comparison to some existing models is then presented in order to illuminate advantages and disadvantages

Since the model is destined for PC application, this report incorporates a description of the necessary modifications and data structures to facilitate the development of the requisite software It is planned that the program be coded in Turbo Pascal and hence, where appropriate, program fragments are given in this language. Upon completion of the software, a more intensive appraisal of the model will be undertaken and reported on To this end, some field and laboratory data are available

B. THE NEED FOR A MODEL

Throughout its history and into the present day, underground coal mining has suffered major disasters in the form of gas and coal dust explosions[1 2 3 4] In the design of mine and/or working section ventilation plans, the prime consideration is the dilution of flammable gases by air to volumetric concentrations below legally permitted maxima since this usually sets a minimum air quantity significantly greater than that dictated by other criteria Secondary considerations include dust production levels, human air requirements and the palliation of noxious gases and heat produced by machinery and mining Methane (CH_4, $\geq 90\%$) is the predominant flammable gas Associated combustible gases include hydrogen (H_2), carbon monoxide (CO) hydrogen sulphide (H_2S) and heavier hydrocarbons, while some non-flammable gases such as carbon dioxide (CO_2), nitrogen (N_2) and helium

(*He*) are also emitted in low concentrations[4,5]. When such a gas mixture disperses in air in a suitable proportion, typically between 5% and 15% by volume, an explosible state is present and a hot spark of 0.3 milliJoules energy suffices to trigger a deflagration. The presence of airborne fine coal particles aggravates the situation by decreasing the lower explosive limit[5].

Coal dust explosions, although more violent and extensive, very rarely occur in isolation, since the minimum explosible airborne dust concentration is seldom present under ordinary conditions, and are almost exclusively the direct result of a methane explosion[3]. These detonations usually result in numerous fatalities and injuries to personnel, because of the heat generated (±2 000 °C), the shockwave, poisonous chemical products (principally carbon dioxide and carbon monoxide) which can disperse in the mine atmosphere and harm other mining crews, and oxygen depletion[7]. Physiological shock and impaired visibility aggravate the situation by provoking inappropriate or delayed reactions. Material damage is multifarious and includes deformed or burnt machinery and electric installations, blown out ventilation stoppings, falls of ground precipitated by the concussion and the ignition of other combustible substances Added to this is the loss of production suffered while the affected area is refurbished and production from it resumed. Thus, such explosions are very costly to the mining operation.

Much of the effort spent on schemes to ameliorate this danger has been reactive in nature in the sense that these are designed to minimise damages in the event of an explosion These schemes include active and passive explosion barriers, underground refuge chambers and first aid stations, compulsory issue of personal self-contained self-rescue equipment, emergency procedures and rescue teams. Efforts to curtail gas ignitions have focused on two main areas Firstly, the sources of such ignitions have been examined and this has resulted in rigorous definitions of and specifications for intrinsically safe and flameproof equipment, improved cutting bit designs and water spray arrangements, and stringent restrictions on blasting techniques and explosives. Secondly, the prerequisites for the existence of an explosible atmosphere have been appraised and this has yielded *inter alia* improved ventilation layouts, legal flammable gas concentration limits, flammable gas detection equipment, warning and automatic cut-out devices for machinery, and procedures for dealing with instances where the gas concentration exceeds applicable limits

Despite the measures outlined above, gas ignitions still occur. The decade 1980 to 1989 averaged 5,5 reported methane incidents *per annum* in South Africa, whereas the previous 50 year average was 2,5 *p a* (the same period saw a rapid increase in total coal production from underground) 75% of these ignitions occurred in the working face area, and 72% were initiated frictionally ie by cutting picks[3]. Frequently, these are localised events without serious consequences, but on occasion a full-scale explosion develops Occurrences of this type require the build-up of fairly extensive gas accumulations in the underground workings, the immediate cause of which is the presence of ventilation inadequacies These sub-standard conditions develop because of a poor understanding of the interrelationships between gas emission, mining layout, coal structure properties etc , and the lack of a suitable tool with which the development of such conditions could be anticipated

In 1989, King and Ertekin[9] reported on a survey of 37 numerical simulators for modelling gas production from geological structures Of these, 16 cater for stationary mining activity, and only eight for stationary and dynamic mining activity Six of these eight require the use of a mainframe computer, effectively putting them beyond the reach of local mining operations, while the remaining two, dating from 1974 and 1964, had not been computerised at the time of the report Dynamic mining activity is known to influence gas emissions significantly[3], so that the applicability of models that exclude it is diminished With regard to the use of mainframe computers, few local coal mining operations have access to such machines and the remainder are unlikely to pursue this in the light of the present trend towards decentralised processing and networking It is thus evident that suitable gas emission prediction techniques are not readily available to local collieries

The standard approach in determining ventilation requirements is to collect field data, usually drill core coal samples, from which the total gas content of the intended mining seam is ascertained This information is then used in conjunction with planned extraction rates to estimate the total methane

release into the working area, and the required air quantities are calculated accordingly. The validity of this practice is questionable in the light of two implicit assumptions it makes, which can only be accepted with reservations. These assumptions are that gas is released almost instantaneously from broken coal only and that the roof and floor do not make any contribution.

The presence of methane in areas that have remained idle for a period indicates that the gas continuously issues from the seam itself, and desorption analyses on various coal samples have shown that gas emission rates are (within certain limits) strongly dependent on the degree of sample comminution[9]. 200μm particles release 80% of their gas in ±20 minutes; 1mm - 3mm particles require in the order of hours to days, and core sized samples several weeks. To a certain extent, the effects of seam gas emission and broken coal gas retention cancel one another, but too many influences remain unconsidered to quantify this. Investigations at Ermelo Mines[13] have revealed that coal seams in the roof and floor can make significant contributions to gas emissions, particularly in the case of overlying seams where the mining method involves goafing. At Majuba Colliery, gas was seen to bubble at a rapid rate through water on the floor over a large area, and roof seam gas pressures as high as 1 750kPa were measured ±10m above the working horizon. Coal was mined from bord and pillar sections which displayed a high incidence of intersection collapse, most probably due to gas pressure causing bed separation in the immediate destressed roof zone These observations indicate that the roof and floor (non-coal) strata are not impermeable to gas, and that gas also migrates in these regions.

European and American empirical prediction models are sometimes applied to local designs, but their relevance to South African conditions has not been examined to any great extent. The geological settings and composition of overseas coal deposits are in general different from those of their South African counterparts, which are also mostly shallower, greater in magnitude, less undulatory and lower in gas content These differences may well be sufficiently pronounced to place local coals outside the ranges of applicability of these models, and so render them unsuitable for local requirements. In addition, empirical models are by their very nature limited to particular mining methods and layouts, and they should be periodically weighed against new data and revised if necessary The fact that this is rarely done leaves questions about their soundness unresolved

Apart from the preceding safety considerations, the development of a general state methane emission prediction model may facilitate commercially viable exploitation of methane as an energy source in South Africa Such a model will enable evaluation of the technical feasibility of different drainage strategies, which may then be implemented either to reduce gas emissions into underground workings or to extract the gas commercially, or both A successful drainage scheme in a mining operation will show additional benefits by reducing the air quantity requirement and thus the cost of its supply this Fan power is nearly proportional to the cube of the volumetric flow rate across it, so that a small reduction in flow rate results in greatly reduced fan power requirements [11] Large scale commercial extraction of methane as a fuel will also be environmentally advantageous in that methane is about 20 times more effective as a greenhouse gas than carbon dioxide, its chief combustion product[12] The environmental impact of its liberation into the atmosphere would be much curtailed

In summary, a methane emission prediction model would be an asset to the South African coal mining industry on the grounds of enhancing safety, and of the commercial and environmental value such a tool could provide

C. THE DESIRABLE FEATURES OF A PREDICTION MODEL

The utility of any model is subject to two primary criteria, namely its ease of application and its reliability As a result of the relatively complex quantitative relationships describing methane transport in geological structures, the application of the model requires a suitable vehicle which simplifies this Model reliability refers largely to the accuracy of the output it generates, which should be relatively simple to understand and of a usable form The widespread use of personal computers and their computational power meets

these requirements to an appreciable extent, although certain encumbrances (chiefly speed and maximum data capacity) place limits on both the range of application and the accuracy of the results, even if the underlying mathematical form of the model does not suffer such drawbacks. The recent advances in PC hardware technology augur well for even more dramatic improvements in this field, so that the development of a model should not be impeded by considerations of current limitations.

Consequently, the model should be as general as possible and include as many of the known (and quantified) influences as possible. This will improve reliability, but also extend the quantity and variety of the required input data. Since the validity of the output is also strongly dependent on the accuracy and detail of the input components, the model should permit this data to be entered to any required degree of (spatio-temporal) resolution, but at the same time accommodate instances where minimal details are given. This is readily accomplished by incorporating a pre-processing phase, wherein suitable interpolations between and extrapolations from known sample points assign values to unknown points.

The introduction of simplifying assumptions should also be avoided during the development stage of the model, since their effect may be detrimental and this will only be evident if a comparison with the unsimplified version is made Such assumptions, if fitting, can then be better motivated and included In the case under consideration, common *a priori* simplifications are isotropy and/or homogeneity in structural and physical properties, reductions in dimensionality, impermeable roof and floor strata, unidirectional gas flow, steady state approximations to unsteady state processes and neglecting secondary interdependencies, such as between fracturing and induced strains.

All of the extant models examined have without exception shown two common traits in their derivations The first of these is the treatment of the geological structure as a continuum, the result of which is the expression of the fundamental transport relationship as a multivariate partial differential equation Upon processing, the geological structure is spatially discretised and a variety of numerical techniques applied to the equation(s). This discretisation is determined on the basis of the complexity and extent of the modelled region, and is done without regard for the actual physical sizes of the fundamentally discrete elements in coal and rock formations The fundamentally discrete nature of such formations is illustrated by their granular composition and the extensive cleating and fracturing of coal, and should, in the author's opinion, be a primary consideration in any model derivation, since this eliminates the otherwise necessary discrete/continuous/discrete transformations and possible errors introduced thereby

The second common characteristic of these models is that they are completely deterministic -ie the same circumstances produce the same results This ought to be regarded with a measure of suspicion because of the presence of basic random variations in virtually all of the parameters needed to describe the phenomenon For example, cleat sizes vary from a few ångstroms to a few millimetres, a range of seven orders of magnitude It is also very unlikely that physical quantities such as diffusion coefficients and intrinsic permeabilities (apart from their dependence on concentrations and fluid pressures) are uniformly distributed in nature It is commonly held that these variations are adequately catered for by the use of averages However, secure knowledge of these averages is scarce and often meaningless as a result of ignorance surrounding the type and dispersion of the distribution of values they represent. To illustrate this further, it has been shown[13] that Darcy's law is the empirical equivalent of the general Navier-Stokes equations statistically averaged in a steady flow regime with negligible inertia, but the demonstration requires assumptions of invariance in certain quantities known not to behave thus Hence, a device that permits the introduction of random (or pseudorandom) fluctuations is deemed to enhance the model's representativeness

The output of the model should be reliable and meaningful Instantaneous gas emission rates are the most immediately important result for ventilation planning, but the behaviour of these rates over time is also consequential in that transient peaks or troughs may occur which, if seen in isolation, would encourage a false perception of the actuality The emission rates are also location-dependent and this is relevant to both the finer details of ventilation plans as well as gas drainage. With regard to drainage, the behaviour over time of in-seam gas pressure and total gas content distributions and the resultant flow vectors will indicate the efficiency of a given strategy and provide clues as to its improvement The initial state of the modelled region and its boundaries should form part of the output for the sake of

completeness.

Evident as it may seem, it must be stated that the model's usefulness is also closely aligned to the time required for the simulation of a given situation. In the extreme case, the processing time could match or exceed the actual period the simulation is required to cover and this is of little use. There is a distinct danger that this might happen as a result of the huge number of computations and the huge amount of data manipulated (currently estimated at 30 to 50 MegaBytes). Few PC installations currently have sufficient random access memory to store such voluminous data, so that work files must be written to, and accessed from, hard disk drives or other non-volatile storage media, adding sizeable read/write time overheads to the execution times. Furthermore, certain conditions on the spatial and temporal increments must be met to ensure stable results. In practise, this means that the number of computations required to model a region over a certain time interval increases by a factor of 32 for each doubling of the spatial resolution, since such a doubling in three dimensions increases the number of elements eightfold, and the stability conditions require the time increment to be reduced to one fourth of its original size.

In summary, a methane emission prediction model should be trustworthy, efficient, simple to apply, cater for a wide variety of circumstances and accommodate input ranging from the minutely detailed to the bare essentials. The output it generates should be readily comprehensible and worthwhile from a practical perspective

D. A QUALITATIVE PORTRAYAL OF THE MODEL

1. GAS ORIGIN AND RETENTION

The more or less ubiquitous presence of methane and hydrogen in coal structures is believed to originate during the initial stages of coalification, from the decay of vegetable matter in the absence of oxygen[1], which is consumed mostly in the formation of oxides of carbon. Tiny gas bubbles adhering to solid matter in colloidal suspension produce a porous microstructure upon gelling. Subsequent drying and deposition of mineral detritus over the forming coalbed results in strain-induced fracturing and cleating of the macrostructure, giving fully formed coal its dual porosity nature. The micropore network is comprised of roughly spherical, occasionally interconnected cavities up to about 400 ångstroms in diameter with an average around 40 ångstroms for South African coals[1], and provides a large internal surface area, typically between 40 and 200m^2 per gram of coal. The macropore network consists of randomly oriented[a] planar discontinuities at moderately regular intervals.

The chemical affinity between carbonaceous material and molecules with protruding hydrogen atoms accounts for adsorption of methane (also water, hydrogen and other hydrocarbons) on free coal surfaces. This effect, coupled with the large micropore surface area, allows coal to retain a large amount of gas, and its capacity in this respect is augmented by pressurised free gas storage in voids. It has been estimated[4] that up to 90% of the total seam gas content is retained by adsorption and the remainder as free gas. Coal structures have remained relatively undisturbed over a long period of time, so that it is reasonable to assume that the amount of adsorbed gas, which depends on the (partial) free gas pressure as quantified by the Langmuir relationship, is in equilibrium with the free gas and remains so until some disturbance upsets this balance.

2. FLOW MECHANISMS

Mining or drilling of the seam disturbs this equilibrium by allowing free gas to escape, creating regions of low pressure and thus altering the in-seam pressure distribution profile. This causes gas molecules

---

[a] Although cleats by definition are not randomly oriented, the presence of many fractures gives the totality of discontinuities this appearance.

to desorb from exposed surfaces within these zones of diminished pressure and to appear as free gas, which in turn changes the adsorbed gas concentration. The macropore network provides the conduits in which free gas migrates under the influence of pressure gradients, and this phenomenon is (within limits) described by the Darcy permeable flow relationship. Changes in the concentration of adsorbed gas on surfaces adjoining or delimiting the macropore structure introduce non-zero concentration gradients within the micropore system. These concentration gradients, in accordance with Fick's first law, drive gas molecules from areas of higher to areas of lower concentration -ie. the internally adsorbed gas diffuses in the micropore network, prevalently migrating towards surfaces where the free gas pressure is at a relative minimum.

It is evident from the preceding discussion that in-seam gas transport occurs as long as there exist either pressure or concentration differences, or both, and that gas will be emitted from any exposed coal surface as long as these conditions hold

3. STRUCTURE IDEALISATION

The planar nature of cleating and fracturing effectively divides the coal into small elemental segments of fairly regular proportions. The interior of each of these segments is exclusively a micropore structure and gas transport therein is purely diffusive. Individual segments are completely bounded by the planar discontinuities of varying gap widths that comprise the macropore system, wherein gas transport is purely Darcy permeable The entire mechanism described thus far may be viewed as a matrix of coal particles separated by interstitial voids in which the particles are the source of gas and the voids allow its displacement. Structurally, the coal may be idealised as shown in Figure 1 Geometrically, the random orientation and more or less regular spacing of cleats and fractures means that a straight line of given length will intersect, on average, equal numbers of discontinuities, irrespective of its direction, and that the coal particles are all of similar size The idealised structure has corresponding properties

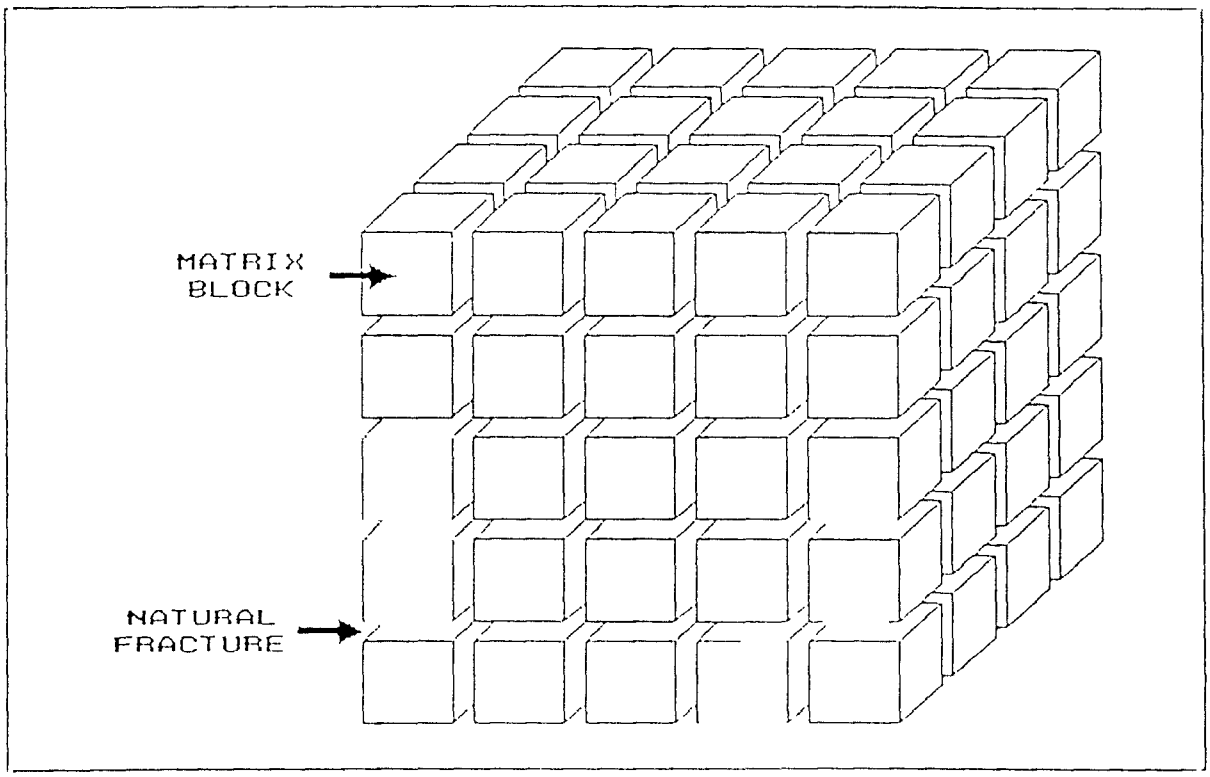

Figure 1: Idealised coal/rock structure

Some evidence suggesting that methane migrates in non coal sediments has been presented earlier (page 3) The direct method of total gas content determination[3] was applied to a 2m long core sample of fine-grained sandstone extracted from directly above a coal seam via a surface borehole at Middelbult

Colliery. Unsurprisingly, the total content was significantly lower than that of an equal mass of coal, but the average emission rate was notably higher. A coal sample of similar proportions emits gradually decreasing quantities of gas over several months, whereas the sandstone was depleted of gas after three days. This indicates that gas in sandstone is predominantly stored as free gas in voids and migrates within a permeable flow regime[a]. Other non-carbonaceous rock types are likely to behave in much the same way. The granular matrix structure of these may also be idealised as shown in Figure 1, but with one essential difference: the particles do not make any gas contribution.

4. STRUCTURE GEOMETRY AND DIMENSIONS

The geometrical arrangement of the idealised structure for the purpose of modelling is thus a matrix of regularly spaced, similarly oriented rectangular prisms of equal size. Physically, it is assumed that diffusion occurs only within these prisms, sorption on their outer surfaces and gaseous flow within the interstices. The model assumes that sorptive processes are sufficiently rapid that at any given instant the adsorbed gas on the outer surface of a prism is in equilibrium with the surrounding gas pressure No quantitative relationship describing the time-dependence of sorption has been found, but it is known not to change instantaneously

The choice of physical dimensions for this pattern is critical to the representativeness of the model, and presents a difficulty in that no guidelines are available. It has been noted[14] that sorption rates of crushed coal samples are apparently independent of average particle sizes in the range from about 20mm to about 3mm. Smaller particles display a dramatic increase in their sorption rate, while that of larger particles gradually decreases The size at which the increased rate begins to appear is termed the 'Fracture Network Size', or FNS. One possible explanation for this effect is that particles larger than the FNS are effectively composed of blocks of this size and provided that the particles are not too large, free gas diffused from the blocks can flow relatively unhindered through the cleats and fractures The larger the particles, the more of these blocks they contain, which increases the distance that free gas migrates over and retards the rate at which gas desorbs and diffuses from the blocks Conversely, particles smaller than the FNS have a greater total free surface area for sorptive phenomena, a reduced average diffusing distance and uninhibited free gas flow, so that release rates are substantially faster.

From the preceding discussion, it is reasonable to deduce that the basic coal particle size is in the order of the FNS, and that this is a suitable starting point for the prism size Selecting a suitable void size presents even greater difficulties since the width of fractures and cleats ranges from a few ångstroms to several millimetres. The presence of these discontinuities accounts for the permeable nature of coal

5. PERMEABILITY

Analytically, it has been shown[13] that the permeability of a material is proportional to its porosity (the ratio of voids volume to total volume) and the square of the average pore size, but the constant of proportionality is indeterminate without knowledge of the permeability Nevertheless, it is clear that the two main factors affecting permeability are (1) the total cross-sectional void area per unit cross-sectional area of the material across which a fluid can migrate and (2) the total internal area per unit volume with which the fluid is in direct contact The precise relationship between these quantities will be derived in the section to follow. It should also be noted that, given the coal permeability, void size need not be determined for the purposes of calculating flow quantities

Intrinsic material permeability displays a fluid pressure dependence attributed to fluid slippage along the internal surfaces of the material, termed the 'Klinkenberg Effect [2]' At low mean fluid pressure, the material shows a higher apparent permeability In the case of coal, much work has been done[4] to investigate the Klinkenberg permeability correction and the data shows a wide range of different slippage factors for different coals In some instances, physically impossible states in the form of negative liquid permeabilities were indicated (ie at theoretically infinite gas pressure) The usefulness of this correction,

---

[3] If sorptive and/or diffusive processes do in fact occur they may be ignored since they are either very rapid or sparse, or both

though it is included in the model as an option, is therefore questionable, and can easiliy be omitted by setting the relevant constants to zero.

A further well-recognised influence on permeability is the state of stress of the region. It is evident that a region that is compressed in all three principal directions will suffer reduced permeability as a result of the reduced width of cleats and fractures. Conversely, at a free coal face, the vertical stress and the horizontal stress in the plane of the face will cause the face to bulge outwards, widening discontinuities and thus increasing the permeability An empirical relationship for South African conditions has been derived[15], relating the depth of the fractured zone in coal pillars to the seam height and depth. The model assumes that the vertical stress increases uniformly in these fractured zones from zero at the face to the peak abutment stress (determined by a suitable empirical relationship) at the limit of fracturing, whence it decays exponentially to the virgin vertical stress. The permeability is corrected on the basis of the strains induced perpendicularly on the cleats and fractures and the relationship between void size and permeability.

The Darcy relationship is strictly speaking valid only in a laminar flow regime The angular nature of the basic coal structure causes local turbulences at edges and corners, which tends to decrease the gas flow rate. A correction for this laminar-inertial turbulence is made, although the quantitative relationship indicates that this effect may be negligible for the generally low *in situ* coal permeabilities observed locally.

Water in the coal structure has a two-fold influence on gas migration. On the one hand, water tends to reduce the permeability of the structure by collecting in voids, but on the other hand, methane solubility in water is directly proportional to the gas pressure at a given temperature, and if water migrates through the structure, it carries dissolved gas with it, which is released upon a pressure decrease. Few South African collieries have a major problem with ingress water, so that the latter transport mechanism is neglected in the current model Also, coal seam permeabilities are measured *in situ* and this takes the water blockage effect on permeability into account

6. GAS BEHAVIOUR

Methane molecules are comparatively small, non-polar and generally not subject to pressure and/or temperature extremes or abrupt changes in these within the scope of the model, and its gaseous phase behaviour may therefore be closely approximated by the ideal gas law Provision is made in the model for describing the gas as a real one, but this requires knowledge of a quantity referred to as the 'supercompressibility fraction', the precise meaning and value of which is not made clear in the reviewed literature For an ideal gas the value of this quantity is unity Presently, the gas flow is taken to be isothermal, since any in-seam temperature variations are envisioned to be very small The model does, however, provide for temperature dependent gas viscosity and density, which may be of value if the structure contains relatively recent geological intrusions and is consequently not in thermal equilibrium

Cyclical atmospheric pressure variations are not currently taken into account, but can be readily included Atmospheric pressure is assumed to be a fixed quantity, and a sensitivity analysis for this parameter will be made when the model has been computerised If it is found that barometric pressure significantly affects release, rates as suggested by some authors, the program will be modified to accommodate this effect

7. MINING ACTIVITY

Dynamic mining activity will be catered for on the assumption that broken coal releases only the free gas it contains This is justified in terms of the relatively short residence time of broken coal in mined areas, during which time only minor amounts of gas are released by diffusion, since the latter process is very slow The adsorbed gas on exposed surfaces will also be released, but this is to an extent compensated for by the fact that broken coal does not in fact release its entire free gas content, as the fragments are considerably larger on average than the FNS The same assumption is made in the case of initial goafing, but subsequent gas release in goafs is then treated as a purely diffusive phenomenon -

ie. gas released from the micropore network appears immediately as free gas at atmospheric pressure in goafs. Non-carbonaceous material broken during mining or goafing will release only the free gas it contains.

8. BOUNDARY AND INITIAL CONDITIONS

Mined areas are small compared to the overall extent of the coal structure. It would be difficult, if not completely unrealistic, to attempt modelling the entire structure. The area of interest is a bounded region within the structure and in order to model such a region, conditions at its boundaries must be specified. Free faces, as described earlier, are assumed to be at atmospheric pressure, and include the roof and floor. The conditions at boundaries internal to rock or coal are generally unknown, but three ideal states are identified. The boundary may be either impermeable, at a constant free gas pressure or maintain a constant pressure gradient. The first of these states implicitly assumes no gas transport across such a boundary, which is inaccurate, especially for small regions. The second assumes that gas is replenished at the same rate as it moves away, and is also inaccurate for small regions The third will result in a variable flux across the boundary without regard for the effect this has on the areas beyond the boundary, and is deemed the most accurate, provided the modelled time interval is not excessively long.

Finally, a set of initial conditions must be specified before processing can commence. These conditions define the overall state of the modelled region at a certain reference time, taken to be time zero, from which modelling proceeds in a series of time steps The initial state of the region is described *inter alia* by its geometry and dimensions, distribution profiles of gas pressures, permeabilities, diffusion coefficients, Langmuir constants, temperatures, coal densities and rock types Gas migration treatment in the model conforms to the law of mass conservation in order to eliminate the additional processing of gas densities required by a volumetric balance, which some existing simulators use

E. MATHEMATICAL MODEL DERIVATION

1. DIFFUSION

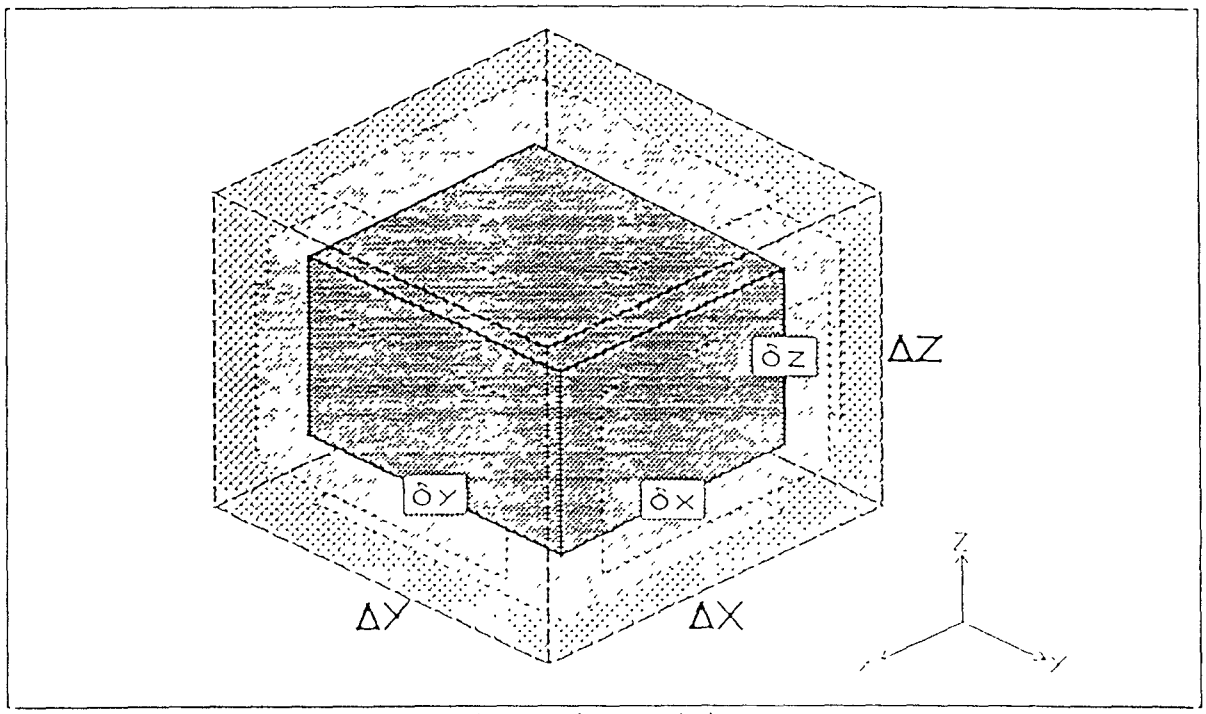

Figure 2: Idealised coal/rock element showing the particle in its surrounding void space

From the preceding outline of the idealised coal structure, it is evident that each matrix block (henceforth referred to as an '**element**') is similar in composition, geometry and dimension. The composition of the elements is assumed to be a homogeneous rectangular prism (henceforth referred to as '**particle**') of coal centrally located in a larger rectangular prism-shaped void (henceforth referred to as '**void space**'). This arrangement is illustrated in Figure 2.

Individual particle homogeneity can be rationalised on the basis of its size. The smaller the particle, the more closely it approaches homogeneity in structure and physical properties. Since the particles are assumed to be in the order of the FNS they are very small, even when compared to a single coal pillar. By way of illustration, a cube of coal with a side length of one metre contains roughly 37 million elements if the FNS is around 3mm. Although an individual particle is assumed to be homogeneous, this does not imply that a collection of them necessarily share the same physical properties.

The behaviour of gas in the particle has been described elsewhere (pages 5, 6 and 8). Bearing this and the idealised coal structure in mind, it is clear that diffusive processes are always subject to similar constraints These constraints are a uniformly distributed initial concentration and an outer surface concentration quantifiable in terms of the surrounding pressure The basic equation describing general state diffusion without sources or sinks is

$$\frac{\partial C}{\partial t} = \nabla(D \cdot \nabla C) \qquad [1.a]$$

where C is the concentration of the diffusing substance in the medium,
t represents time;
D is the (location, concentration, temperature etc dependent) diffusion coefficient, and

$\nabla \equiv \frac{\partial}{\partial x} + \frac{\partial}{\partial y} + \frac{\partial}{\partial z}$ is the scalar *del* operator.

The assumed particle homogeneity also encompasses its physical properties, so that the diffusion coefficient does not vary significantly in the particle, and may hence be treated as a constant In this case, equation [1.a] reduces to

$$\frac{\partial C}{\partial t} = D \nabla^2 C \qquad [1.b]$$

The relative complexity of the above equation disallows a useful analytical and exact solution that satisfies the required initial and boundary conditions Consequently, a numerical technique is required Unfortunately, numerical techniques are time consuming, especially when accuracy is a prime concern, as a result of the stability conditions requiring very small time steps In the proposed model this would be a major inconvenience since solutions must be generated for an enormous number of particles One possible technique which would substantially reduce the computational effort would be to approximate the diffusive gas liberation to within acceptable limits of error

This be achieved by generating solutions to the diffusion problem alone and investigating their behaviour in terms of the governing parameters Suitable regression equations can then be fitted to the results To simplify this process, one additional assumption is made and a series of transformations are applied to the diffusion equation Since permeability is purely a macropore property, the particle in an element can be assumed to be a cube, and the directional dependence of permeability catered for by allowing the width of the void space at various faces of the cube to vary Referring to Figure 2, this means

$$\delta x = \delta y = \delta z = 2\lambda$$

$$\Delta x \neq \Delta y \neq \Delta z$$

where $\lambda > 0$ is half the side length of the cube

The introduction of an orthonormal xyz co-ordinate system, as shown in Figure 3 with its origin at the geometric centre of the cube, oriented so that each cube face is parallel to one of the co-ordinate planes, allows the problem to be reduced to one space dimension This follows from the realisation that gas migration is symmetric with respect to the axes of the coordinate system -ie only one axis, that of

x, need be considered. In addition, the symmetry divides the cube into six equal right pyramids which all behave in the same manner, so that only one of these need be analysed. Diffusion is unidirectional in such a pyramid, from its apex (point O in Figure 3) to its base ($\square$ $ABCD$) and perpendicular to it. For the one-dimensional case, equation [1.b] reduces to

$$\frac{\partial C}{\partial t} = D \cdot \frac{\partial^2 C}{\partial x^2} \qquad \cdots [1.c]$$

There are four parameters that influence the required solution, namely, (1) the cube size λ ; (2) the initial concentration C_0 in the cube; (3) the instantaneous surface concentration C_S on the cube faces and (4) the diffusion coefficient D . The cube size and the diffusion coefficient can be removed as parameters by transforming the actual space and time dimensions. Removing the initial concentration and the surface concentration will be done by transforming the concentration itself, although this will introduce a slight inaccuracy.

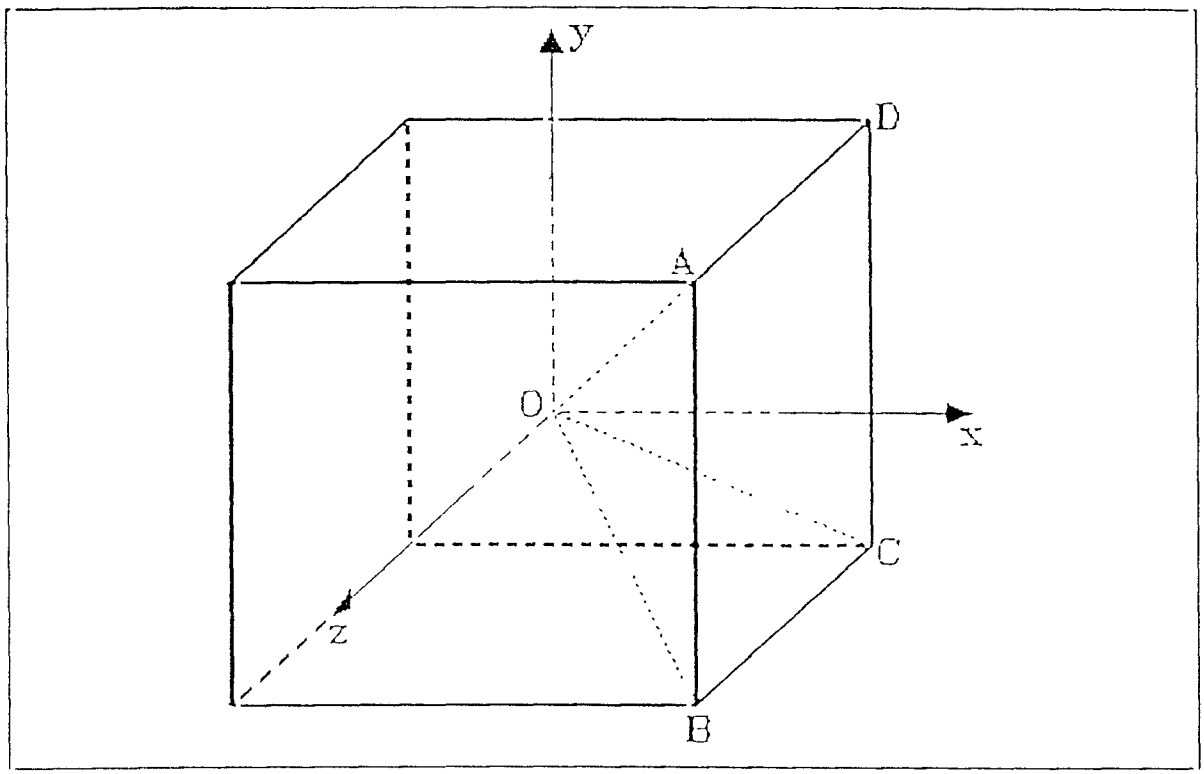

Figure 3: Geometry of a cubic coal particle

Since $-\lambda \leq x \leq \lambda$, normalising x by letting $x = \lambda \xi$, ensures that $-1 \leq \xi \leq 1$ Furthermore, if $\lambda^2 \tau = Dt$, where $\tau \geq 0$, equation [1 c] becomes

$$\frac{\partial C}{\partial \tau} = \frac{\partial^2 C}{\partial \xi^2} \qquad \cdots [1.d]$$

Diffusion coefficients measured thus far[3] are in the range from 10^{-13} to 10^{-7} $m^2 s^{-1}$, which makes diffusion a relatively slow process This indicates that the diffusion rate is not severely affected by small changes in the surface concentration of the cube The complete model progresses by relatively short time steps, during each of which the surface concentration may be considered to remain constant, and successive changes in this parameter will be small This warrants approximating C_S by a constant value, and permits a further simplifying transformation

If $C = C(\xi, \tau)$ is a solution to equation [1 d], then

$$C^* = a_0 + a_1 C(\xi, \tau)$$

is also a solution if a_0 and a_1 are constants and letting

$$C = C_S + (C_0 - C_S)\,C^* \quad \rightarrow \quad C^* = \frac{C - C_S}{C_0 - C_S}$$

eliminates both the surface and initial concentrations as parameters by normalising the initial and boundary conditions, since $0 \le C^* \le 1$. This last condition is guaranteed if gas diffuses only from the cube, and not into it. The nature of the problem renders the required dramatic increase in surface concentration for this to occur highly improbable, so that $C_S \le C \le C_0$ and $C_S < C_0$ for $t > 0$. Thus, the problem has been reduced to solving

$$\frac{\partial C^*}{\partial \tau} = \frac{\partial^2 C^*}{\partial \xi^2} \qquad [1.e]$$

subject to the initial and boundary conditions

$$-1 \le \xi \le 1, \qquad \tau \ge 0$$
$$C^*(\xi,0) = 1 \qquad C^*(-1,\tau) = C^*(1,\tau) = 0$$

For the purpose of the model, the internal concentration distribution of the cube is of no great importance. The only pertinent information required is the total gas content of the cube as a function of time. Since the model will be based on a mass balance, the unit of measure of concentration will be taken as mass of gas per mass of coal -ie. the unit is dimensionless. Mathematically, the total mass of gas in the cube is given by

$$Q = \int_M C\,dm = 3\int_{-\lambda}^{\lambda} C\,\rho_c 4x^2\,\partial x = 24\,\rho_c \lambda^3 \int_0^1 (C_S + (C_0 - C_S)\,C^*)\,\xi^2\,\partial\xi$$

$$= 24\,\rho_c \lambda^3 \left(\frac{C_S}{3} + (C_0 - C_S)\int_0^1 C^*\,\xi^2\,\partial\xi \right) \qquad [1.f]$$

where ρ_c is the (constant) coal particle density, and
dm is a differential of the cube mass

The numerical solution to equation [1.e] proceeds from dividing the pyramid into N slabs of equal width parallel to the base, which are numbered from 1 at the apex to N at the base. Index i refers to the i^{th} slab, while index j refers to the j^{th} time step. The slab width is $\Delta\xi = \frac{1}{N}$ and the time step is $\Delta\tau$. Stability conditions require $0 < \Delta\tau \le \frac{1}{2}(\Delta\xi)^2$, and the numerical solution converges particularly rapidly if $6\,\Delta\tau = (\Delta\xi)^2$ [15]; hence, the time step will be taken as $\Delta\tau = \frac{1}{6N^2}$. The following set of difference equations generates the required solution

$$C^*_{i,0} = 1, \qquad 1 \le i \le N-1$$

$$C^*_{N,j} = 0$$

$$C^*_{i,j+1} = C^*_{i,j} + \frac{1}{12}\left[\left(1 + \left(\frac{2i-1}{2i-3}\right)^2\right)(C^*_{i-1,j} - C^*_{i,j}) - \left(1 + \left(\frac{2i-3}{2i-1}\right)^2\right)(C^*_{i,j} - C^*_{i-1,j})\right]$$

$$2 \le i \le N-1$$

$$C^*_{1,j+1} = \frac{1}{6}(C^*_{1,j} + 5C^*_{2,j})$$

and

$$Q_j = \frac{1}{(2N-1)(2N-3)(N-1)} \sum_{i=1}^{N-1} (2i-1)^2\,C^*_{i,j} \approx \int_0^1 C^*\,\xi^2\,\partial\xi$$

where Q_j gives the amount of gas in the cube at $\tau = j\Delta\tau = j/6N^2$

A Turbo Pascal program (see Appendix A) has been written which generates values of Q for selected values of τ and N. Table 1 reflects the results obtained from this simulation. The program execution time is closely proportional to the cube of the number of slices. Figures 4 and 5 show graphs of the results obtained (Note the log scaling of the quantity axis in Figure 5)

τ	Q					
	N = 25	N = 50	N = 100	N = 200	N = 400	N = 1000
0	0.33333333	0.33333333	0.33333333	0.33333333	0.33333333	0.33333333
0.00026667	0.32506224	0.32045316	0.31707437	0.31528272	0.31437758	0.31383245
0.00053333	0.31823005	0.31235923	0.30892229	0.30717722	0.30630263	0.30577752
0.0008	0.31239674	0.30611809	0.30273114	0.30103060	0.30018084	0.29967132
0.00106667	0.30728464	0.30088473	0.29755959	0.29589883	0.29507029	0.29457387
0.00133333	0.30271258	0.29630425	0.29304072	0.29141582	0.29060603	0.29012108
0.0016	0.29855831	0.29219039	0.28898589	0.28739374	0.28660087	0.28612622
0.00186667	0.29473661	0.28843135	0.28528290	0.28372097	0.28294360	0.28247835
0.00213333	0.29118624	0.28495387	0.28185856	0.28032479	0.27956176	0.27910521
0.0024	0.28786192	0.28170685	0.27866202	0.27715465	0.27640503	0.27595657
0.00266667	0.28472931	0.27865299	0.27565623	0.27417376	0.27343675	0.27299590
0.0032	0.27893808	0.27301818	0.27011123	0.26867483	0.26796105	0.26753421
0.00373333	0.27365745	0.26788876	0.26506445	0.26367005	0.26297739	0.26256325
0.00426667	0.26878397	0.26315980	0.26041218	0.25905652	0.25838328	0.25798080
0.0048	0.26424479	0.25875834	0.25608239	0.25476274	0 25410753	0.25371587
0.00533333	0.25998640	0.25463119	0.25202257	0.25073666	0.25009830	0.24971675
0.00613333	0.25403893	0.24886941	0.24635491	0 24511597	0 24450107	0.24413358
0.00693333	0.24853171	0.24353590	0.24110852	0 23991293	0.23931964	0.23896509
0.00773333	0.24339106	0.23855843	0.23621226	0.23505698	0.23448376	0.23414123
0.00906667	0.23549385	0.23091299	0.22869121	0 22759755	0.22705498	0.22673078
0.0104	0.22828149	0.22393102	0.22182233	0.22078456	0.22026977	0.21996219
0 012	0.22035363	0.21625619	0 21427109	0 21329430	0.21280978	0.21252031
0.01466667	0.20852512	0.20480353	0.20300114	0 20211432	0 20167445	0.20141165
0.01866667	0.19319862	0.18995870	0.18838936	0 18761711	0 18723405	0.18700518
0 02266667	0.17998432	0.17715283	0.17578042	0.17510486	0 17476970	0 17456944
0.02666667	0.16834207	0.16586373	0.16466123	0 16406901	0.16377513	0.16359952
0.032	0.15468818	0.15261444	0.15160628	0 15110933	0 15086262	0.15071515
0 03733333	0.14269937	0 14097098	0.14012846	0 13971266	0.13950612	0 13938263
0.04266667	0.13202872	0.13059871	0 12989918	0 12955339	0 12938150	0.12927868
0.048	0.12243506	0.12126514	0.12069015	0 12040533	0 12026360	0 12017878
0.05333333	0 11374275	0 11280096	0.11233517	0 11210378	0.11198849	0.11191944
0 06133333	0.10211250	0.10146320	0.10113738	0 10097449	0 10089309	0.10084426
0 06933333	0 09188690	0 09148077	0 09127139	0 09116548	0 09111226	0 09108024
0 07733333	0 08282760	0 08262397	0 08251167	0 08245329	0.08242358	0 08240560
0.08533333	0.07475625	0.07472097	0 07468954	0 07467078	0 07466069	0.07465441
0 09333333	0 06753489	0 06763887	0.06767455	0 06768871	0 06769493	0 06769838
0 10666667	0 05709920	0 05738163	0 05750375	0 05756043	0.05758772	0.05760376
0.12	0.04833394	0 04874054	0 04892342	0 04901012	0 04905232	0 04907729
0.13333333	0.04094417	0 04143255	0 04165610	0 04176303	0 04181532	0 04184633
0 14666667	0 03469971	0 03523700	0 03548559	0 03560513	0.03566374	0.03569854
0.16	0.02941562	0 02997667	0 03023825	0 03036451	0 03042653	0.03046340
0 18666667	0.02114807	0 02170490	0.02196743	0 02209484	0 02215760	0 02219495
0 24	0 01093772	0 01138695	0 01160219	0 01170747	0 01175952	0 01179056
0.32	0.00406946	0 00432838	0 00445486	0 00451730	0.00454830	
0 4	0.00151412	0.00164535	0.00171059	0.00174306	0 00175925	
0.53333333	0.00029143	0 00032821	0 00034700	0.00035648	0.00036124	
0 66666667	0.00005609	0 00006547	0 00007039	0 00007291	0.00007418	
0.8	0.00001080	0.00001306	0.00001428	0 00001491	0 00001523	
0 93333333	0.00000208	0 00000261	0.00000290	0 00000305	0 00000313	
1.13333333	0.00000018	0 00000023	0 00000026	0 00000028	0 00000029	
1 33333333	0.00000001	0.00000002	0 00000002	0 00000003	0 00000003	
1 6	0.00000000	0 00000000	0.00000000	0 00000000	0 00000000	
Execution time (H.M.S) 486 DX33	0.00.40	0 05 11	0 41 56	5 36 51	44 58 00	extrapolated 702 51 00

Table 1: Results of the numerical diffusion simulation

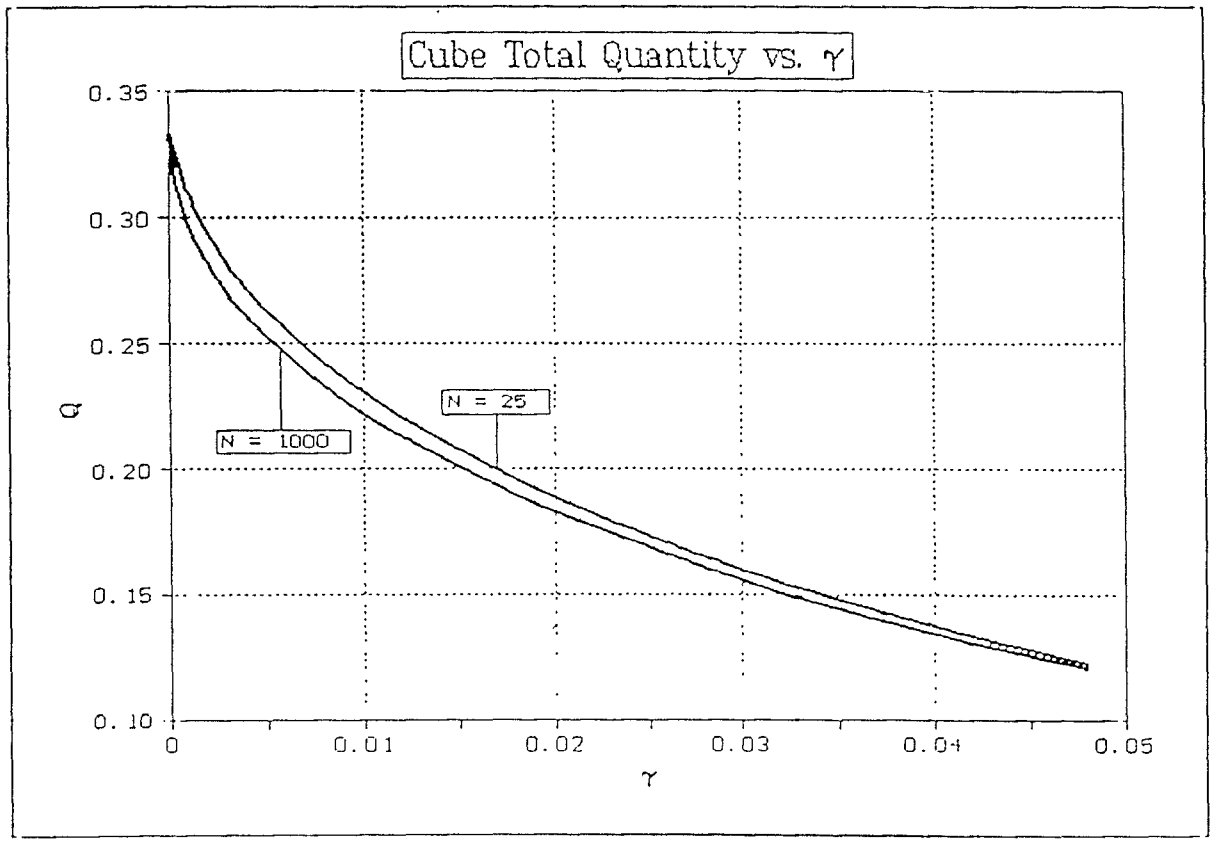

Figure 4: Graph showing the behaviour of Q against γ

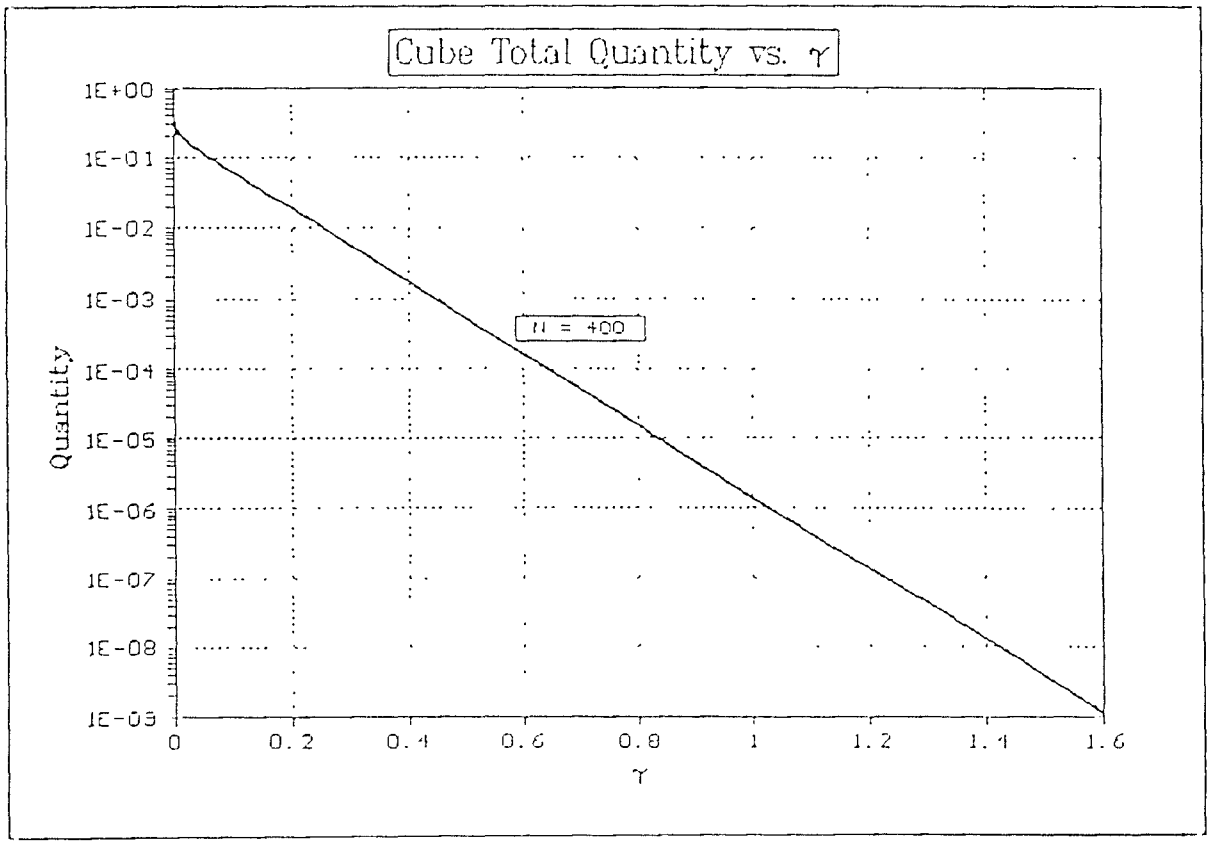

Figure 5: Graph of Q against γ for $N = 400$

The following regression equation was fitted to the data points of $N = 1000$:

$$Q = \frac{1}{3}\exp\left[a_0\tau + a_1\left((1+a_2\tau)^{\alpha} - \frac{a_3}{a_3+(a_4\tau)^{\beta}}\right)^{\frac{1}{\alpha}}\right]$$

$a_0 = 7,263\,945\,44$

$a_1 = -0,512\,791\,213$

$a_2 = 37,168\,346\,3$

$a_3 = 0,691\,627\,618$

$a_4 = 15,830\,837\,2$

$\alpha = 1,875\,653\,24$

$\beta = 1,592\,975\,22$

The regression coefficient for the fitted curve is $r^2 = 0,999\,999\,830\,613$ over 43 data points from $\tau = 0$ to $\tau = 0,24$, with the largest relative error (overestimate by 890ppm) occurring at $\tau = 0,24$.

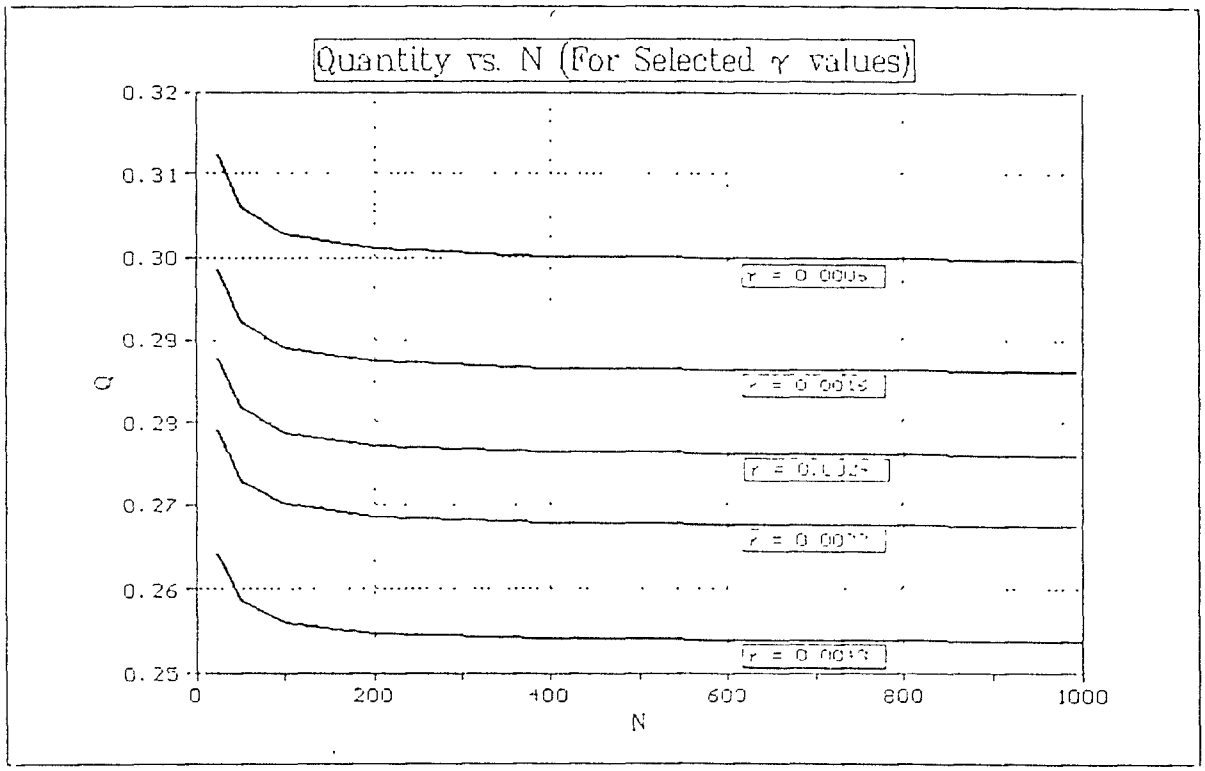

Figure 6: Relationship between Q and N

The relationship between Q and N shows that Q approaches a fixed value asymptotically with increasing N. Figure 6 illustrates this for certain values of τ. Numerical analyses were done on some of these data sets and the best fit asymptotic values were found to agree closely with the values of the regression equation.

A plot of the absolute errors of the regression equation is shown in Figure 7. The same basic regression equation was fitted to the data points of $N = 400$. The values of the constants obtained did not change significantly and the regression coefficient differed in the seventh decimal place, this being slightly less. The graphs for different values of N were plotted on the same set of axes, but the resolution is not fine enough to distinguish them individually over the complete range of τ values. The same shape and trend (Figure 5) was observed in all of these graphs.

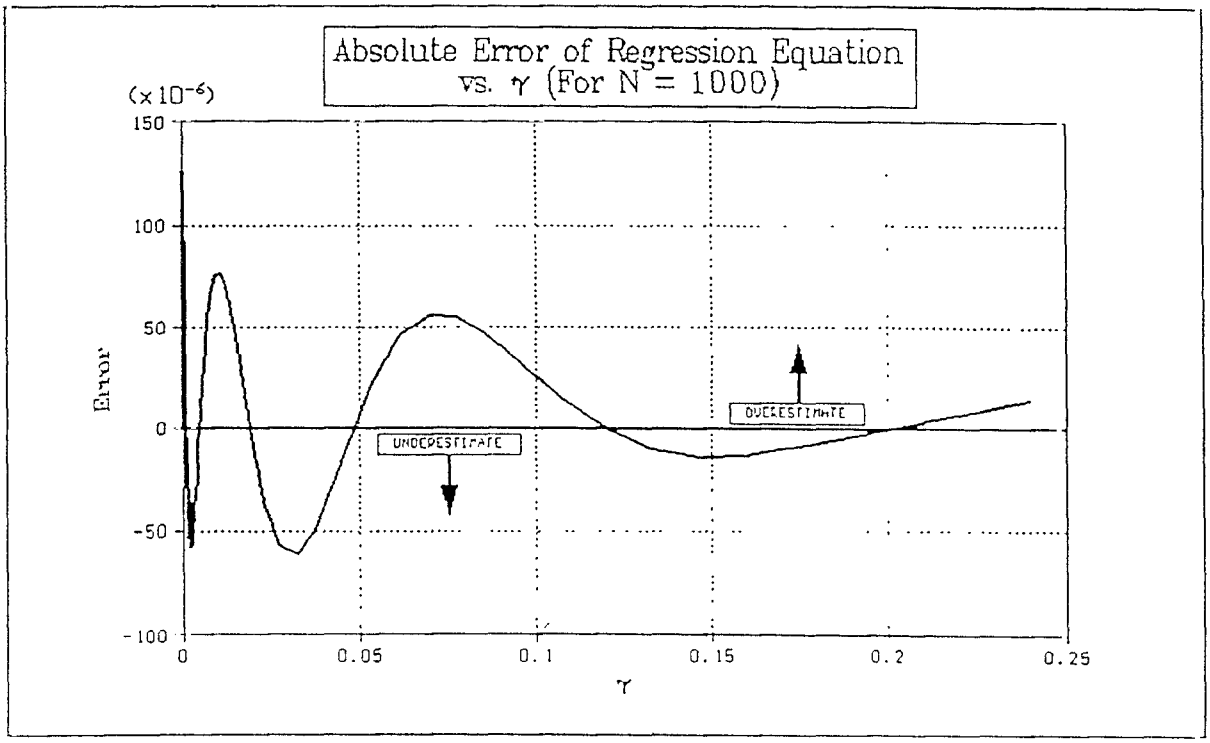

Figure 7: Absolute errors of the diffusion regression equation

Combining the regression equation with equation [1.f] and the relationship between t and τ yields the final diffusion equation that relates the mass of gas as a function of actual time:

$$Q = 8\rho_c\lambda^3\left(C_S + (C_0 - C_S)e^{T}\right)$$

$$T = a_0\tau + a_1\left((1 + a_2\tau)^{\alpha} - \frac{a_3}{a_3 + (a_4\tau)^{\beta}}\right)^{\frac{1}{\alpha}}$$

$a_0 = 7,263\,945\,44$ $\quad a_1 = -0,512\,791\,213$ $\quad a_2 = 37,168\,346\,3$

$a_3 = 0,691\,627\,618$ $\quad a_4 = 15,830\,837\,2$ $\quad \alpha = 1,875\,653\,24$

$\beta = 1,592\,975\,22$

$$\tau = \frac{D}{\lambda^2}t$$

Equation [A]

It should be noted that this equation satisfies the requirements for $t = 0$ and $t \to \infty$ -ie.

$$Q_{t=0} = 8\rho_c\lambda^3 C_0$$

and

$$Q_{t\to\infty} = 8\rho_c\lambda^3 C_S$$

2. SORPTION AND GASEOUS BEHAVIOUR

The surface concentration C_S and the initial concentration C_0 of the particle must now be quantified in terms of the gas pressure surrounding it. A number of relationships whereby this may be done have been proposed. The one used most frequently is the Langmuir isotherm, which relates the total adsorbed

gas volume (at standard temperature and pressure) to the gas pressure. Formally,

$$V_{eq} = m_c \left(\frac{k_1 k_2 p}{1 + k_2 p} \right)$$

where V_{eq} is the equivalent adsorbed gas volume (at STP);
m_c is the coal mass;
k_1, k_2 are the Langmuir constants for the coal, and
p is the actual gas pressure (absolute).

In the above form, however, this equation is of little use, since the model is to be based on a mass balance. Commonly, volumes and corresponding masses are related to each other via density, but in the case under consideration the density is both variable and unknown. This problem is overcome by a slight manipulation of the real gas law

$$pV = \kappa n R T$$

where κ is the gas supercompressibility fraction,
n is the number of moles of the gas;
R is the universal gas constant, and
T is the gas temperature

The actual mass of a volume V of gas under an absolute pressure p is $m = n M_G$, where M_G is the gas molecular mass. Combining these equations and rearranging for explicit gas mass,

$$\frac{m}{m_c} = \left(\frac{p_{STD} M_G}{\kappa R T_{STD}} \right) \left(\frac{k_1 k_2 p}{1 + k_2 p} \right)$$

where p_{STD} is standard pressure, and
T_{STD} is standard temperature

The term on the left hand side of the last equation is a concentration (gas mass per coal mass) as used in the preceding section on diffusion. On the assumption that sorption rates are sufficiently rapid on the outer surfaces of the particle (see page 7), the right hand side of the equation quantifies the surface concentration in terms of the void space gas pressure. Furthermore, this equation can be used to quantify the initial particle concentration in terms of the virgin seam gas pressure p_- (see page 5). Thus,

$$C_S = \left(\frac{p_{STD} M_G}{\kappa R T_{STD}} \right) \left(\frac{k_1 k_2 p}{1 + k_2 p} \right)$$

$$C_0 = \left(\frac{p_{STD} M_G}{\kappa R T_{STD}} \right) \left(\frac{k_1 k_2 p_-}{1 + k_2 p_-} \right)$$

Equations [B]

The actual mass of free gas in an element depends on the gas pressure and the volume of the void space, which is given by the difference between the element volume and the particle volume. Mathematically,

$$m = \left(\frac{M_G (\Delta x \Delta y \Delta z - 8 \lambda^3)}{\kappa R T} \right) p$$

Equation [C]

where Δx, Δy and Δz are the physical dimensions of the element, and
T is the free gas temperature (absolute)

Ideal gas behaviour will be catered for by letting $\kappa = 1$

3. PERMEABILITY

The present section will attempt to relate the element dimensions, specifically those of the void space, to intrinsic permeability. This information will be necessary in order to quantify the amounts of free and adsorbed gas. The fundamental steady state Darcy permeable flow equation for anisotropic permeability is

$$q_s = -\frac{1}{\eta}\left(K_x \frac{\partial p}{\partial x}\bar{i} + K_y \frac{\partial p}{\partial y}\bar{j} + K_z \frac{\partial p}{\partial z}\bar{k}\right)$$

where q_s is the specific discharge -ie. volumetric flow rate per unit cross-sectional area perpendicular to the flow direction;
η is the fluid dynamic viscosity,
K_x, K_y and K_z are the principal material permeabilities in the x, y and z directions;
p is the fluid pressure, and
$\bar{i}$, $\bar{j}$ and $\bar{k}$ are unit vectors in the x, y and z directions

The specific discharge may also be interpreted as the average fluid drift velocity through the medium in the flow direction. For a particular direction ζ within the medium, the Darcy relationship becomes

$$q_\zeta = -\frac{K_\zeta}{\eta}\frac{dp}{d\zeta}$$

This relationship is valid only in a laminar flow regime, which affords an opportunity to equate the permeability to certain geometric properties via the steady state laminar flow law for circular ducts proposed by Poiseuille This law is

$$U = -\frac{1}{4\eta}\frac{dp}{d\zeta}(a^2 - r^2)$$

where U is the fluid velocity along the duct's axis ζ at a distance r from this axis,
a is the radius of the duct, and the other symbols are as before

The total volumetric flow rate for such a duct is obtained by integrating the velocity over the duct area and is given by

$$\dot{V}_\zeta = \int_A U\,dA = \int_0^a -\frac{1}{4\eta}\frac{dp}{d\zeta}(a^2 - r^2)\,2\pi r\,dr = -\frac{\pi}{8\eta}\frac{dp}{d\zeta}a^4$$

It was noted earlier (page 7) that permeability is affected by the cross-sectional area available to flow per unit cross-sectional area of the medium and the internal surface area with which the fluid is in contact per unit volume of the medium For a short cylindrical duct of radius a and length $\Delta\zeta$ through a solid medium of uniform cross-sectional area A_s, the previous relationship can be translated into a more usable form

$$q_\zeta = \frac{\dot{V}_\zeta}{A_s} = -\frac{\pi}{8\eta}\frac{dp}{d\zeta}\frac{a^4}{A_s} = -K_o\frac{1}{\eta}\frac{dp}{d\zeta}\left(\frac{2\pi a\,\Delta\zeta}{A_s\,\Delta\zeta}\right)^{\alpha_0}\left(\frac{\pi a^2}{A_s}\right)^{\alpha_1}$$

$$= -K_o\frac{1}{\eta}\frac{dp}{d\zeta}\left(\frac{A_c}{V_s}\right)^{\alpha_0}\left(\frac{A_f}{A_s}\right)^{\alpha_1}$$

where K_o is a dimensionless constant,
A_c is the internal area with which the fluid is in contact,
V_s is the total volume of the medium,
A_f is the cross-sectional area available to flow, and
α_0 and α_1 are constants

Analysis of the exponents of a and A_s in the above relationship yields

$$\alpha_0 = -2 \qquad \alpha_1 = 3$$
$$K_o = \frac{1}{2}$$

By equating the last relationship with that of Darcy, permeability of a medium with circular ducts can be expressed as

$$K_{\circ} = \frac{1}{2}\left(\frac{A_f}{A_s}\right)^3\left(\frac{V_s}{A_c}\right)^2$$

It can be shown that the specific discharge of a rectangular duct is in the ratio 8.9 with that of a circular duct for the same fluid velocity. Thus, the permeability of a medium with rectangular ducts can be expressed as

$$K_{\square} = \frac{4}{9}\left(\frac{A_f}{A_s}\right)^3\left(\frac{V_s}{A_c}\right)^2$$

From the geometry of the element (see Figure 2) it is evident that the 'ducts' are rectangular, and the following equivalences for the quantities in the above equation in terms of the element dimensions are readily established:

$$A_{fx} = \Delta y\Delta z - 4\lambda^2 \qquad A_{fy} = \Delta x\Delta z - 4\lambda^2 \qquad A_{fz} = \Delta x\Delta y - 4\lambda^2$$

$$A_{sx} = \Delta y\Delta z \qquad A_{sy} = \Delta x\Delta z \qquad A_{sz} = \Delta x\Delta y$$

$$V_s = \Delta x\Delta y\Delta z \qquad A_c = 16\lambda^2$$

Upon substitution of the above into the previous equation, three equations relating the permeabilities in the three principal directions are obtained:

$$K_x = \frac{\Delta x^2\lambda^2}{9\Delta y\Delta z}\left(\frac{\Delta y\Delta z}{4\lambda^2} - 1\right)^3$$

$$K_y = \frac{\Delta y^2\lambda^2}{9\Delta x\Delta z}\left(\frac{\Delta x\Delta z}{4\lambda^2} - 1\right)^3$$

$$K_z = \frac{\Delta z^2\lambda^2}{9\Delta x\Delta y}\left(\frac{\Delta x\Delta y}{4\lambda^2} - 1\right)^3$$

In order to solve the above for Δx, Δy and Δz, the following substitution is useful:

$$\phi_x = \frac{4\lambda^2}{\Delta y\Delta z} \qquad \Delta x = 2\lambda\sqrt{\frac{\phi_x}{\phi_y\phi_z}} \qquad 0 < \phi_x \le 1$$

$$\phi_y = \frac{4\lambda^2}{\Delta x\Delta z} \qquad \Delta y = 2\lambda\sqrt{\frac{\phi_y}{\phi_x\phi_z}} \qquad 0 < \phi_y \le 1$$

$$\phi_z = \frac{4\lambda^2}{\Delta x\Delta y} \qquad \Delta z = 2\lambda\sqrt{\frac{\phi_z}{\phi_x\phi_y}} \qquad 0 < \phi_z \le 1$$

whence

$$K_x = \frac{\lambda^2(1-\phi_x)^3}{9\phi_x\phi_y\phi_z}$$

$$K_y = \frac{\lambda^2(1-\phi_y)^3}{9\phi_x\phi_y\phi_z} \qquad \rightarrow \phi_y = \sqrt[3]{\frac{K_y}{K_x}}\,\phi_x + \left(1 - \sqrt[3]{\frac{K_y}{K_x}}\right)$$

$$K_z = \frac{\lambda^2(1-\phi_z)^3}{9\phi_x\phi_y\phi_z} \qquad \rightarrow \phi_z = \sqrt[3]{\frac{K_z}{K_x}}\,\phi_x + \left(1 - \sqrt[3]{\frac{K_z}{K_x}}\right)$$

By substituting the above expressions of ϕ_y and ϕ_z in terms of ϕ_x into the equation for K_x, a cubic in ϕ_x is obtained which may be solved by Cardano's method (see Appendix B). Back substitution then yields ϕ_y and ϕ_z, and these three values determine Δx, Δy and Δz. For the solution to be physically meaningful, $\Delta x \ge 2\lambda$, $\Delta y \ge 2\lambda$ and $\Delta z \ge 2\lambda$ must be satisfied. In the case of isotropic permeability,

$$\Delta x = \Delta y = \Delta z = 2\lambda\sqrt{1 + \sqrt[3]{\frac{9K}{\lambda^2}}}$$

The above equation may be used to approximate Δx, Δy and Δz in the anisotropic case, provided the principal permeabilities do not differ substantially. Thus,

$$\Delta x \approx 2\lambda \sqrt{1 + \sqrt[3]{\frac{9K_x}{\lambda^2}}} \qquad \Delta y \approx 2\lambda \sqrt{1 + \sqrt[3]{\frac{9K_y}{\lambda^2}}}$$

$$\Delta z \approx 2\lambda \sqrt{1 + \sqrt[3]{\frac{9K_z}{\lambda^2}}} \qquad K_x \approx K_y \approx K_z$$

The *in situ* permeability is affected by the fluid pressure, the presence of liquids (mostly water) and the state of stress in the region. The fluid pressure dependency is known as the 'Klinkenberg Effect' (see page 7) and is given by

$$K_\zeta = K_{\infty\zeta}\left(1 + \frac{b_\zeta}{\overline{p}}\right)$$

where K_ζ is the Klinkenberg corrected permeability,
$K_{\infty\zeta}$ is the permeability at a theoretically infinite fluid pressure;
b_ζ is the Klinkenberg constant, characteristic of both medium and fluid, and
$\overline{p}$ is the mean fluid pressure

The presence of water reduces the permeability of the medium by diminishing the effective duct sizes. It is assumed that any water in the coal is held as a thin uniform film on the outer surfaces of the particle. The moisture content of South African coals rarely exceeds 0 05 (viz 5%) by mass, and water, being a polar molecule with protruding hydrogen atoms, will tend to adhere to free coal surfaces, so that the assumption about the mode of its retention is reasonable All ducts are reduced by the amount $2\delta\lambda$, given by

$$2\delta\lambda = 2\lambda\left(\sqrt[3]{1 + \frac{\mu_w \rho_c}{(1+\mu_w)\rho_w}} - 1\right) \approx \lambda \frac{2\mu_w \rho_c}{3 f_c (1+\mu_w)\rho_w}$$

$$f_c = 1 + \left(0,2681\frac{\rho_c}{\rho_w} + 0,01526\right)\mu_w$$

where μ_w is the moisture content of the coal, and
ρ_w is the density of the water/liquid

The approximation on the right hand side of the above equation is valid where the moisture content is low (less than 20%) and is given as it is computationally simpler than the exact cube root expression.

The stress state of a particular region affects the void sizes via the resultant strains which tend to alter the width of cleats and fractures The derivation to follow assumes that shear stresses and strains are of negligible effect compared to their normal counterparts Free gas in the voids also affects the stress state in that the gas pressure tends to widen the voids Stress and gas pressure together determine the strains in the medium as follows

$$\varepsilon_x = \frac{1}{E}(\sigma_x - \nu\sigma_y - \nu\sigma_z - (1-2\nu)p)$$

$$\varepsilon_y = \frac{1}{E}(\sigma_y - \nu\sigma_x - \nu\sigma_z - (1-2\nu)p)$$

$$\varepsilon_z = \frac{1}{E}(\sigma_z - \nu\sigma_x - \nu\sigma_y - (1-2\nu)p)$$

where ε_x, ε_y and ε_z are the resultant strains in the three directions,
σ_x, σ_y and σ_z are the normal stresses in the three directions,
E is Young's modulus of the material,
ν is Poisson's ratio for the material, and
p is the gas pressure

Compressive stresses in rock engineering are by convention positive and consequently a positive strain

means a shortening of distance. The moisture and stress considerations can be combined since they are quantified in terms of the element geometry. Δx_0, Δy_0, Δz_0 and λ_0 are the element dimensions of a dry, unstressed sample of coal, while Δx, Δy, Δz and λ are the dimensions of an element in a stressed state and with water present.

$$\Delta x = \Delta x_0(1-\varepsilon_x) \qquad \Delta y = \Delta y_0(1-\varepsilon_y) \qquad \Delta z = \Delta z_0(1-\varepsilon_z) \qquad \lambda = \lambda_0 + \delta\lambda$$

The preceding derivations can be succinctly summarized by letting X stand for any one of x, y or z and Υ and Z for the other two in the following set of equations The remaining symbols are as described before.

$$K_X = \frac{\Delta X^2 \lambda^2}{9\,\Delta\Upsilon\,\Delta Z}\left(\frac{\Delta\Upsilon\,\Delta Z}{4\lambda^2} - 1\right)^3$$

$$K_X = K_{\infty X}\left(1 + \frac{b_X}{p}\right)$$

$$\lambda = \lambda_0 \sqrt[3]{1 + \frac{\mu_w \rho_c}{(1+\mu_w)\,\rho_w}}$$

$$\varepsilon_X = \frac{1}{E}(\sigma_X - \nu\sigma_\Upsilon - \nu\sigma_Z - (1-2\nu)p)$$

$$\Delta X = \Delta X_0(1-\varepsilon_X)$$

Equations [D]

4. DARCY PERMEABLE FLOW

The Darcy equation as given in the previous section is, as stated on page 18, valid only in a laminar flow regime In their review of existing simulators, King and Ertekin quote a correction factor for (localised) turbulences in terms of the porous flow Reynold's Number Since Reynold's Number depends on the specific discharge from the medium, the correction requires further analysis. One dimensional Darcy flow is described by

$$q_\zeta = -C_{LIT}\frac{K_\zeta}{\eta}\frac{\partial p}{\partial \zeta}$$

$$C_{LIT} = 1 + \frac{1}{2}\left[\sqrt{1 + 4\,\mathrm{Re}_\zeta} - 1\right]$$

$$\mathrm{Re}_\zeta = \frac{\rho_g \sqrt{K_\zeta}}{\eta} q_\zeta$$

$$\rho_g = \frac{M_G}{\kappa R T} p$$

where C_{LIT} is the correction for laminar-inertial turbulence,
Re_ζ is the porous medium Reynold's Number, and
ρ_g is the gas density

These equations can be combined and rearranged for an explicit expression of the specific discharge

$$q_\zeta = -\frac{K_\zeta}{\eta}\left(1 - \frac{M_G\sqrt{K_\zeta^3}\,p}{\kappa R T \eta^2}\frac{\partial p}{\partial \zeta}\right)\frac{\partial p}{\partial \zeta}$$

Using the same conventions as in *Equations [D]*, the gas mass flow rate is given by

$$\dot{m}_X = \frac{M_G \Delta Y \Delta Z}{\kappa R T} p\, q_X$$

The equations and relationships presented thus far describe the migration of gas between two elements. When considering an element, however, it is clear that gas not only escapes from it to an adjacent element at a lower pressure, but also enters it from an adjacent element at a higher pressure. In addition, gas diffuses from the particle into the void space, increasing the total amount of free gas in the element. Figure 8 shows the geometry and convention for the one-dimensional situation, and the extension into three dimensions is a simple matter of adding similar terms for the remaining two directions due to the symmetries involved.

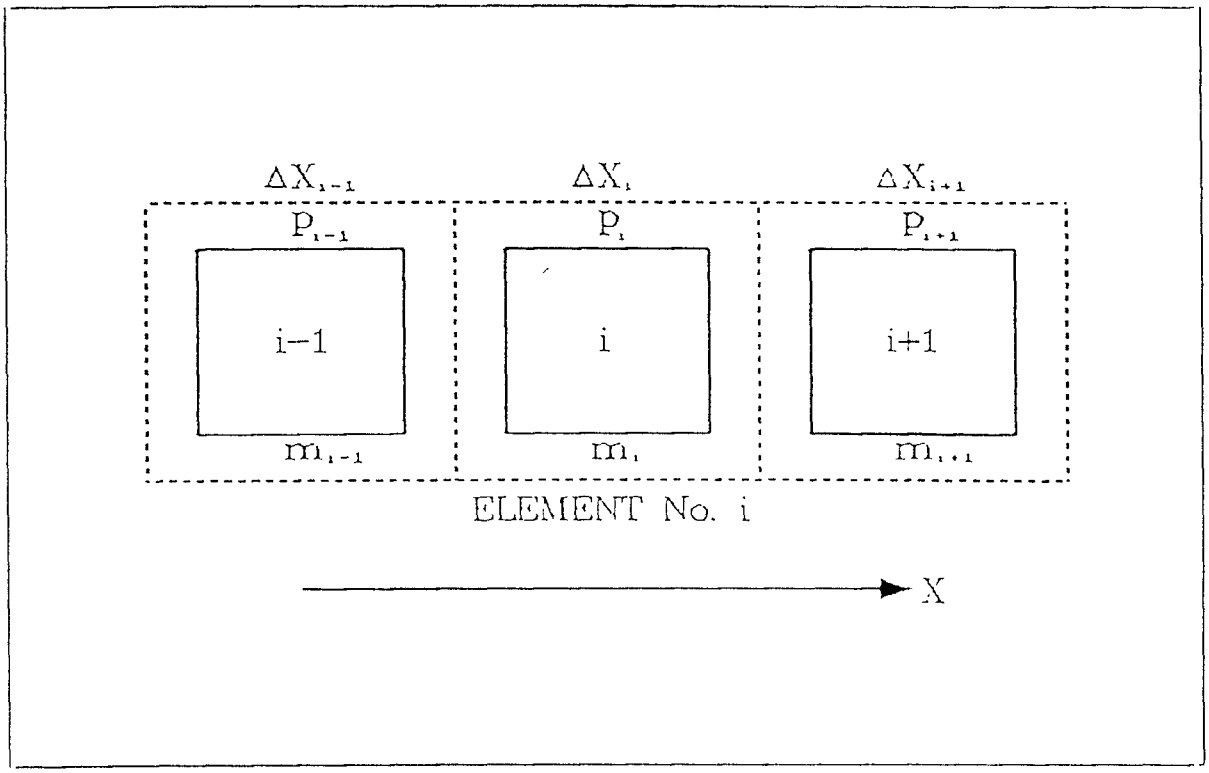

Figure 8: One dimensional Darcy flow geometry

With reference to Figure 8, the mass of gas that diffuses from the particle in the time from t to $t + \Delta t$ is given by

$$\Delta m_D = Q(t + \Delta t) - Q(t)$$

where $Q(t)$ is the function defined by *Equation [A]* and *Equations [B]*

The mass of gas that moves from Element *i-1* to Element *i* in the time increment Δt by permeable flow is given by

$$\delta m_{K_{X\,i}} = -\frac{M_G \Delta Y_i \Delta Z_i K_{X\,i}}{\kappa R T_i \eta_i} p_i \left(1 - \frac{M_G \sqrt{K_{X\,i}^3}}{\kappa R T_i \eta_i^2} p_i \frac{2(p_i - p_{i-1})}{\Delta X_i + \Delta X_{i-1}}\right) \frac{2(p_i - p_{i-1})}{\Delta X_i + \Delta X_{i-1}} \Delta t$$

The mass of gas that moves from Element i to Element $i+1$ in the time increment Δt by permeable flow is given by

$$\delta m_{K_{X\,R}} = -\frac{M_G \Delta Y_i \Delta Z_i K_{X\,i}}{\kappa R T_i \eta_i} p_i \left(1 - \frac{M_G \sqrt{K_{X\,i}^3}}{\kappa R T_i \eta_i^2} p_i \frac{2(p_{i+1} - p_i)}{\Delta X_i + \Delta X_{i+1}}\right) \frac{2(p_{i+1} - p_i)}{\Delta X_i + \Delta X_{i+1}} \Delta t$$

Thus, the gas mass change due to Darcy permeable flow in the X direction during Δt is

$$\Delta m_{K_{X\,i}} = \delta m_{K_{X\,L}} - \delta m_{K_{X\,R}}$$

$$= A_{xI}\left(\frac{p_I - p_{I-1}}{\Delta X_I + \Delta X_{I-1}} - \frac{p_{I-1} - p_I}{\Delta X_I + \Delta X_{I-1}}\right)\left(1 - B_{xI}\left(\frac{p_I - p_{I-1}}{\Delta X_I + \Delta X_{I-1}} + \frac{p_{I-1} - p_I}{\Delta X_I + \Delta X_{I-1}}\right)\right)$$

$$A_{xI} = -\frac{2 M_G \Delta Y_I \Delta Z_I K_{xI}}{\kappa R T_I \eta_I} p_I \Delta t$$

$$B_{xI} = \frac{2 M_G \sqrt{K_{xI}^3}}{\kappa R T_I \eta_I^2} p_I$$

The introduction of the ordinal numbers i, j and k as subscripts of the physical properties of an element distinguishes elements from each other and allows the preceding derivation to be extended to three dimensions. Subscripts i, j and k refer to the x, y and z directions respectively -ie. the subscript ijk refers to the i^{th} element in the x direction, the j^{th} element in the y direction and the k^{th} element in the z direction, where the numberings commence from *1* at a suitable reference point and increase in the same direction the respective axes increase.

Hence, the mass of free gas associated with element ijk is described by the following set of equations:

$$m_{ijk}|_{t+\Delta t} = m_{ijk}|_t - \Delta m_{D\,ijk} + \Delta m_{K\,ijk}$$

$$\Delta m_{D\,ijk} = Q_{ijk}(t+\Delta t) - Q_{ijk}(t)$$

$$\Delta m_{K\,ijk} = A_{ijk}\left(\Gamma_{x\,ijk} + \Gamma_{y\,ijk} + \Gamma_{z\,ijk} + \frac{A_{ijk}}{\eta_{ijk}}\left(\Gamma_{x\,ijk}\Gamma^{\cdot}_{x\,ijk} + \Gamma_{y\,ijk}\Gamma^{\cdot}_{y\,ijk} + \Gamma_{z\,ijk}\Gamma^{\cdot}_{z\,ijk}\right)\right)\Delta t$$

$$A_{ijk} = -\frac{2 M_G}{\kappa R T_{ijk} \eta_{ijk}} p_{ijk}$$

$$\Gamma_{x\,ijk} = K_{x\,ijk}\Delta y_{ijk}\Delta z_{ijk}\left(\frac{p_{ijk} - p_{i-1\,jk}}{\Delta x_{ijk} + \Delta x_{i-1\,jk}} - \frac{p_{i-1\,jk} - p_{ijk}}{\Delta x_{ijk} + \Delta x_{i-1\,jk}}\right)$$

$$\Gamma_{y\,ijk} = K_{y\,ijk}\Delta x_{ijk}\Delta z_{ijk}\left(\frac{p_{ijk} - p_{ij\,1\,k}}{\Delta y_{ijk} + \Delta y_{ij\,1\,k}} - \frac{p_{ij\,1\,k} - p_{ijk}}{\Delta y_{ijk} + \Delta y_{ij\,1\,k}}\right)$$

$$\Gamma_{z\,ijk} = K_{z\,ijk}\Delta x_{ijk}\Delta y_{ijk}\left(\frac{p_{ijk} - p_{ij\,k-1}}{\Delta z_{ijk} + \Delta z_{ij\,k-1}} - \frac{p_{ij\,k-1} - p_{ijk}}{\Delta z_{ijk} + \Delta z_{ij\,k-1}}\right)$$

$$\Gamma^{\cdot}_{x\,ijk} = \sqrt{K^3_{x\,ijk}}\left(\frac{p_{ijk} - p_{i-1\,jk}}{\Delta x_{ijk} + \Delta x_{i-1\,jk}} + \frac{p_{i-1\,jk} - p_{ijk}}{\Delta x_{ijk} + \Delta x_{i-1\,jk}}\right)$$

$$\Gamma^{\cdot}_{y\,ijk} = \sqrt{K^3_{y\,ijk}}\left(\frac{p_{ijk} - p_{ij\,1\,k}}{\Delta y_{ijk} + \Delta y_{ij\,1\,k}} + \frac{p_{ij\,1\,k} - p_{ijk}}{\Delta y_{ijk} + \Delta y_{ij\,1\,k}}\right)$$

$$\Gamma^{\cdot}_{z\,ijk} = \sqrt{K^3_{z\,ijk}}\left(\frac{p_{ijk} - p_{ij\,k-1}}{\Delta z_{ijk} + \Delta z_{ij\,k-1}} + \frac{p_{ij\,k-1} - p_{ijk}}{\Delta z_{ijk} + \Delta z_{ij\,k-1}}\right)$$

Equations [E]

NOTE: The only quantities appearing in *Equations [A]* through *[D]* that are not ijk subscripted are the following

t, p_{STO}, M_G, κ, R, T_{STO} and Δt.

5. METHANE VISCOSITY

Viscosity is a measure of a fluid's resistance to deformation by external forces. In the case of a fluid moving through a medium of given permeability, the flow rate is inversely proportional to the viscosity

For most fluids the viscosity is not constant and depends predominantly on the fluid temperature. Most gases show an increase in this quantity for increasing temperatures and methane is no exception. A graphical representation of the methane viscosity temperature dependence is shown in Figure 9, and an approximate mathematical relationship between these quantities is

$$\eta_{ijk} = \left(4{,}159\,596\ T_{ijk}^{0{,}824\,002} - 35\right) \cdot 10^{-7}$$

The temperature in the above equation is the absolute gas temperature -ie. degrees Kelvin [°K], and the physical unit of the dynamic viscosity is the Pascal-second [Pa•s]. With regard to Figure 9, it can rightly be argued that the temperature range covers a substantially wider scope than can be reasonably expected in a real situation. However, all of the measured values were used in fitting the approximate relationship, and are reproduced mainly for the sake of completeness.

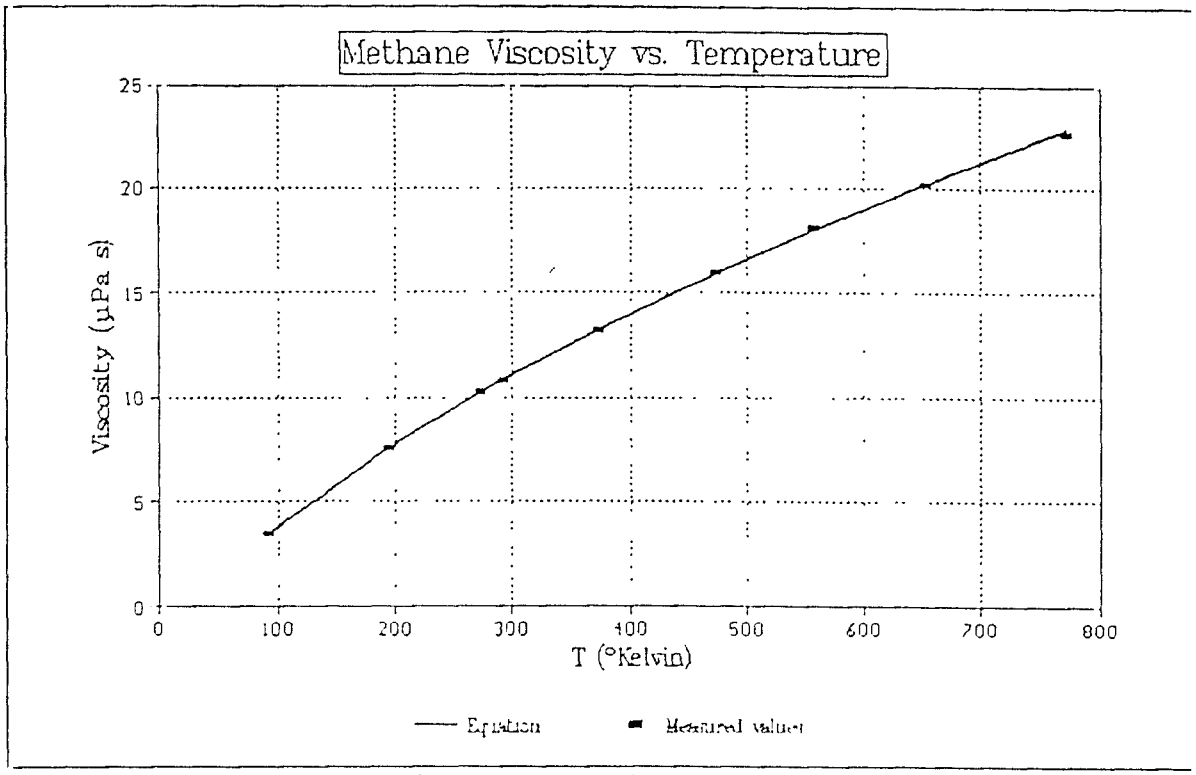

Figure 9: Methane dynamic viscosity as a function of absolute temperature

6. RANDOM VARIATIONS

It was mentioned on page 4 that virtually all quantities involved in the mathematical description of gas transport in a geological structure are subject to variations of an apparently random character. The statistical population of each quantity or parameter is extremely large and this fact allows, by the Central Limit Theorem of Statistics, the distribution of values to be described by a normal or lognormal distribution profile. The choice between a normal or lognormal profile is made purely on the basis of the range of values a quantity or parameter can meaningfully assume. If the range encompasses all real values (negative, zero or positive), then the distribution is normal, while if only non-negative values (zero or positive) are permitted, then the distribution is lognormal.

Although this method of assigning a distribution profile may not be unequivocally valid in a strict sense for certain quantities or parameters, the model will provide this scheme as a default. If data that refute this come to light, suitable modifications are readily implemented to correct this. Table 2 groups the fundamental quantities and parameters dealt with thus far by the distribution type on the basis of the preceding discussion.

NO VARIATION	LOGNORMAL	NORMAL
M_G	$b_{x\,ijk}$ $b_{y\,ijk}$ $b_{z\,ijk}$	$\sigma_{x\,ijk}$ $\sigma_{y\,ijk}$ $\sigma_{z\,ijk}$
p_{STD}	D_{ijk} E_{ijk}	
R	$K_{-x\,ijk}$ $K_{-y\,ijk}$ $K_{-z\,ijk}$	
T_{STD}	$k_{1\,ijk}$ $k_{2\,ijk}$	
t, Δt	$p_{-\,ijk}$ T_{ijk}	
κ	λ_{ijk} $\mu_{w\,ijk}$	
ρ_w	ν_{ijk} $\rho_{c\,ijk}$	

Table 2: Fundamental quantities grouped by distribution type

In order to reproduce these random fluctuations, use is made of a random or pseudorandom number generator that produces random numbers ϱ in the range $0 \le \varrho < 1$. These numbers are uniformly distributed and must therefore be related to the required distribution In the case of a lognormally distributed quantity, the logarithms of the population values are normally distributed, so that it is necessary only to relate the random numbers to the normal distribution. A function is thus required that maps the uniform distribution of random numbers to the normal distribution

The probability density function for the random numbers is

$$\Pi_\varrho = \begin{cases} 1 & \text{if } 0 \le \varrho < 1 \\ 0 & \text{if } \varrho < 0 \text{ or } \varrho \ge 1 \end{cases}$$

and that of the normal distribution is

$$\Pi_N = \frac{1}{\sqrt{2\pi}} e^{-\frac{1}{2}z^2} \quad \text{if } -\infty < z < +\infty$$

NOTE: In this section and this section alone, z does not refer to a spatial dimension, it represents a normalised random variable

The relationship between ϱ and z is established on the basis of equal areas under the curves of the two probability density functions -ie equal cumulative probabilities- within their respective valid ranges Thus,

$$\int_0^{\varrho} \Pi_\varrho \, d\varrho = \int_{-\infty}^{z} \Pi_N \, dz$$

$$\therefore \varrho = \int_{-\infty}^{z} \frac{1}{\sqrt{2\pi}} e^{-\frac{1}{2}z^2} dz = F(z)$$

$F(z)$ in the above equation is the cumulative normal distribution This function cannot be evaluated by analytical means, but statistical tables quote its values for various values of z Figure 10 presents a graph of this function An approximate expression is given by

$$\Phi(z) = \frac{1}{2}\left(1 + \sqrt{1 - e^{-0.609\,28\,z^{1.980\,104}}}\right)$$

$$F(z) = \begin{cases} \Phi(z) & \text{if } z \ge 0 \\ 1 - \Phi(z) & \text{if } z < 0 \end{cases}$$

Theoretically, z should range from $-\infty$ to $+\infty$ to encompass all possible values, but since the range from -4 to +4 includes at least 99 99% of all possible values, these limits are chosen for simplicity to

represent the full range. The relative errors of the approximation range from -1.28% at $z = 0{,}01$ to +2.14% at $z = 0{,}60$. Using the approximation and rearranging,

$$|z| = 1{,}284\,318 \left(Ln \frac{1}{4\,\varrho\,(1-\varrho)} \right)^{0{,}505\,024}$$

The validity of the above equation is substantiated by the fact that it conforms to the intuitive expectation that $|z| \to \infty$ as $\varrho \to 1$ or $\varrho \to 0$, and that $|z| = 0$ for $\varrho = ½$. The choice of negative or positive z is resolved on the basis of whether ϱ is less than or greater than ½, respectively. Furthermore, to ensure that $|z| \leq 4$, $|\varrho - ½| \leq 0{,}499981$ must be satisfied.

If the maximum allowable variation for a particular quantity is υ, then the allowable range of values for the quantity is between $1 - \upsilon$ and $1 + \upsilon$ times its mean value, and these limits correspond to $z = -4$ and $z = +4$ respectively. Random fluctuations are then introduced by multiplying the quantity by the factor

$$f_{\upsilon N} = 1 + ¼\, z\, \upsilon$$

This scheme was programmed and several runs producing between 200 000 and 1.5 million factors in a loop showed the distribution of factors (divided into 51 classes) to be very closely normal with a mean of 1 and a standard deviation of $¼\,\upsilon$. The relative frequency of each of the classes was used in the comparison, and the largest relative aberrations were, as expected, found at the endpoints. The relative errors in the both the mean and standard deviation were better (less) than 0 05%, while the worst relative error in the class frequencies was slightly more than 7%

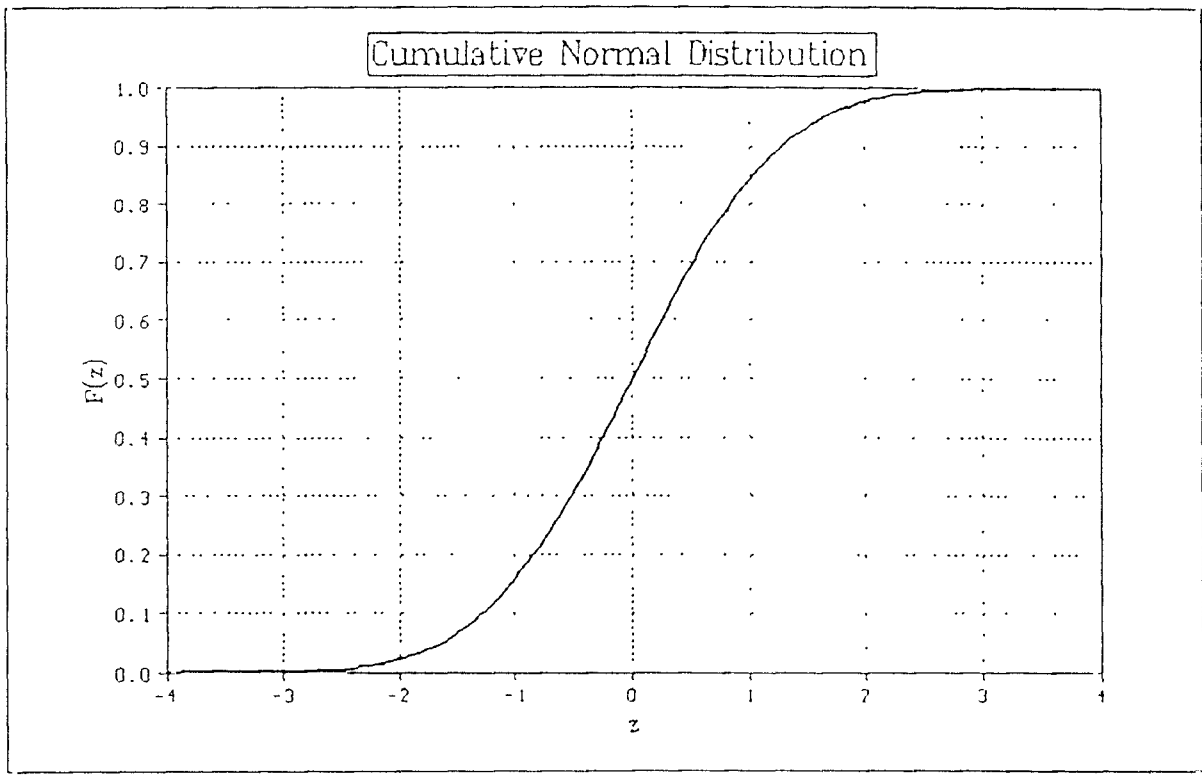

Figure 10: Cumulative normal distribution

In the case of lognormally distributed quantities, it is more convenient to specify the allowable range of values in terms of the number of orders of magnitude N_{OM} that it covers This means that the maximum value the quantity can assume is $10^{N_{OM}}$ times as large as its minimum allowable value, and its mean value is the geometric mean of the minimum and maximum The factor for lognormally distributed quantities is then

$$f_{LN} = 10^{\left(\frac{N_{OM}}{8}\right) z}$$

In summary, random variations are described by

Normal: $Q' = \overline{Q} \cdot f_{uN}$

Lognormal: $Q' = \overline{Q} \cdot f_{LN}$

$f_{uN} = 1 + \frac{1}{4} z u$ $\qquad f_{LN} = 10^{\left(\frac{N_{ou}}{8}\right) z}$

$z = \pm 1{,}284\,318 \left(Ln \frac{1}{4\varrho(1-\varrho)} \right)^{0{,}505\,024}$ $\qquad$ + *if* $\varrho \geq \frac{1}{2}$; − *if* $\varrho < \frac{1}{2}$

$\varrho = 0{,}00001903 + 0{,}99996194 \cdot RN_{|RN|<1}$

Equations [F]

where Q' is the varied quantity;
$\overline{Q}$ is the mean value of the quantity, and
$RN_{|RN|<1}$ is a random number less than 1 and greater or equal to zero

7. BOUNDARY CONDITIONS

Owing to the small size of the elements, all boundaries are composed of whole elements. Two types of boundaries are identified: free faces (ie areas exposed to the atmosphere) and modelled region boundaries (ie the peripheries of the modelled region). In the case of region boundaries, three ideal states were discussed (page 9 - Section D.8). With reference to *Equations [E]*,

(a). At impermeable boundaries gas release is exclusively diffusive in nature Mathematically,

$$\Delta m_{K\,ijk} = 0$$

Equation [G 1]

(b) At boundaries where the pressure remains constant, depending on the location and orientation of the boundary, one or more of the following hold:

Either $p_{ijk} - p_{i-1\,jk} = 0$ *or* $p_{i-1\,jk} - p_{ijk} = 0$

Either $p_{ijk} - p_{i\,j-1\,k} = 0$ *or* $p_{i\,j-1\,k} - p_{ijk} = 0$

Either $p_{ijk} - p_{ij\,k-1} = 0$ *or* $p_{ij\,k-1} - p_{ijk} = 0$

Equations [G 2]

(c) At boundaries where the pressure gradient remains constant, depending on the location and orientation of the boundary, one or more of the following hold

Either $\frac{p_{ijk} - p_{i-1\,jk}}{\Delta x_{ijk} + \Delta x_{i-1\,jk}} = constant$ *or* $\frac{p_{i-1\,jk} - p_{ijk}}{\Delta x_{ijk} + \Delta x_{i-1\,jk}} = constant$

Either $\frac{p_{ijk} - p_{i\,j-1\,k}}{\Delta y_{ijk} + \Delta y_{i\,j-1\,k}} = constant$ *or* $\frac{p_{i\,j-1\,k} - p_{ijk}}{\Delta y_{ijk} + \Delta y_{i\,j-1\,k}} = constant$

Either $\frac{p_{ijk} - p_{ij\,k-1}}{\Delta z_{ijk} + \Delta z_{ij\,k-1}} = constant$ *or* $\frac{p_{ij\,k-1} - p_{ijk}}{\Delta z_{ijk} + \Delta z_{ij\,k-1}} = constant$

Equations [G 3]

The conditions at free faces are more complex in that these are destressed and fractured, and are consequently more permeable An empirical relationship for the depth of pillar fracturing from a free face

in terms of the mining depth and the mining height[15] for South African conditions is

$$d_f = 0{,}615\, h^{1{,}3}\, Ln \frac{H}{44{,}174 + 25{,}92\, h}$$

where d_f is the depth of the fractured zone in metres;
h is the mining height in metres, and
H is the mining depth in metres.

It is assumed that all vertical free (coal) faces are similarly fractured, and that the vertical stress increases linearly with depth into the face up to the limit of fracturing, where its value equals the peak abutment stress behind the free face. Beyond the limit of fracturing, the vertical stress decays roughly exponentially to the vertical virgin value.

An empirical relationship for the peak abutment stress in terms of the fracture zone depth and the mining height[15] is

$$\sigma_p = 1{,}2\, e^{3{,}56\, h^{-0{,}86}\, d_f}$$

where σ_p is the peak abutment stress behind the free face in MPa.

Figure 11 shows a plan view of a pillar which is symmetrically divided into four areas Each of these areas is further subdivided into four regions within each of which the vertical stress distribution can be described in terms of the spatial dimensions The corresponding regions mirrored by the two axes of symmetry in each of the four areas behave similarly to the numbered ones in terms of their stress distribution

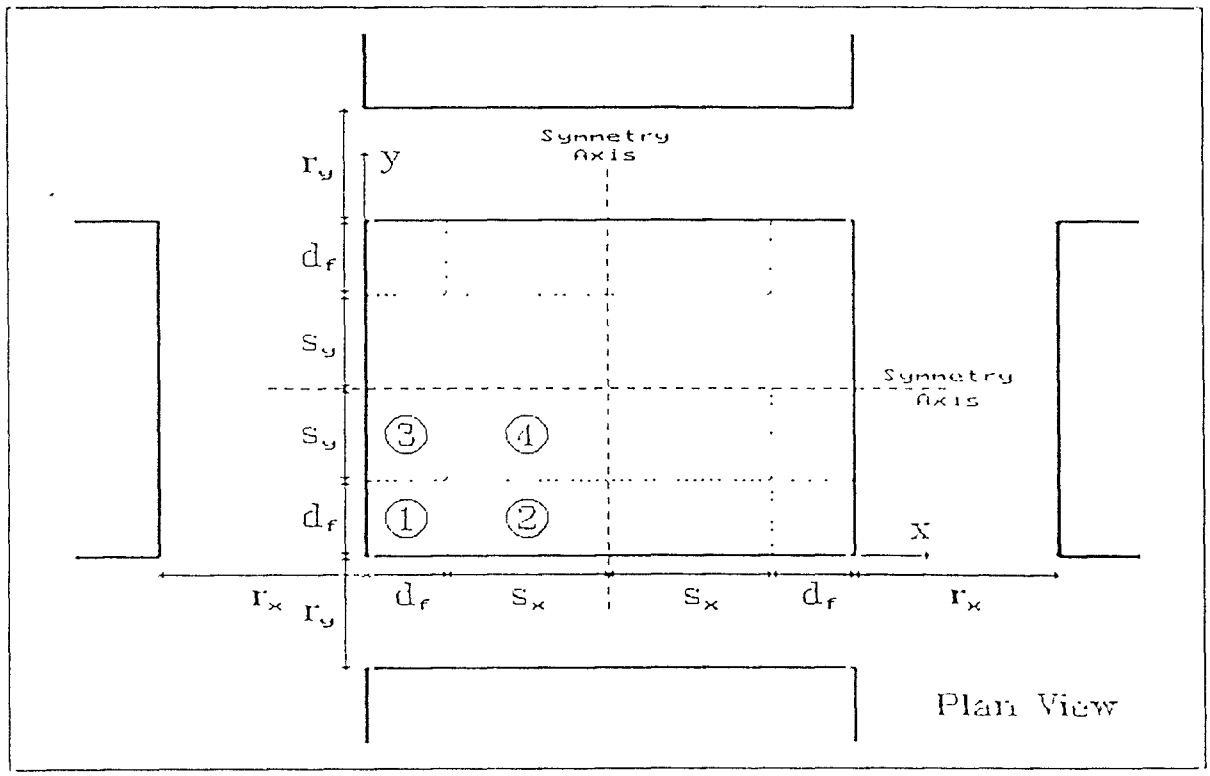

Figure 11: Pillar geometry

The vertical stress distribution in each of the four regions (the numbers in parentheses correspond to the numbered areas in Figure 11) is given by

(1) $\sigma_z = \frac{\sigma_p}{d_f^2}\, xy$

(2) $\sigma_z = \frac{\sigma_p}{d_f}\, y$

$$(3)\ \sigma_z = \frac{\sigma_P}{d_f}\, x$$

$$(4)\ \sigma_z = \sigma_\infty + \left(\sigma_P - \sigma_\infty\right) e^{k_c \sqrt{(x-d_f)(y-d_f)(w_x-d_f-x)(w_y-d_f-y)}}$$

where $w_x = 2(s_x + d_f)$ and $w_y = 2(s_y + d_f)$ are the pillar dimensions;
σ_∞ is the virgin vertical stress ($\approx 0{,}025\,H$ MPa) at the pillar horizon, and
k_c is the stress decay constant.

k_c can be determined from considerations of static equilibrium and is (approximately) given by

$$k_c = \frac{69{,}384\, Ln(0{,}317\,427\, Ln(0{,}318\,428\, F^{1{,}013\,955} + Ln(1 + 59{,}978\,1F)) + 0{,}527\,62)}{(w_x - 2d_f)(w_y - 2d_f)}$$

$$F = \frac{1}{\sigma_P - 0{,}025\,H}\left\{\frac{0{,}025\,H(w_x + r_x)(w_y + r_y) - \sigma_P(w_x + w_y - 3d_f)\,d_f}{(w_x - 2d_f)(w_y - 2d_f)} - 0{,}025\,H\right\}$$

Equation [G.4]

In the case of a free (coal) face that is not part of a pillar (eg. rib or working face), the relationships are somewhat simpler. Again, it is assumed that the vertical stress increases linearly with depth into the face up to the limit of fracturing, and decays roughly exponentially beyond this limit The depth of fracturing and peak abutment stress are assumed to be the same as for pillars The vertical stress distribution in the fractured zone is given by

$$\sigma_z = \frac{\sigma_P}{d_f}\,\xi$$

and beyond this by

$$\sigma_z = \sigma_\infty + \left(\sigma_P - \sigma_\infty\right) e^{-k_c(\xi - d_f)}$$

where ξ is the distance into the free face, measured perpendicularly to it in the plane of the seam

In this case k_c is given by

$$k_c = \frac{\sigma_P - \sigma_\infty}{\sigma_\infty(d_f + h) - \tfrac{1}{2}\, d_f\, \sigma_P}$$

Equation [G 5]

Equation [G.5] applies also to free faces in the case of total extraction methods where goafing is involved, with the slight modification that UCS (the unconfined uniaxial compressive strength of the intact material/coal) replaces the peak abutment stress term σ_P. The reason for this modification is that in the case of goafing, the horizontal confining stresses acting in the plane of the seam will tend to be relieved since there is no roof to transmit them, effectively reducing the load bearing capacity of unbroken material in this plane. In all cases, the two horizontal stresses in these regions are assumed to be equal to one another and in a constant proportion to the vertical stresses, so that $\sigma_x = \sigma_y = c_o\,\sigma_z$, where c_o is the constant of proportionality (usually ≈ 1) between the horizontal and vertical stress, unless otherwise specified.

Horizontal free faces, such as the roof and floor of the excavation, are generally subject to tensile horizontal stresses Where such a free face is composed of carbonaceous material, the assumption is made that the permeability is sufficiently high (due to the relatively high degree of 'stretching') for gas transport to be governed exclusively by sorptive and diffusive processes Where it is composed of non-carbonaceous material, the 'stretching' is insufficient to significantly alter the permeability of the material due to the generally high Young's moduli exhibited by these materials

The gas pressure at any free face is equal to the prevailing atmospheric pressure, so that, depending

on the location and orientation of the free face, one or more of the following hold:

$$\text{Either } p_{i-1\,jk} = p_{atm} = p_{ijk} \quad \text{or} \quad p_{ijk} = p_{atm} = p_{i+1\,jk}$$
$$\text{Either } p_{i\,j-1\,k} = p_{atm} = p_{ijk} \quad \text{or} \quad p_{ijk} = p_{atm} = p_{i\,j+1\,k}$$
$$\text{Either } p_{ij\,k-1} = p_{atm} = p_{ijk} \quad \text{or} \quad p_{ijk} = p_{atm} = p_{ij\,k+1}$$

Equations [G.6]

where p_{atm} is the prevailing atmospheric pressure.

8 TRANSPORT IN NON-CARBONACEOUS ELEMENTS

It was stated on pages 6 and 7 that gas transport in non-carbonaceous regions is purely Darcy permeable In terms of *Equations [E]* this means

$$\Delta m_{D\,ijk} = 0$$

Equation [H]

It is obvious that this applies also at non-carbonaceous free faces of arbitrary orientation

9. DYNAMIC MINING ACTIVITY

The effect of dynamic mining activity on gas release was qualitatively described on page 8 The total mass of free gas held by an element is quantified by *Equation [C]*. The assumption that coal releases the entirety of its free gas upon being broken leads to the following relationship

$$\Delta m_M = \sum_i \sum_j \sum_k \left(\frac{M_G \left(\Delta x_{ijk} \Delta y_{ijk} \Delta z_{ijk} - 8 \lambda_{ijk}^3 \right)}{\kappa R T_{ijk}} \right) \left(p_{ijk} - p_{atm} \right)$$

Equation [I]

where Δm_M is the gas mass released by broken coal in time Δt

The dimensions of the element (Δx_{ijk}, Δy_{ijk}, Δz_{ijk} and λ_{ijk}), as well as the physical properties thereof (T_{ijk}) are taken to be those at the instant just before the coal is broken, and the summation extends only over those elements separated from the seam during the time increment Δt In addition, the freshly exposed face becomes a new boundary, subject to the relationship(s) given in Section E 7 The gas released by coal breaking is added to the total gas emitted at that point, and is calculated *prior* to diffusive and permeable considerations in order to cater for the substantial increase in pressure gradient at the new free face.

It is assumed that the residence time of such mined material in the modelled region is such that subsequent sorptive and diffusive gas release therefrom is insignificant compared to that from the remaining areas

10. GOAFING AND CAVING

Where the extraction of coal involves goafing and/or caving, the effect thereof on gas make depends on the type of material that breaks. In the case of non-carbonaceous material, the gas released is that held in the void spaces of the rock broken by caving/goafing during the time increment Δt, whereafter no further gas is released, and is quantified by *Equation [I]*. In the case of carbonaceous material, the same holds true, except that the material continues to emit gas by purely diffusive means. In terms of the surface concentration C_S of the caved elements, this means

$$C_{S\,ijk} = \left(\frac{p_{STD} M_G}{\kappa R T_{STD}}\right)\left(\frac{k_{1\,ijk}\, k_{2\,ijk}\, p_{atm}}{1 + k_{2\,ijk}\, p_{atm}}\right)$$

Equation [J]

11. INITIAL CONDITIONS

Ideally, a complete specification of the initial conditions from which modelling proceeds would entail a complete spatio-temporal description of the required physical properties and geometric dimensions of the entire region. Needless to say, this is a virtual impossibility from a practical point of view, but an indication of the likely *status quo* of the physical properties and geometry is none the less required for each and every element. Generally, the required quantities are known only at a few isolated points within the region, and this may be used as a basis upon which values may be assigned to other points via a suitable inter- and extrapolation scheme Such schemes usually project values of a certain quantity spatially on the basis of some measure of the distance between points at which the quantity is known and those where it is unknown In the case of a linear inter/extrapolation, the value assigned to an unknown point is the inverse distance-weighted mean of the all the known values within the region considered

This notion may be extended to the general case where the weighting factors are the inverse of the respective distances raised to some power $c \geq 0$ For any quantity Q, the c -weighted distribution yields values of the quantity at unknown points via

$$Q_{ijk} = \frac{\sum_{i=1}^{N_K} Q_{i\,ijk}\, S_{i\,ijk}^{-c}}{\sum_{i=1}^{N_K} S_{i\,ijk}^{-c}}$$

$$S_{i\,ijk} = \sqrt{(X_{i\,ijk} - X_{ijk})^2 + (Y_{i\,ijk} - Y_{ijk})^2 + (Z_{i\,ijk} - Z_{ijk})^2}$$

Equation [K]

where N_K is the total number of points at which the quantity is known,
Q_{ijk} is the value of the quantity at the point with co-ordinates $(x_{ijk}, y_{ijk}, z_{ijk})$, and
$Q_{i\,ijk}$ is the known value at the point with co-ordinates $(x_{i\,ijk}, y_{i\,ijk}, z_{i\,ijk})$

This scheme is applied before the commencement of gas flow processing Practically, the known values can be either field or laboratory observations It should be noted that N_K and $c \geq 0$ may be different for different quantities and that $N_K \geq 1$. Furthermore, the use of this procedure is valid only for the basic data associated with elements of the same *type* (eg assigning diffusion coefficients to carbonaceous elements) It is thus convenient at this point to split the basic data into two groups and to divide the elements into three main categories, and to list with each the associated physical and geometric parameters that are required The two basic data groups distinguish between data that are associated with a particular element and those which are common to all, while the element categories distinguish the element types from one another (see Tables 3 and 4).

GENERAL QUANTITIES AND PARAMETERS		
NAME	SYMBOL	UNIT
(1) Time	t	[s]
(2) Time step increment	Δt	[s]
(3) Orthonormal (Cartesian) co-ordinates	$x\ y\ z$	[m]
(4) Universal gas constant	R	[J·mol^{-1}·°K^{-1}]
(5) Standard atmospheric pressure	p_{STD}	[Pa]
(6) Standard atmospheric temperature	T_{STD}	[°K]
(7) Gas molecular mass	M_G	[kg·mol^{-1}]
(8) Gas supercompressibility fraction	κ	[-]
(9) Water/moisture density	ρ_w	[kg·m^{-3}]

Table 3: Data common to all element types

ELEMENT TYPE	ASSOCIATED PARAMETERS & QUANTITIES		
	NAME(S)	SYMBOL(S)	UNIT(S)
[I] CARBONACEOUS	(1) Element ordinal numbers	$i\ j\ k$	[-]
	(2) Particle half-length	$\lambda_{0\ ijk}$	[m]
	(3) Element dimensions	$\Delta x_{0\ ijk}\ \Delta y_{0\ ijk}\ \Delta z_{0\ ijk}$	[m]
	(4) Particle density	$\rho_{c\ ijk}$	[kg·m^{-3}]
	(5) Diffusion coefficient	D_{ijk}	[m^2·s^{-1}]
	(6) Langmuir constants	$k_{1\ ijk}\ k_{2\ ijk}$	[m^3·kg^{-1}] [Pa^{-1}]
	(7) Free gas pressure	p_{ijk}	[Pa]
	(8) Free gas temperature	T_{ijk}	[°K]
	(9) Principal intrinsic permeabilities	$K_{-x\ ijk}\ K_{-y\ ijk}\ K_{-z\ ijk}$	[m^2]
	(10) Klinkenberg constants	$b_{x\ ijk}\ b_{y\ ijk}\ b_{z\ ijk}$	[Pa]
	(11) Moisture content	$\mu_{w\ ijk}$	[-] or [%]
	(12) Normal stresses	$\sigma_{x\ ijk}\ \sigma_{y\ ijk}\ \sigma_{z\ ijk}$	[Pa]
	(13) Young's modulus	E_{ijk}	[Pa]
	(14) Poisson's ratio	ν_{ijk}	[-]
	(15) Virgin (seam) gas pressure	$p_{-\ ijk}$	[Pa]
[II] NON-CARBONACEOUS	(1) Element ordinal numbers	$i\ j\ k$	[-]
	(2) Particle half-length	$\lambda_{0\ ijk}$	[m]
	(3) Element dimensions	$\Delta x_{0\ ijk}\ \Delta y_{0\ ijk}\ \Delta z_{0\ ijk}$	[m]
	(4) Free gas pressure	p_{ijk}	[Pa]
	(5) Free gas temperature	T_{ijk}	[°K]
	(6) Principal intrinsic permeabilities	$K_{-x\ ijk}\ K_{-y\ ijk}\ K_{-z\ ijk}$	[m^2]
	(7) Klinkenberg constants	$b_{x\ ijk}\ b_{y\ ijk}\ b_{z\ ijk}$	[Pa]
	(8) Moisture content	$\mu_{w\ ijk}$	[-] or [%]
	(9) Normal stresses	$\sigma_{x\ ijk}\ \sigma_{y\ ijk}\ \sigma_{z\ ijk}$	[Pa]
	(10) Young's modulus	E_{ijk}	[Pa]
	(11) Poisson's ratio	ν_{ijk}	[-]
	(12) Particle density	$\rho_{r\ ijk}$	[kg·m^{-3}]
[III] FREE SPACE	(1) Element ordinal numbers	$i\ j\ k$	[-]
	(2) Element dimensions	$\Delta x_{0\ ijk}\ \Delta y_{0\ ijk}\ \Delta z_{0\ ijk}$	[m]
	(3) Atmospheric pressure	$p_{atm\ ijk}$	[Pa]

Table 4: Element types and their associated data

In Table 3, only the water/moisture density is subject to random fluctuations, as outlined in Table 2, Section E.6., while in Table 4 all quantities listed, with exception of the element ordinal numbers, are subject to such variations. The element categorisation as given has the advantage that the modelled region consists in its entirety of elements -ie. no special provisions are required for areas or sub-regions devoid of solid material. In terms of the categorisation, this means that the boundary elements at any free face adjoin type [III] (free space) elements. In addition, type [I] and type [II] elements are sub-classified further as '*broken*' or '*solid*', depending on whether they are located in a sub-region that has caved/ goafed/been mined or not, respectively. In the case of mined elements, these are replaced by type [III] elements once their gas contribution has been evaluated (Section E.9), while goafed/caved elements are displaced vertically in order to preserve spatial accuracy of the gas emission distribution.

A Turbo Pascal TYPE data abstraction that encapsulates the elements is given in Appendix C.

F. COMPARISON WITH EXISTING MODELS

Table 5 shows the differences and similarities between the salient features of the present model and those existing models, listed in the King and Ertekin survey (page 2), which include dynamic mining activity. The reason that this feature is chosen as the admission criterion for the comparison is that its significant effect on overall gas emission is a well established fact, particularly for the seemingly ever increasing production rates achieved by continuous miners and shearers The relevance of those models that do not incorporate this effect is thus substantially reduced.

The information in Table 5 was extracted from three tables in the King and Ertekin report The latter also compares the models with regard to their applicability to single or multiple gas extraction wells. This feature is neglected here since it is considered of lesser importance, but the model does accommodate it, although fractures are not considered separately from permeability

The eight models chosen for the comparison are listed below with their identifying code

[A] BOM (MINES1D)
[B] BOM (MINES2D)
[C] Chen
[D] Intercomp-1
[E] Intercomp-2
[F] Kovalev et al
[G] Lindine et al
[H] Penn State-4
(A complete list of the 37 simulators evaluated in the survey is presented in Appendix D)

The present model is identified by [X]

In terms of the overall model type (property 1), six of the eight are classed as two-phase simulators, since they simulate both gas and liquid (water) transport [X] does not take liquid transport into account for the reasons stated earlier (page 8) The geology catered for (property 2) by the present model is limited only by the amount of information that is available concerning the physical and geometric properties of the material(s) of which it is composed The only distinctions that must be made in this regard are between carbonaceous and non-carbonaceous matter and between solid and broken material

Adsorbed gas in primary porosity regions (applicable only to carbonaceous material) is described only by the Langmuir isotherm in the current model, since Henry's Law isotherm provides for multilayer adsorption, which only occurs at very high gas pressures, and the highest virgin seam gas pressures measured thus far in South Africa do not exceed 2MPa The gas transport in the micropore structure

developing into virgin ground, the effects of varying production rates and goafing of overlying strata on gas emissions are all within the scope of the model. It will not, however, simulate gas dilution and/or removal by ventilation.

It is envisioned that the relevant geometry is input to the program as a series of horizontal sections at various elevations. The following stage will then prompt for the required data (physical properties, values for certain quantities, etc.). The program will then generate a suitable node-mesh (discretisation) on the basis of both the geometry and the data (see also following section) The user will then specify both the interval(s) at which output is desired and the required degree of detail -ie. the most basic output would be the average and total gas emission, while a full report would include the spatial and temporal emission behaviour, concentration and pressure distribution profiles, flow vectors and instantaneous emission rates at selected locations and times.

Provision for standard layouts (eg. bord and pillar workings) and standard reports can be made quite readily. Standard mining layouts would not be part of the model/program *per se*, as these are considered to be part of the input data, but would take the form of data files that can be edited from the program environment. Standard reports would be available as options on the report menu and user specified reports would be configured on the basis of a checklist of available options. Reports can be generated in the form of hard copies (printer or plotter), files or screen output

G. MODIFICATIONS FOR COMPUTERISATION

It was mentioned on page 10 by way of illustration that a cube of coal with a side length of one metre contains in the order of 37 million elements if the FNS is ±3mm For every doubling of the side length of such a cube, the number of elements increases eightfold, so that even modelling a single pillar measuring 30 by 30 by 3 metres (10^{11} elements) with impermeable over- and underlying strata on a supercomputer is a formidable exercise The basic data alone would occupy an estimated 28000 GigaBytes, and the execution time for a single time step would be astronomical Needless to say, it is thus totally impractical to model a region on the basis of single elements

This problem may be substantially reduced by considering an elemental region (henceforth referred to as 'c-element') composed of a collection of elements that all behave in a similar manner Adopting this strategy constitutes an approximation, the validity of which depends on three main factors

- The size of the c-element (geometric dimensions in relation to that of an element),
- The shape of the c-element (dimensional proportions), and
- The prevalent physical conditions in adjacent c-elements at a given instant.

The size of the c-element gives an indication of the total number of elements it contains The larger this number, the less accuracy is achieved by the approximation. The shape of the c-element in conjunction with its size gives an indication of the number of elements a line of arbitrary direction through its geometric centre traverses For a given direction, the larger this number, the less will be the directional accuracy of the approximation The more pronounced the (relative) differences between the physical conditions of adjacent c-elements are, the less accurate is the approximation

For the present model, the choice of c-element shape is unambiguously that of a rectangular parallelIped, considering both the element shape and the Cartesian co-ordinate system within which the coal structure is defined. This arrangement makes for relatively simple subdivision of the region into c-elements

The size of the c-elements will to a large extent be dictated by the computational abilities of the

computer system the model is targeted for. In practice, this will entail discretising the region to be modelled into a fixed number of basic c–elements, the actual dimensions of which will depend on the dimensions of the modelled region, and consolidating these into larger c–elements on the basis of both geometrical conformity and the prevalent gas pressure. Since the latter changes most dramatically at or near free faces, this implies that c–elements at such locations will be smaller than those of regions completely enclosed by coal or rock. The consolidation of the basic c–elements into larger units will be done in such a manner that the pressure *differences* between adjacent c–elements in a given direction are relatively constant, and the region's geometry is preserved.

Each c–element is then uniquely identified by a set of three ordinal numbers, which are fairly readily combined into a single index for each particular c–element. A reference list of such indices indicating the adjacencies of individual c–elements is required to eliminate data replication and to ensure correct data processing. This notion could even be extended so that the c–element configurations are reassessed periodically on the basis of the changing physical quantities (viz. gas pressure). From a computational point of view, it is not especially difficult to merge or split c–elements

Much of the actual processing time will be invested in data transfer, rather than calculation, and this effect can be reduced by making individual data blocks as large as possible, thus percentagewise reducing the disk read/write overheads

A further reduction in processing time may be realised by implementing a short-circuit evaluation strategy, whereby for instance pressure differences are evaluated first, and further calculations done only if these differences are non-zero. Whether or not this strategy is of value must still be assessed, since it may well be the case that the additional time required to process the necessary Boolean values has a detrimental overall effect.

H. CONCLUSIONS AND RECOMMENDATIONS

The model as presented here is expected to provide reasonably accurate and reliable data on the migration of methane gas in South African coal mines Currently, the mathematical descriptions given in Section E are in the process of being coded into a computer program The value of the model's output can only reasonably be appraised once this coding is complete The individual mathematical descriptions are deemed to be correct and suitably accurate as stand alone units, and are linked to one another in a relatively straightforward manner

On the proviso that the coding is successful inasmuch as that all the factors of influence outlined in this report can be efficiently accommodated, the model will permit virtually any mining situation to be simulated with relative ease Upon completion of the coding, model verification will be undertaken with existing field and laboratory data, as well as further data collected for this purpose. Presently, field work is being planned to quantify the directional dependence of *in-situ* coal permeability. A fairly substantial data base of sorptive characteristics for a wide variety of South African coals is available to serve as model input data. Seam gas pressures are also known at a few locations, and overall emission rates are readily calculated from ventilating air quantities and volumetric gas concentrations

Some field work will be required to establish the importance (or otherwise) of considering roof and floor emissions on overall gas make This work should focus primarily on (non-coal) strata permeabilities and total gas contents of such strata If the permeabilities are found to be such that gas contributions are virtually negligible (a fairly common assumption, for or against which no strong evidence has been found), the model may then be modified to consider only two-dimensional flow or three-dimensional flow in limited sub-regions only This will simplify the discretisation and reduce the computational effort

Two other influences neglected in this model, namely those of flowing ground water and barometric pressure variations, may be found to be sufficiently important to warrant inclusion into the model at a

subsequent stage. The development of an apparatus that monitors flammable gas concentrations and barometric pressures simultaneously is underway. Once operational, it will establish the relative importance of barometric pressure variations for gas emission rates Very few local collieries have a significant ingress water problem, which is the reason for neglecting this influence in the first place, but if suitable sites for investigating this come to light, then field data should be collected.

The collection of data concerning the physical properties (particularly those related to sorption, diffusion and permeability) and their statistical distribution characteristics would be of significant benefit in evaluating the practical validity of the theoretical considerations presented in this report. Such data would assist in pinpointing model deficiencies.

Upon completion of the model evaluation/verification and any necessary modifications, the user interfaces will be extended and enhanced for industrial application and user-friendliness, and a complete methane emission prediction software package will be produced which will fill a large gap in the local coal mining industry's tool box.

APPENDIX A: Pascal Diffusion Program

```
PROGRAM     Diffusion;

USES        CRT,Printer;

CONST       N              = 1000,              {No. of slices}
            NBase          = 25;
            No_Of_Stops    = 52;                {No. of datapoints to print}
            Stop : ARRAY [1..No_Of_Stops] OF LongInt
                   = (0, 1, 2, 3, 4, 5, 6, 7, 8, 9, 10, 12, 14, 16, 18, 20, 23, 26, 29, 34, 39, 45, 55, 70,
                   85, 100, 120, 140, 160, 180, 200, 230, 260, 290, 320, 350, 400, 450, 500, 550,
                   600, 700, 900, 1200, 1500, 2000, 2500, 3000, 3500, 4250, 5000, 6000);
                                                {List of steps at which to print results}

VAR         i, k           : Word,
            j              : LongInt,
            C              : ARRAY [1..N] OF Real,
            QT, k1, k2, T  : Real,

BEGIN
 FOR i := 1 TO (N-1) DO C[i] := 1,
 C[N] := 0,                                     {Initialise concentrations}
 FOR k := 1 TO No_Of_Stops DO
   Stop[k] := trunc(N/NBase*N/Nbase+0.5)*Stop[k]; {Initialise Stops}
 j := 0;                                        {Initialise counter}
 WriteLn(LST,'              ',N:4,' Slices'),
 WriteLn(LST,'      tau          Q');          {Write printer heading}
 FOR k := 1 TO No_Of_Stops DO
 BEGIN
   Writeln('BUSY with step ',k,' ', Stop[k]),
   WHILE (j < Stop[k]) DO
   BEGIN
     inc(j),                                    {Increment time step counter}
     FOR i := (N-1) DOWNTO 2 DO
     BEGIN
       k1 := (2.0*i+1)/(2.0*i-1),
       k1 := (sqr(k1)+1)/12,
       k2 := (2.0*i-3)/(2.0*i-1),               {Compute new concentration}
       k2 := (sqr(k2)+1)/12;
       C[i] := C[i]+k1*(C[i+1]-C[i])-k2*(C[i]-C[i-1]),
     END,          {FOR}
     C[1] := (C[1]+5*C[2])/6;
   END,            {WHILE}
   T := j/6/N/N,
   QT := 0,                                     {Compute total quantity}
   FOR i := 1 TO (N-1) DO QT := QT + sqr(2.0*i-1)*C[i],
   QT := QT/(2.0*N-1)/(2.0*N-3)/(N-1),
   WriteLn(LST,'    ',T:12:8,'  ',  QT:12:10),  {Print results}
 END,              {FOR}
END                {PROGRAM Diffusion}
```

APPENDIX B: Cardano's Method for Cubics

In order to find one root of a general cubic of the form

$$Ax^3 + Bx^2 + Cx + D = 0$$

let

$$x = y - \frac{B}{3A}$$

$$E = \frac{1}{3}\left(\frac{B^2}{3A^2} - \frac{C}{A}\right)$$

$$F = \frac{BC}{3A^2} - \frac{2B^3}{27A^3} - \frac{D}{A}$$

The cubic then becomes

$$y^3 - 3Ey - F = 0$$

This has a solution in

$$y = \sqrt[3]{\tfrac{1}{2}\left(F + \sqrt{G}\right)} + \sqrt[3]{\tfrac{1}{2}\left(F - \sqrt{G}\right)} \qquad \text{if } G \geq 0$$

$$y = 2\sqrt[3]{\tfrac{1}{2}\sqrt{F^2 - G}}\cos\theta \qquad \text{if } G < 0$$

where

$$G = F^2 - 4E^3$$

$$\theta = \frac{1}{3}\arctan\left(\frac{\sqrt{-G}}{F}\right)$$

Back substitution yields one root of the original cubic as x_1. Letting

$$H = B^2 - 4AC - 3A^2x_1^2 - 2ABx_1$$

the other two roots are given by

$$x_2 = \frac{-B - Ax_1 + \sqrt{H}}{2A}$$

and

$$x_3 = \frac{-B - Ax_1 - \sqrt{H}}{2A}$$

APPENDIX C: Turbo Pascal Element Type Declaration

```
TYPE    Region      = (Coal, Rock, Space);
        Modus       = (Intact, Broken);
        Place       = (Periphery, Internal);
        Boundary    = (FreeFace, Impermeable, ConstPressure, ConstPressGrad);

        ThreeDims   = RECORD
                X,Y,Z               : Real;
                    END;

        Ordinal3    = RECORD
                I,J,K               : Word;
                    END;

        CElmType    = RECORD
                Index               LongInt,
                Subscripts,
                NoOfElms            Ordinal3;
                Position,
                Delta               ThreeDims,
                GasPress,
                GasTemp             Real,
                CASE ElmType    . Region OF
                   Coal,Rock        (Lambda,
                                     PartDens       . Real,
                                     CASE State     Modus OF
                                        Intact      : (MoistCont,
                                                       YoungMod,
                                                       PoissRatio       : Real,
                                                       NormStress,
                                                       Permeablity
                                                       KlinkConst       ThreeDims,
                                                       CASE Locus       Place OF
                                                          Periphery     (Nature : Boundary)));
                   Coal             (VirgGasPress,
                                     DiffusCoeff,
                                     LangmuirC1,
                                     LangmuirC2     Real)
                     END, {CElement}

    DataBlock       = ARRAY [1..7,1..7,1..7] OF CElmType;
```

APPENDIX D: List of Numerical Simulators Assessed by King and Ertekin

Airey-1
Airey-2
ARRAYS(1D)
ARRAYS(2D)
Bayels et al
Bumb
Bumb et al
BOM (MINES1D)*
BOM (MINES2D)*
Chase
Chen*
COMET
Federov et al
Gorbachev et al
Intercomp-1*
Intercomp-2*
Karagodin et al
Kissell
Kovalev et al*
Kuchuk et al
Lindine et al*
McFall et al
McKee et al
Owili-Eger
Penn State-1
Penn State-2
Penn State-3
Penn State-4*
Serra et al
Smith et al
Spencer et al
SUGAR
SUGARMD
SUGARWAT
Nottingham-1
Nottingham-2
Vorazhtsov et al

* - Models used in comparison -ie those catering for dynamic mining activity

Details and specifications of these simulators can be found in the King and Ertekin survey (Reference [8])

REFERENCES

[1] Marais D. Practical Aspects of Methane Measurements. Symposium on Methane Detection and Explosion Prevention. The Mine Ventilation Society of South Africa, Johannesburg. 1988/1989.

[2] Viljoen PLJ. Case Histories and Preventative Measures with Relevance to Methane Ignitions/ Explosions. Symposium on Methane Detection and Explosion Prevention. The Mine Ventilation Society of South Africa, Johannesburg. 1988/1989.

[3] Phillips HR and Landman GvR. The Explosion Potential of Methane/Dust Mixtures at the Coal Face. Fifth International Mine Ventilation Congress. The Mine Ventilation Society of South Africa, Johannesburg. 1992.

[4] Stripp GP. Methane Emission Characteristics of South African Coal Seam Strata. PhD Thesis. University of the Witwatersrand, Johannesburg. 1989.

[5] Gardiner LR. Methanometry in Mining - A South African Case Study Symposium on Methane Detection and Explosion Prevention. The Mine Ventilation Society of South Africa, Johannesburg. 1988/1989.

[6] Kononov VA Infrared Methane Monitoring CSIR Division of Mining Technology Internal Report, Johannesburg. 1993

[7] Pardoe DR and Baker RH. An Analysis of Six Colliery Fires and Explosions with Reference to the Lifesaving Potential of Self-rescuers Coal Mining Laboratory, Chamber of Mines of South Africa Research Organisation, Johannesburg Research Report No 7/86 1985.

[8] King GR and Ertekin T. State-of-the-Art Modeling of Unconventional Gas Recovery. SPE Joint Rocky Mountain Regional/Low Permeability Reservoirs Symposium and Exhibition. Society of Petroleum Engineers, Inc , Denver, Colorado 1989

[9] Cook AP and Erwee EC Methane Properties of South African Coals Part 1: Sorption Characteristics Coal Mining, Chamber of Mines Research Organisation, Johannesburg. Reference Report No 16/91 1991

[10] Cook AP Methane Characteristics of the Coal Seams at Ermelo Mines Coal Mining, Chamber of Mines Research Organisation, Johannesburg Consultancy Report No 27/92. 1992

[11] Le Roux WL. Le Roux's Notes on Mine Environmental Control, 4th Edition The Mine Ventilation Society of South Africa, Johannesburg 1990

[12] Leibowitz AG. The Greenhouse Effect and the South African Coal Mining Industry Coal Mining, Chamber of Mines Research Organisation, Johannesburg Project Proposal Report No 30/91. 1991.

[13] De Wiest RJM (Ed) Flow Through Porous Media Academic Press New York 1969

[14] Cook AP The Methane-emission Characteristics of South African Coals MASSMIN '92 Symposium The South African Institute of Mining and Metallurgy Symposium Series S12, Johannesburg 1992

[15] Ozan TT The Determination of the Depth of Fractured Zones around Coal Pillars MASSMIN '92 Symposium The South African Institute of Mining and Metallurgy Symposium Series S12, Johannesburg 1992

[16] Ames WF. Numerical Methods for Partial Differential Equations. Thomas Nelson and Sons Ltd, London. 1969.

[17] Piaggio HTH. An Elementary Treatise on Differential Equations and their Applications. Bell's Mathematical Series, G Bell and Sons Ltd, London. 1958.

[19] Janas HF. Ermittlung des Flözgasdrucks anhand von Desorbomessungen (Seam Gas Pressure Determination by Desorption Measurements). Glückauf-Forschungshefte 54 Nr. 1. 1993.

[20] Hanson DR and Holub RF. Methane Release from Actively Yielding Coal and its Implications for Yield Zone Determination. International Journal of Rock Mechanics, Mining Science and Geomechanics, Vol. 27, No. 3. 1990.

[21] Linzer P. An Outline of the Adopted Strategy towards an Approximated Solution for a General State Methane Flow Model within a Coal Structure. Coal Mining, Chamber of Mines Research Organisation, Johannesburg. Technical Note No. 15/93. 1993.

[22] Budavari S (Ed). Rock Mechanics in Mining Practice The South African Institute of Mining and Metallurgy Monograph Series No 5, Johannesburg 1983

[23] Wylie Jr CR. Advanced Engineering Mathematics, 3rd Edition McGraw-Hill Book Company, Tokyo. 1966.

[24] Burden RL and Faires JD. Numerical Analysis Prindle, Weber & Schmidt, Boston, Massachusetts 1985

[25] Burrows J (Ed.). Environmental Engineering in South African Mines The Mine Ventilation Society of South Africa, Johannesburg 1982

[26] Salmon WI Structures and Abstractions - An Introduction to Computer Science with Turbo Pascal Richard D. Irwin, Inc , Homewood, Illinois 1992

[28] Collins J Data Structures - An Object Oriented Approach Addison-Wesley Publishing Company, Reading, Massachusetts 1992

[29] Weast RC (Ed) CRC Handbook of Chemistry and Physics, 63rd Edition, 1982-1983 CRC Press, Inc , Boca Raton, Florida 1982

[16] Ames WF. Numerical Methods for Partial Differential Equations. Thomas Nelson and Sons Ltd, London. 1969.

[17] Piaggio HTH. An Elementary Treatise on Differential Equations and their Applications. Bell's Mathematical Series, G Bell and Sons Ltd, London. 1958.

[19] Janas HF. Ermittlung des Flözgasdrucks anhand von Desorbomessungen (Seam Gas Pressure Determination by Desorption Measurements). Glückauf-Forschungshefte 54 Nr. 1. 1993.

[20] Hanson DR and Holub RF. Methane Release from Actively Yielding Coal and its Implications for Yield Zone Determination. International Journal of Rock Mechanics, Mining Science and Geomechanics, Vol. 27, No. 3. 1990.

[21] Linzer P. An Outline of the Adopted Strategy towards an Approximated Solution for a General State Methane Flow Model within a Coal Structure. Coal Mining, Chamber of Mines Research Organisation, Johannesburg. Technical Note No. 15/93. 1993.

[22] Budavari S (Ed.). Rock Mechanics in Mining Practice. The South African Institute of Mining and Metallurgy Monograph Series No. 5, Johannesburg. 1983.

[23] Wylie Jr CR. Advanced Engineering Mathematics, 3rd Edition. McGraw-Hill Book Company, Tokyo. 1966.

[24] Burden RL and Faires JD. Numerical Analysis. Prindle, Weber & Schmidt, Boston, Massachusetts. 1985.

[25] Burrows J (Ed.). Environmental Engineering in South African Mines. The Mine Ventilation Society of South Africa, Johannesburg. 1982.

[26] Salmon WI. Structures and Abstractions - An Introduction to Computer Science with Turbo Pascal. Richard D. Irwin, Inc., Homewood, Illinois. 1992.

[28] Collins J. Data Structures - An Object-Oriented Approach. Addison-Wesley Publishing Company, Reading, Massachusetts. 1992.

[29] Weast RC (Ed.). CRC Handbook of Chemistry and Physics, 63rd Edition, 1982-1983. CRC Press, Inc., Boca Raton, Florida. 1982.

APPENDIX B5

REPORT BACK OF EUROPEAN VISITS TO DETERMINE THE POSITION OF THE MININGTEK'S METHANE EMISSION MODEL

PREAMBLE

A twofold purpose was served by the visits undertaken by Mr Linzer during September 1995. Firstly, a technical paper authored by Mr Linzer was presented at the 26th International Conference of Safety in Mines Research Institutes held in Katowice, Poland during the first week of September. The prime objective of the remaining visits to various institutes was to determine the merit of the theoretical considerations employed in the derivation of Miningtek's methane emission simulator and to gauge this work against similar work undertaken or currently in progress in Europe. Below is a brief summary of the salient points raised at each location.

(1) 26th INTERNATIONAL CONFERENCE OF SAFETY IN MINES RESEARCH INSTITUTES (POLAND)

Subsequent to the presentation of his paper, Mr Linzer was invited by Professor Noack of the German company D.M.T. to join a special interest group which he directed. This interest group's purpose is to consolidate and disseminate the latest developments in all areas of computational fluid dynamics throughout the world from and to interested parties.

Personal communications with delegates from Germany, UK and Poland did not reveal any instances of similar work currently in progress in any of these countries. In Germany and Poland, empirical and semi-empirical models are used by some organisations, but generally their application is very limited, since they are recognised to be relatively inaccurate. More commonly, the accepted practise is to measure or estimate seam gas contents and to design ventilation quantities to deal with the expected gas emissions at peak production rates.

(2) UNIVERSITÉ DE LOUVAIN (BELGIUM)

A senior lecturer in the Department of Thermodynamics, Dr E. J. Jacques, had received a copy of the draft report titled "A General State Model of Methane Transport in Coal Structures" (Linzer, 1994) at the 7th US Mine Ventilation Symposium (Lexington 1995) for the purposes of evaluation thereof. He was visited in order to obtain feedback on this report, as well as to provide information on similar work being done by one of his students. His assessment was that the emission model described in the report was more sophisticated than most other models of its type he had come across. He anticipates that the computerisation thereof will present difficulties.

Regarding the work done by his student, this is limited in scope to the emission of seam gases into shafts and tunnels during their excavation and is thus of relatively little use to South African collieries. Dr Jacques is not aware of any other similar work currently in progress anywhere in Europe.

(3) INERIS (FRANCE)

Mr C. Tauziède (Department Head - Surface and Underground Ecosystems) had also received a copy of the report mentioned in (2). His assessment of the work was that it is sufficiently complex in the sense that it accounts for most of the known influences in order to provide answers of good accuracy, and at the same time sufficiently general to accommodate any practical mining situation. He expressed surprise that the report was the work of one person only.

Mr Tauziède is not aware of any similar work currently in progress anywhere in Europe, but handed over a copy of a report on work completed by INERIS in 1988 on a numerical simulator for

modelling gas drainage via boreholes. He mentioned that the simulator was not very successful, and that no further work along these lines was planned.

(4) BRUNEL UNIVERSITY (ENGLAND)

Dr D. W. Dixon, a lecturer in the Department of Mechanical Engineering, Brunel University, had also received a copy of the report mentioned in (2). He was very impressed with the novel treatment of permeability, the inclusion of random variations as a facility of the model and the compactness of the overall model formulation. He did, however, express reservations about the computerisation thereof - he feels that the phenomenal number of calculations required by the model may not render a personal computer an optimal platform for the model. It is his opinion that a more powerful computer (eg. a Sun Box) might be required. He expressed surprise that this work was not being done towards a PhD degree.

Dr Dixon asserted that to the best of his knowledge no similar work was currently in progress in Europe. He said that the (British) National Coal Board at one time used an empirical model to gauge seam gas emissions into underground workings, but the accuracy of this model left a great deal to be desired. He also is of the opinion that Miningtek's work may in the future be of appreciable value in Europe, since he predicts an increase in European coal production and a commensurate increase in private mining consultancies who would use the work.

(5) IOM (SCOTLAND)

Dr A. Jones of the Institute of Occupational Medicine, Edinburgh, had also received a copy of the report mentioned in (2). He had been requested to examine the report for both mathematical correctness and consistency as well as overall report clarity. He had identified two instances in the report which appear to be mathematically deficient. One of these resulted from a misunderstanding on his part, and is correctly formulated in the report. The other is in fact a mathematical deficiency in the differential equation describing diffusion in a pyramidal region, but no revision of the model is necessary as a result of this, since the difference equations that were derived for the numerical solution incorporate the omitted effect.

Dr Jones' found the report generally clear and interesting and has forwarded a further copy to Dr J. Edwards of Nottingham University.

APPENDIX B6

EVALUATING THE METHANE GAS CONDITIONS IN UNDERGROUND SOUTH AFRICAN COAL MINES

Alan P. Cook

Coal Mining division, COMRO, Johannesburg, South Africa

The Coal Mining division of COMRO has developed a range of *in situ* and laboratory techniques to quantify the methane conditions on collieries. *In situ* measurements are made of seam gas pressures, in-seam gas flow velocities and directions, as well as methane drainage volumes. Seam pressures are measured using borehole packers, and in-seam flow using packers in conjunction with SF_6 tracer gas. Methane drainage is monitored in terms of pressure decay and volume flowrate. South African seam pressures are rarely above 1000 kPa, with corresponding contents of 8 m^3/t. Methane drainage rates average 440 $m^3/m/year$. Methane adsorption and desorption potentials are determined using a gravimetric sorption laboratory. South African coals exhibit adsorption potentials similar to those of coals from other countries, but have slower desorbing rates.

INTRODUCTION

To fully understand the behaviour and movements of methane within a coal seam it is necessary to identify and quantify several individual parameters. These are the methane adsorption and desorption potentials of a coal; the macropore and micropore flow characteristics; and the methane pressure and content of a coal seam. These all combine to govern the methane characteristics of a seam. The Coal Mining division (CM) of COMRO has developed a range of *in situ* and laboratory techniques which measure these parameters for coals and coal seams.

In situ techniques make use mostly of boreholes and borehole packers. These are used to identify seam pressures and methane flow directions within a seam, or surrounding strata. Laboratory techniques make use of a gravimetric sorption laboratory, where the methane properties of a coal are obtained by adsorbing and desorbing methane under controlled conditions.

The effects of each of the individual parameters are combined mathematically to model methane flow within and emission from a seam.

UNDERGROUND TECHNIQUES

Boreholes are a relatively simple means of gaining access to coal seams or surrounding strata underground. They can be drilled either horizontally or vertically, and then equipped to monitor pressures, pressure decays, flowrates and flow directions. Inflatable borehole packers provide a suitable means of sealing holes to monitor pressures, and can be used in conjunction with a tracer gas to obtain flow directions. Borehole flowrates are measured with rotameter type flowmeters.

Borehole Packers

CM has several types of borehole packer available, three developed by the division and three others commercially available. All are reuseable, and are inflated with inert nitrogen gas when installed. Essentially they comprise of an inflatable rubber tube, sealed at the ends, with

trailing lines for inflation and pressure monitoring, see Figure 1. Those developed by CM are 70 mm diameter for use in boreholes of 80 mm. They are pushed into position in a borehole using extension rods that screw togethe

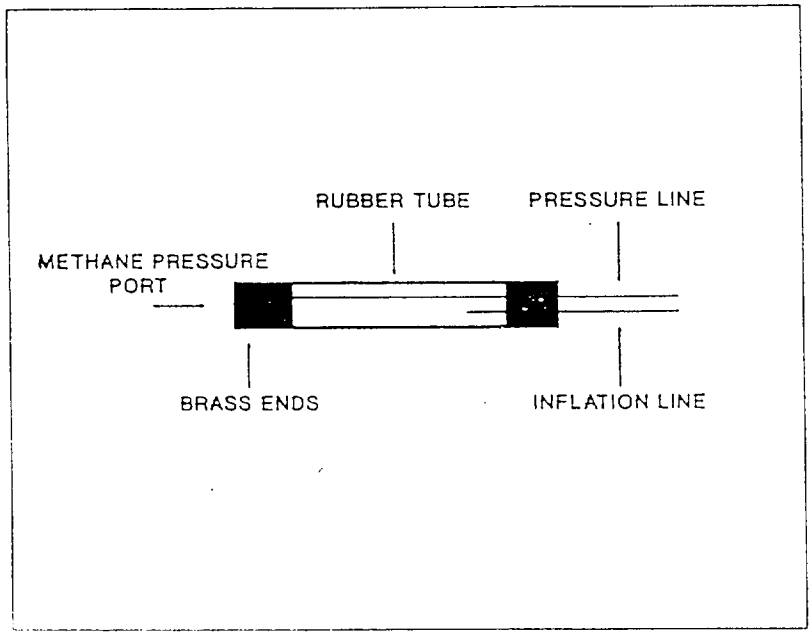

Figure 1. SCHEMATIC INFLATABLE BOREHOLE PACKER

Single Packers. These are used to seal off a length of borehole beyond the packer itself, and measure gas pressure over that length of the borehole, see Figure 2. They can be installed horizontally or vertically, with the vertical application normally being to just below an adjacent seam. Pressure is measured through a port in the end of the packer.

Double Packers. These comprise two inflatable sections, with the methane monitoring point between the two, see Figure 3. This enables the pressure at an exact position in a hole to be obtained. This, for example, is applicable to measuring pressure gradients with distance into sidewall or roof.

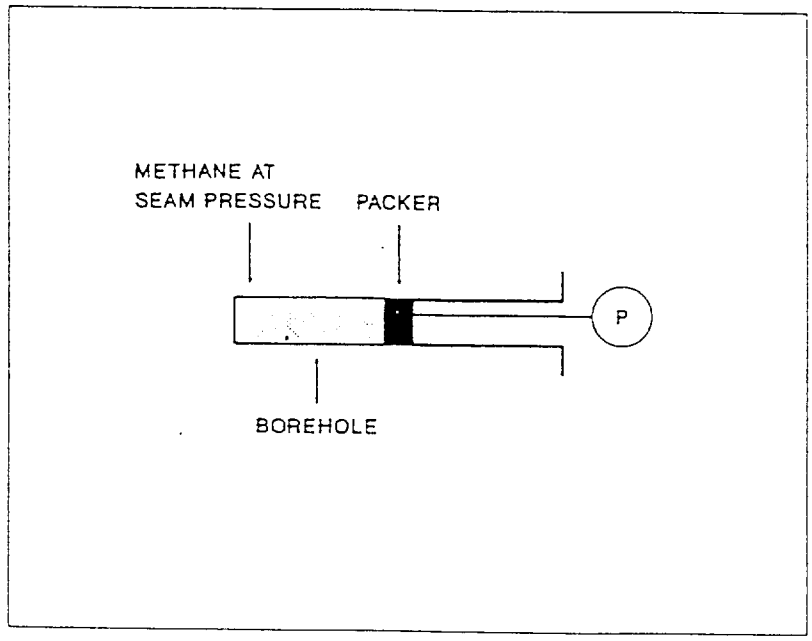

Figure 2. SINGLE PACKER

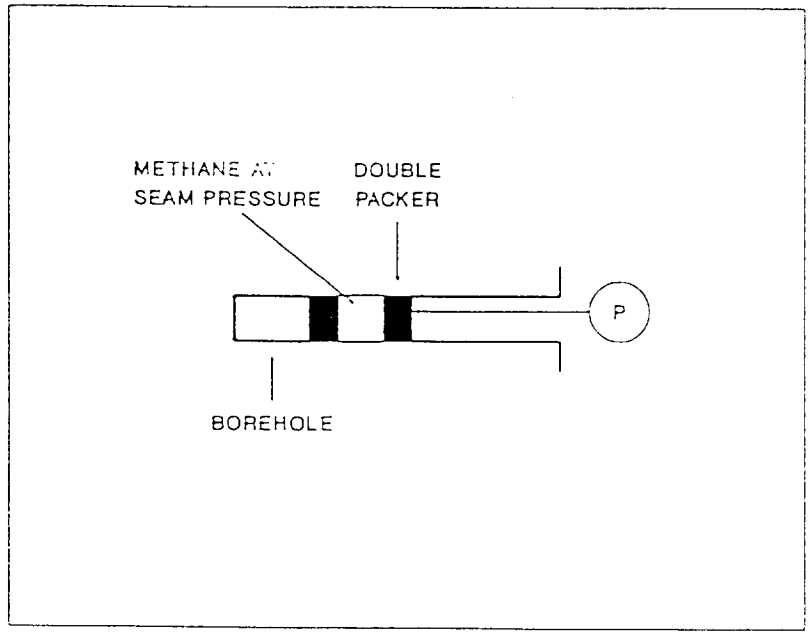

Figure 3. DOUBLE PACKER

Series Packers. These have been developed to permit simultaneous measurement of pressure at several points within a borehole, see Figure 4.

Each of the packers can be used separately, or as one of a series of up to five.

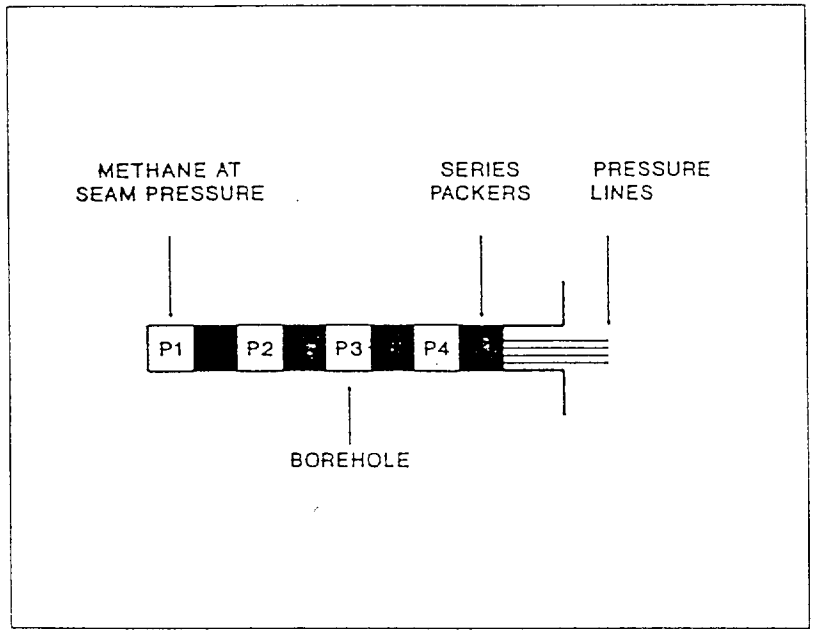

Figure 4. SERIES PACKERS

Tracer Gas

Tracer gas inserted into a seam is carried by the free methane as it flows through the micropore fracture system. It can be used to measure both flow directions and flow velocity, and this is combined with a known pressure difference to calculate the fracture permeability. CM uses sulphur hexafluoride (SF_6) as it is an artificial gas, detectable in parts per trillion.

Figure 5 shows a simple method to monitor velocity and permeability. Two parallel borehole are drilled and one is sealed with a packer. Whe the pressure has stabilised, tracer gas is injected through the packer, and gas samples collected, a regular time intervals, from the other hole. Thes are analysed for SF_6 content and the gas velocity thus obtained from the time of arrival and the distance travelled. This has been used successful to measure the increase in permeability followin borehole fracturing to attempt to increase methane drainage flow.

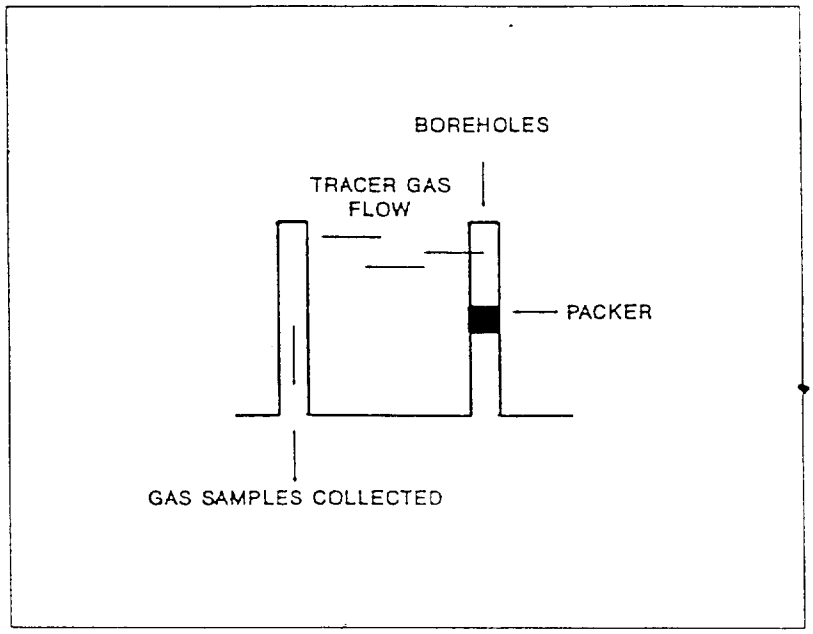

Figure 5. MONITORING IN-SEAM FLOW VELOCITY

Figure 6 shows a test carried out to monitor in-seam flow directions. Tracer gas was injected at the centre hole, of a network of bleeder holes, drilled vertically up from a production seam through a 1 m parting and into a roof coal seam. Gas samples were collected at each of the other holes and analysed for tracer gas, which allowed contours to be plotted for the gas flow, some examples of which are shown in Figure 7 (Leibowitz and Cook, 1992).

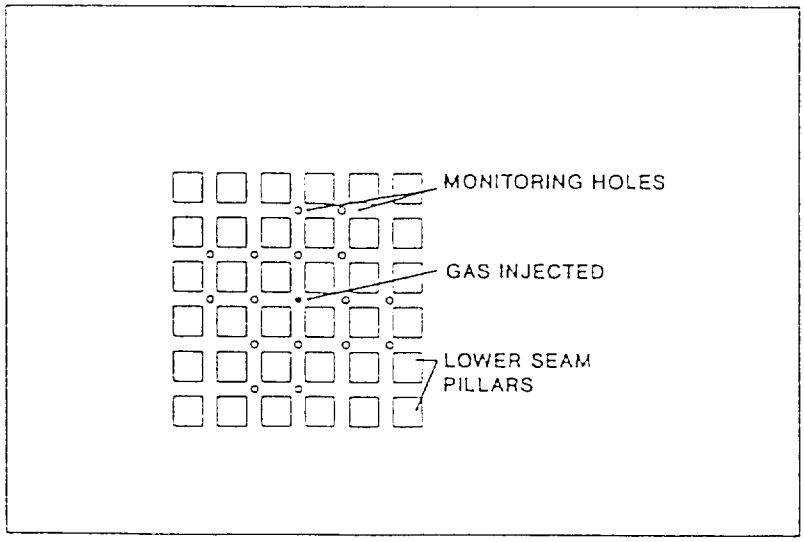

Figure 6. MONITORING IN-SEAM FLOW DIRECTIONS

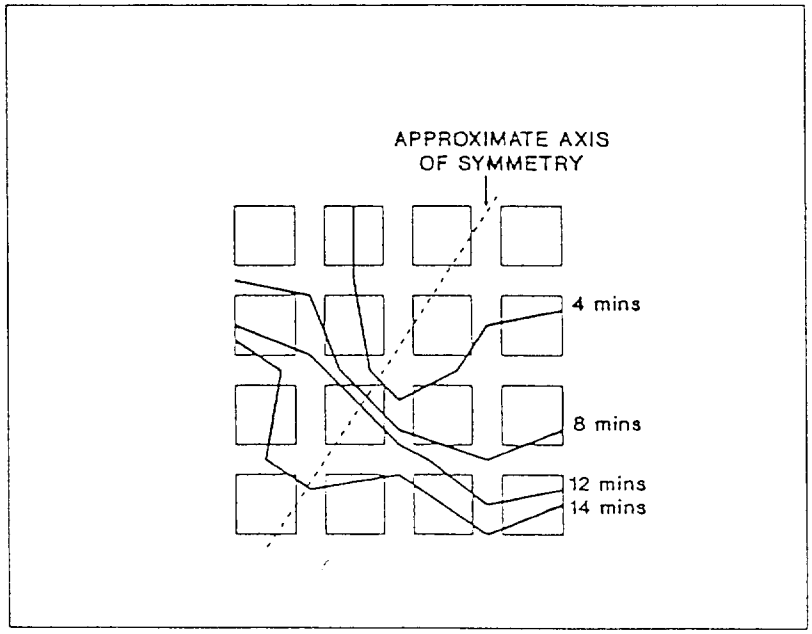

Figure 7. IN-SEAM FLOW CONTOURS

Interference tests

Borehole interference tests are a relatively simple means of optimising drainage borehole spacing. A series of parallel boreholes is drilled and all are sealed, either with packers or standpipes. When the pressures have stabilised one of the holes is opened and pressure decays monitored in the others. The rate of pressure drop at different radii from the open hole is obtained, and this is used to predict the spacing required between boreholes, depending on the draining time available. Figure 8 shows typical results, with the effect of increasing distance seen by the reduced pressure drops at greater distances. The pressures do however gradually all reach the same levels, in this case taking about 100 days.

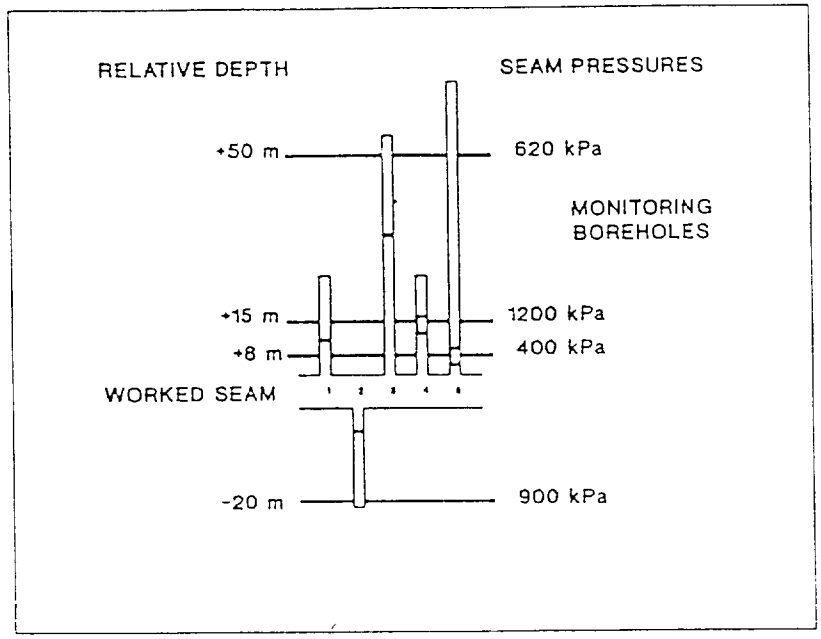

Figure 9. SEAM PRESSURES IN SURROUNDING SEAMS

Methane Drainage Rates

Methane drainage is not yet widely practised in South African mines, but the interest is increasing, particularly as a localised necessity for high methane areas. Monitoring is presently being carried out of an existing methane drianage network, comprising numerous in-seam horizontal boreholes linked to a central drainage column to surface. Flowrates from the boreholes are measured using a rotameter flowmeter installed between the borehole and the drainage column.

Specific volume flowrates (m^3 of gas drained per metre length of borehole per year) range from less than 100 $m^3/m/yr$ to more than 900 $m^3/m/yr$, with the average being 440 $m^3/m/yr$. Table 1 shows typical range of flowrates for a number of holes draining at any one time. These values are considerably lower than those reported for US and European mines, but may not be reprentative of SA as a whole as the values are for a low permeability seam.

Table 1. SPECIFIC VOLUME FLOWRATES

B/H No	LENGTH (m)	FLOW (m^3/hr)	SPECIFIC FLOWRATE (m^3/m/y)
A	137	5	320
B	279	15	471
C	228	10	384
D	564	30	466
E	859	10	102
F	597	5	73
G	285	30	922
H	996	40	352
I	306	30	859

LABORATORY TECHNIQUES

All laboratory results are obtained from the gravimetric sorption apparatus shown in Figure 10. Coal samples are crushed and sieved to 200 μm, sealed in the test capsules and pressurised with methane at a set temperature. The mass of methane adsorbed by the coal at a range of pressures (usually up to 4 MPa) is used to plot an adsorption isotherm, before the methane is desorbed to atmosphere to get the desorbing rate. The desorption rate is then used to calculate a diffusion coefficient (D) which is a mathematical definition of the rate of methane diffusion through the micropores of the coal. The apparatus and procedures are described in more detail by Erwee and Cook, 1991.

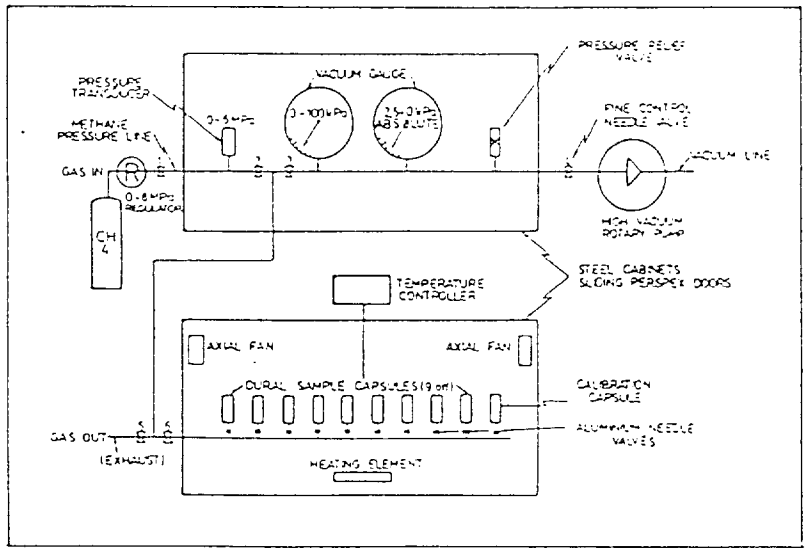

Figure 10. GRAVIMETRIC SORPTION LABORATORY

SOUTH AFRICAN COAL METHANE CHARACTERISTICS

Adsorption Potentials

Figure 11 shows a range of adsorption curves for SA coals, tested at 20°C. The curves are not dissimilar to those for similar type coals in other countries. So the adsorption properties of the coals themselves are no different, only the actual *in situ* circumstances affect the methane conditions in South Africa compared to other countries.

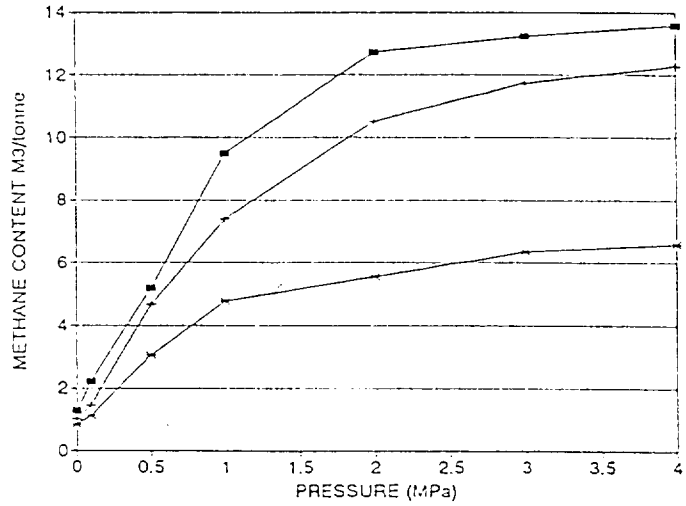

Figure 11. ADSORPTION CURVES

Diffusion Coefficients

Figure 12 shows the range of diffusion coefficients for SA coals. The majority (approximately 2/3) lie within the range of E-09, with the remainder less than this. The lower the value the slower the diffusion rate of methane. A generally quoted value for calculation purposes is E-10, so the results are not too dissimilar from this. However, values quoted for US coals are E-07 (Kissel and Bielicki, 1972) and for Australian coals are E-04 (Lama and Nguyen, 1987), considerably faster. It would appear therefore that SA coals tend to have a relatively slow potential for methane diffusion.

Fracture Network Size

Also important for calculating the rate of methane release from coal is the effective methane diffusing distance, or the fracture network size (FNS). This is the distance between the microfractures in a coal, consisting of the micropores of the coal containing the adsorbed gas.

By testing the rate of methane adsorption and desorption across coal particle sizes ranging from 200 um to 10 000 um, the fracture network size for three SA coals has been obtained, and all are around 3 mm (Cook, 1992).

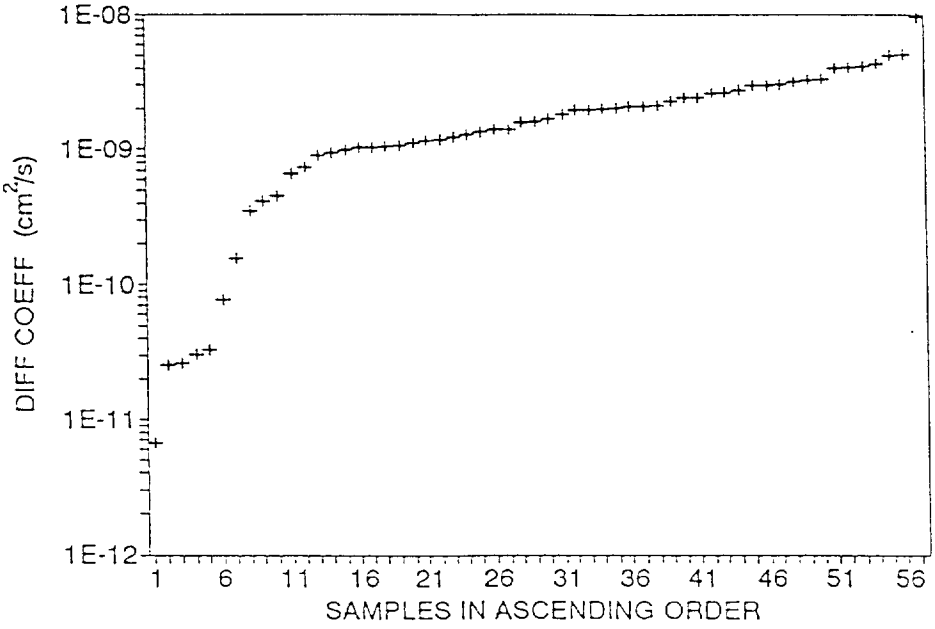

Figure 12. DIFFUSION COEFFICIENTS

MATHEMATICAL MODELLING

The main objective of quantifying each of the individual parameters is to be able to predict methane emission rates from coal seams. The models being developed combine the effects of the parameters and how they interact, considering basically two distinct flow regimes within a seam; diffusive flow within the micropore matrix, and permeable flow within the macropore structure, with sorption processes as a link between the two. This is based on four basic assumptions (Linzer, 1993):

1) Methane diffuses through the micropore network of the coal matrix on the basis of the instanteneous concentration gradient, which is governed by the initial concentration within the matrix and the concentration on the surface of a (homogeneous) element.

2) The outer surface of each such coal matrix element is a boundary of the macropore network, the gas pressure in which governs the concentration of methane on this outer surface by sorption.

3) The pressure distribution within the macropore network in turn determines the behaviour of the gaseous methane confined therein by permeable flow.

4) The geometry, coal seam, roof and floor properties and initial conditions determine the pressure distribution in the macropore network of the coal, and determine the gas emission for this coal structure.

The models will be suitable for both prediction from exposed faces into workings, and for flowrate prediction from boreholes and the effect this will have on the surrounding coal seam.

CONCLUSIONS

It is possible to quantify the methane characteristics of coals and coal seams using the laboratory and *in situ* techniques developed by the Coal Mining division of COMRO. The laboratory determines the sorption and diffusive properties of a coal, and underground methods measure the pressure and permeability of a seam.

Inflatable packers make effective gas seals in boreholes and can be used to measure pressures and pressure decays. Injecting tracer gas through the packers allows both methane flow velocity and direction to be monitored.

Seam gas pressures in South African collieries are generally below 1000 kPa, but pressures of 1600 kPa are measured at 300 m depth. These pressures correspond to gas contents of up to 12 m^3/t, but these are more commonly less than 8 m^3/t. Methane drainage rates from in-seam boreholes average 440 $m^3/m/year$, substantially less than those of other countries.

Diffusion coefficients range from E-12 to E-09, indicating relatively slow methane diffusive rates through the micropores of the coals. This tends to support the low methane drainage rates. Adsorption potentials of the coals are similar to those of coals from other countries.

REFERENCES

Cook, A.P., 1992, "The Methane Emission Characteristics of South African Coals", Proceedings, MASSMIN 92, Johannesburg, SAIMM, 1992. pp 469-472.

Erwee, E.C., and Cook, A.P., 1991, "Methane Sorption Properties of South African Coals and Their Determination by Means of a Gravimetric Sorption Laboratory", Proceedings, 24th International Conference of Safety in Mines Research Institutes, Donetsk USSR, 1991. Part 1 pp 48-57.

Kissel, F.N., and Bielicki, R.J., "An *In Situ* Diffusion Parameter for the Pittsburgh and Pocahantas No.3 Coalbeds", USBM Report of Investigation RI 7668, 1972.

Lama, R.D., and Nguyen, V.U., 1987, " A Model for Determination of Methane Flow Parameters in Coal From Desorption Tests", Proceedings, Twentieth International Symposium on the Application of Computers and Mathematics in the Mineral Industries, Johannesburg, SAIMM, 1987. Volume 1: Mining pp 275-282.

Linzer, P., 1993, "An Outline of the Adopted Strategy Towards an Approximated Solution for a General State Methane Flow Model", CM Technical Note SC9314 No.93/15 (Restricted), COMRO, Johannesburg, 1993.

Leibowitz, A.G., and Cook, A.P., Proceedings, "The Directional Dependence of Coalbed Permeability and Its Implications for Methane Emission Into Workings", 5th International Mine Ventilation Congress, Johannesburg, 1992.

APPENDIX B7

TYPICAL VALUES FOR SOUTH AFRICAN COAL PROPERTIES AS METHANE EMISSION PREDICTION MODEL INPUTS.

			Diffusion	Bulk	Proximate analysis (%)			Fixed
	Langmuir constants:		Coefficients	Density	Moisture	Volatiles	Ash	carbon
Mine No.	k1=(m^3/t)	k2=(1/kPa)	cm^2/s	g/cm^3	%	%	%	%
1	14.07	1.064	2.070E-09	1.34	2.5	29.1	16.2	52.2
2	10.48	0.988	3.230E-09	1.52	3.4	26.3	23.4	46.9
3	11.30	1.328	1.460E-09	1.36	1.7	38.4	18.7	41.2
4	11.96	1.392	1.440E-09	1.31	1.7	35.2	18.0	45.1
5	10.85	1.243	1.750E-09	1.42	1.7	27.3	20.9	50.1
6	11.33	1.714	1.500E-09	1.39	2.0	24.2	22.2	51.6
7	10.81	1.122	3.660E-10	1.77	2.6	14.6	57.0	25.9
8	6.24	1.705	2.300E-09	1.98	2.8	16.2	51.1	29.9
9	7.15	2.278	1.590E-09	1.77	2.2	34.4	20.5	42.9
10	16.29	1.175	1.800E-09	1.47	1.5	31.2	7.7	59.6
11	18.48	1.007	2.080E-09	1.36	2.7	22.1	31.7	43.5
12	14.64	1.049	1.350E-09	1.55	2.1	21.2	28.0	48.7
13	10.90	1.059	5.720E-09	1.39	2.0	44.4	16.4	37.2
14	14.64	1.049	9.420E-10	1.68	1.9	19.2	32.5	46.4
15	13.15	0.525	1.190E-09	1.74	1.4	14.2	46.3	38.1
16	14.93	0.691	1.410E-09	1.94	1.9	18.1	32.8	47.2
17	15.20	1.075	5.790E-10	1.33	2.6	24.4	28.7	44.3
18	12.24	1.011	1.020E-09	1.42	2.6	22.3	33.3	41.8
19	8.31	1.809	1.610E-09	1.47	5.5	11.9	28.1	54.5
20	21.64	0.526	1.840E-09	1.43	5.8	12.3	25.0	56.9
21	9.55	1.239	1.440E-09	1.43	5.7	9.3	28.2	56.8
22	15.20	1.075	6.860E-10	1.56	3.2	17.1	22.1	57.6
23	16.05	1.610	2.790E-10	1.55	3.2	31.0	21.8	44.0
24	13.20	1.473	2.370E-10	1.47	3.8	21.9	17.8	56.5
25	13.63	0.916	4.330E-09	1.67	1.6	34.5	27.0	36.9
26	7.78	0.822	9.910E-10	1.68	1.1	35.7	38.9	24.3
27	13.50	0.989	1.160E-09	1.34	1.2	28.1	21.1	49.6
28	10.42	1.365	1.110E-09	1.45	1.1	9.3	30.9	48.7
29	13.93	0.645	3.550E-09	1.43	4.1	17.6	27.2	51.1

APPENDIX C

C1. A.P. Cook, Methane Safety Research for Continuous Miners in South Africa, 7th US Mine Ventilation Symposium, June 1995, CSIR Division of Mining Technology.

C2. A.P. Cook, Simulations of Methane Flow Around a Continuous Miner Part 1 : Comparison with Dust Flow for a Full Heading Development with Jet Fan Ventilation, Interim Report, July 1994, CSIR Division of Mining Technology.

C3. A.P. Cook, Simulations of Methane Flow Around a Continuous Miner Part 2 : Full Split Development with Jet Fan Ventilation, Interim Report, September 1994, CSIR Division of Mining Technology.

C4. A.P. Cook and C.F. Meyer, Simulations of Methane Flow Around a Continuous Miner Part 3 : Different Heading Development Stages with Jet Fan Ventilation, Interim Report, November 1994, CSIR Division of Mining Technology.

C5. F.J. van Zyl, Methane Monitoring Around an Operational Continuous Miner at Mine A, Technical Report, October 1994, CSIR Division of Mining Technology.

C6. F.J. van Zyl, Methane Monitoring Around an Operational Continuous Miner at Mine B, Technical Report, December 1994, CSIR Division of Mining Technology.

C7. F.J. van Zyl, Methane Monitoring Around an Operational Continuous Miner at Mine C, Technical Report, September 1994, CSIR Division of Mining Technology.

C8. C.F. Meyer and F.J. van Zyl, Methane Simulations Around a Continuous Miner Part 4: Comparison of Methane Behaviour Under Various Ventilation Conditions in a Partially Developed Heading, Interim Report, December 1995, CSIR Division of Mining Technology.

APPENDIX C1

Chapter 9

METHANE SAFETY RESEARCH FOR CONTINUOUS MINERS IN SOUTH AFRICA

Alan P. Cook

CSIR Miningtek, Johannesburg, South Africa

Methane levels have been measured around continuous miners and compared with computer simulations of methane flow. A multi-channel data logger, reading continuously from six methanometers, has shown methane levels to vary at different positions around a continuous miner, with the cutting drum and the immediate face area not necessarily recording the highest concentrations. Methane levels in the driver's cabin are generally low compared with the return side. Computer simulations, using computational fluid dynamics, have been supported by the measured data, and have shown that methane behaviour within the first few metres of the face varies considerably for different bord and pillar development stages. Methane is diluted rapidly to acceptable levels, but the distance required for this is extended when ventilation flow to the face is restricted.

INTRODUCTION

Methane ignitions caused by cutting picks during mechanised mining operations remain a hazard both in South African and worldwide coal mining. A significant proportion of South African methane and explosion research carried out by Miningtek (the CSIR Division of Mining Technology) is therefore directed at reducing the number of these incidents, with a major objective being improved methane monitoring on and around continuous miners. The initial work is to quantify methane flow and behaviour around continuous miners during mining, and then to optimise monitoring positions and procedures.

Quantifying methane requires the ability to monitor effectively at various positions during mining, and to do this an intrinsically safe data logger has been built which presently records from six methanometers throughout a shift.
The recorded data are compared with computer simulations generated through computational fluid dynamics (CFD), and the CFD can then used to quickly evaluate differing mining and ventilation conditions.

METHANE MONITORING AND DATA LOGGER SYSTEM

The system presently consists of six methanometers connected to an intrinsically safe multi-channel data logger. It was designed and constructed by Miningtek specifically for use on and around continuous miners, but can be applied in any underground situation, and with any suitable output sensors.

The methanometers operate continuously, and the logger reads from each of them every 10 seconds. Power consumption and data memory were designed to give 10 hours of continual operation under these conditions, but a maximum of 10 days can be obtained with reduced sensors and extended sampling intervals.

Figure 1 is a diagrammatic representation of the system showing the methanometers, connected by 12 m cables to the main case which houses the battery, recording station and data logger. Sampling intervals and data calculations for the logger are programmed from a PC, and the data downloaded to a PC via a milking station.

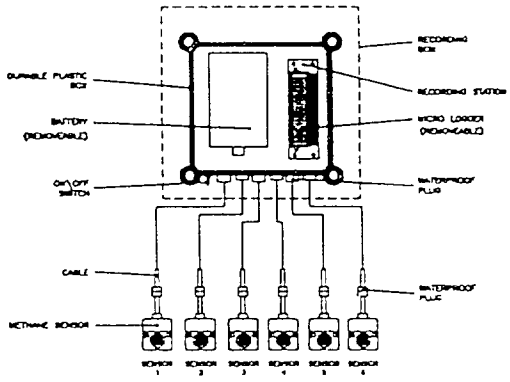

Figure 1. DATA LOGGER AND SENSORS

The sensors are positioned on the CM to give comparative methane levels between easily accessible positions, such as the driver's cab, and less accessible positions such as close to the cutting drum. The six positions used in the tests reported here are shown in Figure 2. Two sensors were positioned as close to the drum as possible, either side of the boom; one at the scrubber intake; one at the cab; one mid way down on the left hand (return) side of the boom; and one at the left rear. Results are from a CM equipped with a directional spray system, an on-board scrubber, and with additional force ventilation from a jet-fan.

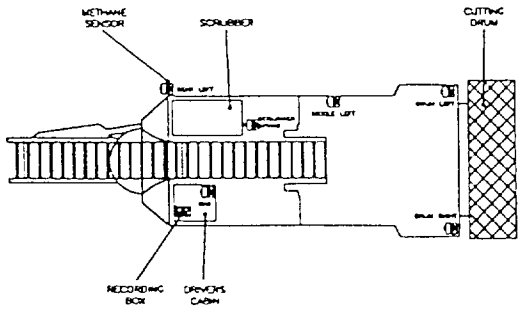

Figure 2. SENSOR POSITIONS ON CM

METHANE LEVELS AROUND CONTINUOUS MINERS

Results from on-board methane monitoring are given in Figures 3 - 6. These show plots of methane concentrations against time, measured at the six positions. Figures 3 and 4 are for two hour periods, and figure 5 and 6 for full shifts.

Figure 3 gives results cutting first a left hand pass, and then a right side pass. Mining the pass began at approximately 09:40 and 10:40 respectively, and in both cases methane levels show a slight upward trend as the CM advances. Levels are generally between 0.2 % and 0.7 %, with a peak at the drum left sensor of 1.3 % at the completion of the first pass. A little surprising is the mininmal difference in methane levels between the passes, as during the first, the CM is confined, and ventilation more restricted. There is no significant differences between the six sensor positions, although the drum left and middle left sensors are generally highest, with the cabin recording lowest. The cabin sensor was positioned beside the driver's own methanometer, so his readings were continually less than the levels around the drum.

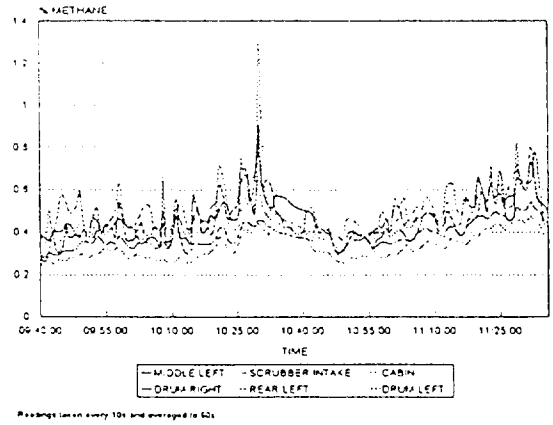

Figure 3. METHANE LEVELS AROUND CM

Figure 4 also shows a two hour period, but with greater variation between the sensors. The methane range is from 0.1 % to 0.5 %, with a peak at 0.6 %. The highest readings are from the middle left and scrubber intake sensors, with the left and right drums being lowest. This indicates that methane is

being removed from the face to the return side of the CM by the face scraping action of the directional sprays. This result has also been seen in the CFD simulations for headings.

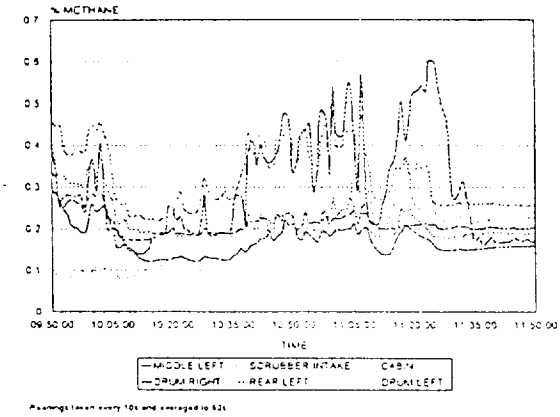

Figure 4. METHANE LEVELS AROUND CM

Figure 5 shows results over a six hour period, with methane readings from 0.05 % to 0.5 %, but with distinct differences between the six sensor positions. The highest levels are recorded at the scrubber intake, but the lowest at the middle left. However it is likely that the middle left had become choked with dust and sludge by this point of the test. During the next shift it again began functioning correctly after cleaning. The cabin recorded second highest with the drum sensors again being low.

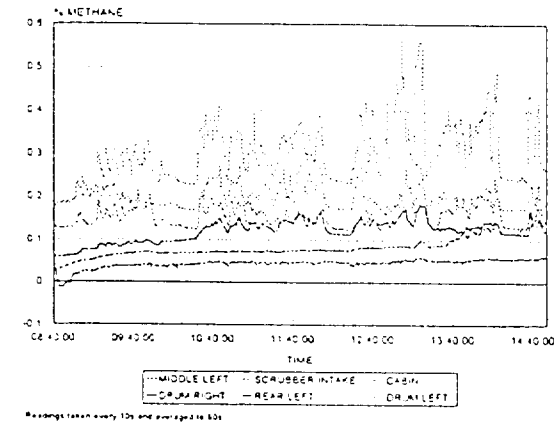

Figure 5. METHANE LEVELS AROUND CM

Figure 6 shows results over a seven hour period, and from a week later than those in Figure 6. By this time four of the sensors were still functioning well, but the two at drum left and middle left were recording consistently low, again due to lack of maintenance on these two sensors which were blocked.

Methane levels are considerably higher, with the cabin recording between 1 % and 3 %, and the drum right recording between 1 % and 2 %. Both these sensors were functioning well and within calibration limits, so there is no reason to doubt the readings. The return side sensors, at the scrubber and rear left, show much lower levels. Unfortunately there is no record of what operations the CM was carrying out during this period, or of the ventilation conditions, but the normal intake side to return side methane readings were reversed. Similar levels of methane were recorded on other shifts, but on the return side of the CM; as yet however, there is insufficient data to confirm how common these levels are around CMs.

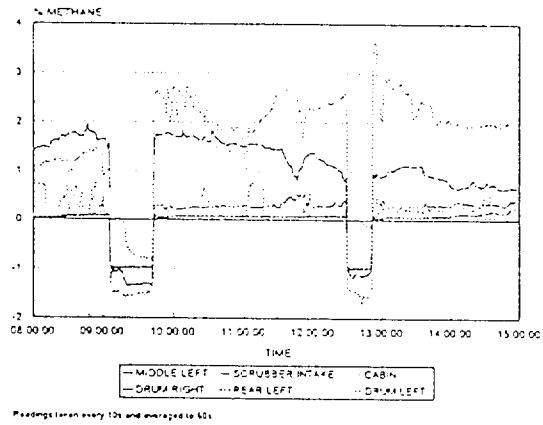

Figure 6. METHANE LEVELS AROUND CM

SIMULATIONS OF METHANE FLOW

Computer simulations are also carried out using CFD. The work forms part of a project comparing and evaluating different ventilation practices for continuous miner sections. Methane simulations have been completed for fully and partially developed headings and splits using jet-fan ventilation. Results are produced as velocity flow vectors for ventilation, and as percentage contours for methane.

Figures 7 - 11 show examples of the type of result obtained for a CM with a shuttle car (SC) positioned immediately behind it. The methane percentages in the figures are approximately three times higher than those measured underground. This is because the emission rates were exaggerated in the simulations to ensure sufficient contours to identify methane flow patterns.

Figure 7 shows velocity vectors taken on a horizontal plane in a full heading at operator height. Last through road velocity is right to left with the jet fan on the floor at the right hand side of the heading. The longer vectors along the right sidewall are the influence of the jet-fan, and those returning over the shuttle car are from the scrubber.

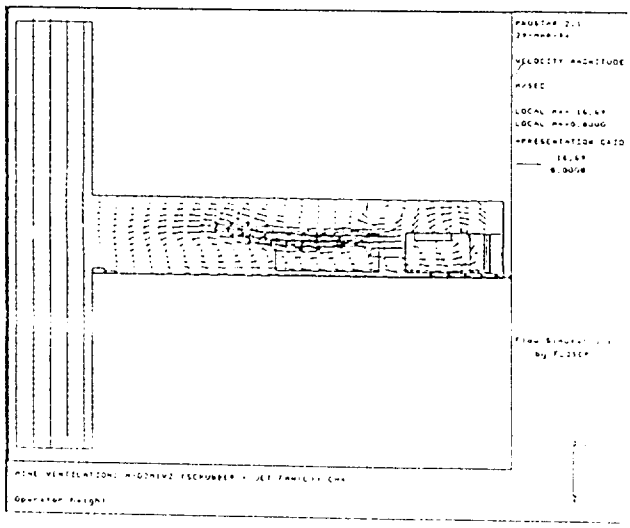

Figure 7. VELOCITY VECTORS, FULL HEADING

Figure 8 shows methane contours at operator height for a heading. The highest levels are to the left side of the drum. These are from methane released immediately on the drum and removed by the directional sprays. The contours then continue along the left side of the CM, similar to the high methane levels recorded at the mid boom position with the data logger.

Figure 9 shows a three-dimensional view of a partly developed heading with methane contours of methane released at the face, mostly from the immediate vicinity of the cutting drum. The highest methane contours are all confined to the first few metres, around the drum and boom, with levels dropping rapidly to a general body level of about 0.5 % in the heading.

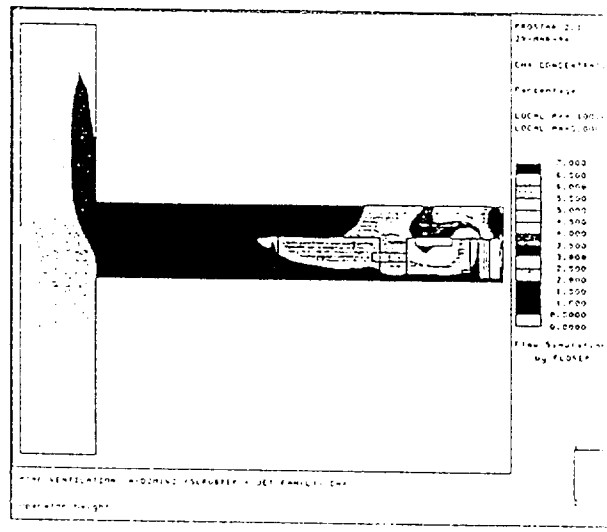

Figure 8. METHANE CONTOURS, FULL HEADING

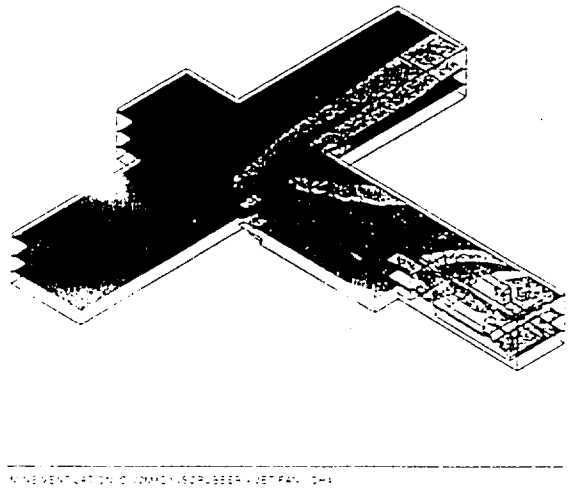

Figure 9. METHANE CONTOURS, PARTLY DEVELOPED HEADING

Figures 10 and 11 show detail around the CM and SC for a fully developed split to the right; only the face area is shown. Methane contours are given on horizontal planes in Figure 10 and vertically in Figure 11. The methane levels drop within the first few metres of the face to below 1 %, although a level of +2 % does extend along the right hand side of the CM. However this contour is at floor level and not against the roof. Intake or recirculating air against the roof pushes the methane downwards.

This lack of layering is evident in all the simulations, showing that as long as ventilation is provided, methane mixes rapidly into the air and shows no tendency to layer.

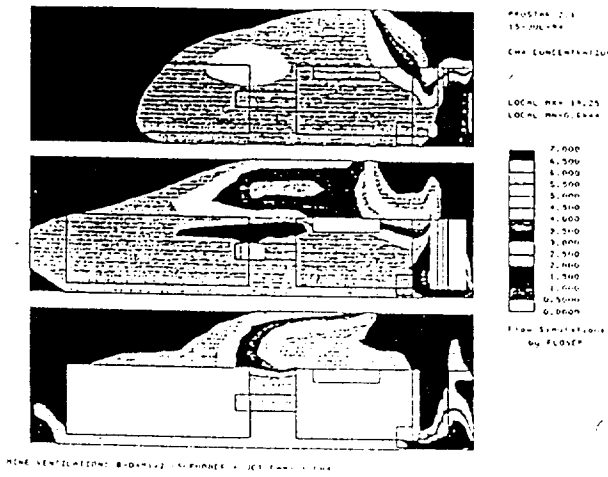

Figure 10. HORIZONTAL METHANE CONTOURS, SPLIT TO RIGHT

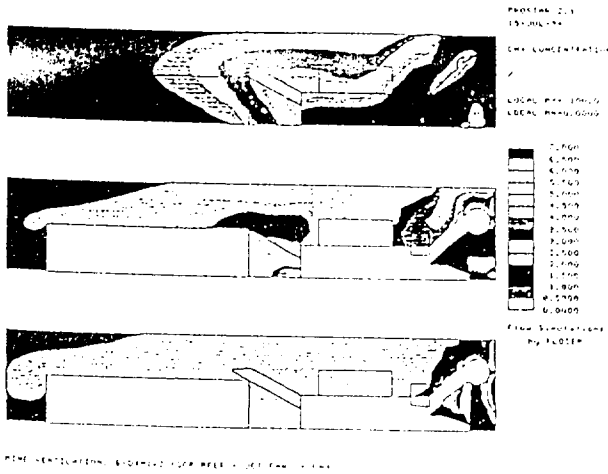

Figure 11. VERTICAL METHANE CONTOURS, SPLIT TO RIGHT

DISCUSSION

Methane levels are not consistent around continuous miners during mining operations. The return side sensors generally record higher levels than those on the intake, although, by the left rear of the CM, levels have returned to those of the cabin. The highest levels are usually recorded at the middle left position of the boom, these being more than double those in the cab.

When the left hand side of the CM is not confined by the sidewall, such as cutting the second pass on the right, the directional sprays effectively remove methane from the face to the left of the CM, and the drum sensors record lower levels. The main source of ignition, the picks, are therefore not in methane levels that will be ignited. However, in some tests the drum sensors did record the highest levels, and this is also seen in the computer simulations when the air from the directional sprays is confined by the sidewall. This is also evident in a split, when less fresh air reaches the face, so a greater distance is required to dilute the methane.

There is no evidence of methane layering against the roof, either in the simulations or from actual results. The turbulent flow provided by the ventilation mixes the methane into the air, not allowing it to flow separately and layer. Dilution to acceptable levels is rapid and occurs within the first few metres of the face, although when ventilation to the face is restricted the drum and boom can be in an atmosphere of + 2 %.

The driver's cabin sensor and the scrubber intake sensors generally, but not always, record similar values, and these initial results suggest that these are reasonable positions for methane sensors. They are removed from the less friendly environment close to the drum, and operate with less maintenance. However, they do not record the maximum methane levels being experienced, and, as they mostly record about half of the level at the middle left of the boom, this may require adjusting alarm levels for methanometers in such positions.

CONCLUSIONS

Methane levels have been recorded around operating continuous miners using the data logger system designed by Miningtek. In general the CMs operated in acceptable conditions, of less than 0.6 % methane, but levels as high as 3 % were recorded.

Methane levels around the drum are generally not the highest, due to the scraping effect of the directional sprays, which remove the methane to the return side where the sensor at the middle of the boom recorded high levels.

Sensors placed in the driver's cab and at the scrubber intake would appear to give a good evaluation of methane levels, although not recording the maximum level.

CFD simulations show the reduced effect of directional sprays on clearing the immediate face when the flow is restricted against a sidewall. This results in the drum and boom being in an atmosphere of +2 %.

Methane around a ventilated and operating CM shows no tendency to layer against the roof. It is diluted to acceptable levels within the first few metres of the face, and remains mixed.

ACKNOWLEDGEMENT

This work is carried out with the support of the Safety in Mines Research Advisory Committee (SIMRAC), and the author acknowledges the contribution made by the members of SIMRAC, SIMCOL, SIGEH and SIGDS.

APPENDIX C2

SIMULATIONS OF METHANE FLOW AROUND A CONTINUOUS MINER.
Part 1: Comparison with dust flow for full heading development with jet fan ventilation.

A.P. COOK

INTERIM REPORT
SIMRAC PROJECT COL 030
JULY 1994

SUMMARY

Simulations of methane flow around a continuous miner have been completed using computational fluid dynamics. These initial results are for a CM and SC in a heading with jet fan ventilation. Methane concentration contours are compared with those of dust to evaluate the possible use of dust contours as a means of determining methane flow.

Methane and dust liberated at the face during cutting behave significantly differently. Methane mixes to acceptable levels within the first few metres, and remains mixed for the length of the heading to the last through road. It shows no tendency to layer back over the CM. Dust requires a greater distance to dilute and rolls back over the CM.

Dust contours cannot be used to predict methane flow patterns.

CONTENTS page

FIGURES page

INTRODUCTION

Miningtek is presently carrying out a large and detailed simulation programme using CFD to compare five different ventilation systems for continuous miner (CM) headings and splits. This work is part of SIMRAC projects COL030 and COL027, reducing the hazards of both methane and dust.

The simulations predict ventilation flow around the CM and a shuttle car (SC), and also methane or dust concentrations. Input data is based on industry-wide average ventilation values, and measured or calculated methane emission and dust generation. Dust values as input are presently more accurate and therefore more reliable than those for methane. The methane values are reliant on the further development of methane monitoring and data logging systems being developed by Miningtek, and also of methane emission predictions from the model and software being developed. These are all objectives of COL030.

The full simulation programme is presently scheduled for 85 simulations, but this will be extended as further detailed work is identified. It is intended that CFD becomes an accepted and respected means of determining ventilation flow for mining situations. It can quickly and relatively cheaply provide solutions to rapidly changing ventilation or mining conditions, without time and manpower consuming physical underground tests. Miningtek has used CFD as a ventilation tool since 1990, developing simulation models to their present detailed standard for continuous miners and road headers.

Methane has been simulated on previous occasions, but without guaranteed input data for emission rates. It is intended that results produced from this programme will give true methane values in the ventilation around a CM. However, initial work must identify methane flow and behaviour patterns, without necessarily predicting actual methane values. This will provide information as to suitable measuring positions for methanometers to later quantify actual levels and to verify the simulations.

As the ventilation and dust data are presently more reliable, it was intended to possibly relate these results to methane. This report describes simulations carried out to relate methane and dust behaviour for identical ventilation conditions.

OBJECTIVE

The objective of this comparison simulation was to relate the methane contours to the ventilation vectors and the dust contours. It was intended to identify any particular methane behaviour relative to air flow or dust flow, and by this means evaluate flow vectors and dust contours in terms of methane.

SIMULATED MINING AND VENTILATION CONDITIONS

The mining situation and ventilation values are given in Figure 1. The simulation is that of a CM and SC in a heading, with ventilation provided by a jet fan (4 m^3/s), on board scrubber (10 m^3/s) and directional sprays. The LTR velocity is 1,5 m/s

SIMULATED METHANE EMISSIONS

As the main objective was to relate methane flow patterns and behaviour to the ventilation and dust, the methane input values were not significant in terms of actual methane percentages in the air. More important were the release points to determine the methane flow patterns after release. The input figures therefore were based on information from a range of coal seams and were not a specific situation.

The main methane emissions were considered to be immediately in front of the drum at 7 $l/s/m^2$, and from the freshly exposed face above the drum at 1 $l/s/m^2$. Methane was also added from the face below the drum and from the broken coal at the gathering

arms at 0,2 l/s/m^2. Methane concentration at the scrubber inlet was fixed at 0,8 %.

No emissions were considered from the sidewalls, roof, floor or shuttlecar as comparisons with the generated dust contours were required, and no dust was simulated from these positions.

PRESENTATION OF RESULTS

Results are produced as velocity flow vectors, indicating relative velocity and direction; methane concentration contours; and dust concentration contours. These are produced on horizontal and vertical planes taken at predetermined positions within heading. They were chosen to give good representation across the full width and height of the heading and are shown in Figure 2.

METHANE PERCENTAGES: ACTUAL AND SIMULATED

Information from two sites has been used to equate the relative contours produced by the simulations to actual methane percentages in the ventilation. At Matla No. 3 Mine, a data logger installed at the intake to the scrubber recorded a relatively consistent 0,7 % - 0,8 % throughout a shift. At Goedehoop, Hope Mine, the methanometer in the operator's cab was observed to read 0,5 % to 0,7 % throughout the shift.

Equating these values to the simulation contours gives 2,5 at the scrubber inlet equal to 0,8 %, and 2,0 at the operator position to 0,7 %. Both observed values are approximately one third that of the simulation, so this calculation was applied throughout to all simulation contours.

In this report the contour value is quoted with the equivalent methane percentage after it in parenthesis, e.g. 2,5 (0,8%).

FIGURE 1 Mining situation simulated

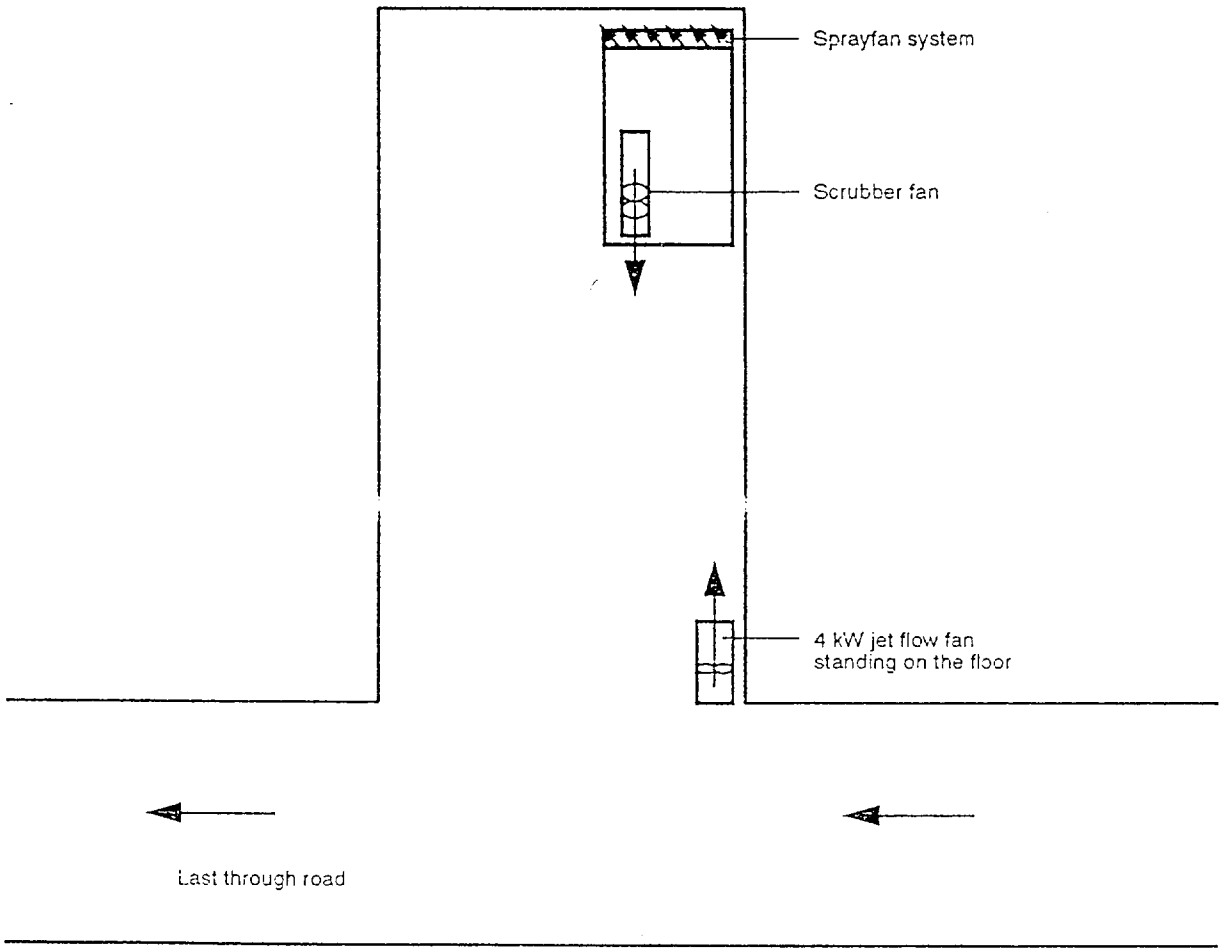

FIGURE 2 Positions of horizontal and vertical data planes

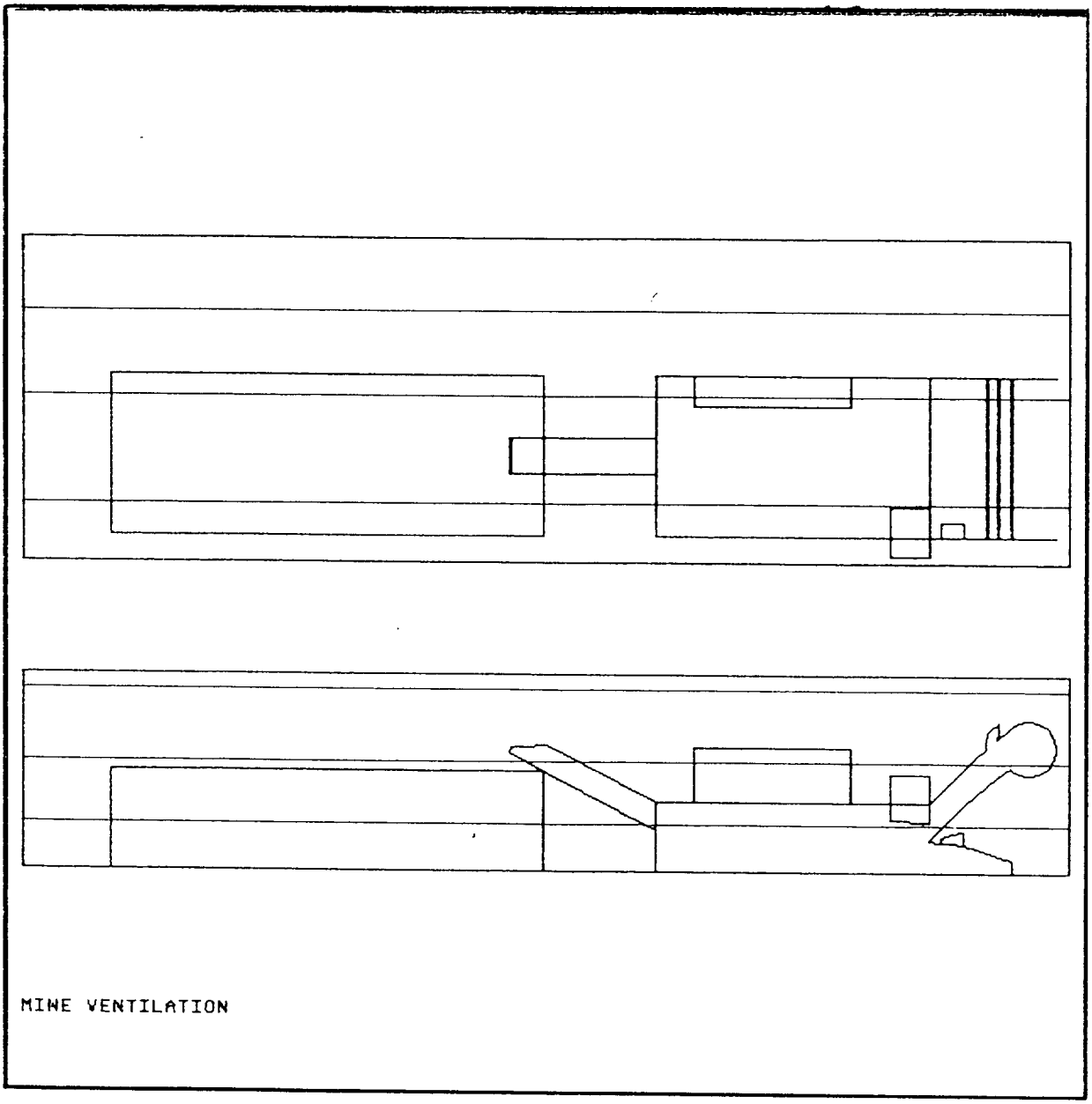

RESULTS OF SIMULATIONS

Overall situation in heading

Figure 3 shows a three dimensional view of the heading and last through road (LTR). The contours are of methane concentrations on the three horizontal planes. Almost the entire heading is at a constant methane percentage, the contour value being 1,5 - 2,0 (0,5% - 0,6%). The only high value contours are in the immediate vicinity of the face, these being as high as 7,0 (2,5%), with values above and around the CM and SC generally being 1,5 - 3,0 (0,5% - 1,0%).

This indicates that methane is mixed with the ventilation within a few metres of the face, and remains mixed at constant levels within the full volume of the heading.

Full heading

Figures 4, 5 and 6 show ventilation flow vectors and corresponding methane and dust contours for the full heading, taken on the plane just above the gathering arms.

The vectors show good scraping of the face by the sprays, and fresh air from the jet fan on the r-h side of the CM. Some entrainment occurs behind the shuttle car, causing some areas of very slow air movement. There are also opposing air flows on the l-h side of the CM and SC. However none of these flow patterns have any significant effect on the methane contours. From the front of the SC to the LTR, the contours are constant. On the face a very narrow zone records as high as 7,0 (2,5%), but this drops very quickly to 3,5 (1,2%) and less. The l-h side of the CM shows contours of 2,5 - 3,5 (0,8% - 1,2%), which reduce to 2,0 (0,7%) by the rear of the CM.

Dust contours show much greater variation and distribution, with less immediate mixing and dissipation. The l-h side of the CM and SC show 50 % of the face concentrations, and these continue on the l-h side of the heading well beyond the SC.

FIGURE 3 3-D global view showing horizontal methane contours

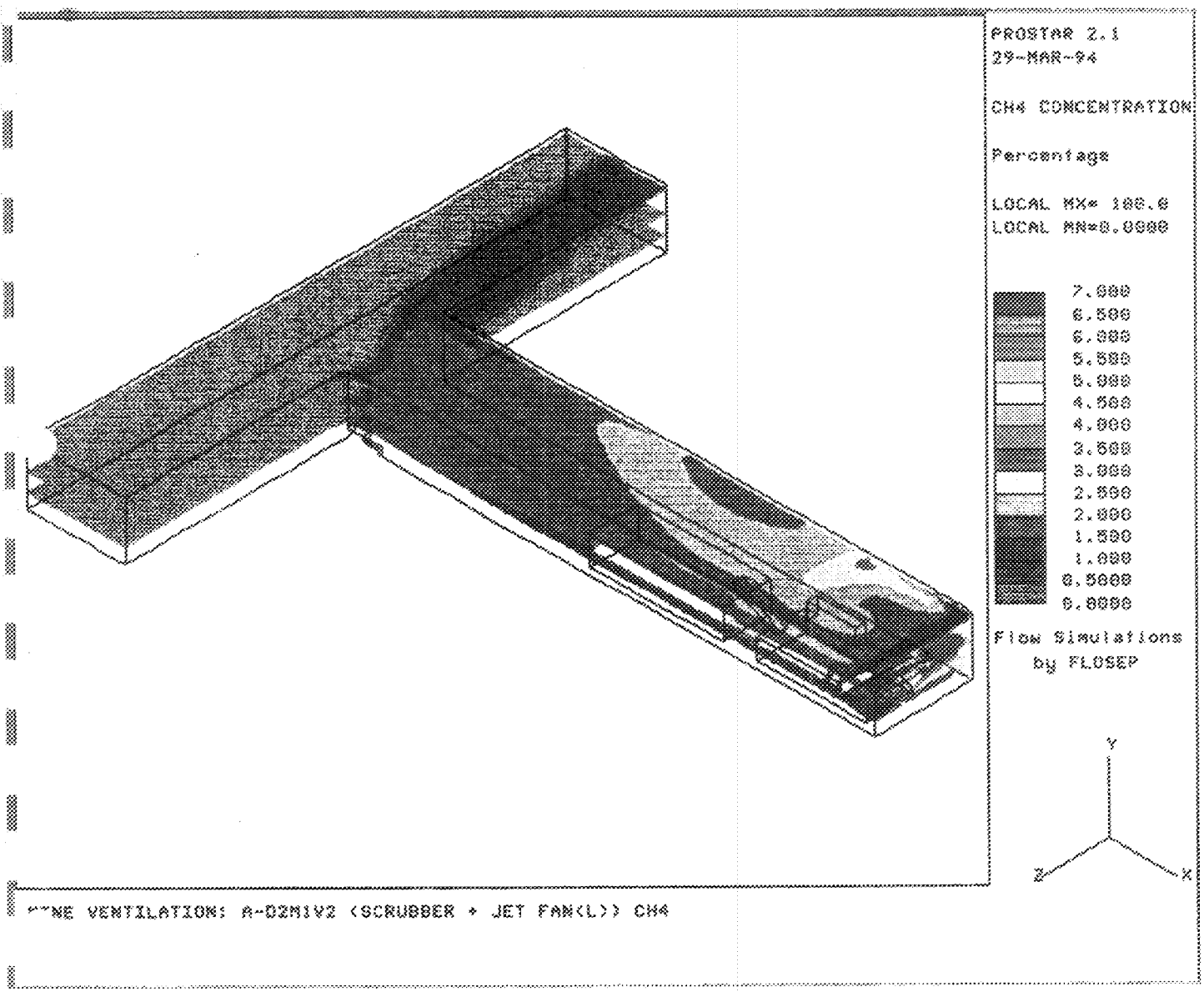

FIGURE 4 Velocity vectors above gathering arms

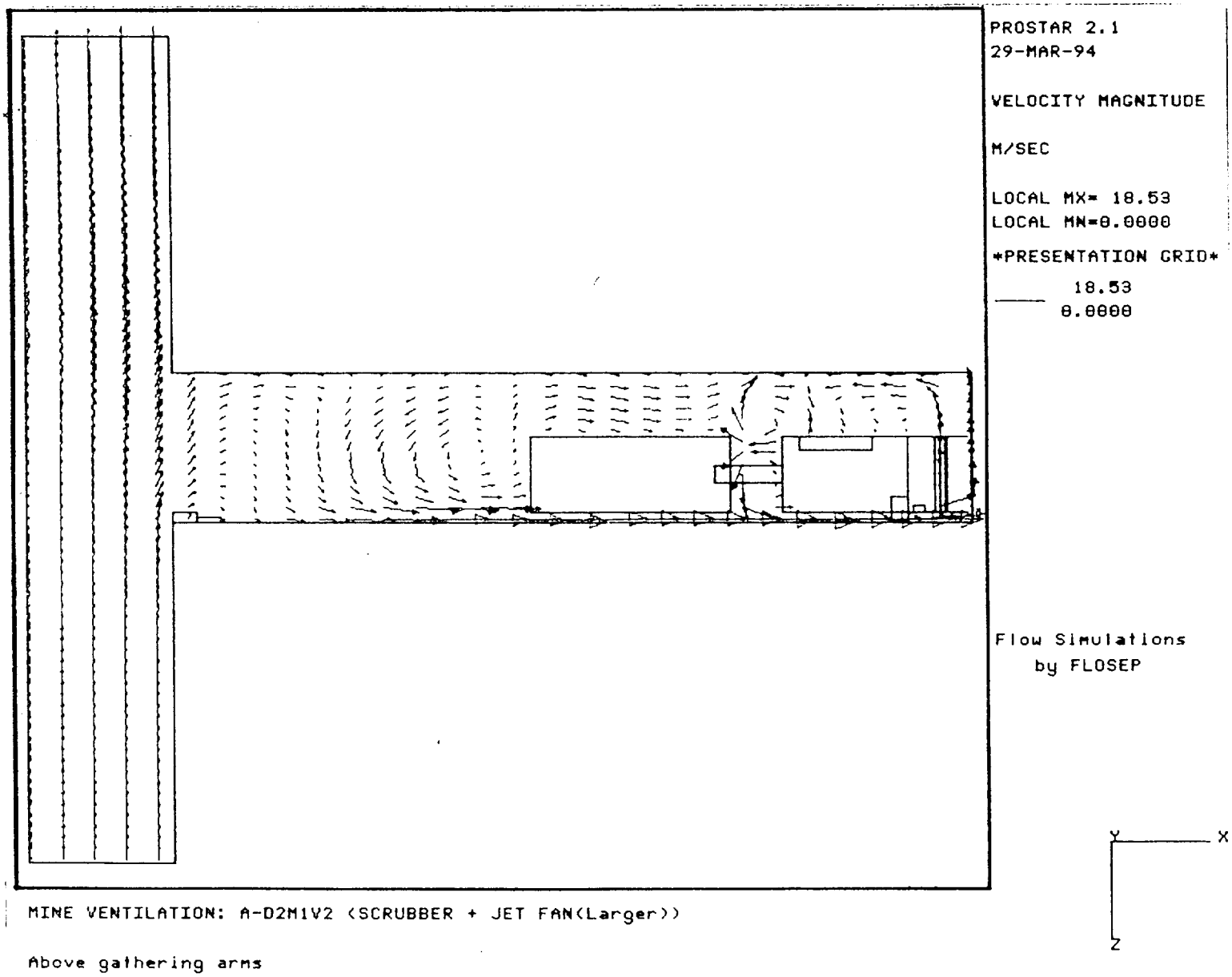

FIGURE 5 Methane contours above gathering arms

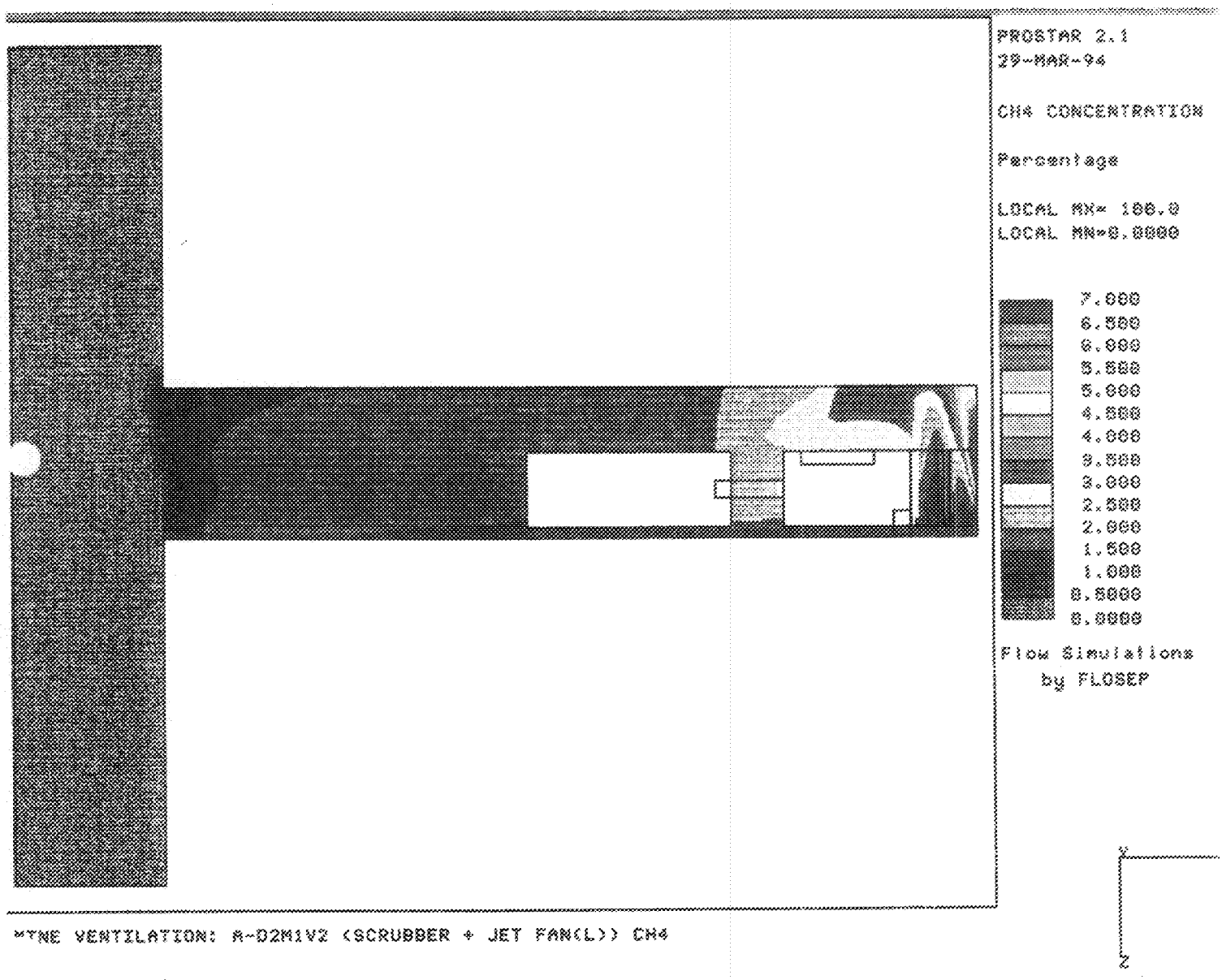

FIGURE 6 Dust contours above gathering arms

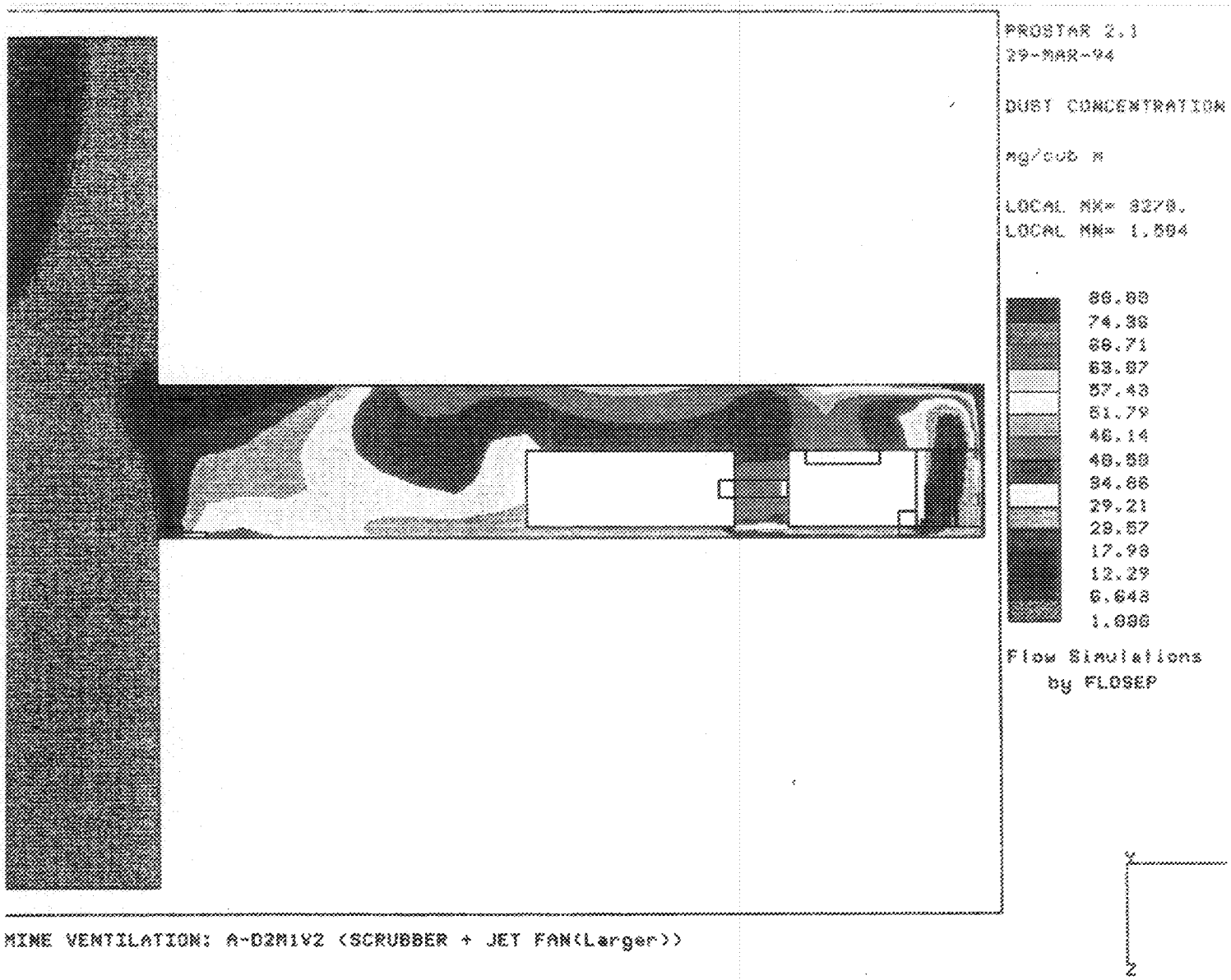

Figures 7, 8 and 9 show the same vectors and contours, but taken at the operator height. The flow vectors show a much more positive return flow of air to the LTR, due to the scrubber, although there is still considerable intake air movement from the jet fan. There is good air flow over the CM, returning on the l-h side.

The methane contours are more obvious close to the face at this level, but, are again reduced within the length of the CM. The contours on the l-h side of the CM are extended out over the SC by the entrained air from the scrubber, however the level is now reduced to 2,0 (0,7%). From the SC to the LTR methane levels are very constant, at 1,5 (0,5%).

Again the dust contours show greater variation than the methane, indicating slower dilution. Levels remain at 50 % of the face value down the l-h side of the heading, almost to the LTR. Dust enters the LTR ta 20 % - 30 % of the face value.

Figure 10, 11 and 12 show the same vectors and contours but taken near to the roof. The flow vectors show a general outflow of air at this height, but there is still fresh air from the jet fan. There is also some entrainment of return air.

The methane contours show very consistent methane concentrations over the full length of the heading. There is a zone of 2,5 (0,8%) above the CM and SC, but most is below 1,5 (0,5%). Even on the immediate face the contours are very low, at 1,0, due to the sweeping of the spray fans above the drum. The methane is released into the LTR at 0,5 (0,2%).

The dust contours again show much greater variations, over the heading, and with 20 % to 50 % of face levels being emitted into the LTR. The most significant difference in the dust is the zone of high concentration over the CM. This is caused by the sweeping action of the spray fans carrying dust generated at the drum across the face and upwards.

FIGURE 7 Velocity vectors at operator height

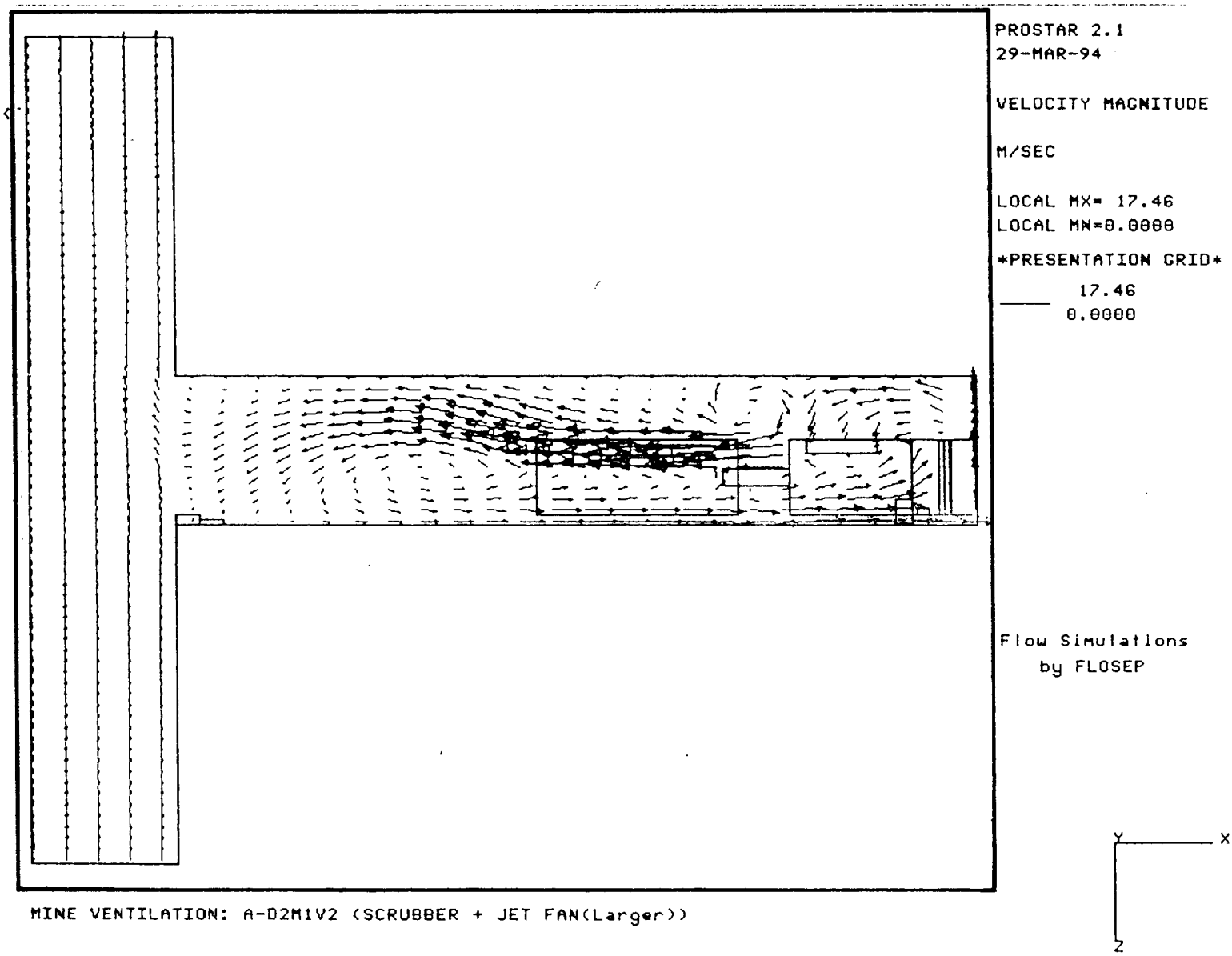

FIGURE 8 Methane contours at operator height

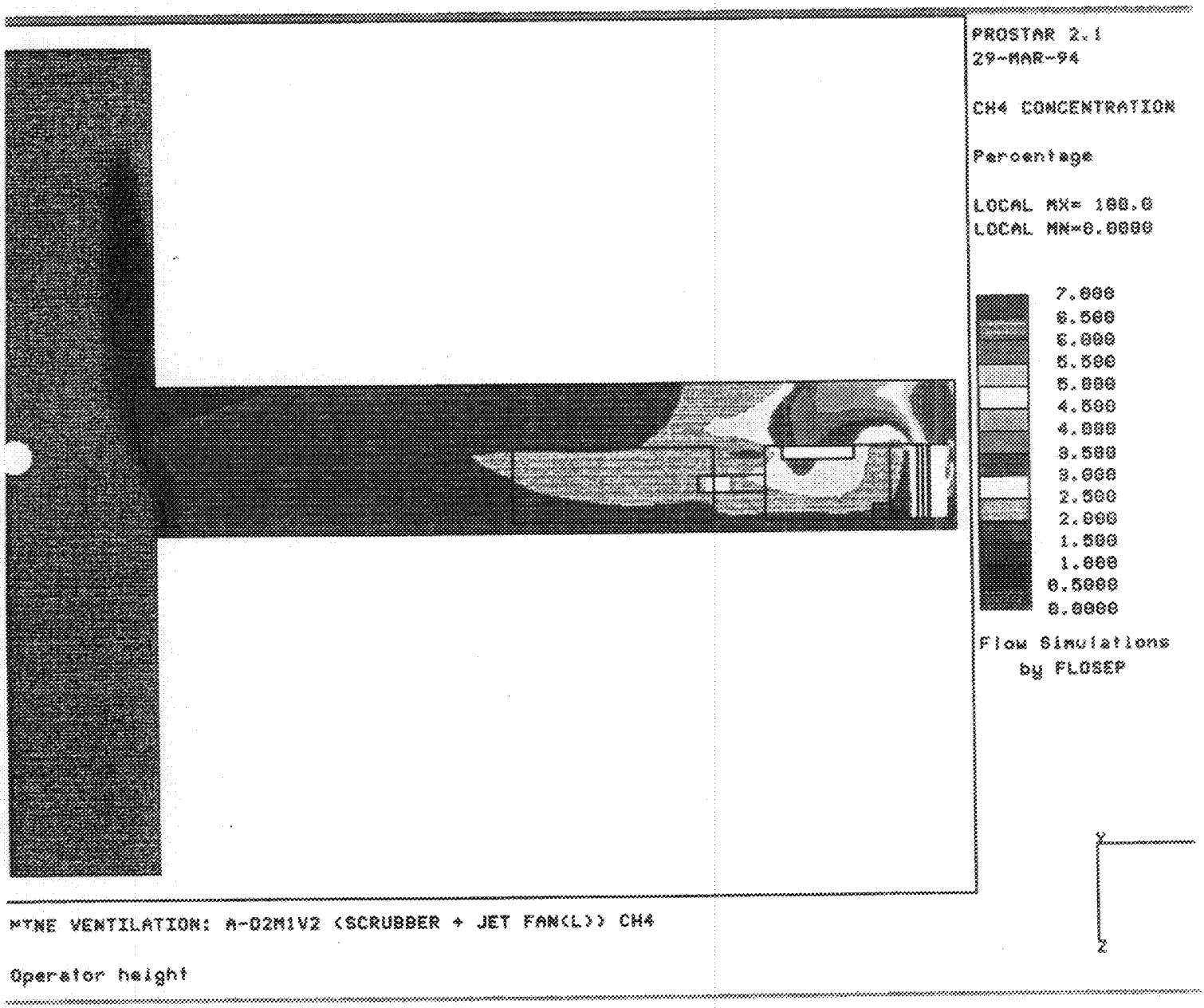

FIGURE 9 Dust contours at operator height

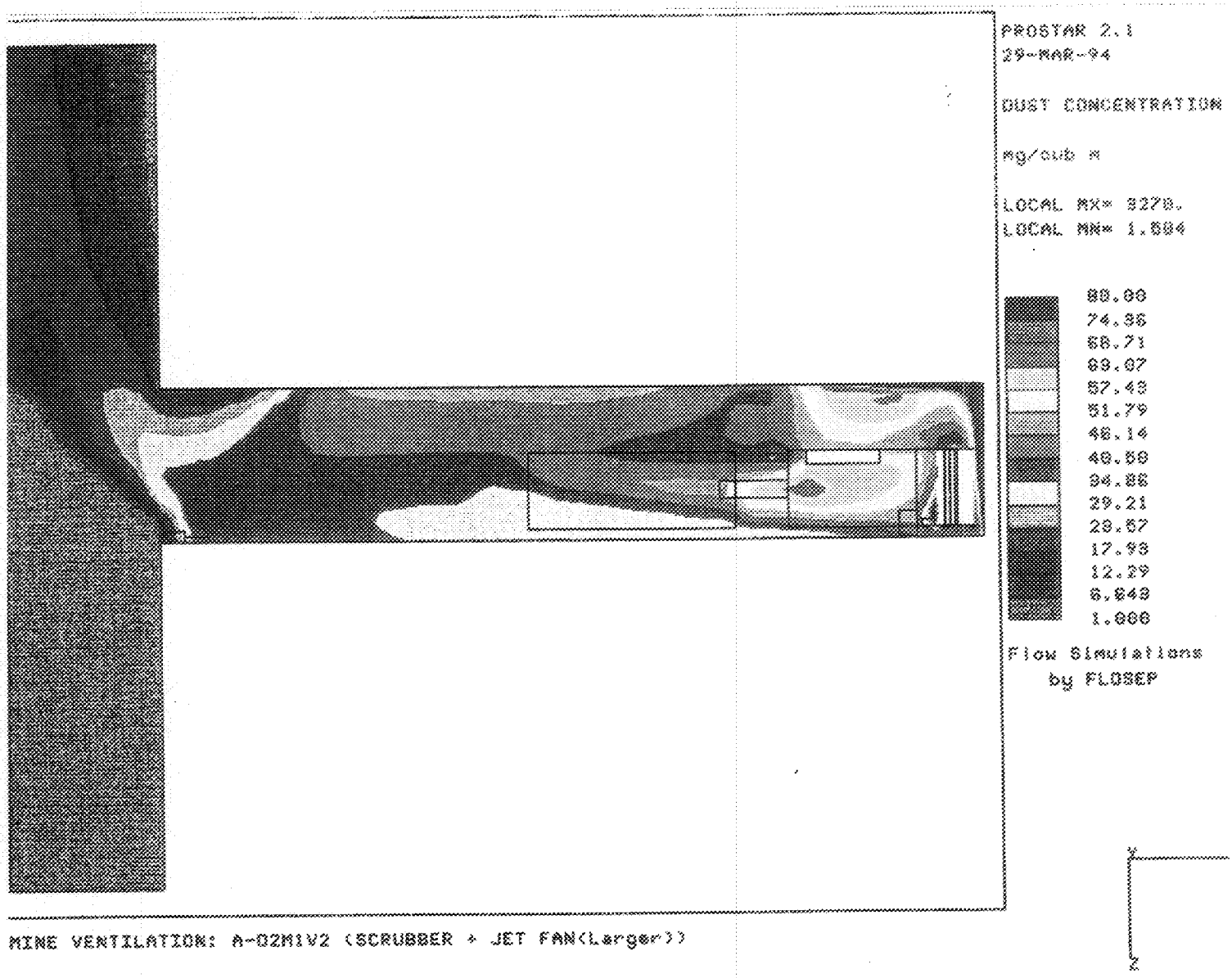

FIGURE 10 Velocity contours close to roof

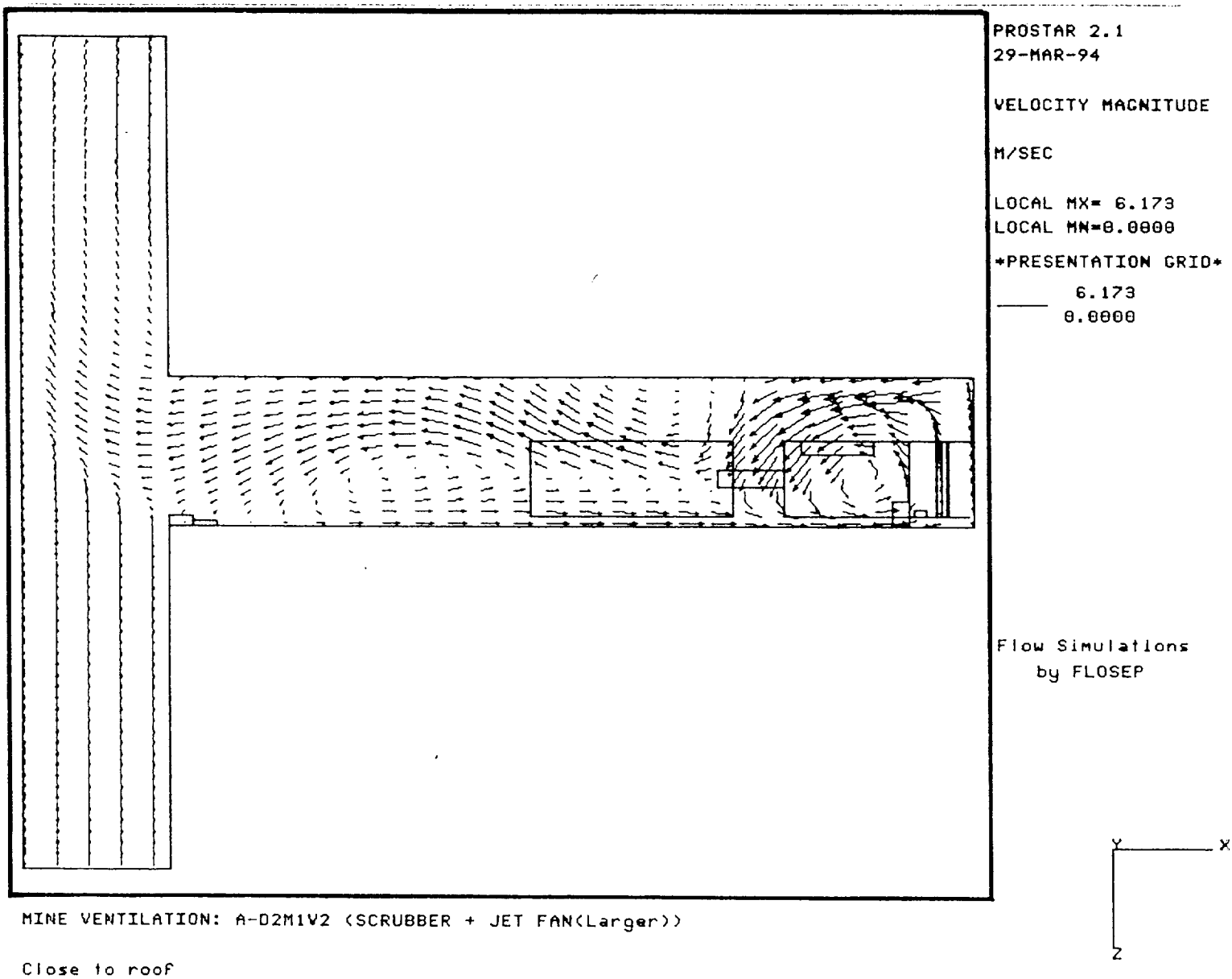

FIGURE 11 Methane contours close to roof

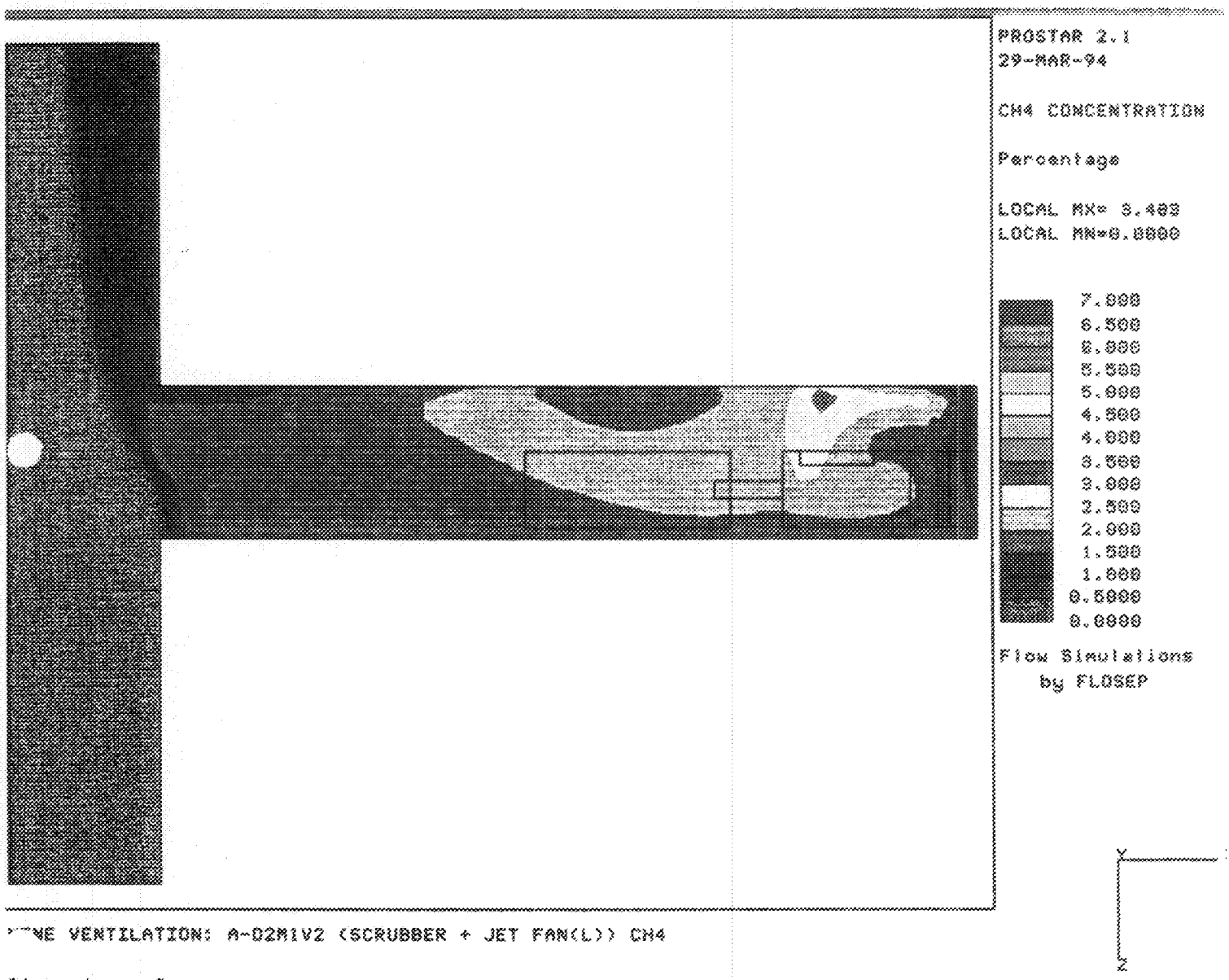

FIGURE 12 Dust contours close to roof

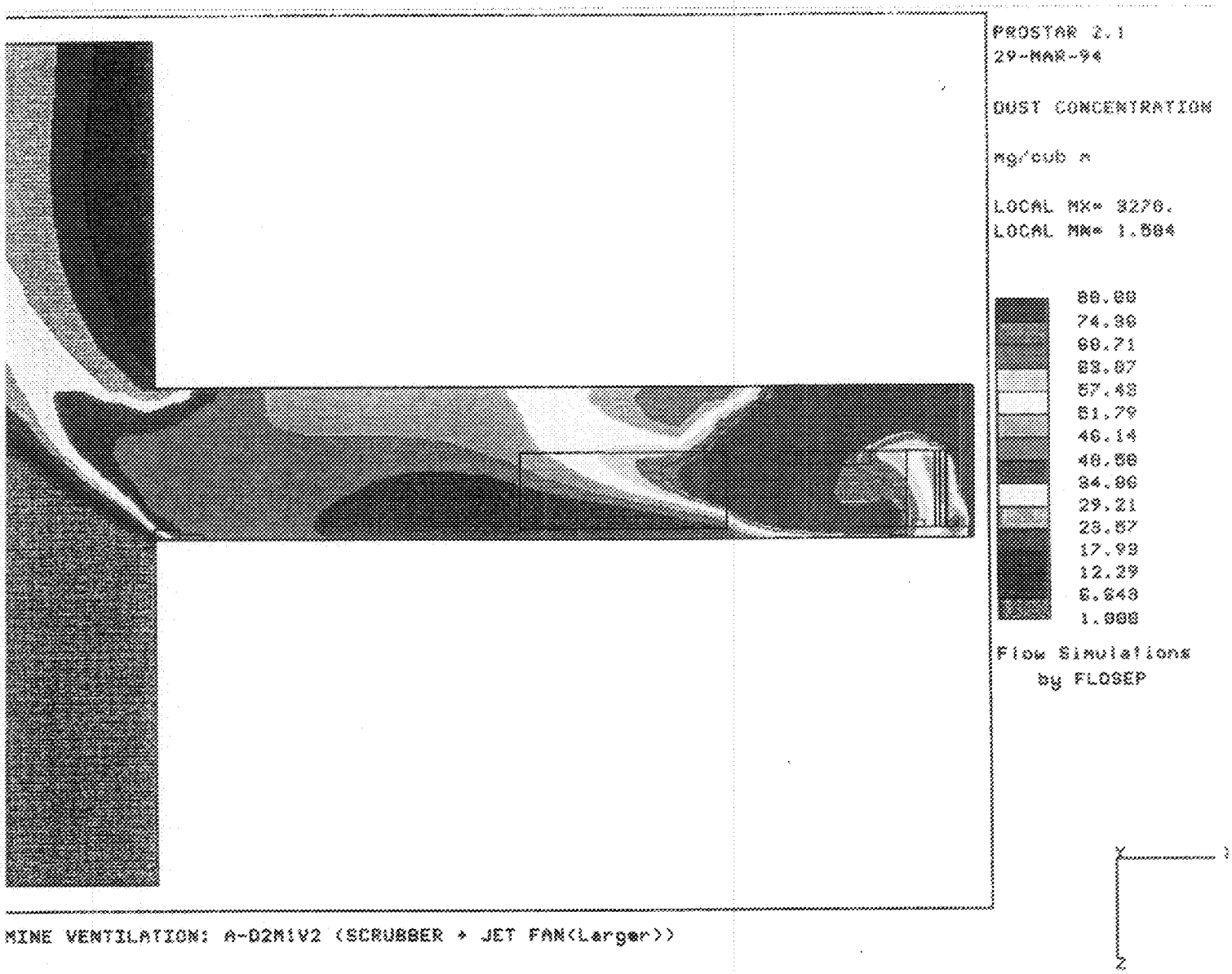

CM detail

Figures 13 - 18 show more detail of the ventilation, methane and dust around the CM and SC, taken on three horizontal and three vertical planes.

Figure 13 and 14 show the ventilation vectors. The most obvious occurrence is the return air from the scrubber outlet. However it is important to note that a significant volume of air returns past the l-h side of the CM, bypassing the scrubber inlet. This meets intake air and is pushed up to the roof and recirculated above the CM.

Figures 15 and 16 show the corresponding methane contours. The highest levels of gas occur around the cutting drum and to the left of the drum. Drum rotation is pushing the contours downwards and under the boom, and the spray fans carry the gas to the l-h side. However the ventilation movements up and over the CM have little effect on the methane, the gas levels reduce quickly, and only low methane levels are seen above the CM and SC. The spray fans are very effective in reducing methane levels on the face above the drum, showing conto[illegible] - 2,0 (0,2% - 0,7%), and these low values extend back against the roof.

The scrubber has very little influence on the methane contours, although its effect on the ventilation is significant. The extended tail of the 2,0 (0,7%) contour, from the scrubber outlet back over the SC, may be due to entrainment of intake 1,5 (0,5%) mixtures with the 2,5 (0,8%) exiting the scrubber. But these levels are only slightly above the level of 1,5 (0,5%) in the general body.

FIGURE 13 Velocity vectors around CM, horizontal planes

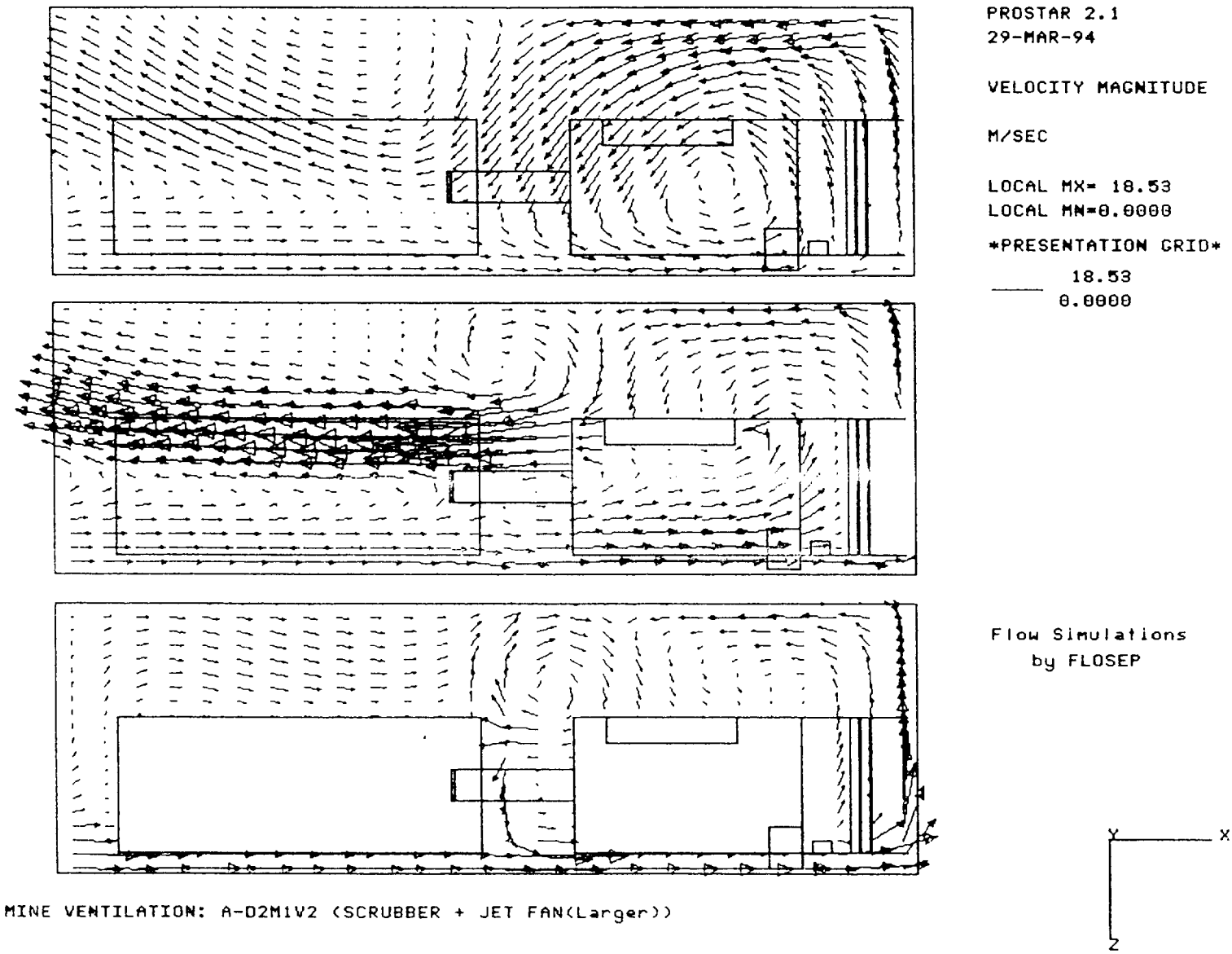

FIGURE 14 Velocity vectors around CM, vertical planes

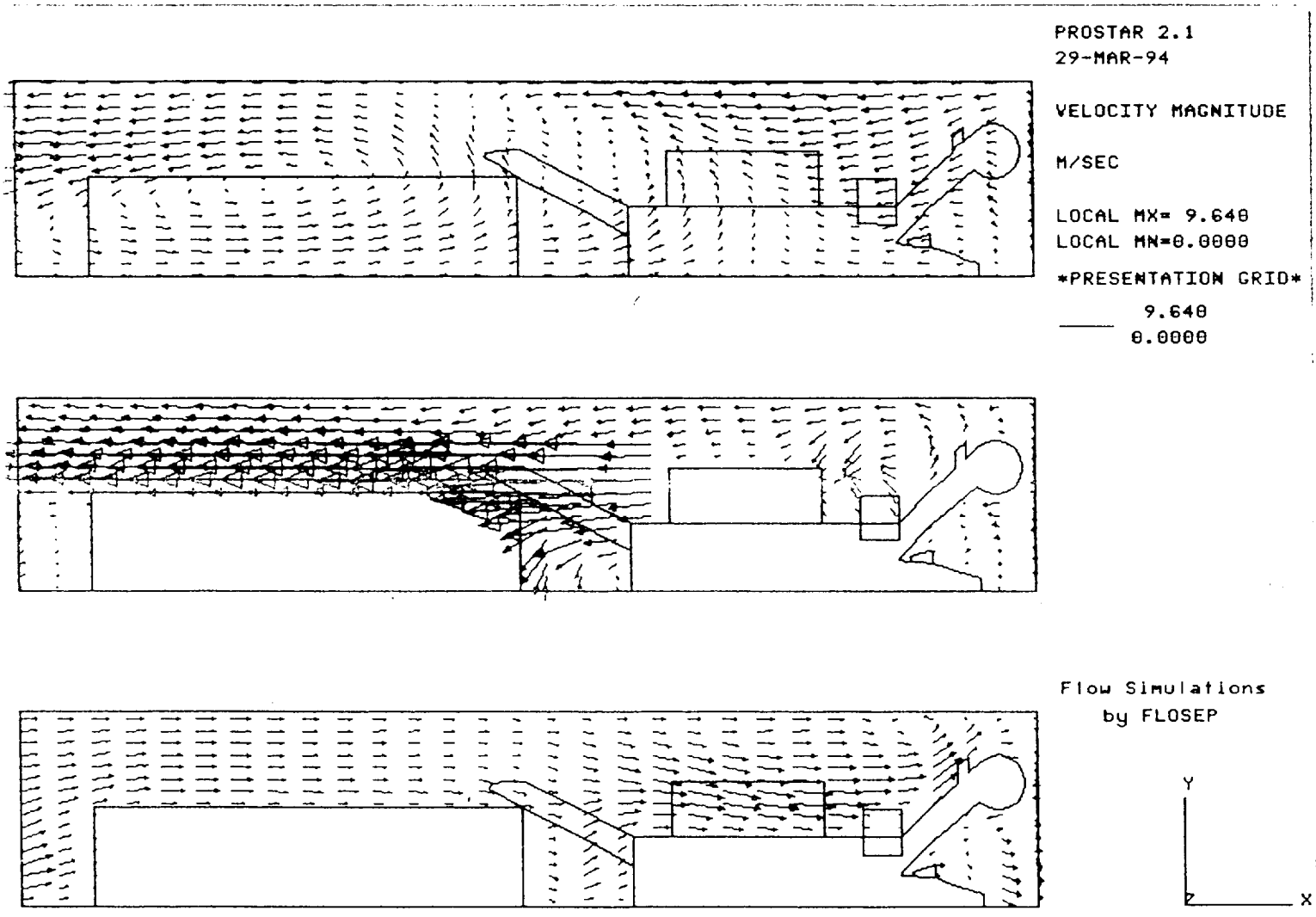

MINE VENTILATION: A-D2M1V2 (SCRUBBER + JET FAN(Larger))

FIGURE 15 Methane contours around CM, horizontal planes

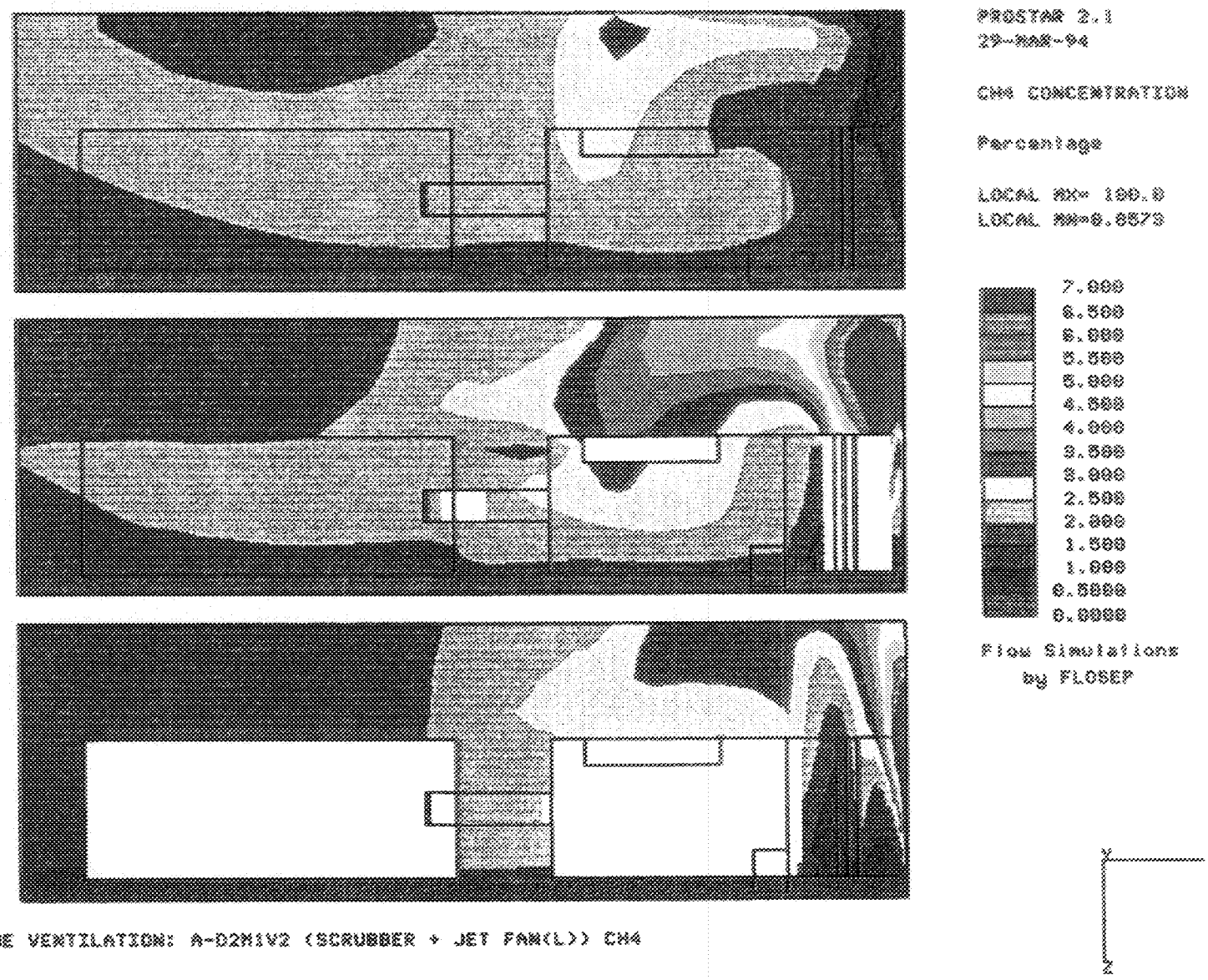

FIGURE 16 Methane contours around CM, vertical planes

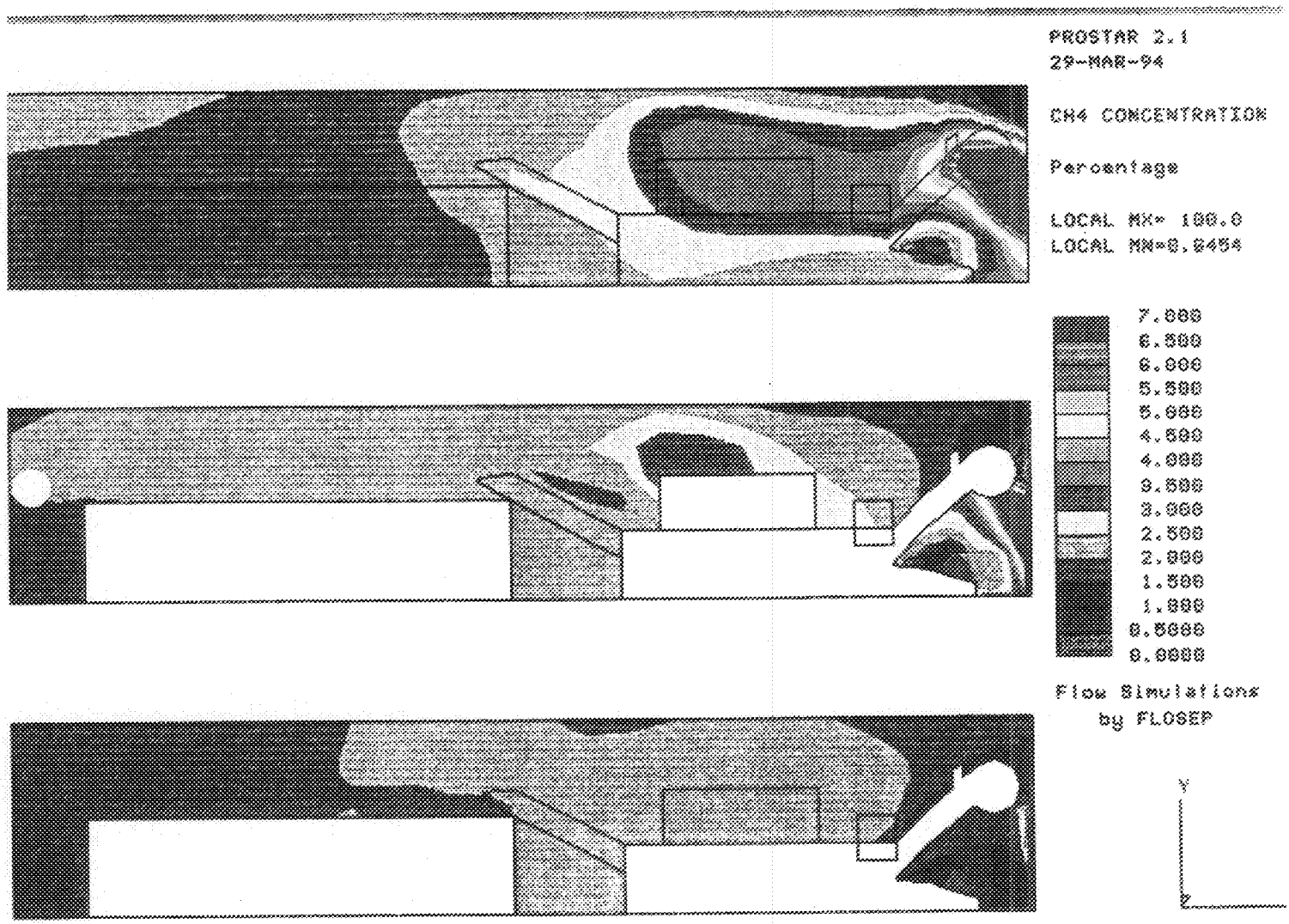

MINE VENTILATION: A-02M1V2 (SCRUBBER + JET FAN(L)) CH4

FIGURE 17 Dust contours around CM, vertical planes

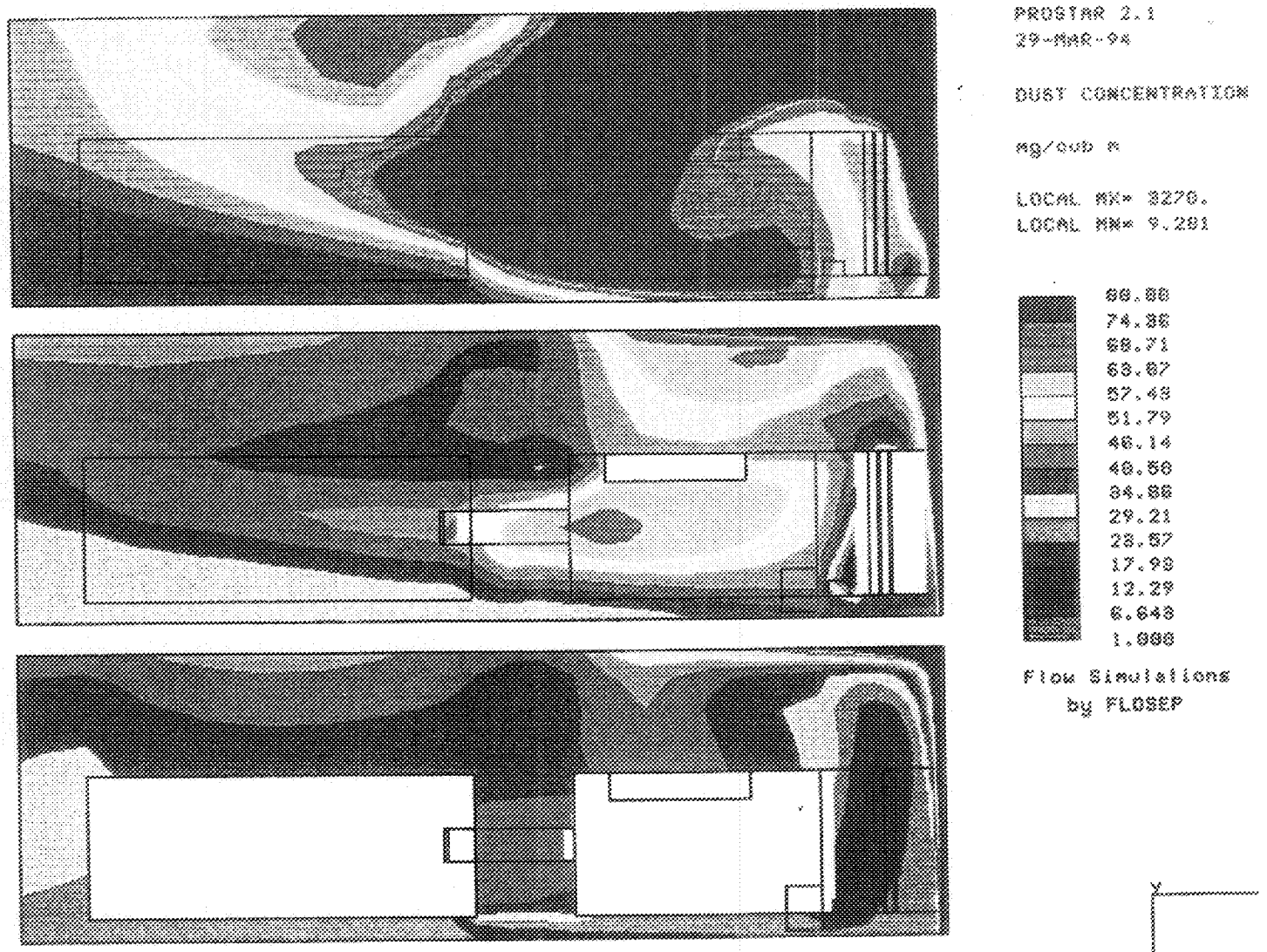

MINE VENTILATION: A-02M1V2 (SCRUBBER + JET FAN(Larger))

FIGURE 18 Dust contours around CM, horizontal planes

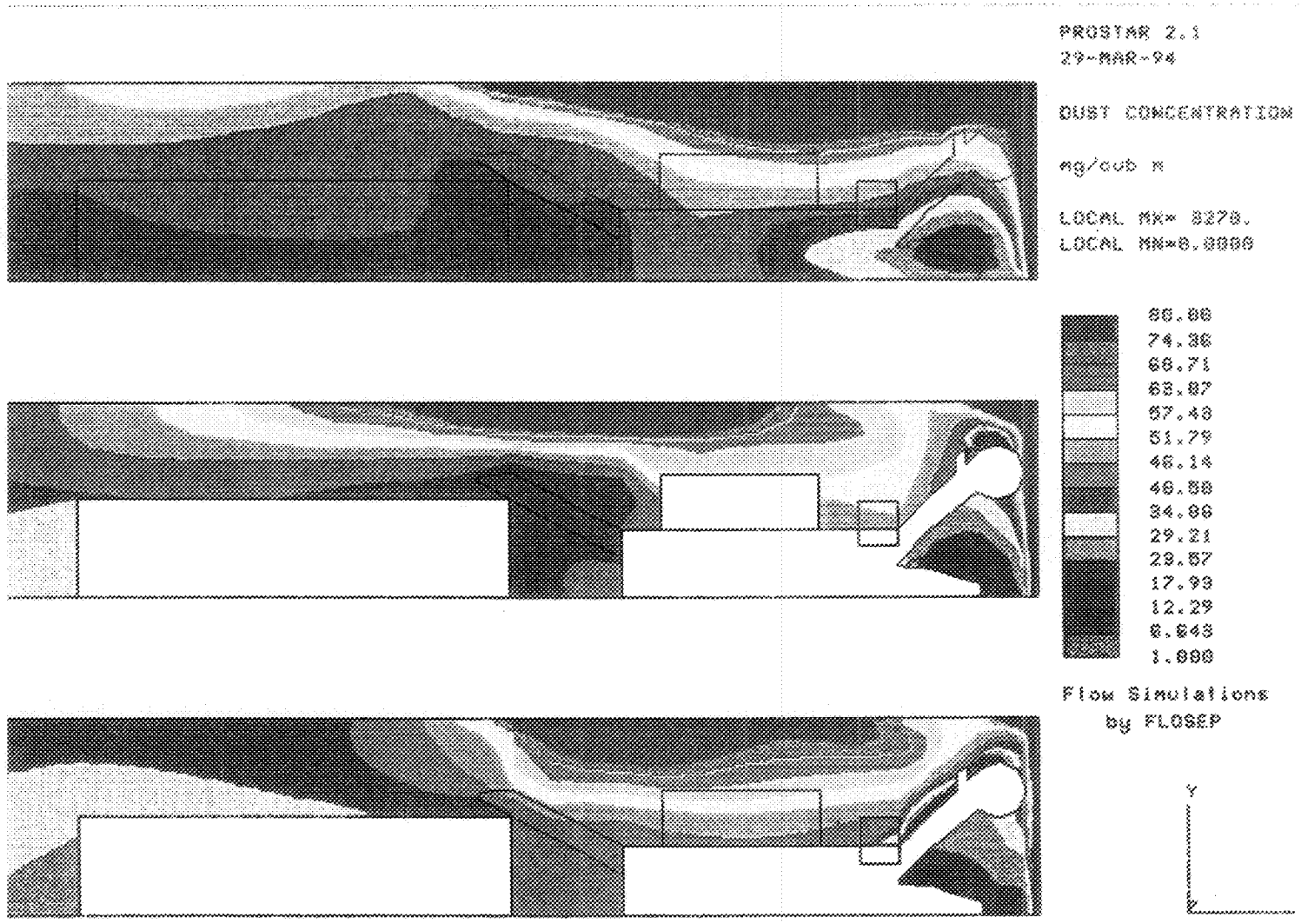

MINE VENTILATION: A-D2M1V2 (SCRUBBER + JET FAN(Larger))

Figures 17 and 18 show the detailed dust contours. These again show the different behaviour of the dust to the methane. Low level contours are seen on the r-h side, with high levels on the l-h side and above the CM. The most obvious difference to methane is the extensive area of higher dust concentrations along the roof. The dust does not mix in the air as the methane does, but is transported by the ventilation, being diluted with time and distance.

DISCUSSION OF RESULTS

Full heading

Methane mixes into the ventilation air within a few metres of the face, being rapidly diluted to manageable levels. The heading is predominantly filled with a constant level of methane, with higher contours only being present on the immediate face. There is no evidence of methane layering against the roof, although there are slightly higher concentrations above the CM and SC. However, these higher levels are only 2,0 - 3,0 (0,7% - 1,0%) and not much more than the 1,5 (0,5%) in the general body of the heading. The contours on the face dissipate r[illegible] l-h side of the CM.

Dust contours are more varied than the methane, and show greater differences between the three heights. Lower concentrations are seen on the floor, influenced by the fresh air from the jet fan, and higher concentrations occur against the roof. High concentrations of dust occur over the CM, caused by the flow of air across the face and upwards.

CM detail

Methane and dust behave quite differently in the first few metres from the face, with the methane mixing rapidly and remaining mixed at low levels, but the dust being carried by the ventilation. This results in a relatively consistent gas level around the CM, but considerable variations in dust levels, with

much higher values against the roof. Methane shows no obvious signs of layering against the roof.

CONCLUSIONS

Methane gas liberated at the face during CM operations does not behave in the same manner as dust generated at the same time. The methane mixes with the ventilation air, and remains mixed at constant percentages throughout the heading. Dust does not mix so readily, and is rather carried by the airflow.

Methane percentages drop rapidly within the first few metres of the face, and have effectively stabilised before the back of the CM. Higher values occur on the face, mostly below and to the left of the drum. The drum rotation draws the methane downwards and the spray fans remove it to the left. Without spray fans scraping the face more methane would be retained under the boom.

Low methane concentrations were recorded above the drum and against the roof. This rapid dilution is the result of the good air movement across the face from the spray fans.

The scrubber has no significant effect on the methane contours. Dilution due to mixing has largely taken place between the face and the scrubber intake, so the ventilation from the scrubber outlet is all in the general body of the heading, and at constant methane levels.

Dust contours show much greater variation than methane, and dilution takes place at greater distances from the face. The most significant difference is the high dust concentrations against the roof above the CM.

Methane concentrations and flow patterns show very little correlation to the flow vectors or the dust contours. This means that dust results cannot be used to predict methane flow. The main difference in behaviour is the rapid mixing of methane to constant levels within a few metres of the face, and the longer time and distance required for dust dilution. This results in the dust being carried by the ventilation flow, so the dust contours are more closely related to the flow vectors.

The most significant methane contours originated from the relatively high emissions immediately in front of the drum. The face and broken coal emissions were quickly mixed and diluted by the face ventilation and spray fans.

CONTINUING WORK

Release from SC and broken coal

It was a concern that the freshly mined coal was making a more significant contribution of methane than was simulated. Laboratory tests were carried out on CM produced coal lumps to determine their rate of gas release from 1000 kPa (equivalent to a seam depth of approximately 150 m). The rate of release was surprisingly slow, and two underground sites were then tested to verify this. Newly cut coal was sampled from SCs at Goedehoop and New Denmark collieries, and the rate of gas emission measured. In both cases the results supported the laboratory data, and it is now concluded that the emission form freshly broken coal is not significant in terms of the total emission into a heading. CFD simulations will continue without broken coal emissions.

Data logger monitoring system

This system is now operating and the first results are available, although too late for inclusion in this report. This will provide invaluable information in terms of verification on the CFD.

Input values

The initial input values are intended more to identify flow behaviour patterns rather than actual methane values, although results to date suggest they are not too inaccurate. The input values shall be adjusted and improved as more actual data becomes available. Results reported by the USBM suggest that 50 % of the total emission is from the face and 50 % from the sidewalls. This type of information will all be included when appropriate.

Ventilation and mining conditions

This first run will be repeated for a split, with no alterations to the input parameters. Later simulations will consider alternative ventilation systems, and any particular methane problems.

APPENDIX C3

SIMULATIONS OF METHANE FLOW AROUND A CONTINUOUS MINER.
Part 2: Full split development with jet fan ventilation.

A.P. COOK

INTERIM REPORT
SIMRAC PROJECT COL030
SEPTEMBER 1994

SUMMARY

Simulations of methane flow around a continuous miner in a fully developed split to the right show that methane released at the face is rapidly diluted by the ventilation. Methane mixes readily into the air and remains mixed to the last through road.

The highest concentrations, of above 2%, occur within the first few metres of the face, and extend down the left hand side of the continuous miner for its full length. These concentrations are along the floor, not the roof, caused by recirculating ventilation in the split.

CONTENTS **PAGE**

LIST OF FIGURES **PAGE**

INTRODUCTION

A major objective of project COL030 is to evaluate methane flow around continuous miners. Some of this work is being carried out using CFD, as part of the detailed ventilation simulation programme. The CFD results are initially being used to identify methane flow behaviour and patterns, as a guide to installing the on-board data logger system. Later simulations will use actual recorded values as input, as well as predicted emission values, to improve the accuracy of the calculated methane levels.

The second phase of the simulation work (Phase 2), was CFD modelling of methane flow for a CM and SC in a fully developed split to the right. This report describes the results and compares them with those of Phase 1, for a heading. Results are given as methane contours and velocity flow vectors taken on horizontal and vertical planes chosen to give representation across the full width and height of the roadways.

OBJECTIVE

The objective of the Phase 2 simulations was to evaluate methane flow around a CM in a fully developed split.

SIMULATED MINING AND VENTILATION CONDITIONS

The mining and ventilation situations are given in Figure 1. The simulation is that of a CM and SC in a split, with ventilation from a jet fan (4 m^3/s), on board scrubber (10 m^3/s) and directional sprays. The LTR velocity is 1,5 m/s.

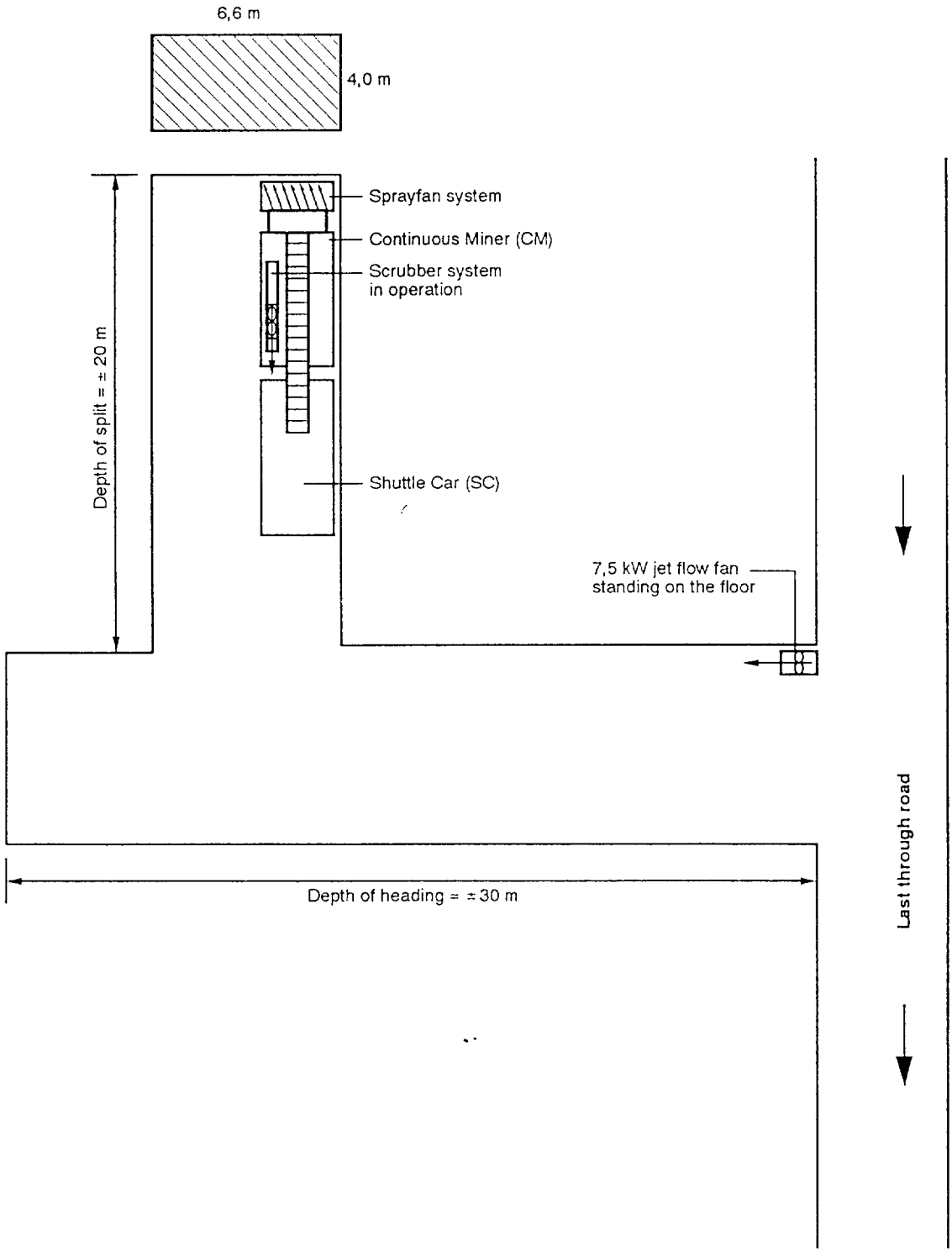

FIGURE 1: Mining situation simulated

SIMULATED METHANE EMISSIONS

As the main objective remains the evaluation of methane flow, rather than determining actual methane levels, the emission rates were the same as in the heading simulations. Immediately in front of the drum at 7 l/s/m², from the exposed face above the drum at 1 l/s/m², and from the broken coal at 0,2 l/s/m². The methane level at the scrubber inlet was set at 0,8 %.

RESULTS OF SIMULATIONS

As in Phase 1, the methane results are quoted as the contour value from the simulation, followed by the equivalent actual value based on underground observations, e.g. 2,5 (0,8 %).

Results are given on the planes shown in Figure 2.

Overall situation in split

Figure 3 shows a three dimensional global view of the split and heading back to the last through road. The contours are of methane concentrations, and it is seen that these are at reasonably constant values in the split and again in the straight. In the split, the level drops rapidly to 2,5 (0,8 %), and by the straight has dropped further to 0,5 (0,2 %). Higher readings, of 7,0 (2,5%) and above, occur in the immediate face area, and to the left hand side of the CM.

Full split

Figures 4 through 9 show horizontal planes taken over the entire simulated area. Figures 4, 5 and 6 show methane contours and Figures 7, 8 and 9 show velocity flow vectors.

Methane contours decrease rapidly after release at the face, but can be seen extending down the left hand side of the CM and SC, particularly in Figure 4 taken just above the gathering arms.

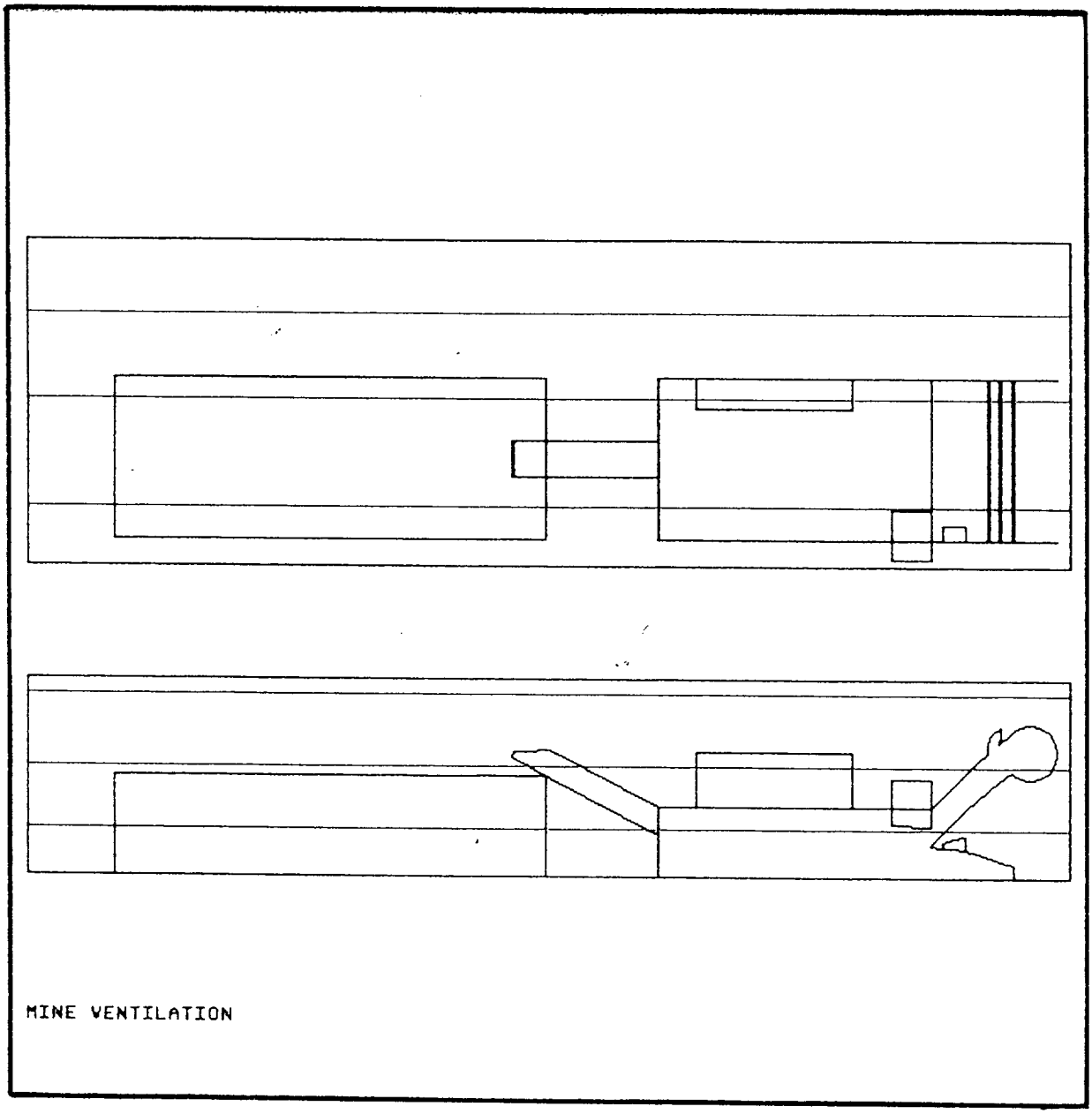

FIGURE 2: Positions of data planes

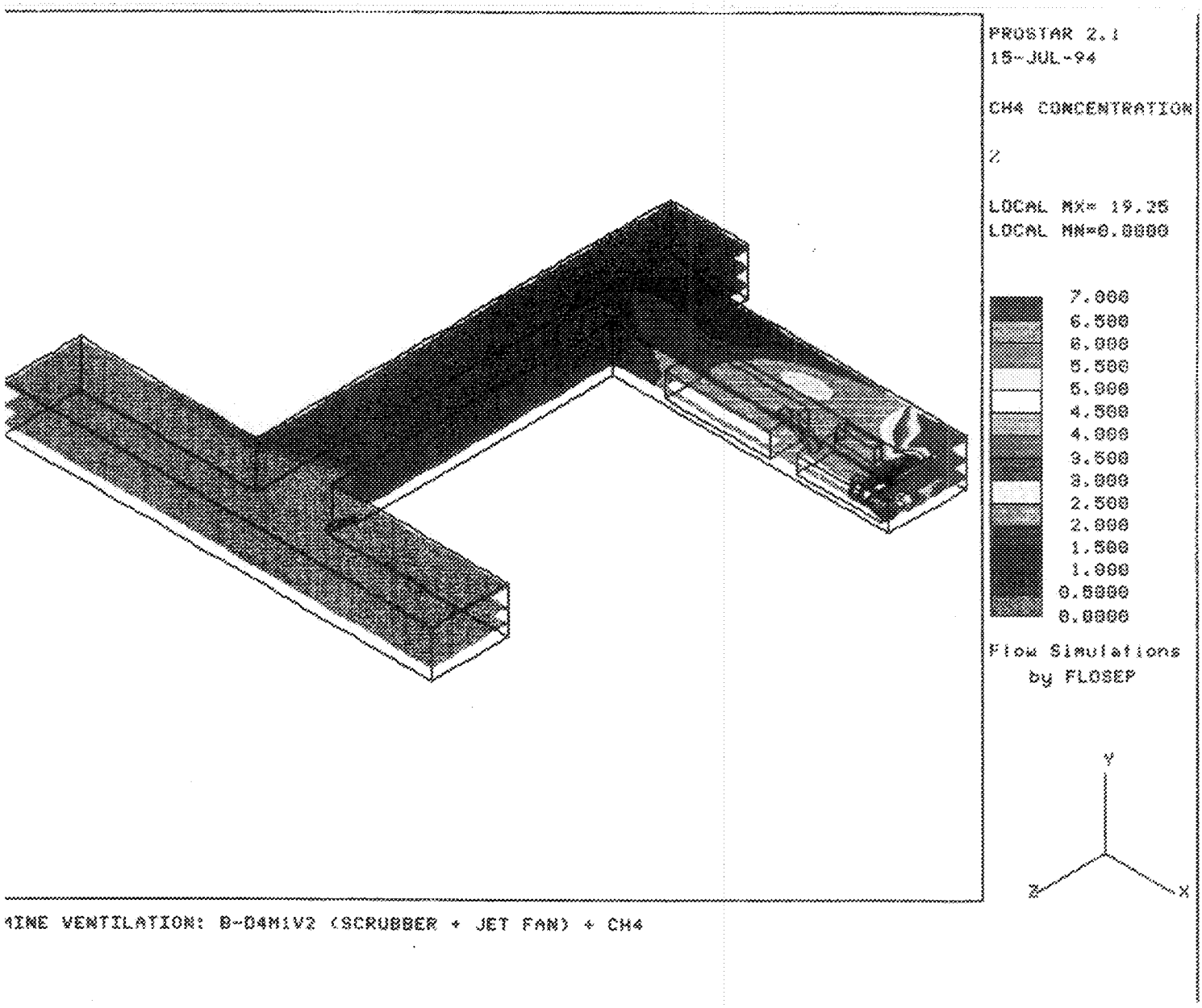

FIGURE 3: 3-D global view of split

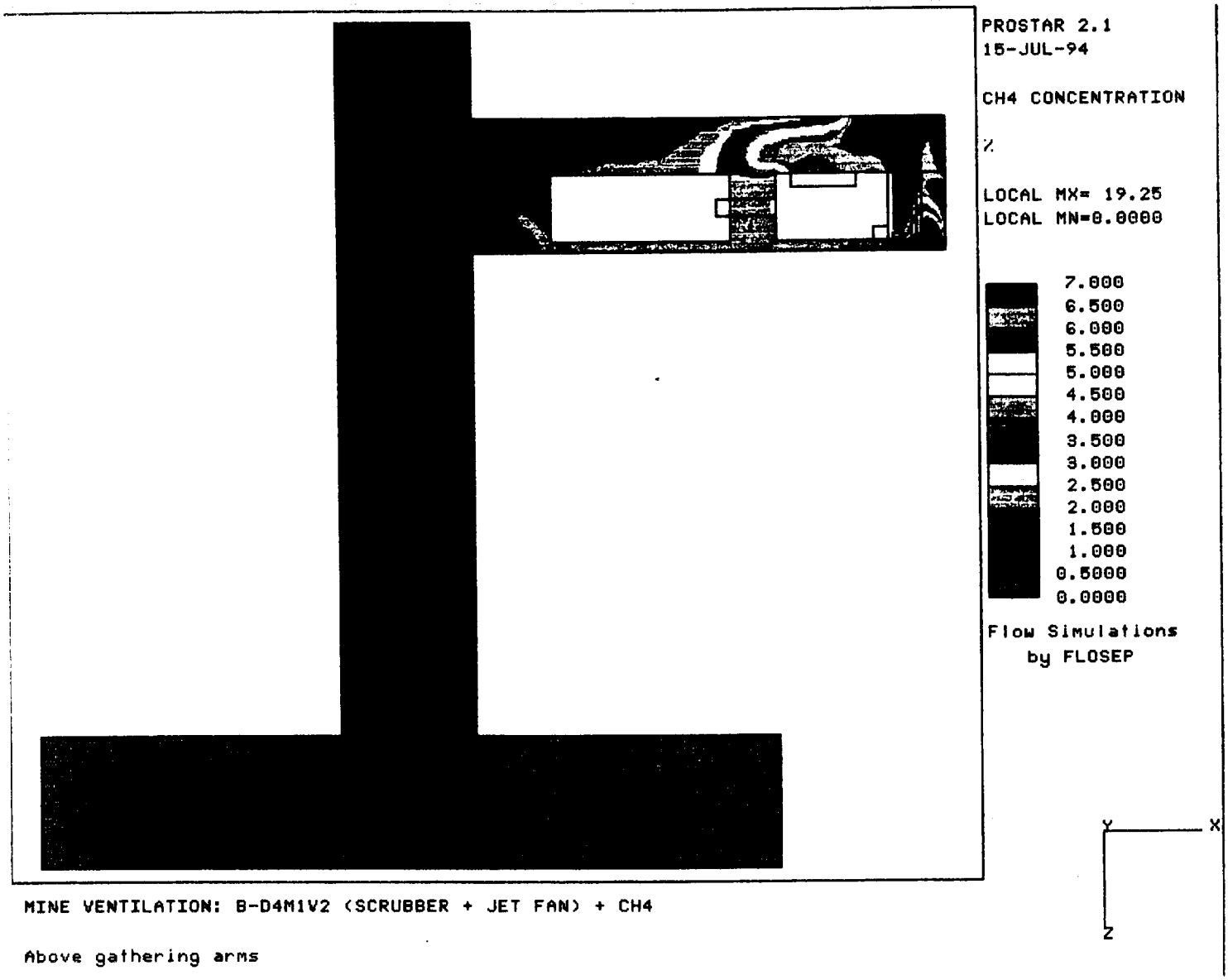

FIGURE 4: Methane contours above gathering arms, full split

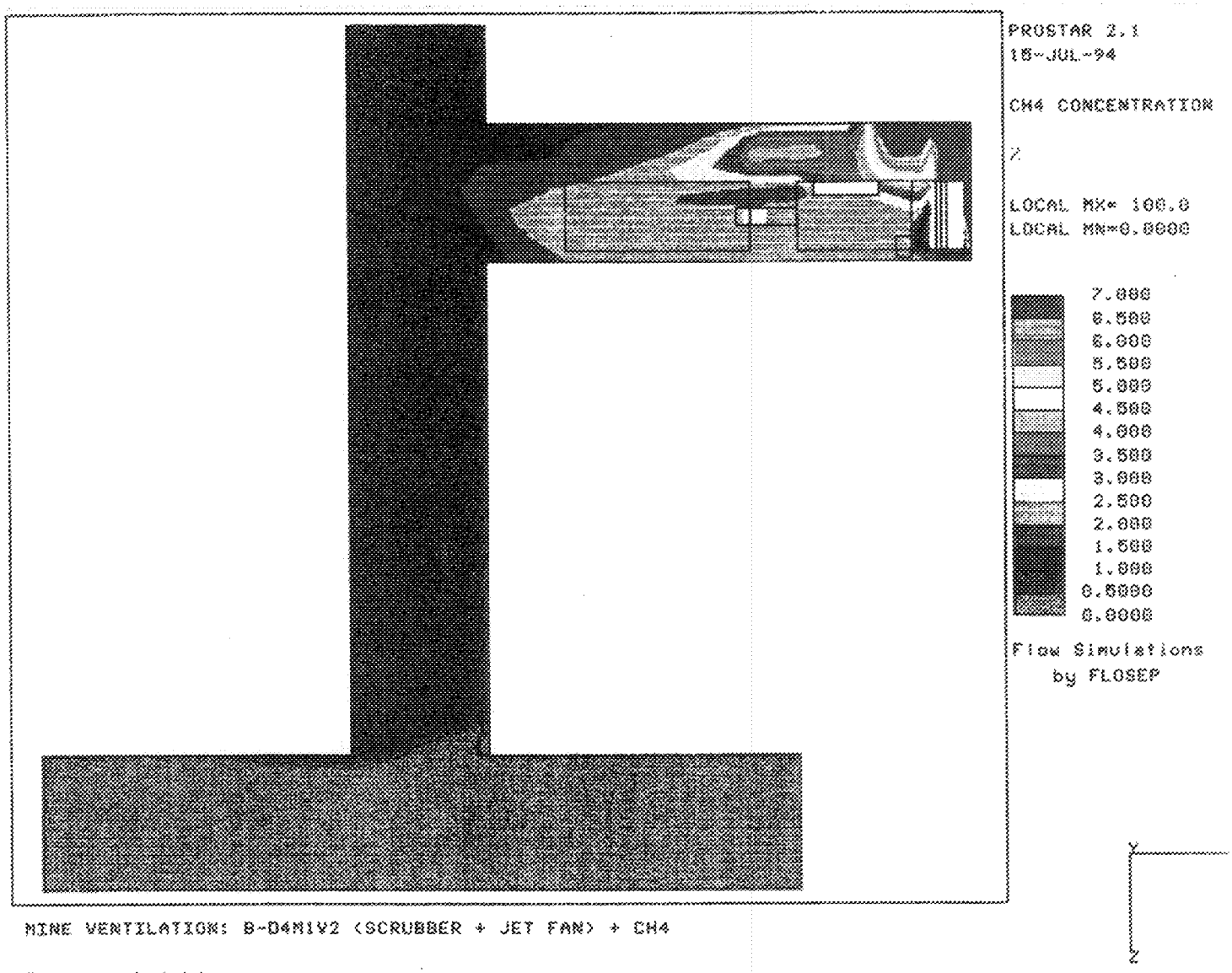

FIGURE 5: Methane contours at operator height, full split

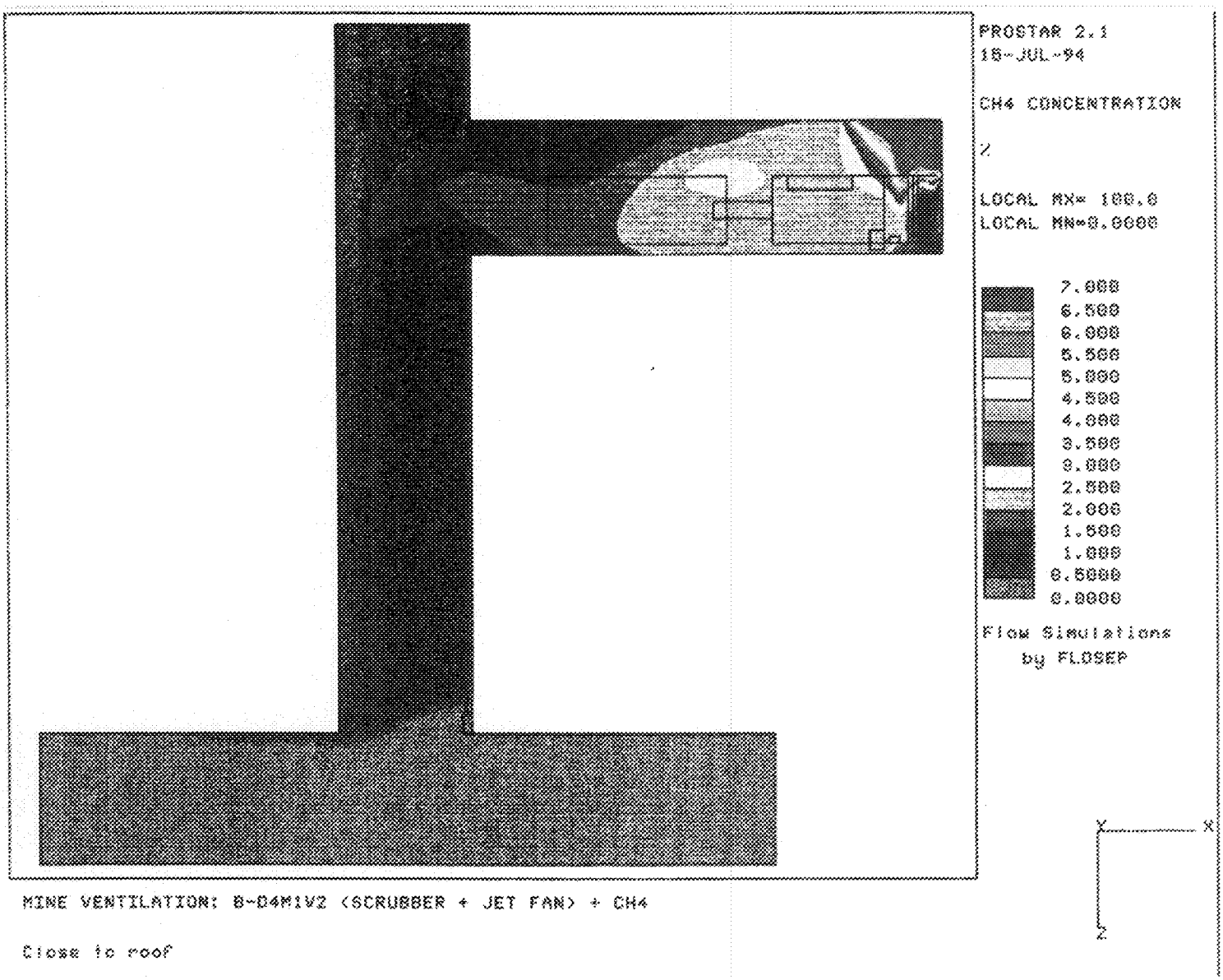

FIGURE 6: Methane contours close to roof, full split

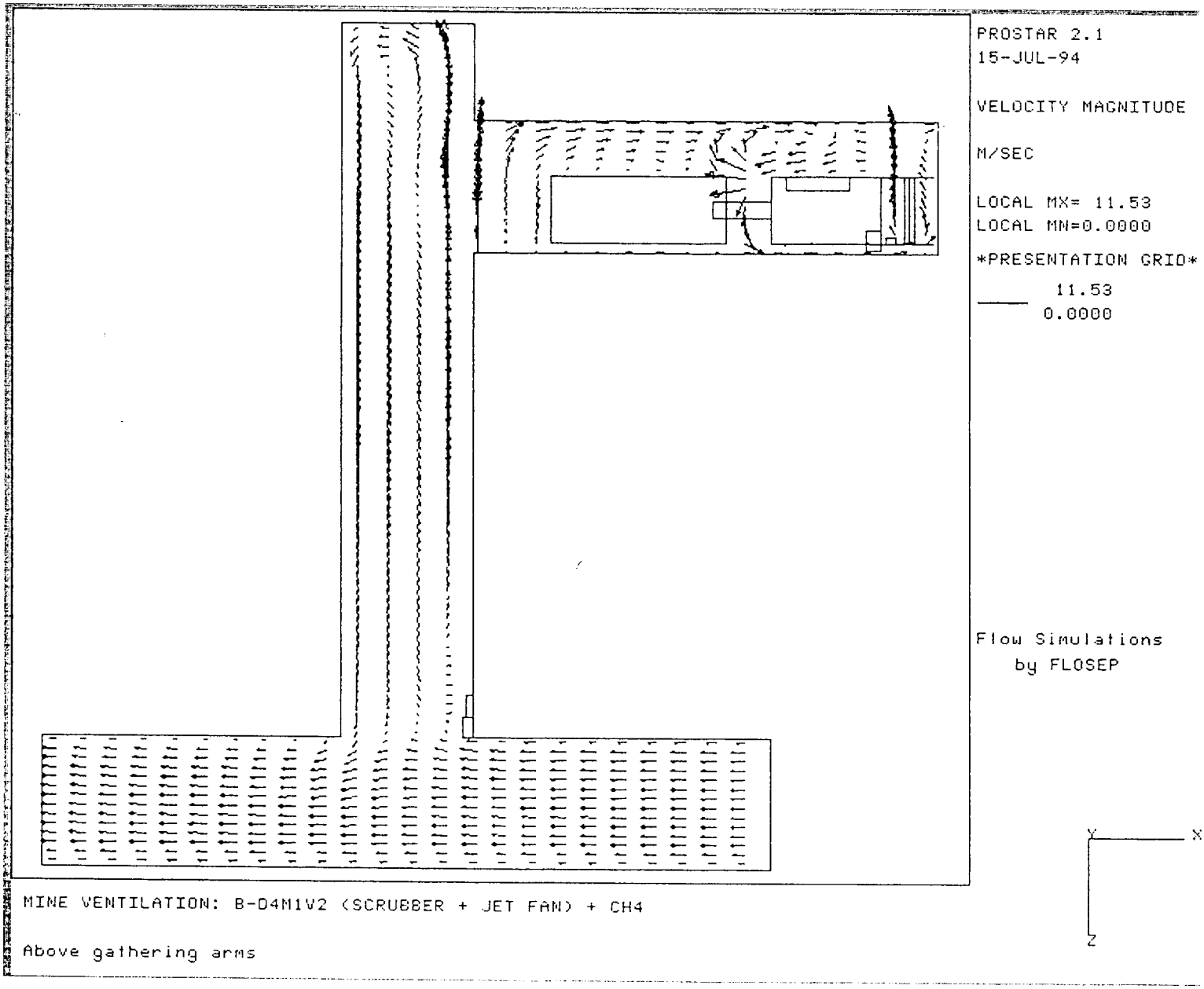

FIGURE 7: Velocity vectors above gathering arms, full split

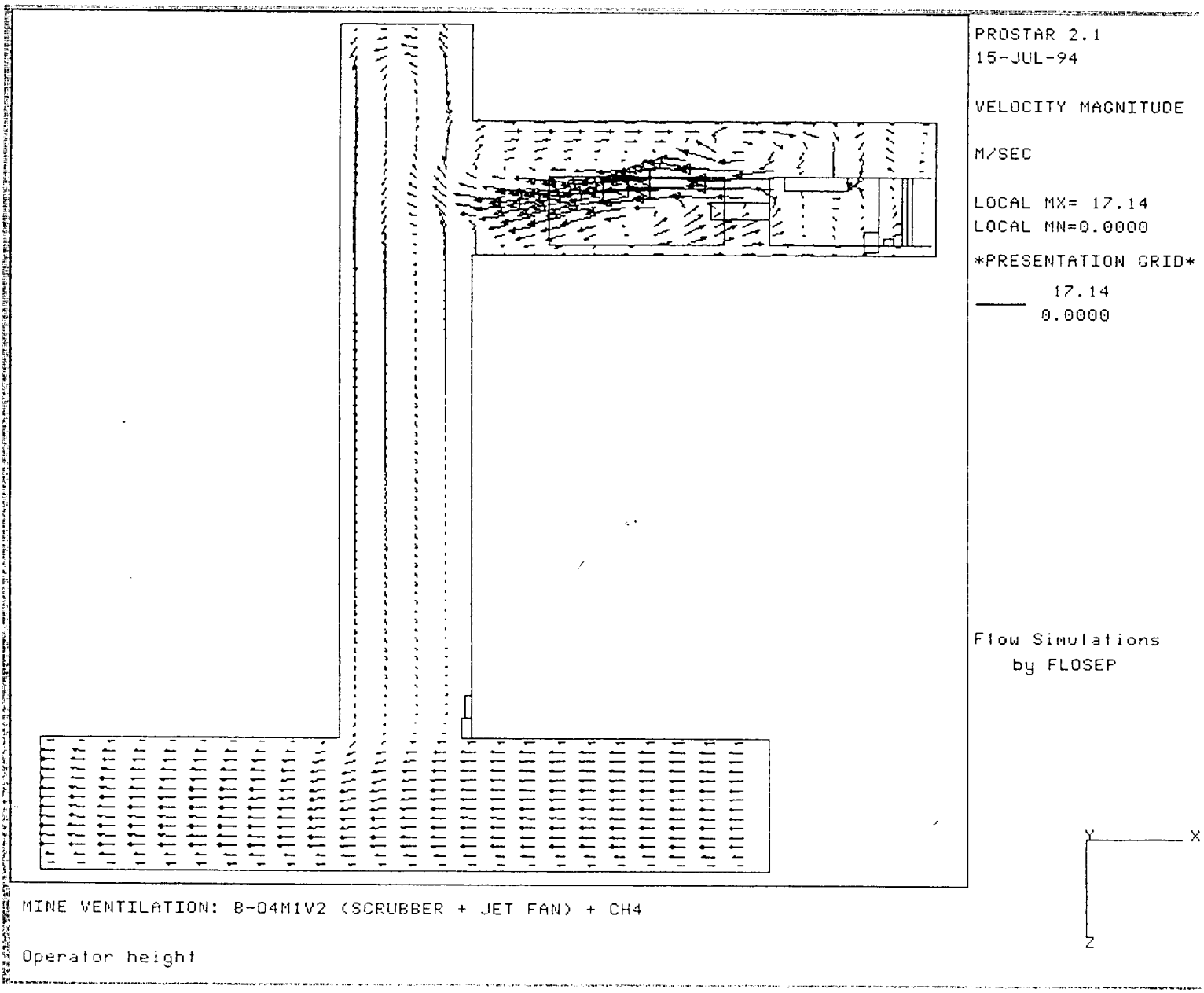

FIGURE 8: Velocity vectors at operator height, full split

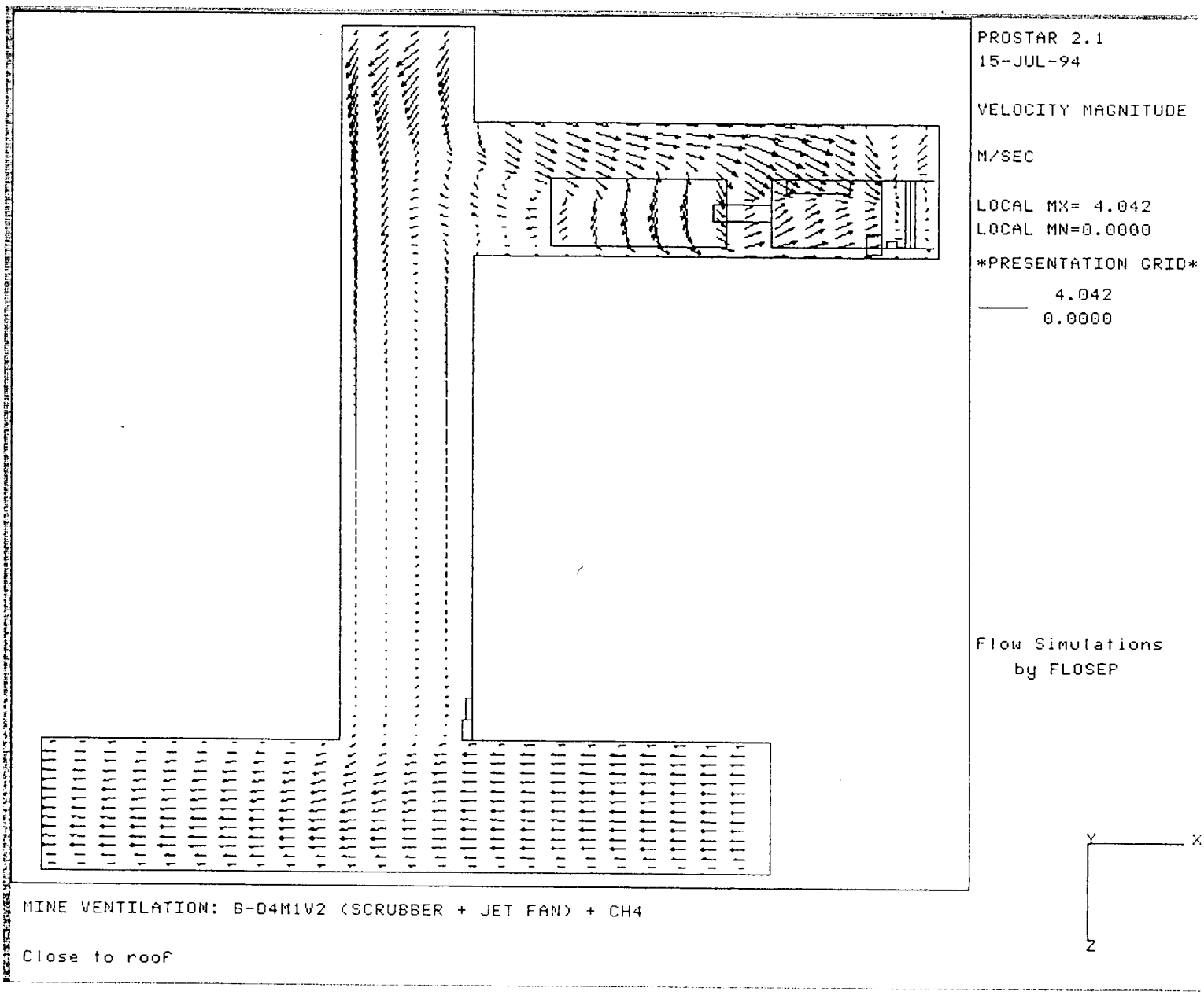

FIGURE 9: Velocity vectors close to roof, full split

Ventilation flow vectors show the scrubber having the most significant effect in the split, with the jet fan at the heading entrance having little influence. The jet fan does appear to create an air curtain affect across the end of the split, especially near to the floor, and this results in recirculation within the split.

CM detail

Figures 10 and 11 show methane contour detail around the CM and SC, and Figures 12 and 13 show the same detail for ventilation flow vectors.

Figure 11 shows vertical planes, and the extent of the contours can be clearly seen, particularly to the left hand side (the top figure). An important result is the high contour, 7,0 (2,5 %) being on the floor and not against the roof. This appears to contradict the common suggestion that methane, being lighter than air tends to layer back against the roof. The centre plane clearly shows the methane being rolled down under the boom by the drum rotation, from where the directional sprays remove it to the left.

The ventilation flows in Figure 13 explain the shape of the methane contours. The plane to the left hand side of the CM clearly shows air against the roof moving towards the face, meeting air returning from the face and being pushed downwards and along the floor beside the CM.

COMPARISON OF SPLIT AND HEADING RESULTS

Figure 14 shows the three dimensional view of methane contours in a heading. More detailed results from the heading simulations can be obtained from Part 1 of this report.

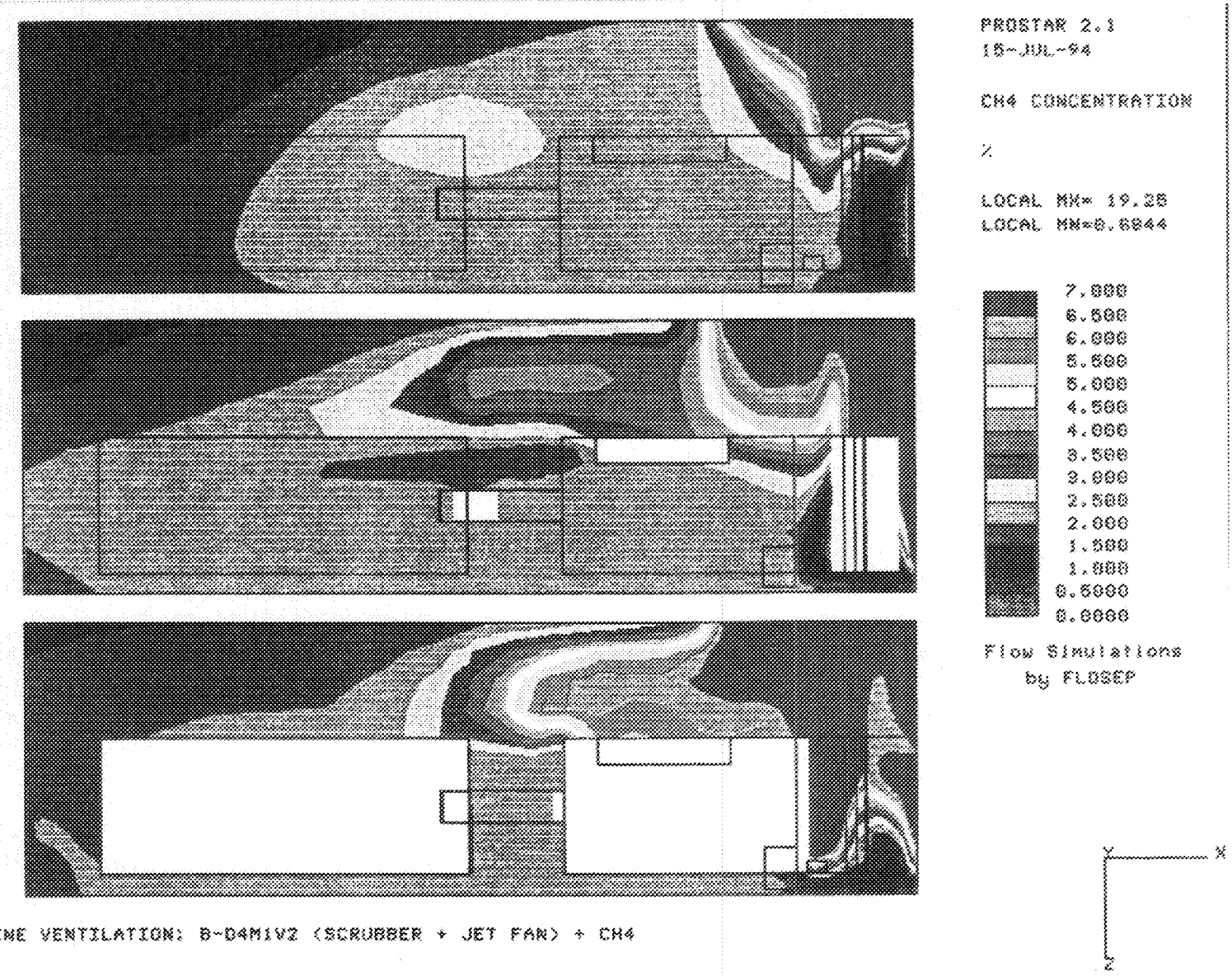

FIGURE 10: Horizontal methane contours, CM detail

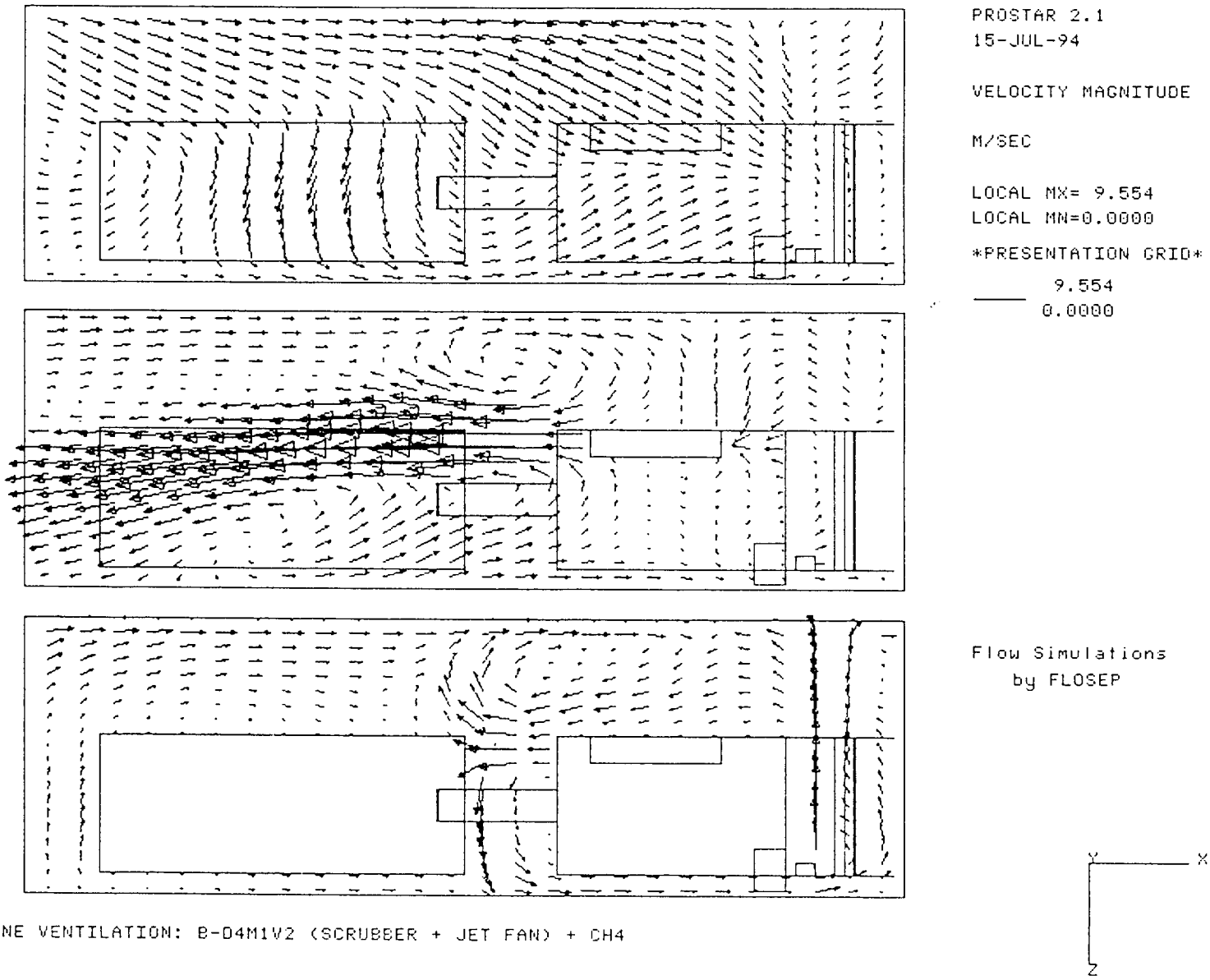

FIGURE 11: Horizontal velocity vectors, CM detail

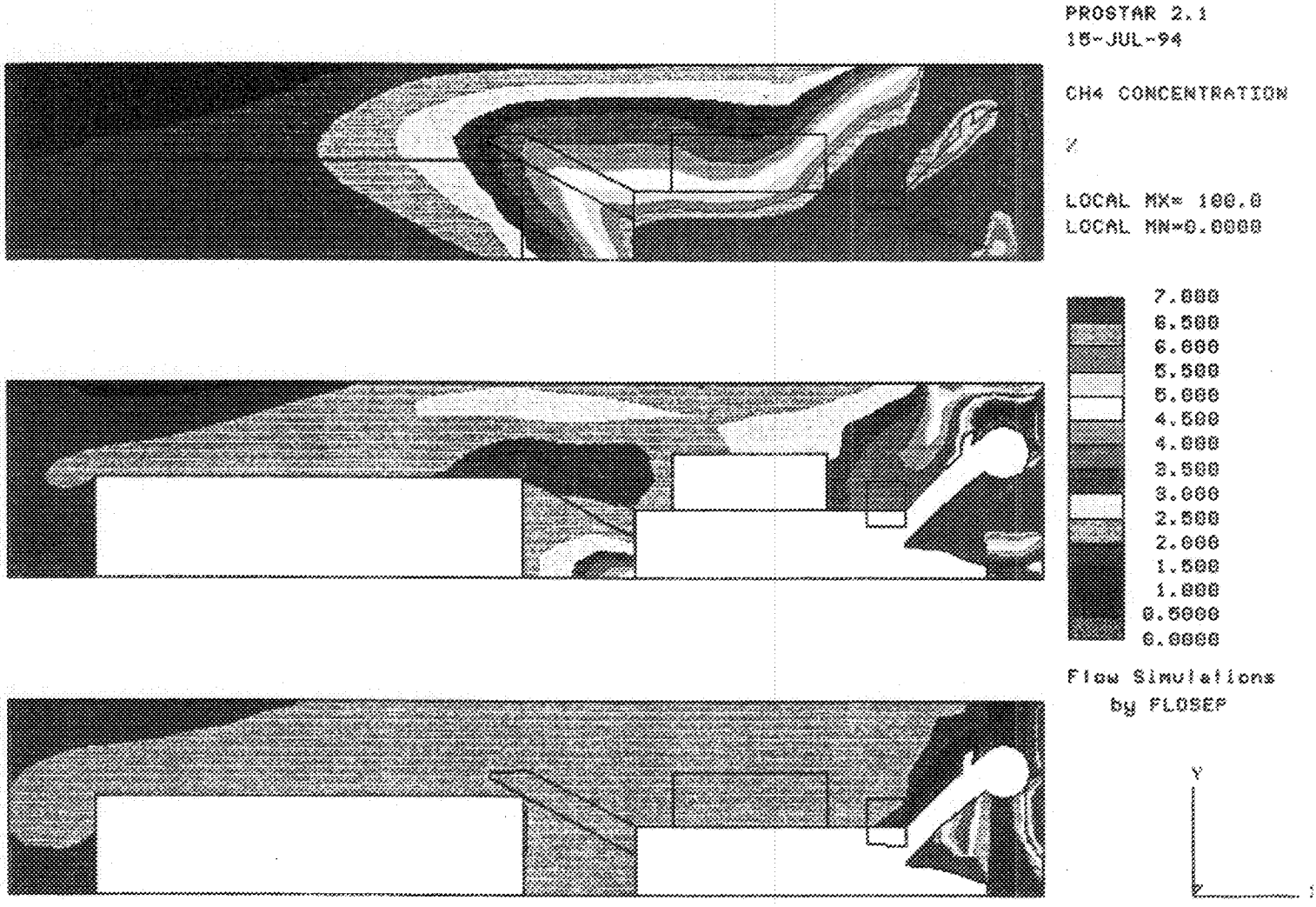

MINE VENTILATION: B-D4M1V2 (SCRUBBER + JET FAN) + CH4

FIGURE 12: Vertical methane contours, CM detail

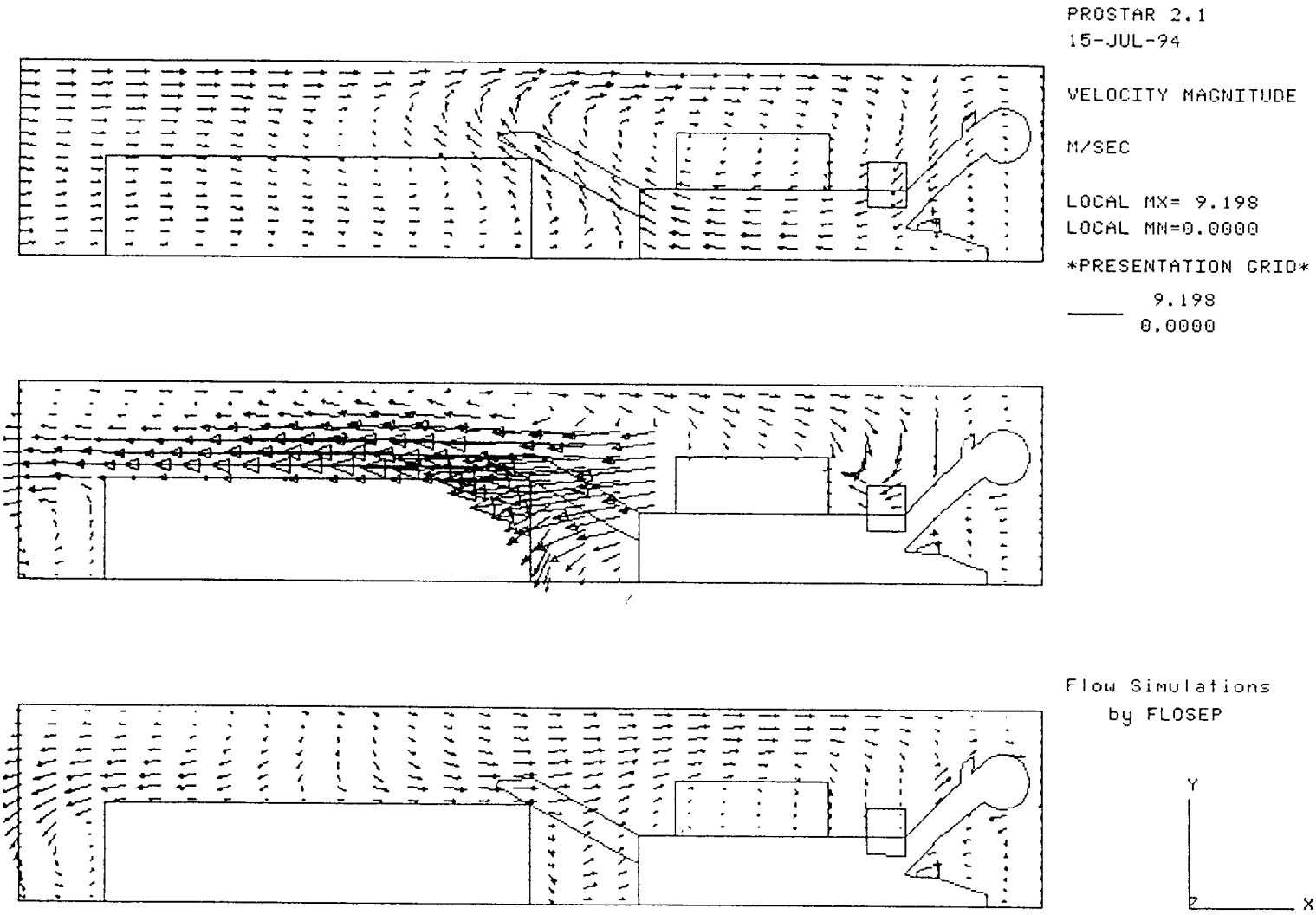

MINE VENTILATION: B-D4M1V2 (SCRUBBER + JET FAN) + CH4

FIGURE 13: Vertical velocity vectors, CM detail

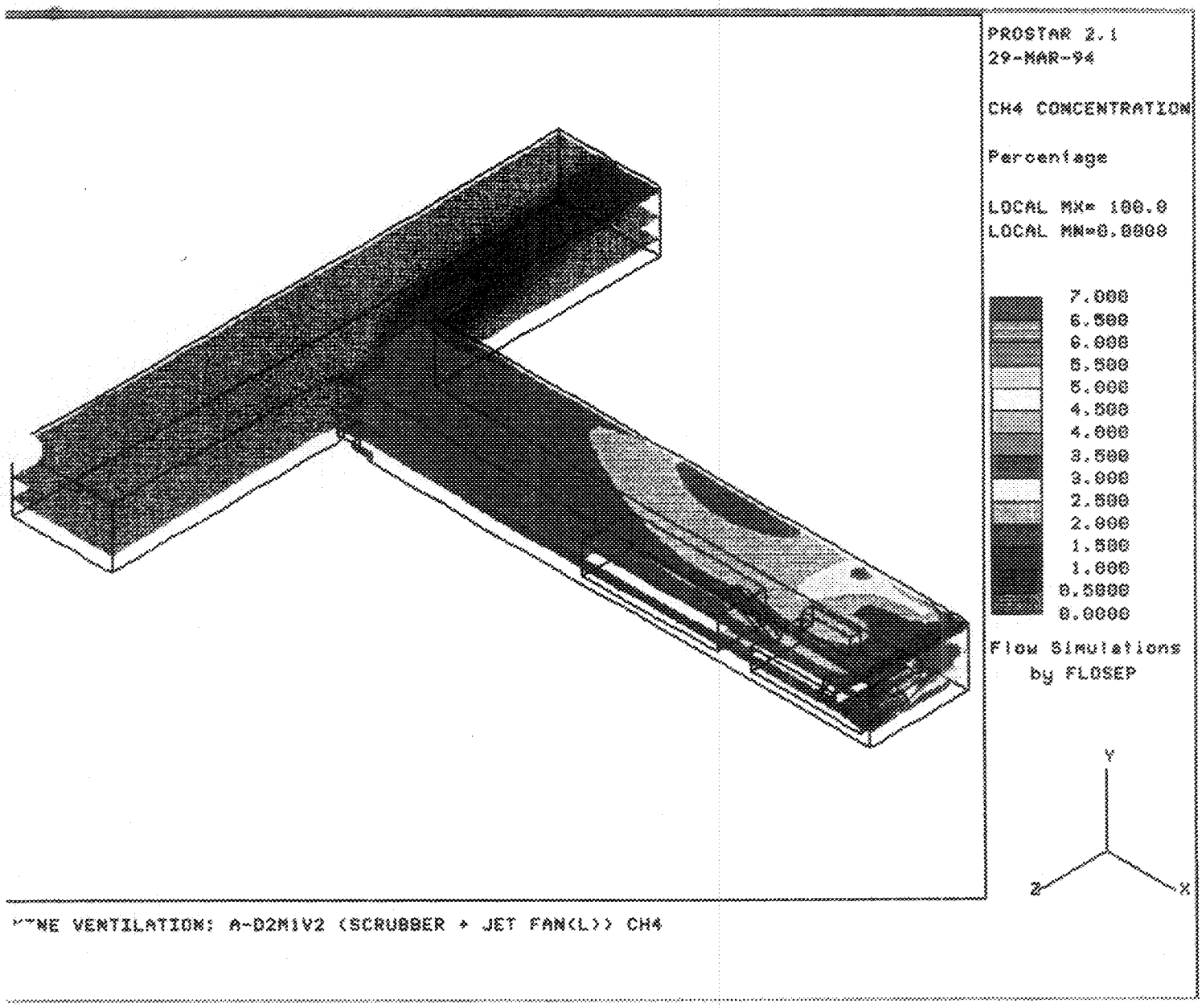

FIGURE 14: 3-D global view of heading

In the heading, methane mixes readily after release at the face, and the contours decrease within a few metres of the face. In the split the contours extend further from the face, due to the reduced volume of fresh air available on the immediate face. Beyond the rear of the CM the methane values are very similar in both the heading and split, being around 2,5 (0,8 %).

CONCLUSIONS

Methane mixes with the ventilation air, and is diluted to manageable levels within a few metres of the face. Once mixed it remains so to the LTR. The general levels in the split were 2,5 (0,8 %), and in the straight were slightly lower at 0,5 (0,2 %). Higher levels were recorded close to the face, with the the 7,0 (2,5 %) contour extending back along the l-h side for the full length of the CM. There is no tendency for the methane to layer against the roof, and at the l-h side of the CM, the highest methane levels occur against the floor, the result of the recirculating ventilation moving towards the face against the roof.

The main difference between the Phase 1 heading simulation, and the Phase 2 split simulation is the distance from the face the 7,0 (2,5 %) contour extends. Less fresh air reaching the face of the split means that the methane levels take longer to dilute, but still do not extend beyond the rear of the CM.

CONTINUING WORK

The same methane emission values and ventilation conditions will next be used for three simulations from Phase 3 of the programme, namely the incomplete stages of the heading, and of the split, and for the full split to the left. This will give methane comparisons for a jet fan in all the mining stages modelled to date.

As more results become available from the on-board data logger system these will be used to further verify the CFD simulations, and to improve the accuracy of the contours. Initial results indicate that the simulated flow patterns are correct, as the relative readings between sensors mounted at various positions on a CM correspond with the relative contours.

APPENDIX C4

SIMULATIONS OF METHANE FLOW AROUND A CONTINUOUS MINER. Part 3: Different heading development stages with jet fan ventilation.

A P COOK / C F MEYER

INTERIM REPORT
SIMRAC PROJECT: COL030
NOVEMBER 1994

SUMMARY

This report deals with the simulations of methane concentrations in a heading and splits at different development stages with a jet fan as the ventilation system. The results showed that at no stage did any methane build-up occur. With the split developed to the left of the heading and the jet fan situated at the right entrance of the heading, large amounts of air recirculation caused methane dilution not to be very effective, but again no methane build-up occurred.

With the heading and the split to the right only partially developed, the small space around the CM tends to keep the methane around the cutting head, only moved around by the sprayfan action and the fresh air flowing into the scrubber inlet. With these particular situations the fresh air from the jet fan could not reach the face and assist in removing the methane.

CONTENTS PAGE

LIST OF FIGURES PAGE

1 INTRODUCTION

The methane project, COL030, used computer simulations (CFD) to determine the methane flow behaviour in a continuous miner heading using specific ventilation systems. Parts 1 and 2 of the project looked at the methane conditions inside a full heading and a full split to the right of the heading while a jet fan and on-board scrubber were used.

This report describes the behaviour of the methane and airflow patterns inside a heading and split at different development stages. Three different development stages with the jet fan and scrubber are discussed.

2 METHANE EMISSIONS AND CONTOURS

As was the case in phases 1 and 2, the objective was to determine the methane behaviour and not concentrate on the actual methane levels. The emission rates were simulated as being 7 l/s/m² immediately in front of the cutting drum, 1 l/s/m² from the exposed face above the drum and 0,2 l/s/m² from the broken coal. The methane level at the scrubber inlet was set at 0,8 %. Methane results are given as the simulation contour value, followed by the equivalent actual percentages as parethesis, e.g. 2,5(0,8%), based on measured underground values compared with the simulations.

3 DIFFERENT DEVELOPMENT STAGES

In all three stages that will be discussed, partial heading; partial split to the right and full split to the left, the same ventilation conditions prevailed. The last through road air velocity was set at 1,0 m/s flowing from right to left past the heading. The jet fan delivered an air quantity of 4,0 m³/s and the on-board scrubber handled a quantity of 10 m³/s. Directional sprays were installed around the cutting drum.

3.1 Development stage 1

Figure 1 shows a partial heading developed ± 20 m from the last through road with the detail of the jet fan, continuous miner (CM) and shuttle car (SC). It also shows the heading dimensions.

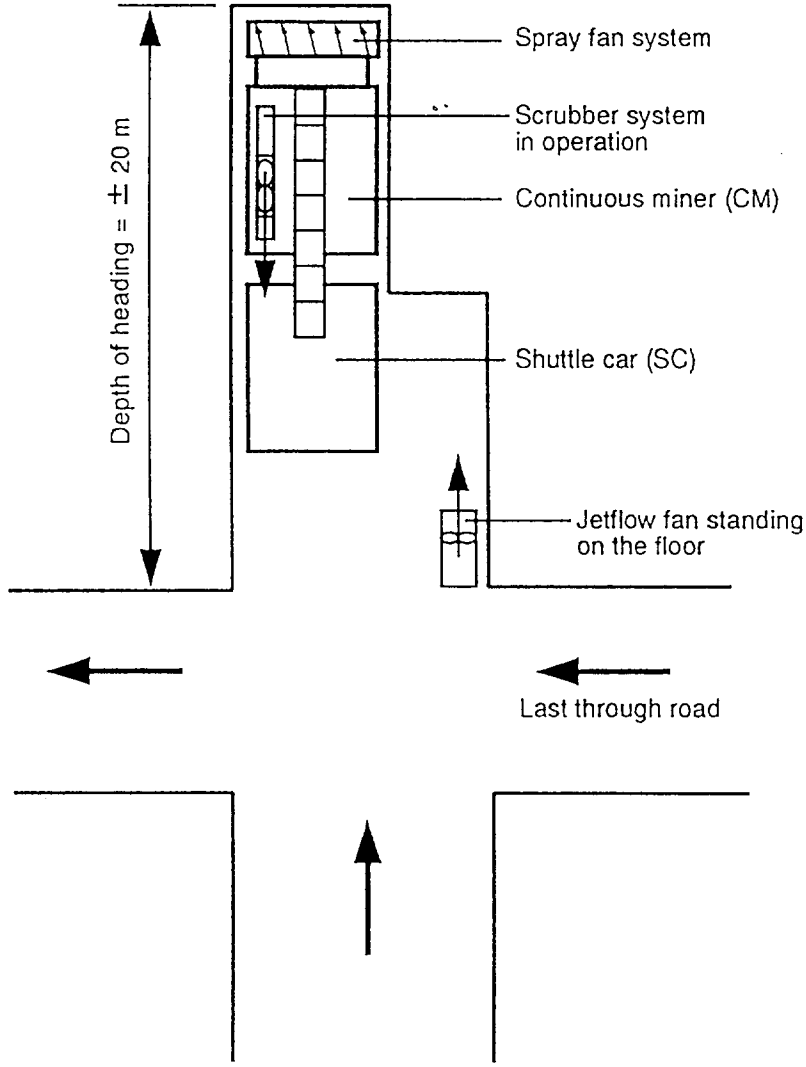

Figure 1: Sketch showing the layout for development stage 1

3.1.1 OVERALL CONDITIONS

Figure 2 shows the airflow vectors at floor level just above the gathering arms. At this level the jet fan is pushing air into the heading against the shoulder of the heading with some fresh air flowing towards the CM. Figure 3 shows the methane contours at this level. Levels of 0,5(0,15%) towards as much as 2(0,6%) are shown towards the back of the CM with 7(2,5%) and more at the face around the cutting area.

Figure 4 and 5 show the airflow vectors and the methane contours at the operator level. At this level the scrubber dominates the airflow patterns with the methane levels being somewhat higher at the back of the SC at 1,5(0,45%) to 2(0,6%). The zone of 7(2,5%) and more has moved backwards over the CM towards the drivers position.

Figures 6 and 7 show the airflow and methane conditions at roof level. Much turbulence is present at this level with a large amount of airflow out of the heading. Methane levels remain at between 1(0,3%) and 2(0,6%) up to the CM with the high levels contained in the face area.

Figure 8 shows a three-dimensional view of the methane contours in this first development stage.

3.1.2 CM DETAIL

Figures 9 and 10 show the detail on the horizontal plane around the CM and SC with regard to the airflow vectors and methane contours. Large amounts of air turbulence and some air recirculation is present in this part of the heading. Because of the position of the jet fan, the scrubber and sprayfan system is dominating the airflow around the CM. The methane contours show that the methane is distributed evenly over the full area of the face. Because of the position of the CM and the resulting airflow patterns, the sprayfan is not successful in removing the gas to the one side of the CM and out of the heading.

Figures 11 and 12 demonstrates the same phenomenon on the vertical plane with the very turbulent airflow patterns and the methane distributed evenly around the cutting head.

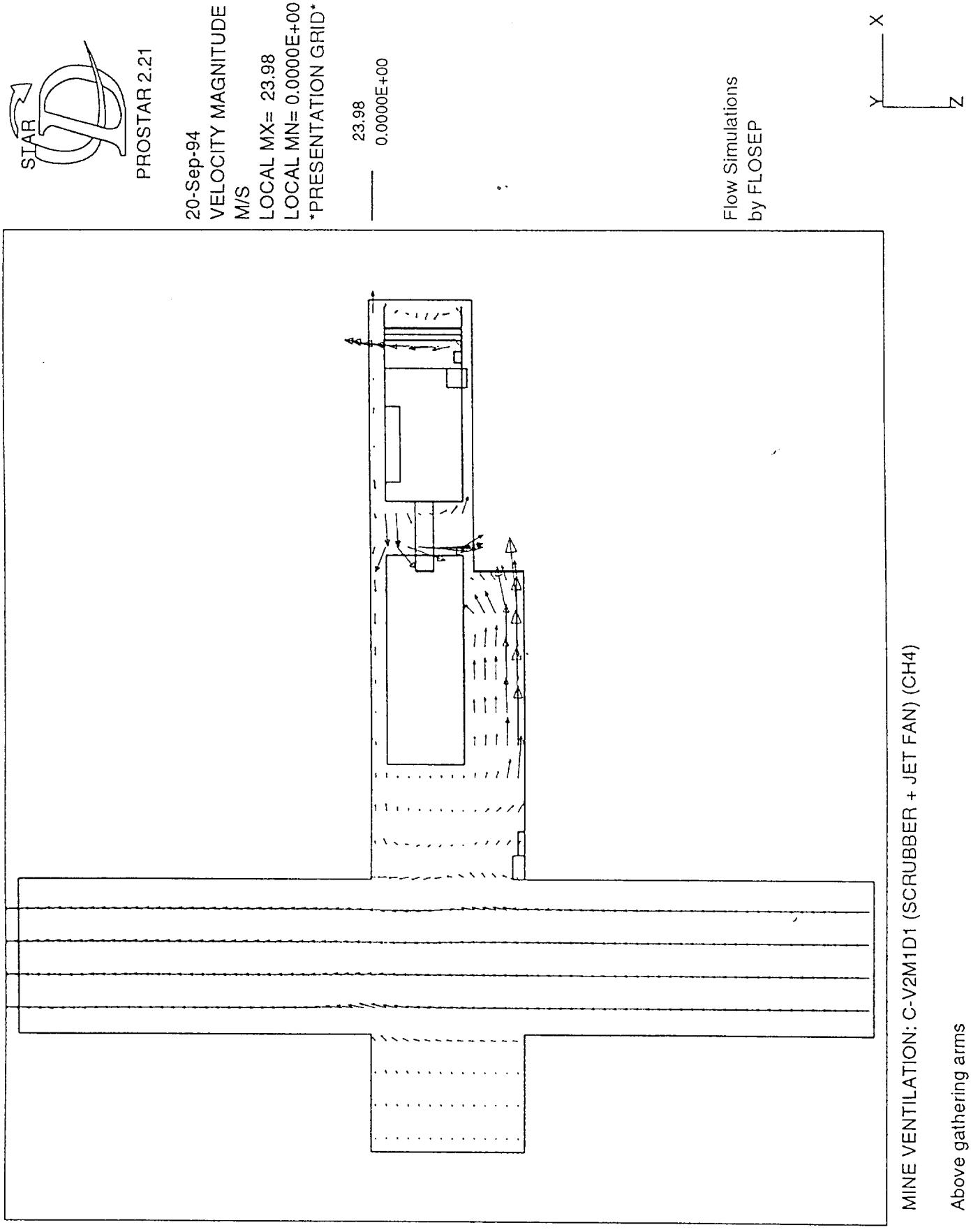

Figure 2: Airflow vectors at floor level for development stage 1

Figure 3: Methane contours at floor level for development stage 1

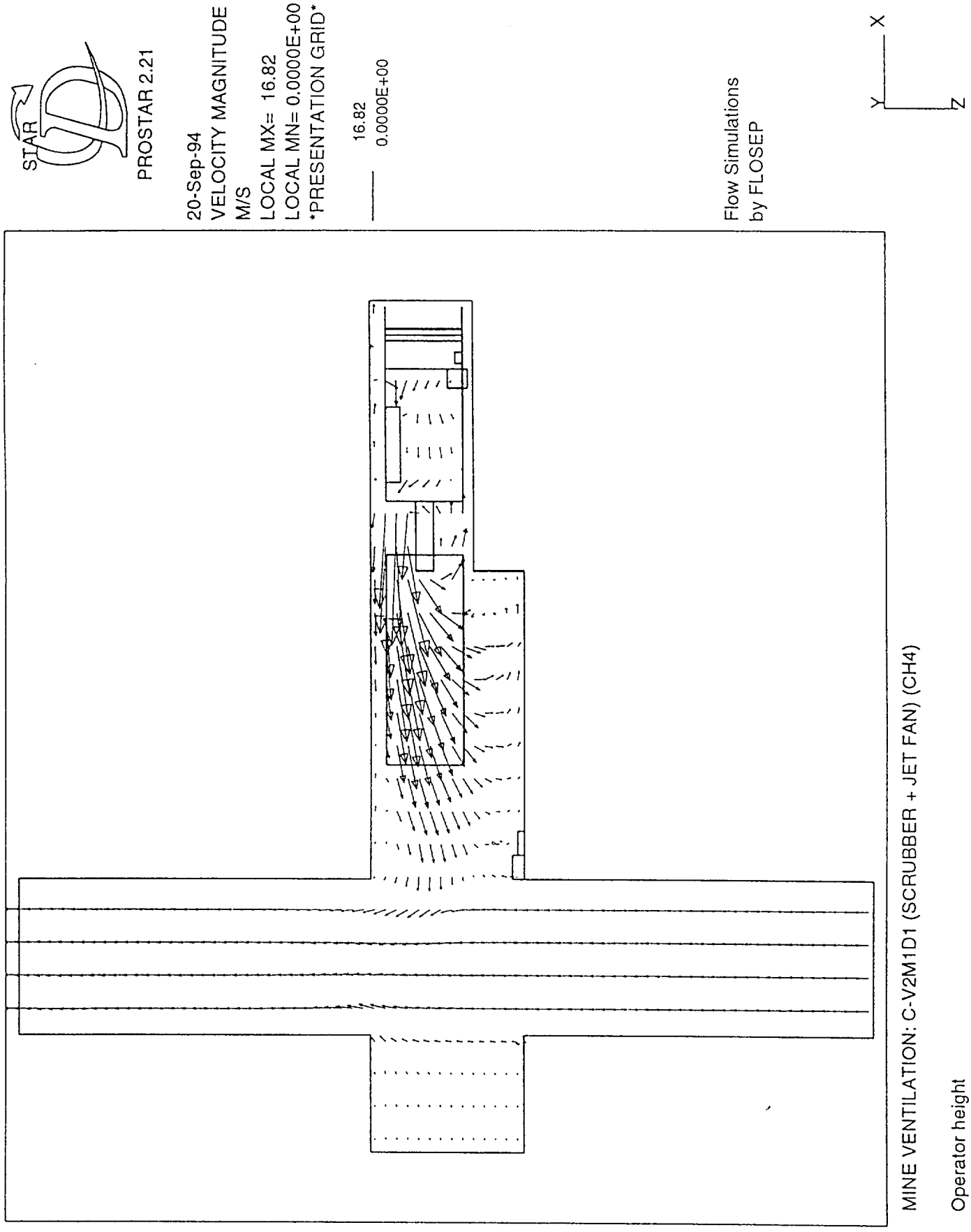

Figure 4: Airflow vectors at operator height for development stage 1

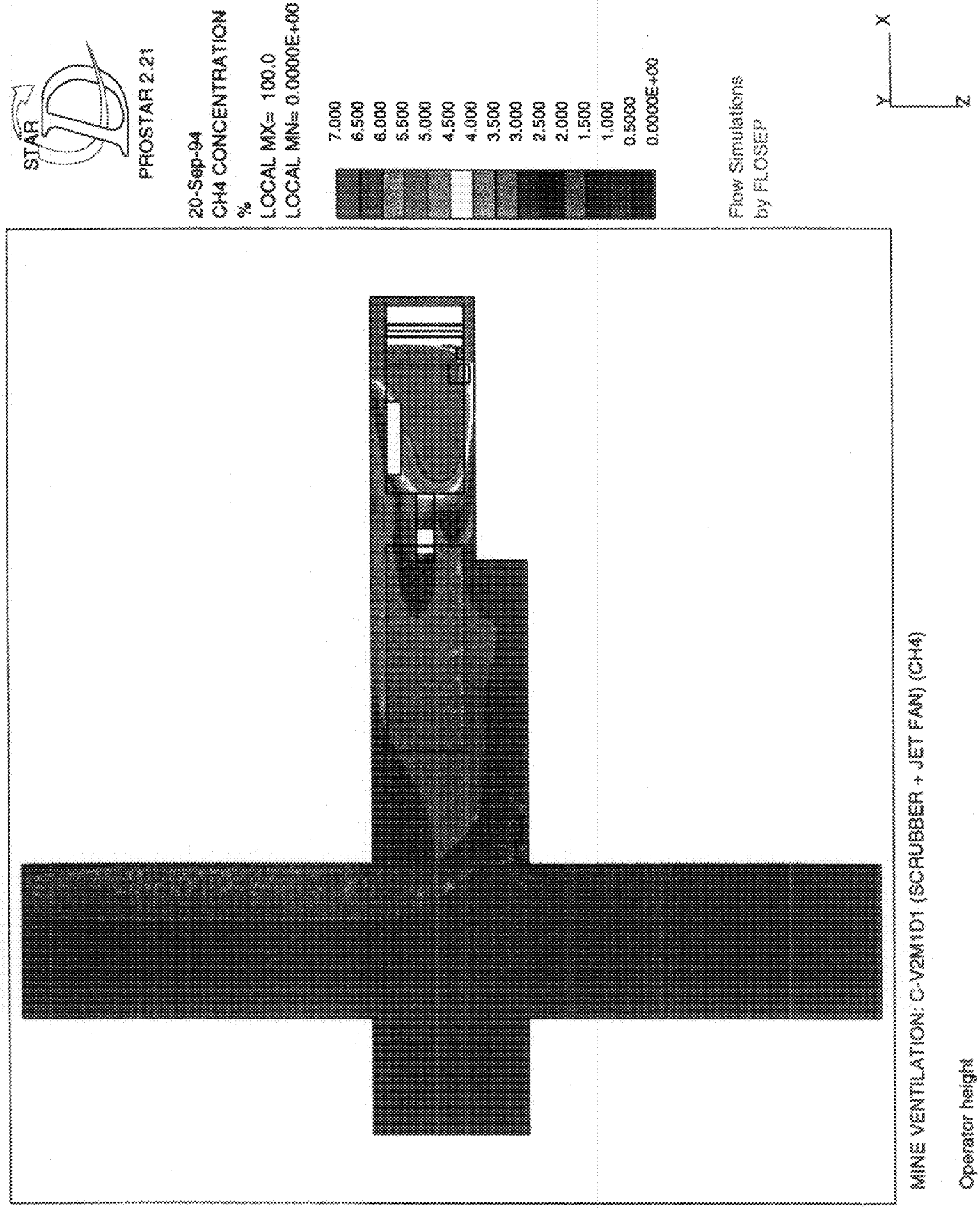

Figure 5: Methane contours at operator height for development stage 1

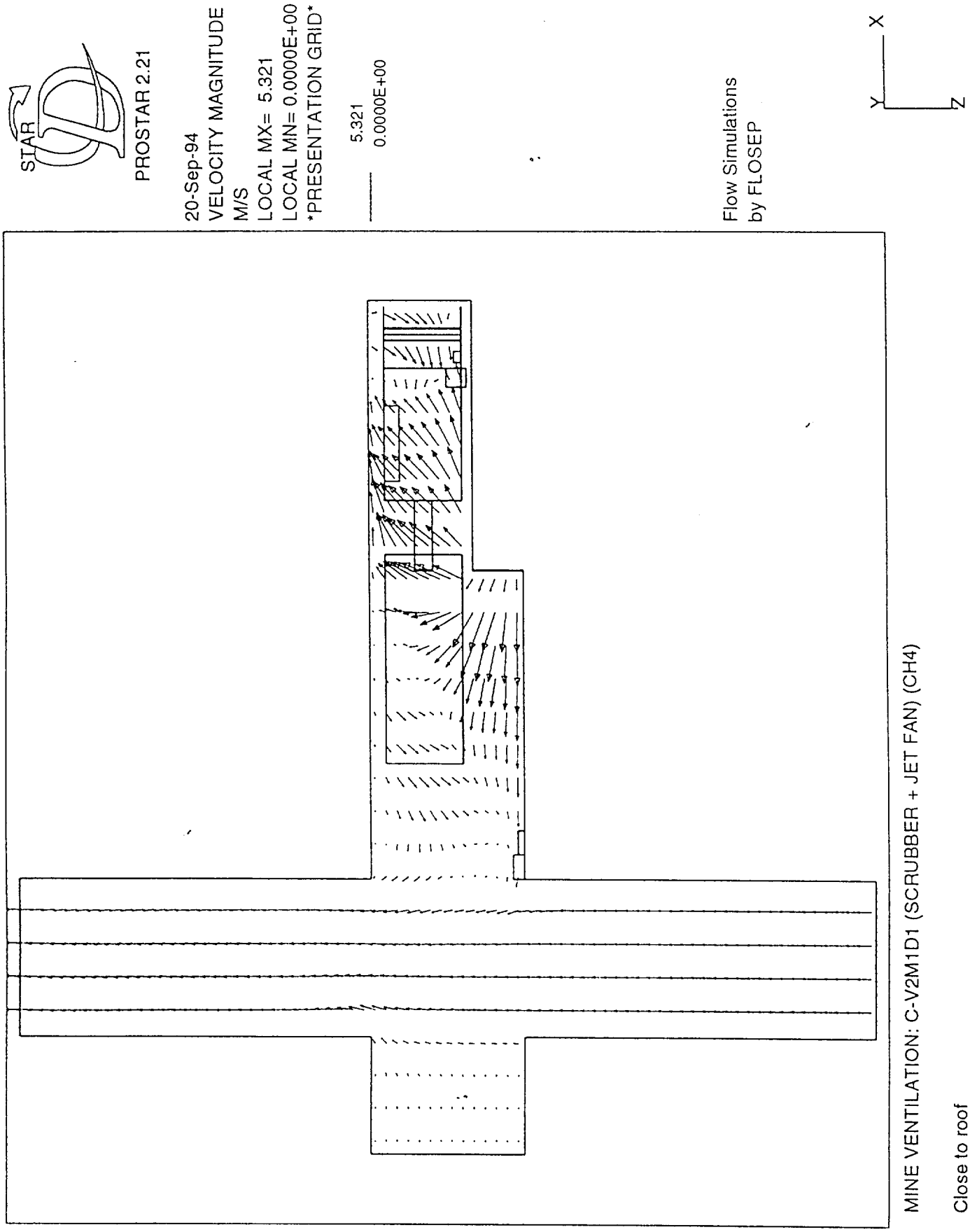

Figure 6: Airflow vectors at roof level for development stage 1

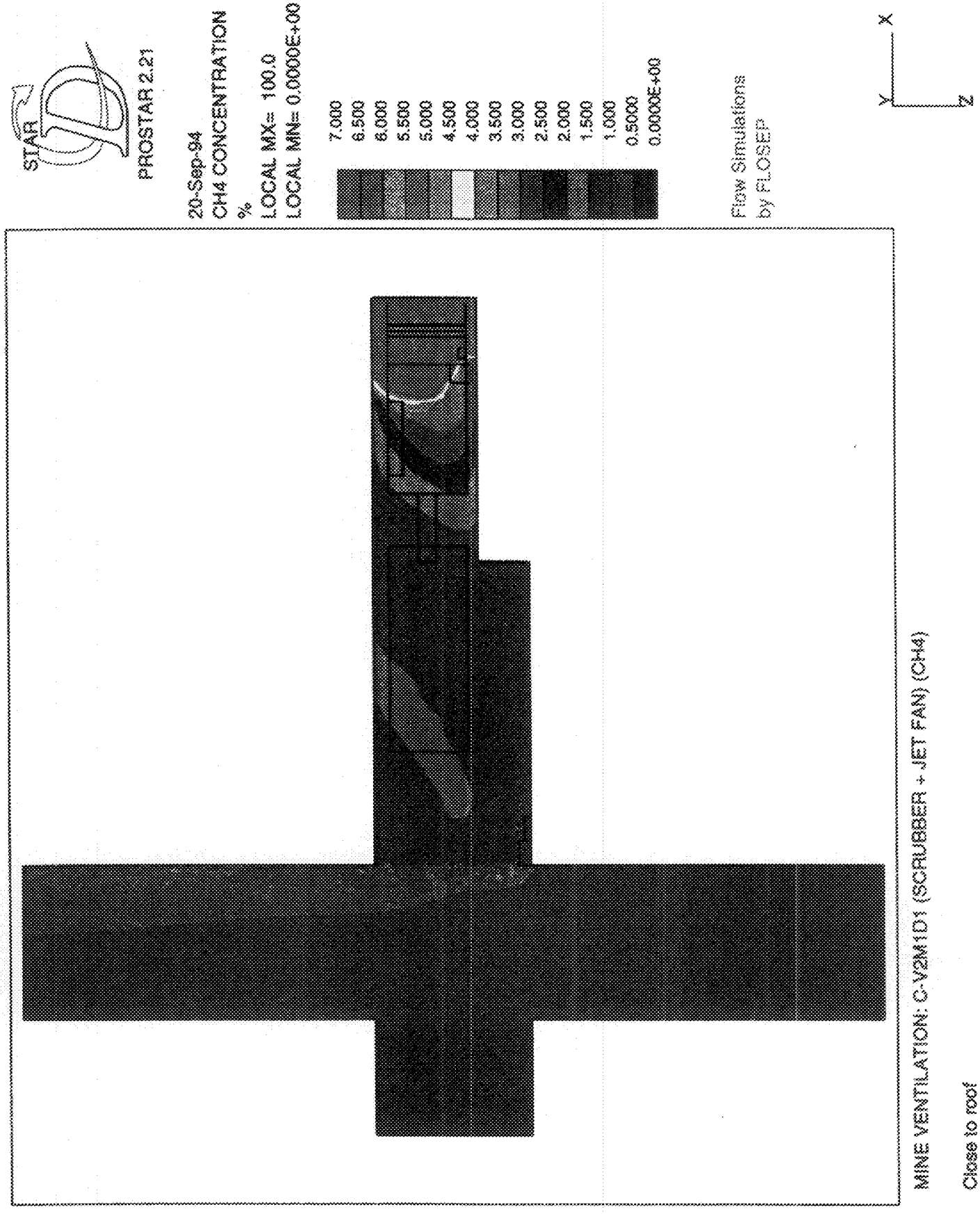

Figure 7: Methane contours at roof level for development stage 1

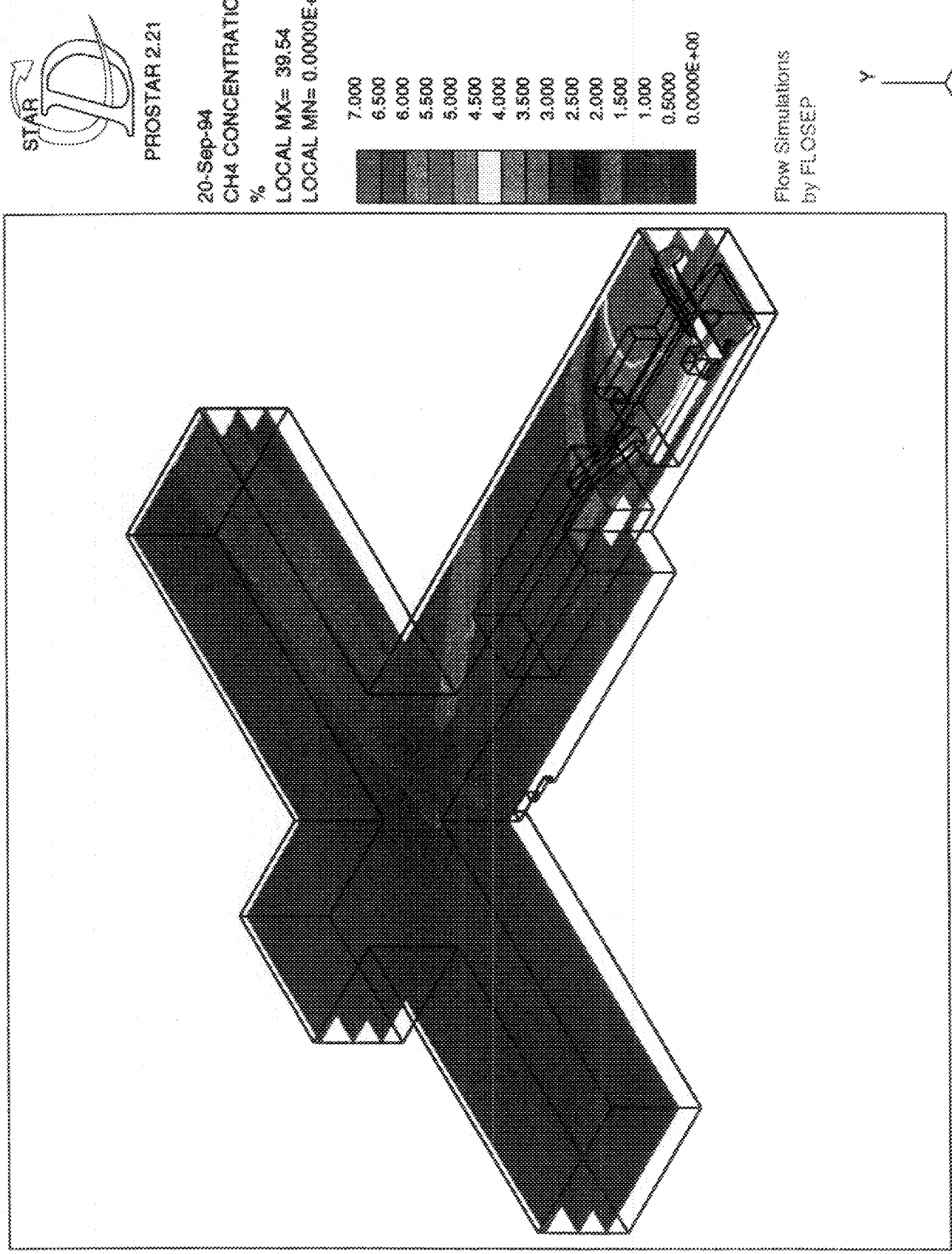

Figure 8: Three-dimensional view of the methane contours for development stage 1

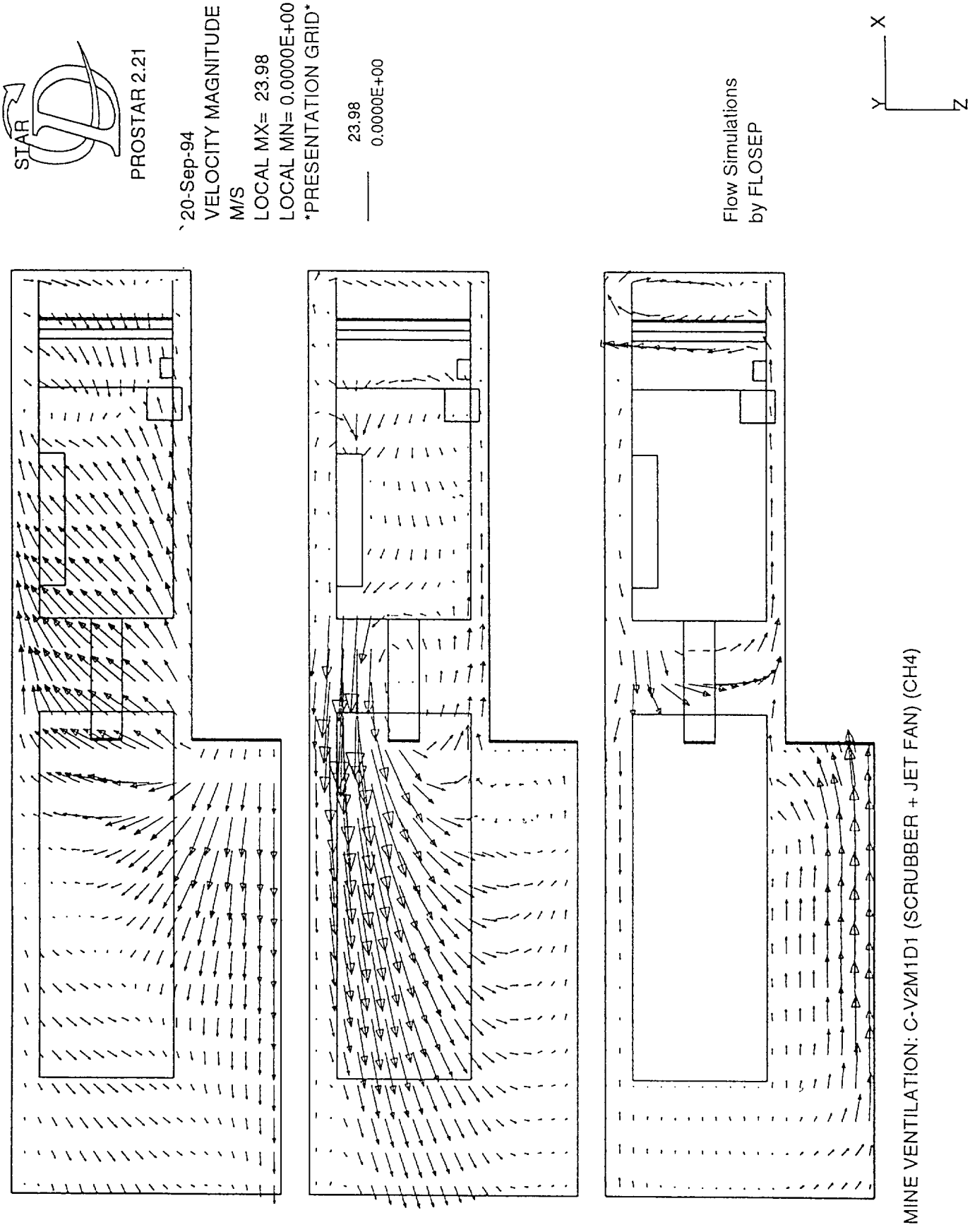

Figure 9: Detail of the airflow vectors around the CM and SC on the horizontal plane

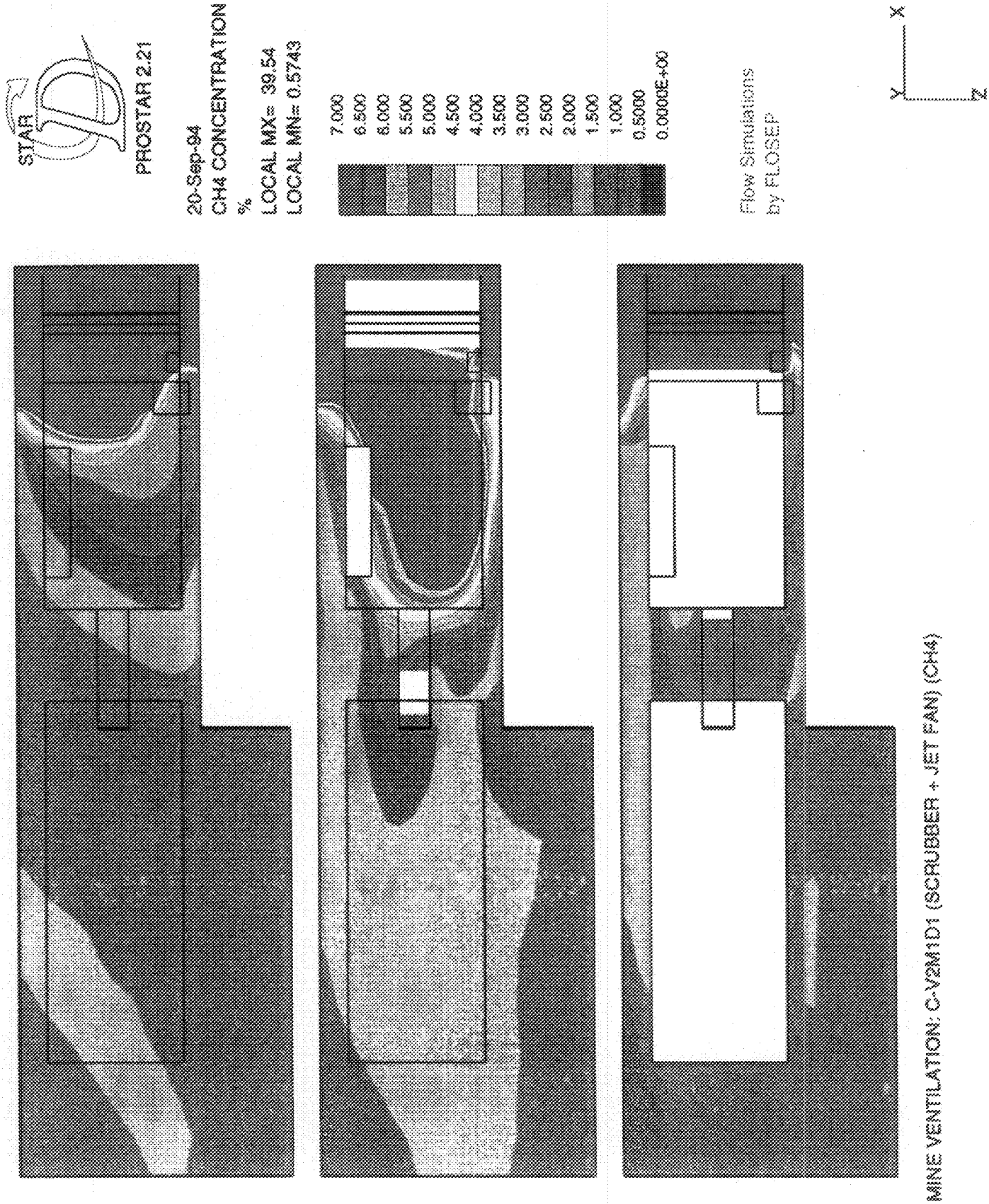

Figure 10: Details of the methane contours around the CM and SC on the horizontal plane

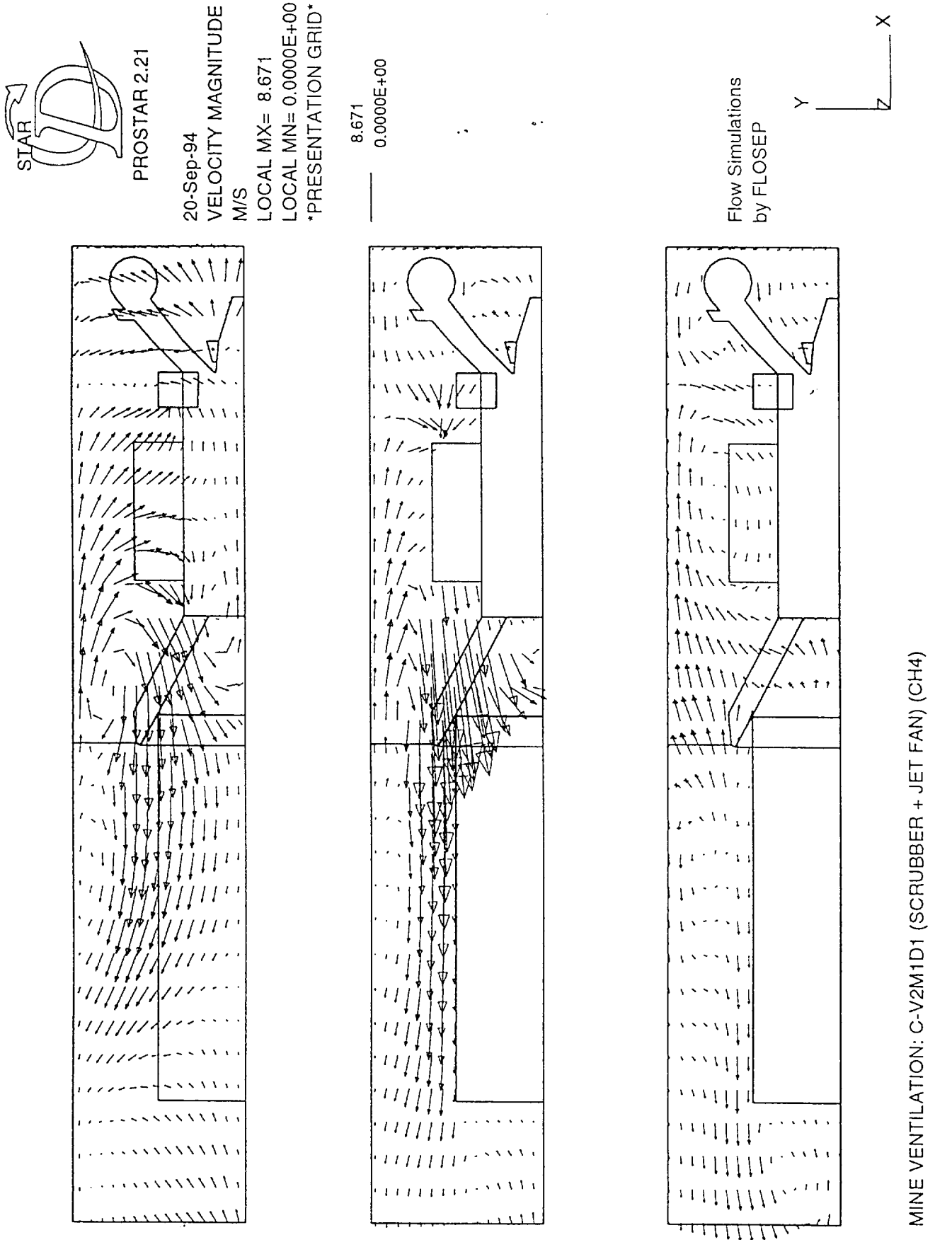

Figure 11: Details of the airflow vectors around the CM and SC on the vertical plane

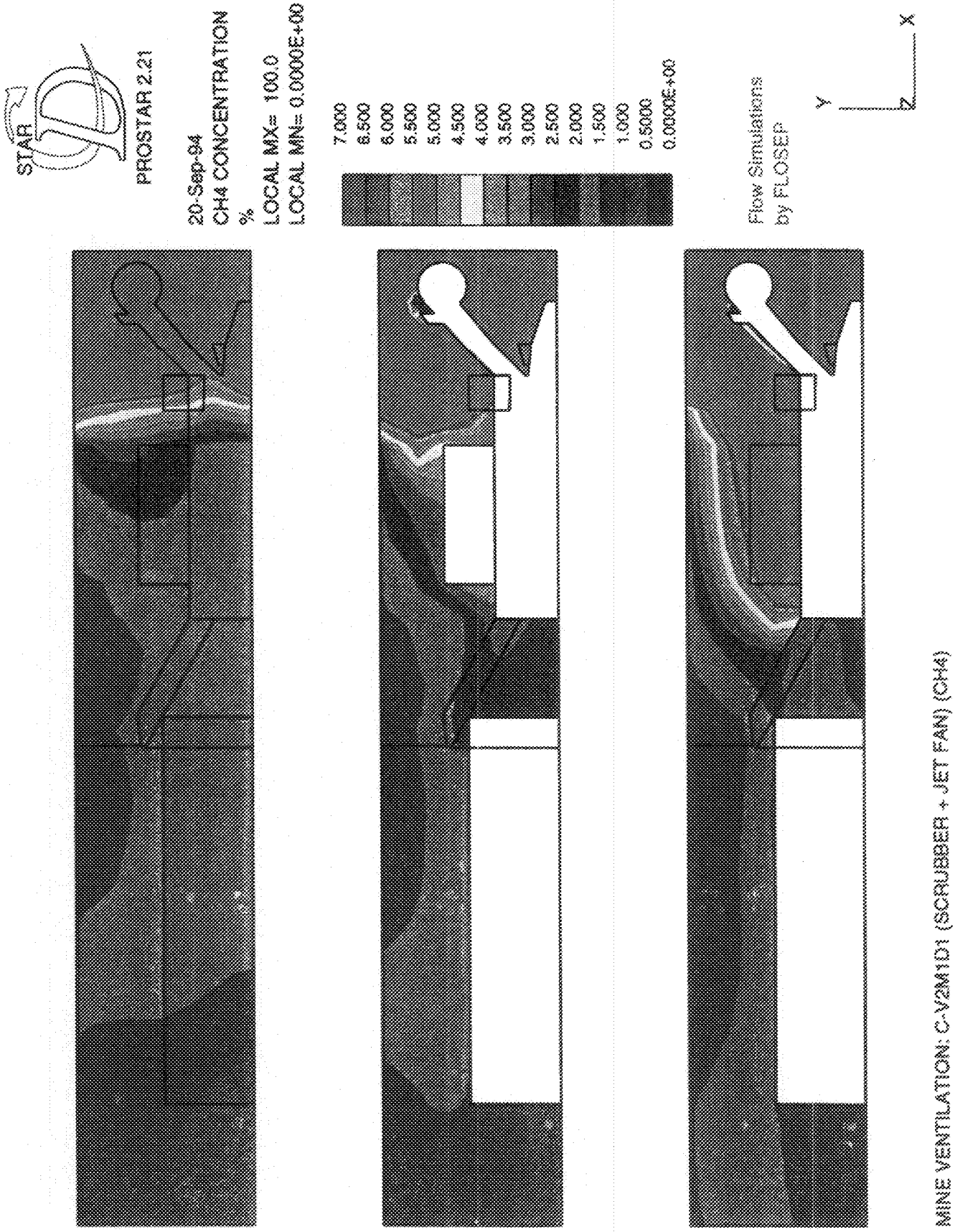

Figure 12: Details of the methane contours around the CM and SC on the vertical planes

3.1.3 INTERIM CONCLUSIONS

The results show that the methane does not layer or accumulate at any specific position. The turbulent airflow patterns around the CM and SC provides for quick and effective dilution of the methane to levels as low as 0,5(0,15%). Even with a small amount of the air from the jet fan reaching the face area, dilution rates are still high. The methane extends back over the CM at operator height caused by recirculating air against the roof. The entire cutting drum and boom are within the highest contour 7(2,5%), so the effectiveness of the sprayfans is reduced by the enclosed space around the CM. These simulation results emphasises the importance of the correct mining sequence with regard to the fan position (See paragraph on mining sequence at the end of this report.)

3.2 **Development stage 2**

Figure 13 shows the detail of the second development stage. This sketch demonstrates a partial split developed to the right of the heading with the CM and SC in the left corner of the face. The jet fan remained at the entrance of the heading in the upstream position.

3.2.1 OVERALL CONDITIONS

Figures 14, 15 and 16 show the airflow vectors at the floor, operator and roof levels. The jet fan is blowing the air past the entrance of the split creating an air curtain at this position. Because of this, the scrubber and sprayfan dominate the airflow patterns inside the split, causing similar conditions to prevail inside the face area than in development stage 1. Figures 17, 18 and 19 further demonstrates this statement in that the methane contours are similar in the split area. The concentration of 7(2,5%) and more is confined around the cutting drum with the levels in the rest of the split area diluting to 0,5(0,15%) and 0(0%) when reaching the entrance of the split.

See Figure 20 for a three-dimensional view of the methane contours inside the split and heading.

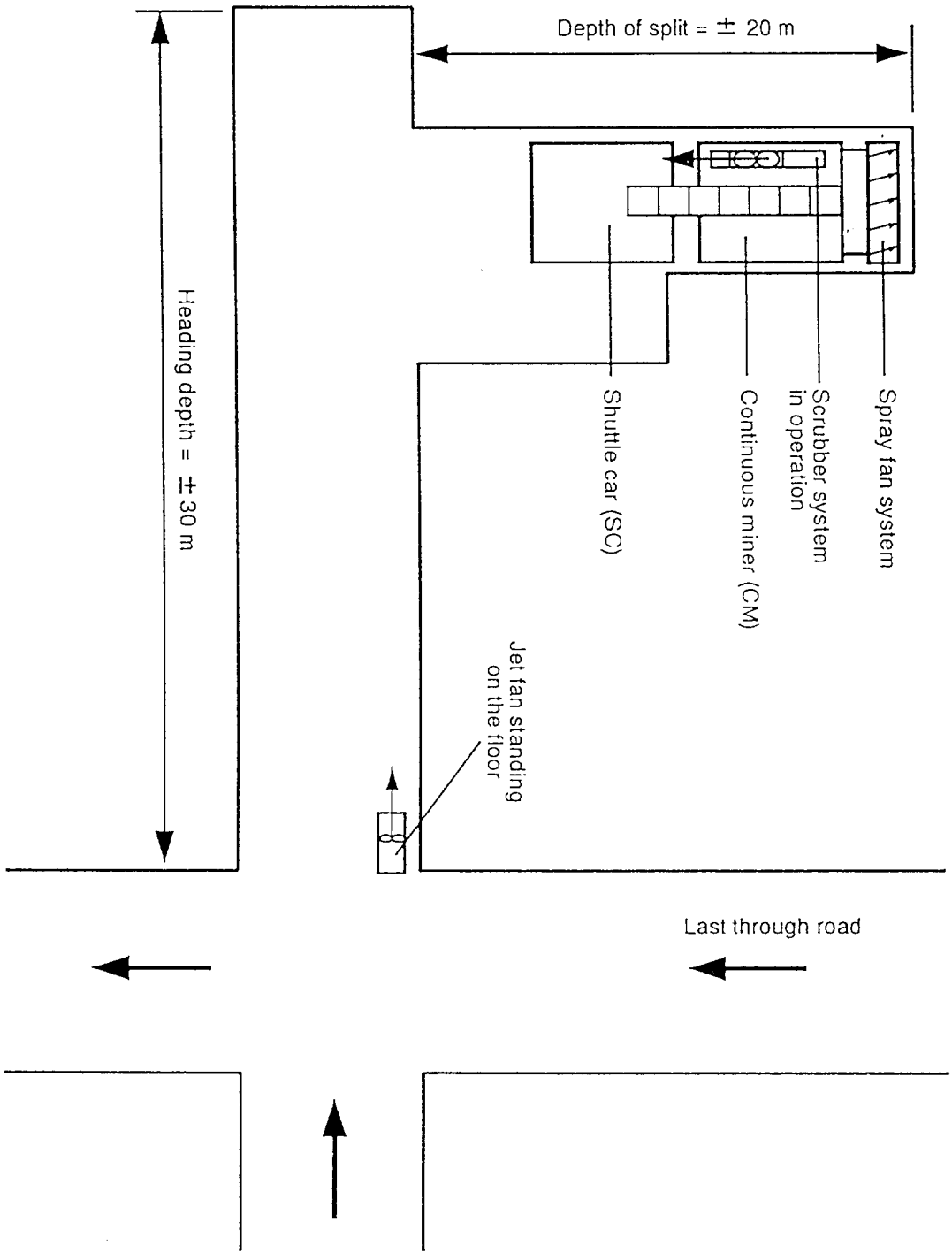

Figure 13: Sketch showing the layout for development stage 2

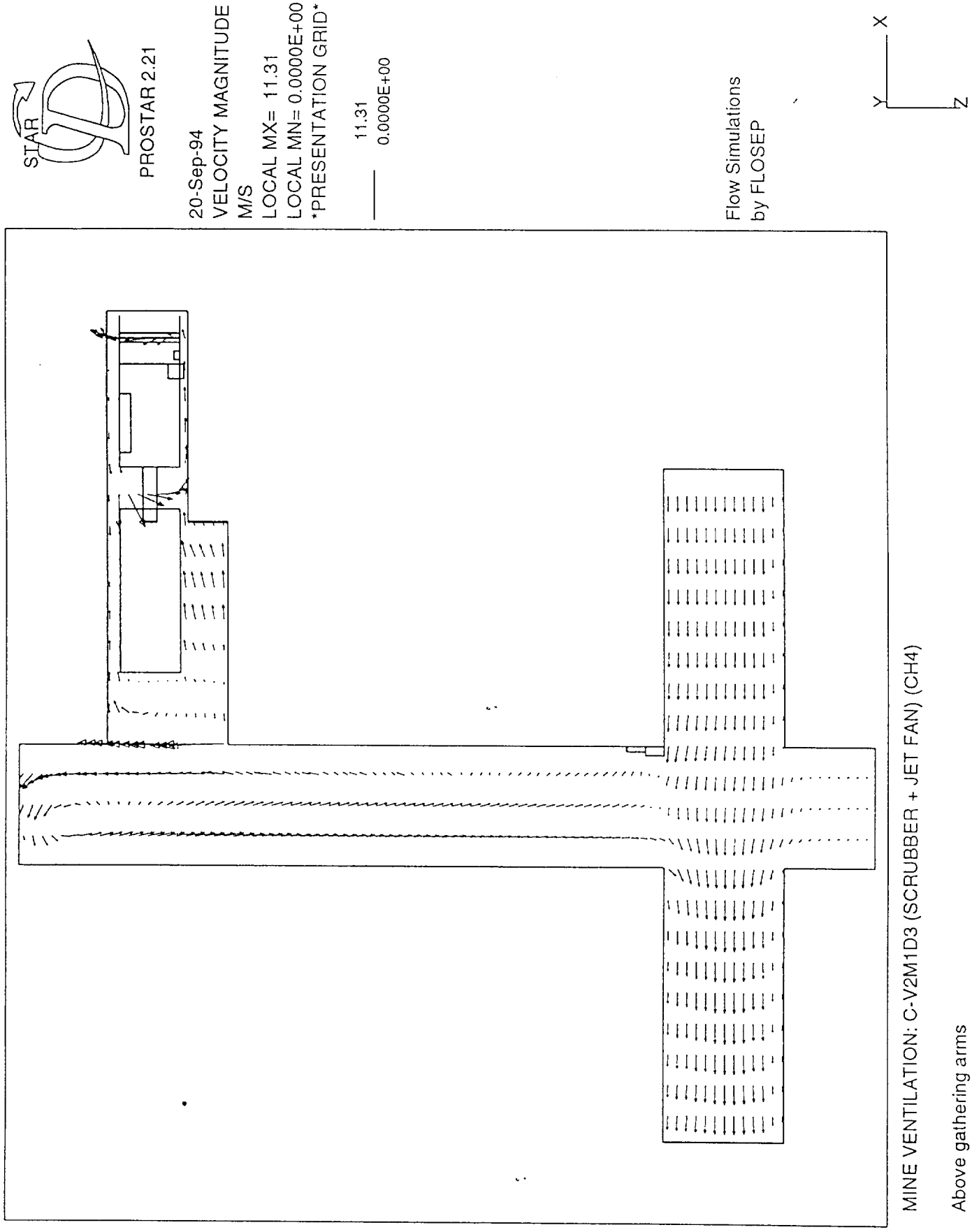

Figure 14: Airflow vectors at floor level for development stage 2

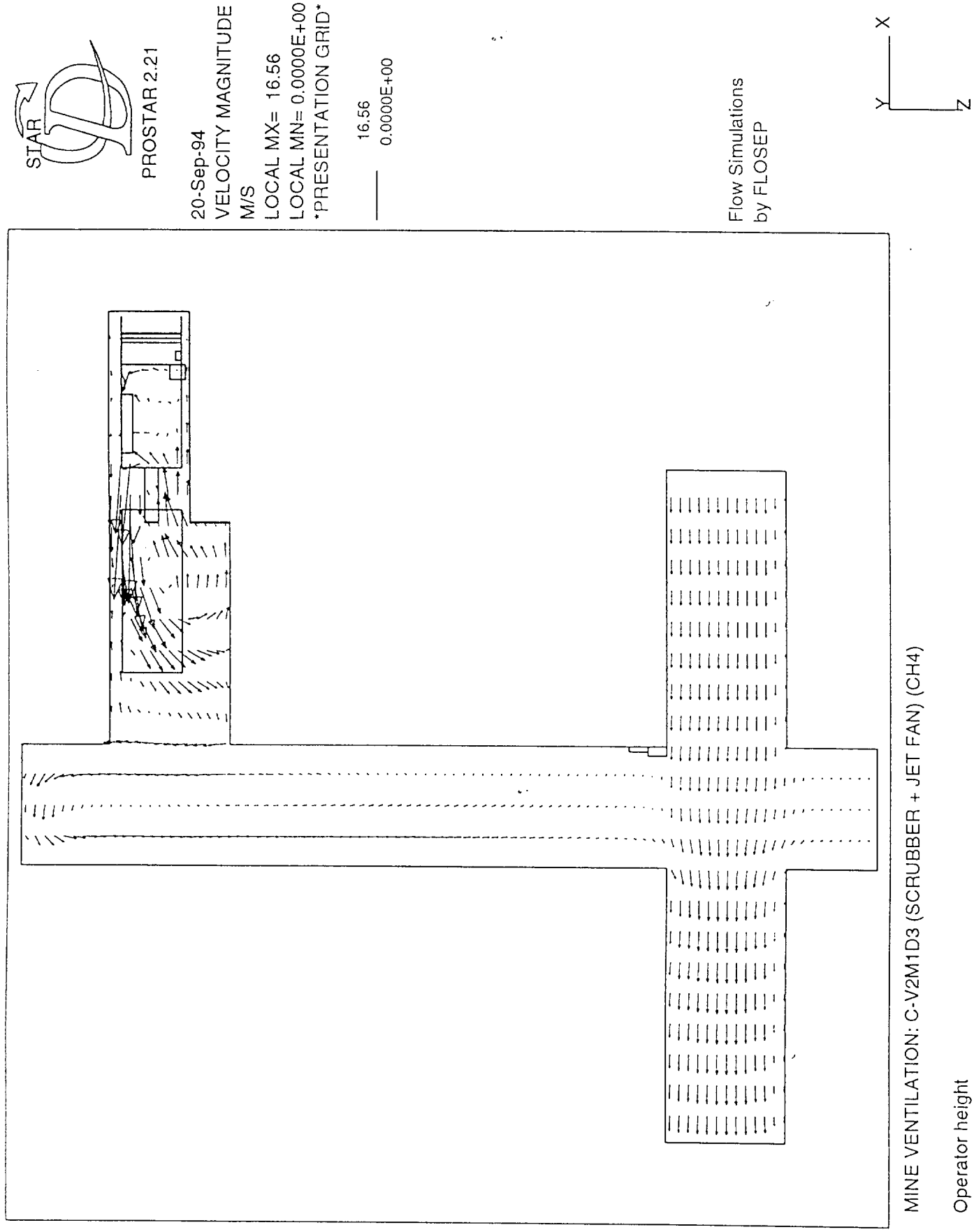

Figure 15: Airflow vectors at operator height for development stage 2

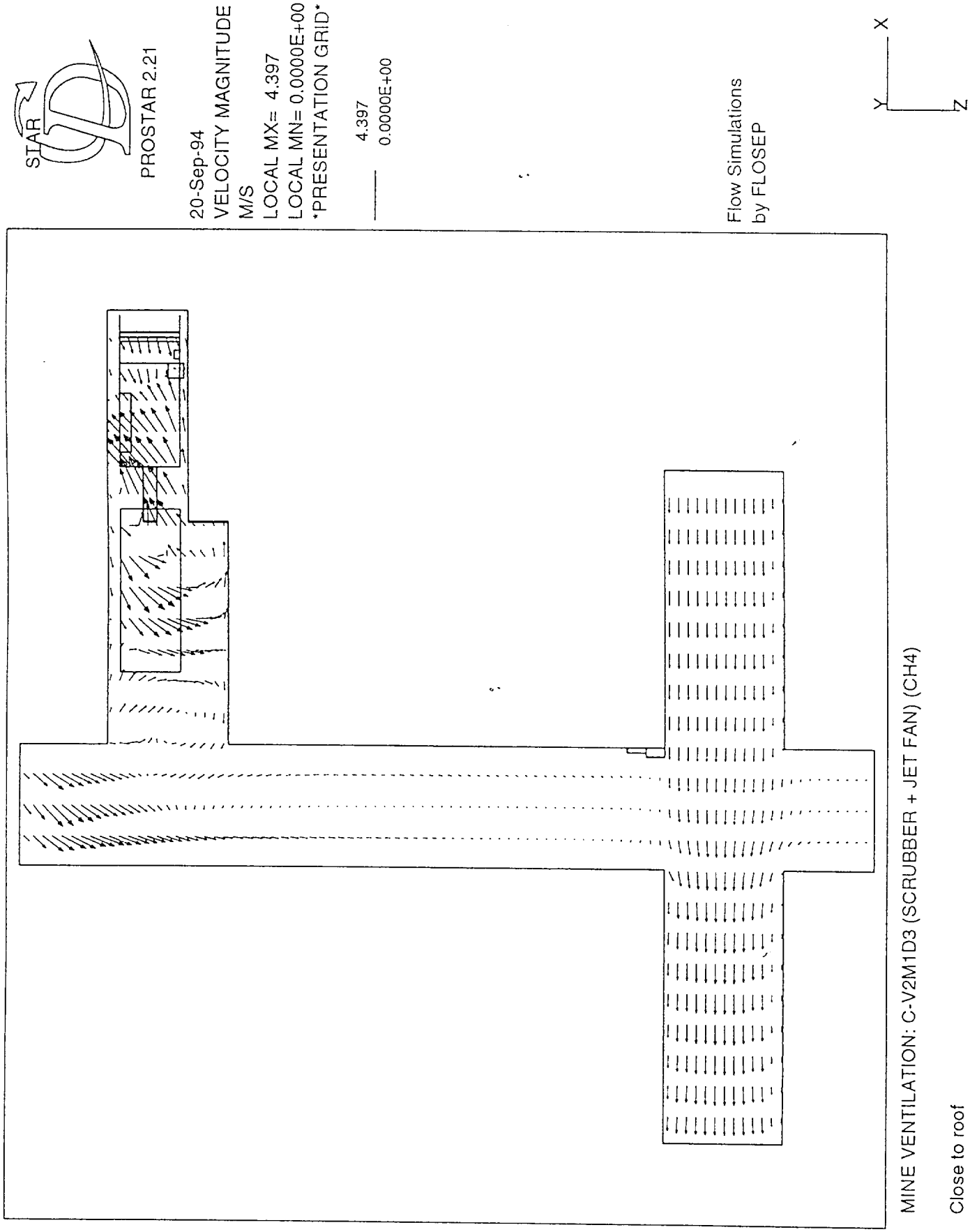

Figure 16: Airflow vectors at roof level for development stage 2

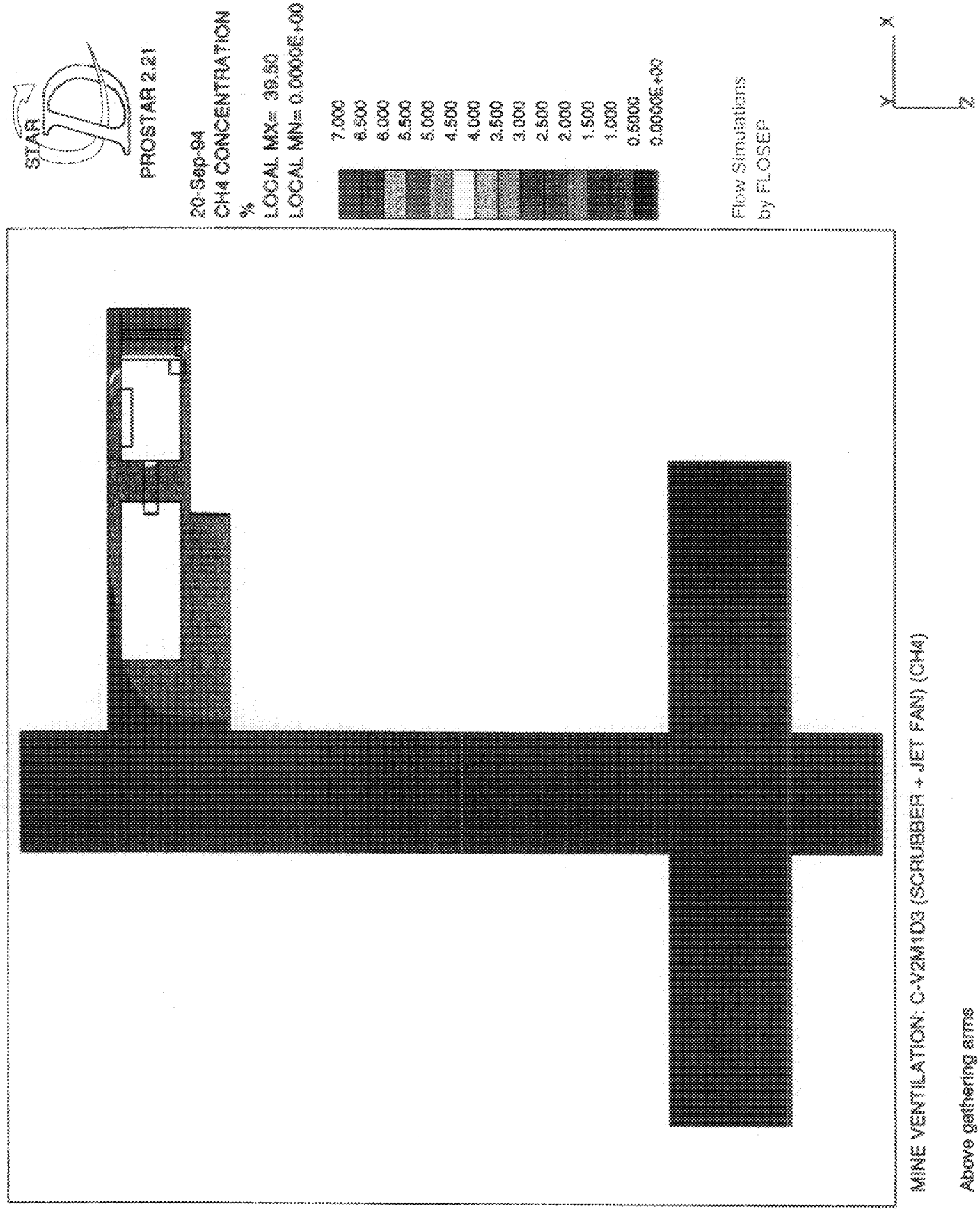

Figure 17: Methane contours at floor level for development stage 2

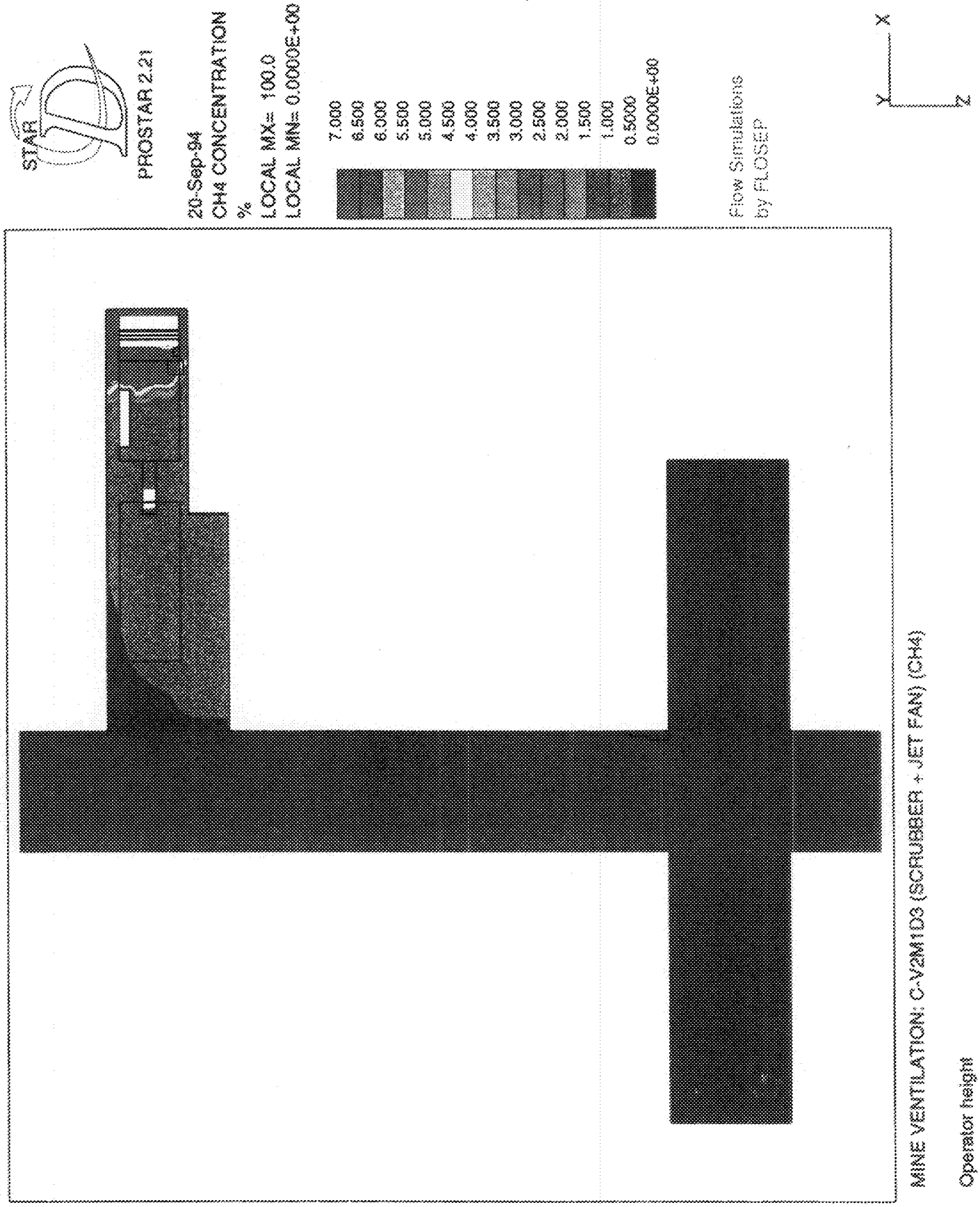

Figure 18: Methane contours at operator height for development stage 2

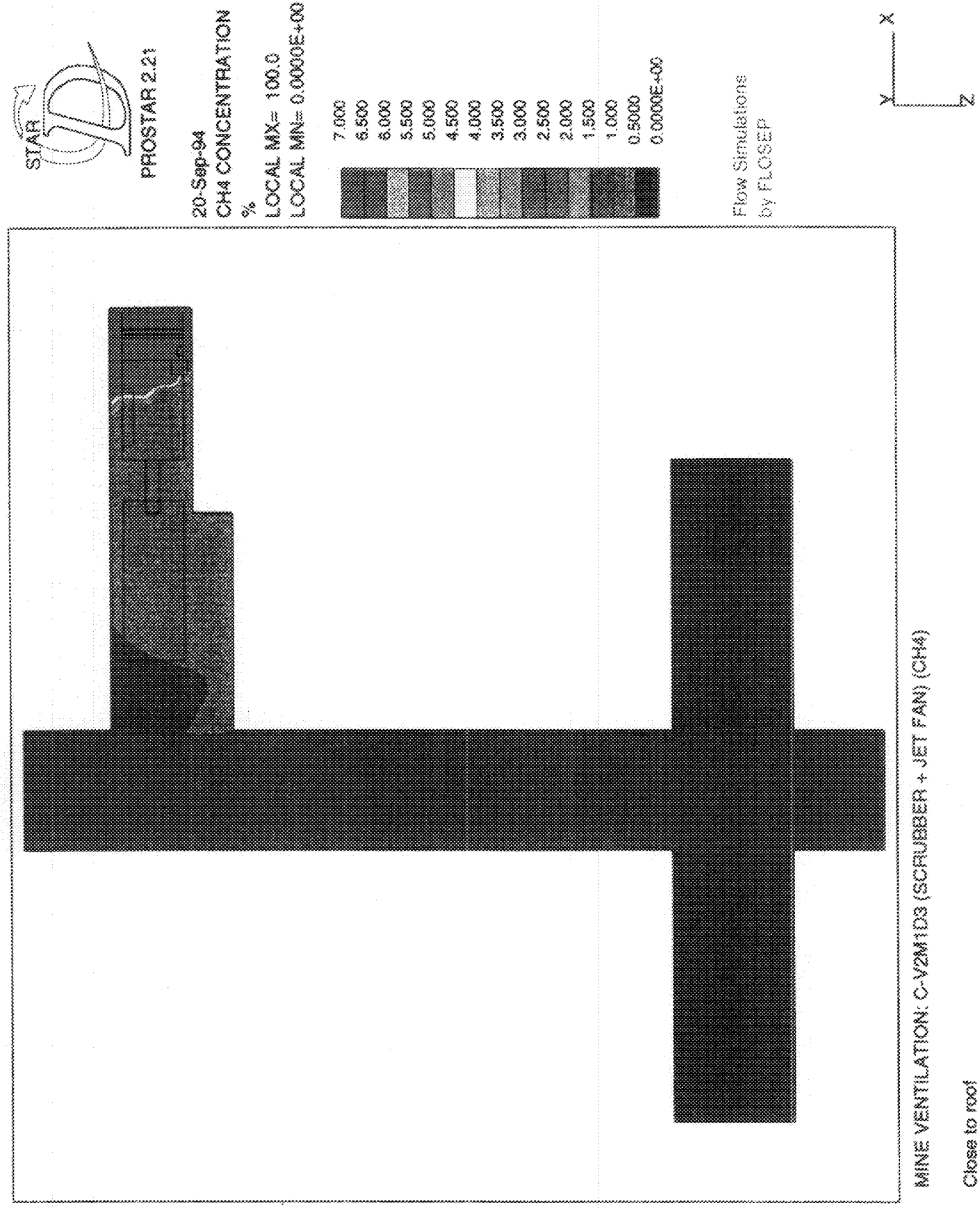

Figure 19: Methane contours at roof level for development stage 2

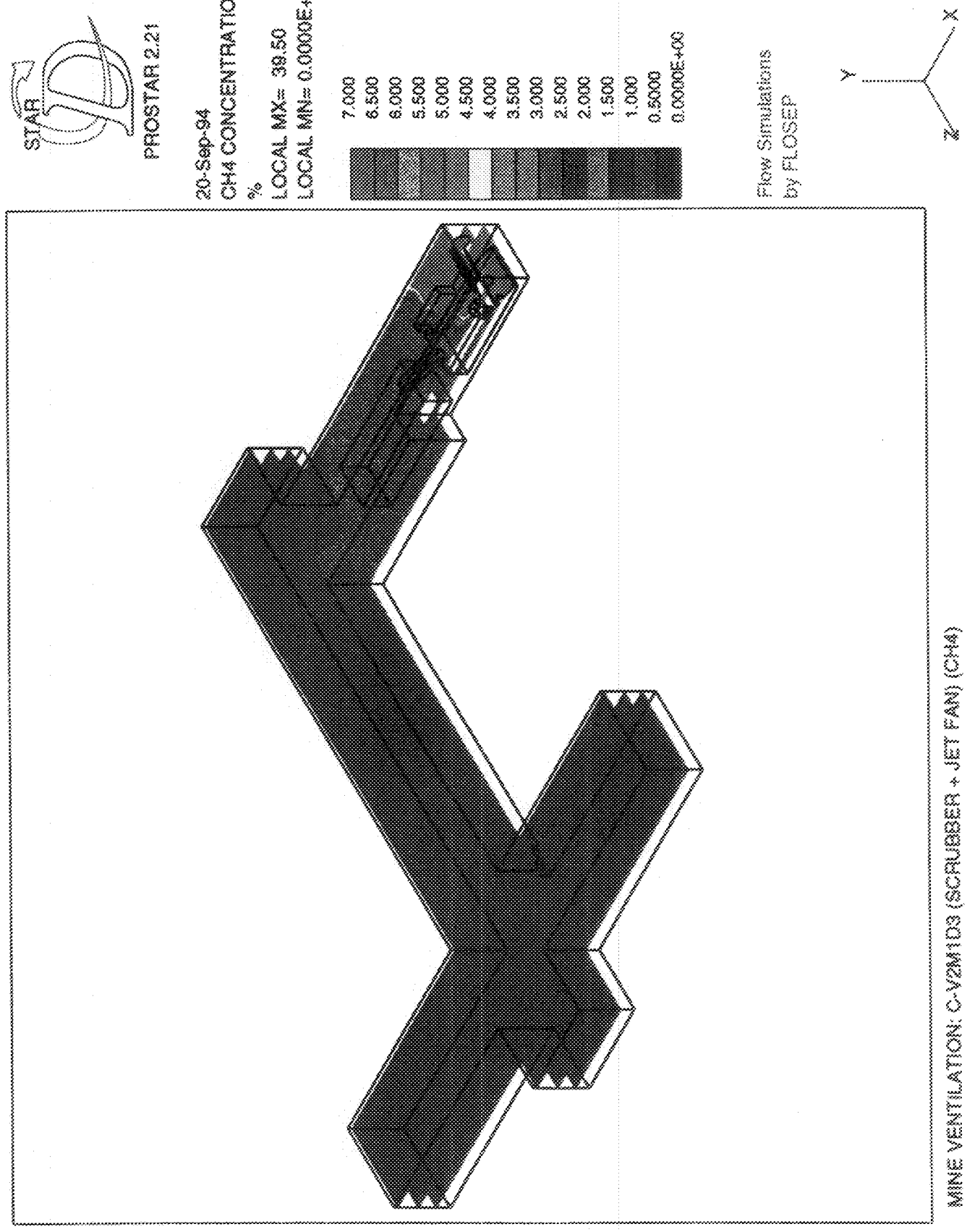

Figure 20: Three-dimensional view of the methane contours for development stage 2

3.2.2 CM DETAILS

Figures 21 and 22 show the detail of the airflow and methane contours around the CM and SC on the horizontal planes at floor, operator and roof levels. Figure 21 demonstrates the turbulent flow patterns and as well as the air recirculation caused by the scrubber. Figure 22 shows the resulting methane contours which demonstrates the rapid dilution of the methane from 7(2,5%) to 0,5(0,15%) midway down the CM.

Figures 23 and 24 also demonstrates the turbulence and air recirculation with the resulting methane contours from a vertical point of view. These clearly show the high levels of methane, 7(2,5%), around the drum and boom, but being confined to this area.

3.2.3 INTERIM CONCLUSIONS

Again the air from the jet fan is not influencing the flow patterns inside the split area although the methane contours indicate that fresh air is indeed flowing into the split. The scrubber and the sprayfan system is causing a large amount of turbulence inside the split and is causing effective dilution of the methane. The air recirculation caused by the scrubber does not cause any accumulation of methane at any point and if anything is assisting the dilution rate of the methane. Because of the position of the scrubber and CM, relative to the jet fan position and the resulting airflow patterns, the sprayfan system could not perform the normal removal of the methane from the right side of the CM to the left. The methane contours show that no layering or accumulation of the methane occurs at any position.

3.3 **Development stage 3**

Figure 25 shows the situation for the final development stage. The sketch shows a full split developed to the left of the heading with the CM and SC in the left corner of the face. The jet fan remained at the same position as before.

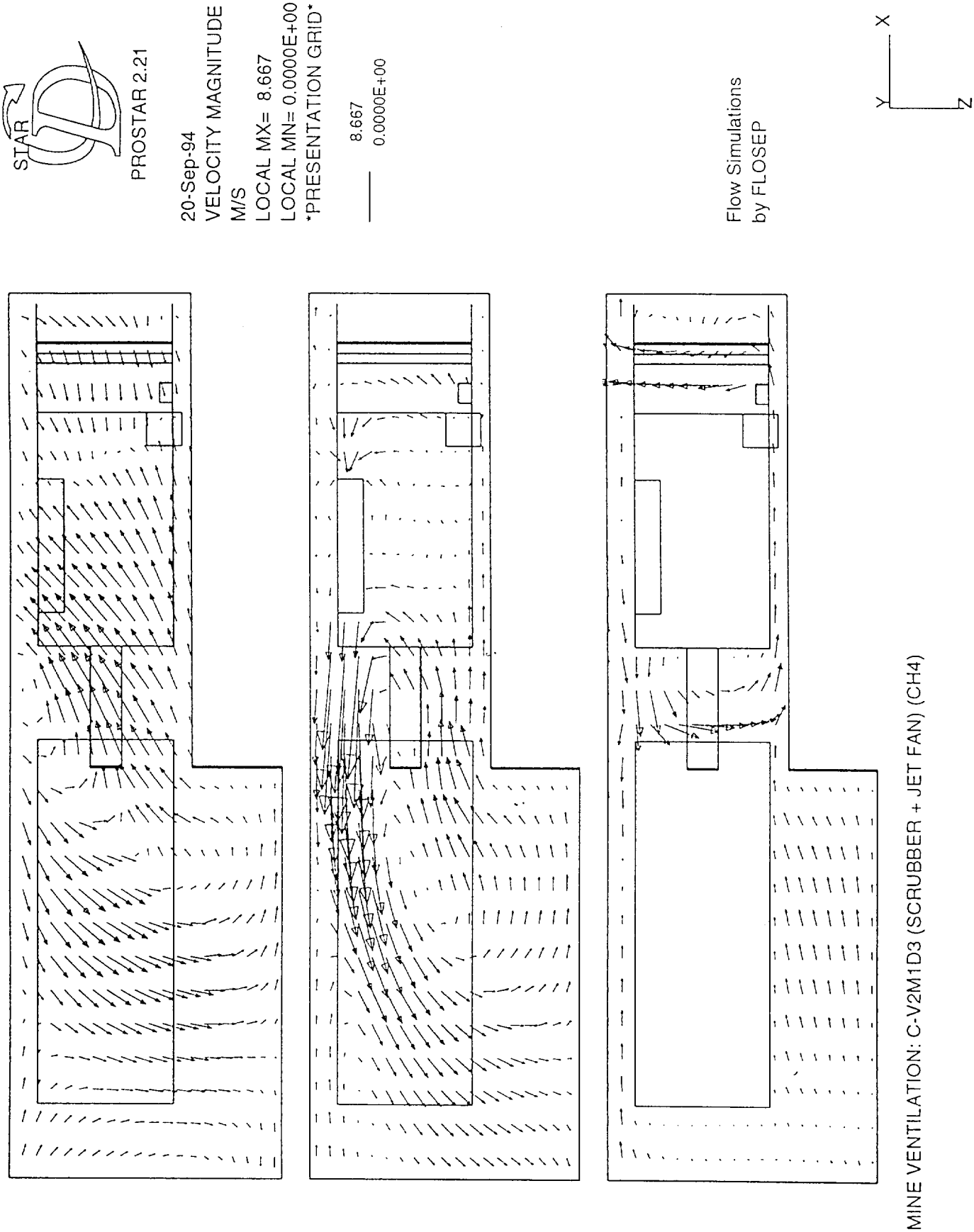

Figure 21: Details of the airflow vectors around the CM and SC on the horizontal plane

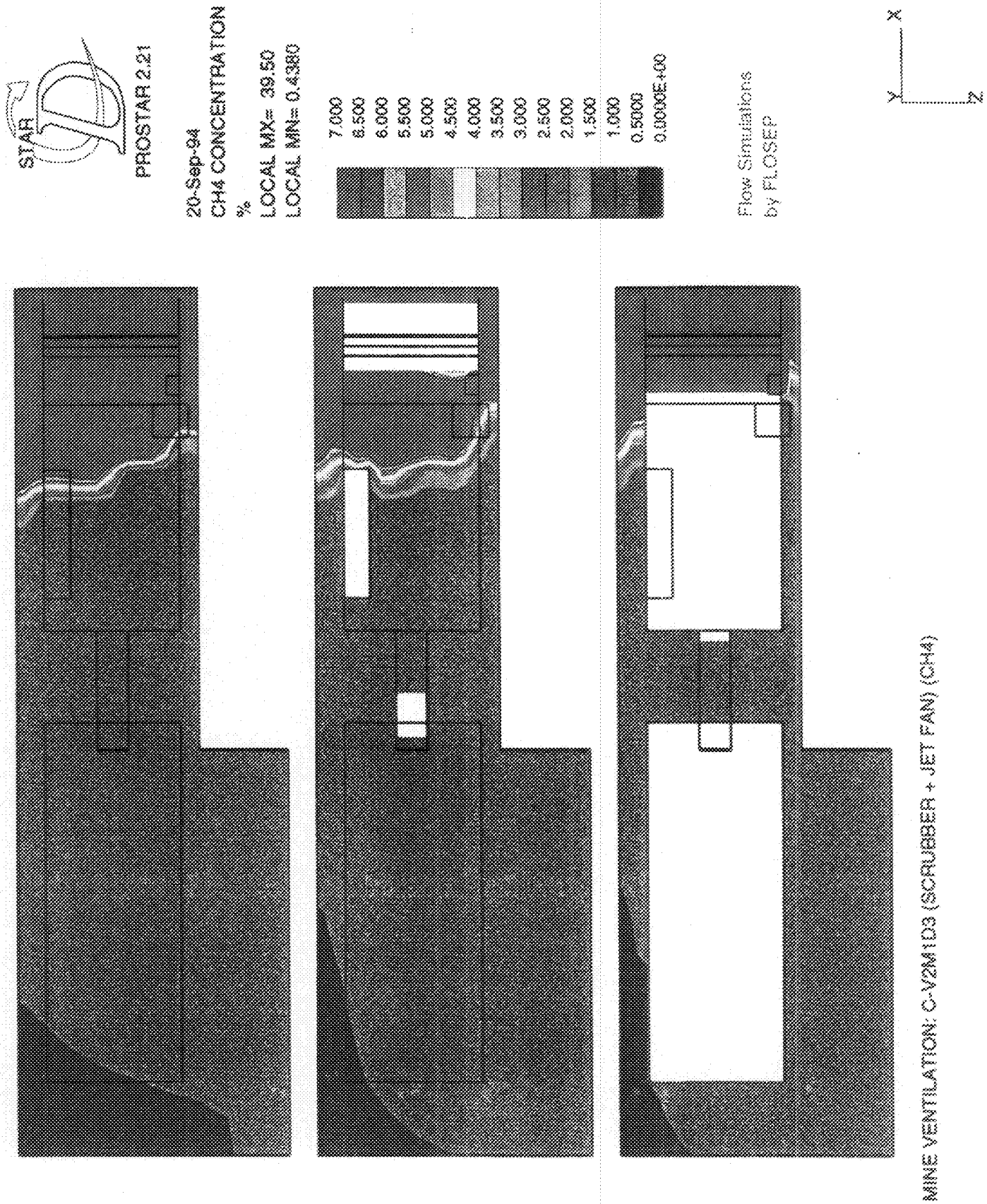

Figure 22: Details of the methane contours around the CM and SC on the horizontal plane

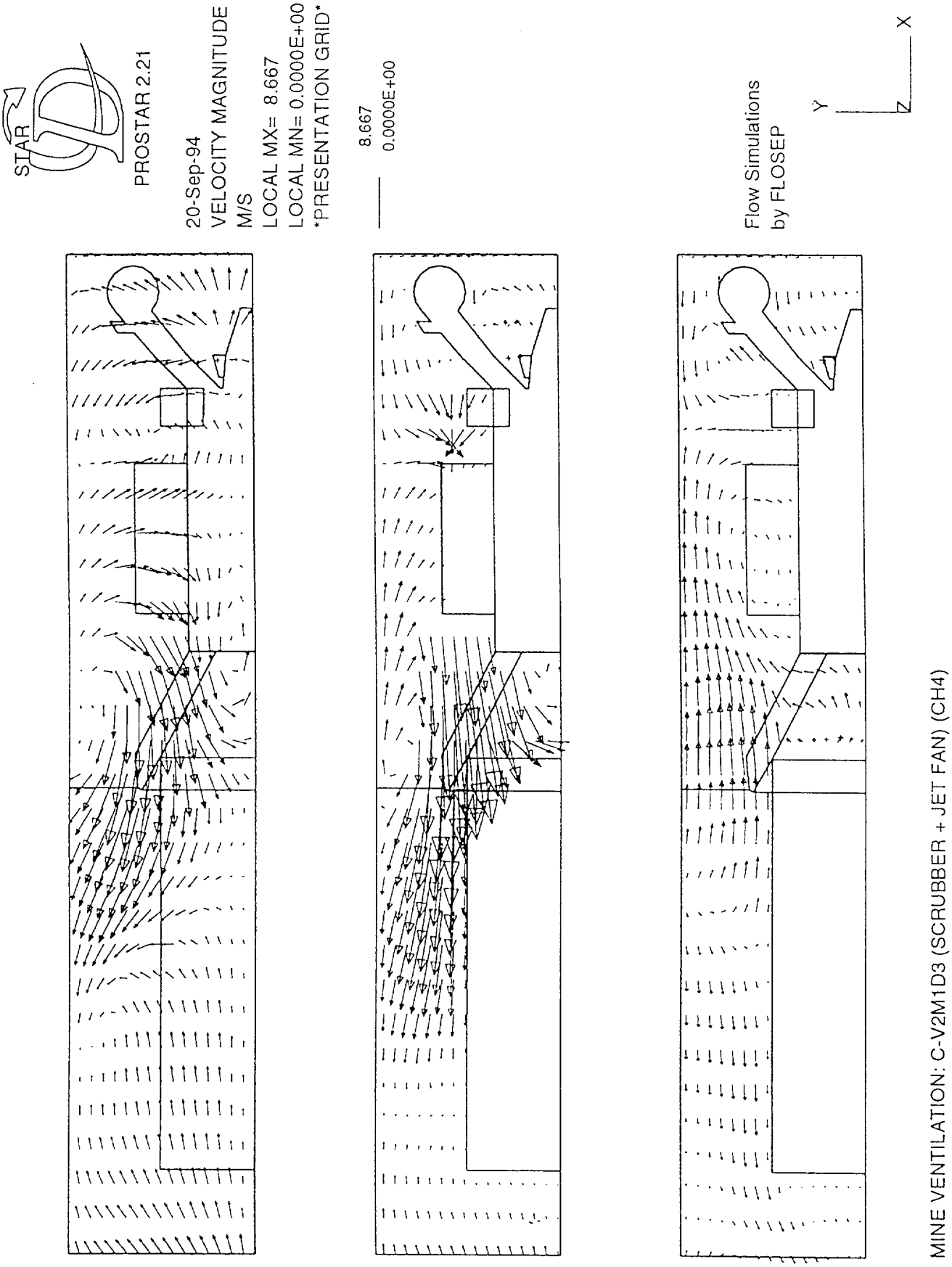

Figure 23: Details of the airflow vectors around the CM and SC on the vertical plane

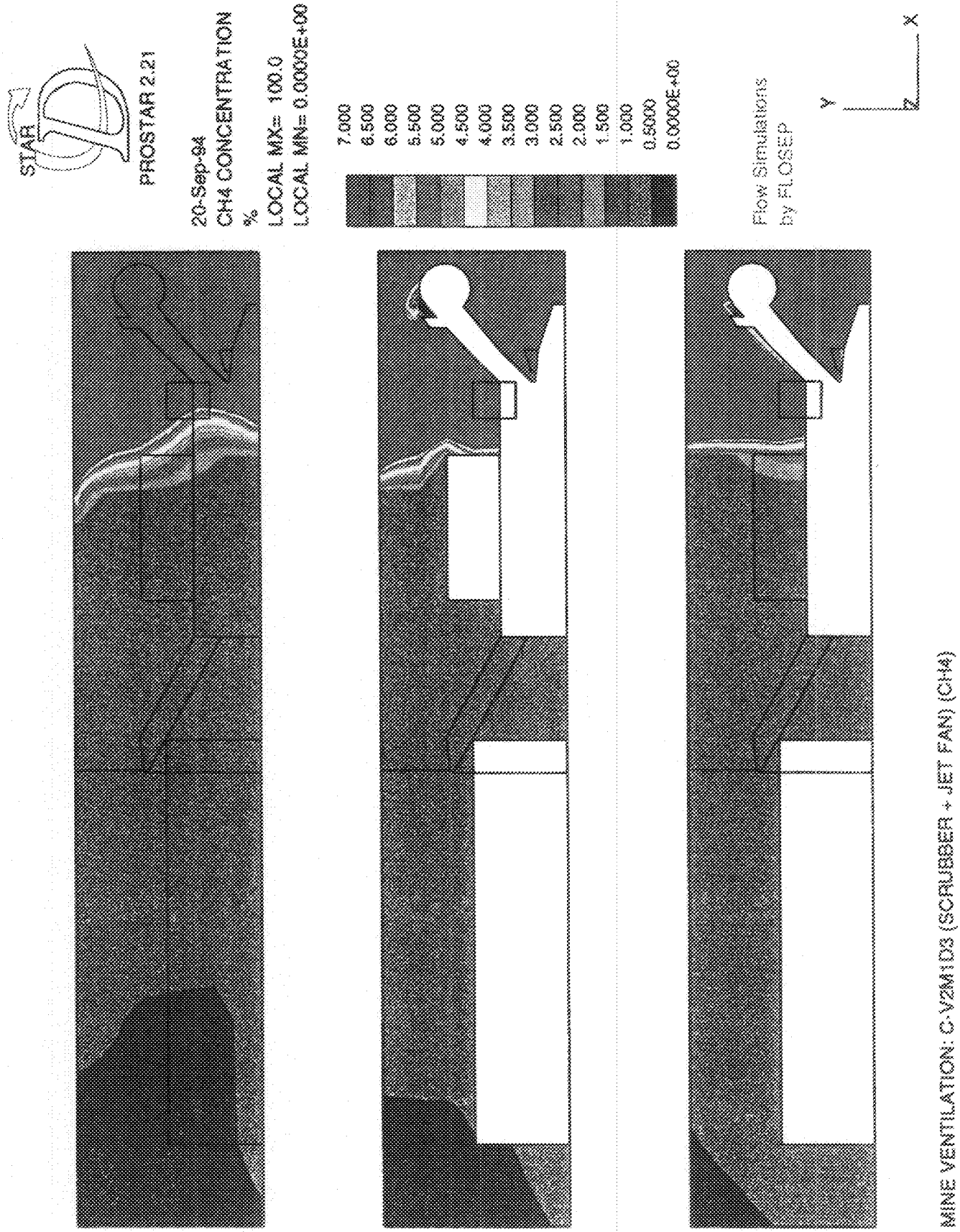

Figure 24: Details of the methane contours around the CM amd SC on the vertical plane

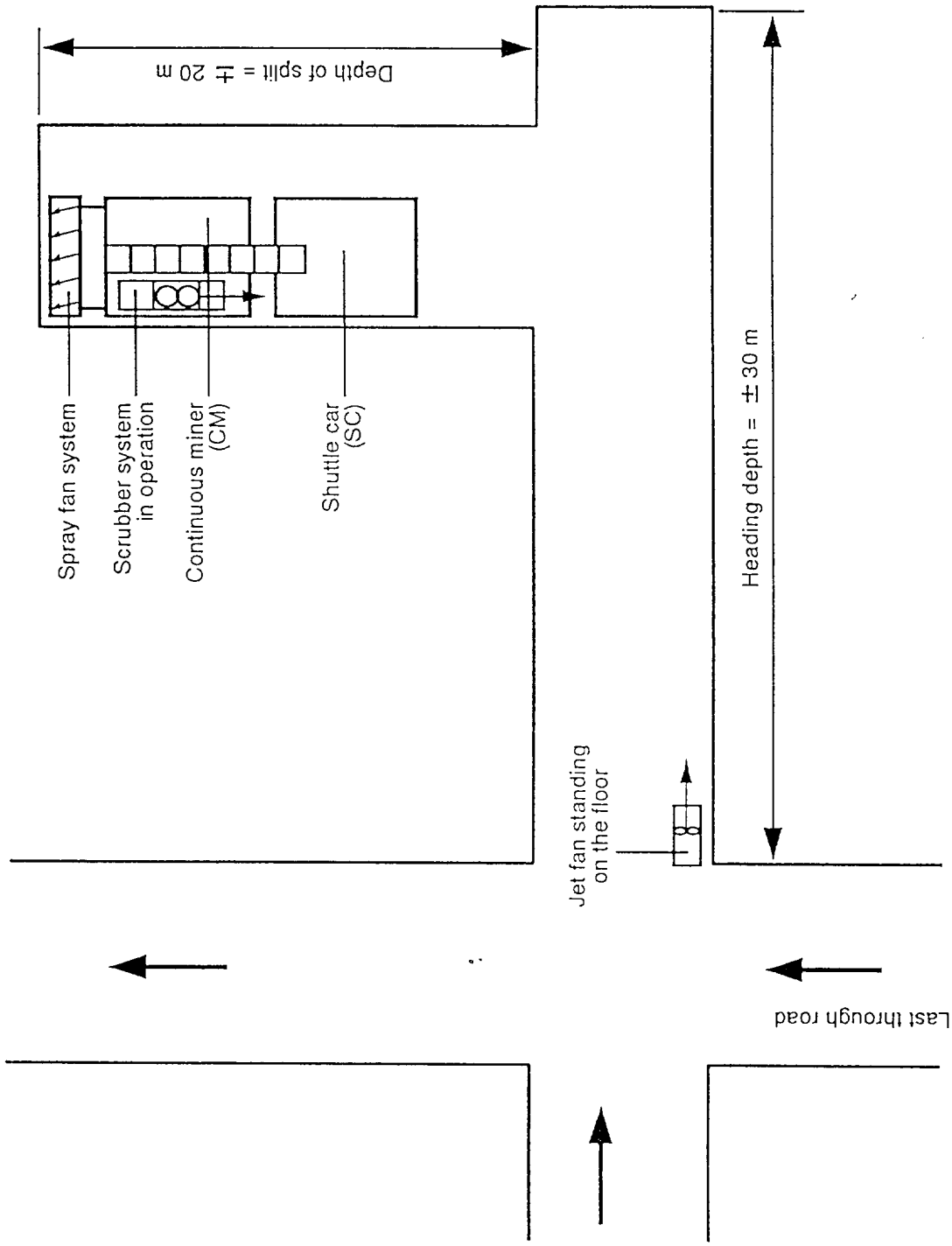

Figure 25: Sketch showing the layout for development stage 3

3.3.1 OVERALL CONDITIONS

Figure 26, 27 and 28 shows the airflow vectors for the floor, operator and roof levels. With the jet fan in this position relative to the scrubber position, the air from the scrubber seems to be pushed back into the split at floor level by the air from the jet fan. At the other two levels, it seems that the air from the scrubber is flowing out of the split towards the jet fan where it is again re-induced into the heading by the air from the jet fan. This indicates that the whole system is recirculating and that a very small amount of fresh air is introduced into the heading and split.

The methane contours as shown in Figures 29, 30 and 31 demonstrates the lack of fresh air in that the dilution rates of the methane is not as effective as the previous two scenarios. The methane levels ranged between 2(0,6%) and 7(2,5%) from the entrance of the heading to the face of the split. The contours show that the turbulence is dispersing the methane and that no layering or accumulation is occuring. The lack of fresh air inside the turbulent flow that is a result of the recirculation is, however, causing the methane levels not to drop as low as 0,5(0,15%).

Methane is again concentrated around the drum and boom, but the influence of the scrubber is clearly seen by the extended contours, and higher levels down the left hand side of the CM. Apart from the immediate at the left hand side, the general methane concentration in the split is slightly lower than in the heading, 2(0,6%) compared with 2,5(0,75%).

See Figure 32 for a three-dimensional view of the methane contours inside the heading and split.

3.3.2 CM DETAILS

Figures 33 and 34 show the airflow vectors and methane contours around the CM and SC on the horizontal planes.

Figures 35 and 36 show these details from a vertical point of view. Because of the CM position in the face area and the resulting airflow patterns, the sprayfan system is pushing the air/methane mixture from the right side of the CM to the left of the CM towards the entrance of the split.

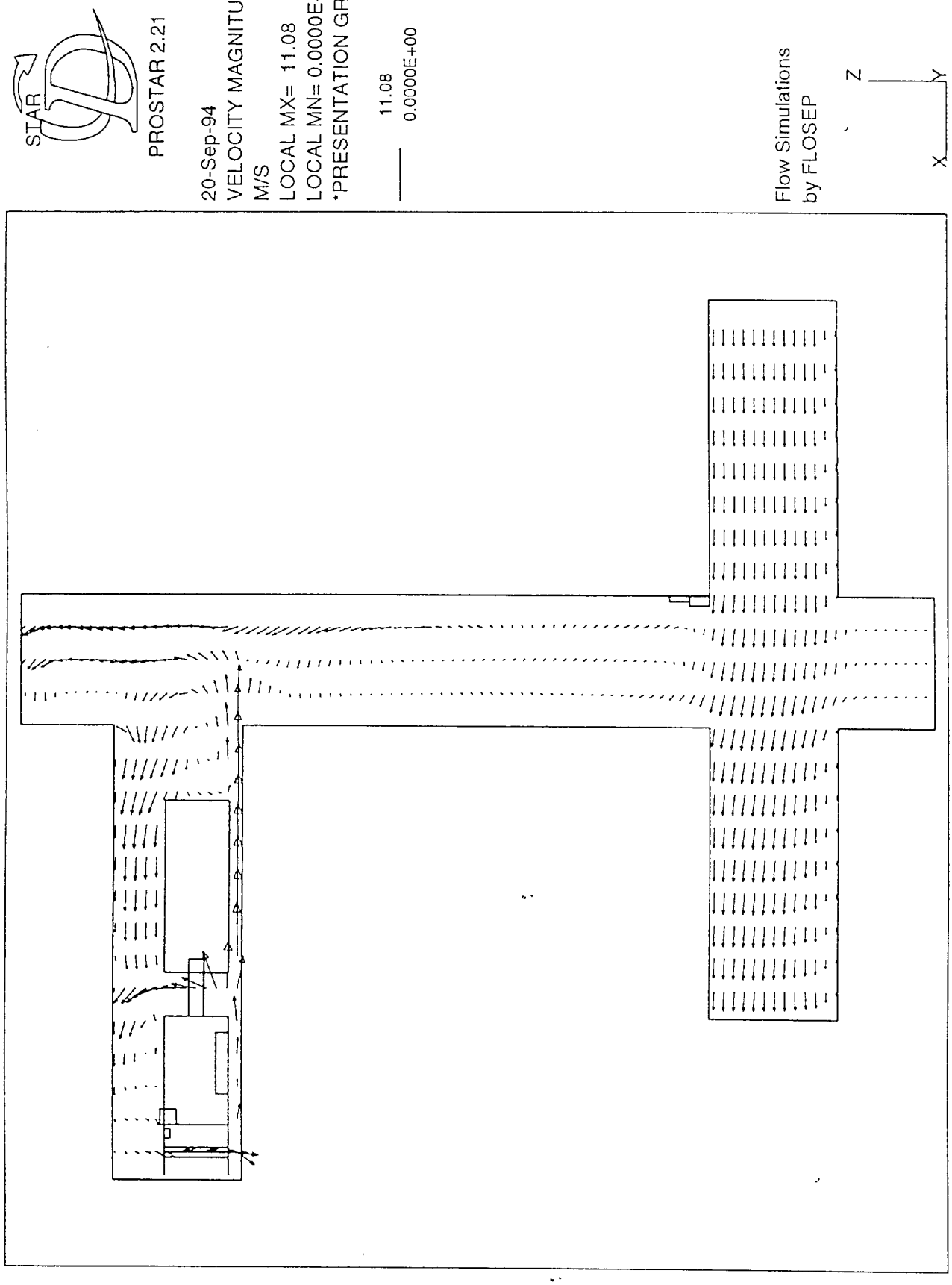

Figure 26: Airflow vectors at floor level for development stage 3

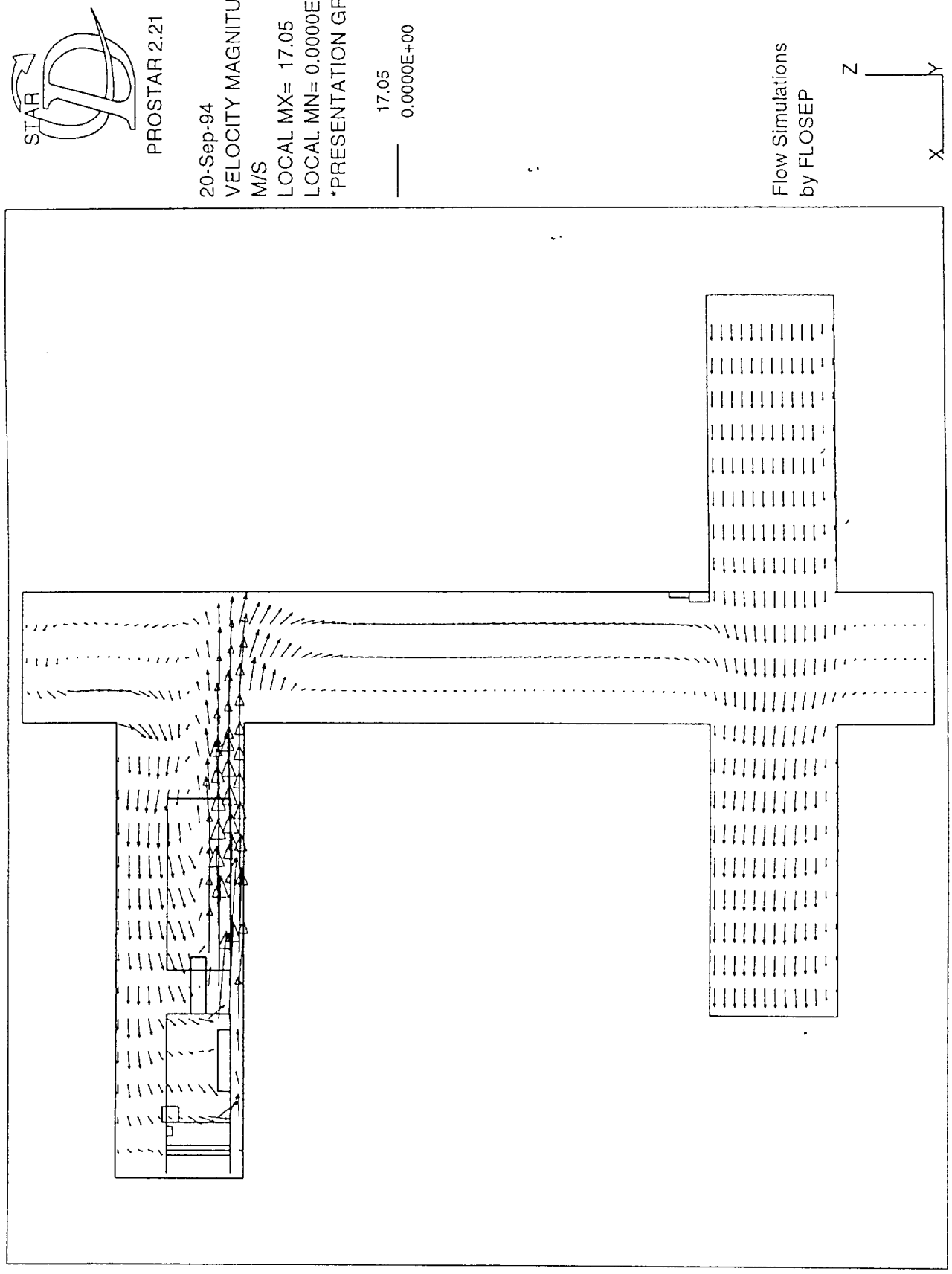

Figure 27: Airflow vectors at operator height for development stage 3

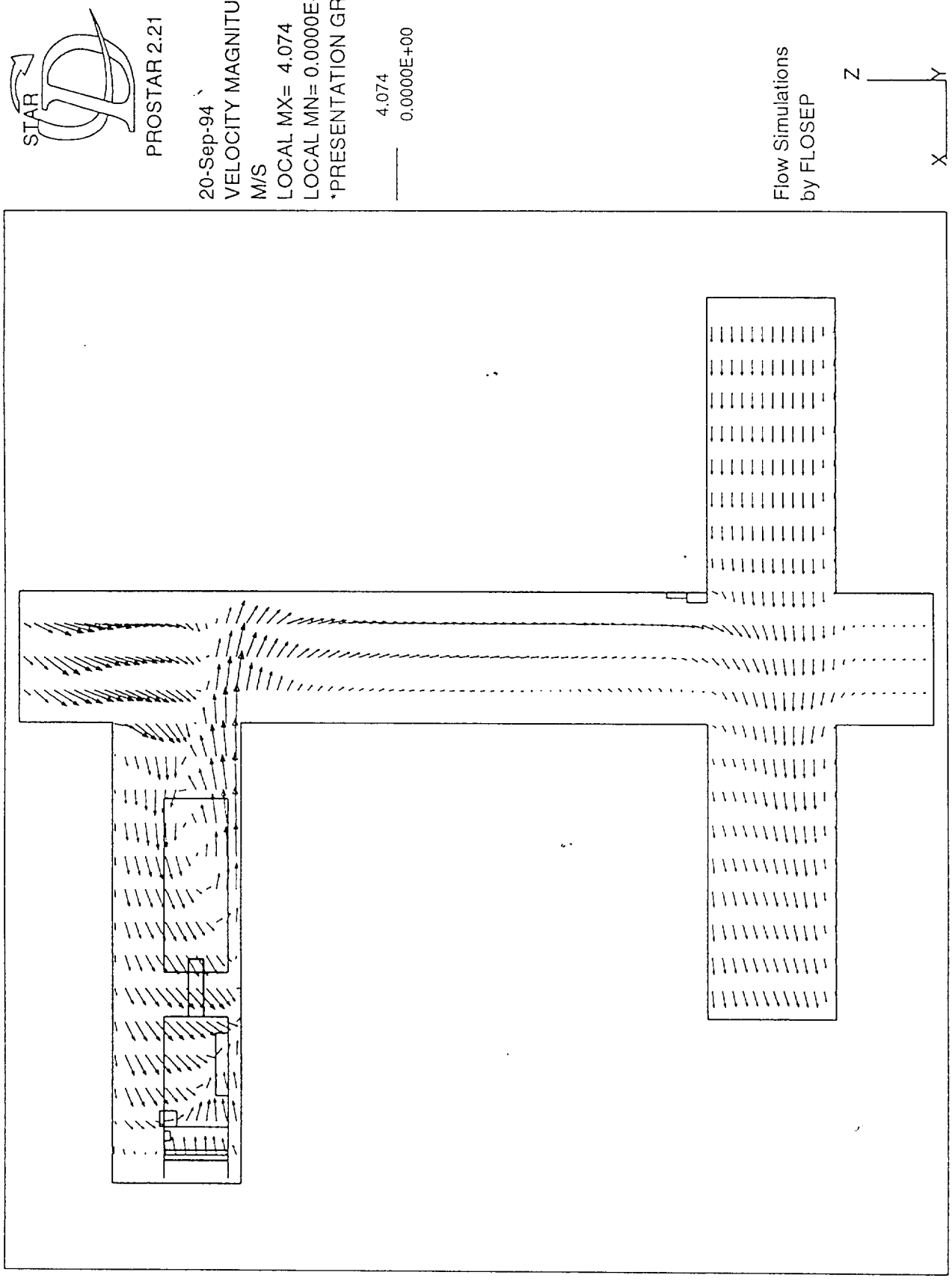

Figure 28: Airflow vectors at roof level for development stage 3

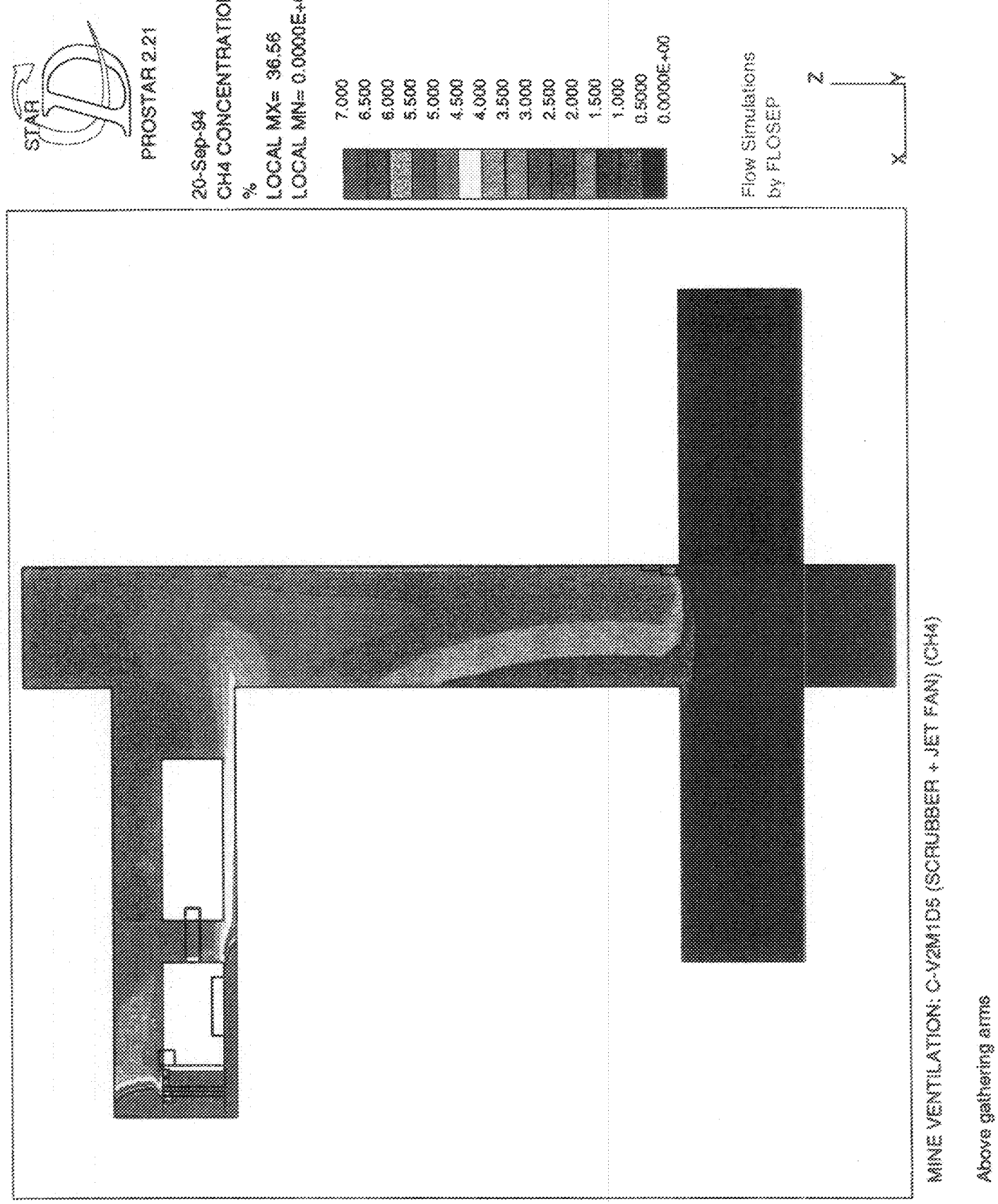

Figure 29: Methane contours at floor level for development stage 3

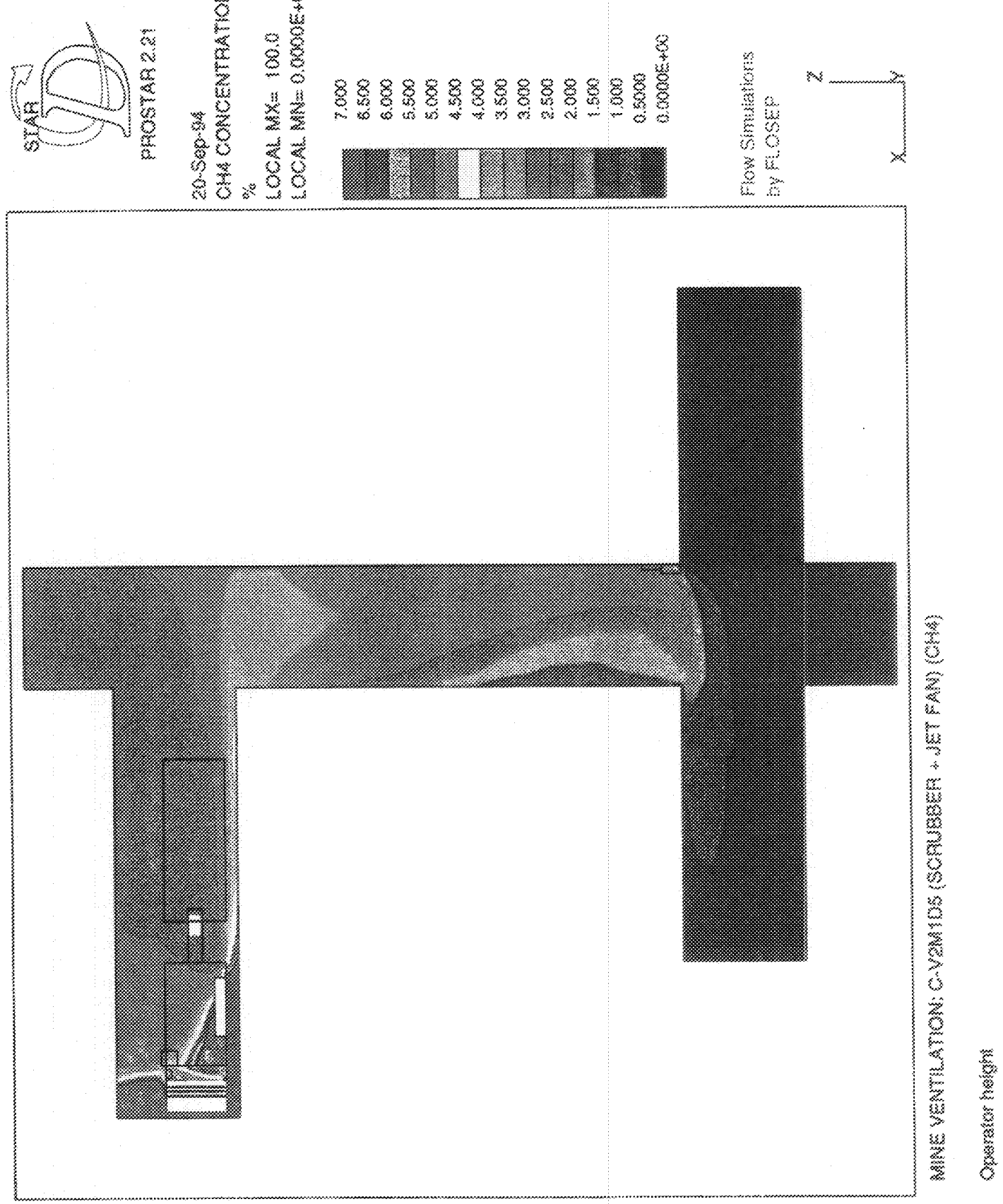

Figure 30: Methane contours at operator height for development stage 3

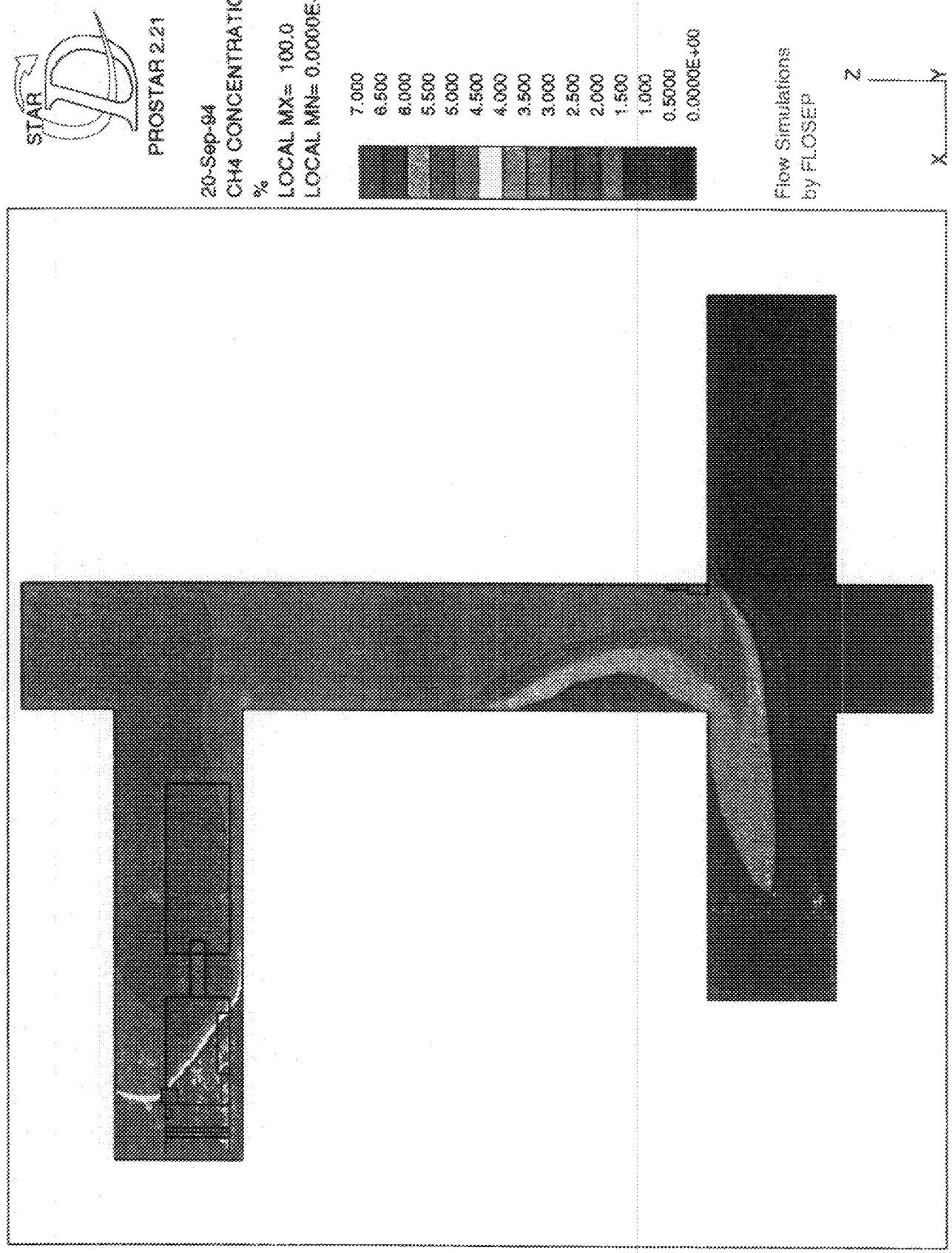

Figure 31: Methane contoursn at roof level for development stage 3

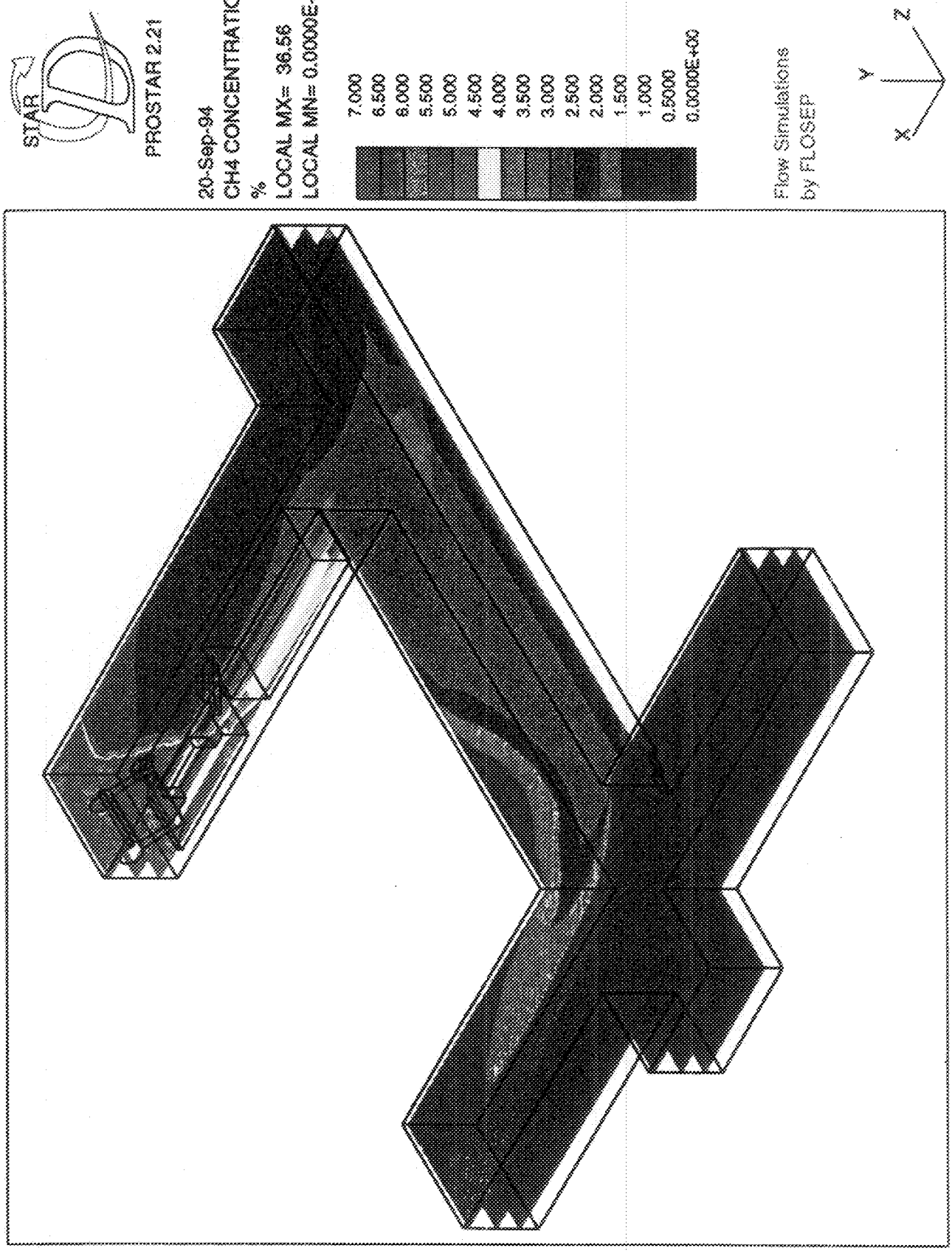

Figure 32: Three-dimensional view of the methane contours for development stage 3

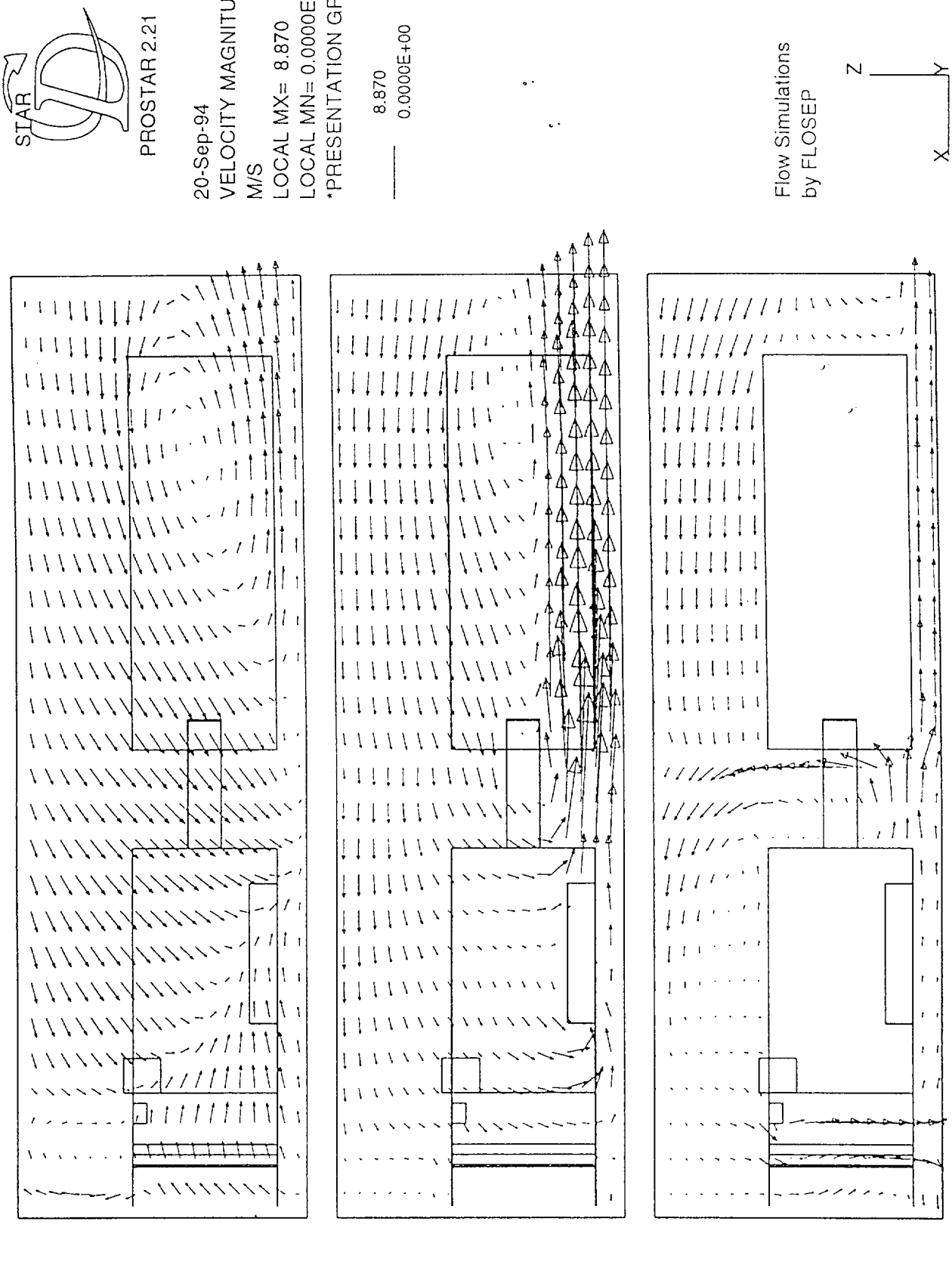

Figure 33: Details of airflow vectors around CM and SC on the horizontal plane

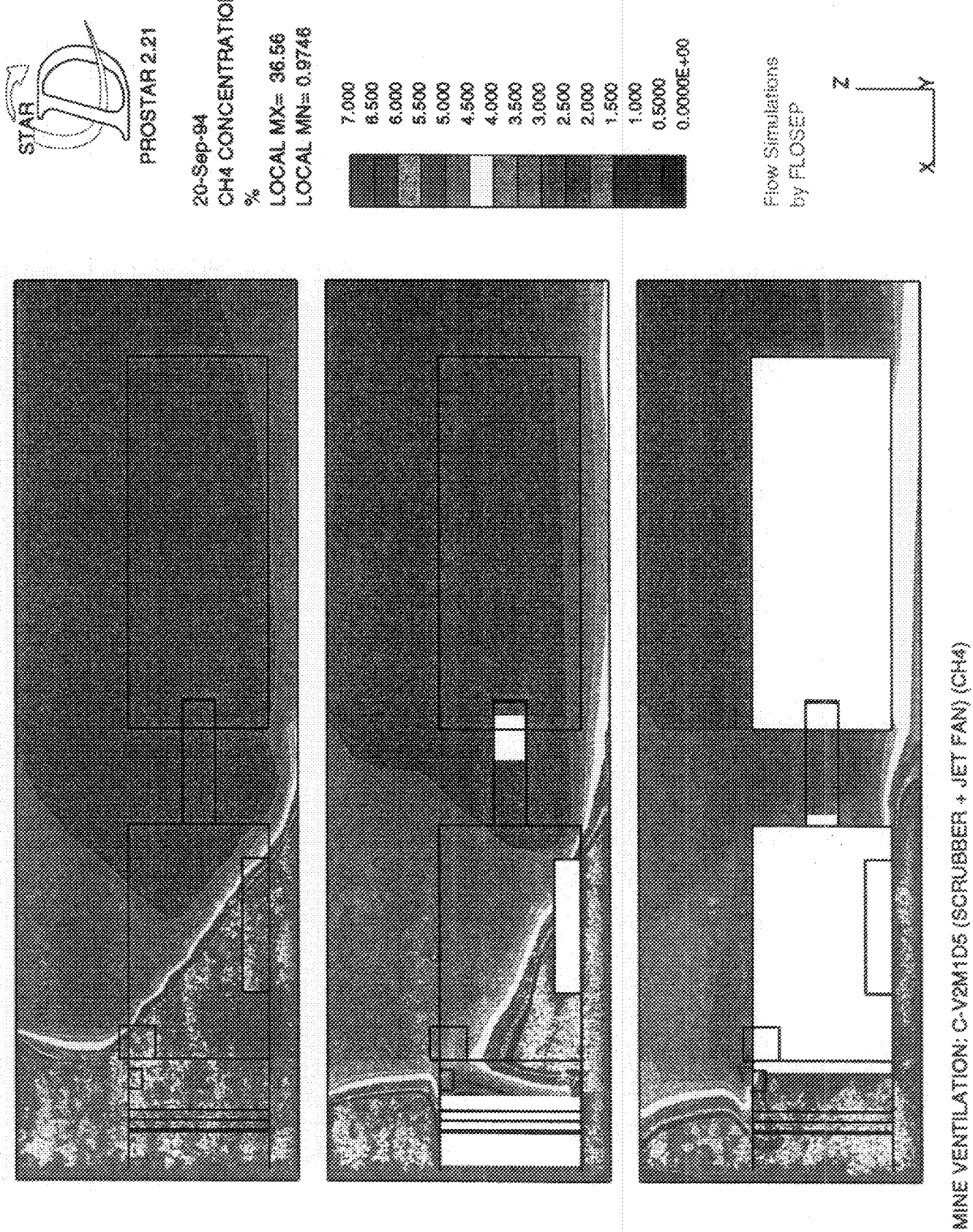

Figure 34: Details of the methane contours around the CM and SC on the horizontal plane

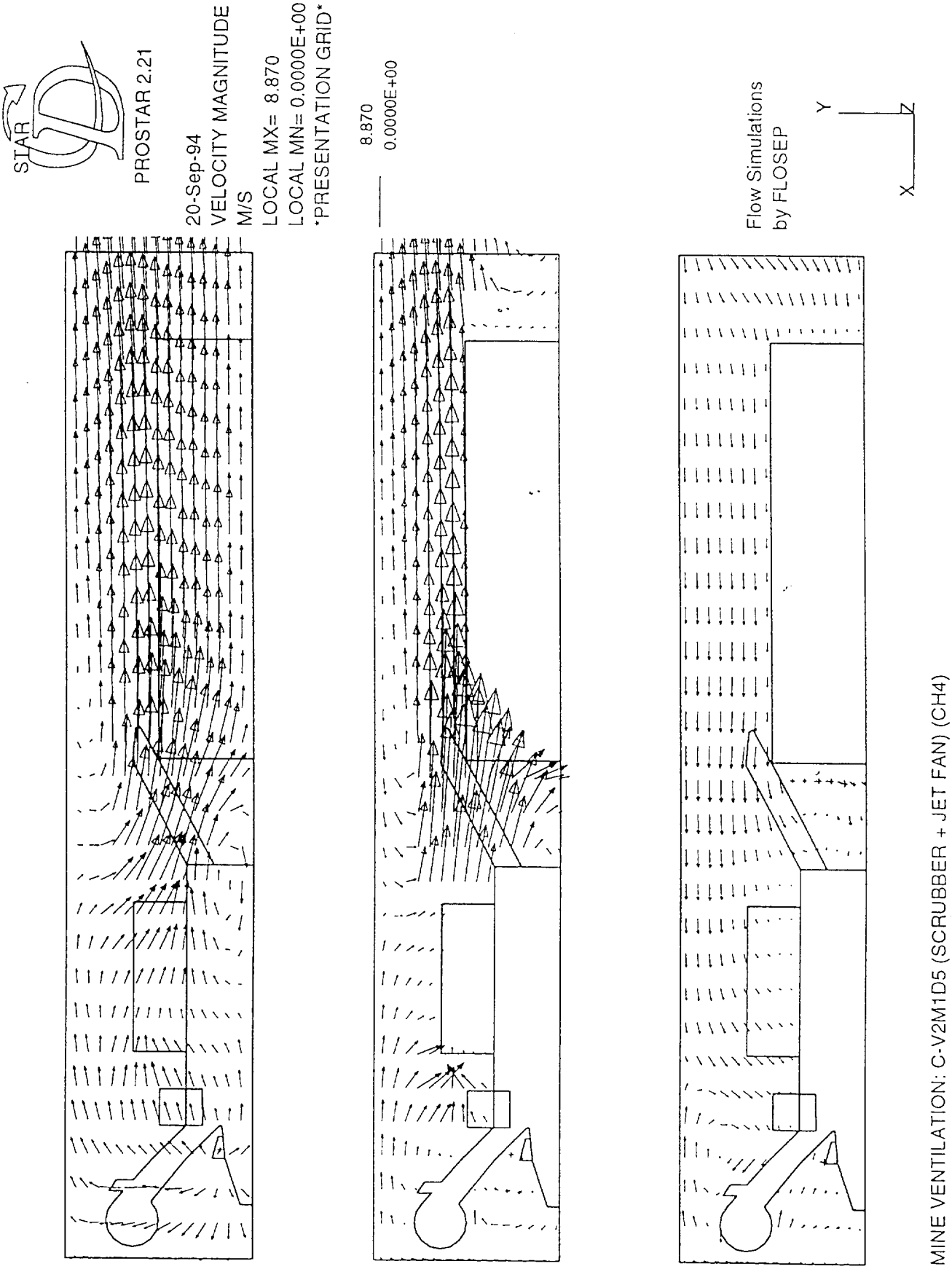

Figure 35: Details of the airflow vectors around CM and SC on the vertical plane

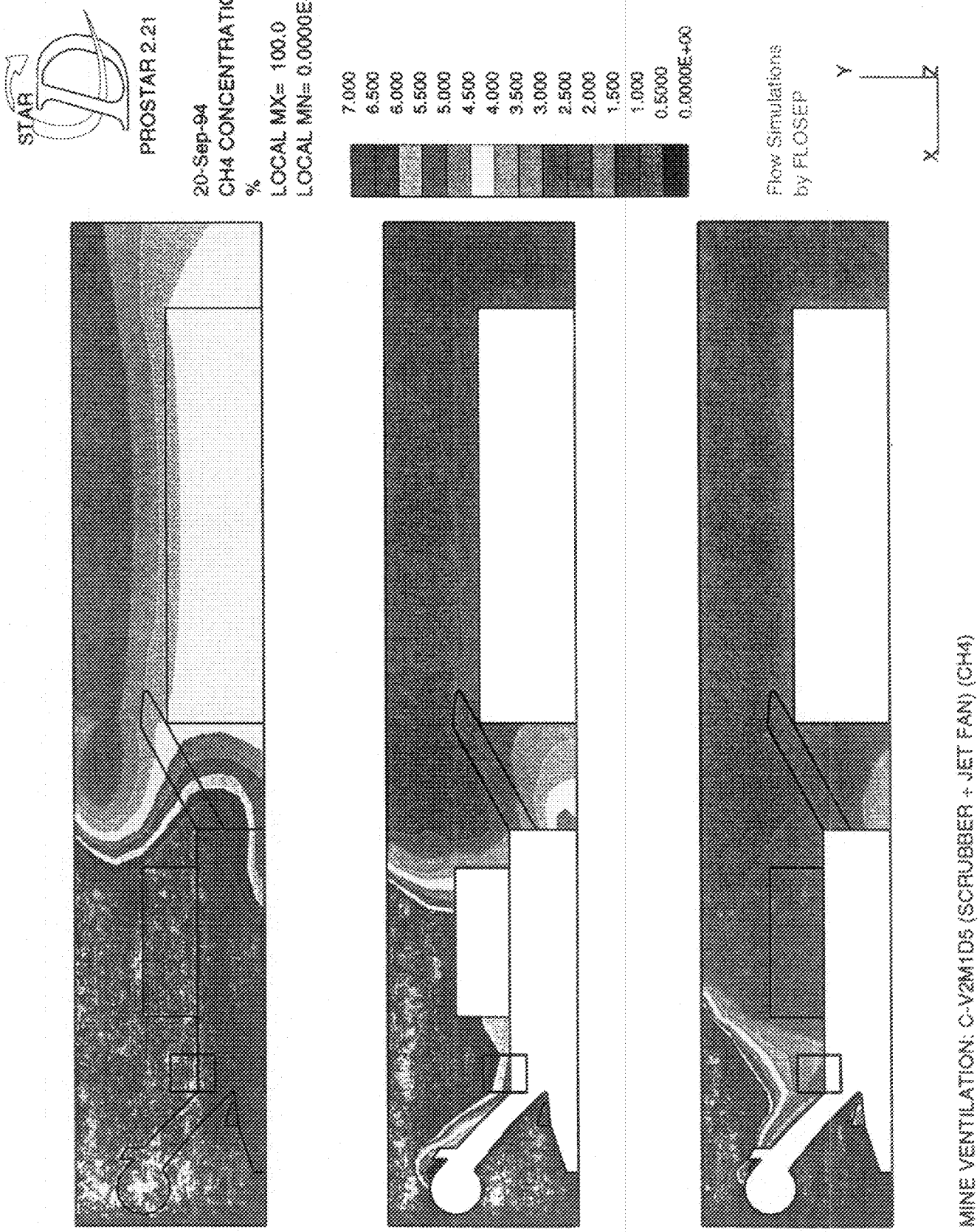

Figure 36: Details of the methane contours around the CM and SC on the vertical plane

4 CONCLUSIONS

In all three conditions, no methane accumulations or methane layering occurred at any position, and where sufficient fresh air was introduced into the face area, the dilution rates of the methane was rapid and effective. The methane contours emphasises the importance of the correct mining sequences with regard to the fan positions. The results of this project show that methane will not layer or accumulate as long as there is something that will cause some turbulence that could cause dilution.

Much greater area of 7(2,5%) around the cutting drum and boom is due to the confined area around the CM and the fact that fresh air does not reach the face. Because of the confined space, the sprayfan system can not perform as expected in removing the methane.

5 CONTINUING WORK

Future work will involve further investigations into the actual accuracy of predicting methane levels by using CFD. Future simulations will involve more realistic methane release rates, changing emission patterns and zones. Other areas that will be investigated will include recirculation patterns of air and methane, different boom positions and different mining cycles for sections as well as headings.

6 MINING SEQUENCE

The mining sequence that was used in the simulations showed the CM removed and sheltered from the air from the jet fan causing the methane to remain in the face area and causing the sprayfan to struggle in removing the methane. The sequence that is suggested is to cut the first part of the heading on the side of the ventilation system, being a jet fan or force duct. This way the ventilation system can assist in ventilating the face during this first cutting cycle. During the second cycle, the area will have been opened up for the air from the ventilation system to reach the face.

METHANE MONITORING AROUND AN OPERATIONAL CONTINUOUS MINER AT MINE A

Technical report

F.J. VAN ZYL

1994-10-25

SUMMARY

This report discusses the introductory tests done with a multi channel data logging system. The equipment and test procedures used to determine the methane distribution around an active continuous miner are explained. The results from the preliminary tests are shown in graph form. Sensor protection was found lacking in the first test but with suitable protection good results were obtained during the second test. From the levels recorded it can be seen that the methane levels at the cabin is substantially lower than the levels recorded at the boom and other forward positions on the continuous miner. Levels recorded by individual sensors also vary in relation to time. This indicates that the methane levels around a continuous miner is dependant on its movements in a section. For future tests the movements of the continuous miner will have to be recorded and the data logging system maintained to ensure a more comprehensive date set.

TABLE OF CONTENTS

1. INTRODUCTION

During continuous miner (CM) operations, methane gas is released. A common and convenient place to measure the methane levels is in the driver's cabin (cab). Because of the size of a CM and the air movement around it during the mining process, it is reasonable to assume that the methane around a CM is not uniform. For this reason it can be said that the level recorded in the cab is probably not representative of the methane levels around the CM. To get a representative picture the methane levels at various positions must be measured and from such data a comparison can then be drawn between levels at the various positions. Once this is known, it will be possible to predict what levels of methane can be expected around a CM when the methane level is recorded at one position. It will also give an indication of were the maximum level of methane is likely to occur and what levels can be expected.

CSIR Miningtek has developed an intrinsically safe, self contained, 6 sensor methane data logging system. The system is capable of recording methane levels at 6 different positions over a full shift at preset time intervals, of down to 1 second. This system will enable a study to made of the relationship between methane levels at various positions around a CM during normal working conditions.

This report describes the data logging unit and the results obtained from the two tests that were run at Mine A, with the 6 sensors placed on a CM.

2. THE 6 CHANNEL DATA LOGGING UNIT

The data logging unit is an intrinsically safe, self contained unit that is capable of recording methane levels of up to 4%, from 6 independent methane sensors. Along with the methane levels the unit also records the date, time and location of the system. This information can be down loaded onto a PC and imported to a spread sheet for analysis.

The data logging unit consists of four main components :

I. Recording box.

ii. 6 methane sensors and their cables.

iii. PC milking station.

iv. Micro logger.

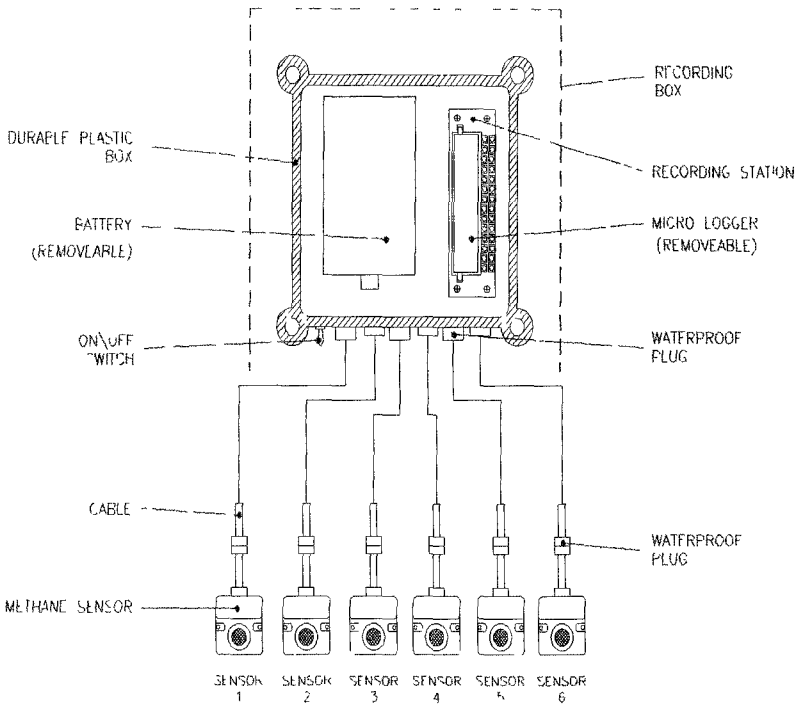

Figure 2.1 The 6 channel data logging unit.

2.1 The Recording Box

The recording box consists of three main parts :

i. A power supply that powers the 6 methane sensors and the micro logger. The power supply is a rechargeable 12V battery that is capable of supplying power to the unit for at least 10 hours of continuous use, when fully charged.

ii. A recording station into which the micro logger is placed when the system is in operation.

iii. A set of 6 plugs that connects the cables from the methane sensors to the recording box.

The unit is also supplied with a manual ON/OFF switch that is used to switch off the unit when not in operation to save battery life. The components are contained in a plastic box that is filled with foam rubber to protect the recording box from excessive vibrations.

2.2 The Methane Sensors and Cables

Trolex TX3261 MkII methane sensors with a range from 0% - 4% methane in air are presently used with the system. The overall accuracy of the sensors are ±0.1% of methane for the range 0% to 1.25% methane in air and ±8% for the range 1.25% to 4% methane in air. The response time for the sensors is 10s. This specific methane sensor was decided on only because of its low power consumption, which allows the unit to operate for at least 10 hours continuously. Miningtek does not approve or endorse the use of this sensor over any other type.

The sensors are wrapped in a rubber jackets and supplied with an additional external filter to protect the sensors against minor impacts and excessive dust. Two of the sensors are also supplied with demister hoods to protect them from excessive exposure to water sprays and coal dust.

The cables that are used are 6 core reinforced screened cables, fitted with waterproof plugs.

2.3 The PC Milking Station

The PC milking station is the connection between the micro logger and the PC, and is connected via the serial port. The milking station is used to down load the recorded data from the micro logger to the PC and alternately to programme the micro logger through the PC.

2.4 The Micro Logger (ML)

The micro logger (ML) is used to record the data from the methane sensors. The ML is programmed and milked through a PC with dedicated software.

The ML records the date, time and levels of methane for each of the 6 sensor when a set of readings are taken. The time intervals between readings are programmed into the ML via a PC. This time intervals can range from seconds to minutes to hours.

The ML can record up to 60 000 data points before the memory is full and the ML switches off automatically, saving the recorded data.

3. TEST SETUP AND PROCEDURES

Before a test is done the system is checked and calibrated. The methane sensors are fitted with new activated carbon filters to ensure that the recorded data is accurate. After each test the system is also checked to ensure that the methane sensors are still with in specifications and the cables intact. This is done to verify or discard the results obtained from the preceding test.

The data logging unit was taken to Mine A where it was fitted to a HM21 CM. The 6 sensors were placed on the CM so as to cover all the major areas that was thought would give a fair indication of the methane distribution around the CM and rendered reasonable protection to the sensors. Two sensors were placed either side just backward of the cutting drum, one sensor was placed at the scrubber intake and one at the scrubber outlet, one sensor was placed in the middle of the boom on the return air side and the remaining sensor was placed in the drivers cab of the CM. The recording unit was also located in the drivers cab (See figure 3.1).

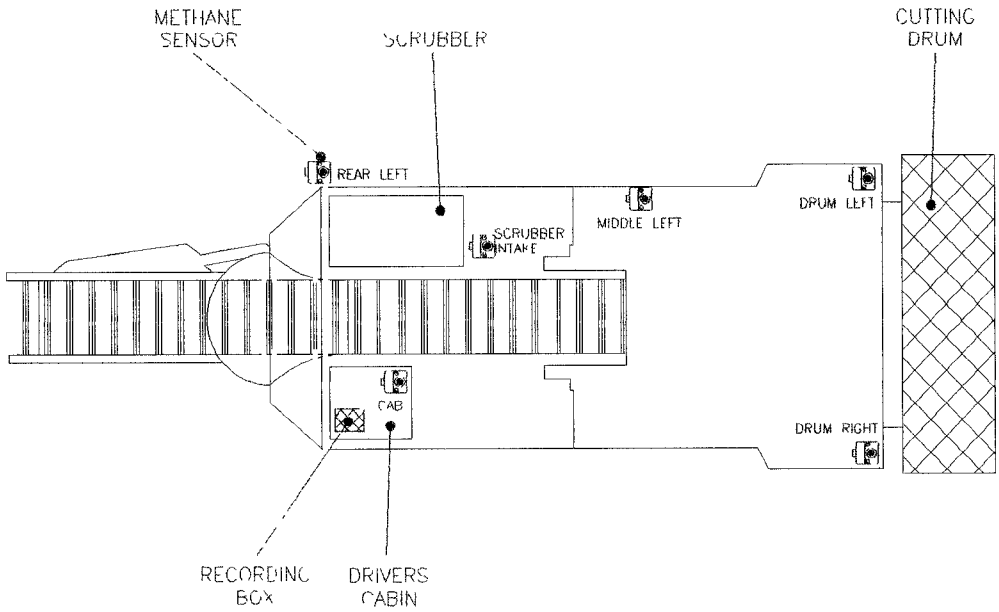

Figure 3.1 Placement of the 6 methane sensors around the CM.

After the system was fitted to the CM the recording of the methane levels commenced. The methane levels for a shift or part of a shift were recorded after which the recording unit was taken to the surface and the ML down loaded onto a PC. The ML's memory was cleared and reprogrammed for the next shift. The battery pack of the ML and the system battery were then charged after which it was ready for the next shift. This procedure was repeated after each set of recordings were taken. After a test period was completed the system was removed from the CM and taken to the laboratory for inspection and calibration. After both the tests the system was checked and the methane sensors were all with in specifications.

4. TEST RESULTS

Two tests were conducted at Hope Shaft, Section 7/8. The first test was conducted between 07/07/1994 and 15/07/1994 and the second between 21/09/1994 and 03/10/1994.

In both cases the ML was set to record the methane levels every 10s, which corresponds to the

response time of the Trolex methane sensors. Because of the vast number of data points generated during a shift, the average of every 6 readings were taken which provided the average methane level per minute during a shift for each sensor. This was done to save time during analysis of the results and no apparent difference can be observed between the graphs of a full data set and an averaged data set.

4.1 TEST 1

From test 1 three sets of results were obtained.

07/07/1994

On 07/07/1994 the system was installed and allowed to recorded for 1 hour to test the system (fig. 4.1).

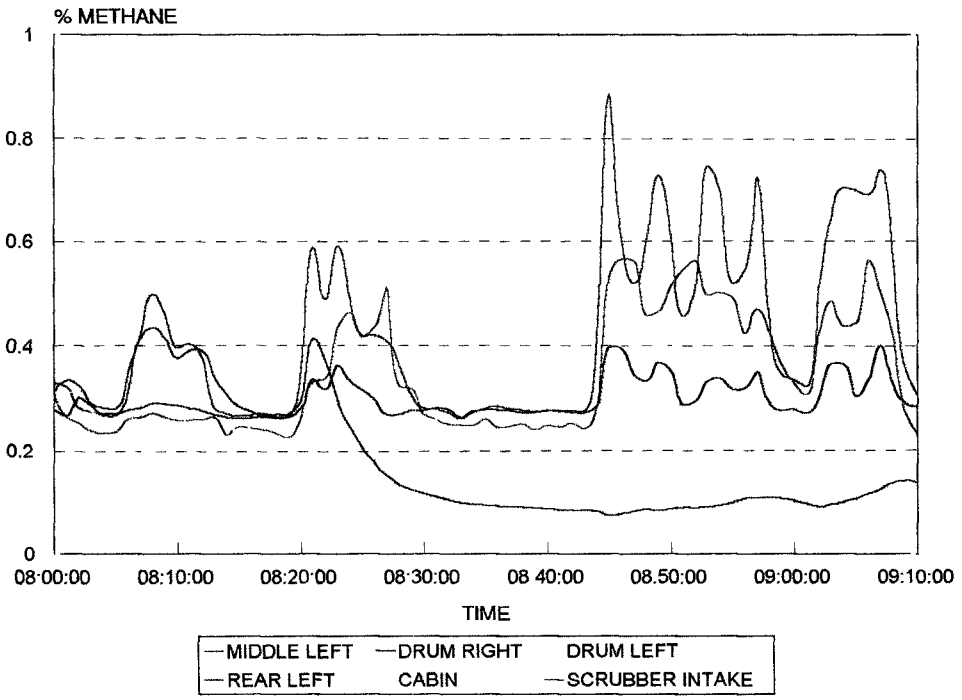

Figure 4.1 Results from 07/07/1994 (Shift 1)

From the results obtained it can seen that the levels recorded by the two sensors near the drum

dropped to nearly 0% after 6 and 21 minutes respectively. This was caused by the sensors failing due to excessive exposure to water spray and coal dust. The remaining four sensors recorded for the full duration of the test period. For the first 42 minutes of the test period levels of around 0.3% methane were recorded by all the sensors with two definitive peaks after 8 and 20 minutes that reached maximum levels of 0.5% and 0.6% respectively. Both the maximum levels were recorded on the return air side near the middle of the boom.

During the last 25 minutes of the test period a marked increase in the methane levels can be detected. The maximum level recorded of 0.9% methane, was again recorded on the return air side near the middle of the boom. For this active period there is a distinct difference in levels recorded by the various sensors. The sensor on the return air side near the middle of the boom (middle left sensor) and the sensor at scrubber intake show a marked increase in methane levels recorded, both in peaks and average levels. The maximum level recorded by the middle left sensors is 0.9% and that of the scrubber intake sensor is 0.56%. The peaks recorded by the middle left sensor tends to be ±25% higher than that recorded by scrubber intake sensor. The levels recorded by the cab and rear left sensors also show a increase in activity but considerably less than that of the other two sensors. There is no marked increase in the average level recorded by these two sensors which behaved very similar through out the test period.

The two sensors backward of the cutting drum were not fitted with the demister hoods as these hoods were introduced as a result of this failure of the two sensors.

08/07/1994

On 08/07/1994 the system recorded for 1 hour (fig 4.2).

From these results it can be seen that the two sensors near the cutting drum were still choked and that the sensor at the scrubber intake also got choked.

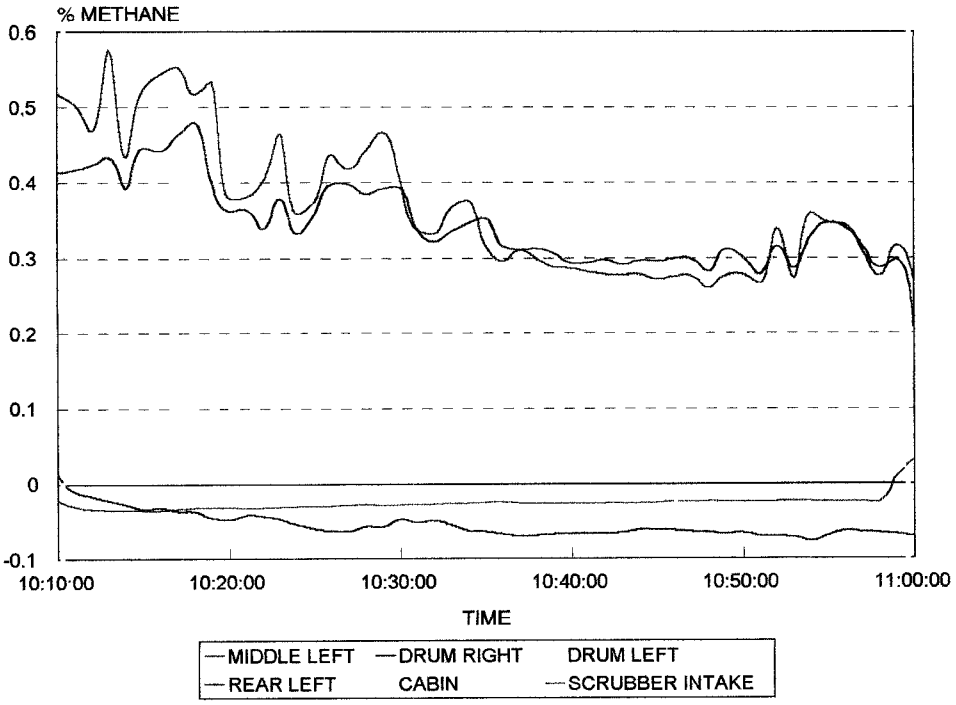

Figure 4.2 Results from 08/07/1994 (Shift 2)

The three remaining sensors recorded for the full hour. All three senors recorded much the same levels of methane through out the recording period. The maximum level for the shift was recorded by the middle left sensors (0.58%). There is a general downward trend evident during the recording period from ±0.45% to 0.3% with each sensor recording the maximum recorded level at one time during the hour.

15/07/1994

The next set of readings were taken on 15/07/1994 when the system recorded for the duration of a 8 hour shift (fig.4.3). At this stage the sensors near the boom and at the scrubber intake malfunctioned which can be seen as the flat line at 4% in fig 4.3.

During the shift the methane levels varied extensively and extremely high methane levels were recorded in comparison with the first two data sets. The middle left sensor consistently recorded the highest methane level and repeatedly reached levels of 4% plus near the end of the shift. The levels recorded by the middle left sensor tended to be twice as high as than that recorded by the sensors in the cab and rear left. The sensor at the rear left recorded slightly higher methane levels

than the sensor in the cab throughout the shift.

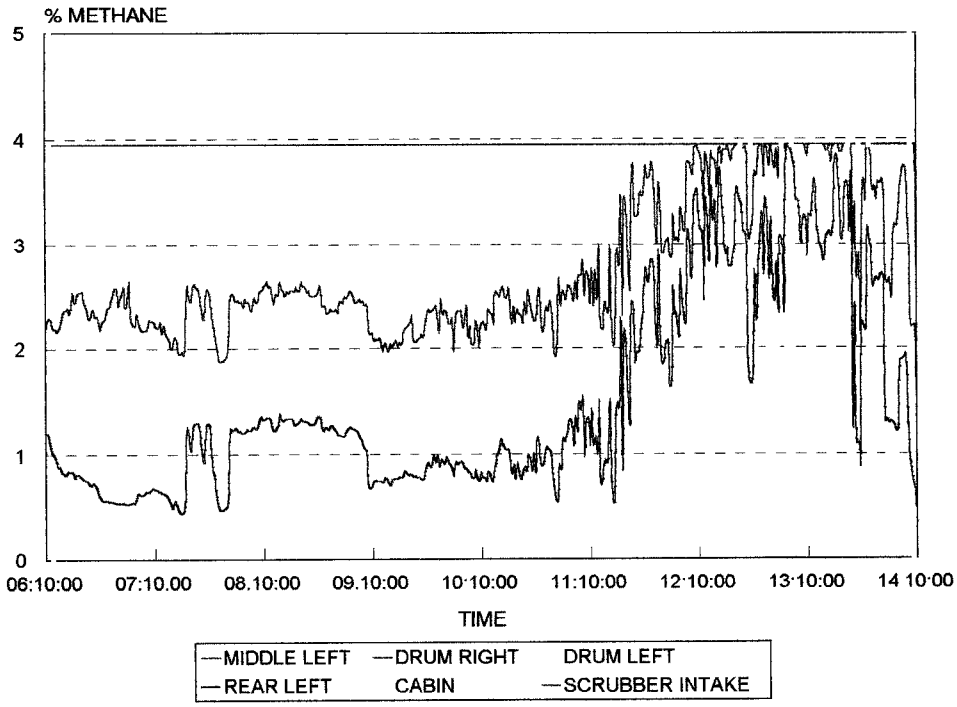

Figure 4.3 Results from 15/07/1994 (Shift 3)

During the first 5 hours the middle left sensor recorded levels of 2.3% methane on average and the sensor at the rear left approximately 1% with the sensor in the cab on an average of 0.7%. The next 3 hours of the shift was marked by a sharp increase in methane activity with the middle left sensor recording levels in excess of 4% on several occasions. The sensor at the rear left also recorded a level of 4% and the maximum level recorded in the cab sensor was 3.5% methane. The last 30 minutes there seems to be a decrease in the methane levels recorded with all three sensors recording values corresponding to values recorded earlier in the shift.

4.2 TEST 2

From test 2 five sets of data were recorded during the test period.

21/09/1994

On 21/09/1994 the system was installed and allowed to record for 2 hours (fig 4.4). The two sensors near the boom were fitted with demister hoods and the sensor near the scrubber intake was positioned so as not to be in the direct spray path of the water sprays. All the sensors recorded for the full 2 hours.

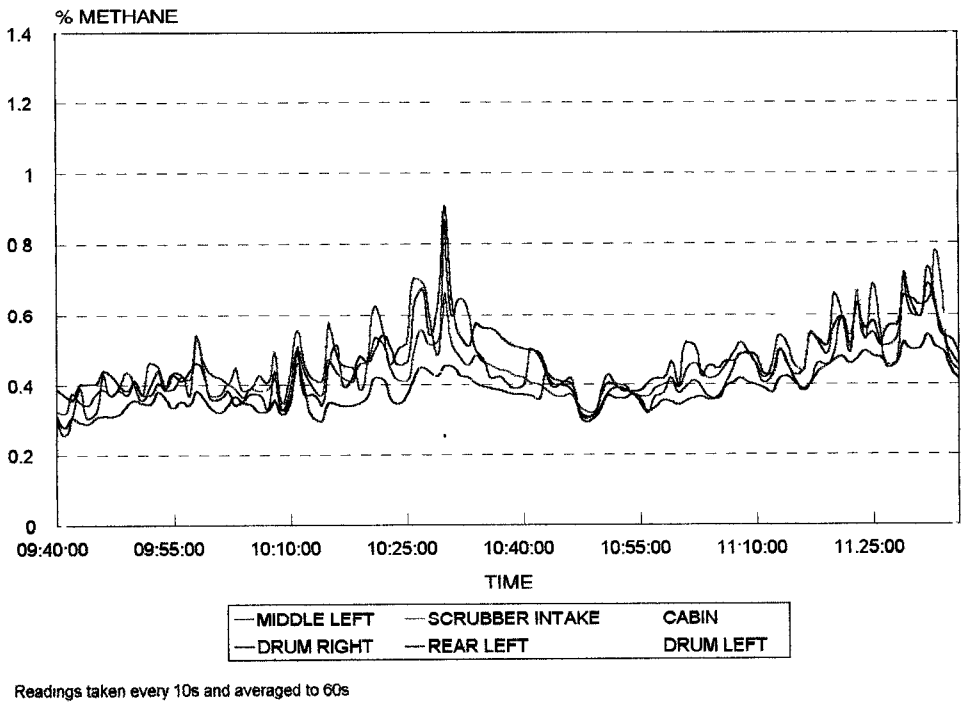

Figure 4.4 Results from 21/09/1994 (Shift 1)

During the first 45 minutes of the shift the methane levels ranged from 0.25% in the cabin to 0.7% measured just backward of the drum on the return air side (drum left sensor). During this time the CM was cutting the first web. At 10H30 a sharp peak occurs in the readings taken by the sensors near the drum, the sensor at the scrubber intake and the middle left sensor. The drum left sensor recorded the highest level of 1.3% with the boom right and middle left sensor recording 0.9% and 0.87% respectively. The scrubber intake sensor recorded a peak of 0.66% while the cabin and rear left sensor does not show a peak at this time with recorded values of 0.44% and 0.45% respectively. This peak occurred as the CM was pulling out of the first cut and preparing for the second cut.

After the peak a slight drop in recorded methane levels can be observed for all the sensors in relation to the values recorded preceding the peak. After this initial drop a moderate but steady increase is evident for all the sensors as the CM was making the second cut. The left boom sensor shows an increase in methane levels from 0.37% to 0.81% in a 45 minute period. In the same period an increase from 0.25% to 0.46% was measured by the cab sensor. The highest level recorded for this second period after the peak was 0.81% at the drum left sensor. The middle boom, drum right and scrubber intake sensors followed the trend of the drum left sensor and recorded maximum values of 0.78%, 0.72% and 0.75% respectively. The cab and rear left sensor does not show the distinct peaks recorded by the other four sensors that is situated closer to the cutting face but does show the steady rise in the methane level.

22/09/1994

The second set of data was taken on 22/09/1994 (fig. 4.5). All the sensors were still operational and recorded for just over 6 hours continuously.

For this data set the sensor at the scrubber intake recorded the highest methane levels for the duration of the shift with a maximum of 0.58% methane. The levels recorded in the cabin was second highest (max. 0.29%) for most of the shift with the left boom sensor slightly exceeding the cab value briefly on 10 occasions. The drum right sensor recorded the fourth highest level (max. 0.18%) for most of the shift following the drum left sensor closely during the middle part of the shift. The rear left sensors recorded levels below 0.1% for most of the shift with no apparent peaks evident. The last hour of the shift an increase is evident in the levels recorded by the rear left sensor with definite peaks visible reaching a maximum of 0.16% methane. The middle left sensor recorded sub 0.1% methane levels for the duration of the shift with no peaks visible.

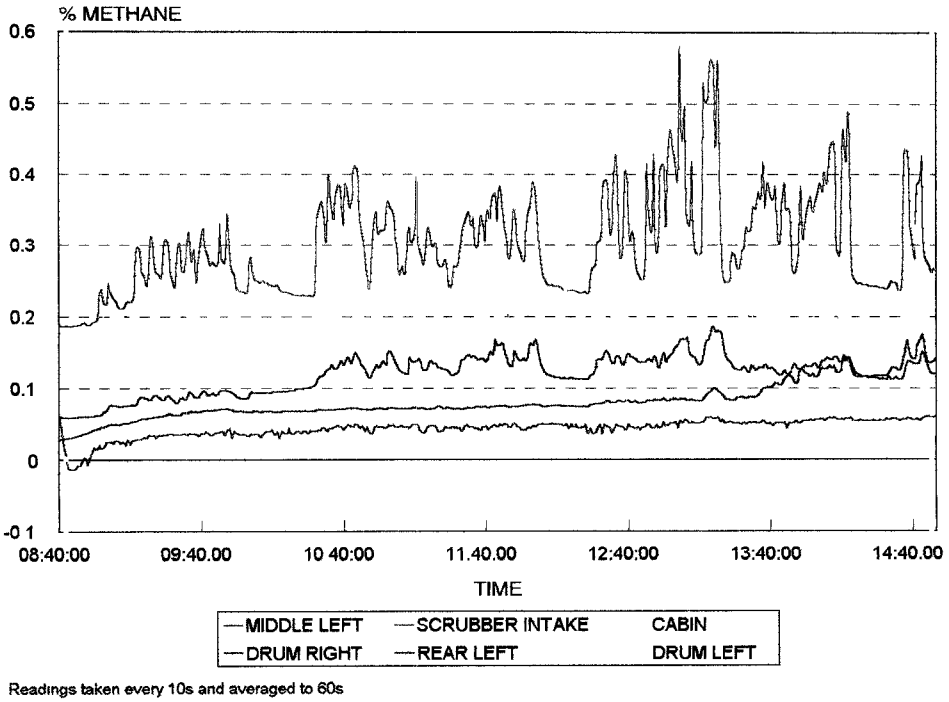

Figure 4.5 Results from 22/09/1994 (Shift 2)

23/09/1994

The third set of data was recorded on 23/09/1994 (fig 4.6) and covered a period of 5 hours during which all the sensors recorded.

During the first hour and a half of the shift distinct peaks can be observed for all the sensors with the middle left sensor recording the highest methane level of 0.6% for the shift. During this period the middle left and scrubber intake sensors recorded the highest methane levels and followed each other for most of this period. The cabin and rear left sensors also followed each other closely for this period but recorded lower levels than that of the middle left and scrubber intake sensors reaching maxima of 0.4% and 0.28% respectively. The drum left sensor recorded the lowest level (0.09%) for the shift right at the start and showed a steady increase for the first hour and half of the shift reaching a level of 0.37% methane.

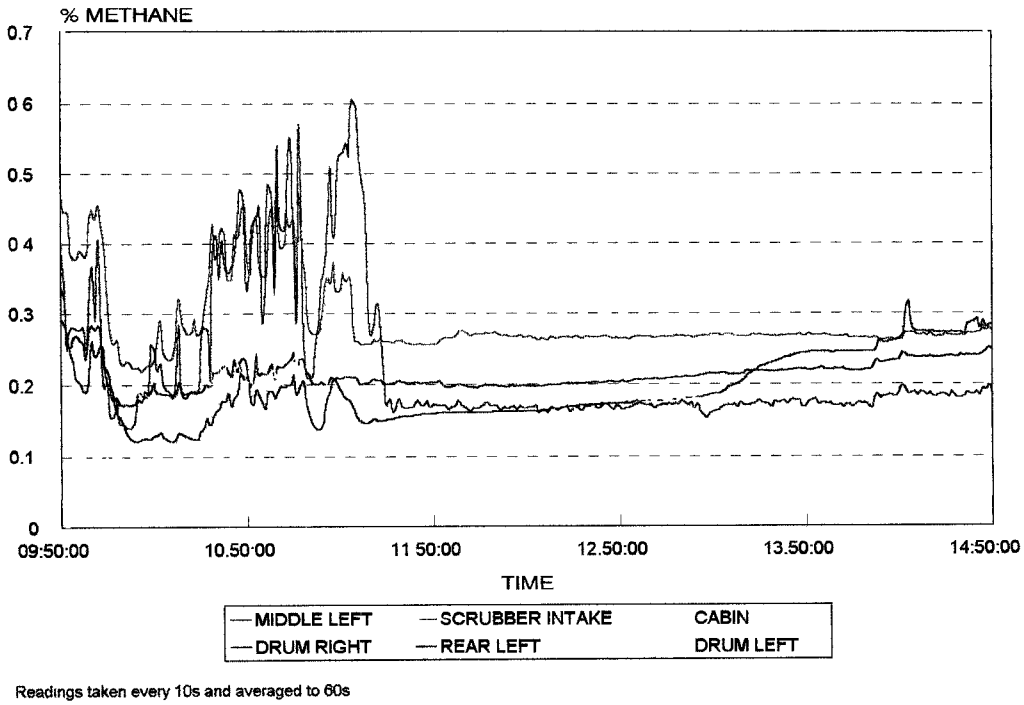

Figure 4.6 Results from 23/09/1994 (Shift 3)

After the this active period all the sensors stabilised between 0.29% and 0.17 % methane for the rest of the shift with the scrubber intake being the highest and the cab and middle left sensors the lowest. During the last hour and a half the right drum sensor showed an increase from 0.29% to 0.31%.

27/09/1994

For the fourth data set, which was recorded on 27/09/1994, the data logger recorded for 7 hours (fig 4.7). During the recording period the logger was switched off twice, the first interruption in the power supply occurring between 09H05 to 09H42 and the second between 12H29 and 12H46. All the sensors were still recording although the middle left and drum left sensors appears to be choked with coal dust because it gives very constant low level readings without any significant peaks.

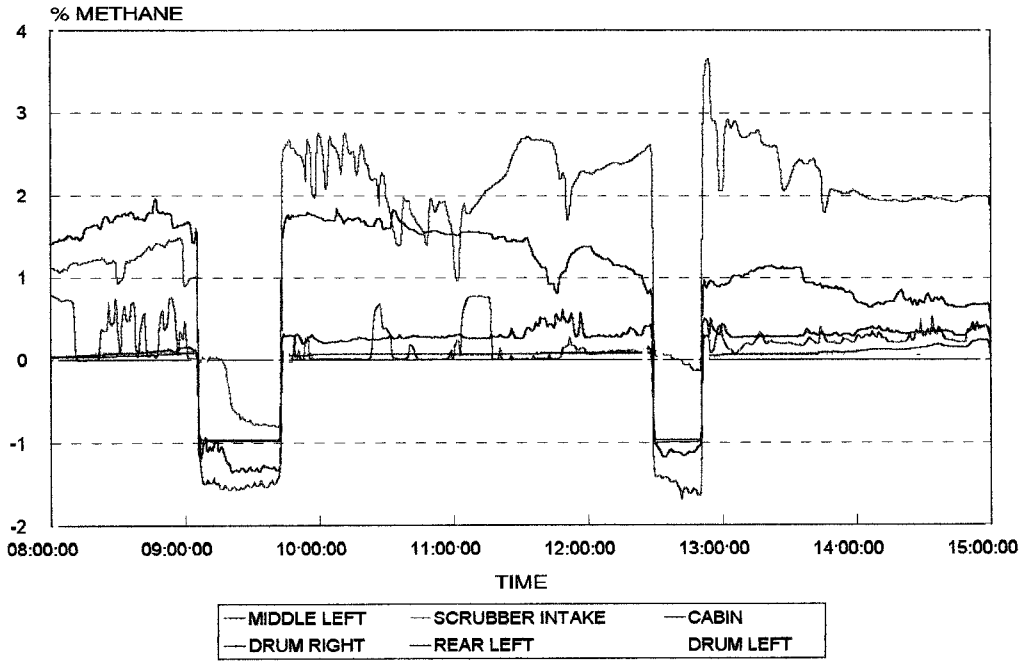

Figure 4.7 Results from 27/09/1994 (Shift 4)

During the shift recorded methane levels varied from 0% to 3.6 %. For the shift there is a definite difference between the levels recorded by the cabin and drum right sensors compared to the remaining four sensors. The levels recorded by these two sensors tends to be 2 to 3 times higher than that of the other sensors. The maximum level recorded by the cabin sensor is 3.6% with an average of 2% throughout the shift with sharp peaks between 09H40 and 11H00. The maximum level recorded by the drum right sensor is 2.95% at the beginning of the shift with a steady decline during the shift to a level of 0.6% at the end of the shift without any sharp peaks occurring. The only other sensor that recorded significant levels of methane is the scrubber intake sensor with a maximum of 0.8%. It is interesting to note that the recorded levels for this sensor is either 0% or in the region of 0.7 - 0.8% for the first 5 hours of the shift. After this there seems to be an increase in the average level recorded by the sensor to a level of 0.2%. The rear left sensor shows a marginal increase from 0% to 0.15% during the first hour of the shift before levelling out at around 0.3% the rest of the shift with no large peaks is visible for the 7 hour period. The levels recorded by the middle left and drum left sensors are low compared to the levels recorded by the cab and drum right sensors.

03/10/1994

The last set of results for this test was recorded on the 03/10/1994 and covered a period of 6 hours (fig 4.8). All the sensors was operational for this period. The scrubber intake and drum left sensor recorded levels close to 0% which indicates that these sensors might have been choked with coal dust.

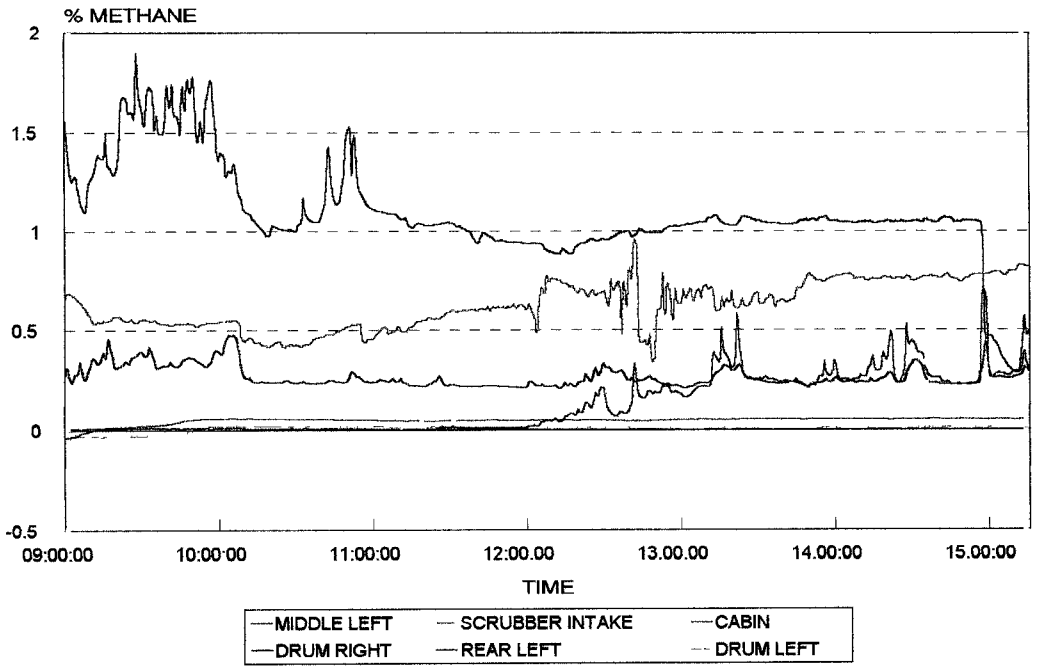

Figure 4.8 Results from 03/10/1994 (Shift 5)

The highest level for this shift was recorded by the drum right sensor to the value of 1.9%. Sharp peaks can be observed for this sensor during the first two hours of the shift after which it levelled out at 1% with a sharp drop to 0.25% after 05H50. The second highest level was recorded by the cabin sensor (1.0%) with peaks recorded between 12H30 and 13H15. An upward trend can be identified for the cabin sensor for the duration of the shift from 0.5% to 0.8%. The rear left sensor recorded consistent levels of methane in the region of 0.25% with a few minor peaks. The middle left sensor recorded 0% methane for the first half of the shift after which a definite increase in the methane level transpire. This increase closely follow the recorded levels for the rear left

sensor with more definite peaks evident. The levels recorded by the scrubber intake and drum left sensors are constant and nearly 0% for the duration of the shift.

5. DISCUSSION

TEST 1

The data obtained from the sensors just backward of the boom of sub 0.1% readings indicates that the sensors might have been choked by the combination of water spray and coal dust. This choking lead to the introduction of the demister hoods in the second test for the drum sensors and proved successful. The choking of the scrubber intake sensor prompted the sensor to be moved away from the water spray system of the scrubber and proved effective.

From the results obtained it can be seen that two sensors at the back of the CM i.e. the cabin and rear left sensor recorded the lowest levels for all three shifts. It can also be noted that when measuring levels in the region of 1% and lower no significant peaks is formed by these two sensors in contrast with the two sensors closer to the cutting face on the return air side of the CM measuring in the same methane level region.

The third set of data show a dramatic increase in methane levels around the CM compared to the first two sets of results. The two sensors at the back of the CM recorded ±50% less methane than the middle left boom sensor. These high readings were measured 8 days after the system was installed on the system. No maintenance was done on the sensors and the condition of the sensors at the time of the measurements is unknown. The sensors were however removed from the CM six days later after a roof fall and taken to the laboratory where they were inspected. All the sensors were still within specification but the cables were damaged by the roof fall so their condition prior to the roof fall could not be determined.

TEST 2

For the first three days of the test, levels of below 1% methane were recorded except on the first

day when the CM retreated from its first cut. During shift 4 and 5 levels of up to 2.7% and 1.9% methane were measured. These levels were recorded 7 and 14 days after the system was installed on the CM with no maintenance to the sensors. After the test period the sensors were removed from the CM and taken to the laboratory for inspection. All the sensors were still with in specification and the cables intact.

During the first three shifts the two sensors near the cutting drum recorded methane levels of much the same magnitude. After this period the drum left sensor choked. No apparent trend is visible for the cutting drum sensors other than that they tend to measure much the same levels.

The scrubber intake sensor was inclined to measure the highest or close to highest methane levels recorded during a shift. It appears as if the scrubber intake sensor was choked by the 5th shift.

Over the five shift period the rear left sensor and the cabin sensor seems to follow each other to some extent. The exception is shift 5 when the cab recorded the highest methane levels.

The sensor near the middle of the boom on the return air side also tends to be one of the sensors that records high levels of methane. At this position the sensor also gets choked easily as can be seen from the results of shift 2. It would appear that at this position the sensor also tends to lose the material that causes it to choke as can be seen by comparing the results of shift 2 with that of shift 3. For shift 2 the sensor appear to be choked and for shift 3 it records peaks. This is more clearly shown during shift 5 when the recorded level goes from 0% to 0.25% with definite peaks present.

6. CONCLUSIONS AND FUTURE WORK

From the results it can be seen that the 6 channel methane data logging unit is capable of recording the methane levels at 6 different positions on a CM for the duration of a 8 hour shift. No definite conclusions can be drawn from the results obtained in these two tests because of a lack of information. Information that would be required to make more reliable conclusions would

be the state of the sensors at various stages of the test and also the operations performed by the CM during the shift. Furthermore a wider data base must be established by conducting further tests to be able to examine all aspects of CM operations with relation to methane levels around the CM.

The high levels recorded during test 1 and 2 on last days of the test could indicate that the sensors need some form of maintenance after a certain period but this can not confirmed before further test are done and the condition of the sensors monitored over a period of time. For this reason the results for the last days of each test cannot be confirmed nor discarded at this stage.

In future tests the sensors would need to be inspected and maintained at regular intervals. This would ensure that data from the various shifts would be comparable as far as sensor condition is concerned. Also the operations of a CM during a shift must be monitored and logged to be able to try and identify various methane related trends surrounding each operation.

Form the results obtained thus far it would seem possible to identify a position that would give a better indication of the methane levels around a CM and what safety factor to apply. A fair amount of work still have to be done to reach this goal but encouraging results have been obtained thus far.

APPENDIX C6

METHANE MONITORING AROUND AN OPERATIONAL CONTINUOUS MINER AT MINE B

Technical report

F.J. VAN ZYL

1994-12-06

SUMMARY

This report discusses the equipment and test procedures used to determine the methane distribution around an active continuous miner. The results from the preliminary tests are shown in graph form. Low levels of methane were recorded for the duration of the test with no apparent trend identified between the various sensors. For future tests the movements of the continuous miner will have to be recorded and the data logging system maintained to ensure a more comprehensive date set.

TABLE OF CONTENTS

1. INTRODUCTION

During continuous miner (CM) operations, methane gas is released. A common and convenient place to measure the methane levels is in the drivers cabin (cab). Because of the size of a CM and the air movement around it during the mining process, it is reasonable to assume that the methane around a CM is not uniform. For this reason it can be said that the level recorded in the cab is not representative of the methane levels around the CM. To get a representative picture the methane levels at various positions must be measured and from such data a comparison can then be drawn between levels at various positions. Once this is known, it will be possible to predict what levels of methane can be expected around a CM when the methane level is recorded at one or two position. It will also give an indication of were the maximum level of methane is likely to occur and what levels can be expected.

CSIR Miningtek has developed an intrinsically safe, self contained, 6 sensor methane data logging system. The system is capable of recording methane levels at 6 different positions for 10 hours continuous at preset time intervals, of down to 1 second. This system will enable a study to be made of the relationship between methane levels at various positions around a CM during normal working conditions.

This report describes the data logging unit and the results obtained from the test done atMine B, with 6 sensors placed on a CM.

2. THE 6 CHANNEL DATA LOGGING UNIT

The data logging unit is an intrinsically safe, self contained unit that is capable of recording methane levels of up to 4%, from 6 independent methane sensors. Along with the methane levels the unit also records the date, time and location of the system. This information can be down loaded onto a personal computer (PC) and imported to a spread sheet for analysis.

The data logging unit consists of four main parts:

I. The recording box

ii. Methane sensors (X 6)

iii. PC milking station

iv. Micro logger

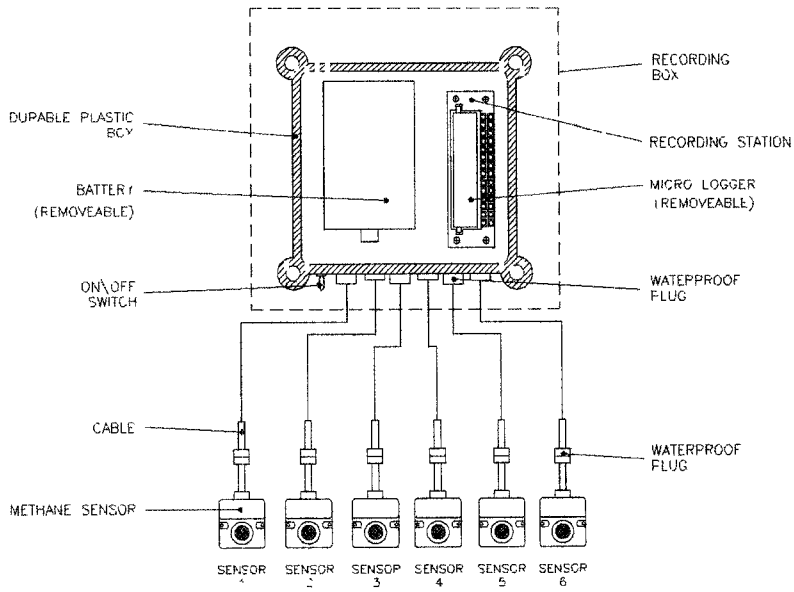

Figure 2.1 Schematic drawing of 6 channel methane data logger.

2.1 The Recording Box

The recording box contain three principal parts :

I. A power supply that powers the 6 methane sensors and the micro logger. The power supply is a rechargeable 12V battery that is capable of supplying power to the unit for at least 10 hours of continuous use, when fully charged.

ii. A recording station into which the micro logger is placed when the system is in operation.

iii. A set of 6 plugs that connects the cables from the sensors to the recording box.

The unit is also equipped with a manual ON/OFF switch that is used to switch off the unit when

not in operation to save battery life. The components are housed in a plastic box that is packed with foam rubber to protect the components from excessive vibrations.

2.2 The Methane Sensors and Cables.

Trolex TX3261 MkII sensors with a range of 0% - 4% methane in air are presently used with the system. The over all accuracy of the sensors are ±0.1% of methane in air for the range 0% to 1.25% methane in air and ±8% for the range 1.25% to 4% methane in air. The response time of the sensors are 10s. This specific methane sensor was decided on because of its low power consumption, which allows the system to operate for a minimum of 10 hours. Miningtek does not approve or endorse the use of this sensor over any other type.

The sensors are wrapped in protective rubber jackets and supplied with an additional external filter to protect them against minor impacts and excessive dust. Two of the sensors are also supplied with demister hoods to protect them from excessive exposure to water spray and coal dust.

The cables that are used are 6 core reinforced screened cables, fitted with waterproof plugs at both ends.

2.3 The PC Milking Station

The PC milking station is the interface between the micro logger and the PC, and is connected via the serial port. The milking station is used to down load recorded data from the micro logger to the PC and alternately to programme the micro logger through the PC.

2.4 The Micro Logger (ML)

The micro logger (ML) is used to record the data from the methane sensors in the recording box on site. The ML is programmed and milked via a PC with custom software.

The ML records the date, time and methane levels for each of the 6 sensors when a set of readings are taken. The time intervals between readings is constant and can range from seconds to minutes to hours.

The ML is capable of storing 60 000 bits of information before the memory is full and the ML switch of automatically, saving the recorded data.

3. TEST SETUP AND PROCEDURES

Before a test commence the system is checked, calibrated and the methane sensors fitted with new activated carbon filters to ensure that the recorded data is accurate. After each test the system is rechecked to ensure that the sensors are still with in specification and the cables intact. This is done to verify or discard the recorded data obtained during the monitoring period.

The data logging unit was taken toMine B were it was fitted to a CM. The 6 sensors were placed so as to cover all the major areas that was thought would give a fair indication of the methane distribution around the CM and also rendered reasonable protection for the sensors. Two sensors were placed either side just backward of the cutting drum, one sensor was placed at the scrubber intake and one at the scrubber outlet at the back of the CM. One sensor was also placed near the middle of the boom on the return air side and the remaining sensor was placed in the drivers cabin. The recording box was also placed in the drivers cab (See fig 3.1)

After the system was fitted to the CM monitoring of the methane levels commenced. The methane levels for a shift or part of a shift were recorded after which the recording box was removed from the CM and taken to the surface. On the surface the ML was removed from the recording box and the recorded data down loaded onto a PC. After this the ML was reprogrammed for the next shift and its battery pack charged. The system battery was also charged during this period after which the system was ready for the next shift. This procedure was repeated after each set of data was recorded.

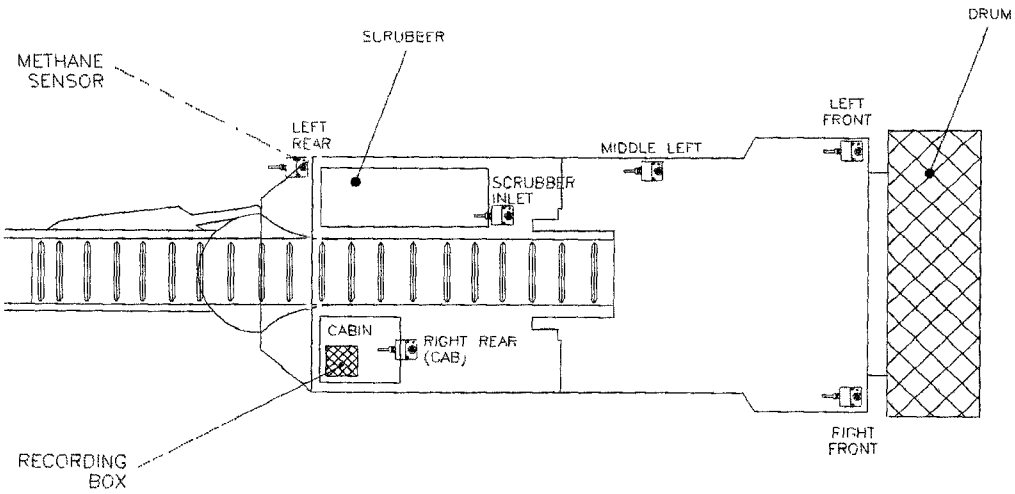

Figure 3.1 Placement of the 6 methane sensors around the CM

After the monitoring period was over the system was removed from the CM and taken to the laboratory for inspection.

3.1 Post Test System Inspection Results

During inspection it was found that the cable of the cab sensor was damaged and this resulted in the cab readings being high. For this reason the cab readings were discarded during the evaluation of the results. Table 3.1 contains the results from the post test inspection for all the sensors used during the test. (The sensors that don't comply with the specifications are printed bold.)

The post test system inspection entails that the sensors be exposed to a known air/methane mixture and the resulting output voltage of the sensor measured and compared to the specified output voltage for the sensor. This then indicates if the sensor is still with in range or not. The specified air/methane mixtures for the testing of the sensors are 0% and 2.5%. The sensors are firstly exposed to a 0% mixture, then to a 2.5% mixture and then again to the 0% mixture, as specified. In each case the sensors are allowed to stabilize before the output voltage is taken.

POST TEST SENSOR INSPECTION RESULTS

SPECIFIED VOLTAGE READINGS:

0% CH_4 : 0.40±0.01 V
2.5% CH_4 : 1.40±0.01 V

SENSOR	READINGS		
	0% CH_4 (V)	2.5% CH_4 (V)	0% CH_4 (V)
REAR LEFT	0.41	1.41	0.41
SCRUBBER INTAKE	**0.42**	1.39	**0.42**
CAB	**0.61**	**1.45**	**0.60**
MIDDLE LEFT	0.39	**1.38**	0.39
DRUM LEFT	0.39	1.39	0.39
DRUM RIGHT	**0.38**	**1.38**	0.39

*Test done with full length cable and voltages measured at entry to data logger.

Table 3.1 Post test inspection voltages for Trolex sensors.

Of the remaining 5 sensors checked, 3 were not with in specification. The scrubber intake sensor error was 2.5% high for the 0% mixture but within specification for 2.5% mixture. The sensor near the middle of the boom on the return air side (middle left sensor) had an error of 2.3% low for the 2.5% mixture but was with in specification for the 0% mixture. The sensor just backward of the boom on the air intake side (drum right sensor) had an error of 2.3% low and 2.5% low for the 2.5% and 0% mixtures respectively. The sensor at the back of the CM on the return air side (rear left sensor) and the sensor just backward of the boom on the return air side (drum left sensor) were both within specification.

4. RESULTS AND DISCUSSION

The data logging system was installed at Matla 3 on 13/10/1994 and stayed on the CM for 12 days after which it was removed. During this period 3 sets of results were obtained. The first set of results was obtained on 18/10/1994, the second on 19/10/1994 and the last set on 20/10/1994. From these dates it can be seen that for the first 5 days no results were obtained. This was caused by the incorrect procedures followed during the down loading of the micro logger.

For the duration of the test period the ML was set to record the methane levels every 10s, which

corresponds to the response time of the Trolex sensors. Because of the vast number of data points generated during a shift the average of every 6 readings were taken which then provided the average methane level per minute for the shift for each sensor. This was done to reduce the processing time during analysis of the results and no apparent difference can be observed between the graphs of a full data set and that of an averaged set.

18/10/1994

The data obtained during this shift spans a 8 hour period. The results are shown in graphs 4.1 & 4.2. In graph 4.1 it can be seen that the cab sensor was reading in the region of 0.8% for most of the shift while the remaining 5 sensors recorded levels of between 0% and 0.25%.

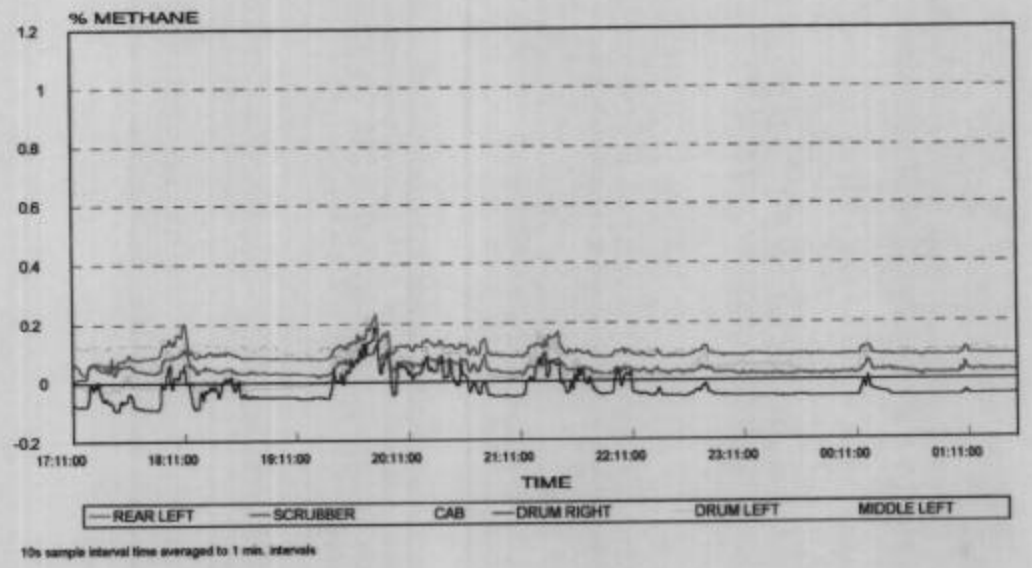

Graph 4.1 Results from 18/10/1994

In graph 4.2 the levels recorded by the cab sensor was discarded and a better indication of the results recorded by the remaining sensors were obtained. From the post test inspection it was established that the cab sensor cable was damaged and this caused the cab sensor to read high. For this reason the data recorded by the cab sensor was discarded for this analysis.

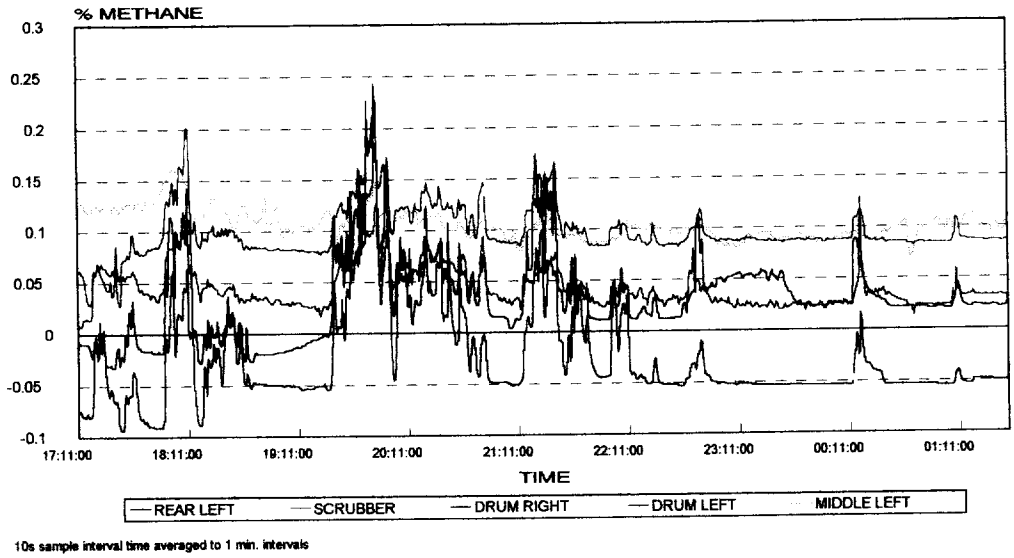

Graph 4.2 Results from 18/10/1994 excluding the cab results.

From graph 4.2 it can be seen that low levels of between 0% and 0.25% were measured for the duration of the shift. The right drum sensor was recording levels below 0% which corresponds to the post test inspection results for this sensor. Because of the small deviations occurring in the specifications for 3 of the 5 sensors and the low levels of methane recorded no apparent trend can be observed for this period

19/10/1994

The next set of data was recorded over a period of 5 hours during which the system was switched off once at 11H05 for approximately 1 minute. The results for this period are shown in graph 4.3 & 4.4. From graph 4.3 it can be seen that the cab sensor was recording levels in the region of 0.6% and the remaining 5 sensors levels below 0.2%. A damaged sensor cable caused the high cab readings with the result that these readings had to be discarded for this analysis.

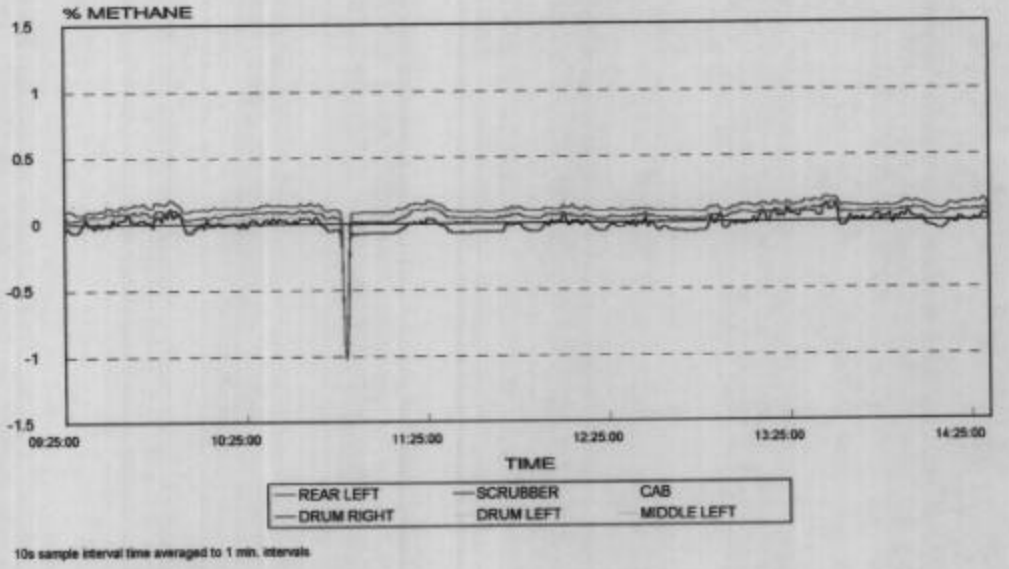

Graph 4.3 Results from 19/10/1994

Graph 4.4 shows the results for the remaining 5 sensors. It can be seen that levels below 0.2% were recorded for the duration of period. The sub 0% levels recorded by the drum right sensor corresponds to the post test inspection results for this sensor. Because of the small deviations occurring in the specifications for 3 of the 5 sensors and the low levels of methane recorded no apparent trend can be observed for this period.

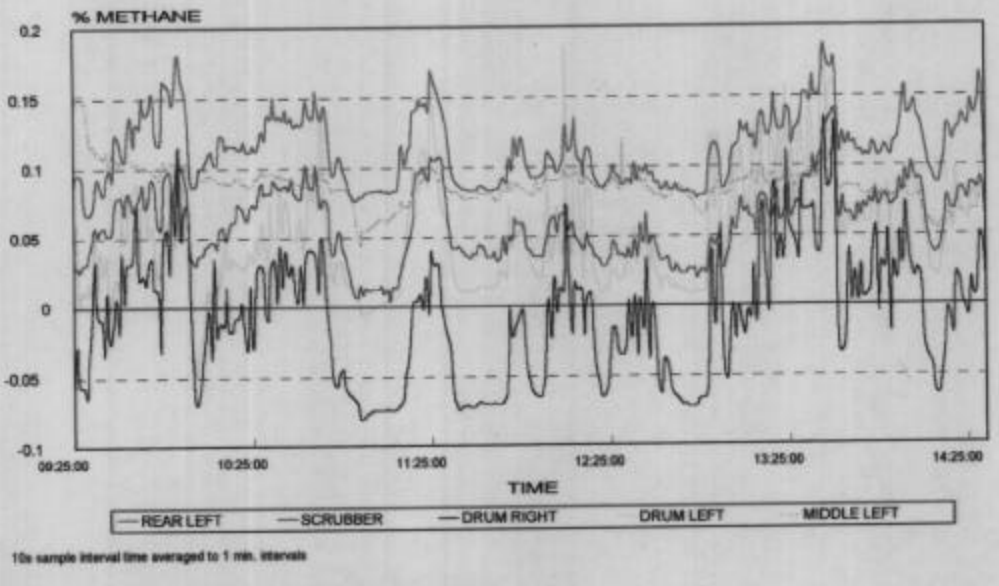

Graph 4.4 Results from 19/10/1994 excluding the cab data

20/10/1994

The last set of data was recorded on 20/10/1994 and spanned a period of 5 hours. Sub 0.2% levels were recorded for the duration of the test by all the sensors. Graph 4.5 contains the results for this test period.

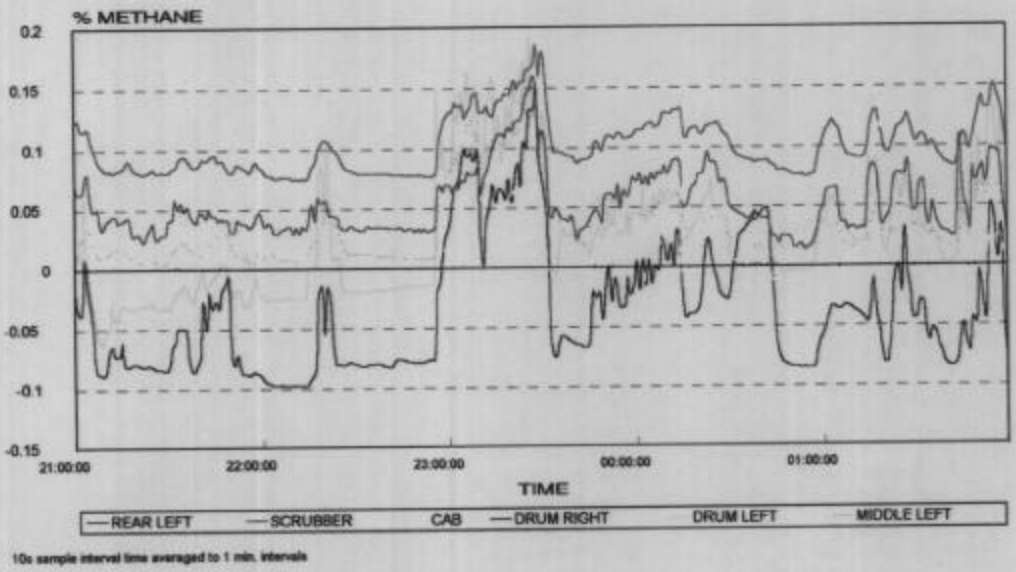

Graph 4.5 Results from 20/10/1994

The level recorded by the cab sensor was below 0.2% but has to be discarded because the post test inspection showed the cable to be damaged. The sub 0% levels recorded by the drum right sensor was caused by the sensor recording low as indicted by the post test inspection. Because of the small deviations occurring in the specifications for 3 of the 5 sensors and the low levels of methane recorded no apparent trend can be observed for this period.

5. CONCLUSION

For the duration of the test period sub 0.25% methane levels were recorded. Such low recorded levels will be influenced by slight deviations in the specifications for the sensors and from the post test inspection 3 of the 5 sensors showed a slight deviation from the specifications. This deviation will result that the sensors will still record variations in the methane levels but their absolute values will be incorrect. Because such low methane levels were recorded this variation in the absolute value makes it impossible to compare the results obtained.

The best results for the methane monitoring system is obtained during the first 3 to 4 days after the installation of the system, if no maintenance is done on the system. During this period the sensors will still be within specification and the filters will still be relatively free of dust, which tends to impede the responsiveness of the sensors.

All the sensors functioned for the duration of the test with the exception of the cab sensor. The cab sensor cable was damaged which caused the sensor to read high.

From the results it can be seen that the methane levels recorded around the CM was low for all the recording positions with the result that no obvious trend between the various positions can be identified. To be able to make a better assessment of the methane conditions around the CM, data from the first few shifts is essential for future tests. The movements of the CM also needs to be recorded for the duration of the test period and maintenance needs to be carried out on the data logging system to ensure a comprehensive data set for future tests.

APPENDIX C7

METHANE MONITORING AROUND AN OPERATIONAL CONTINUOUS MINER AT MINE C

Technical Report

F.J. VAN ZYL
MINING OPERATIONS AND ENVIRONMENT
CSIR MININGTEK

1995-09-22

SUMMARY

This report discusses the two tests done with a multi channel methane data logging system. The equipment and test procedures used to determine the methane distribution around an active continuous miner are explained. The results from the tests are presented in graph form. From the results and the logsheets of CM movements it appears as if their is a tendency for methane accumulation under the boom. During certain ventilation conditions it seems as if the ventilation assists in this apparent buildup by not suppling the heading with adequate amounts of fresh air. It was also found that ventilation variations can have a significant influence on methane levels in an active heading. It seems as if sporadic instances of increased methane emissions occur on a seemingly random basis. The results also indicate that the majority of methane in an active heading is produced by the freshly cut coal. These are preliminary findings from the limited data available. To be able to make a comprehensive assessment of the various factors that influence methane levels and behaviour in an active heading, further tests have to be done. These tests will be designed to investigate particular factors that were identified as possible problem areas. From this test data possible solutions can be found, if it deems necessary.

TABLE OF CONTENTS

1. INTRODUCTION

When the methane content in air is within the explosive range and an ignition source is supplied an explosion will result. In an active heading in a colliery both these elements are ever present and if left unchecked could have disastrous consequences. To avoid this scenario one of the two contributing elements must be removed. As it is currently not possible to avoid hot spots developing on the picks and sparks forming when other materials are accidentally cut e.g. sandstone, the industry strive to keep methane levels below the explosive range. In order to ensure that the methane levels is below the explosive range, it has to be measured. In the past it was common practise to measure the methane levels in the drivers cabin (cab) of a CM. This was done because the cab provide a certain degree of protection to the sensor and so reducing maintenance requirements. If we assume that the most methane gas is librated from the coal being cut in a heading (more exposed surface area) and we take into account the physical size of a CM and the ventilation conditions in a heading, it is reasonable to assume that the methane levels recorded in the cab is not representative of the methane levels surrounding the CM. Under these conditions it might be possible for pockets of methane in the explosive range to form, with potentially dangerous consequences. To be able to get a clearer picture of methane behaviour around an active CM, levels have to recorded at various positions on the CM during the mining process. This information will then indicate if areas of high methane levels exist or can potentially exist and what the relation is with levels at various other positions on the CM.

CSIR Miningtek developed a intrinsically safe methane data logging system. The systems consists of 6 methane sensors linked to a datalogger via cables. The system is totally self contained to ensure ease of use and portability. The datalogger is fully programable and can record methane levels over a 8 hour shift, with recording intervals down to 1 s. This system enable Miningtek to continuously monitor and analyse the methane levels around an active CM to determine if any patterns or trends can be identified. From this results it is hoped that a quantitative assessment can be made, which would indicate if the current procedures applied by the colliery is adequate. From the data it is also hoped that future recommendations can be made with regard to sensor placements, maintenance and alarm levels, if it deems necessary.

Two tests were run at Mine C in conjunction with the environmental department. Both tests ran for approximately 15 days. During the first test some logistical problems were experienced and less data were retrieved than from the second test. Both tests produced reliable data and combined with the manual recording of CM operations, by colliery staff, a general picture of the methane distribution and behaviour can be formed.

2. THE 6 CHANNEL DATA LOGGER SYSTEM

The data logging unit is an intrinsically safe, autonomous unit that is capable of recording methane levels from six different sensors. Each methane sensor measures methane in the range 0-4%. Along with the methane levels the data logger also records the date and time. This information is down loaded onto a PC and imported to a spreadsheet for analysis.

The four main parts of the system is the recording box, methane sensor and cable assemblies, PC milking station and micro logger.

2.1 Recording Box

The recording box contains the 12V system battery, the on site termination station, connecting plugs for the sensor cables and an ON\OFF switch. The micro logger is plugged into the termination station during the test and removed on completion of the test, to be down loaded onto a PC. The system battery can also be removed for recharging purposes. Because the micro logger and battery can be removed from the recording box or the cables can be disconnected from the recording box the option exist to either remove the entire box or just the battery and micro logger after a test. This adds to the flexibility of the system, which can be of vital importance if space is limited. The recording box is lined with foam rubber to protect it against excessive vibrations.

2.2 Methane Sensor and Cable Assembly

The Trolex TX3261 MkII methane sensors with a range of 0 - 4% methane are presently used with the system. The overall accuracy of this sensors is ±0.1% for the range 0 -

1.25% methane in air and ±8% for the range 1.25 - 4.00% methane in air. The response time of the sensors is 10s. These sensors are used because of their low power consumption, which allow the system to operate for ±9 hours continuously. Miningtek does not approve or endorse the use of this product over any other type.

Three of the sensors are fitted with protective hoods. These hoods provide some protection to the sensors in extreme environmental conditions of dust and water spray e.g. behind the cutting drum.

The cables that are used is 6 core screened armoured cables. Connection to the recording box is established trough waterproof screw on plugs.

2.3 Milking Station

The PC milking station is the termination station that is used to down load recorded data from the micro logger to a PC. The termination station is connected to a serial port of a PC via a RS232 cable. Dedicated software exist for down loading and converting of data into a format that is accepted by most spreadsheet software e.g. Lotus123, QuatroPro, Excel etc.

2.4 Micro Logger (ML)

The ML is a self powered, of the shelf data logger that has been made intrinsically safe by Miningtek. The ML has 8 analog channels and 2 digital channels for recording purposes.

The ML is programmed via a PC with dedicated software. During the programming procedure the memory is cleared, internal clock checked and recording intervals set. The recording intervals can range from seconds to hours.

The ML has 64K bytes of memory available for recording purposes. This will enable the data logger to record the data of the 6 methane sensors, at 10 s intervals, for approximately 22 hours. This period is much longer than the system battery can sustain during full operation. When the memory of the data logger is filled the logger switches

off automatically, saving the recorded data.

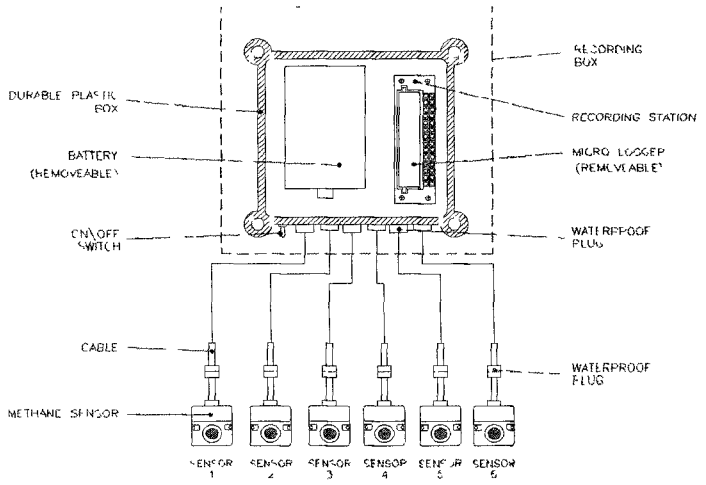

Figure 2.1 Schematic drawing of 6 channel methane data logger.

3. DATA- ACQUISITION PROCEDURE

Before each of the two test periods the data logger system was examined and the methane sensors calibrated. New activated carbon filters were fitted to the methane sensors to minimize errors during the recording of methane levels. Three of the sensors were also fitted with protective hoods. These protective hoods shields the sensors against excessive water spray and dust, typically found in the measuring positions near the cutting drum. These hoods have been tested under laboratory and operational conditions and it was found that they do not influence to the response time of the methane sensors if kept reasonably clean. The big advantage arise from the fact that the hoods allow for methane levels to be recorded right behind the cutting drum for up to 14 days with a ± 25% chance of sensor failure after about 8-12 days. Without the hood a 100% failure rate is obtained after 1 shift.

The system was installed on a 14CM9 continuous miner at Mine C for both tests. This was done to try and establish continuity between test 1 and 2 because of the problems experienced during the first run. The CM was used for long wall development in a seam height of approximately

2.2m. The CM was not fitted with directional sprays nor was an onboard scrubber system present. The ventilation setup consisted of a forced column in conjunction with an exhaust column. During one shift a jet fan was employed to ventilate the work area.

To establish a data base sensor placements are kept as constant as possible from test to test, conditions and equipment allowing. The sensor positions, as currently employed, attempt to cover all the main points of interest, as far as methane levels around an active CM is concerned. These positions are shown in figure 3.1. The sensor in the cabin is used as reference to measurements typically taken on a CM in the industry. The two sensors behind the cutting drum would in theory detect the highest levels of methane because of methane liberated from the broken

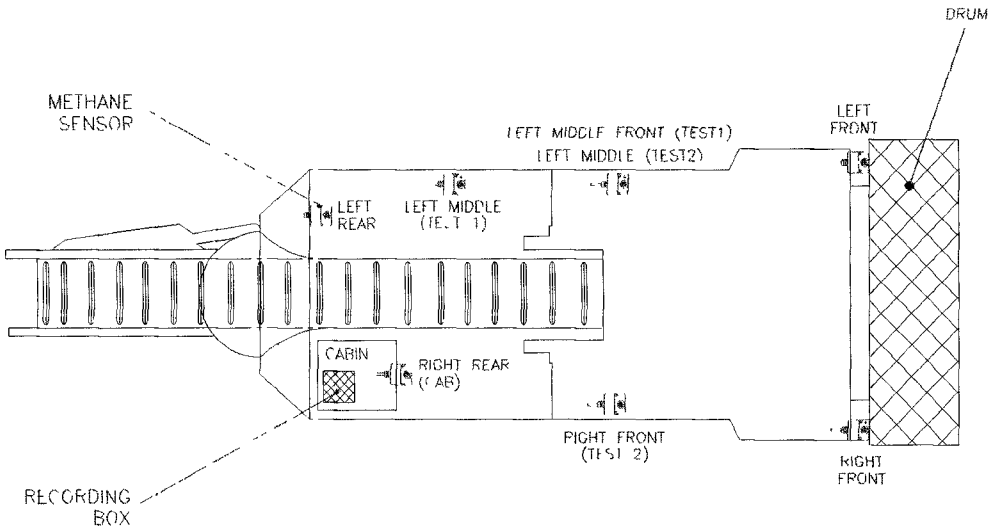

Figure 3.1 Methane sensors placements on the CM for test 1 & 2.

coal during the cutting process. These two sensors are placed in this harsh environment to try and determine what the maximum methane levels are in the heading during the mining process. The sensor in the middle of the CM, on the return air side is mainly used to determine the dilution rate from the drum to the middle of the CM. The sensors in front and behind of the scrubber (or would be scrubber) are mainly employed to determine if there is a marked difference in methane levels across the scrubber of the CM during its various operations and movements .

Secondary information can also be extracted from the recorded data. Any correlation that may exist between the air intake and return air side of the CM can be identified as well as any gradients across the length of the CM. The influence of mining activity and ventilation on methane levels can also be studied, if monitoring conditions allow. Because of the continuous nature of the test the life span of the various sensors can also be monitored. From this data a profile of sensor life for the various monitor positions can be compiled. This profile, in combination with the relative methane levels recorded at this position, can be used to determine the optimum methane monitoring position/s on a CM and the maintenance requirements to ensure reliable operation.

The sensor placements from test 1 to 2 were slightly different because of the absence of an onboard scrubber system. The sensor in front of the would be scrubber was moved to the middle of the CM on the air intake side for the second test (fig 3.1). This move was prompted because of the similarity in methane levels recorded at this position and the middle return air side position. This move would allow for a better parallel to be drawn between the air intake and return air side of the CM.

It is reasonable to expected that the various mining operations and ventilation conditions in a section will influence the methane levels around a CM. For this reason a logsheet of CM movements for all the shifts were kept. These logsheets were recorded manually and also contained general notes on prevailing conditions e.g. ventilation conditions, irregular incidents etc. These logsheets are used in conjunction with the recorded data to analyse the methane levels around the CM.

After each of the tests the system was taken to the laboratory and the system and sensors inspected to ensure that the system was still functional and within specifications. This is done to eliminate any major errors that may have been incurred during the monitoring period.

4. TEST RESULTS

Two tests were conducted at Mine C. The first test was conducted from 1995-03-07 to 1995-04-02 and the second from 1995-07-31 to 1995-08-14. Monitoring intervals were set to 10s and

averaged to 1 minute during down loading of the data. This averaging of the data reduces the computer time significantly during analysis without a loss in detail and accuracy to the graphs.

4.1 TEST 1

The first test at Mine C spanned a period of 26 days. This period is longer than the prescribed 14 days, but the system was calibrated in situ in an effort to retrieve more data from the test. During this period only 2 sets of data were retrieved. This low return of data was caused by various unforseen incidents during the test period. Apart from the expected frequent belt extensions that had to be performed, causing the CM to be stationary, other uncommon and critical system breakdowns played a significant part in the low data return. A broken system battery cable, a destroyed methane sensor, damaged sensor cables, data logger failure and PC hardware failure were the main attributers to the monitoring problems.

The first set of data was recorded 2 days into the test and the 2nd during the 9th day. The right drum sensor was destroyed during this shift which rendered the last part of the shift's data invalid. The sensor was not replaced for the remainder of the test.

The results from test 1 is contained in appendix A1.

4.2 TEST 2

The second test yielded 5 sets of results from the 15 day test period. During the third shift of monitoring the right drum sensor was damaged. This occurred during the third day of the test period. It seems as if the sensor head were exposed to extreme water spray and coal dust which choked the hood and consequently subjected the sensor head to water causing it to fail. The sensor was not replaced for the duration of the test.

The results from test 1 is contained in appendix A2.

5. DISCUSSION

TEST 1

During the recording of the first set of data a jet fan provided the ventilation . The CM was busy clearing up after holing through a split. The CM started of in the unrestricted path way of the split, were it received the full extend of the ventilation. During the first hour of the monitoring period the CM was clearing the corner of a pillar to the left and moved into the heading, 3-4 metres. During the clearing of the corner the left front sensor was effectively cut off from the ventilation which in induced an accumulation of methane in this area, with levels reaching 2.5%. From the position of the CM relative to the jet fan during this period, ventilation conditions over the top of the CM must have been close to normal, which leads to a conclusion that the majority of methane must have accumulated under the boom. A combination of factors most likely contributed to this accumulation occurring under the boom. Firstly the rotation of the cutting drum would tend to drag some of the released methane from broken coal under the boom. In conjunction with this the position of the CM next to the wall effectively caused a cavity to be formed between the wall, boom and the floor, restricting ventilation to pass freely underneath the boom. This caused a reduction in the fresh air supplied to this area, creating favourable conditions for methane buildup. The absence of directional sprays also contributed to this buildup by not inducing air movement towards the left of the boom, which could have assisted the already weakened ventilation conditions.

As the CM worked its way around the corner (turning left) and started into the heading, a slight decrease in the general effectiveness of the overall ventilation across the CM can be observed. Although a decrease is evident for the left front sensor, caused by the CM straightening up and aligning more with the ventilation, an increase in methane levels recorded by the remaining sensors positioned towards the front of the CM (RF, LF, LMF & LM) can be observed. Towards the end of the cut, the two sensors behind the cutting drum were recording peaks of ± 1%, with the two sensors towards the middle of the CM, on the return air side recording peaks ±60% lower. The two sensors at the back of the CM, which were still exposed to normal ventilation conditions in the last through road (LTR), did not record any significant peaks during this period. This would confirm the decrease in the overall effectiveness of the ventilation as the CM moves into a heading.

For the second data set the CM was cutting a split to the right with the right front sensor missing. A force column and exhaust column provided ventilation during the shift. An interesting observation is the 2.1% methane that was recorded by the left front sensor while the general body of methane around the CM was 0.25%. The CM was parked with its left side next to the side wall with no external ventilation in the section when the peak occurred. This peak was most probably caused by a very localised area were methane was desorbing at a high rate (blower).

A drop in the general methane level can be observed as the power was restored to the ventilation fans. As the CM moved into the split for the first pass a general increase in methane levels for all the sensors were recorded. The peaks recorded by the front left sensor increased by ±123% during the first pass, with a maximum of 1.42% at the end. As expected the left front sensor recorded the highest methane levels on average with the two left middle sensors, which followed each other closely, recording on average levels ±25% lower than the left front sensor. The peaks of the left rear sensor is much less pronounced than for those closer to the boom. This is because the rear of the CM is more exposed to ventilation conditions than the front sensors, so allowing for better dilution. This trend can also be seen for right rear (cabin) sensor. The methane levels recorded by this sensor also remains fairly constant until the sensor moves into the developing split and by doing so out of the ventilation conditions sustained in the LTR. When this happens the peaks become more pronounced possible because of a reduction in ventilation effectiveness. When the CM pulls out of the heading the levels return to the previously recorded levels in the LTR. At this time the force column was moved around the pillar corner to supply more ventilation into the heading resulting in an overall reduction in methane levels for the remainder of the test. The flat line recorded for the middle left sensor for the last half of the test indicates that the sensor most probably got choked.

TEST 2

For all of the 5 recorded shifts straight cuts were made i.e. no splits cut. Ventilation was supplied by a force and exhaust column combination. The only exception being the third shift when only a force column was utilised for heading ventilation. Methane levels recorded for this shift show very cyclic behaviour with peaks forming every ±3 minutes for the sensors on the return air side of the CM. The peaks formed by the front sensor were approximately twice the value of the lows

preceding it. A steady increase in peak methane levels, as the CM moves into the heading, is also evident, followed by a subsequent drop as the CM retreats. A definite difference between the recorded lows and peaks are evident for the sensors placed on the return air side of the CM. Peaks at the front of the CM is much more pronounced than the peaks formed by the rear left sensor. The cabin sensor and to a lesser extend the right middle sensor, being in the direct fresh air stream, do not exhibit this cyclic behaviour of methane levels. This indicates that the peaks could possibly be related to the ventilation conditions. As the CM was cutting on the right side of the heading ventilation from the force column over the CM must have been substantial. It is reasonable to assume that the ventilation under the boom was reduced because of the constraints the side walls and boom itself presented to effective air flow. To aggravate this situation the CM was not equipped with directional sprays. As the intervals between peaks roughly coincide with the time it takes to do one sump and shear action it is conceivable that they might be related. As the boom is lifted to do a sump at roof level an under ventilated region is formed under the boom. From computational fluid dynamic (CFD) simulations it seems as if the rotation of the drum tends to drag methane released under the boom. Also fresh surface area is exposed during the shear action and the broken coal accumulates at the gathering arms, all contributing to increased methane emissions in this area. By bringing the boom down the area under the boom decreases and the air and methane mixture is pushed out from under the boom. With air escaping during the downward movement of the boom as the area under boom decreases, less air is available for the dilution of the fresh supplies of methane introduced to the under boom area by the rotation of the drum and the newly exposed coal. To worsen the scenario the air present under the boom meant for the dilution of the newly added methane, already contains increased levels of methane accumulated from the start of the shear operation. As the boom moves down this effect becomes progressively worse, possibly explaining the dramatic increase (up to twice the initial level) in recorded methane levels over a short period of time. As the boom now moves up surrounding fresh air is pulled in to expanding under boom area diluting the high methane concentration. As the CM moves into the heading the general heading ventilation deteriorates, supplying less quantities of fresh air to the heading for methane dilution. This means that the air which replaces the methane rich air under the boom already contains a certain amount of diluted methane. This can be seen from the general increase in the recorded methane levels for the sensors as the CM moves into the heading.

Ventilation can also play a possible part in methane buildup in a heading by failing to supply adequate quantities of fresh air for methane dilution. This situation can be seen from the last shifts data. The CM was cutting its first pass on the left with force and exhaust columns active. The force column was entering air on the right hand side of the heading, blowing onto the face directly in front. This most likely caused the air supplied by the force column to blow across the face of the heading, reducing the effectiveness of the exhaust column, especially when the CM moves into the pass. This can be seen from the rapid increase in methane levels at the front and left middle sensor positions, as the CM moves into the pass. An increase from 0.25% to 2.25% for the front sensor was recorded in less that 20 minutes. The middle left sensor recorded an increase from 0.25% to 1.33% for the same period. The same 3 minute cycle can be observed but with much less definite peaks because the air replacing the under boom air also contains elevated levels of methane caused by the lack of fresh air supplied to the heading. It is unlikely that abnormal methane emissions were responsible for the high recorded levels since when the CM performed the second pass, recorded levels were half of the previous maximums.

For all of the shifts the sensors just back of the cutting drum recorded the highest methane levels. The levels recorded at the left middle sensor position were ±45% lower than that of the front sensors for most of the mining activities during the test. Sporadic fluctuations in this status quo do however occur on a seemingly random basis, not related to any obvious ventilation changes. This can be seen from the 4% plus recorded by left front sensor during the first shift. The left and right front sensors recorded much the same levels for the duration of the shift, except for this 16 minute period. The chances of equipment failure is unlikely. Also during the fourth recorded shift the only sensor that registered any significant gas activity was the front sensor (1%) for the last 1.5 hours of the shift, with levels 5 times higher than middle sensors and 10 times that of the back sensor readings. This occurred after all the sensor showed much the same levels for the preceding 2.5 hours of the shift. This increase could have been caused by the CM mining past depth of the the first pass, creating walls on either side of the CM. This is unlikely as the CM only advanced ±1.5m into the face and the increase is to sudden to be caused by buildup.

It is evident that the methane released during the mining process is very significant compared to the methane released form the roof, floor and side walls, normal ventilation in the section

prevailing. This is the most clearly illustrated in shift two were in distinctive drop in methane levels is evident when the CM is not operational.

Apart from the definite peaks and highs in the methane levels that form, it seems as if the prevailing methane levels recorded in the cabin is in the region of 0.2%. Compared to the maximum of 2% plus recorded at 6 occasions for the 5 shift test period, it can be appreciated that methane monitoring in the cabin seems inadequate.

6. CONCLUSIONS

1. It appears as if the high methane levels recorded at the back of the cutting drum is caused by methane buildup under the boom. Poor ventilation conditions prevailing under the boom, combined with reduced ventilation effectiveness as the CM moves into a pass, can be held responsible for this buildup. Properly placed directional sprays can possibly reduce this effect.

2. Ventilation conditions has a significant influence on methane levels. When ventilation conditions do not allow for fresh to be supplied to an active heading, methane buildup can occur due to a lack of dilution. Thus situations when ventilation systems oppose each other, or is not well directed, can induce methane buildup. The position of the CM relative to the ventilation flow can also have a major influence on potential methane buildup.

4. Apart from the expected methane buildup in an active heading, significant sporadic methane occurrences do take place. It is difficult at this stage to determine the frequency or nature of such occurrences.

5. From the results it appears that the worst methane buildup can be expected during a pass where there is no open side to the CM. Adding to this problem would be opposing ventilation conditions, reducing the fresh air supply to the heading. This situation can realised when the first pass is taken on the left with a force column on the right and an exhaust column on the left supplying ventilation.

6. Most methane emissions occur during the cutting process. The results indicate that methane emissions from the roof, floor and side walls are negligible when related to the methane emitted during the cutting process, normal section ventilation prevailing.

8. For a more detailed and accurate evaluation of the effects of boom movement on methane buildup, the influence of ventilation conditions on methane buildup etc. a more detailed observation database must be established.

APPENDIX C8

SIMULATIONS OF METHANE FLOW AROUND A CONTINUOUS MINER

Part 4 : Comparison of methane behaviour under various ventilation conditions in a partly developed heading.

C.F. Meyer / F.J. van Zyl

INTERIM REPORT
SIMRAC PROJECT : COL030
DECEMBER 1995

CONTENTS **PAGE**

LIST OF FIGURES PAGE

1) INTRODUCTION

As a continuation of the project on methane behaviour and monitoring, a number of scenarios were tested to determine the effect of different ventilation systems on methane flow and behaviour.

It has already been established that dust and methane do not behave in the same manner for the same situation. In the dust programme, various simulations have been conducted using different test configurations. Some of these situations have been chosen at random for the methane project and the dust concentrations replaced with methane emissions.

This report will in short describe the results of the simulations done on five different situations for phase 4 (final phase for the dust programme), one situation from phase 1 (30 m heading development) and one situation from phase 2 (20 m split development). The detail in the full heading and full split development has been altered in the sense that the shuttle car (SC) has been removed from the heading and the boom position is down at all times.

2) RELATED METHANE LEVELS

In part 1 of these tests it was found that the modelled methane values are roughly three times the value of actual levels recorded. This calculation was applied to all the simulation contours and the corrected methane percentages supplied in parathesis throughout the report.

3) RESULTS: PHASE 1 AND 2

3.1) **Phase 1: Full Heading Development (30 m)**

This scenario shows a full heading developed 30 m from the last through road (LTR). The continuous miner (CM) is cutting in the right hand corner of the face and the SC has been removed. The ventilation system in use consists of an 11 kW jet fan standing on the floor of the heading. The on-board scrubber on the machine is in operation and is delivering ±10 m^3/s. The usual sprayfan system that has been simulated, has been replaced with normal watersprays, not simulating any directional air movement caused by these watersprays as would be the case with the sprayfan system. The fact that these watersprays do not move the air across the face, is visible on the simulation results.

At floor level, CH_4 is shown to be trapped underneath the boom and concentrations as high as 14% (5%) are shown. On the left of the CM in the open space, the concentrations are diluted from 9% (3%) at the face to 3% (1%) at the back of the CM. From this point, the fresh air and the existing air turbulence, is diluting the CH_4 to levels between 1% (0,3%) - 2% (0,7%) and this situation prevails into the LTR.

At operator level, the influence of the scrubber is visible in that the air flowing towards the scrubber inlet, is diluting the gas levels to concentrations between 3% (1%) - 10% (3,3%). The simulations show very high concentrations immediately in front of the cutting drum against the face. This can prove to be a very dangerous situation and this also demonstrates that no fresh air is reaching the face position in front of the cutting drum. Again the simulations show CH_4 concentrations of between 1% (0,3%) - 2% (0,7%) flowing into the LTR.

The simulation runs against the roof show high concentrations of CH_4 in excess of 14% (>5%) rolling backwards against the roof above the CM position. It seems that the supply of fresh air towards the face position is limited to that flowing towards the scrubber intake which is then mainly concentrated at the operator level. All these results again show the importance of a sprayfan system being installed on the machine to enable fresh air flowing towards the face position. This is particularly true for heading distances of 20 m and more. Figures 1 and 2 show the airflow vectors at the right side of the CM, through the scrubber and on the left of the CM with the resulting methane concentrations at these positions respectively. The sketch at the bottom of the page is the slice on the right of the CM. The sketch in the middle is the slice through the scrubber position and the top sketch is on the left of the CM.

The results also show that the jet fan used in the simulations does not deliver air to the face position in the 30 m heading as was previously thought. As the CFD model was developed, the characteristics of the air delivered by the jet fan was defined more accurately resulting in a more accurate simulation, and thus the difference in performance. Figure 3 gives a three-dimensional horizontal view of the methane concentrations.

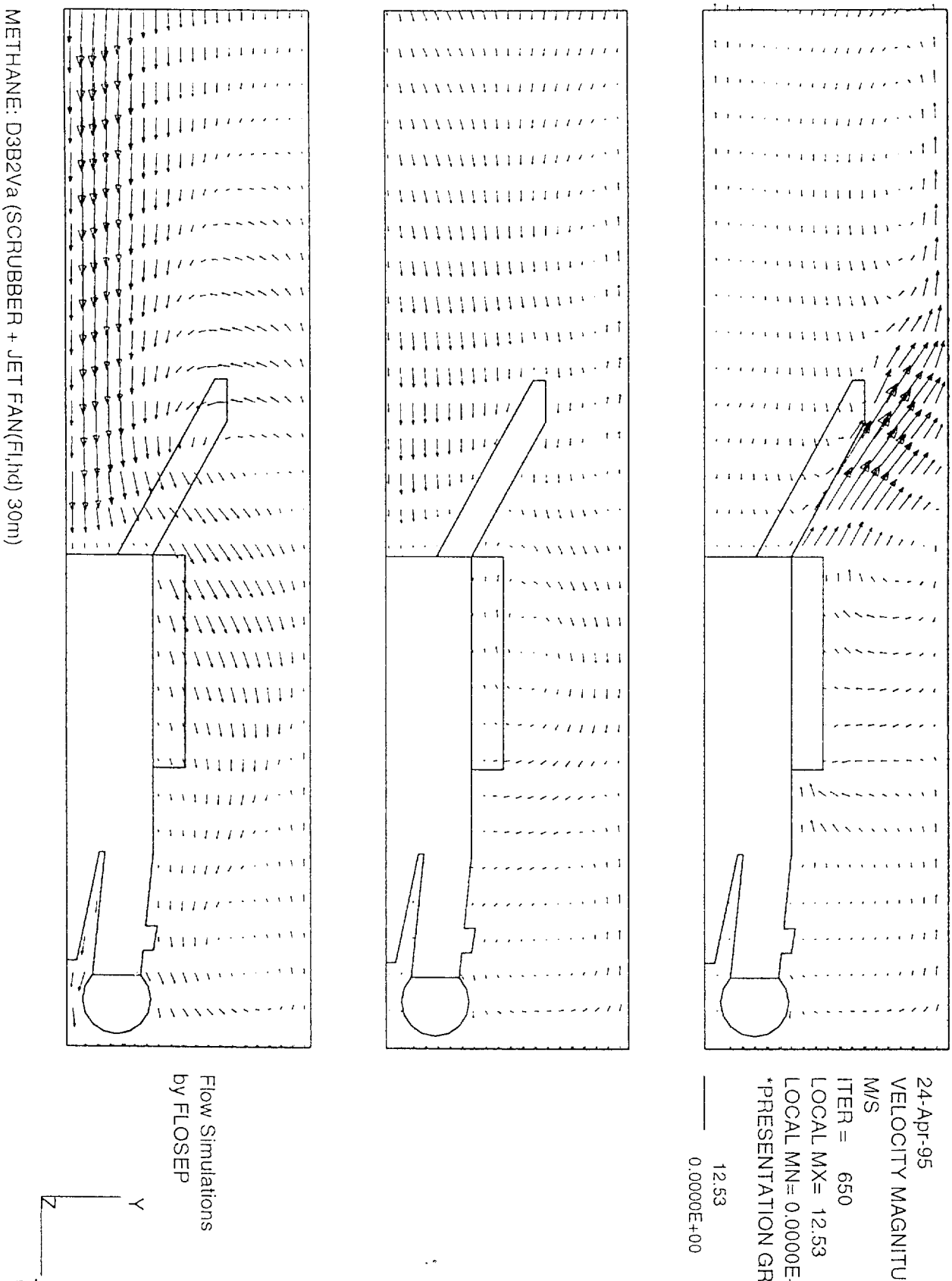

Figure 1: Sketch showing the airflow vectors at three vertical positions through the heading for the 30 m heading development

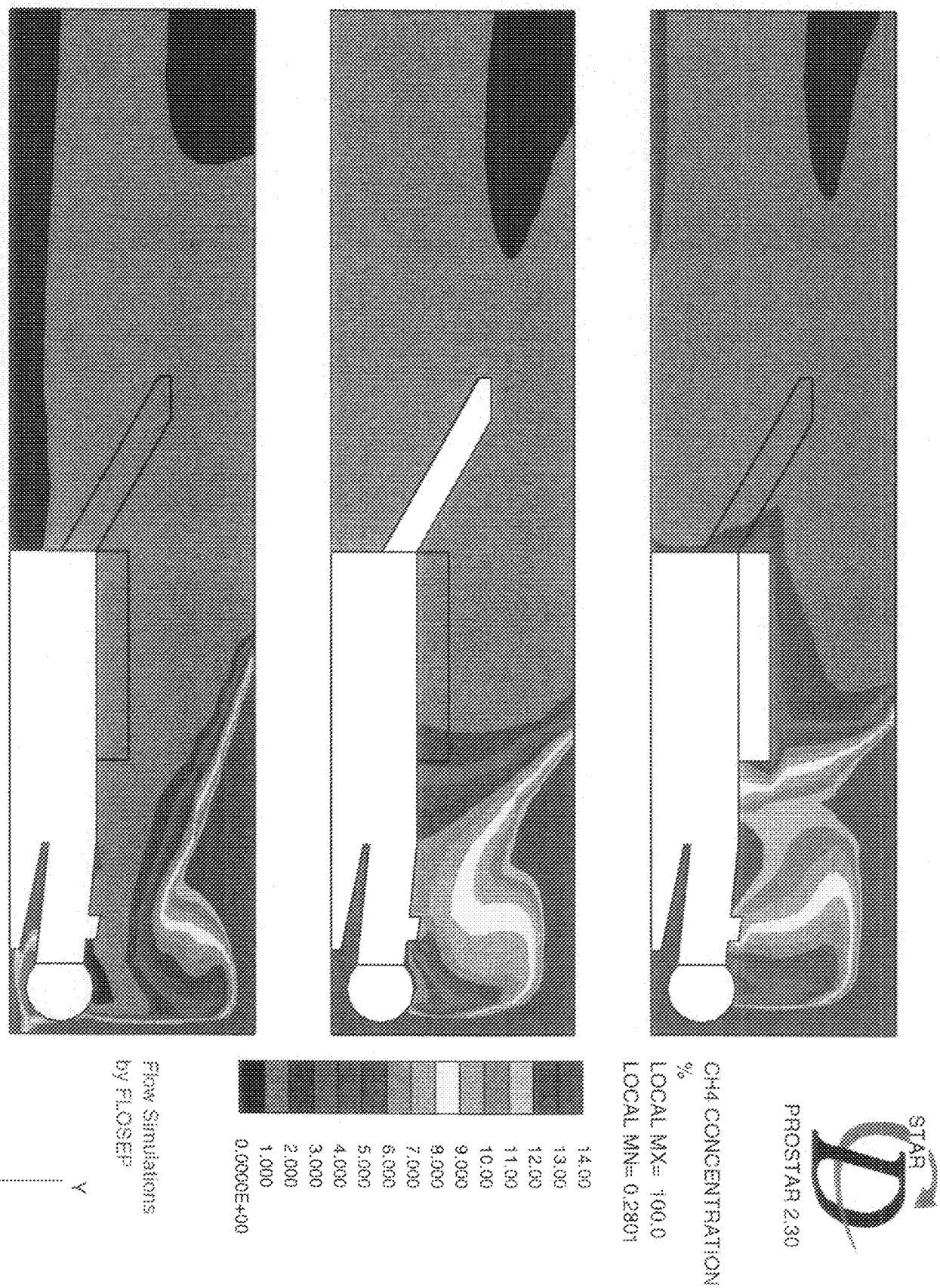

Figure 2 : Sketch showing the methane concentration contours at three vertical positions through the heading for the 30 m heading development.

Figure 3 : Sketch showing the three-dimensional view of the methane concentration contours for the 30m heading development.

3.2) **Phase 2: Full Split Development 20 m To The Right Of The Heading**

This scenario shows a full split developed to the right of the heading. The CM is cutting in the right hand corner of the split. The CM cutting drum, as in the previous scenario, is only equipped with normal watersprays instead of the sprayfan system. An 11 kW jet flow fan is placed on the floor at the entrance of the heading. the air flowing from the outlet of the on-board scrubber is angled at 30° to the left and 30° upwards. This is visible by looking at the airflow vectors at the exhaust of the scrubber.

At gathering arm level the airflow vectors show that the air from the jet fan is mainly ventilating the heading and forming an air curtain at the entrance to the split. Inside the split the airflow patterns are dictated by the scrubber and the air flowing towards the scrubber inlet controls the methane concentrations. As before, the absence of the sprayfan system is evident, in that high concentrations of methane are visible underneath the boom. To the left of the CM towards the scrubber inlet, the methane concentrations are diluted from 9% (3%) down to 5% (2%). From this position backwards the CH_4 concentrations are constant being between 4% (1,3%) - 1% (0,3%) from inside the split to the LTR. The results show no flow of CH_4 into the LTR at this level.

At operator level, the condition differs somewhat in that more fresh air flows towards the face position and the scrubber inlet. More turbulence is also visible at this level as a result of the air that is exiting from the scrubber and recirculating back to the intake of the scrubber. High methane concentrations are still visible in front of the cutting head against the face. The simulations show lower concentrations over the CM and to the left of the CM, being between 5% (2%) and 10% (3,3%). This is mainly caused by the turbulence and the fresh air supply at this level. From the CM backwards, the CH_4 are again constant between 4% (1,3%) - 1% (0,3%) with more methane shown to be flowing into the LTR. Figures 4 and 5 show the airflow vectors in three different vertical positions, on the right of the machine, in the middle and on the left of the CM with the resulting methane concentration contours in these positions.

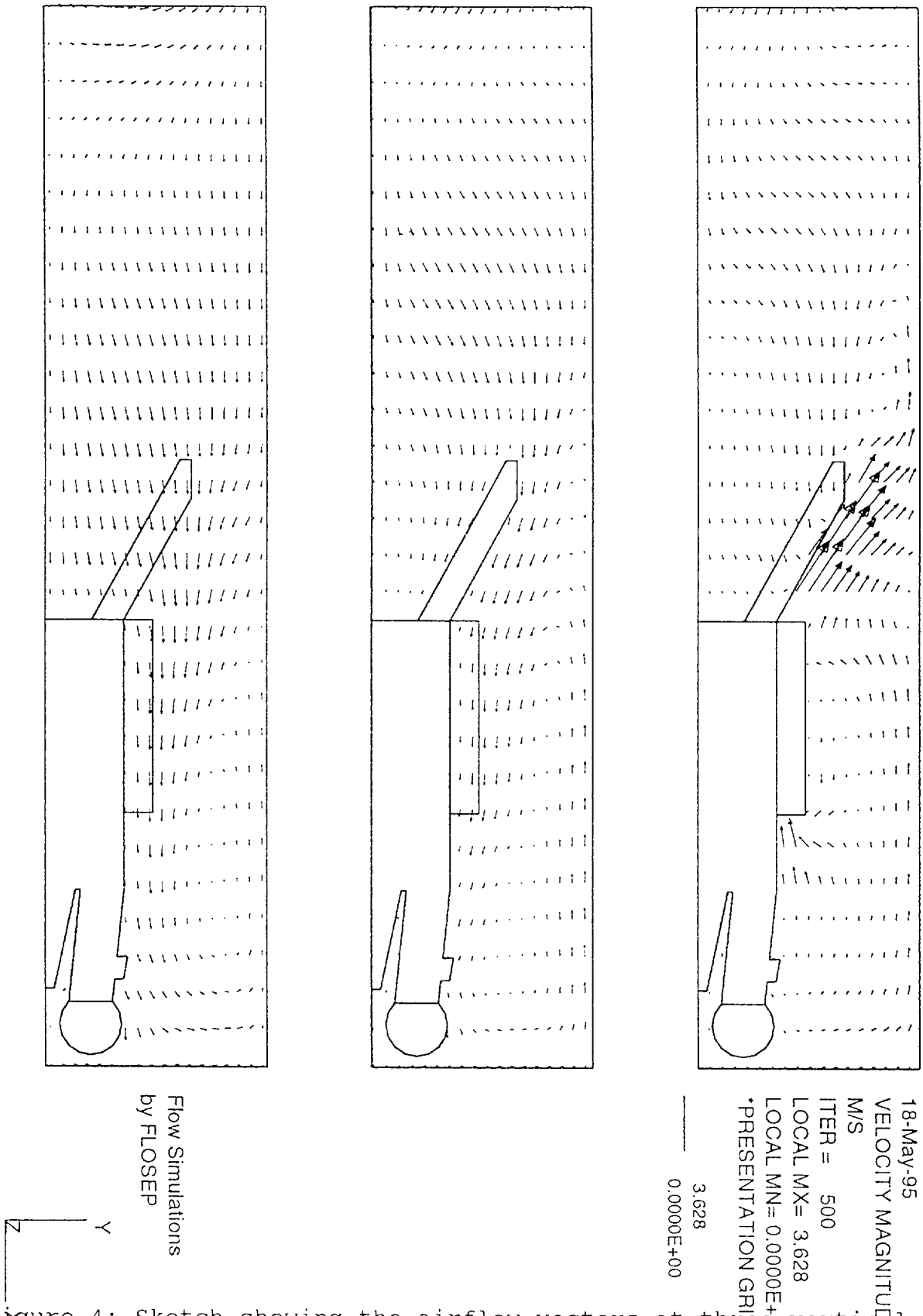

Figure 4: Sketch showing the airflow vectors at three vertical positions through the heading for the 20 m split development

Figure 5 : Sketch showing the methane concentration contours at three vertical positions through the heading for the 20 m split development.

At roof level, more air is shown to be flowing out of the split and heading by the airflow vectors as well as the CH_4 contours. High concentrations of more than 14% (5%) are shown to be rolling back against the roof above the CM. Dilution is really shown to be happening from the CM back towards the LTR. Air from the scrubber is shown to contain between 4% (1,3%) - 5% (2%) methane which is then diluted down to between 1% (0,3%) - 2% (0,7%) inside the LTR. Figure 6 show a three-dimensional horizontal view of the methane concentrations.

4) DISCUSSION PHASE 1 AND 2

In both the split and the heading, high levels are recorded at the roof. These highs are caused by recirculating air which tend to trap some of the methane released from the face in this region. In the heading the jet fan assist in the dilution of the CH_4 released effectively "pushing" back the point where recirculation starts. This is obtained by the stronger airflows into the heading by the jet fan which is not the case in the split, hence the greater area of high CH_4 levels against the roof.

It has been seen from previous simulations that when released methane is "trapped" by the ventilation (no air for dilution), the transition gradient from high to levels of CH_4 is very steep. This is again evident as no definite recirculation can be identified around the CM at operator and gathering arm level. Gentle gradients of CH_4 transition can be observed.

5) RESULTS PHASE 4 SIMULATIONS: 20 m PARTIAL HEADING DEVELOPMENT

In these simulations, five ventilation systems were compared to determine their ability to control methane. During all these simulations the directional sprayfan system was in use. The situation shows a partial heading developed to the right of the heading with the face being 20 m from the LTR. A CM and SC is present at the face with the cutting drum cutting against the floor at 52 rpm.

Figure 6 : Sketch showing the three-dimensional view of the methane contours for the 20 m split development.

The five ventilation systems compared includes the following:

- Jet fan (floor position) and on-board scrubber
- Jet fan (roof position) and on-board scrubber
- Force column against the roof, 10 m from the face and on-board scrubber
- On-board scrubber system only
- Trailing exhaust connected to the outlet of the scrubber

5.1) **Air In At Roof Level**

The following two scenarios show a jet fan and a force duct suspended from the roof. Both systems are delivering air quantities of 5,0 m^3/s into the heading. The difference is that the force duct is 10 m from the face of the heading and the jet fan is placed in the LTR 20 m from the face.

The jet fan, being against the roof, is blowing air over the SC towards the face. The airflow vectors show that the air from the fan is pushed downwards by air movement from the face by mainly the air leaving the scrubber outlet. This occurs between the SC and the CM. Fresh air supply is indicated to be limited in the region of the CM. The methane contours show that the methane is pushed towards the roof, and the dilution capabilities of the air appears to be insufficient in the face area. The jet fan and the scrubber is opposing each other, creating two ventilation systems to operate inside the heading. This cause the typical high transfer gradient from high to lower levels of methane indicating possible entrapment of released CH_4.

Dilution of the methane is fairly high upto the scrubber inlet, from where the contours show that methane concentrations of more than 14% (5%)are present towards the face. The sprayfan system causes substantial air movement in showing that areas for possible layering are limited. Fresh air supply to this area needs to be improved to support CH_4 dilution. A possible reason for the insufficient supply of fresh air to the face can be the limited open area around the CM restricting air from the jet fan to enter the partial heading. See Figures 7 and 8 for horizontal slices through the heading at floor level, middle level and roof level showing the airflow vectors and the methane concentrations for the jet fan.
Figure 9 show the three-dimensional horizontal view of the methane concentrations for the jet fan.

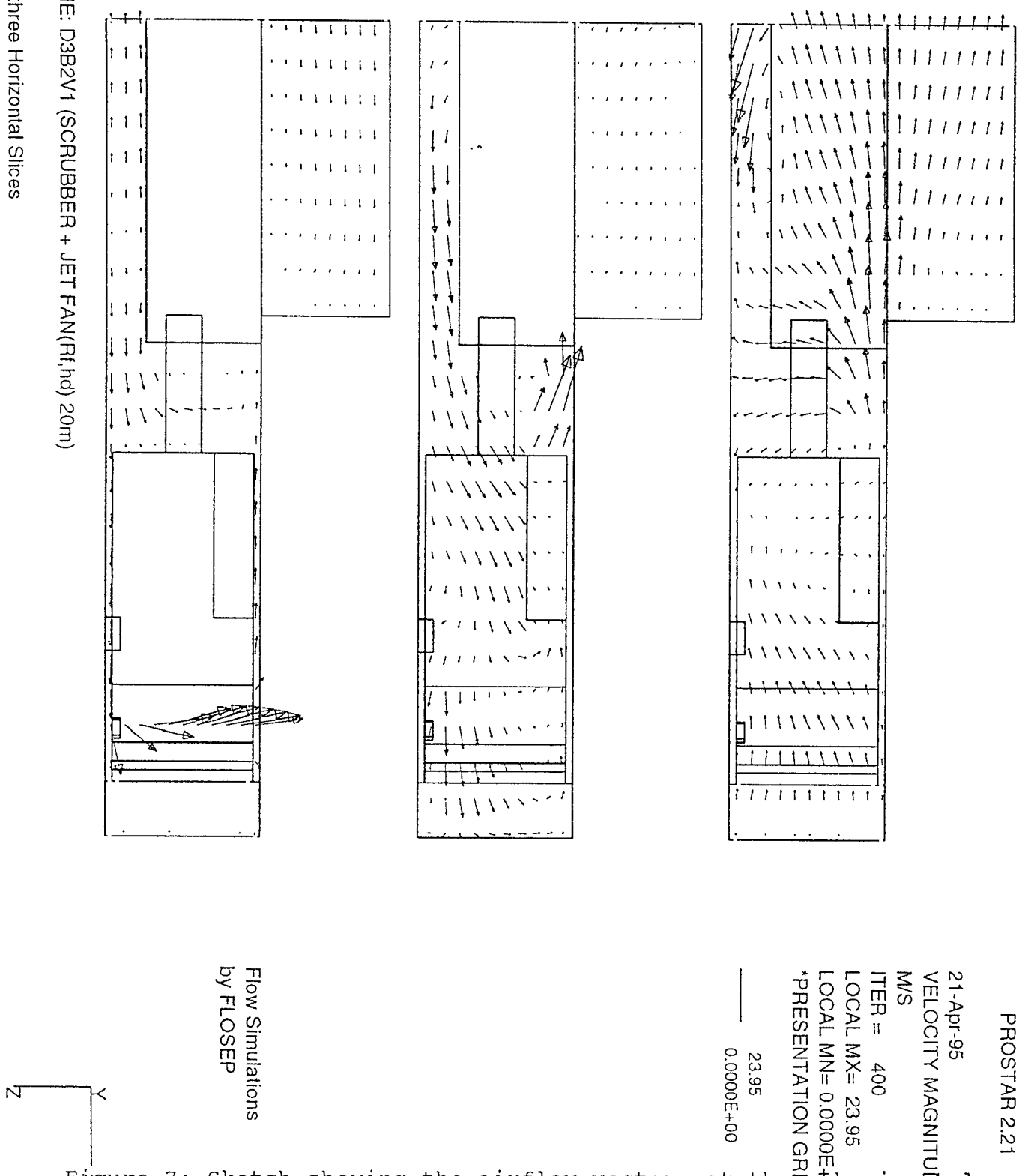

Figure 7: Sketch showing the airflow vectors at three horizontal positions through the heading with the jet fan against the roof

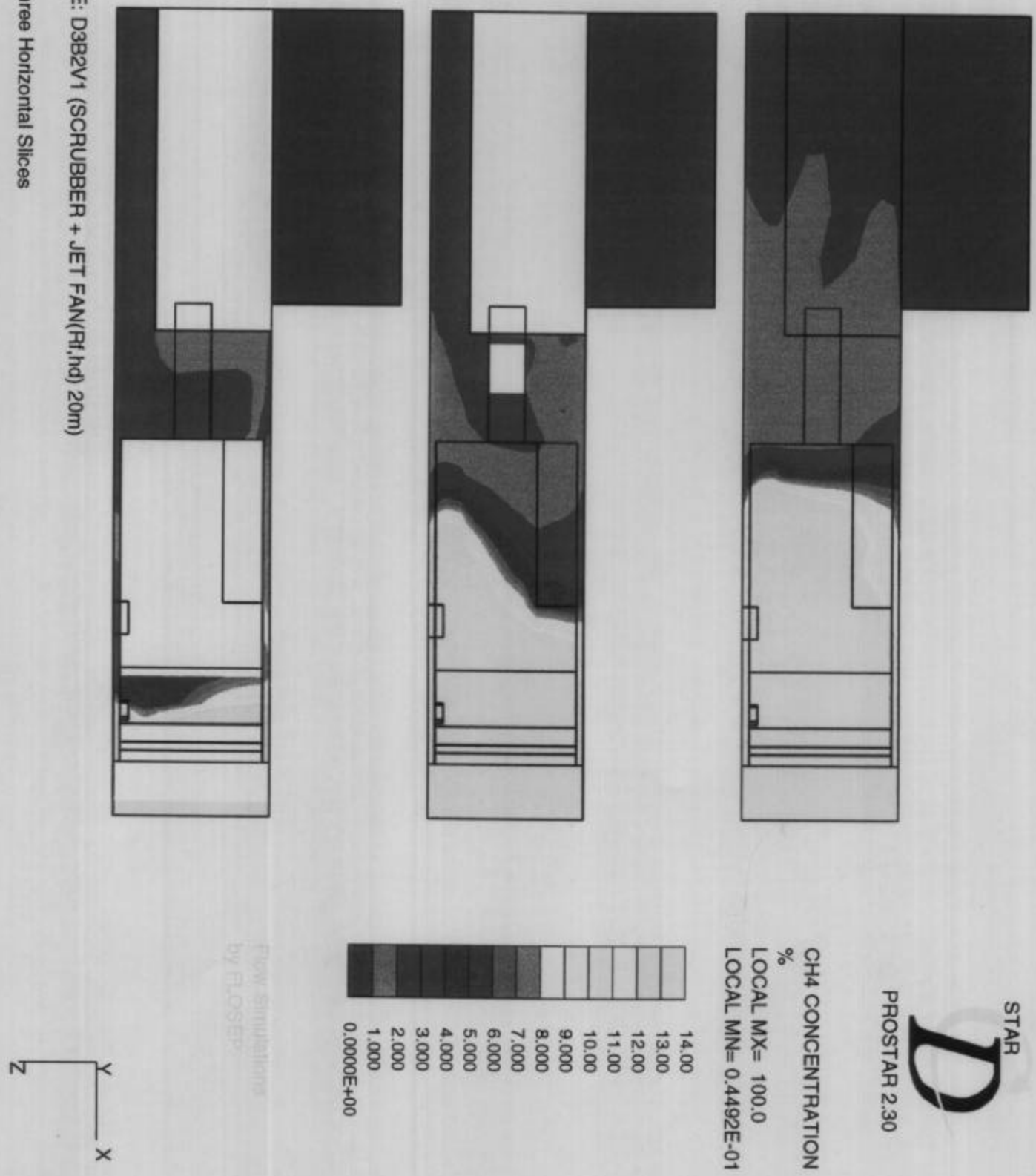

Figure 8 : Sketch showing the methane concentration contours at three horizontal positions through the heading with the jet fan against the roof.

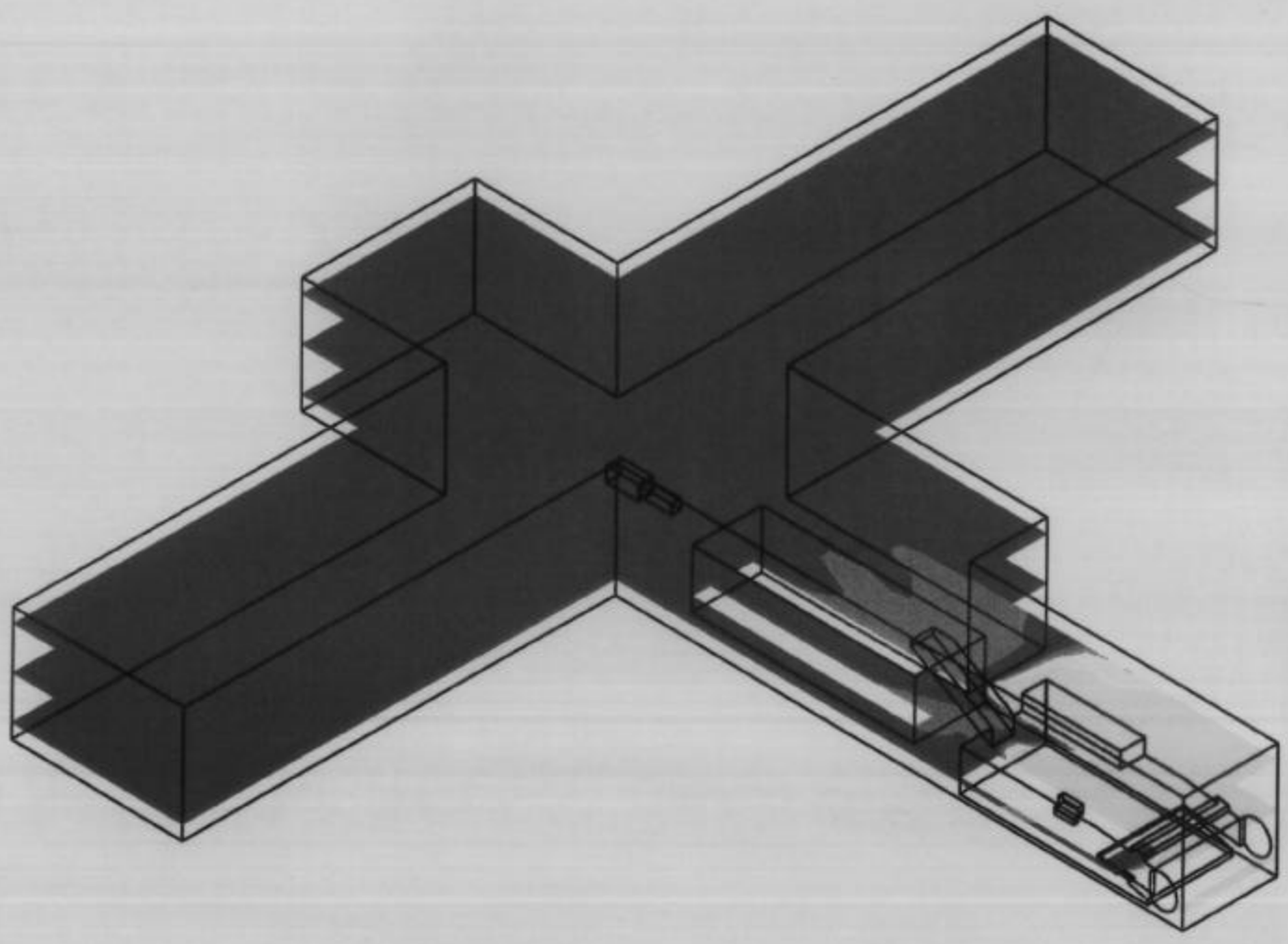

Figure 9 : Sketch showing the three-dimensional view of the methane contours with the jet fan against the roof.

The methane contours show different behaviour with the force duct in use. The outlet of the force duct is closer to the face and the air is delivered onto the face. The airflow vectors show, however, that the air from the scrubber outlet is again influencing the air from the duct. The air recirculation patterns above the CM is again preventing the fresh air from flowing into the face area, resulting in the high methane levels above the CM. Levels of more than 14% (5%) is shown in this area, but methane is also pushed out of this area by the high air input velocities. The transition gradients from high to lower CH_4 levels is not as pronounced as with the jet fan indicating that more air is leaving the heading, carrying CH_4 with it. Levels of between 14% (5%) and 3% (1%) are shown to fill the heading. It seems that the additional fresh air (5 m^3/s) that is supplied by the force duct, is not sufficient to dilute the high methane concentrations to acceptable levels. Again it is shown that the different systems inside the heading are working against each other which result in different zones which does not favour the removal and dilution of the methane. See Figures 10 and 11 for three horizontal slices through the heading with the resulting methane concentration contours for the force duct.
Figure 12 for a three-dimensional horizontal view of the methane contours for the force duct.

5.2) Air In At Floor Level

The next scenario shows the air jet fan on the floor. Air is showing to be flowing into the face area on floor level CM. Much of the fresh air from the fan is restricted by the actual position of the CM and the SC. The small amount that manages to pass the CM, assists the sprayfan system to push the methane up and back towards the scrubber intake. Immediate dilution of the methane is shown at the back of the CM which indicates sufficient fresh air supply, but seems to be less than with the jet fan against the roof. This might be caused by the seemingly high amounts of air from the scrubber that is recirculated back into the heading. This means less fresh air, lower levels of dilution and a lower gradient in the transfer from high to low levels of CH_4. The methane contours show that high methane concentrations are still present above the CM. The dilution rates of the methane is not acceptable in these regions and care should be taken to force more fresh air into these regions. The jet fan and the scrubber are again opposing each other, because of their relevant position as a result of this particular mining sequence. See Figures 13 and 14 for three horizontal slices through the heading showing the airflow vectors and the resulting methane concentration contours for the jet fan.
Figure 15 show the three-dimensional horizontal view of the methane contours for the jet fan.

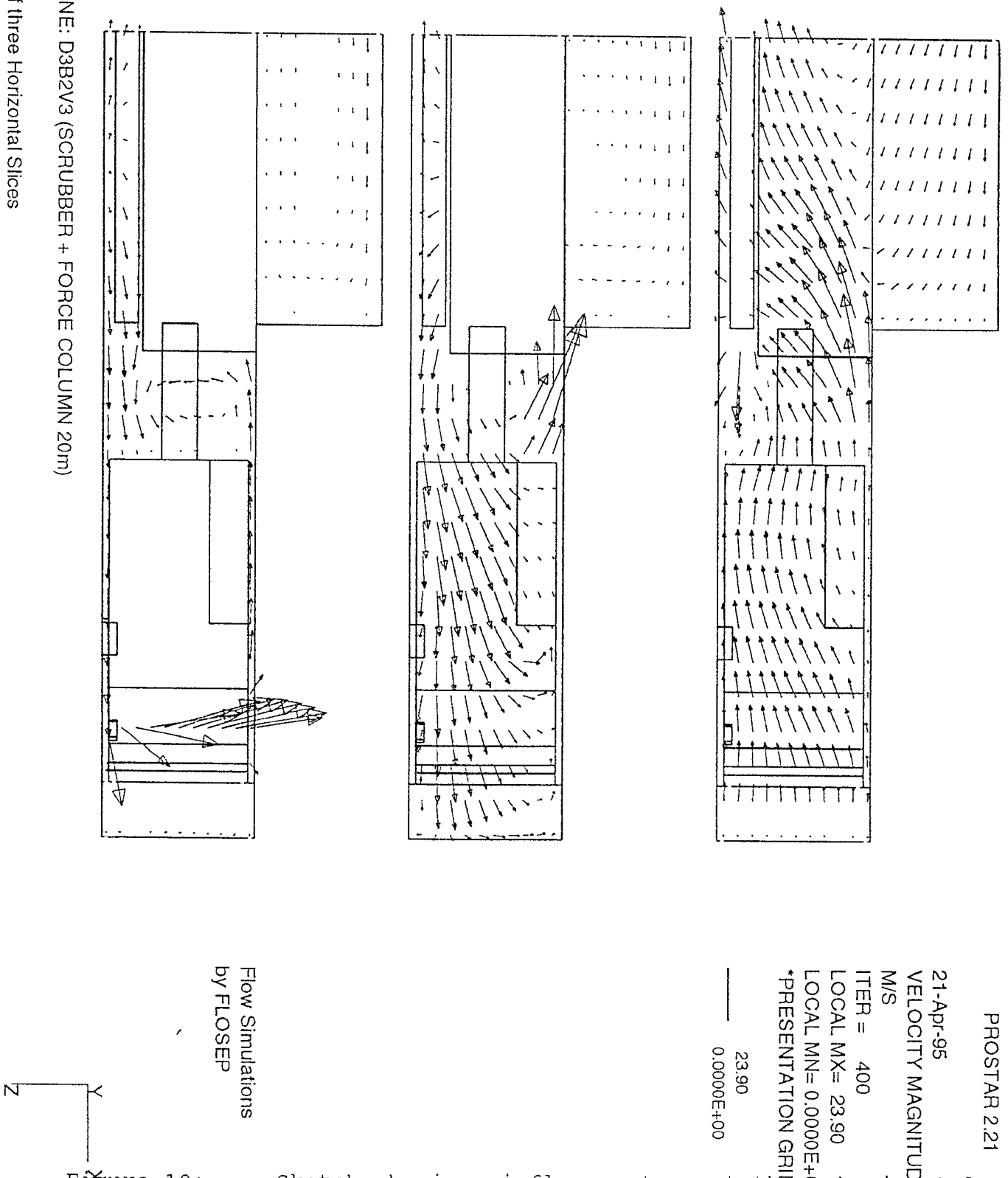

Figure 10: Sketch showing airflow vectors at three horizontal positions through the heading with the force duct

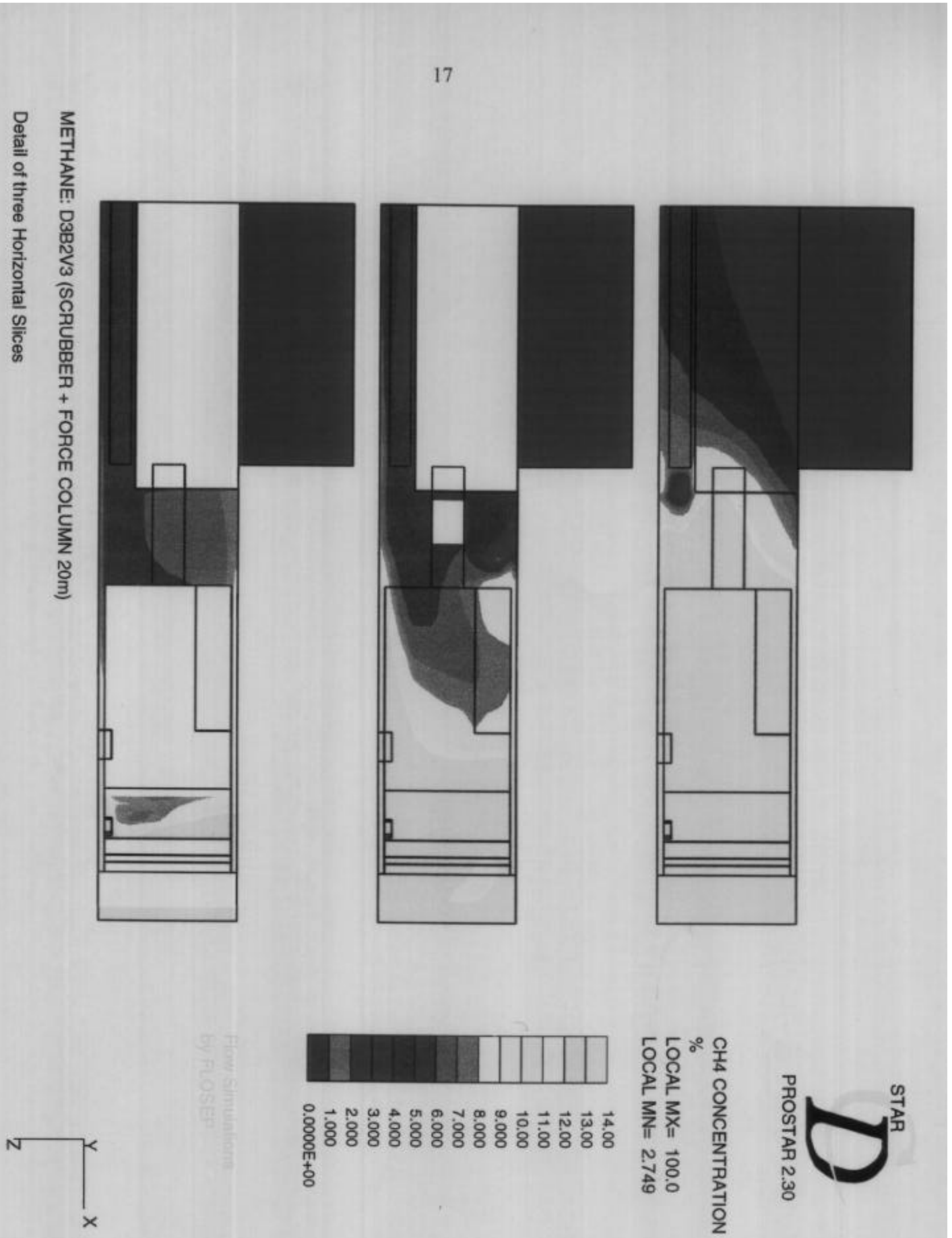

Figure 11 : Sketch showing the methane concentration contours at three horizontal positions through the heading with force duct.

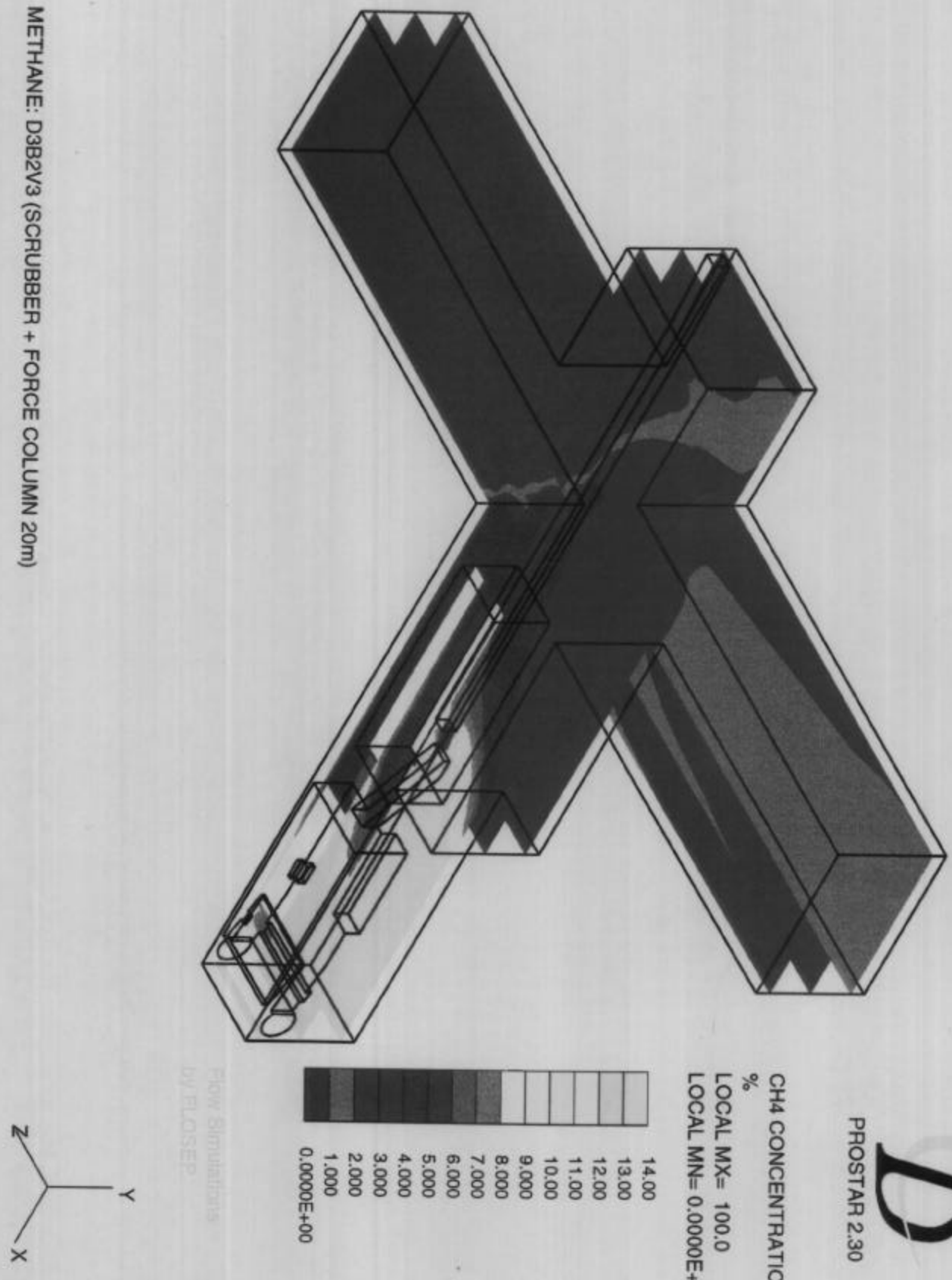

Figure 12 : Sketch showing the three-dimensional view of the methane contours with the force duct.

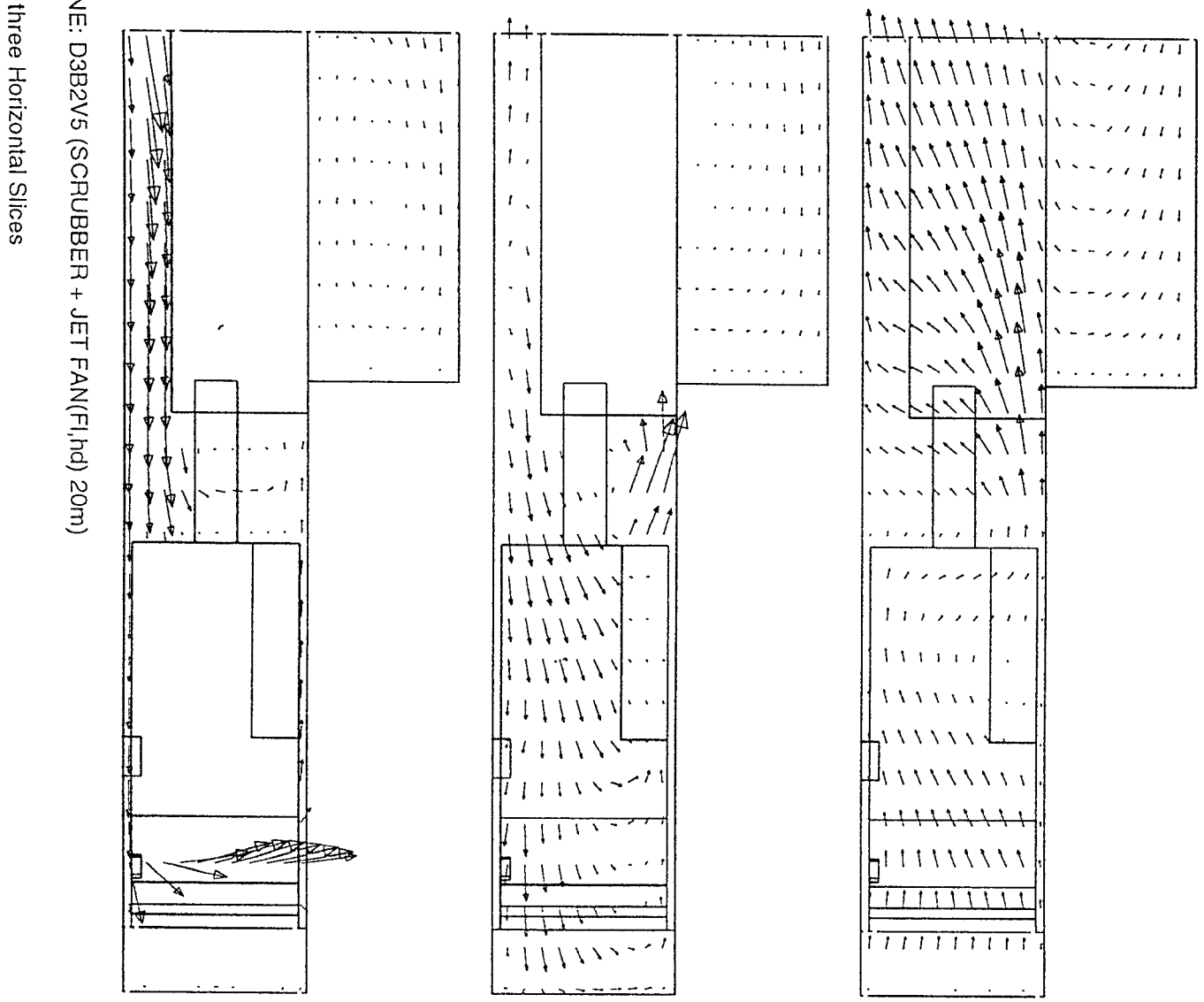

Figure 13: Sketch showing the airflow vectors at three horizontal positions through the heading with the jet fan at the floor

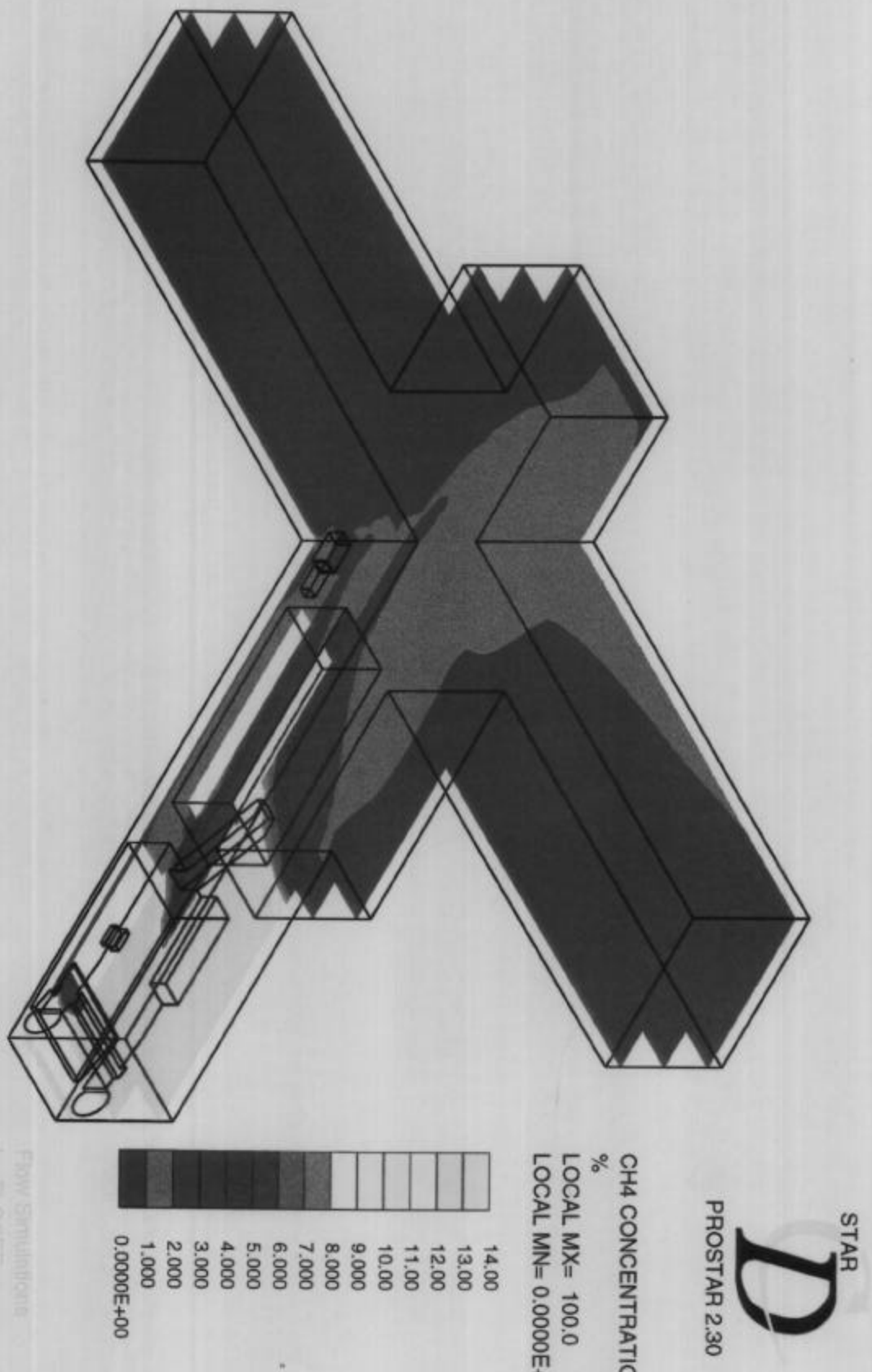

Figure 15 : Sketch showing the three-dimensional view of the methane contours with the jet fan at the floor.

5.3) No Force Auxiliary Ventilation

The next two scenarios show the on-board scrubber only and also the trailing exhaust that is connected to the outlet of the scrubber and extends to the LTR. Of all the systems discussed thus far, these two systems show the best results with regard to the methane levels and methane behaviour. See Figures 16, 17 and 18 for the vertical slices showing the airflow vectors, methane contours as well a three-dimensional view of the methane contours for the scrubber only system.

Air is shown to flow into the heading towards the scrubber intake with high dilution of the methane upto this point. The methane is again confined in the front area of the face with high air movement caused by the sprayfan system as well as the rotation of the cutting head. The airflow vectors show that some of the fresh air flowing towards the scrubber intake reaches the face, assisting the sprayfan system to keep the face ventilated. The fresh air supply in these areas are again not sufficient to completely dilute the methane down to acceptable levels. As in the previous situations, the contours again show the methane levels in these areas to be in excess of 14% (5%). It is interesting to note the effect of the exhaust of the scrubber has on the general airflow. Without the trailing exhaust recirculation occurs, coinciding with slightly higher CH_4 levels at the rear of the CM. This indicate that recirculating air can cause increased levels of methane when they do occur. See Figures 19, 20 and 21 for the three vertical slices through the heading showing the airflow vectors, methane contours as well a three-dimensional view of the methane concentration contours.

6) REMARKS AND RECOMMENDATIONS

All these simulations were done to compare the different ventilation systems with regard to methane behaviour and not as much the actual methane concentrations. In order to be able to do that, additional investigations will have to be conducted into the behaviour of methane and the research approach will have to be moved from generic to detail and in-depth studies.

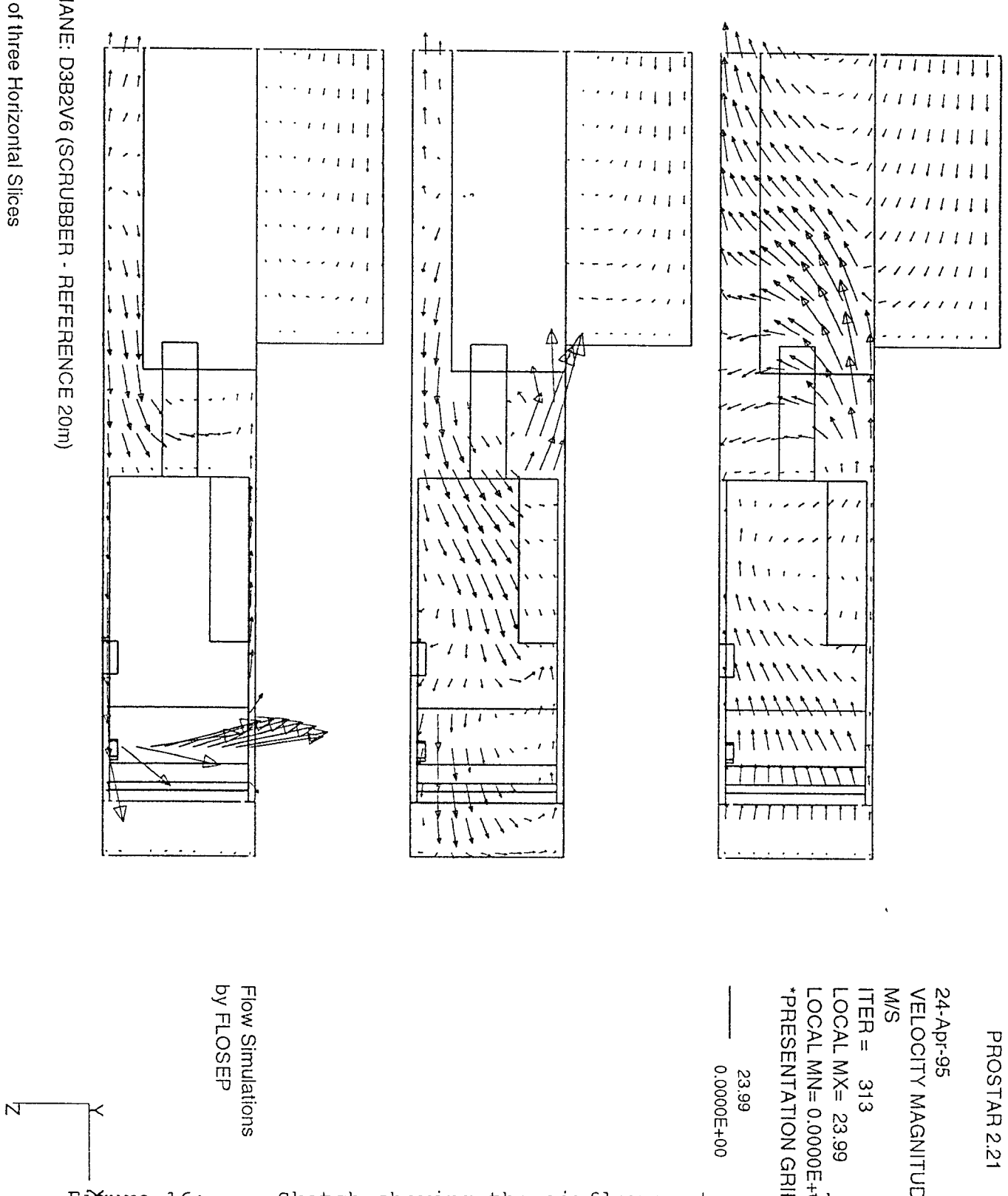

Figure 16: Sketch showing the airflow vectors at three horizontal positions through the heading for the scrubber system

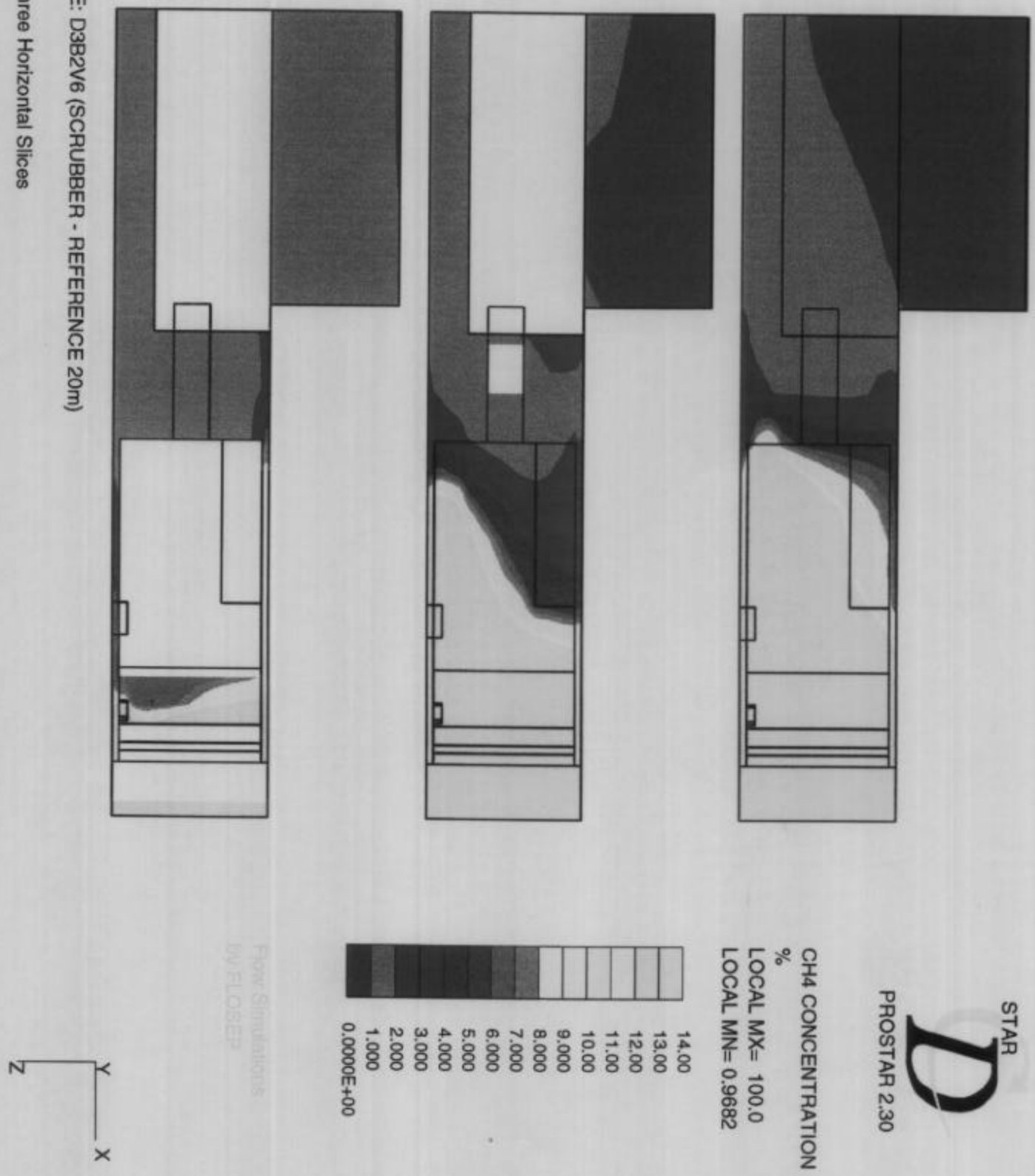

Figure 17 : Sketch showing the methane concentration contours at three horizontal positions through the heading for the scrubber system.

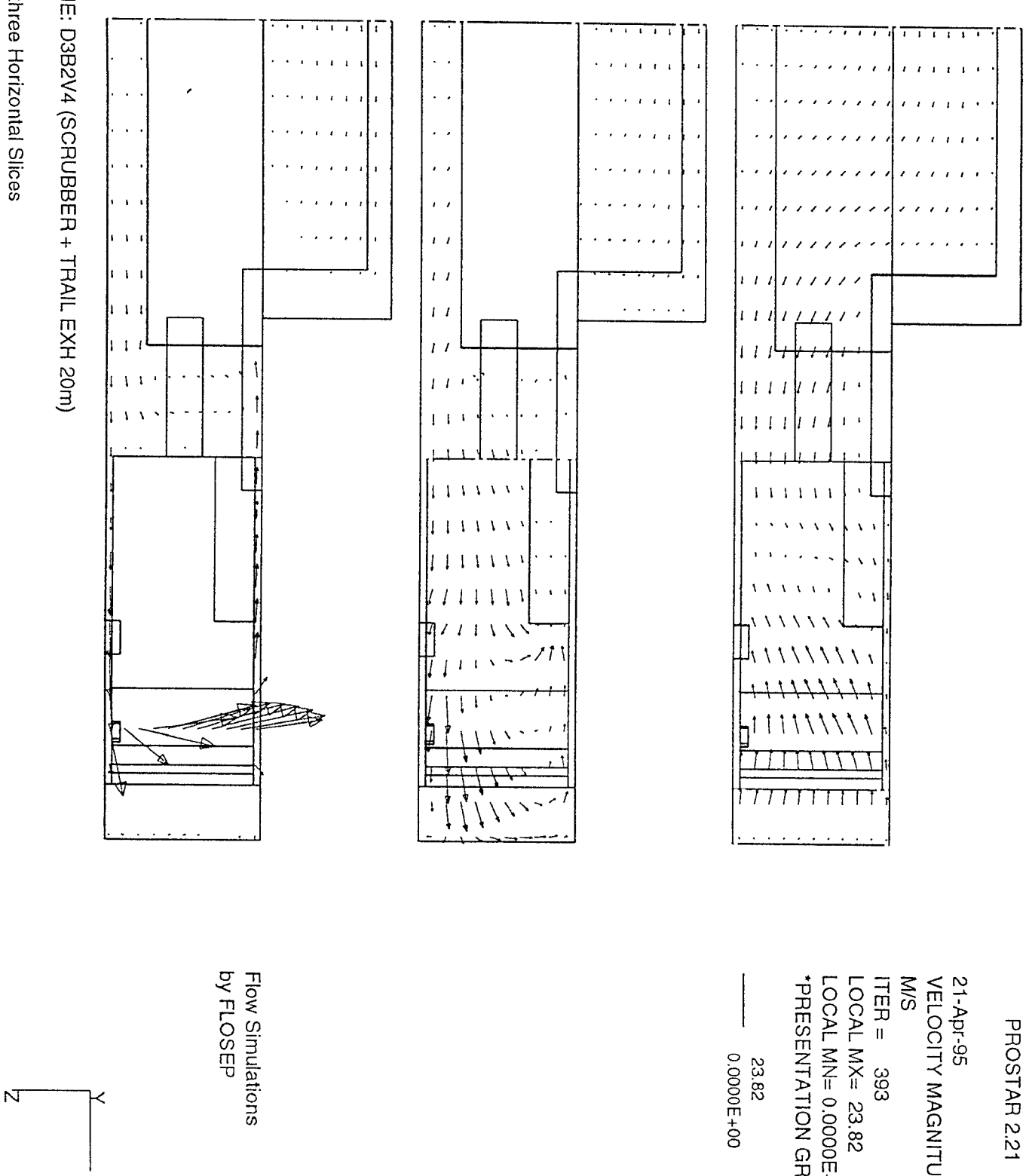

Figure 19: Sketch showing the airflow vectors at three horizontal positions through the heading for the trailing exhaust

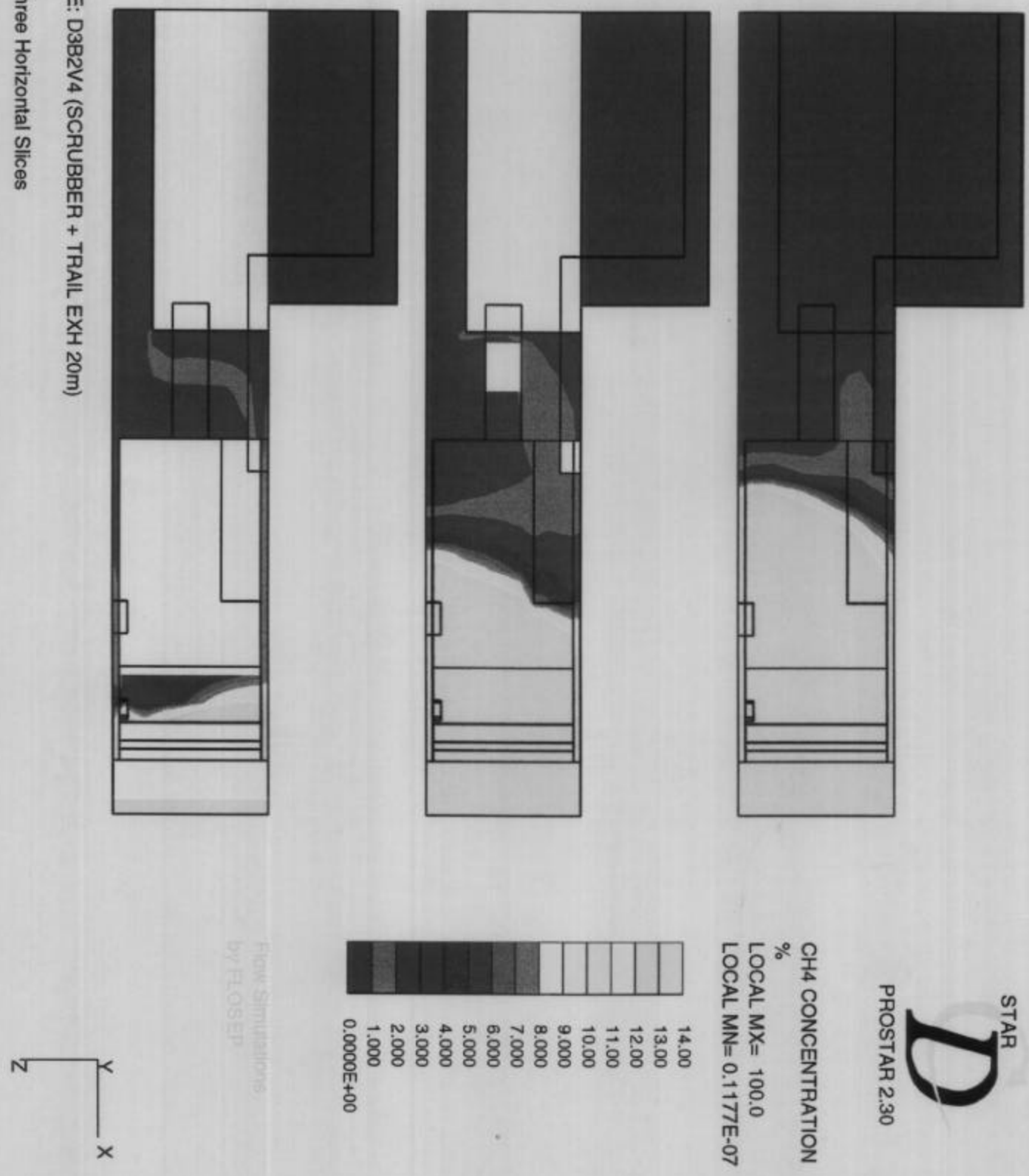

Figure 20 : Sketch showing the methane concentration contours at three horizontal positions through the heading for the trailing exhaust.

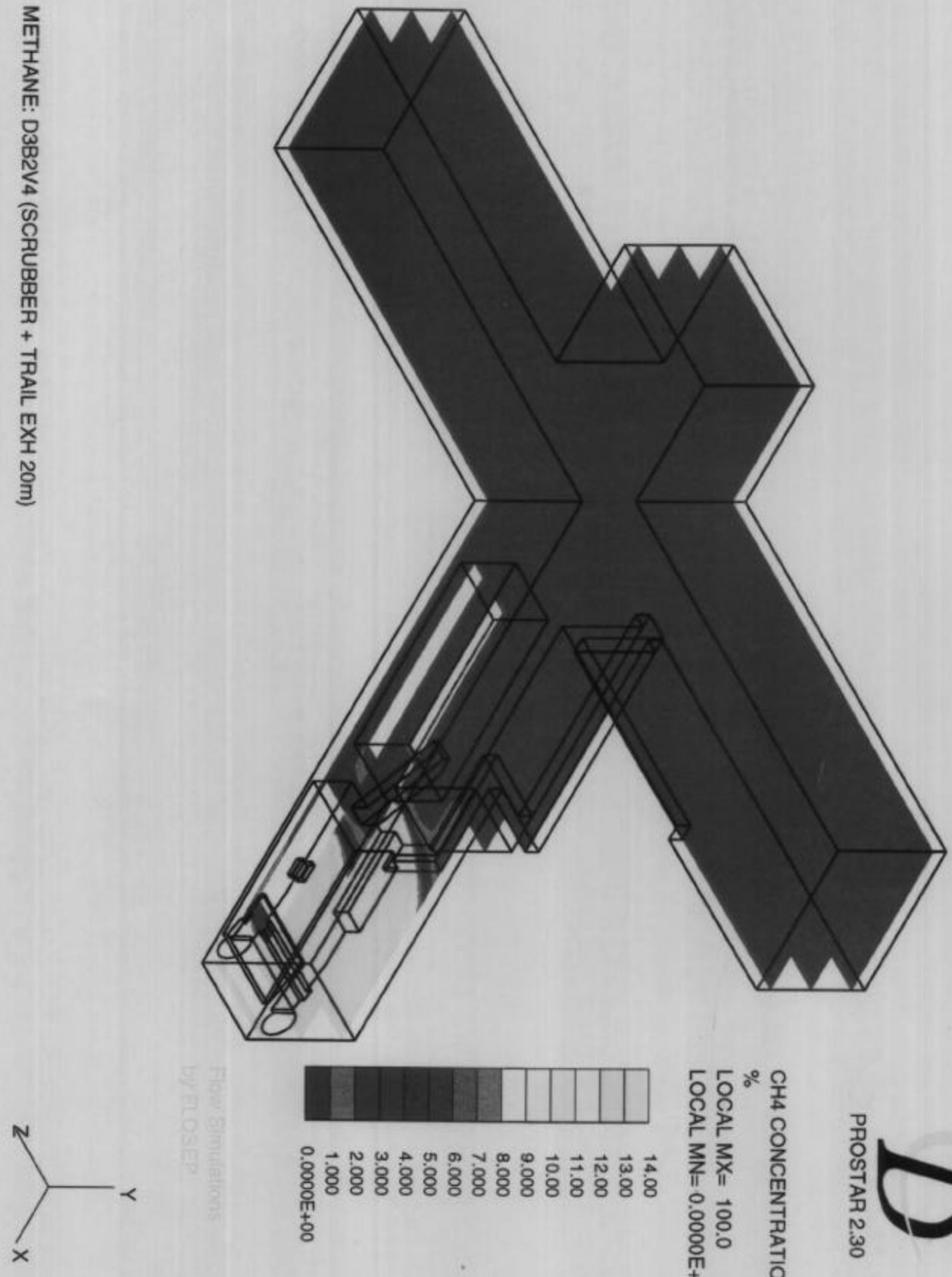

Figure 21 : Sketch showing the three dimensional view of the methane contours for the trailing exhaust.

These simulations have shown that when a CM is cutting the first web, during the development cycle, it is very difficult to ventilate the face area and to get sufficient fresh air into these areas. The on-board scrubber has shown to be the best solution for these particular scenario with regard to keeping the methane under control. It is, however, suggested that the intake of the scrubber be moved forward and perhaps enlarged in order for the fresh air zone to be moved closer to the face. The sprayfan system is causing sufficient air movement on the face and above the machine to prevent any layering or possible accumulations of the methane in this area, but still needs the fresh air to be able to dilute the methane.

All the simulations that have been conducted up to date, have been used to identify problem areas. It is time to start concentrating on finding solutions for these problem areas and to provide guidelines on how to cope with high methane concentrations in these small areas.

The results indicate the CH_4 behaviour can be closely related to the prevailing ventilation conditions. As ventilation flow patterns can be easily diverted and changed, it is necessary to investigate this aspect to minimise areas of recirculation. CFD simulations will allow for all aspects to be investigated in a cost effective and time saving manner to determine optimum ventilation conditions for each unique underground environment.

past 100 years.

Other contributing factors that were not considered for this preliminary study were factors such as the coalfield being mined, the mining method used, the production rate, the source of the ignition, the location of the incident (face, non-face or abandoned areas) and the number of fatalities and injuries caused by the explosion. These factors were considered not to be of importance for this study because the aim of this study was to determine if there is a direct link between barometric pressure fluctuations and gas related incidents.

2. BAROMETRIC PRESSURE FLUCTUATIONS

Before a study of this nature can be undertaken a basic understanding of barometric pressure variations must be reached. The diurnal barometric pressure fluctuates continually with a daily cyclic nature and reaches daily maxima and minima. When the average for the daily barometric pressure variations is taken a definite trend exists. This daily average barometric pressure trend can be sustained for several days and even weeks. From this we can see that there is a variation not only on a hourly basis for the barometric pressure (diurnal variations), but also on a day to day basis for the average daily barometric pressure.

Diurnal variations in barometric pressure are the result of the differential cooling and heating of the surface of the earth. For a simplified understanding of these processes, it is accepted that an increase in the temperature of the surface of the earth during the day causes the air above it to heat up, expand, become less dense and rise, causing the barometric pressure to drop. Conversely, if the temperature of the surface of the earth cools down during the night as heat is radiated from surface, the air above it cools down, contract, become more dense and an increase in barometric pressure is observed.

To explain the average daily barometric pressure trends, which can be either upward, downward or neutral, over any number of days, the meteorological position of South Africa must be considered. South Africa is situated in a high pressure belt skirted to the south by the circumpolar westerly airstream. The weather in South Africa is almost entirely under the influence of this

westerly circulation and weather changes are largely dominated by disturbances in the southern hemisphere. On the earth's surface this appears as a succession of cyclones and anti-cyclones. A cyclone is a low pressure system and an anti-cyclone is a high pressure system[2]. Thus when a cyclonic system is in influence a downward trend in barometric pressure is observed and when an anti-cyclonic system moves across the country, and is in influence an upward trend in barometric pressure is observed.

On a global scale diurnal pressure fluctuations tend to increase nearing the equator. The height above sea level also tend to increase diurnal pressure fluctuations. These two factors would suggest that South African Collieries are subjected to bigger diurnal pressure fluctuations than coal producing countries which are situated further away from the equator[3].

3. METHOD OF INTERPRETATION OF BAROMETRIC PRESSURE VARIATIONS

In order to have norms against which to measure and analyse barometric pressure variations prior to an incident, it is necessary to have a quantitative appreciation of the "normal" diurnal variation in barometric pressure. In order to achieve this a stratified random sample of 720 days, consisting of 60 sample days of each month of the year, was drawn from the meterological database at Jan Smuts Airport for the period 1970-1989. From this data the yearly average daily barometric pressure drop was found to be 270 Pa. This drop was found to be seasonally dependant with an average daytime drop of 328 Pa in November and 239 Pa in July for this period[4].

The barometric pressure data that was directly considered in this analysis, to identify a relationship between barometric pressures variations and gas related explosions in coal mines, were the following :

i. The daily average and diurnal barometric pressure trend that was apparent when the incident occurred (upward, downward or neutral), and the number of days for which this trend was evident leading up to the incident.
ii. The diurnal pressure drop on the day preceding the incident.
iii. The maximum daily barometric pressure fluctuation in the days preceding an incident.

and number of days before an incident it occurred.

iv. The time the of the day the incident occurred. This would indicate if the incident occurred on a decreasing or increasing diurnal pressure trend.

The data for the 35 incidents studied is given in Appendix 1.

4. RESULTS

4.1 Pressure trends

The first set of data that was considered was the pressure trends leading up to an incident. The daily average barometric pressure trend and the diurnal pressure trend leading up to an incident, were analysed. Three trends were identified namely an upward, downward or neutral trend, also called a plateau. A percentage value for each trend was calculated based on the number of incidents studied. The results are shown in fig 4.1 a&b.

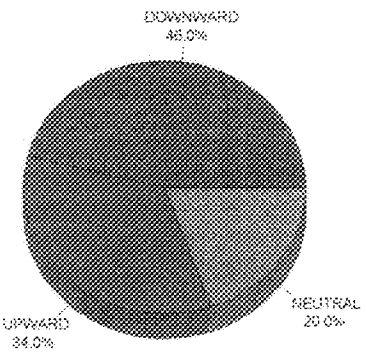

Figure 4.1a Daily average barometric pressure trends before an incident.

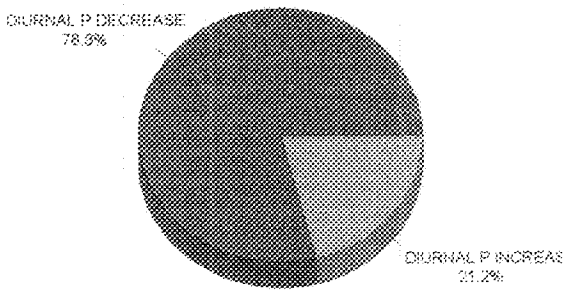

Figure 4.1b Diurnal barometric pressure trends before an incident.

4.2 Daily barometric pressure drop

The next set of data that was examined was the maximum daily barometric pressure drop the day

preceding an incident. The daily pressure drops were divided into four categories so as to be able to clearly identify the trends that occur. The categories decided on consists of daily barometric pressure drops of between 0-0.199 kPa, 0.2-0.299 kPa, 0.3-0.399 kPa and drops greater than 0.4 kPa. The categories were chosen based on the spread of data points and the measuring units used. The percentage of incidents for each category was then calculated. The results are shown in fig 4.2.

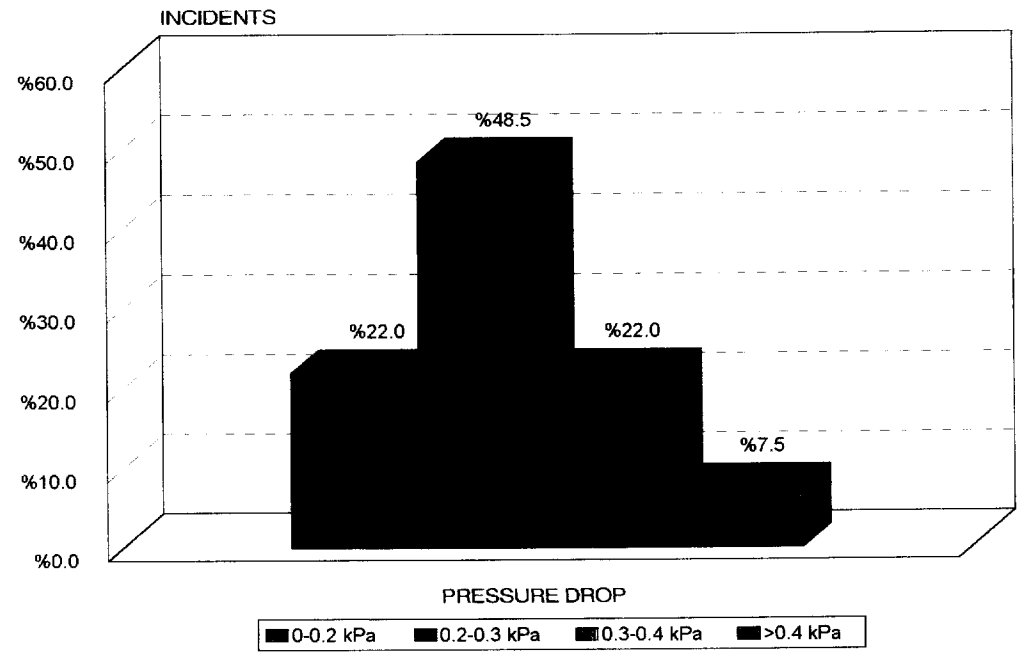

Figure 4.2 Barometric pressure drop the day before an incident.

4.3 Maximum barometric pressure drop

The maximum barometric pressure drop preceding an incident was also investigated. The aspect of the maximum barometric pressure drop that was of interest was the time elapsed, in days, between the recording of the maximum diurnal barometric pressure drop and the incident occurring.

A maximum barometric pressure drop preceding an incident was classified as a substantial drop in diurnal pressure in relation to the diurnal pressure drops during the days surrounding the incident. The maximum barometric pressure drops for this study varied between 290Pa and 620Pa with a average of 350Pa. See fig 4.3.

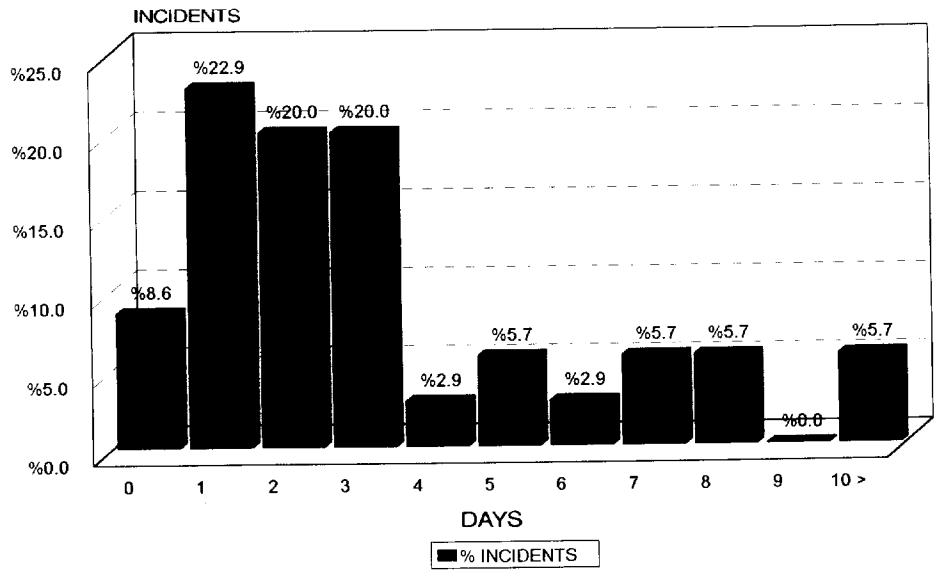

Figure 4.3 Number of days before an incident the maximum barometric pressure drop was recorded.

4.4 Distribution of incidents during the week

Data that was also considered to be of importance was the day of the week the incident occurred. Although this would not give a direct indication of the influence of barometric pressure variation on gas related incidents it could be used to see if there is a relation between incidents and the day of the week. This could be of some significance if a trend could be identified between the incidents and the working days on the mines. This in turn could give an indication of possible methane build up in the mine if the mine is inactive. The results are contained in fig 4.4.

4.5 Hourly distribution of incidents

In order to get an idea of what hour of the day the most incidents occur, the time the incidents occurred were noted. A percentage value for each hour of the day was calculated for the incidents considered. The time for an incident was taken on the hour. Incidents occurring 30 minutes before the hour and 29 minutes after the hour was taken for the hour. To get a more comparative graph, all the gas related incidents from 1970 -1989 were also included in the graph[5]. Super imposed onto these two sets of data is an average diurnal pressure fluctuation. This diurnal pressure

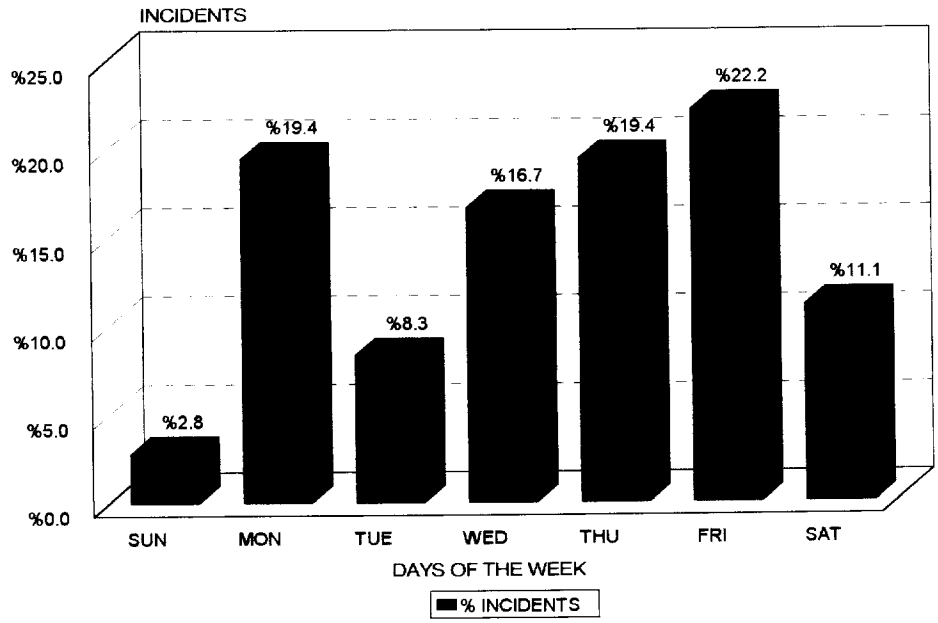

Figure 4.4 Distribution of incidents during the week.

variation is purely a qualitative view of a daily barometric pressure variations, as predicted by the stratified sample taken from the period 1970-1989 (See para. 1). The results are contained in fig.4.5.

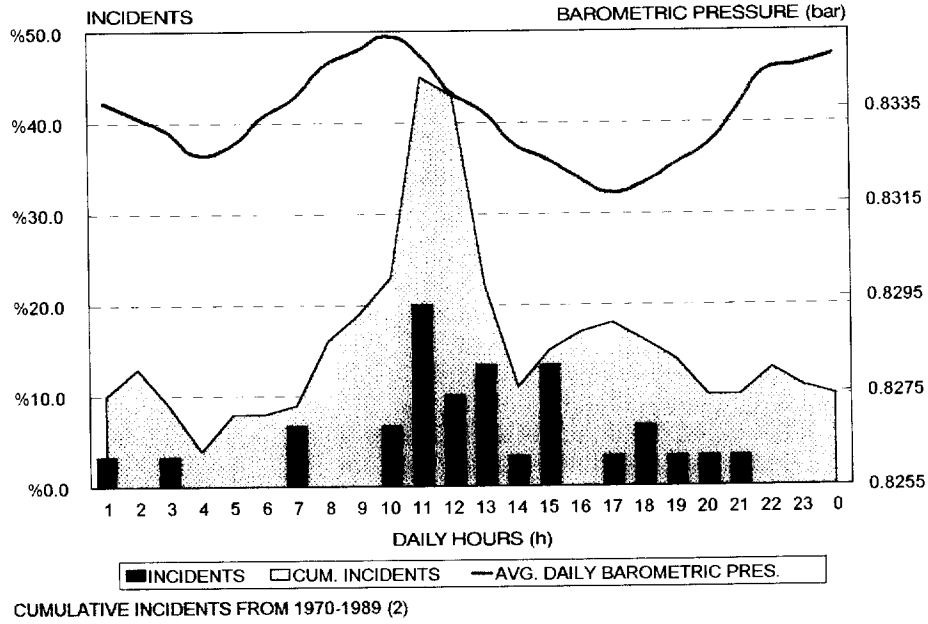

Figure 4.5 Hourly distribution of the 35 incidents studied for this study and the cumulative hourly distribution of all gas related incidents for the period 1970-1989. A typical daily barometric pressure curve is also shown.

4.6 Monthly distribution of incidents

Barometric pressure fluctuations varies for the different seasons[2]. To see if there was a trend evident from season to season a plot of the monthly distribution of incidents was made. All gas related incidents from 1970 to 1989 were considered[5]. All the gas related incidents for this period was considered because the incidents for this study was chosen to cover a full calender year and would thus not render a true picture for the seasonal distribution of incidents.

To get an indication of the relationship between incidents and barometric pressure fluctuations from season to season the average monthly barometric pressure for the highveld was obtained. This average barometric pressure was compiled from the data received from the weather bureau for their weather stations in the highveld region.

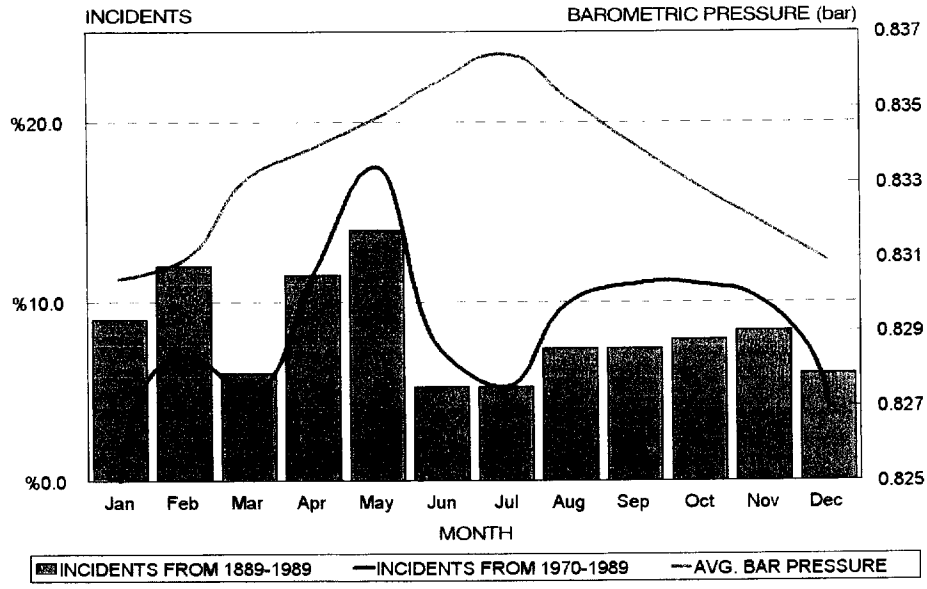

Figure 4.6a Monthly distribution of incidents compared with the average monthly barometric pressures.

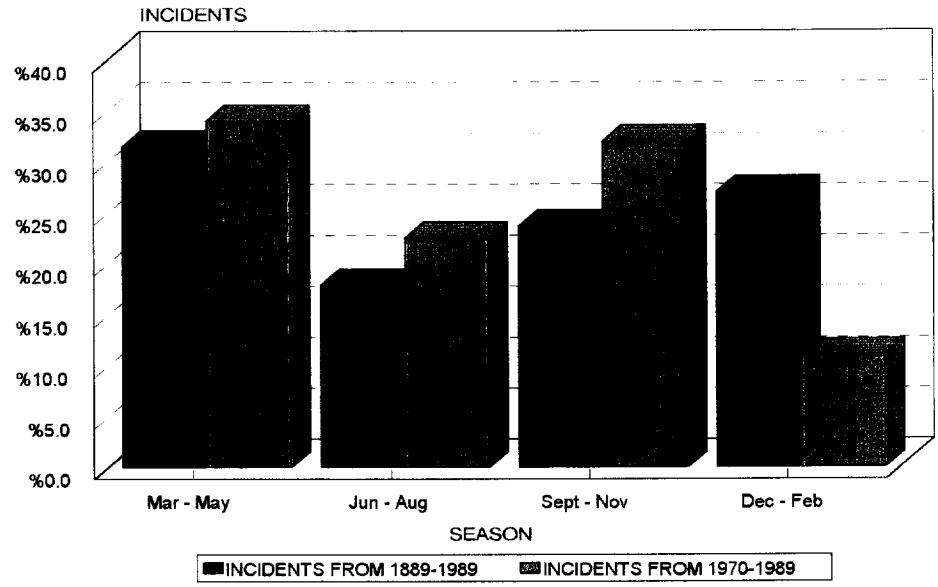

Figure 4.6b Seasonal distribution of incidents.

5. DISCUSSION

5.1 Pressure trends

From figure 4.1 we see that approximately 50% of all the incidents investigated, occurred on a downward trend for the average daily barometric pressure. Also nearly 80% of the incidents occurred on a diurnal pressure decrease. From these two observations it seems that incidents tend to occur on a downward daily average barometric pressure trend coupled with a downward diurnal pressure trend.

An explanation for this tendency for incidents to occur on a downward trend for daily average barometric pressures can be found in the old workings. Barometric pressure fluctuations on the surface is transferred to the underground environment of the colliery with no significant time lag[6]. This might not be the case for the old workings which is sealed off for ventilation purposes. If this is true, a drop in barometric pressure will manifest it self as pressure gradient between the old and active workings. This will cause air, that may contain methane[6], to flow from the old to the active workings and over loading the ventilation system. A similar phenomena is observed in a goaf. A

drop in barometric pressure induces a outflow of air from the goaf because of the pressure gradient that is created by a drop in barometric pressure and the delayed transfer of this drop in barometric pressure to the centre of the goaf[6].

5.2 Daily barometric pressure drop

From figure 4.2 it can be seen that there is definite tendency for the incidents considered to occur after a diurnal barometric pressure drop of 0.2 to 0.3 kPa the preceding day. Nearly 50% of the incidents considered occurred in this region. The remainder of the incidents are reasonably evenly spread out on either side of this. It thus seems that a diurnal pressure drop of between 0.2 kPa to 0.3 kPa favours a incident occurring the following day.

5.3 Maximum barometric pressure drop

For the maximum barometric pressure drop, the time elapsed between the pressure drop occurring and the incident occurring was analysed. From figure 4.3 it is obvious that over 70% of the incidents occurred within 3 days after the maximum diurnal barometric drop was recorded. The day after the pressure drop was recorded there is a dramatic increase in incidents occurring for the following 3 days. After 4 days there is a sharp decrease in the percentage of incidents occurring.

The average maximum barometric pressure drop for the incidents considered was 350 Pa with a minimum of 250 Pa in July and a maximum of 620 Pa in February. This maximum value was recorded 16 days before an incident occurred. The second highest value for the maximum diurnal barometric pressure drop that was recorded was 540 Pa in January, three days before an incident. For the incidents occurring within 3 days of the maximum diurnal barometric pressure being recorded, the average maximum drop in pressure was 375 Pa. This value is 6.6% higher than the average maximum daily barometric pressure drop recorded for the incidents considered.

From this data it can be said that for a diurnal pressure drop in the region of 375 Pa or greater, the chances of a gas related incident occurring during the following 3 days are increased.

5.4 Distribution of incidents during the week

In considering figure 4.4 it can be seen that there is a sharp increase in incidents occurring on a Monday in relation to the surrounding two days. There is also a steady increase in incidents occurring from a Tuesday to a Friday, with a maximum of 22% of the incidents occurring on a Friday. Approximately 19% of the incidents occur on a Monday and a Thursday. Landman[5] in his study of Coal Mine Explosions found that 38% of all major gas explosions occur on a Monday for the period 1970 -1989. (A major explosion was classified as an explosion where 5 or more people were killed.)

A possible explanation of this can be that on Mondays most mines did not produce over the weekend, and a methane build up occurred[7].

5.5 Hourly distribution of incidents

From figure 4.5 it is obvious that most of the gas related incidents occur between the hours of 10h00 and 15h00 of the day. This corresponds to a diurnal pressure drop for an average day. This trend seems to tie up with figure 4.1b which also suggests that incidents occur on a downward trend for diurnal barometric pressure. During these hours the mine is also at its busiest with the highest production rate and most men under ground.

The other 3 peaks that are observed at 02h00, 18h00 and 22h00 are less evident and do not seem to be directly related to barometric pressure variations.

5.6 Monthly distribution of incidents

Figure 4.6a indicates that there are peaks during the January/February and April/May periods. After these two peak periods there is a drop during June/July with a gradual increase towards the end of the year. These results do not correspond to results obtained by Dr. J.N. van der Merwe of Sasol[8] and a survey done by R.F. Boyer on the monthly frequency of major American coal mine disasters[9]. Both these reports suggests that incidents occur more frequently during the winter months, when the yearly barometric pressure is at a maximum and diurnal pressure drops tend to

be lower[2]. This tendency do not hold true for figure 4.6b.

7. CONCLUSION

The preliminary aim of this report was to determine if there is a direct link between barometric pressure fluctuations and gas related incidents in South African Collieries. From the data studied in this report there seems to be a definite tendency for incidents to occur during a downward daily average barometric trend. Coupled with a diurnal barometric pressure drop, this creates the most favourable conditions for a gas related incident to occur.

The most favourable conditions for a gas related incident occurring, from a barometric pressure point a view, can now be broadly identified. During a downward average daily barometric pressure trend, or within 2 days after a downward trend during a neutral trend, conditions are most favourable. In this period if a diurnal barometric pressure drop of between 0.2 to 0.3 kPa occurs during the day and a maximum diurnal pressure drop was recorded the previous 2 days, the following day can be described as a potentially dangerous day for a gas related incident occurring. If this potentially dangerous day is a Monday, the chances of an incident occurring are increased by 35%. During a potentially dangerous day the time for an incident to occur, is most probable during a diurnal pressure drop. This correlates to a probable time of between 11h00 and 15h00. This prediction is purely based on barometric pressure related data. No other factors such as the location of the incident, ignition source, coalfield being mined or related data was taken into account. Fan stoppages, which influence underground pressure more severely than barometric pressure fluctuations[7], was also not considered in this study.

From the nature of the study no conclusion between actual volumes of methane released and barometric pressure variations can be reached. The reason for this is that only incidents were studied. From the incidents no direct data can be extracted that would give an indication of methane release rates. To find a correlation between methane gas release rates and barometric pressure fluctuations a direct testing method should be devised. Ideally a study should be made where the variations in barometric pressure, on the surface and underground, must be recorded. The methane release during these barometric pressure fluctuations must then be monitored in the

absence of any outside interferences such as ventilation and equipment movement. This should be repeated for various coal fields to establish the influence of barometric pressure fluctuations on methane release rates.

8. FUTURE WORK

1. A factor that must be investigated is the influence of barometric pressure changes on the movement of the air and methane mixture in goafs and old workings. The origin and influence of a possible pressure gradient between old and active workings should also be studied. The magnitude and factors influencing such a pressure gradient must also be determined. The methane content of, and distribution within goafs and old workings must also be investigated.
2. In this report a preliminary study was made of the relationship between barometric pressure fluctuations and gas related incidents. There seems to be a relation between the two but other important non barometric factors should now also investigated in conjunction with barometric pressure fluctuations. Factors such as, ignition source, location of the incident, coalfield mined, average methane levels in the mine, total methane content of the coal, ventilation system, fan stoppages, air velocities, sealing methods of the old workings and its effectiveness, geological conditions, seam depth and production rate during incident.
3. A factor that is important in gas related incidents and coal mining in general is the methane release. To get a better understanding of the relationship between methane release rates and barometric pressure fluctuations definite tests will have to be done. Such tests will entail the measuring of the barometric pressure changes on the surface and underground, and the measuring of the accompanying methane release rates in the absence of external factors such as ventilation and movement of equipment and men. These results in conjunction with the coal characteristics could shed more light on this question.
4. The influence that fan stoppages have on the underground environment pressure must also be investigated. These pressure fluctuations tend to be more severe than barometric pressure fluctuations[7] and the influence that these stoppages have on the under ground

environment must be quantified and investigated.

5. A system to assist in the quantification of methane release and pressure changes has been developed. The system consists of a station with remote methane and pressure sensors which logs the readings simultaneously onto a data logger. This data can be used to determine the actual relationship between methane release and pressure fluctuations at various locations.

REFERENCES

1. Joubert, F.E. Fuel Research Institute of South Africa, Technical Memorandum No. 34, 1968, p1.

2. Schulze, B.R. Climate of South Africa, Part 8, General Survey, Weather Bureau, Department of Transport, Pretoria, 1965, Reprint 1974, pp1-10.

3. Personal contact, Mr. Lang, Weather Bureau, Pretoria, June 1994.

4. Fauconnier C.J. Increased Under Ground Extracrion of Coal, S.A.I.M.M., Johannesburg, 1982.

5. Landman G.V.R. Ignition and Initiation of Coal Mine Explosions, Progress Report, University of the Witwatersrand, 1990.

6. Stevenson, J.W. Effects of Bleeder Entries During Atmospheric Pressure Changes, Mining Engineering, June 1968, p62.

7. Stripp, G.P. Methane Emission Characteristics of South African Coal Seam Strata, University of the Witwatersrand, Chapter 6, 1990.

8. Van der Merwe, Dr. J.N. Analyses of Methane Gas Occurrences At Secunda Collieries, Sasol Mining (Pty.) Ltd., Coal Division, October 1993.

9. Boyer, R.F. Coal Mine Disasters: Frequency by Month, Science, Vol. 144, 19 June 1964, p1448.

APPENDIX 1

MONTHLY DATA FOR BAROMETRIC PRESSURE CASE STUDIES

JANUARY

INCIDENT NO.	1	2	3	4		
DATE:	07-01-81	14-01-81	09-01-89	21-01-89		
DAY:	WED.	WED.	MON.	SAT.		
TIME:	-	11H15	-	-		
COLLIERY:	BAL-GRAY	ERMELO	DELMAS	DNC		
PRESS. TREND:	DOWN	DOWN	UP	PLAT.		
DIURNAL PRESS. TREND:	-	DOWN	-	-		
MAX. PRESS. FLUCTUATION:	430 Pa	540 Pa	380 Pa	360 Pa		
NO. DAYS BEFORE:	1	3	3	5		
FATALITIES:	0	0	0	0		

TABLE A1

FEBRUARY

INCIDENT NO.	5	6	7	8	9	10
DATE:	01-02-89	21-02-68	12-02-80	15-02-80	28-02-81	28-02-81
DAY:	THUR.	WED.	TUES.	FRI.	SAT.	SAT.
TIME:	-	15HOO	-	10H40	07H20	-
COLLIERY:	NATAL COAL	KILBRA-CHAN	COAL-BROOK	USUTU	SPRING-FIELD	BOSJE-SPRIUT
PRESS. TREND:	DOWN	UP	UP	UP	DOWN	DOWN
DIURNAL PRESS. TREND:	UP	DOWN	DOWN	DOWN	UP	DOWN
MAX. PRESS. FLUCTUATION:	380Pa	620Pa	520Pa	520Pa	330Pa	330Pa
NO. DAYS BEFORE:	1	16	5	8	1	1
FATALITIES:	0	0	0	-	2	0

TABLE A.2

MARCH

INCIDENT NO.	11	12				
DATE:	19-03-66	29-03-66				
DAY:	SAT.	TUES.				
TIME:	13H00	12H3O				
COLLIERY:	KILBRA-CHAN	INDMENI				
PRESS. TREND:	DOWN	PLAT				
DIURNAL PRESS. TREND:	DOWN	DOWN				
MAX. PRESS. FLUCTUATION:	420Pa	310Pa				
NO. DAYS BEFORE:	2	2				
FATALITIES:	0	0				

TABLE A.3

APRIL

INCIDENT NO.	13	14	15	16		
DATE:	06-04-81	25-04-81	23-04-79	27-04-79		
DAY:	MON.	SAT.	MON.	FRI..		
TIME:	-	11H00	11H00	13H20		
COLLIERY:	DNC	ERMELO	BAL-GRAY	BAL-GRAY		
PRESS. TREND:	DOWN	DOWN	DOWN	UP		
DIURNAL PRESS. TREND:	DOWN	DOWN	DOWN	DOWN		
MAX. PRESS. FLUCTUATION:	270Pa	300Pa	400Pa	400Pa		
NO. DAYS BEFORE:	0	2	8	12		
FATALITIES:	0	0	2	2		

TABLE A.4

MAY

INCIDENT NO.	17	18	19	20	21	22
DATE:	04-05-84	29-05-84	31-05-84	06-05-81	15-05-81	22-05-81
DAY:	FRI..	TUES.	THUR.	WED.	THUR.	FRI.
TIME:	15H15	11HOO	18H00	12H00	14H15	11H45
COLLIERY:	TWIST-DRAAI	DNC	DNC	PLATB-NEWC.	BAL-GRAY	PLATB-NEWC.
PRESS. TREND:	DOWN	UP	DOWN	PLAT.	UP	DOWN
DIURNAL PRESS. TREND:	DOWN	DOWN	DOWN	DOWN	DOWN	DOWN
MAX. PRESS. FLUCTUATION:	300Pa	400Pa	300Pa	320Pa	310Pa	340Pa
NO. DAYS BEFORE:	3	6	0	3	2	7
FATALITIES:	0	0	0	0	0	0

TABLE A.5

JUNE

INCIDENT NO.	23	24	25			
DATE:	02-06-62	21-06-85	12-02-80			
DAY:	SAT.	FRI.	TUES.			
TIME:	07H00	03H00	20H15			
COLLIERY:	NATAL NAVIG.	SPRING-FIELD	BRAND-SPRUIT			
PRESS. TREND:	DOWN	UP	DOWN			
DIURNAL PRESS. TREND:	UP	DOWN	UP			
MAX. PRESS. FLUCTUATION:	330Pa	320Pa	290Pa			
NO. DAYS BEFORE:	1	3	2			
FATALITIES:	10	0	0			

TABLE A.6

JULY

INCIDENT NO.	26	27				
DATE:	17-07-81	22-07-81				
DAY:	FRI.	WED.				
TIME:	12H45	18H15				
COLLIERY:	DNC	BAL-GRAY				
PRESS. TREND:	DOWN	UP				
DIURNAL PRESS. TREND:	DOWN	UP				
MAX. PRESS. FLUCTUATION:	250Pa	280Pa				
NO. DAYS BEFORE:	2	3				
FATALITIES:	0	0				

TABLE A.7

AUGUST

INCIDENT NO.	28					
DATE:	12-08-85					
DAY:	MON.					
TIME:	12H00					
COLLIERY:	MIDDEL-BULT					
PRESS. TREND:	DOWN					
DIURNAL PRESS. TREND:	DOWN					
MAX. PRESS. FLUCTUATION:	330Pa					
NO. DAYS BEFORE:	1					
FATALITIES:	34					

TABLE A.8

OCTOBER

INCIDENT NO.	29					
DATE:	25-10-84					
DAY:	THUR.					
TIME:	21H15					
COLLIERY:	ERMELO					
PRESS. TREND:	DOWN					
DIURNAL PRESS. TREND:	DOWN					
MAX. PRESS. FLUCTUATION:	310Pa					
NO. DAYS BEFORE:	4					
FATALITIES:	6					

TABLE A.9

NOVEMBER

INCIDENT NO.	38	31	34	33		
DATE:	12-11-82	04-11-83	06-11-83	21-11-83		
DAY:	FRI.	FRI.	SUN.	MON.		
TIME:	10H00	10H40	15H00	18H50		
COLLIERY:	ERMELO	SPRING-FIELD	ERMELO	DELMAS		
PRESS. TREND:	UP	PLAT.	DOWN	PLAT		
DIURNAL PRESS. TREND:	DOWN	DOWN	DOWN	UP		
MAX. PRESS. FLUCTUATION:	330Pa	430Pa	470Pa	350Pa		
NO. DAYS BEFORE:	2	3	1	7		
FATALITIES:	11	0	1	0		

TABLE A.10

DECEMBER

INCIDENT NO.	34	35				
DATE:	15-12-76	23-12-76				
DAY:	WED.	THUR.				
TIME:	15H15	16H35				
COLLIERY:	USUTU	DNC				
PRESS. TREND:	DOWN	UP				
DIURNAL PRESS. TREND:	DOWN	DOWN				
MAX. PRESS. FLUCTUATION:	460Pa	300Pa				
NO. DAYS BEFORE:	0	1				
FATALITIES:	0	2				

TABLE A.11

APPENDIX D

D1. V.A. Kononov and A.P. Cook, Multi Purpose Data Logging Stations for Underground Environmental Monitoring, 26th International Conference of Safety in Mines Research Institutes, September 1995, CSIR Division of Mining Technology.

D2. F.J. van Zyl and A.P. Cook, A Preliminary Review of the Influence of Barometric Pressure on 35 Methane Related Incidents, Interim Report, June 1994, CSIR Division of Mining Technology.

D3. A.E. Vidal da Silva, An Evaluation of the Relation Between Barometric Pressure Fluctuations and Methane Concentrations, Interim Report, December 1995, CSIR Division of Mining Technology.

APPENDIX D1

MULTIPURPOSE DATA LOGGING STATIONS FOR UNDERGROUND ENVIRONMENTAL MONITORING

Dr V.A.KONONOV and A.P.COOK
CSIR MINING TECHNOLOGY,
Johannesburg, South Africa

ABSTRACT: Two intrinsically safe environmental monitoring stations for underground coal mine applications have been developed to satisfy various scientific and industrial needs.

The first station continuously monitors and logs information from 8 methane and/or dust sensors over a twelve hours period in autonomous mode. The second station comprises of barometric and methane sensors together with an intrinsically safe 65K Data Logger, a power pack and a controller and provides more than 10 days of programmable periodic monitoring and logging of information in an autonomous mode. Special measures provide reliable battery charge/discharge cycles.

This instrumentation is a new development in South Africa and provides a unique degree of precision information relating to coal dust and methane flows around a continuous miner and on methane liberation as a function of atmospheric pressure. Both stations could be designed to comply with any national intrinsic safety requirements.

1. INTRODUCTION

Methane gas remains a hazard in mechanized coal sections in South Africa. The Mining Technology Division, Miningtek, of the CSIR is carrying out a wide ranging research programme aimed at reducing methane hazard in underground coal mining. Work is being done towards methane prediction, continuous miner section ventilation and the effects of atmospheric pressure.

The main effort of this work is directed at continuous miners (CM) and the immediate face environment, using both actual recorded data and ventilation simulations. Real time measurement of methane level at various positions around a continuous miner whilst it is operating, are almost impossible to achieve manually and the limited information from one or two methanometers normally used on a production machine is not sufficient to extrapolate over

a full shift or an entire machine. A remote sampling method was therefor required, capable of recording methane level at several positions on and around CM over an extended time period. Such system had to be intrinsically safe (IS), fully self contained, independent of the power supply of the CM and does not interfere with normal operation.

A further advantage of developing such systems was its potential for application in other areas of the project, particularly when remote recording is required over a period of time. This made it suitable for logging the effects of changes in atmospheric pressure on methane levels where it was intended to record methane and pressure simultaneously over a week period. Future developments will include different environmental sensors, initially the addition of dust sensors to monitor hybrid dust and methane mixtures.

2. DATA LOGGING

The main problem which was faced during development of instrumentation for underground coal mining environmental monitoring was to obtain IS Data Logger (DL) small enough to be accommodated in different equipment, universal and user friendly to be handled by mining personal. A DL enables to collect information without permanent presence of the researchers or mine staff in very hostile and hazardous underground coal mine environment.

Initial analysis identified the main requirements to such DL and facilitated in development of the IS DL with the following specification:

* 8 analog inputs 0-2 V;
* fully programmable;
* real time records;
* 65 K memory;
* 12 Bits resolution;
* recording speed from 1 second to 24 hours.

To prevent the DL against deliberate or accidental unauthorized access to records or to initial setting it was decided that the DL itself would contain no monitoring, display or control function. The DL is incorporated in a 95x115x29 mm plastic enclosure with a plug which connects the DL to a measurement system (Fig.1).

The DL requires a PC to be programmed before use and for retrieving data from it. For these purposes the DL needs to be plugged into a surface termination unit which enables the DL to communicate with PC by RS232 code at speed 9600 Baud. Retrieved information can be presented in a table or graphs. Being programmed, the DL starts logging information only after to be plugged in a station termination unit in testing site. Every monitoring instrument has got a station termination unit with encoded ID, therefor, while data are retrieved on the surface they are clearly identified.

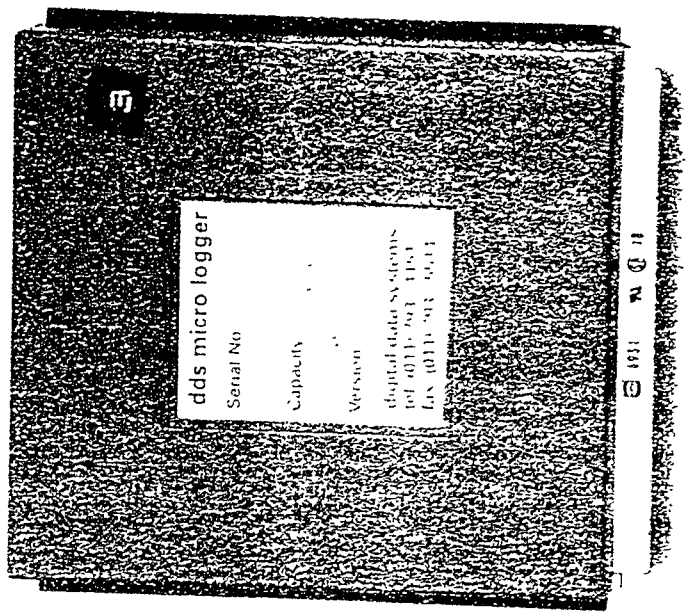

Fig.1 Intrinsically safe Data Logger

In-built 7.5 V rechargeable battery keeps recorded information for up to one week during transportation of the DL between the test site and the place where data should be retrieved. During data recording the DL is supplied with trickle current from the monitoring system.

The DL contains no inductive components and total amount of capacitance does not exceed 10 μF, therefore, only battery current limiting resistor and protective charging diodes are used as IS measures [1].

3. MULTICHANNEL METHANE MONITORING STATION.

Multichannel Methane Monitoring Station (MMMS) is designed for real time monitoring and logging information from eight methane sensors during one shift. Instead of methane sensors other sensors, such as dust sensors could be used.

The station consist of IS rechargeable 12 V, 12 A/h battery, IS DL and 8 sockets are positioned in a 300x300x180 mm plastic enclosure. Up to 8 sensors could be plugged to the station.

The station provides continuous operation during 12 hours period. Operation time is limited by the IS battery which supplies all 8 methane sensors with total current consumption about 0.7 A. The station records methane level every 5-10 seconds that is reasonable record speed taking into account an

average response time of methane sensors. The operation time and/or record speed could be increased by limitation of amount of using sensors.

To study methane distribution around a continuous miner methane sensors should be positioned at different parts of the machine and connected to the station in the cabin. Typically methane sensors are positioned either side of the boom, close to the cutting drum and on the intake and return sides of the CM. Results obtained to date indicate that methane levels are generally higher on return side and close to the drum. Actual levels vary depending on the depth of CM into the heading or split [2].

Off-board applications for the unit are typically to monitor methane build up rates in an unventilated heading and the dilution rate when the ventilation is restored.

Every shift the IS battery must be changed. Having its own IS battery makes the station independent of the machine and enables it to be used without any interaction with machine or mining operation. By the end of the shift the DL also should be brought on the surface for information recovery and a new one must be plugged in the station termination unit.

4. BAROMETRIC AND METHANE MONITORING STATION.

The barometric and methane monitoring station (BMMS) provides real time monitoring and record on mining atmospheric pressure and methane level for scientific and mining safety purposes. The station enables the determination of the definite relation between the atmospheric pressure and level of methane liberation under different mining geological and technical conditions.

To make the station widely applicable for different mine areas the following main requirements were implemented during the development:

1. To obtain reliable information on pressure/level data it is necessary to provide continuous monitoring for at least one week.
2. The station must be portable and selfpowered as it should be positioned in limited space place in underground and where power is not available.
3. The station must not interfere with normal mining operation.
4. The station should be easy to operate and maintain by mining personnel.

At Fig.2 the general view of the station is given. The station comprises of barometric (BS) 1 and methane (MS) 2 sensors, the IS DL 3, IS power pack 4 and the controller 5 which are incorporated in a plastic enclosure 180x180x300 mm.

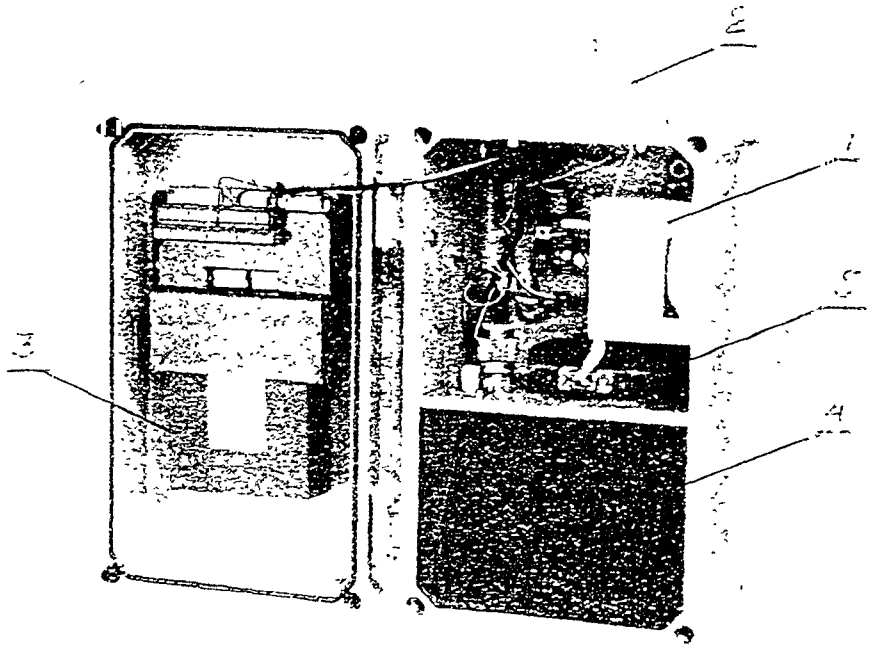

Fig.2 Barometric and Methane Monitoring Station.
General view with open cover.

In Fig.3 the electrical block diagram is presented. The power pack, which includes NiCd rechargeable battery and the DC/DC convertor to supply 24 V to the BS, determines the weight and size of the station. To keep both in a reasonable range 9 V, 7.5 A/h battery was accepted. To provide one week autonomous operation of the station under condition when total current consumption is about 0.12 A, a cyclic method of operation was proposed when atmospheric pressure and methane level are measured for one minute in four minutes interval. Hence, more than 10 days of programmable periodic monitoring and logging of information in an autonomous mode is possible.

To provide long battery life and giving to mining personnel clear indication about battery discharge the station has got no power switch but the fuse F which is blown when the battery is fully discharged. After battery recharge a new fuse must to be installed to start next measuring cycle.

Because of the DL is designed as an universal unit for environmental instrumentation to make no difference for mining personal to use it for different application the controller is developed. The controller is programmable and provides cycling measuring interval. As clocks in the controller and in the DL are not synchronized the controller provides also intermediate analog-digital-analog memory of previous signal level from sensors while they are not powered.

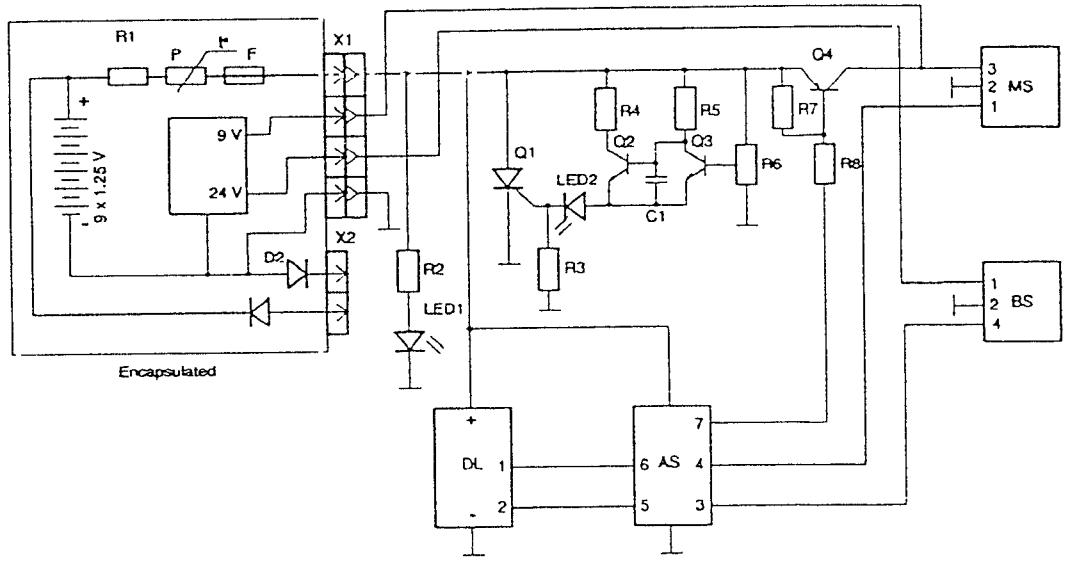

Fig.3 Barometric and Methane Monitoring Station
Electrical Diagram

IS measures includes current limiting resistors R1 and a poliswitch P for 9 V output and current limiting resistors for input/output for 24 V DC/DC convertor. In the station IS Trolex Methane Sensors TX3261 Mk II is used. Using the barometric sensor AD 1000 from Halstrup brought some complication to the station design such as introduction of the DC/DC up-conversion and IS modification of the sensor itself [1].

5. CONCLUSION.

Development of IS Data Logger and application of two types of instruments for environmental monitoring in underground conditions of coal mine enables the obtaining of unique information and hence to improve safety in a coal section.

Developed instrumentation provides real time information on methane (and later dust flow) around a continuous miner, the results being used to confirmed the accuracy of CFD simulation computer models, and facilitates to improving of ventilation in a coal section. New level of knowledge about methane liberation from strata and goafs as a function of atmospheric pressure makes a great impact at a coal section ventilation system design.

REFERENCES

1. SABS IEC 79-0 South African Bureau of Standards. Electrical Apparatus for Explosive Gas Atmospheres. Part 0: General Requirements.

2. Cook, A.P., 1995, "Methane Monitoring Using a Multipurpose Data Logging Station", Proceeding of the 26th International Conference of Safety in Mines Research Institutes, Katowice, Poland, 4-8 September, 1995.

APPENDIX D3

AN EVALUATION OF THE RELATION BETWEEN BAROMETRIC PRESSURE FLUCTUATIONS AND METHANE CONCENTRATIONS

ABSTRACT: This study was undertaken to determine if a relationship between barometric pressure and methane level fluctuations in South African collieries exists. The atmospheric pressure and methane levels at various underground positions were recorded by means of a dedicated unit and the data analysed. Although a relation could not be accurately quantified, a range in which sudden changes in barometric pressure corresponds with noticeable changes in methane levels were identified.

COMPILED BY: A. E. Vidal da Silva
A. de Kock

CONTENTS

1 - INTRODUCTION

The objective was to determine if a relationship exists between periodical and diurnal fluctuations in atmospheric pressure and the methane emission levels in the underground workings of a mine.
For this purpose an underground monitoring station for methane level and atmospheric pressure monitoring was developed and positioned underground in a colliery.
Results obtained were compared with the findings of other studies done in South Africa related to this subject.
Although several sets of data were lost due to technical problems, the data available was analysed to determine if any trends could be identified.

2 - DATA - ACQUISITION PROCEDURE

2.1 - Equipment

The barometric and methane monitoring station provides real time monitoring and records atmospheric pressure and methane level.
The following requirements were specified for the system development:

1 - To obtain reliable information on atmospheric pressure and methane level data trends it was deemed necessary to provide continuous monitoring for at least one week. This will ensure that smaller short term variations do assume undue relevance and ensure at least part of the long term trends are recorded for analysis.
2 - The station must be portable and self-powered as it would be positioned in limited space underground and in locations where power is not available.
3 - The station must not interfere with normal mining operations.
4 - The station should be easy to operate and maintain by mining personnel.

Figure 1 gives a general view of the station. The station comprises the atmospheric pressure and methane sensors, the Intrinsically Safe Data Logger (ISDL), the Intrinsically Safe Power Pack (ISPP) and the controller. The ISPP is incorporated in a sealed plastic enclosure 180x180x300 mm.

In Figure 2 a block diagram of the unit is presented. The ISPP, which includes a NiCd battery and a DC/DC converter to supply 24 volt to the barometric pressure sensor as well as the circuit monitoring the operation of the battery, determines the weight and the size of the station. To keep these in a reasonable range a 9V, 7.5 A/h battery is required. The purpose of the encapsulation is to maintain the battery, and the circuit regulating the level of charge of the battery is made an integral part of this component.

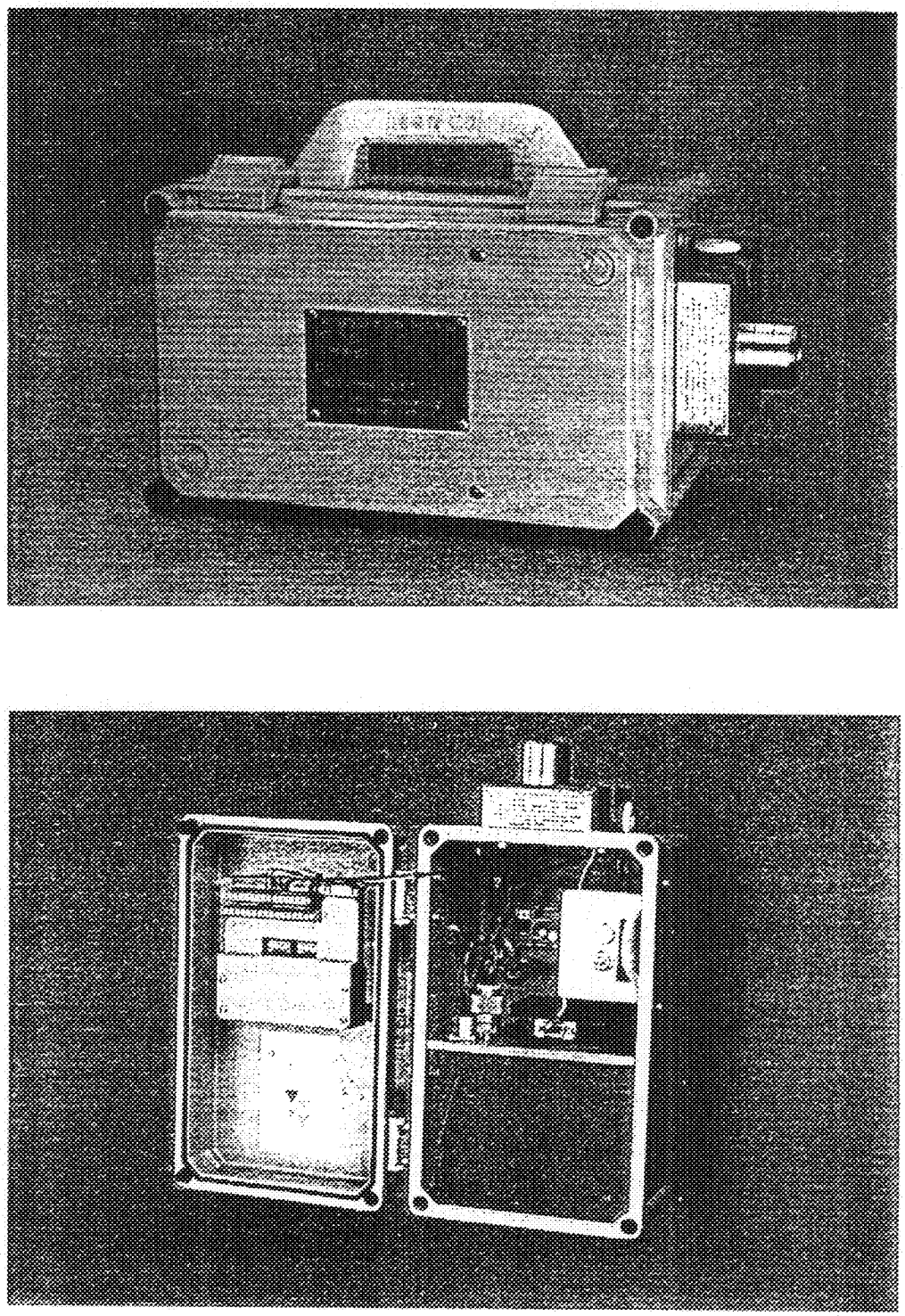

Figure 1 - General View of the Atmospheric Pressure and Methane Unit

To provide one week autonomous operation of the station under the conditions when the total current consumption is in the vicinity of 120 mA, a cyclical method of operation was adopted. The atmospheric pressure and methane level are measured every five minutes with the system dormant for four minutes periods in between. This process allows over 10 days of monitoring and logging of information.

To provide maximum battery life and give the mine personnel a clear indication when the battery is discharged the station has a fuse which is blown by the circuit incorporated in the ISPP when the battery level drops below 9V. After each battery recharge a new fuse must be installed to allow the operation of the unit and start a new measuring cycle.

As mentioned in the preceding paragraphs the system is dormant for four minutes periods between readings to preserve battery life. This feature is achieved by the use of a programmable controller able to provide cyclical measuring intervals. Every four minutes, the controller sends a signal to the control circuit that enables the supply of power for a minute to both sensors. To minimise the risk of data loss the controller was designed with a analog - digital - analog temporary memory. The barometric pressure and methane level readings are recorded on the temporary memory at the end of the one minute cycle. The data logger then records the data stored in the temporary memory of the controller. The reason for this mode of operation is that the four minute dormant period is sufficient for allow for clock drift between the clocks in the data logger and in the controller over a 10 day period.
Also, this setup allows for the "plugging in" of other instruments with a minimum of modifications and also for variations in the recording intervals.

An intrinsically safe methane sensor Trolex TX3261 Mk II is used to take the methane level readings. It is a catalytic combustion sensor with a 10 second response time. The measuring range is 0% to 4% methane, with the following tolerances:

0% to 1.25% CH_4	+/- 0.1% of CH_4
1.25% to 4%	+/- 0.8% of range

The sensor is of the bridging type with an output value of 0.4 Volt to 0% of methane. The occasional negative methane concentration that can be seen in the graphs, occurring immediately after a sudden drop in methane concentration is within the tolerance values and caused by an over compensation of the bridge system.

To obtain barometric pressure readings the sensor used is the AD 1000 from Halstrup. The reading range of this sensor is 80 kPa to 120 kPa. This particular range was decided upon because of the high altitude at which the coal mines are situated. The tolerance of the readings is +/- 1%.
The use of this sensor required the introduction of the 12 to 24 Volt DC/DC converter and modifications of the sensor itself as to meet the intrinsic safety requirements of the SABS IEC 79-0.

The control circuit in the centre of the block diagram contains the switch that opens and closes the circuit that supplies power to both sensors, as well as the circuit that determines when the lower limit of charge in the battery has been reached. When this occurs, the circuit on which the fuse is installed is closed and the fuse blows. From this moment onwards power will only be supplied to the data logger until such time as the battery is recharged and the fuse replaced.

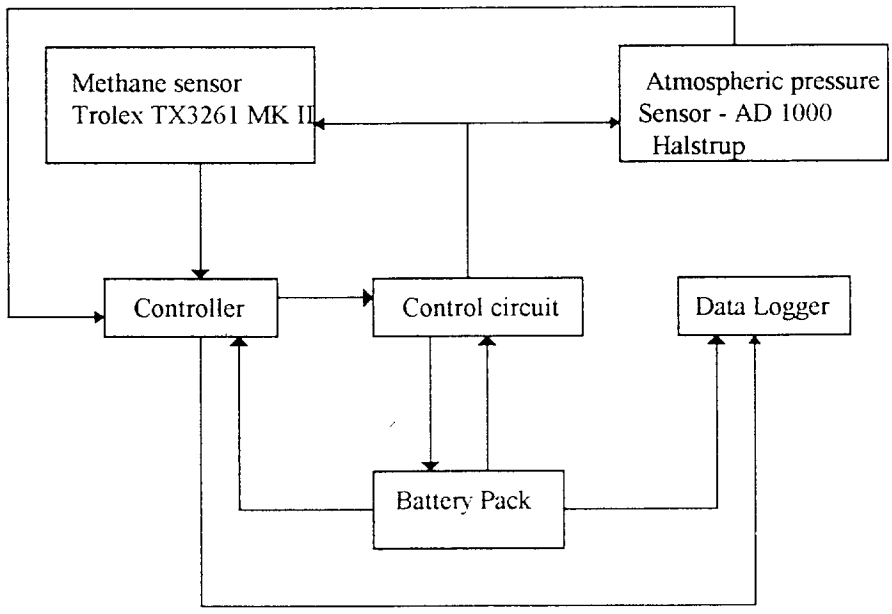

Figure 2 - Block diagram of the atmospheric pressure recording unit

The atmospheric pressure and methane sensors are switched on and enough time is allowed for the methane sensor to reach operating temperature as this is required to achieve reliable results. To keep the design simple, and because the power consumption of the atmospheric pressure sensor is low, both sensors are switched on at the same time. The readings of both sensors are kept in the controller until the time they are read by the logger unit. After this cycle is completed the unit goes into sleep mode, until it is time to take another recording. When it switches on again the controller's temporary memory is cleared before the new readings are downloaded into it. The total time of each cycle is in the order of one minute.

2.2 - Process

The installation procedure is as follows:

The unit is positioned underground, in the middle of the cross-section of the airway, approximately 2.0 meters from the floor with the methane sensor facing the airflow. The position of the unit was chosen so as to avoid as much as possible interference with normal mining activities. The position of the methane sensor was chosen due to being a calibration requirement that the position of the sensor

in relation to the air stream at the time of calibration be as close as possible to the position when in operating conditions.
At the end of the logging period the logger unit is brought to surface and the data downloaded to a PC.

2.3 - Tests - Locations

Two test sites were initially available: Site A, in the return airway of a working section and Site B in a return airway passing by several sealed off goafs as shown in Figure 3 and 4 respectively.
Test 1 was the only test done at Site A that achieved usable results. After the data of subsequent tests was found to be corrupted due to the methane sensor being rendered inoperational it was decided to move the unit to Site B. Tests 2, 3 and 4 were done at this location.
To achieve representativity in the data to be analysed it was decided that Site B would be a suitable location for future tests.

Problems encountered during the initial tests:
- Failures of the sensor due to exposure to silicone vapours, which is specifically warned against by the manufacturer. This happened twice, causing loss of two sets of data.
- Miningtek relied on mine personnel to do the physical installation of the unit in the mine as well to its recovery, and, obviously the production problems took precedence. This caused that from the ten sets of data collected, only four are usable.

From studies previously done[1] with recordings taking place at 15 minutes interval it had been concluded that this interval did not provide an accurate picture, as the pressure variation caused by a stoppage of the main ventilation fans far exceeds the natural variations and, as this seldom occurs for periods as long as fifteen minutes, a distortion in the results occurs.
Despite this, as the equipment was still on its experimental phase, the first test recordings were made at fifteen minutes intervals. After it had been confirmed that that the system would support 10 days recordings at five minutes intervals, the settings were changed to this standard, allowing a more accurate picture of the events.

3 - RESULTS

Test 1 - 7 to 11 September 1994

Chart 1 displays the results for the full test period, and charts 9 to 16 display the daily data collected during this period. With exception of charts 9 and 16, which show the data of the first and last day of recording respectively, the time periods in the charts are from midnight to midnight.

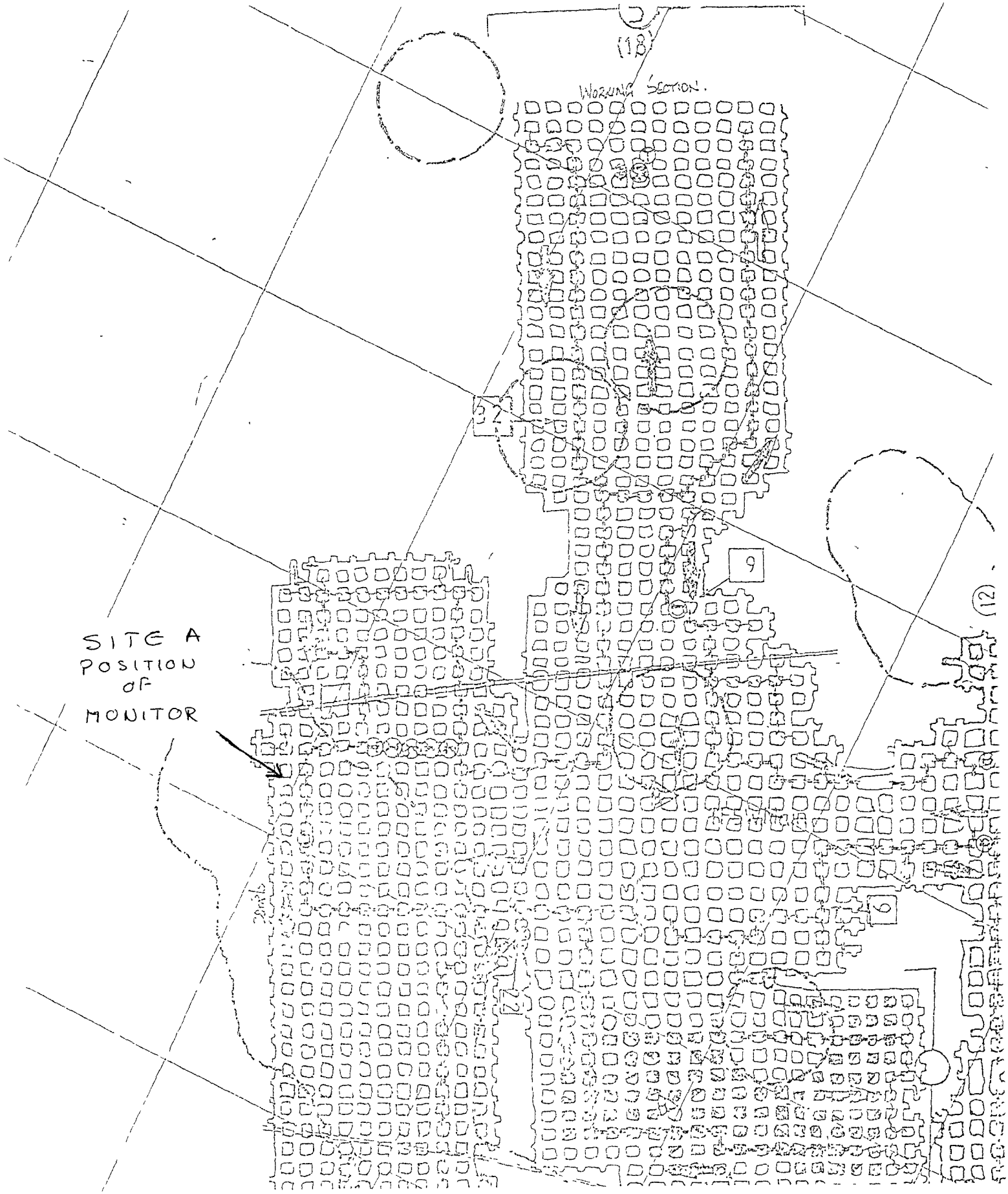

Figure 3 - Location of Site A

Test 2 - 12 December 1994 to 7 Jan 1995

Chart 2 displays the results obtained during this test. This values are an indication that no output signal was received from the sensors during the test period. This was due to an electrical fault.

Test 3 - 2 to 14 Feb. 1995

Chart 3 displays the recorded results for this period. It can be seen that although the atmospheric pressure sensor worked, no output signal was recorded from the methane sensor. On inspection it was found that the cause was poisoning of the methane sensor most likely caused by silicone vapours.

Test 4 - 7 to 14 March 1995

Chart 4 displays the results for this test. It can be seen that the output signal of the methane sensor is intermittent. It varies from a value of - 0.95 (no signal from the sensor) to apparently normal values. On examination it was found that remnants of silicone were still adhering to the outside of the unit which could have caused the erratic results.

Test 5 - 4 to 11 April 1995

Chart 5 displays the recorded values for this test. It can be seen that again the signal from the methane sensor is intermittent, although this time the values vary from nearby zero to seemingly normal values. Although on examination of the equipment no fault was found, the regularity of the drop to zero is suspicious. Attempts were made to try to relate the drop to activities within the shift, but the drops occur even over weekends when no work was taking place. No other reason was found other then an intermittent fault in the methane sensor.

Test 6 - 9 to 16 May 1995

Chart 6 displays the recorded results for this test. As it can be seen, no output signal was recorded from the methane sensor during the full test period. The sensor was inspected and found with no fault and a full inspection of the unit took place. The atmospheric pressure sensor was found not to be working properly. The earth wire on the sensor was loose but the cause of the fault is unknown.

Test 7 -14 to 21 June 1995

Chart 7 displays the results for the whole test period. Detailed results for each day can be found in Charts 17 to 24. With exception of Charts 17 and 24, representing the respectively the first and last day of the test, the time period in this charts is from midnight to midnight.

Test 8 - 25 July to 6 August 1995

Chart 8 displays the results for the full period of this test.
As in the previous case, the time span on charts 25 to 37 is from midnight to midnight and charts 25 and 37 display the results from the first and last day of the recording period respectively .

Test 9 - 15 to 24 August 1995

Chart 9 displays the results for the full term and charts 38 to 47 display more detailed results in a daily basis. Again, the time period displayed in the charts is from midnight to midnight with exception of charts 38 and 47

Test 10 - 1 to 15 December. 95

No data was recorded by the data logger during this period. The cause of the malfunction is being currently investigated.

4 - ANALYSIS

Test 1 - Charts 1 and 9 to 16

Examination of the overall test period as displayed in Chart 1 shows seven distinct peaks in the methane concentration occurring, with a increase of methane levels from below 1% to levels just below 2% and above. In all instances the drop in pressure was greater than 0.4 kPa within a period of 15 minutes. This is a daily occurrence with the exception of the 3rd and 4th day.
Daily occurrences can also be seen where a sudden increase in atmospheric pressure corresponds to a significant drop in the levels of methane released. This increase can be as low as 0.2 kPa in fifteen minutes (Charts 13 and 14), and be associated with a drop of methane levels to 0%, but is in general a series of steps of larger periods of time that can go up to three hours.

Test 7 - Charts 7 and 17 to 24

In this set of data, the first thing to note is the very defined periodic variation of atmospheric pressure. As it can be seen in Chart 7, the atmospheric pressure starts with a downward trend, reaches its lowest point on the afternoon of the 15th, and from here starts an upward trend that lasts up to the night of the 19th and the last two days of the test fall within a new downward trend.
The recorded methane levels follow a sinusoidal like variation with two daily lows occurring in the vicinity of 09:30 and 21:30 while the highs points occur in the vicinity of 02:00 and 15:00.

The short term changes in barometric pressure during this period are less accentuated then on the previous test. The maximum variation within any one day does not exceed 0.5 kPa, and the highest individual change within this period not exceeding 0.3 kPa. Also, there is only one instance when a sudden drop in the level of methane is recorded. This drop takes place on the 16th between 17:00 and 19:00 (Chart 19) and, at the same time, an increase in barometric pressure in the range of 0.3 kPa is recorded. This is the only situation in this test in which the variations in methane level and atmospheric pressure are similar to the situations found in test 1. However, less pronounced increases and decreases in methane level, with the correspondent decreases and increases in atmospheric pressure are virtually a daily occurrence.

The barometric pressure in this test period follows an opposite phase sinusoidal, that is, being at its highest point when methane levels are lowest and at its lowest point when methane levels are high.

Test 8 - Charts 8 and 25 to 37

On this set of results we find drops in atmospheric pressure corresponding with noticeable increases in the levels of methane are virtually a daily occurrence as it can be seen in Charts 25 to 37. The three more accentuated drops occur in the 29th of July at 06:30 and 09:30 (Chart 29), and on the 5th of August at 11:45 and 12:15 (Chart 36). In all three cases a drop in atmospheric pressure of 0.5 kPa in a short time span (max. of 30 min) occurs simultaneously with an increase in methane levels of approximately 1 %.

On the same dates but at different times, we can see that a sudden increase in barometric pressure (approximately 1 kPa on the 29th of July and 0.5 kPa on the 5th of August) occurs simultaneously with a drop in methane levels recorded to values near to zero.

Apart from the more drastic changes in barometric pressure and methane levels the same pattern that was observed in test 2 can be seen: an oscillation of the general attitude of the methane curve that can be characterised by a sine function while the atmospheric pressure function has a step characteristic in an opposite phase to the methane function.

Test 9 - Charts 8A and 38 to 47

During this period, the atmospheric pressure and methane levels kept fairly constant, with almost no sudden variations.

As it can be seen in Chart 42, the exception in the methane curve is the accentuated drop on the 19th to close to 0%, between 07:45 and 08:10 There is no increase in barometric pressure associated with this drop. From 08:10 the level of methane raises steadily, and again there is no associated drop in barometric pressure.

On the atmospheric pressure curve only two noticeable drops are visible: the first on the 17th, between 11:20 and 12:35 (Chart 40) and the second in the 21st between 09:45 and 15:15 (Chart 44). Associated with both these drops are an increase in methane levels in the order of 0.2-0.3%.

The sinusoidal characteristic of the methane curve is again visible in these data, and the atmospheric pressure maintains its step characteristic. An analysis of the daily graphs shows that, as before, the curves are out of phase.

5 - DISCUSSION

As it can be seen from the graphs, the atmospheric pressure has a step characteristic while the methane curves are more erratic and could be characterised by a sine function.
In the methane curve the majority of variations of up to 0.5% in themselves do not seem to be related in any way with atmospheric pressure, although the trend on which these smaller variations occur might be. These variations can be due to changes in the methane content of the air stream passing by the sensor due to turbulence, or simply the normal workings of the mine.
However, the fact that they exist poses serious problems when trying to find a correlation between the two sets of data. The correlation factor in Charts 48 to 50 exemplifies the range of correlation factors for the methane and atmospheric pressure data series, and no meaningful correlation can be found, either to their being none or to being hidden by scatter.

Several methods of analysis were attempted, the first being curve fitting. It was attempted to fit polynomial curves of increasingly higher order to both the methane and the atmospheric pressure curves.
Some of the more successful results of shown in Charts 48 to 50.
Some success was achieved with an attempt to fit a sinusoidal curve to the methane curve, as it can be seen in Chart 51, but any sudden drops in methane concentration rend this method inappropriate for long term analysis.

Smoothing of curves was also attempted, to try to eliminate the perceived more erratic variations, but no positive results were achieved.

Another attempt was made by dividing both the atmospheric pressure and the methane curves variations in groups by size and observing if there is a relation between both variations.
This was done by establishing an arbitrary lower limit bellow which any variation would be regarded as meaningless and separating the variations above this lower limit in groups. The two sets of variations were then plotted against the same time axis and analysed.
Charts 52 to 54 show some of the results of this attempt. In all the charts of this group, Atmospheric Pressure Base and Methane Base represent the lower limits considered.
Only the data of the first tests showed some results. As it can be seen in Chart 52, each variation in atmospheric pressure corresponds to a sudden variation in methane levels.

Charts 53 and 54 are representative of the results obtained when applying the same method to the other sets of data. Although no applicable results were forthcoming, one point that must be mentioned is the high difference between lower limits for atmospheric pressure variation values between these sets of data and the data on Chart 52.

Stripp[1] suggests that natural barometric pressure fluctuations have a relatively insignificant effect on methane monitored. However, he cautions against a too wide interpretation of this result and notes that fan stoppages were found to enhance methane emission flowrates when fans were switched back on, inducing sudden pressure drops. He suggests that is not as much the range of the barometric pressure variation that influences the level of methane in the workings but the time span over which it takes place.
He further refers to the sympathetic relation between variations in atmospheric pressure and methane emission from gas reservoirs at or near to atmospheric pressure, and suggests that the gas ingress associated with the fan stoppages incidents originated from gas reservoirs of this type.

Van Zyl[2] made an analysis of the relation between barometric pressure and gas related incidents. He identified the most likely situation for a methane related incident as the time after a diurnal barometric pressure drop of 0.2-0.3 kPa in an average daily barometric downward trend. He also predicted that the likelihood of the accident occurring is higher between 11:00 and 15:00.

The origin of the variations of atmospheric pressure is not known at this stage, but the fact that it appears to be associated with a clearly noticeable short term methane variation agrees with the results obtained by Stripp.

6 - CONCLUSIONS AND FUTURE WORK

- **Short Term Variations**

The analysis of the test done in Site A, (Test 1) shows that, for this site and during the periods recorded, for each atmospheric pressure variation of 0.2 kPa within 15 minutes a noticeable variation in methane level takes place.
For the tests in Site B (Tests 7,8 and 9) similar results are found. Although the values differ from test to test, it can be said that for a variation in atmospheric pressure in the range 0.2 to 0.4 kPa within a time span of 30 minutes or less there is a high probability that a variation in methane levels in the opposite direction will occur. This probability increases in the same direction as the size of the atmospheric pressure variation and in the opposite direction of the time span. This is, the higher the

atmospheric pressure variation and the shorter the time span, the higher will be the probability of a variation in methane level be associated with a variation in atmospheric pressure.
This variation does not occurs during the other tests, or at least not as clearly defined. There are, however, in all the other tests instances where a sudden variation in atmospheric pressure was associated with a variation in methane level that does not fit into a more general pattern

- **Long Term Variations**

On a daily basis, the methane levels at the recording locations, seem to follow a sinusoidal type of curve, except for the sudden variations already mentioned. Two daily lows and two highs can be clearly observed for both methane and atmospheric pressure levels each day.
The methane curve has an attitude opposite to the general attitude of the atmospheric pressure curve, meaning, the steady increase of pressure appears to be associated with an equally steady decrease in methane levels and inversely.

- **Origin of methane**

One question that remains open, of course, is the origin of the methane detected.
At this stage, no solutions are available, but several hypothesis are possible:

- Methane in the goaf leaking through the seals
- Methane in areas barricaded or bratticed of, where ventilation flow is enough to keep it below the standard limits, but can "spill" into other areas due to a sudden drop in barometric pressure.
- Methane in the fault systems of the coal itself.

More tests need to be done with multiple test units in different locations and environments as to assure the representativity of any conclusions achieved in a general colliery domain, while trying to determine with more precision the laws that govern the overall influence of atmospheric pressure in the levels of methane in the ventilation flow.

REFERENCES

[1] Graham Peter Stripp, "Methane emission characteristics of South African coal seam strata", PhD thesis, University of Witwatesrand, Johannesburg, 1989

[2] Van Zyl FJ and Cook, AP , "A Preliminary Review of the Influence of Barometric Pressure on 35 Methane Related Incidents", Interim Report, CSIR Division of Mining Technology, June 1994

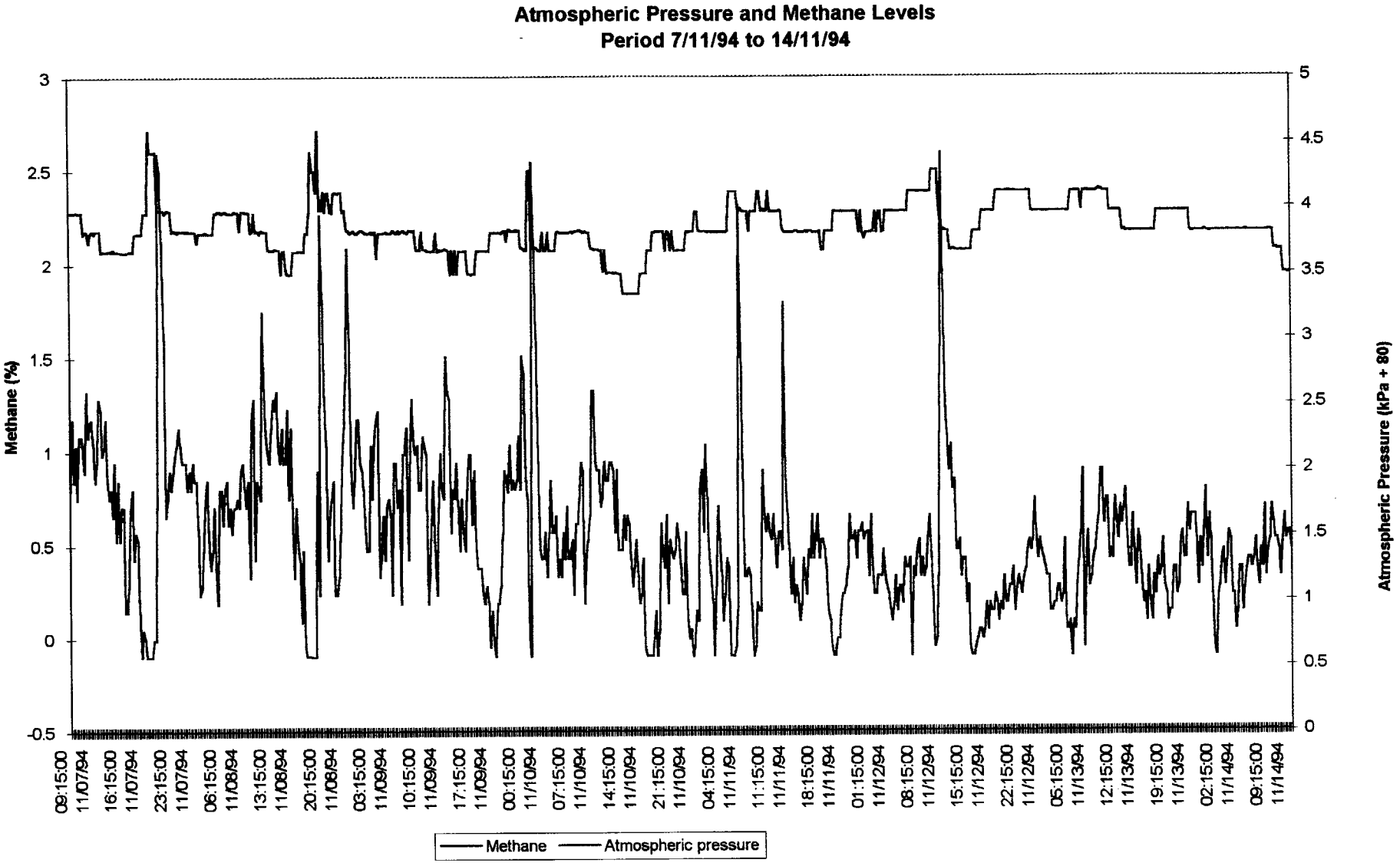
Atmospheric Pressure and Methane Levels
Period 7/11/94 to 14/11/94
Methane (%)
Atmospheric Pressure (kPa + 80)
3
2.5
2
1.5
1
0.5
0
-0.5
5
4.5
4
3.5
3
2.5
2
1.5
1
0.5
0
09:15:00 11/07/94
16:15:00 11/07/94
23:15:00 11/07/94
06:15:00 11/08/94
13:15:00 11/08/94
20:15:00 11/08/94
03:15:00 11/09/94
10:15:00 11/09/94
17:15:00 11/09/94
00:15:00 11/10/94
07:15:00 11/10/94
14:15:00 11/10/94
21:15:00 11/10/94
04:15:00 11/11/94
11:15:00 11/11/94
18:15:00 11/11/94
01:15:00 11/12/94
08:15:00 11/12/94
15:15:00 11/12/94
22:15:00 11/12/94
05:15:00 11/13/94
12:15:00 11/13/94
19:15:00 11/13/94
02:15:00 11/14/94
09:15:00 11/14/94
Methane
Atmospheric pressure

Chart 1

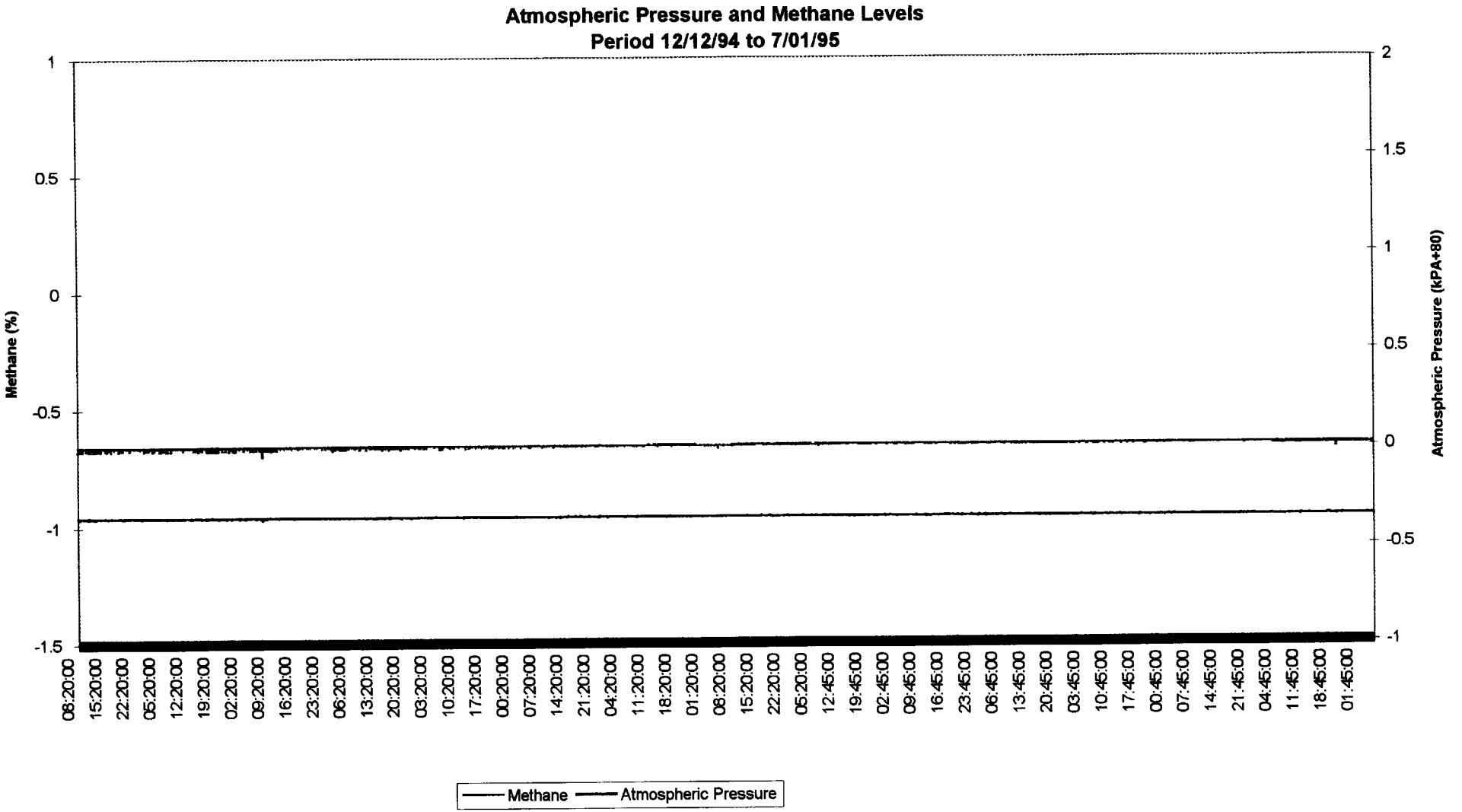
Atmospheric Pressure and Methane Levels
Period 12/12/94 to 7/01/95
Methane (%)
Atmospheric Pressure (kPA+80)
1
0.5
0
-0.5
-1
-1.5
2
1.5
1
0.5
0
-0.5
-1
08:20:00
15:20:00
22:20:00
05:20:00
12:20:00
19:20:00
02:20:00
09:20:00
16:20:00
23:20:00
06:20:00
13:20:00
20:20:00
03:20:00
10:20:00
17:20:00
00:20:00
07:20:00
14:20:00
21:20:00
04:20:00
11:20:00
18:20:00
01:20:00
08:20:00
15:20:00
22:20:00
05:20:00
12:45:00
19:45:00
02:45:00
09:45:00
16:45:00
23:45:00
06:45:00
13:45:00
20:45:00
03:45:00
10:45:00
17:45:00
00:45:00
07:45:00
14:45:00
21:45:00
04:45:00
11:45:00
18:45:00
01:45:00
Methane
Atmospheric Pressure

Chart 2

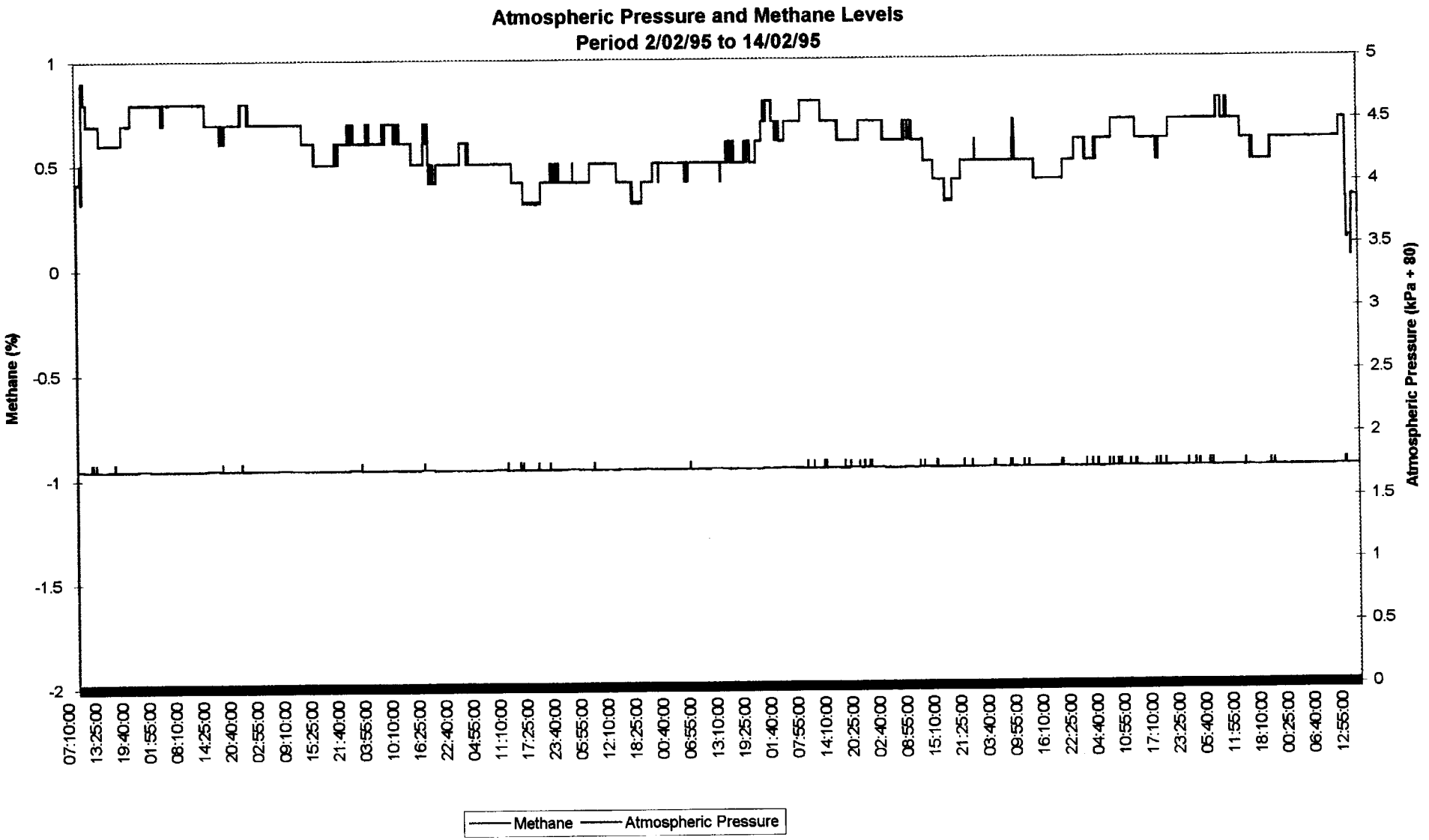
Atmospheric Pressure and Methane Levels
Period 2/02/95 to 14/02/95
Methane (%)
Atmospheric Pressure (kPa + 80)
1
0.5
0
-0.5
-1
-1.5
-2
5
4.5
4
3.5
3
2.5
2
1.5
1
0.5
0
07:10:00
13:25:00
19:40:00
01:55:00
08:10:00
14:25:00
20:40:00
02:55:00
09:10:00
15:25:00
21:40:00
03:55:00
10:10:00
16:25:00
22:40:00
04:55:00
11:10:00
17:25:00
23:40:00
05:55:00
12:10:00
18:25:00
00:40:00
06:55:00
13:10:00
19:25:00
01:40:00
07:55:00
14:10:00
20:25:00
02:40:00
08:55:00
15:10:00
21:25:00
03:40:00
09:55:00
16:10:00
22:25:00
04:40:00
10:55:00
17:10:00
23:25:00
05:40:00
11:55:00
18:10:00
00:25:00
06:40:00
12:55:00
Methane
Atmospheric Pressure

Chart 3

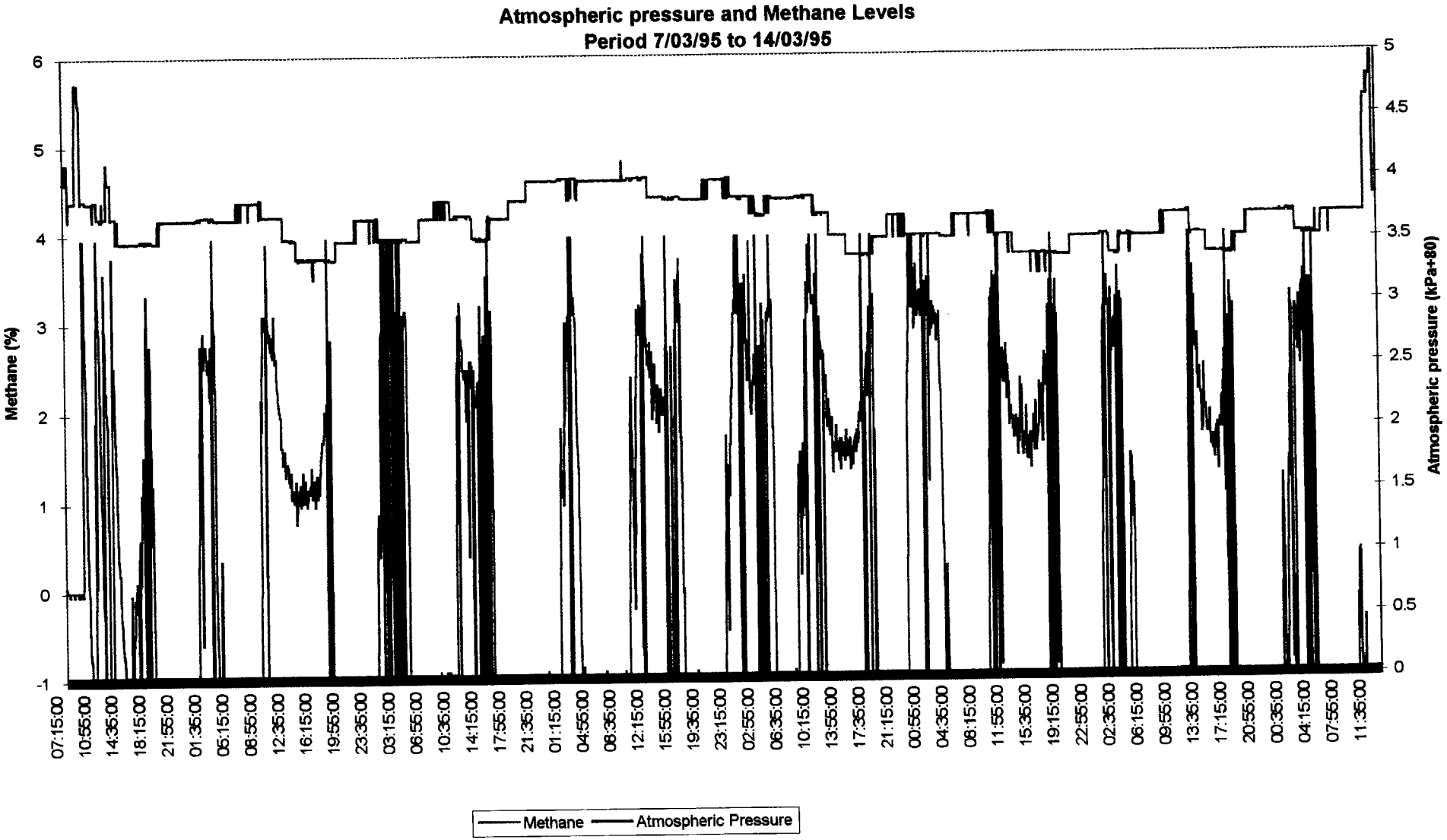
Atmospheric pressure and Methane Levels
Period 7/03/95 to 14/03/95
Methane (%)
Atmospheric pressure (kPa+80)
6
5
4
3
2
1
0
-1
5
4.5
4
3.5
3
2.5
2
1.5
1
0.5
0
07:15:00
10:55:00
14:35:00
18:15:00
21:55:00
01:35:00
05:15:00
08:55:00
12:35:00
16:15:00
19:55:00
23:35:00
03:15:00
06:55:00
10:35:00
14:15:00
17:55:00
21:35:00
01:15:00
04:55:00
08:35:00
12:15:00
15:55:00
19:35:00
23:15:00
02:55:00
06:35:00
10:15:00
13:55:00
17:35:00
21:15:00
00:55:00
04:35:00
08:15:00
11:55:00
15:35:00
19:15:00
22:55:00
02:35:00
06:15:00
09:55:00
13:35:00
17:15:00
20:55:00
00:35:00
04:15:00
07:55:00
11:35:00
Methane
Atmospheric Pressure

Chart 4

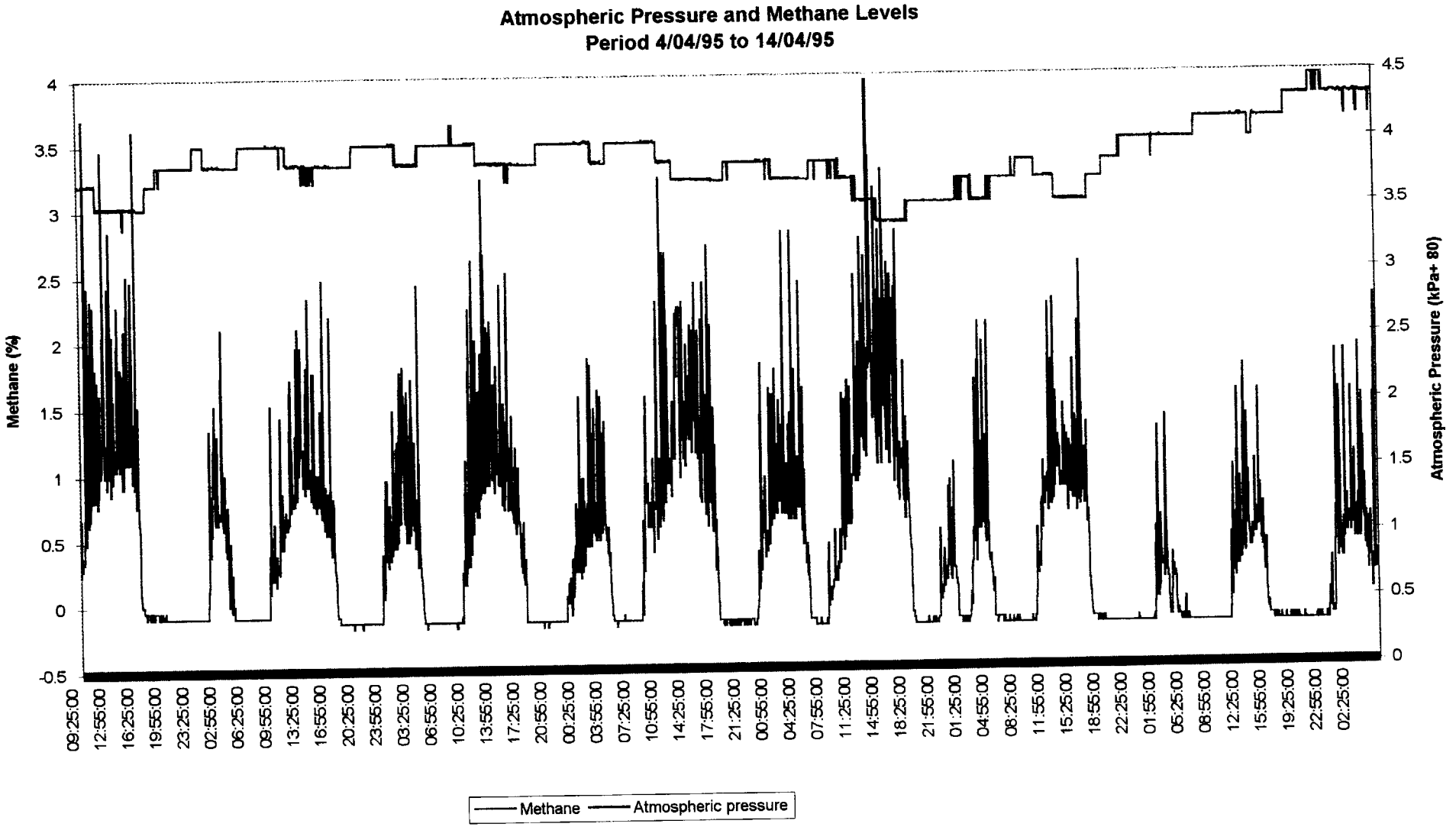
Atmospheric Pressure and Methane Levels
Period 4/04/95 to 14/04/95
Methane (%)
Atmospheric Pressure (kPa+ 80)
4
3.5
3
2.5
2
1.5
1
0.5
0
-0.5
4.5
09:25:00
12:55:00
16:25:00
19:55:00
23:25:00
02:55:00
06:25:00
09:55:00
13:25:00
16:55:00
20:25:00
23:55:00
03:25:00
06:55:00
10:25:00
13:55:00
17:25:00
20:55:00
00:25:00
03:55:00
07:25:00
10:55:00
14:25:00
17:55:00
21:25:00
00:55:00
04:25:00
07:55:00
11:25:00
14:55:00
18:25:00
21:55:00
01:25:00
04:55:00
08:25:00
11:55:00
15:25:00
18:55:00
22:25:00
01:55:00
05:25:00
08:55:00
12:25:00
15:55:00
19:25:00
22:55:00
02:25:00
Methane
Atmospheric pressure

Chart 5

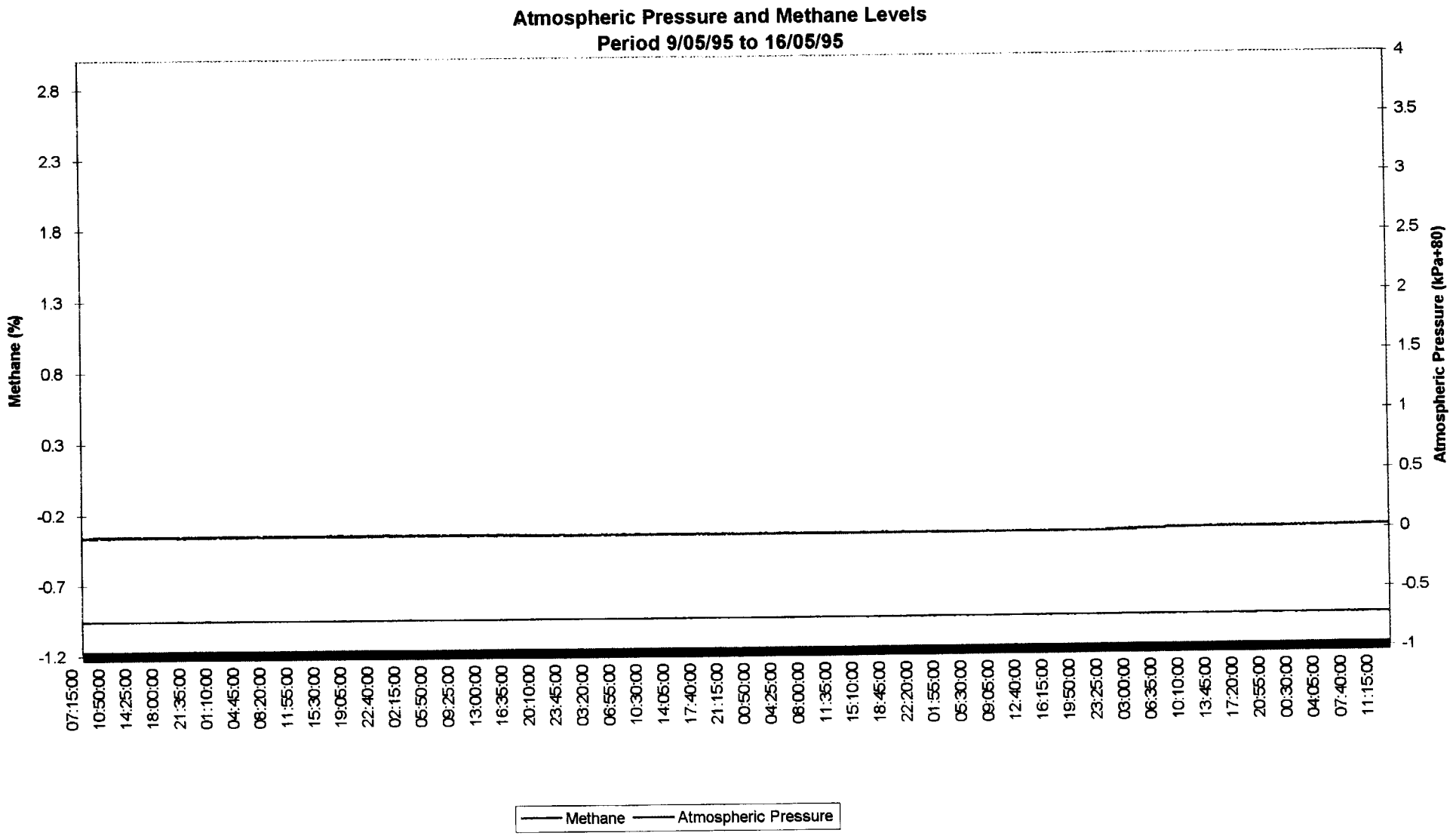
Atmospheric Pressure and Methane Levels
Period 9/05/95 to 16/05/95
Methane (%)
2.8
2.3
1.8
1.3
0.8
0.3
-0.2
-0.7
-1.2
Atmospheric Pressure (kPa+80)
4
3.5
3
2.5
2
1.5
1
0.5
0
-0.5
-1
07:15:00
10:50:00
14:25:00
18:00:00
21:35:00
01:10:00
04:45:00
08:20:00
11:55:00
15:30:00
19:05:00
22:40:00
02:15:00
05:50:00
09:25:00
13:00:00
16:35:00
20:10:00
23:45:00
03:20:00
06:55:00
10:30:00
14:05:00
17:40:00
21:15:00
00:50:00
04:25:00
08:00:00
11:35:00
15:10:00
18:45:00
22:20:00
01:55:00
05:30:00
09:05:00
12:40:00
16:15:00
19:50:00
23:25:00
03:00:00
06:35:00
10:10:00
13:45:00
17:20:00
20:55:00
00:30:00
04:05:00
07:40:00
11:15:00
Methane
Atmospheric Pressure

Chart 6

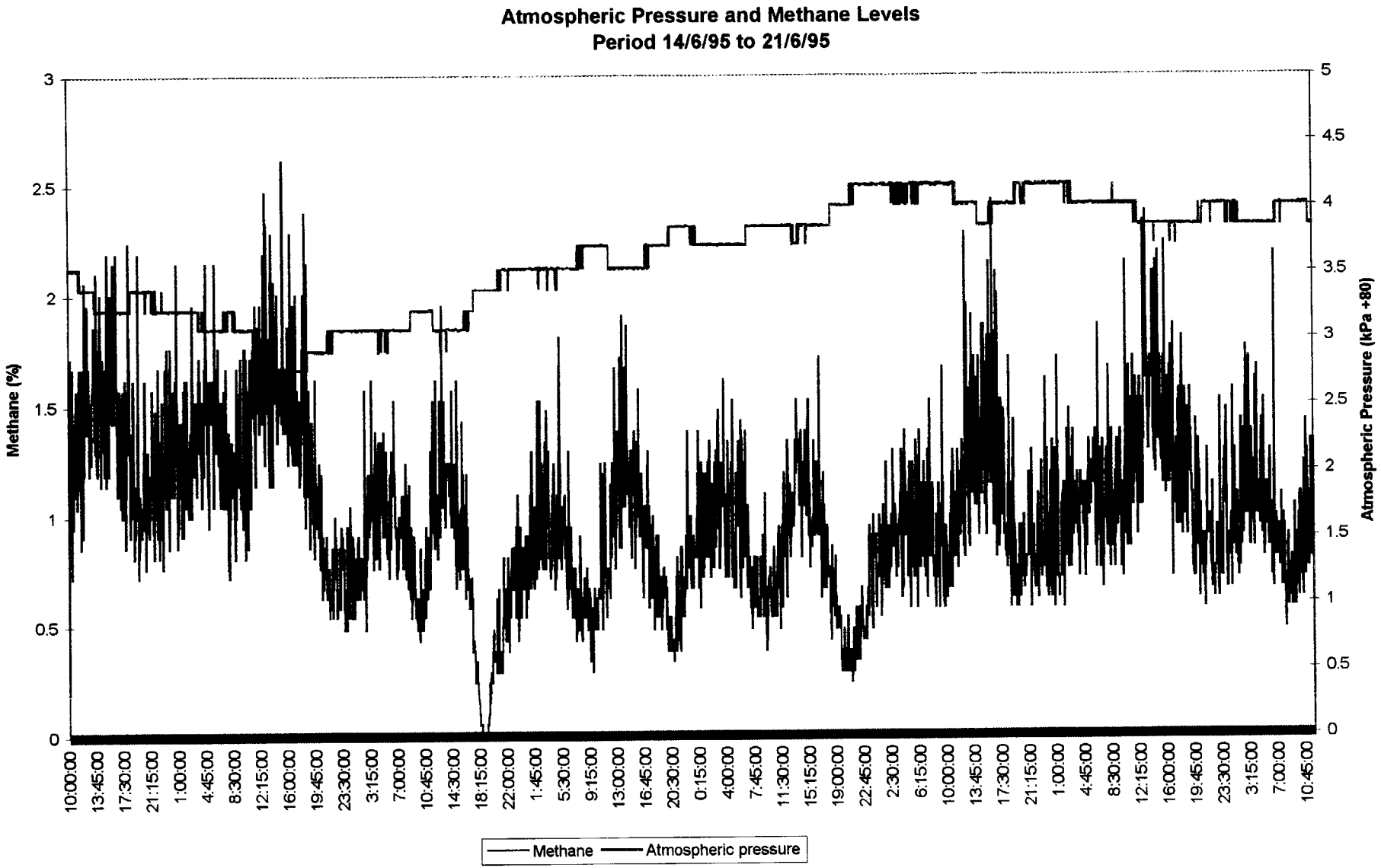
Atmospheric Pressure and Methane Levels
Period 14/6/95 to 21/6/95
Methane (%)
Atmospheric Pressure (kPa +80)
0
0.5
1
1.5
2
2.5
3
0
0.5
1
1.5
2
2.5
3
3.5
4
4.5
5
10:00:00
13:45:00
17:30:00
21:15:00
1:00:00
4:45:00
8:30:00
12:15:00
16:00:00
19:45:00
23:30:00
3:15:00
7:00:00
10:45:00
14:30:00
18:15:00
22:00:00
1:45:00
5:30:00
9:15:00
13:00:00
16:45:00
20:30:00
0:15:00
4:00:00
7:45:00
11:30:00
15:15:00
19:00:00
22:45:00
2:30:00
6:15:00
10:00:00
13:45:00
17:30:00
21:15:00
1:00:00
4:45:00
8:30:00
12:15:00
16:00:00
19:45:00
23:30:00
3:15:00
7:00:00
10:45:00
Methane
Atmospheric pressure

Chart 7

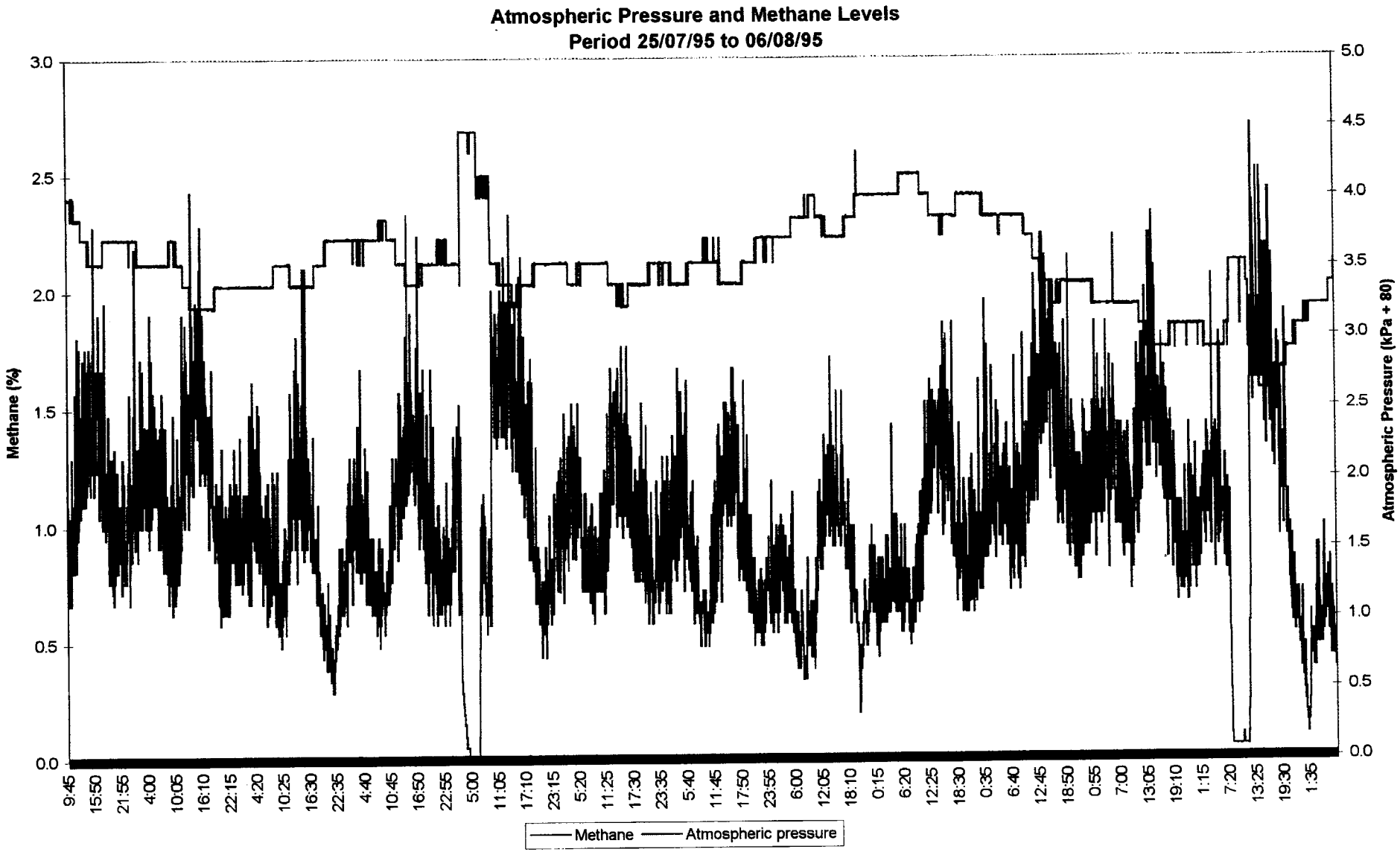
Atmospheric Pressure and Methane Levels
Period 25/07/95 to 06/08/95
Methane (%)
Atmospheric Pressure (kPa + 80)
3.0
2.5
2.0
1.5
1.0
0.5
0.0
5.0
4.5
4.0
3.5
3.0
2.5
2.0
1.5
1.0
0.5
0.0
9:45
15:50
21:55
4:00
10:05
16:10
22:15
4:20
10:25
16:30
22:35
4:40
10:45
16:50
22:55
5:00
11:05
17:10
23:15
5:20
11:25
17:30
23:35
5:40
11:45
17:50
23:55
6:00
12:05
18:10
0:15
6:20
12:25
18:30
0:35
6:40
12:45
18:50
0:55
7:00
13:05
19:10
1:15
7:20
13:25
19:30
1:35
Methane
Atmospheric pressure

Chart 8

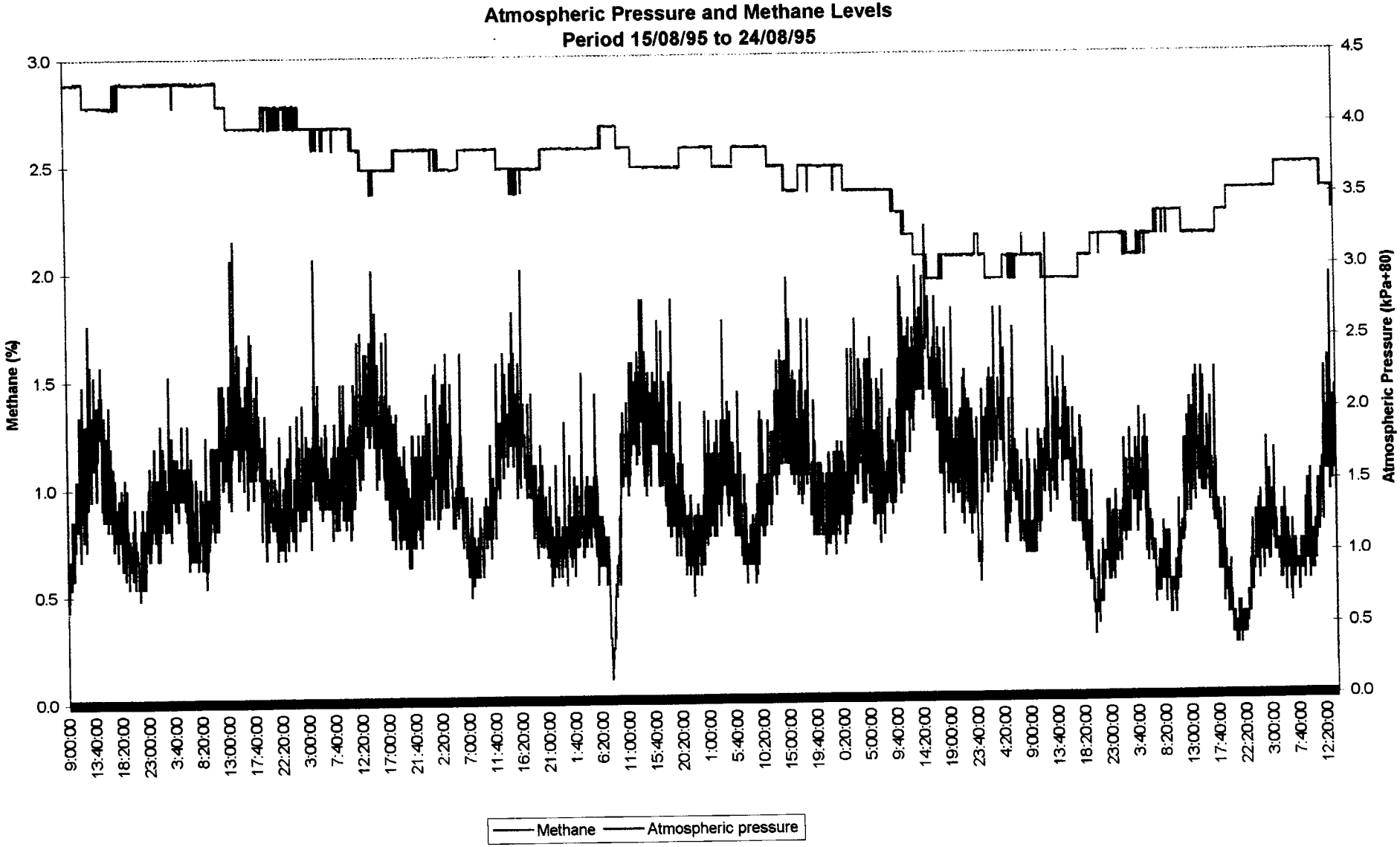
Atmospheric Pressure and Methane Levels
Period 15/08/95 to 24/08/95
Methane (%)
Atmospheric Pressure (kPa+80)
3.0
2.5
2.0
1.5
1.0
0.5
0.0
4.5
4.0
3.5
3.0
2.5
2.0
1.5
1.0
0.5
0.0
9:00:00
13:40:00
18:20:00
23:00:00
3:40:00
8:20:00
13:00:00
17:40:00
22:20:00
3:00:00
7:40:00
12:20:00
17:00:00
21:40:00
2:20:00
7:00:00
11:40:00
16:20:00
21:00:00
1:40:00
6:20:00
11:00:00
15:40:00
20:20:00
1:00:00
5:40:00
10:20:00
15:00:00
19:40:00
0:20:00
5:00:00
9:40:00
14:20:00
19:00:00
23:40:00
4:20:00
9:00:00
13:40:00
18:20:00
23:00:00
3:40:00
8:20:00
13:00:00
17:40:00
22:20:00
3:00:00
7:40:00
12:20:00
Methane
Atmospheric pressure

Chart 8A

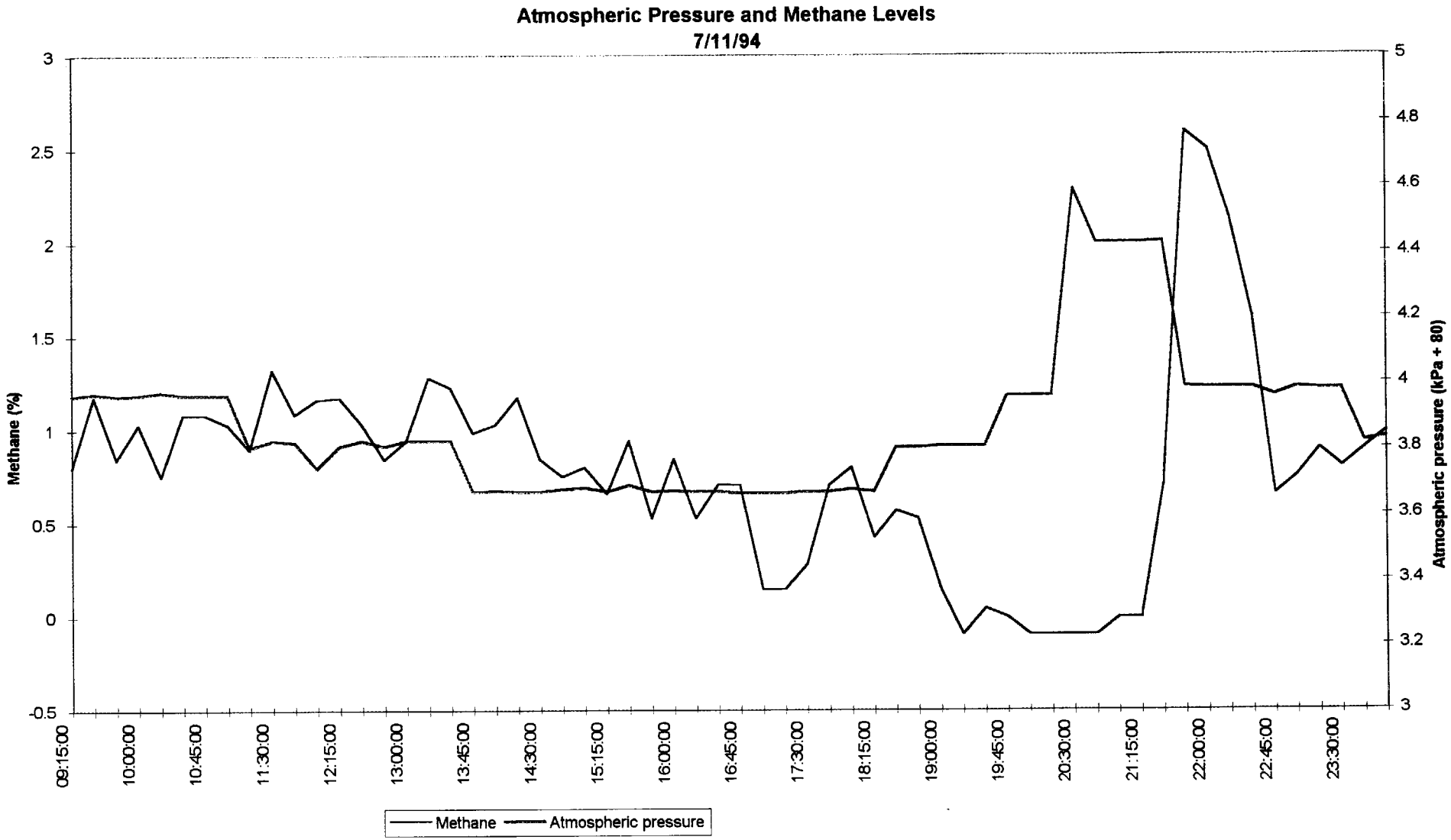
Atmospheric Pressure and Methane Levels
7/11/94
Methane (%)
Atmospheric pressure (kPa + 80)
3
2.5
2
1.5
1
0.5
0
-0.5
5
4.8
4.6
4.4
4.2
4
3.8
3.6
3.4
3.2
3
09:15:00
10:00:00
10:45:00
11:30:00
12:15:00
13:00:00
13:45:00
14:30:00
15:15:00
16:00:00
16:45:00
17:30:00
18:15:00
19:00:00
19:45:00
20:30:00
21:15:00
22:00:00
22:45:00
23:30:00
Methane
Atmospheric pressure

Chart 9

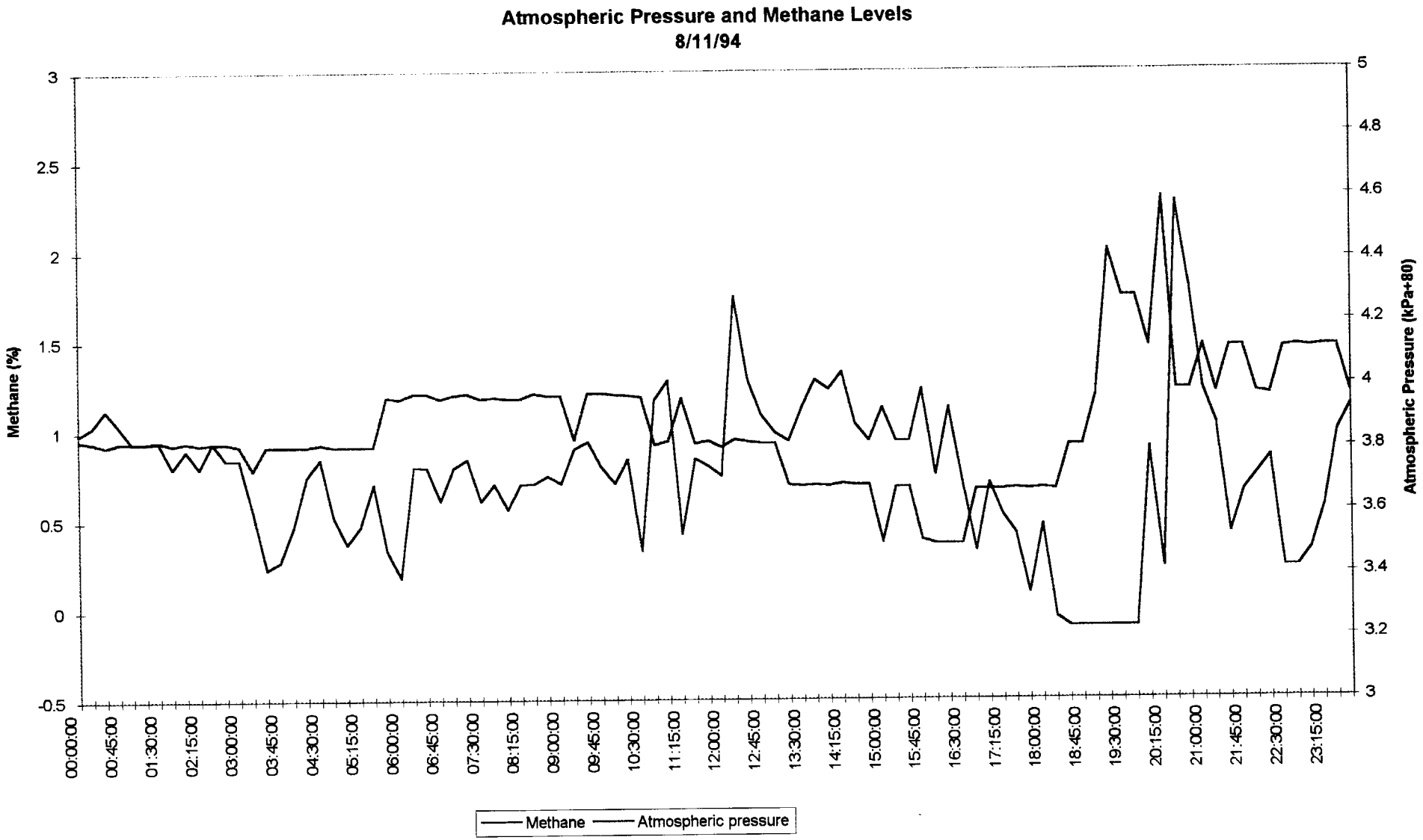
Atmospheric Pressure and Methane Levels
8/11/94
Methane (%)
Atmospheric Pressure (kPa+80)
3
2.5
2
1.5
1
0.5
0
-0.5
5
4.8
4.6
4.4
4.2
4
3.8
3.6
3.4
3.2
3
00:00:00
00:45:00
01:30:00
02:15:00
03:00:00
03:45:00
04:30:00
05:15:00
06:00:00
06:45:00
07:30:00
08:15:00
09:00:00
09:45:00
10:30:00
11:15:00
12:00:00
12:45:00
13:30:00
14:15:00
15:00:00
15:45:00
16:30:00
17:15:00
18:00:00
18:45:00
19:30:00
20:15:00
21:00:00
21:45:00
22:30:00
23:15:00
Methane
Atmospheric pressure

Chart 10

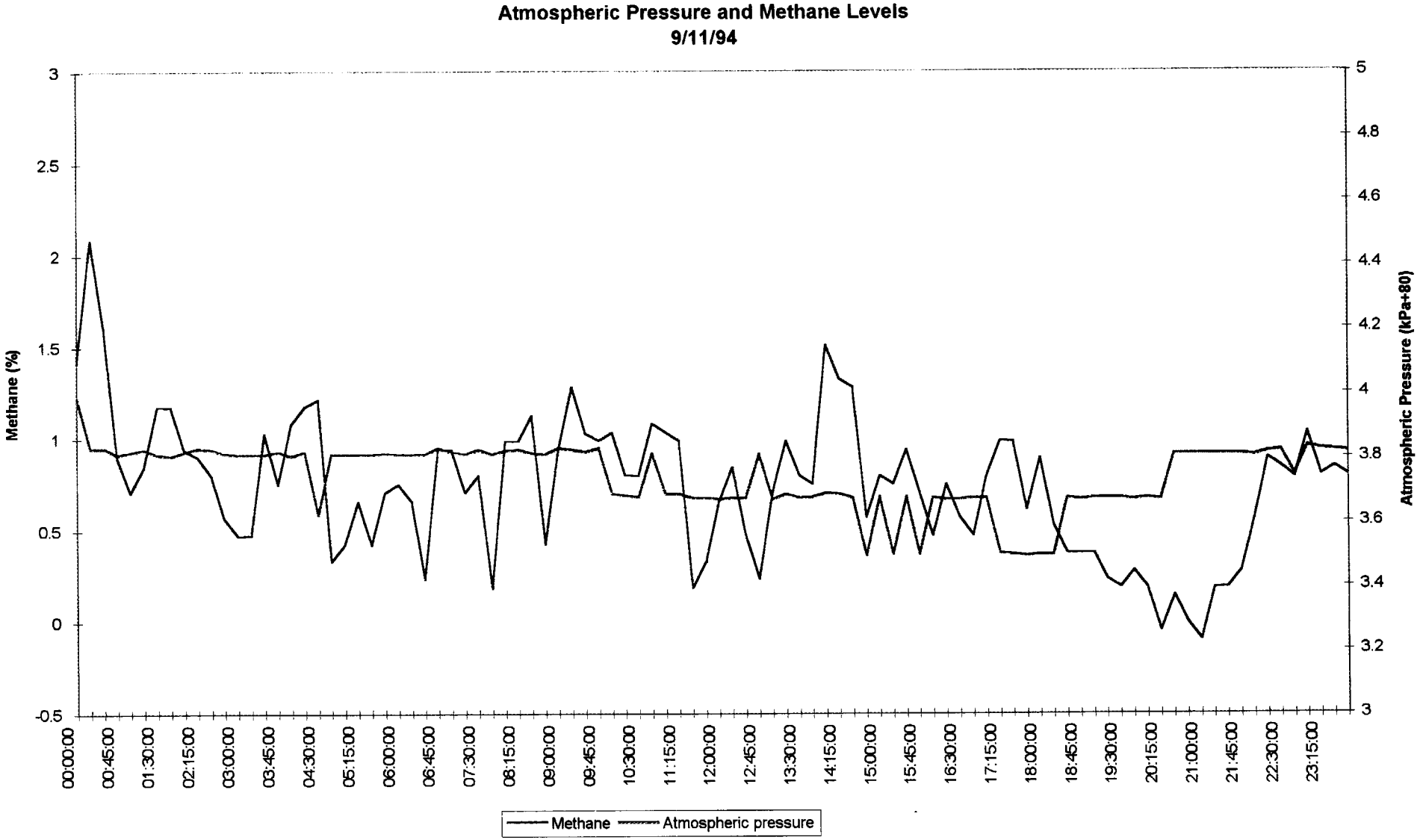
Atmospheric Pressure and Methane Levels
9/11/94
Methane (%)
Atmospheric Pressure (kPa+80)
3
2.5
2
1.5
1
0.5
0
-0.5
5
4.8
4.6
4.4
4.2
4
3.8
3.6
3.4
3.2
3
00:00:00
00:45:00
01:30:00
02:15:00
03:00:00
03:45:00
04:30:00
05:15:00
06:00:00
06:45:00
07:30:00
08:15:00
09:00:00
09:45:00
10:30:00
11:15:00
12:00:00
12:45:00
13:30:00
14:15:00
15:00:00
15:45:00
16:30:00
17:15:00
18:00:00
18:45:00
19:30:00
20:15:00
21:00:00
21:45:00
22:30:00
23:15:00
Methane
Atmospheric pressure

Chart 11

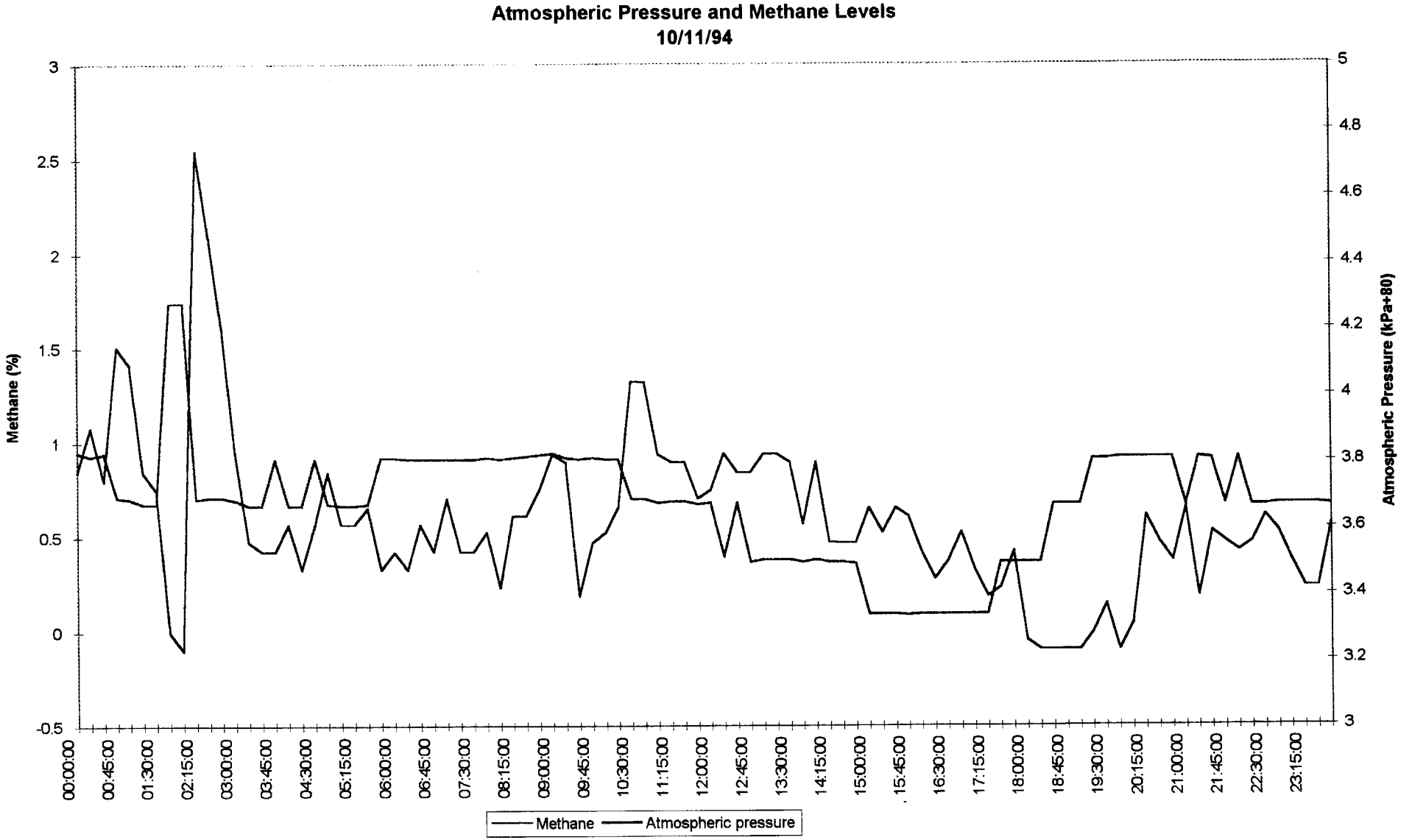
Atmospheric Pressure and Methane Levels
10/11/94
Methane (%)
Atmospheric Pressure (kPa+80)
3
2.5
2
1.5
1
0.5
0
-0.5
5
4.8
4.6
4.4
4.2
4
3.8
3.6
3.4
3.2
3
00:00:00
00:45:00
01:30:00
02:15:00
03:00:00
03:45:00
04:30:00
05:15:00
06:00:00
06:45:00
07:30:00
08:15:00
09:00:00
09:45:00
10:30:00
11:15:00
12:00:00
12:45:00
13:30:00
14:15:00
15:00:00
15:45:00
16:30:00
17:15:00
18:00:00
18:45:00
19:30:00
20:15:00
21:00:00
21:45:00
22:30:00
23:15:00
Methane
Atmospheric pressure

Chart12

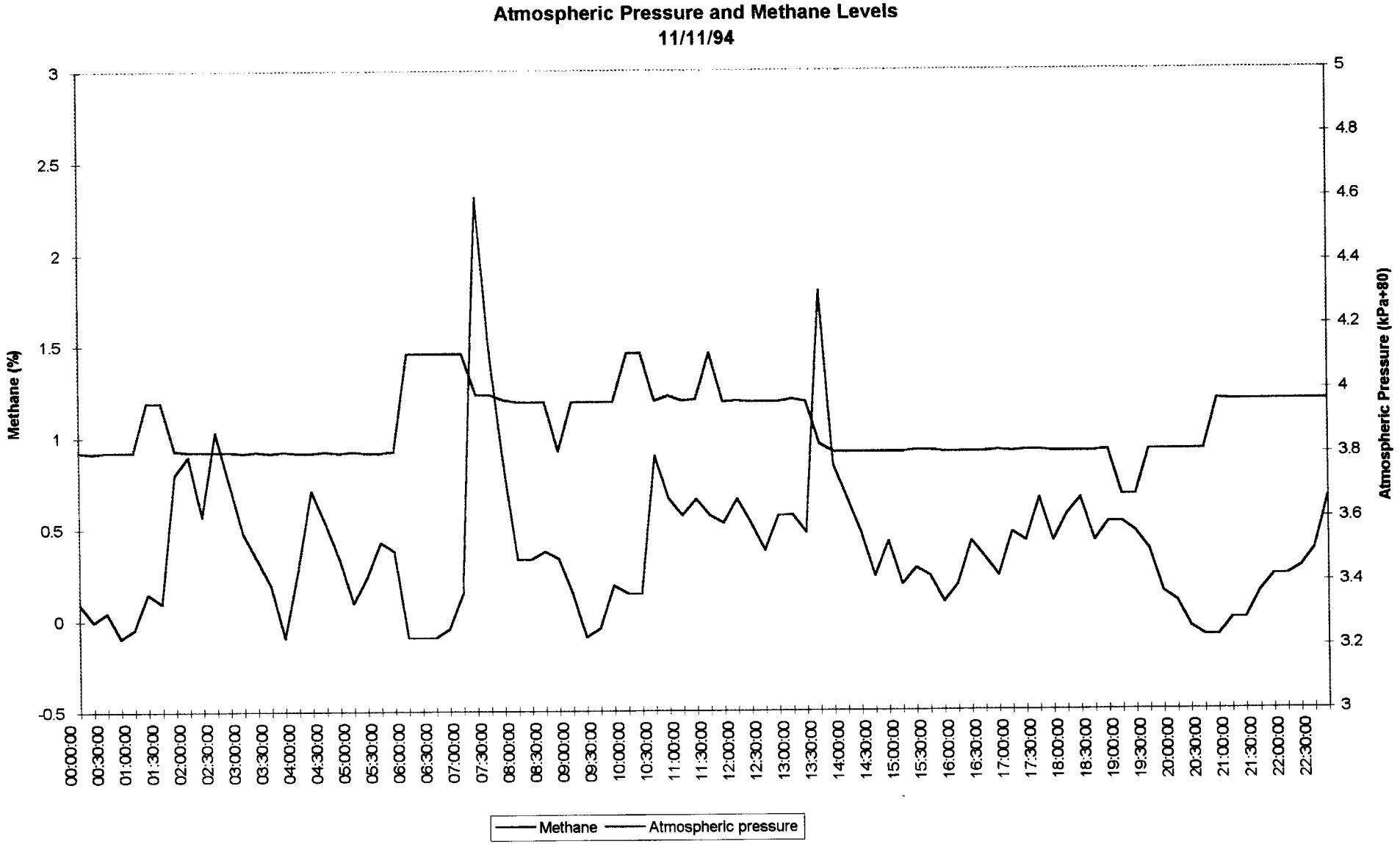
Atmospheric Pressure and Methane Levels
11/11/94
Methane (%)
Atmospheric Pressure (kPa+80)
3
2.5
2
1.5
1
0.5
0
-0.5
5
4.8
4.6
4.4
4.2
4
3.8
3.6
3.4
3.2
3
00:00:00
00:30:00
01:00:00
01:30:00
02:00:00
02:30:00
03:00:00
03:30:00
04:00:00
04:30:00
05:00:00
05:30:00
06:00:00
06:30:00
07:00:00
07:30:00
08:00:00
08:30:00
09:00:00
09:30:00
10:00:00
10:30:00
11:00:00
11:30:00
12:00:00
12:30:00
13:00:00
13:30:00
14:00:00
14:30:00
15:00:00
15:30:00
16:00:00
16:30:00
17:00:00
17:30:00
18:00:00
18:30:00
19:00:00
19:30:00
20:00:00
20:30:00
21:00:00
21:30:00
22:00:00
22:30:00
Methane
Atmospheric pressure

Chart 13

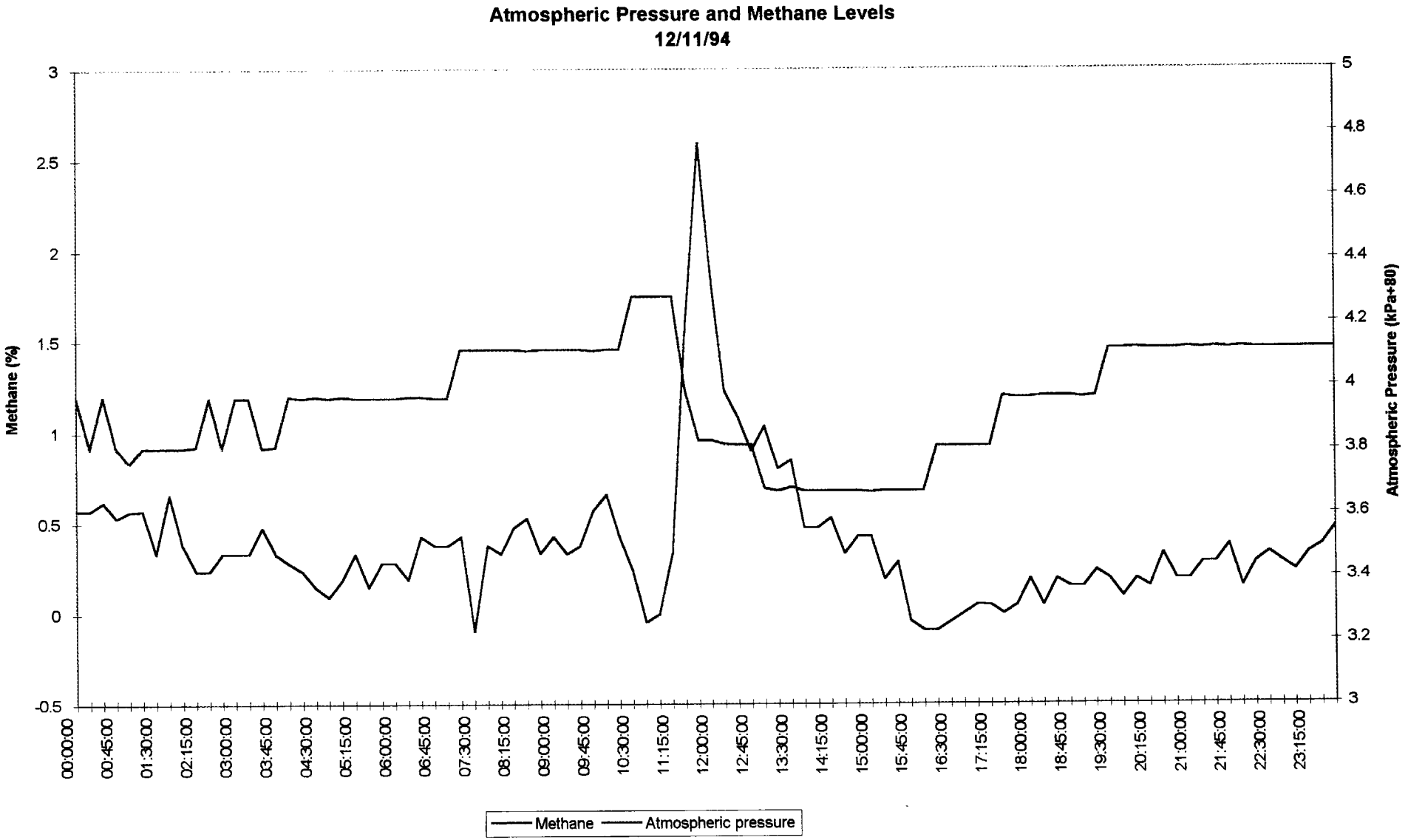
Atmospheric Pressure and Methane Levels
12/11/94
Methane (%)
Atmospheric Pressure (kPa+80)
3
2.5
2
1.5
1
0.5
0
-0.5
5
4.8
4.6
4.4
4.2
4
3.8
3.6
3.4
3.2
3
00:00:00
00:45:00
01:30:00
02:15:00
03:00:00
03:45:00
04:30:00
05:15:00
06:00:00
06:45:00
07:30:00
08:15:00
09:00:00
09:45:00
10:30:00
11:15:00
12:00:00
12:45:00
13:30:00
14:15:00
15:00:00
15:45:00
16:30:00
17:15:00
18:00:00
18:45:00
19:30:00
20:15:00
21:00:00
21:45:00
22:30:00
23:15:00
Methane
Atmospheric pressure

Chart 14

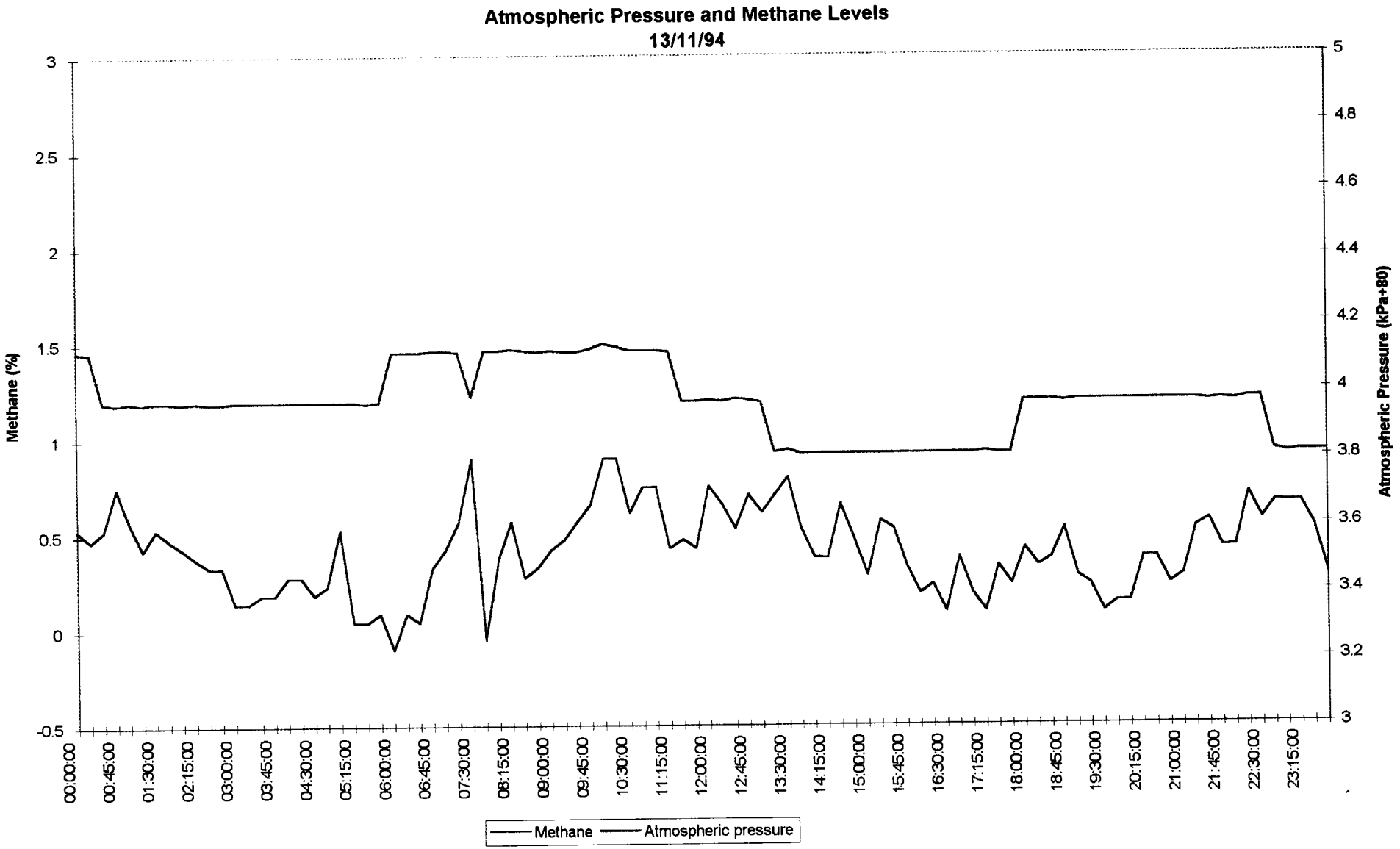
Atmospheric Pressure and Methane Levels
13/11/94
Methane (%)
Atmospheric Pressure (kPa+80)
3
2.5
2
1.5
1
0.5
0
-0.5
5
4.8
4.6
4.4
4.2
4
3.8
3.6
3.4
3.2
3
00:00:00
00:45:00
01:30:00
02:15:00
03:00:00
03:45:00
04:30:00
05:15:00
06:00:00
06:45:00
07:30:00
08:15:00
09:00:00
09:45:00
10:30:00
11:15:00
12:00:00
12:45:00
13:30:00
14:15:00
15:00:00
15:45:00
16:30:00
17:15:00
18:00:00
18:45:00
19:30:00
20:15:00
21:00:00
21:45:00
22:30:00
23:15:00
Methane
Atmospheric pressure

Chart 15

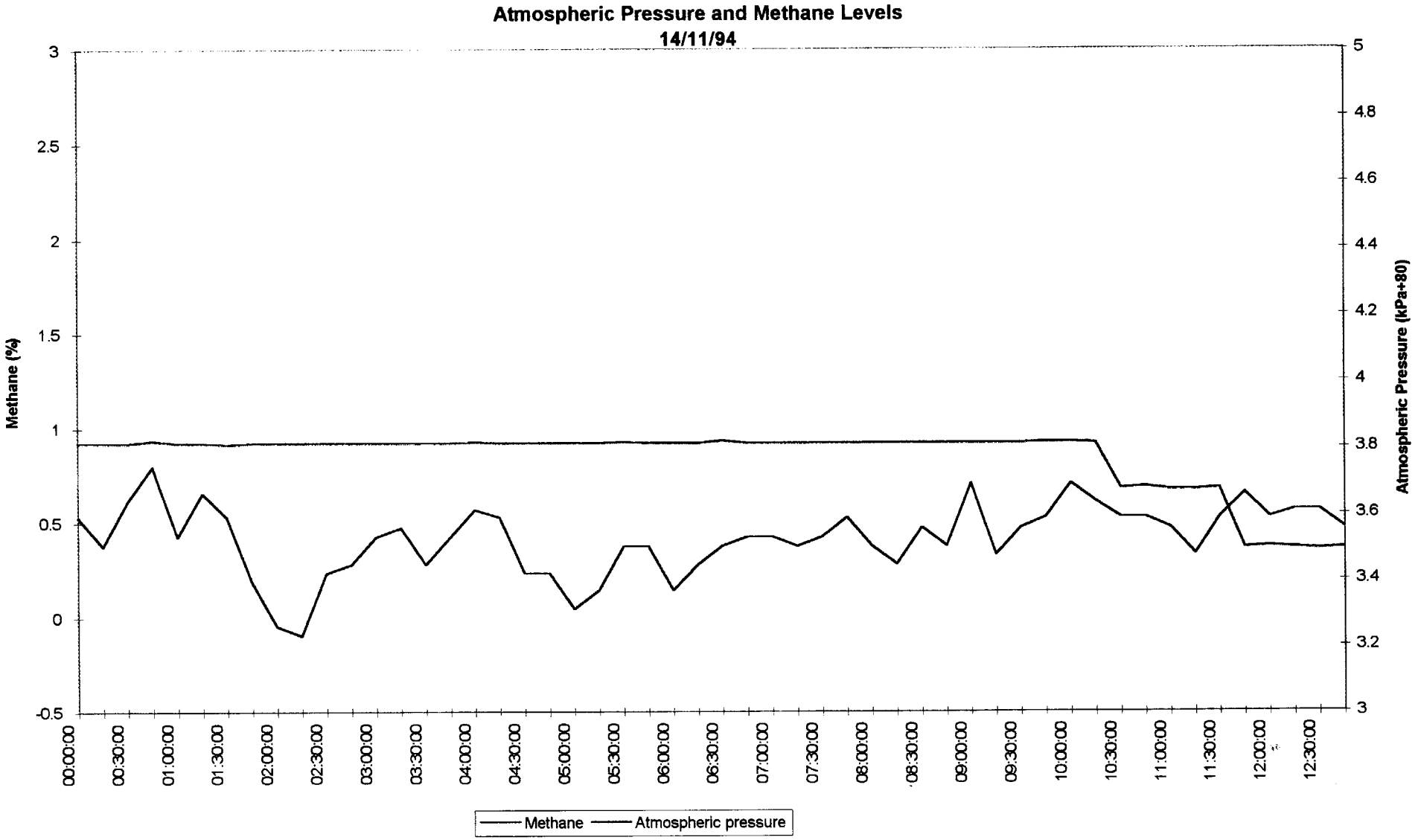
Atmospheric Pressure and Methane Levels
14/11/94
Methane (%)
Atmospheric Pressure (kPa+80)
3
2.5
2
1.5
1
0.5
0
-0.5
5
4.8
4.6
4.4
4.2
4
3.8
3.6
3.4
3.2
3
00:00:00
00:30:00
01:00:00
01:30:00
02:00:00
02:30:00
03:00:00
03:30:00
04:00:00
04:30:00
05:00:00
05:30:00
06:00:00
06:30:00
07:00:00
07:30:00
08:00:00
08:30:00
09:00:00
09:30:00
10:00:00
10:30:00
11:00:00
11:30:00
12:00:00
12:30:00
Methane
Atmospheric pressure

Chart 16

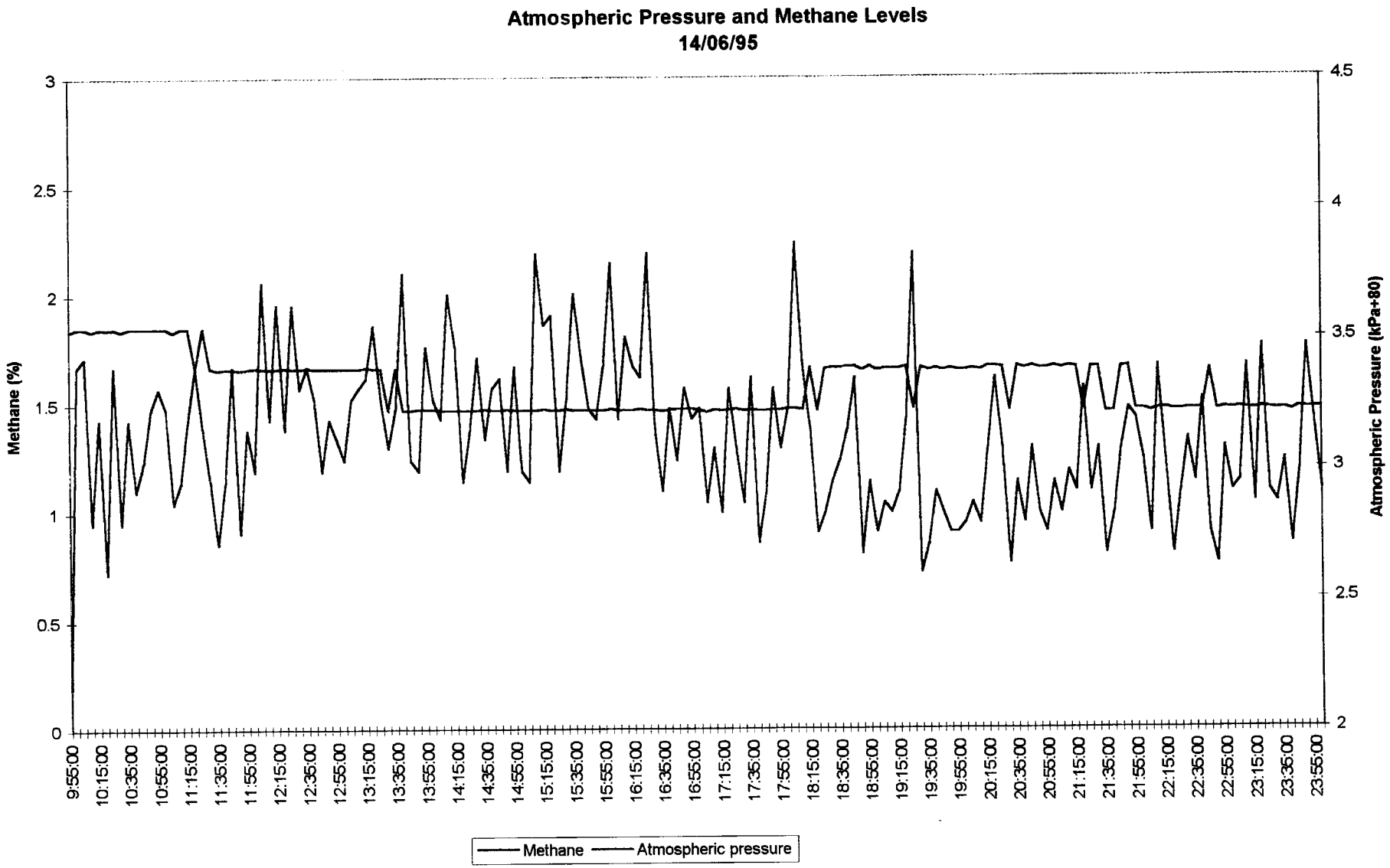
Atmospheric Pressure and Methane Levels
14/06/95
Methane (%)
Atmospheric Pressure (kPa+80)
3
2.5
2
1.5
1
0.5
0
4.5
4
3.5
3
2.5
2
9:55:00
10:15:00
10:35:00
10:55:00
11:15:00
11:35:00
11:55:00
12:15:00
12:35:00
12:55:00
13:15:00
13:35:00
13:55:00
14:15:00
14:35:00
14:55:00
15:15:00
15:35:00
15:55:00
16:15:00
16:35:00
16:55:00
17:15:00
17:35:00
17:55:00
18:15:00
18:35:00
18:55:00
19:15:00
19:35:00
19:55:00
20:15:00
20:35:00
20:55:00
21:15:00
21:35:00
21:55:00
22:15:00
22:35:00
22:55:00
23:15:00
23:35:00
23:55:00
Methane
Atmospheric pressure

Chart 17

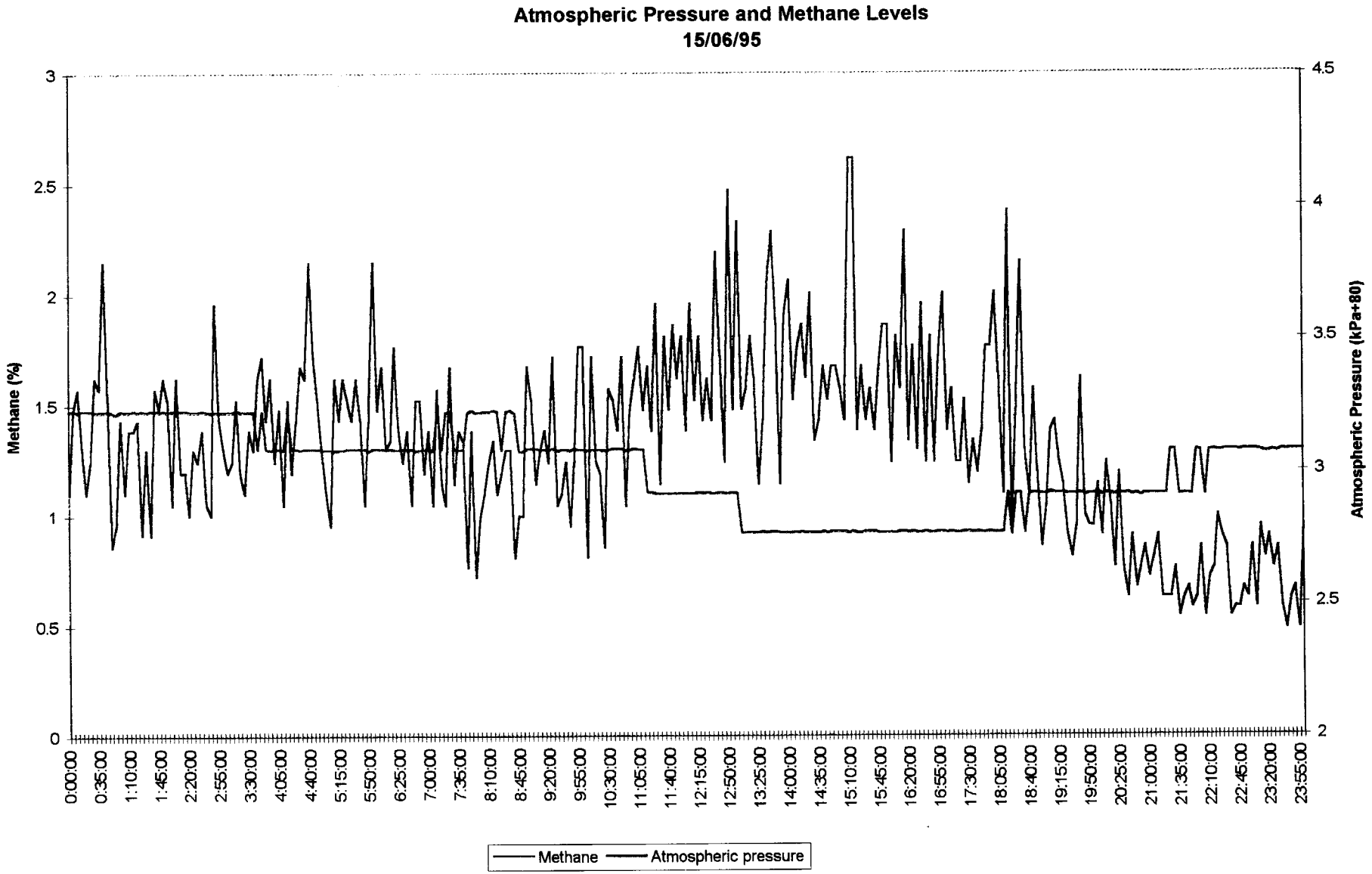
Atmospheric Pressure and Methane Levels
15/06/95
Methane (%)
Atmospheric Pressure (kPa+80)
3
2.5
2
1.5
1
0.5
0
4.5
4
3.5
3
2.5
2
0:00:00
0:35:00
1:10:00
1:45:00
2:20:00
2:55:00
3:30:00
4:05:00
4:40:00
5:15:00
5:50:00
6:25:00
7:00:00
7:35:00
8:10:00
8:45:00
9:20:00
9:55:00
10:30:00
11:05:00
11:40:00
12:15:00
12:50:00
13:25:00
14:00:00
14:35:00
15:10:00
15:45:00
16:20:00
16:55:00
17:30:00
18:05:00
18:40:00
19:15:00
19:50:00
20:25:00
21:00:00
21:35:00
22:10:00
22:45:00
23:20:00
23:55:00
Methane
Atmospheric pressure

Chart 18

Atmospheric Pressure and Methane Levels
16/06/95

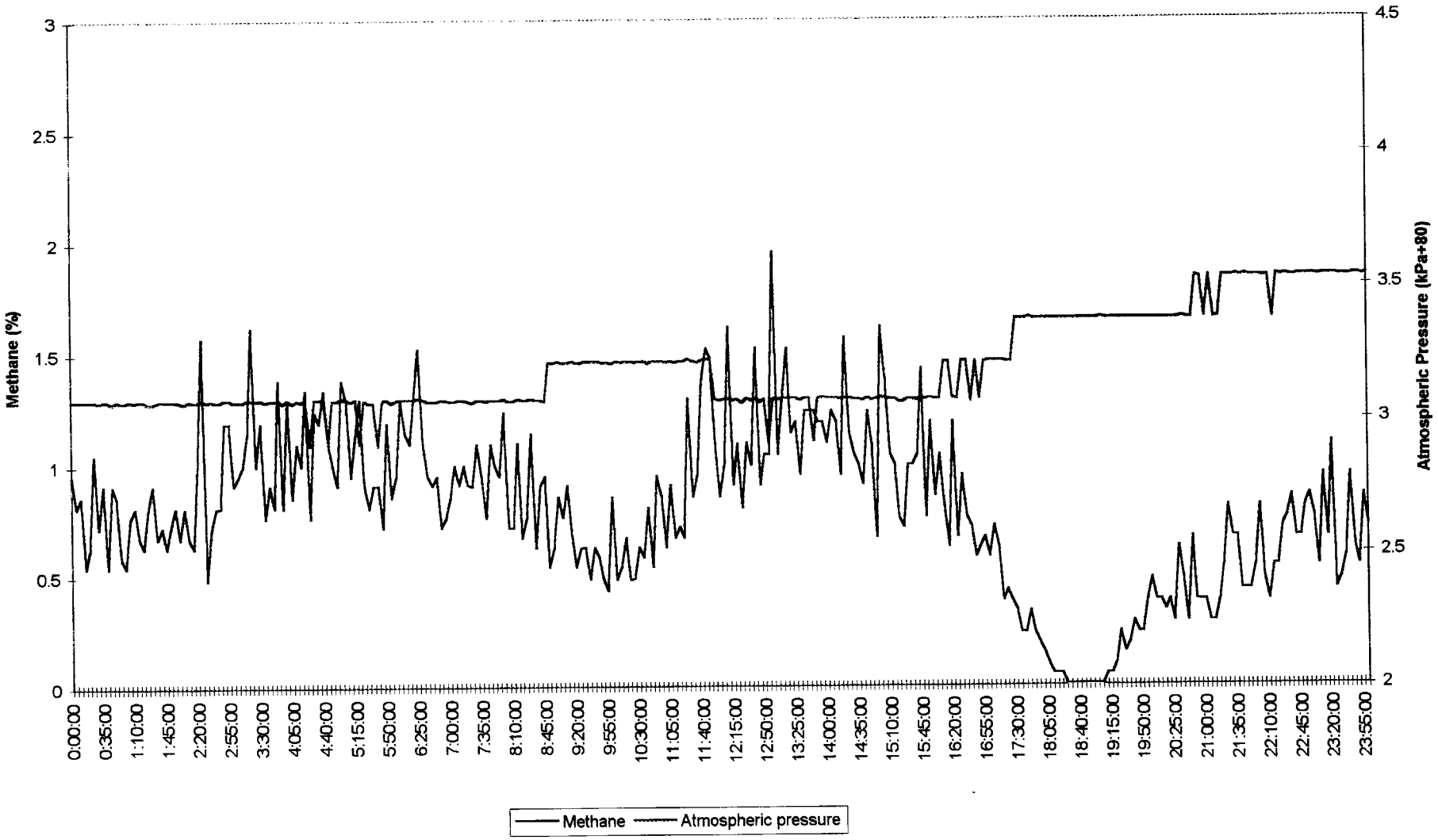

Chart 19

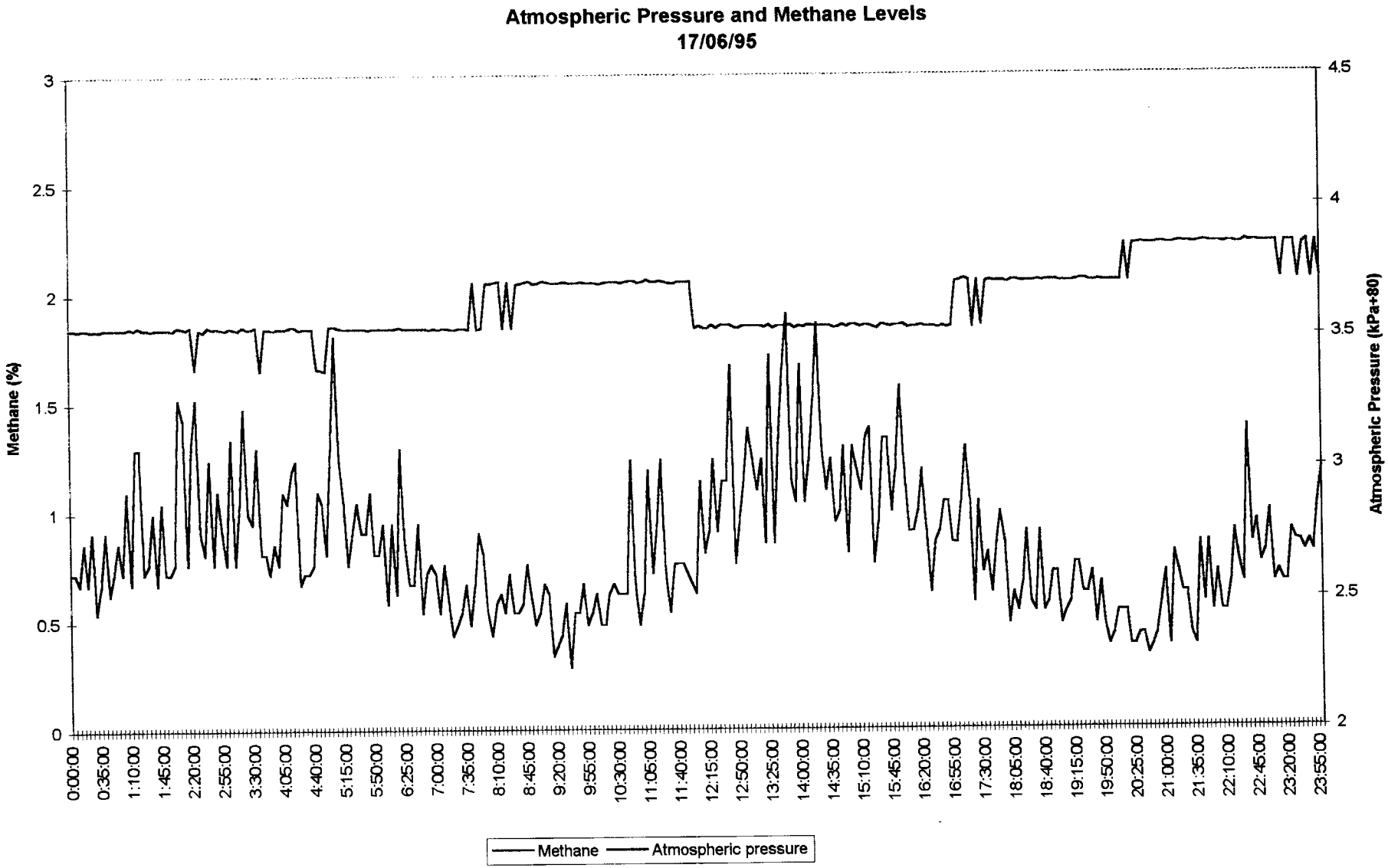
Atmospheric Pressure and Methane Levels
17/06/95
Methane (%)
Atmospheric Pressure (kPa+80)
3
2.5
2
1.5
1
0.5
0
4.5
4
3.5
3
2.5
2
0:00:00
0:35:00
1:10:00
1:45:00
2:20:00
2:55:00
3:30:00
4:05:00
4:40:00
5:15:00
5:50:00
6:25:00
7:00:00
7:35:00
8:10:00
8:45:00
9:20:00
9:55:00
10:30:00
11:05:00
11:40:00
12:15:00
12:50:00
13:25:00
14:00:00
14:35:00
15:10:00
15:45:00
16:20:00
16:55:00
17:30:00
18:05:00
18:40:00
19:15:00
19:50:00
20:25:00
21:00:00
21:35:00
22:10:00
22:45:00
23:20:00
23:55:00
Methane
Atmospheric pressure

Chart 20

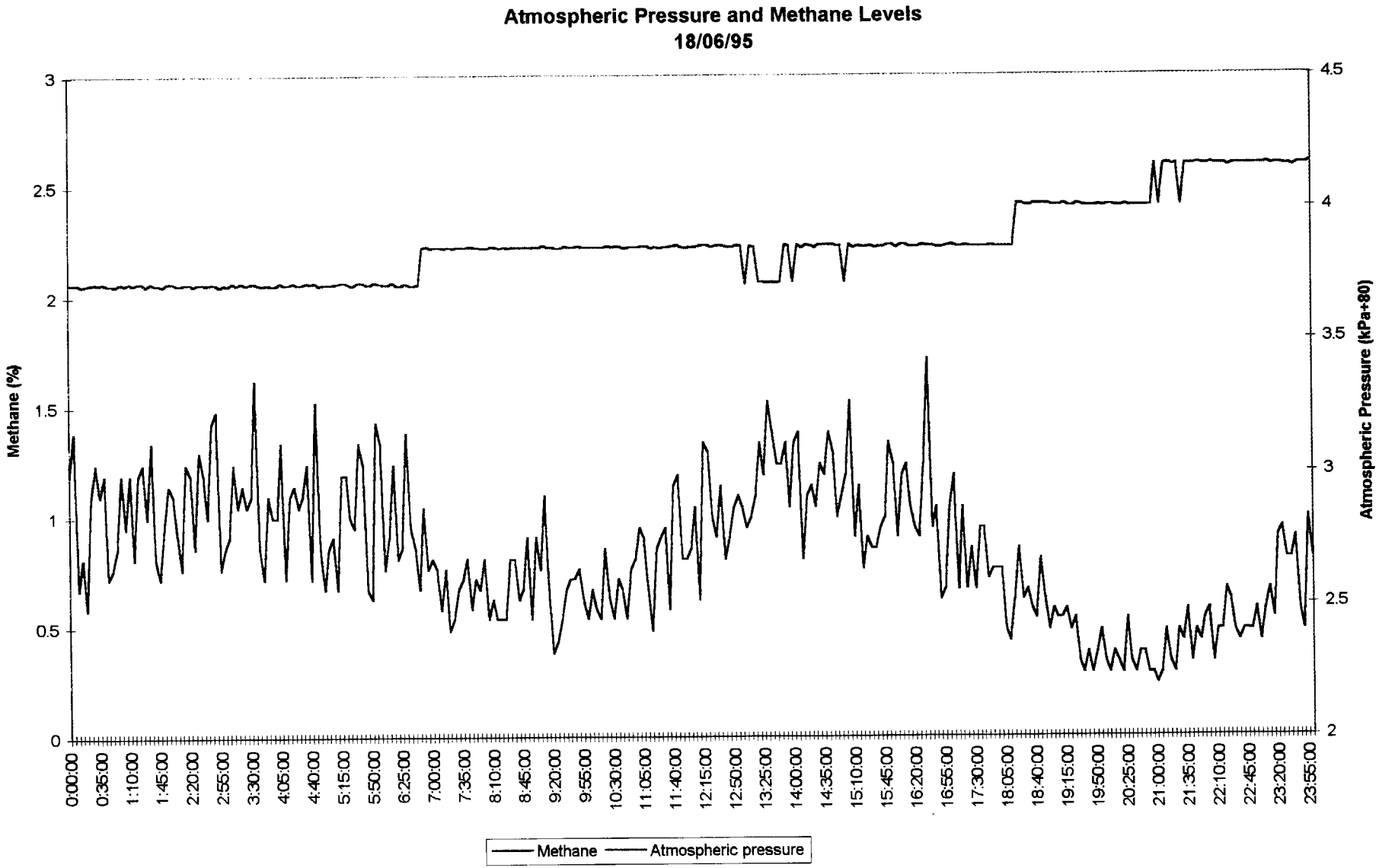
Atmospheric Pressure and Methane Levels
18/06/95
Methane (%)
Atmospheric Pressure (kPa+80)
3
2.5
2
1.5
1
0.5
0
4.5
4
3.5
3
2.5
2
0:00:00
0:35:00
1:10:00
1:45:00
2:20:00
2:55:00
3:30:00
4:05:00
4:40:00
5:15:00
5:50:00
6:25:00
7:00:00
7:35:00
8:10:00
8:45:00
9:20:00
9:55:00
10:30:00
11:05:00
11:40:00
12:15:00
12:50:00
13:25:00
14:00:00
14:35:00
15:10:00
15:45:00
16:20:00
16:55:00
17:30:00
18:05:00
18:40:00
19:15:00
19:50:00
20:25:00
21:00:00
21:35:00
22:10:00
22:45:00
23:20:00
23:55:00
Methane
Atmospheric pressure

Chart 21

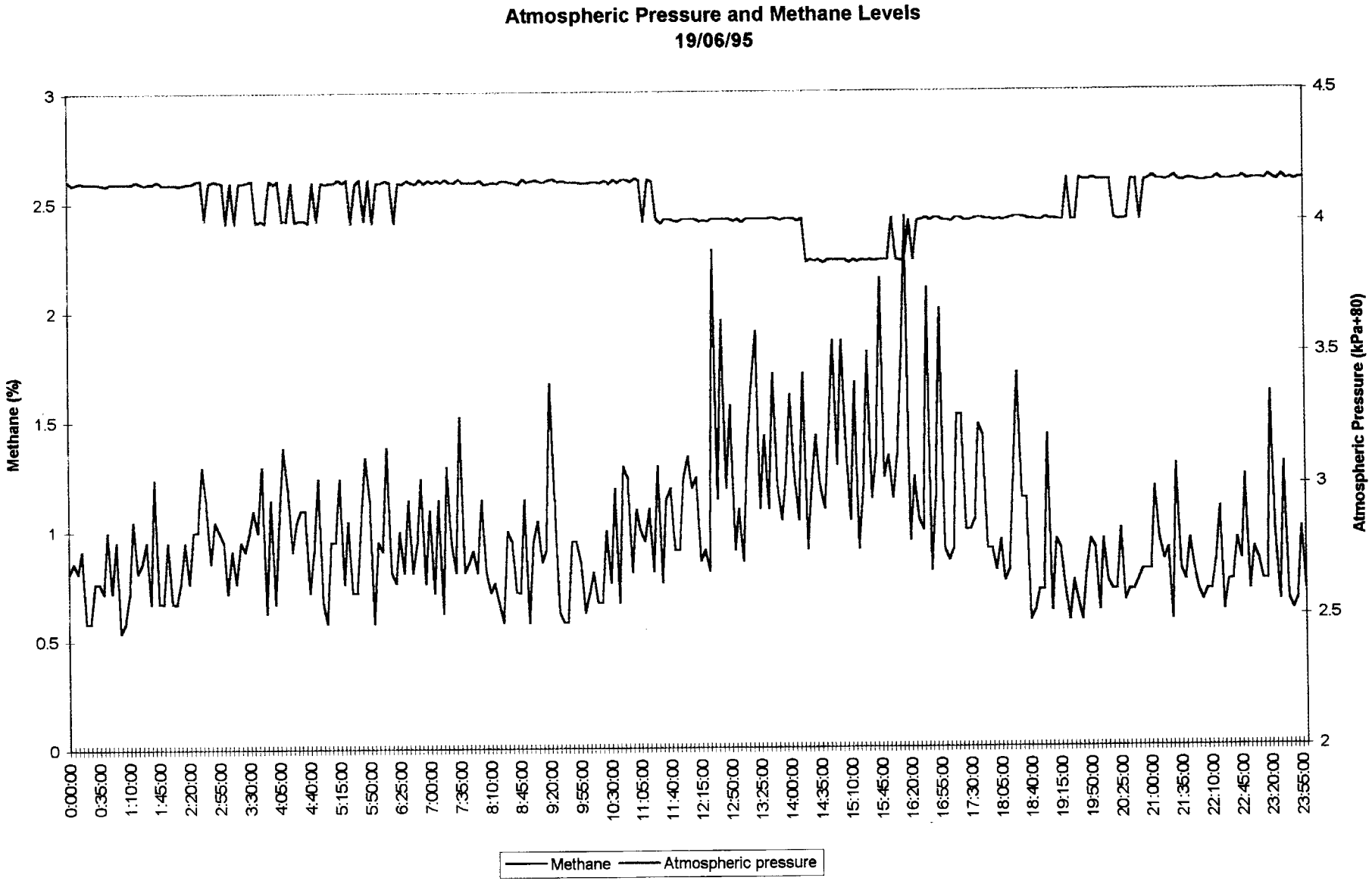
Atmospheric Pressure and Methane Levels
19/06/95
Methane (%)
Atmospheric Pressure (kPa+80)
3
2.5
2
1.5
1
0.5
0
4.5
4
3.5
3
2.5
2
0:00:00
0:35:00
1:10:00
1:45:00
2:20:00
2:55:00
3:30:00
4:05:00
4:40:00
5:15:00
5:50:00
6:25:00
7:00:00
7:35:00
8:10:00
8:45:00
9:20:00
9:55:00
10:30:00
11:05:00
11:40:00
12:15:00
12:50:00
13:25:00
14:00:00
14:35:00
15:10:00
15:45:00
16:20:00
16:55:00
17:30:00
18:05:00
18:40:00
19:15:00
19:50:00
20:25:00
21:00:00
21:35:00
22:10:00
22:45:00
23:20:00
23:55:00
Methane
Atmospheric pressure

Chart 22

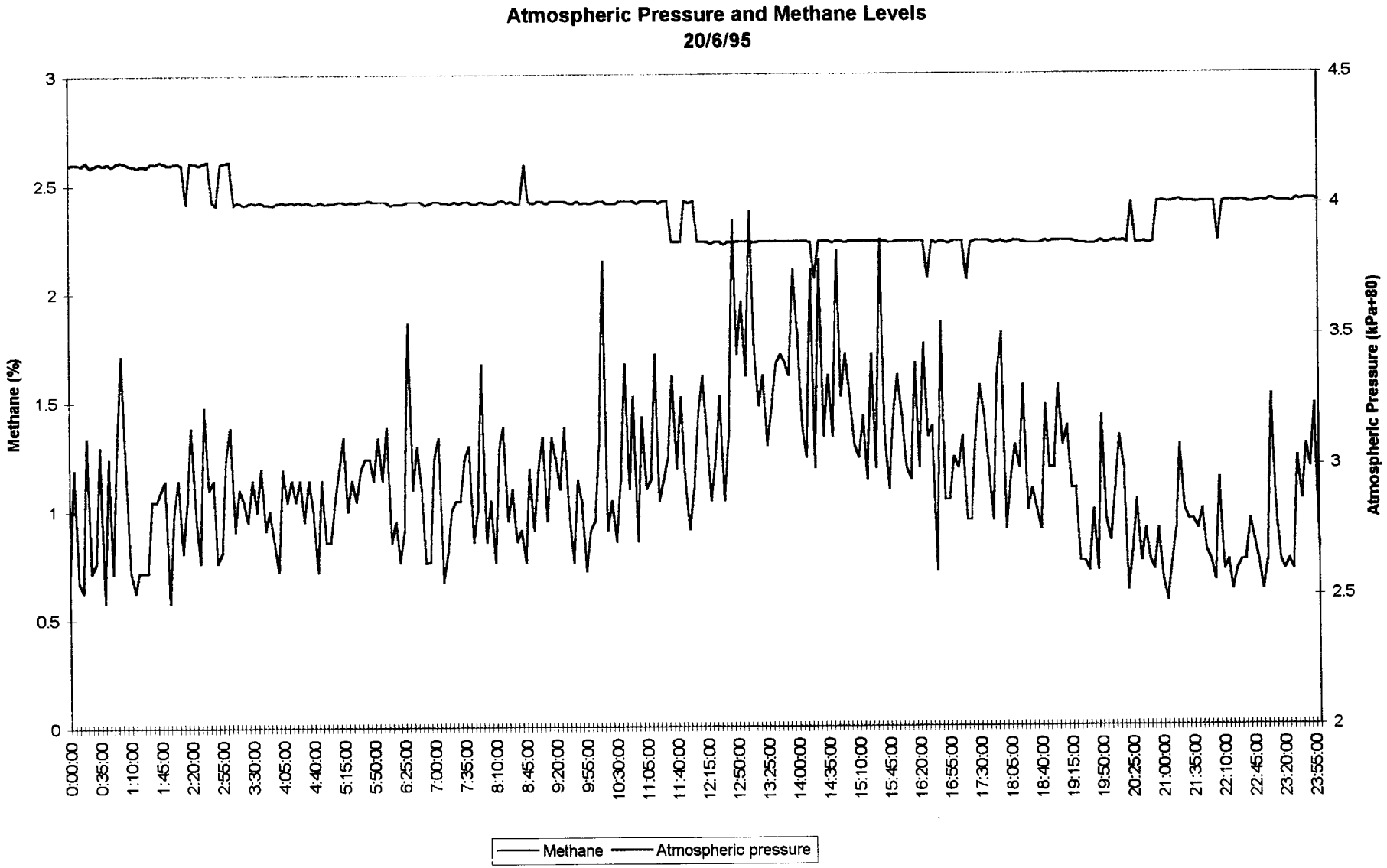
Atmospheric Pressure and Methane Levels
20/6/95
Methane (%)
Atmospheric Pressure (kPa+80)
3
2.5
2
1.5
1
0.5
0
4.5
4
3.5
3
2.5
2
0:00:00
0:35:00
1:10:00
1:45:00
2:20:00
2:55:00
3:30:00
4:05:00
4:40:00
5:15:00
5:50:00
6:25:00
7:00:00
7:35:00
8:10:00
8:45:00
9:20:00
9:55:00
10:30:00
11:05:00
11:40:00
12:15:00
12:50:00
13:25:00
14:00:00
14:35:00
15:10:00
15:45:00
16:20:00
16:55:00
17:30:00
18:05:00
18:40:00
19:15:00
19:50:00
20:25:00
21:00:00
21:35:00
22:10:00
22:45:00
23:20:00
23:55:00
Methane
Atmospheric pressure

Chart 23

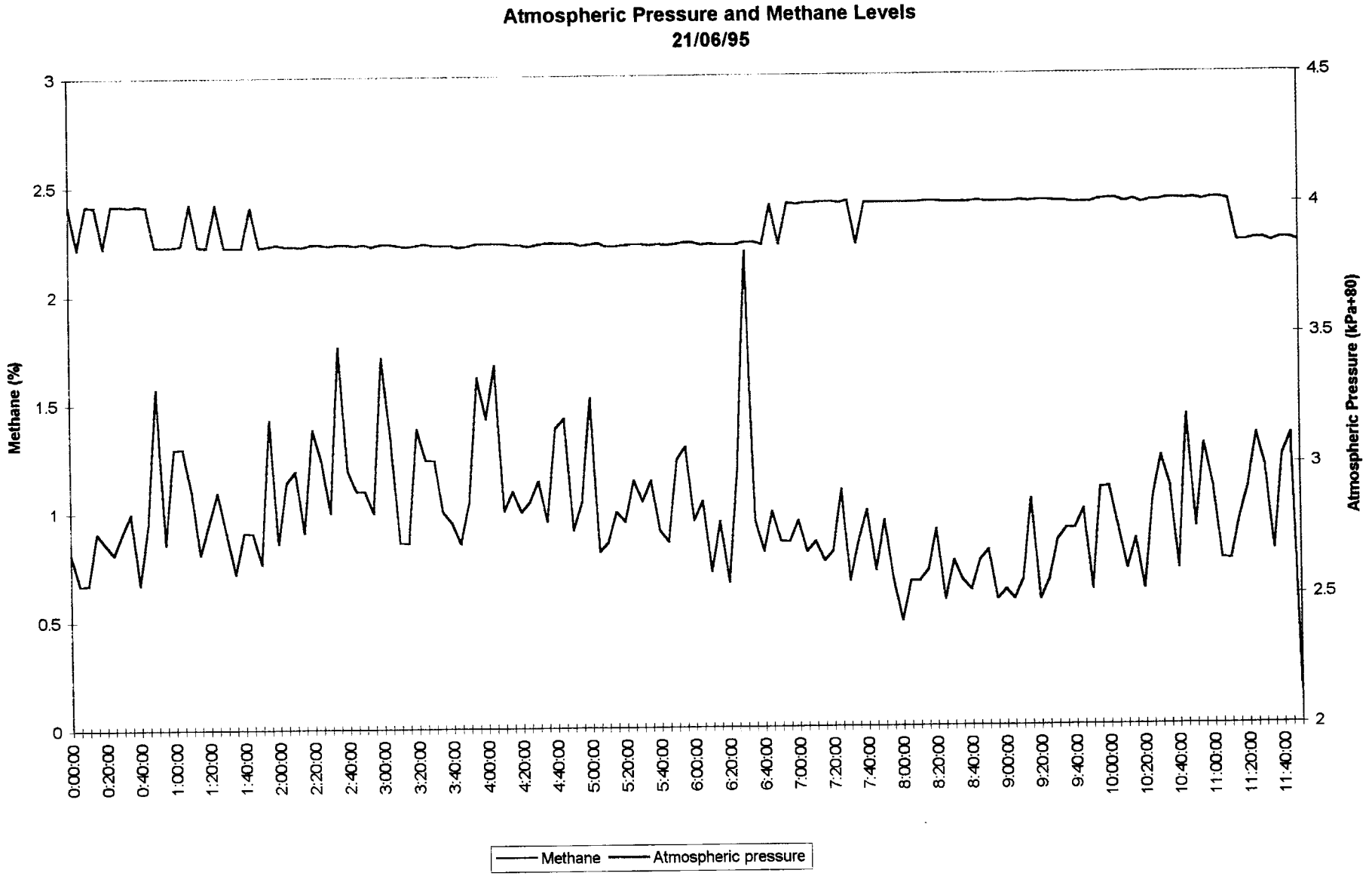
Atmospheric Pressure and Methane Levels
21/06/95
Methane (%)
Atmospheric Pressure (kPa+80)
3
2.5
2
1.5
1
0.5
0
4.5
4
3.5
3
2.5
2
0:00:00
0:20:00
0:40:00
1:00:00
1:20:00
1:40:00
2:00:00
2:20:00
2:40:00
3:00:00
3:20:00
3:40:00
4:00:00
4:20:00
4:40:00
5:00:00
5:20:00
5:40:00
6:00:00
6:20:00
6:40:00
7:00:00
7:20:00
7:40:00
8:00:00
8:20:00
8:40:00
9:00:00
9:20:00
9:40:00
10:00:00
10:20:00
10:40:00
11:00:00
11:20:00
11:40:00
Methane
Atmospheric pressure

Chart 24

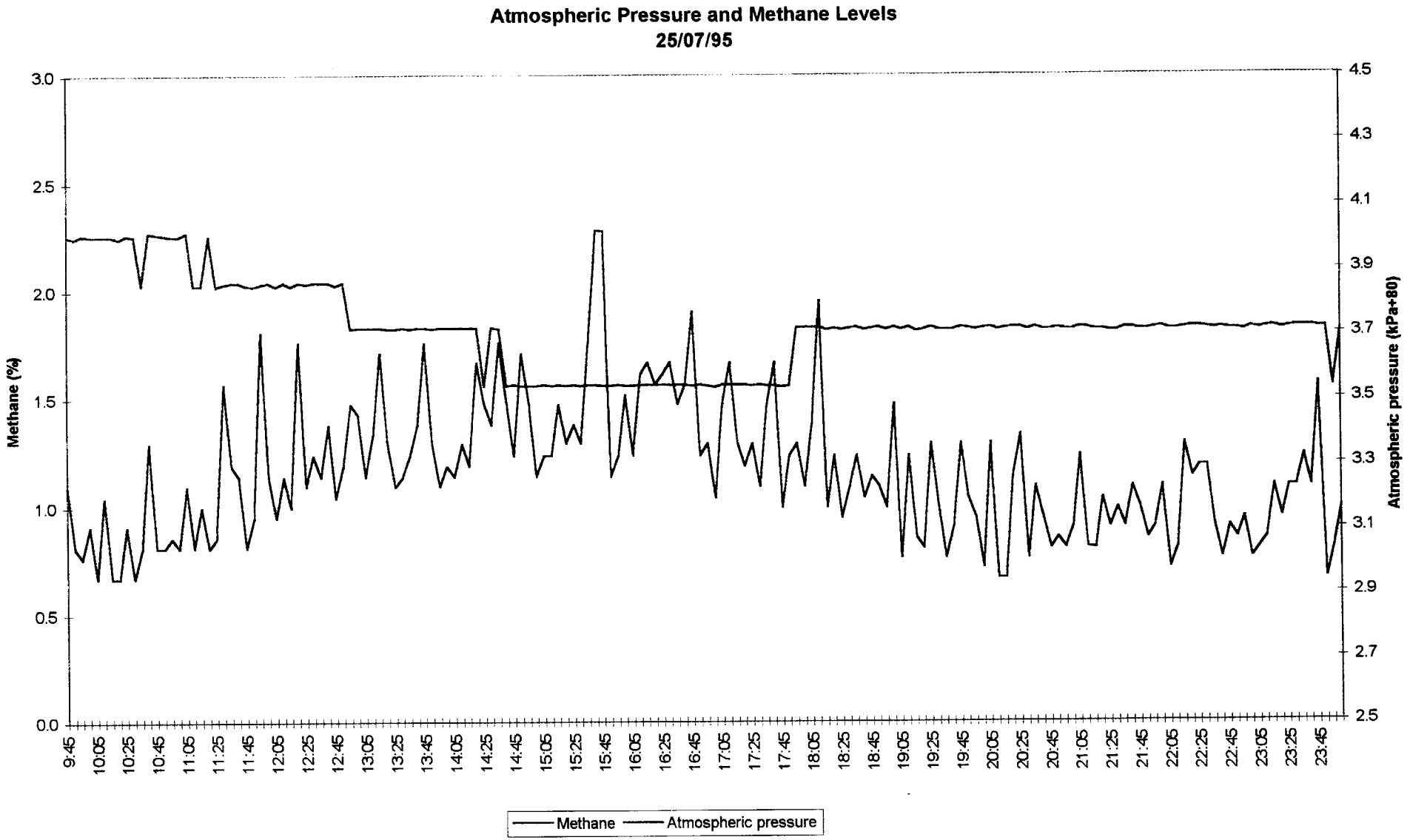
Atmospheric Pressure and Methane Levels
25/07/95
Methane (%)
Atmospheric pressure (kPa+80)
3.0
2.5
2.0
1.5
1.0
0.5
0.0
4.5
4.3
4.1
3.9
3.7
3.5
3.3
3.1
2.9
2.7
2.5
9:45
10:05
10:25
10:45
11:05
11:25
11:45
12:05
12:25
12:45
13:05
13:25
13:45
14:05
14:25
14:45
15:05
15:25
15:45
16:05
16:25
16:45
17:05
17:25
17:45
18:05
18:25
18:45
19:05
19:25
19:45
20:05
20:25
20:45
21:05
21:25
21:45
22:05
22:25
22:45
23:05
23:25
23:45
Methane
Atmospheric pressure

Chart 25

Atmospheric Pressure and Methane Levels
26/07/95

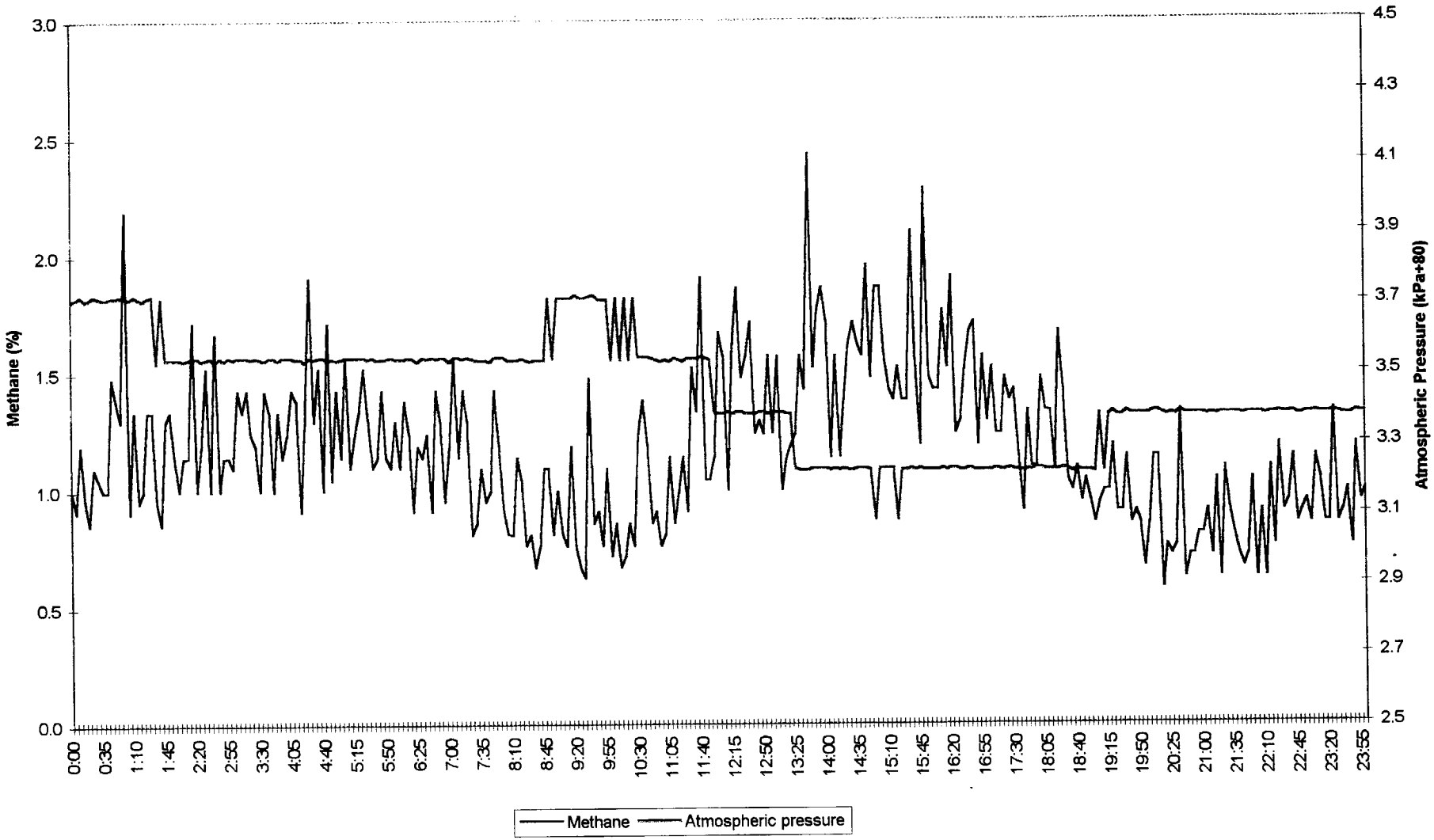

Chart 26

Atmospheric Pressure and Methane Levels
27/07/95

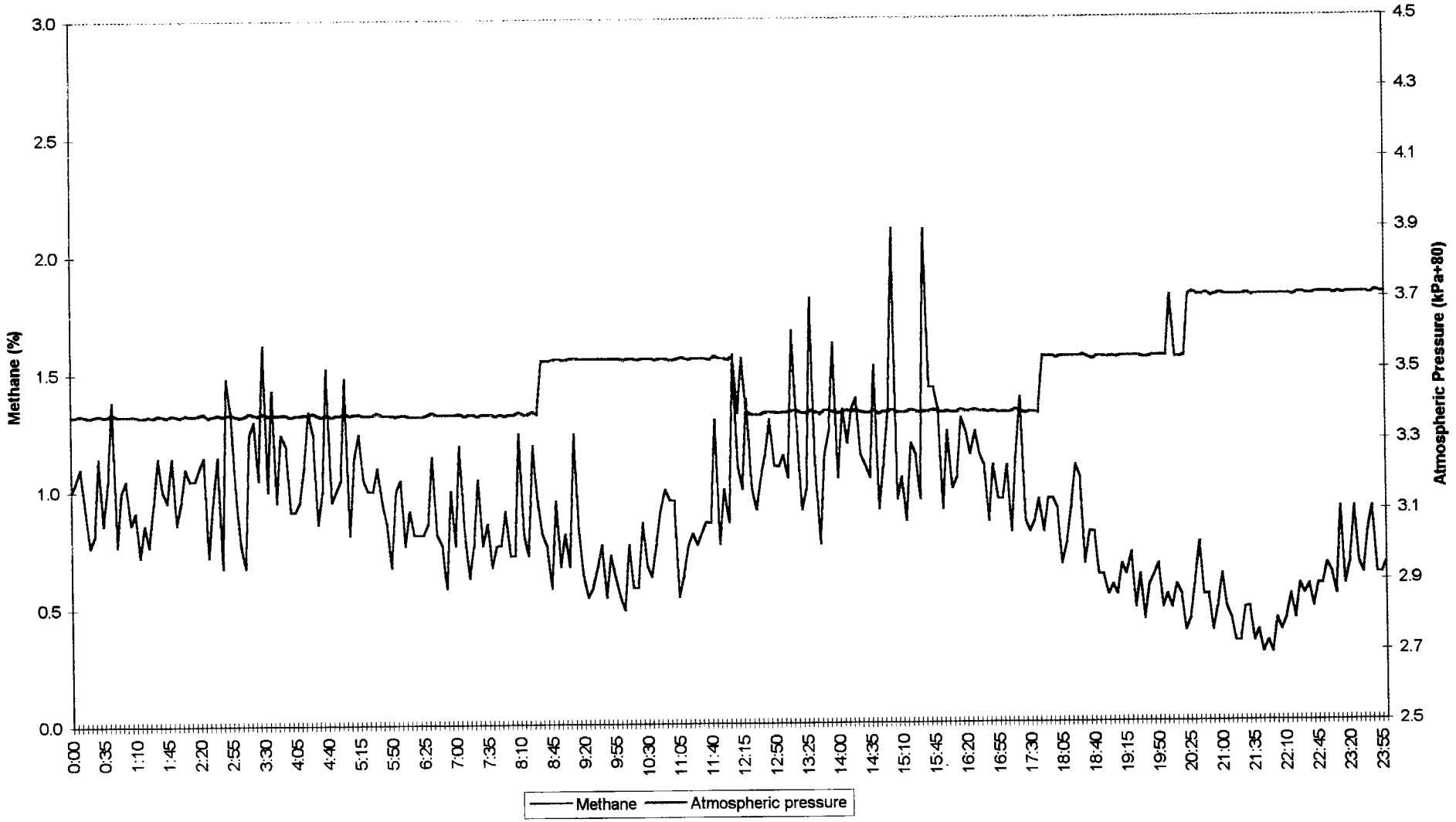

Chart 27

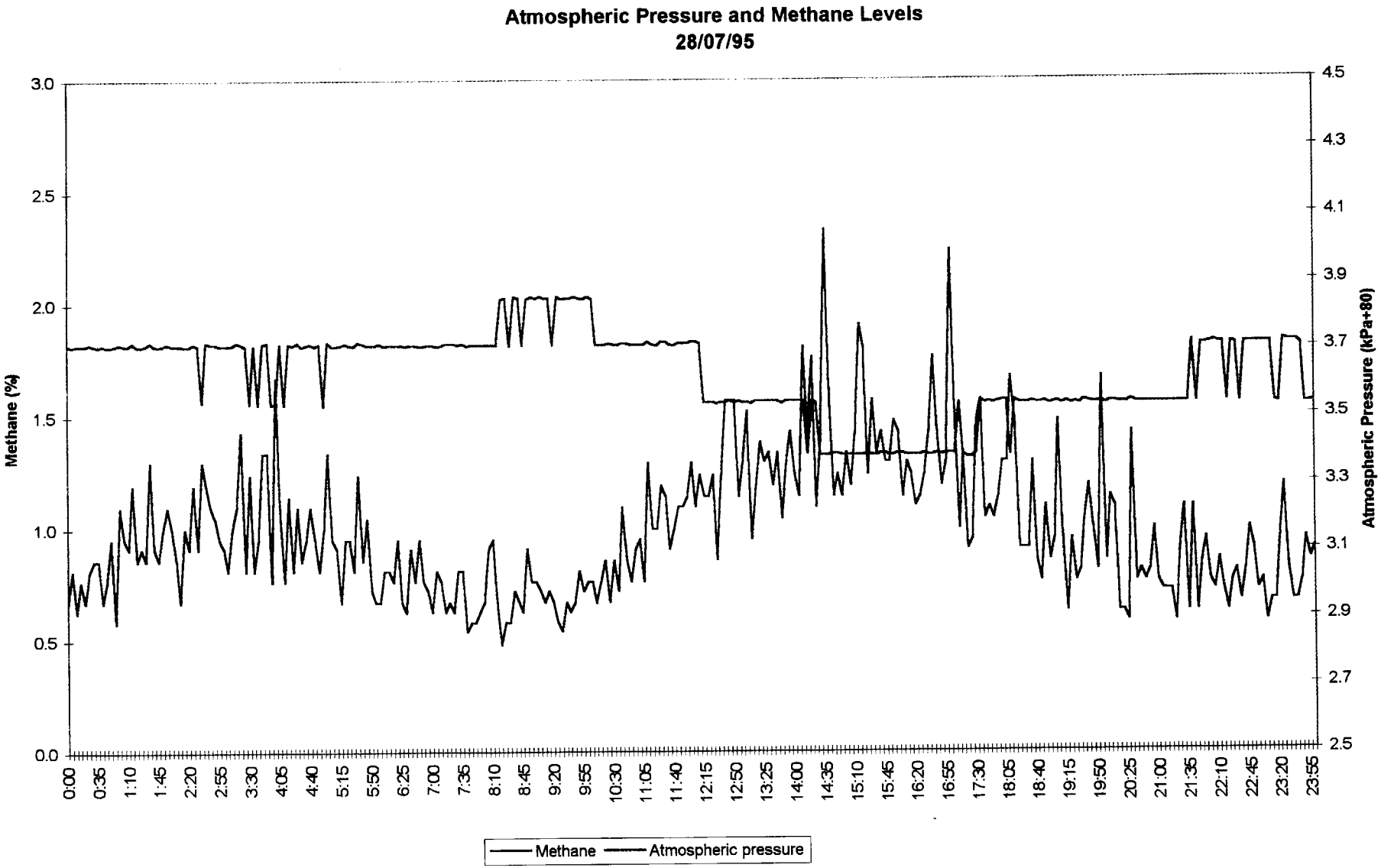
Atmospheric Pressure and Methane Levels
28/07/95
Methane (%)
Atmospheric Pressure (kPa+80)
3.0
2.5
2.0
1.5
1.0
0.5
0.0
4.5
4.3
4.1
3.9
3.7
3.5
3.3
3.1
2.9
2.7
2.5
0:00
0:35
1:10
1:45
2:20
2:55
3:30
4:05
4:40
5:15
5:50
6:25
7:00
7:35
8:10
8:45
9:20
9:55
10:30
11:05
11:40
12:15
12:50
13:25
14:00
14:35
15:10
15:45
16:20
16:55
17:30
18:05
18:40
19:15
19:50
20:25
21:00
21:35
22:10
22:45
23:20
23:55
Methane
Atmospheric pressure

Chart 28

Atmospheric Pressure and Methane Levels
29/07/95

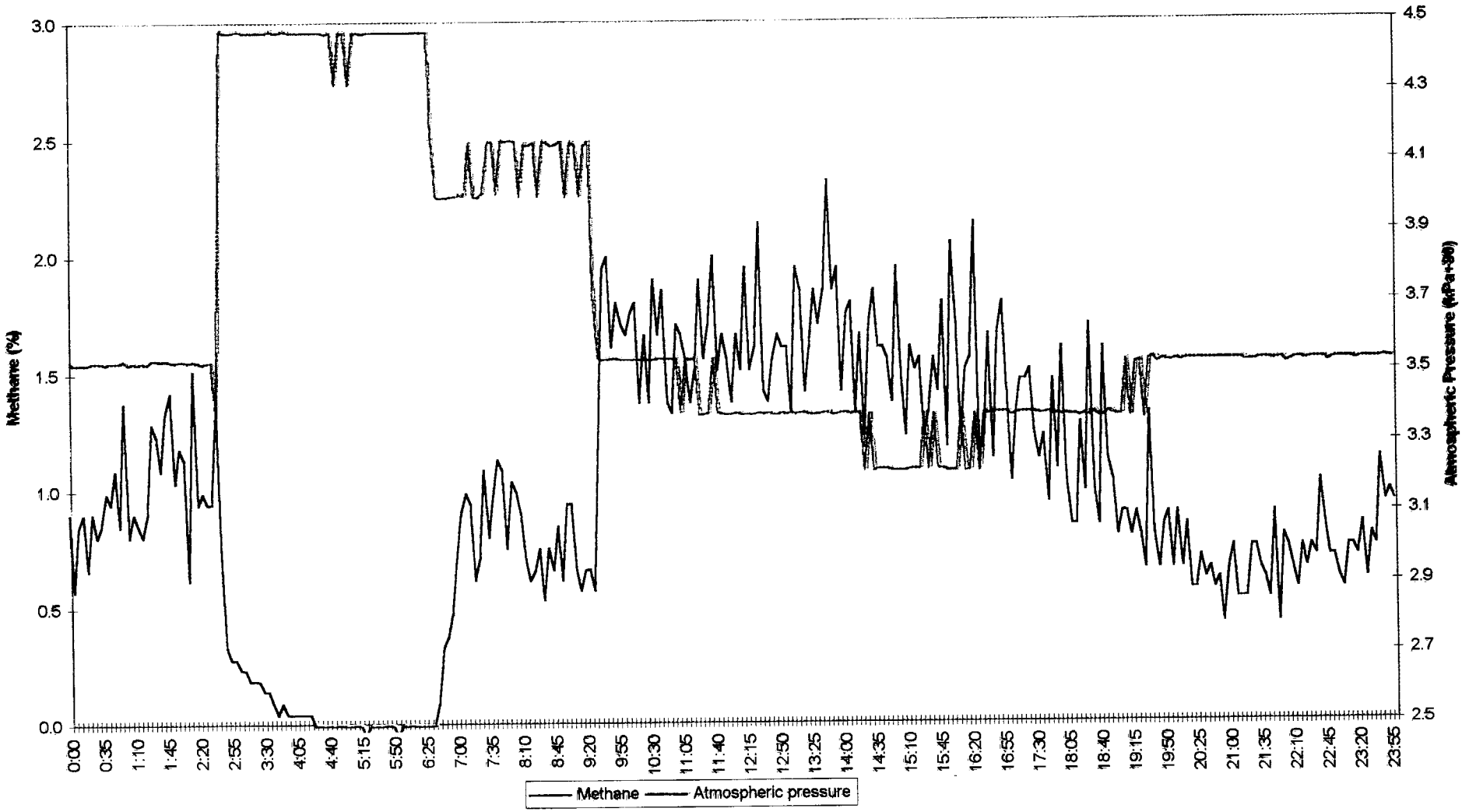

Chart 29

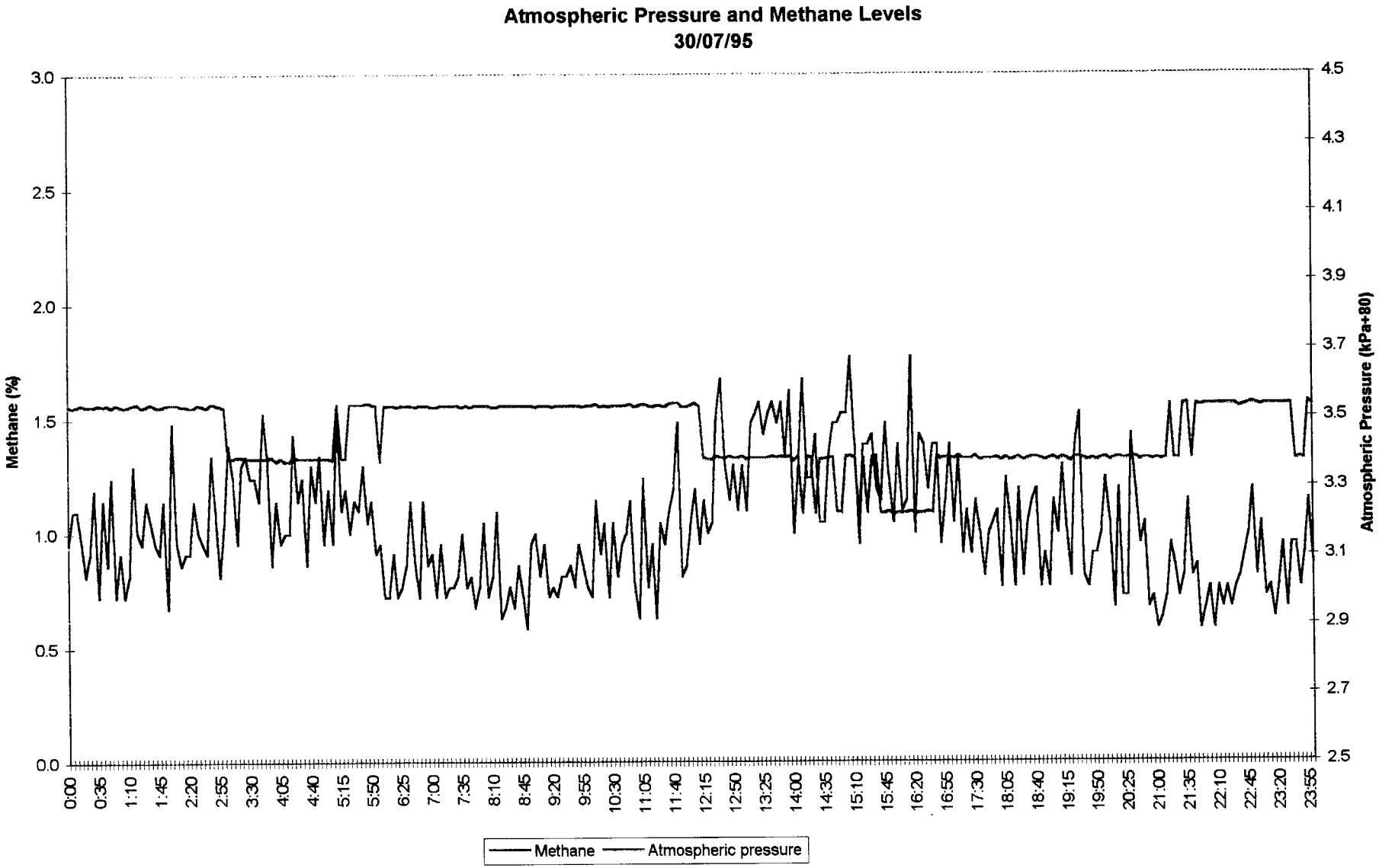
Atmospheric Pressure and Methane Levels
30/07/95
Methane (%)
Atmospheric Pressure (kPa+80)
3.0
2.5
2.0
1.5
1.0
0.5
0.0
4.5
4.3
4.1
3.9
3.7
3.5
3.3
3.1
2.9
2.7
2.5
0:00
0:35
1:10
1:45
2:20
2:55
3:30
4:05
4:40
5:15
5:50
6:25
7:00
7:35
8:10
8:45
9:20
9:55
10:30
11:05
11:40
12:15
12:50
13:25
14:00
14:35
15:10
15:45
16:20
16:55
17:30
18:05
18:40
19:15
19:50
20:25
21:00
21:35
22:10
22:45
23:20
23:55
Methane
Atmospheric pressure

Chart 30

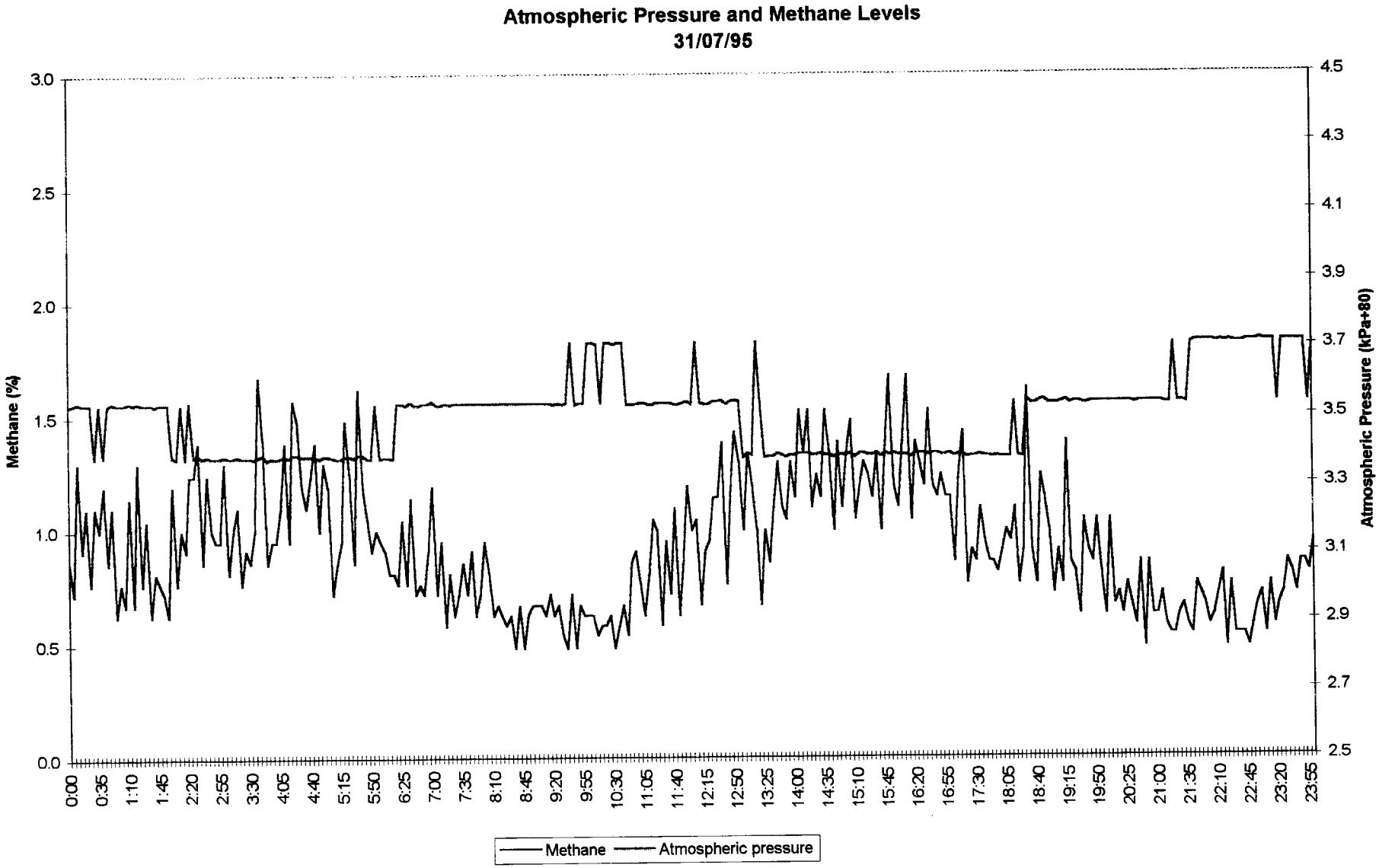
Atmospheric Pressure and Methane Levels
31/07/95
Methane (%)
Atmospheric Pressure (kPa+80)
3.0
2.5
2.0
1.5
1.0
0.5
0.0
4.5
4.3
4.1
3.9
3.7
3.5
3.3
3.1
2.9
2.7
2.5
0:00
0:35
1:10
1:45
2:20
2:55
3:30
4:05
4:40
5:15
5:50
6:25
7:00
7:35
8:10
8:45
9:20
9:55
10:30
11:05
11:40
12:15
12:50
13:25
14:00
14:35
15:10
15:45
16:20
16:55
17:30
18:05
18:40
19:15
19:50
20:25
21:00
21:35
22:10
22:45
23:20
23:55
Methane
Atmospheric pressure

Chart 31

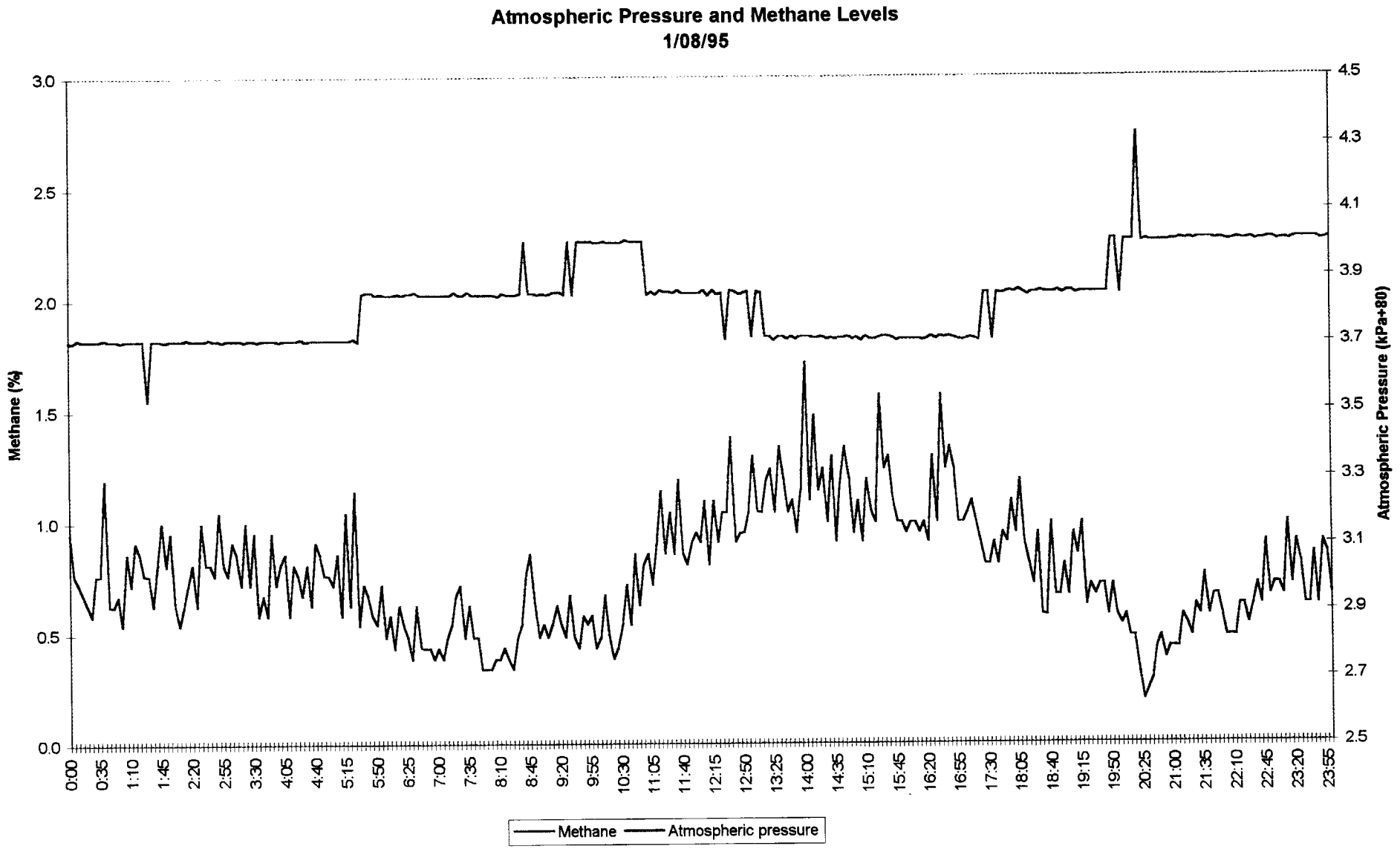
Atmospheric Pressure and Methane Levels
1/08/95
Methane (%)
Atmospheric Pressure (kPa+80)
3.0
2.5
2.0
1.5
1.0
0.5
0.0
4.5
4.3
4.1
3.9
3.7
3.5
3.3
3.1
2.9
2.7
2.5
0:00
0:35
1:10
1:45
2:20
2:55
3:30
4:05
4:40
5:15
5:50
6:25
7:00
7:35
8:10
8:45
9:20
9:55
10:30
11:05
11:40
12:15
12:50
13:25
14:00
14:35
15:10
15:45
16:20
16:55
17:30
18:05
18:40
19:15
19:50
20:25
21:00
21:35
22:10
22:45
23:20
23:55
Methane
Atmospheric pressure

Chart 32

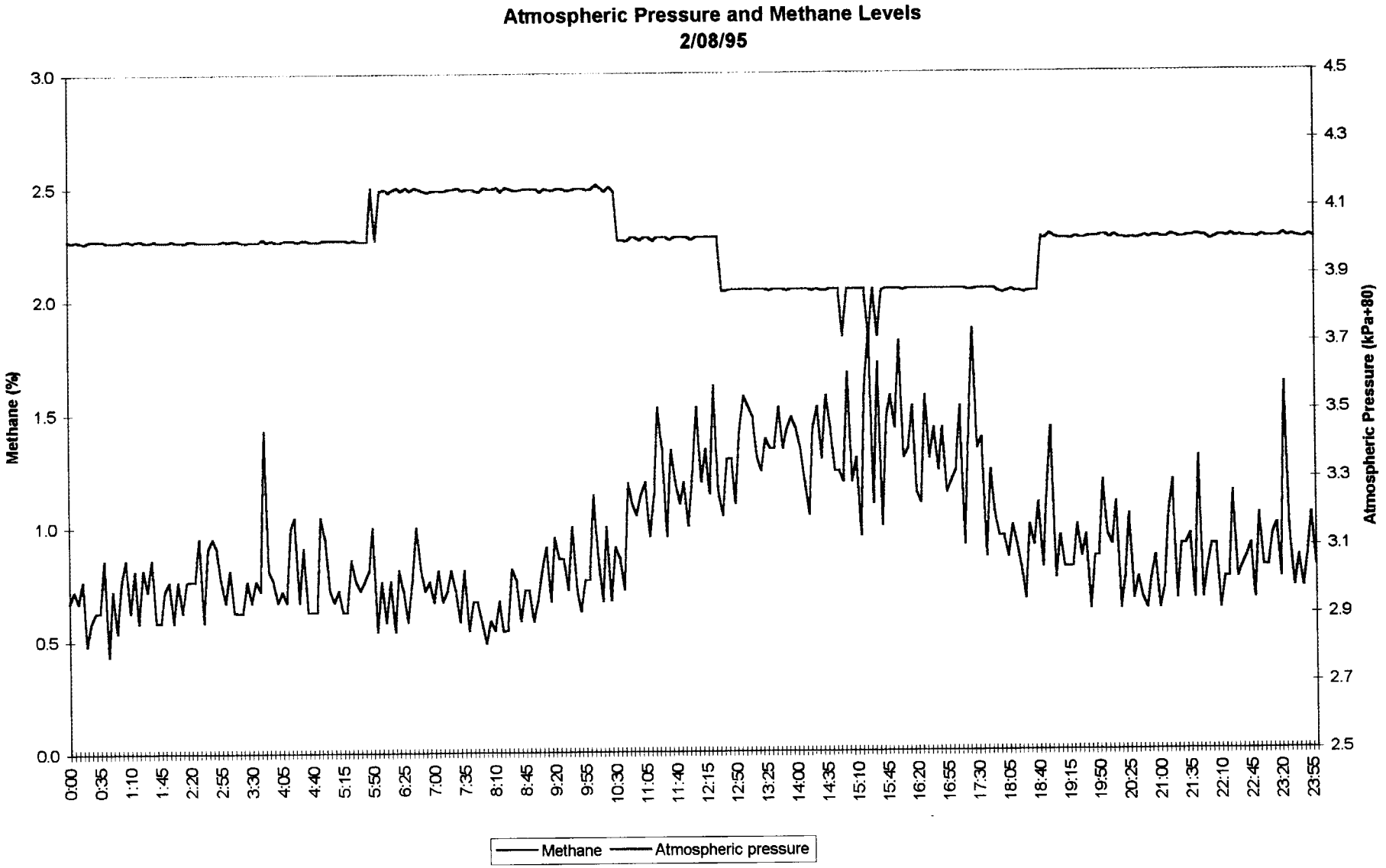
Atmospheric Pressure and Methane Levels
2/08/95
Methane (%)
Atmospheric Pressure (kPa+80)
3.0
2.5
2.0
1.5
1.0
0.5
0.0
4.5
4.3
4.1
3.9
3.7
3.5
3.3
3.1
2.9
2.7
2.5
0:00
0:35
1:10
1:45
2:20
2:55
3:30
4:05
4:40
5:15
5:50
6:25
7:00
7:35
8:10
8:45
9:20
9:55
10:30
11:05
11:40
12:15
12:50
13:25
14:00
14:35
15:10
15:45
16:20
16:55
17:30
18:05
18:40
19:15
19:50
20:25
21:00
21:35
22:10
22:45
23:20
23:55
Methane
Atmospheric pressure

Chart 33

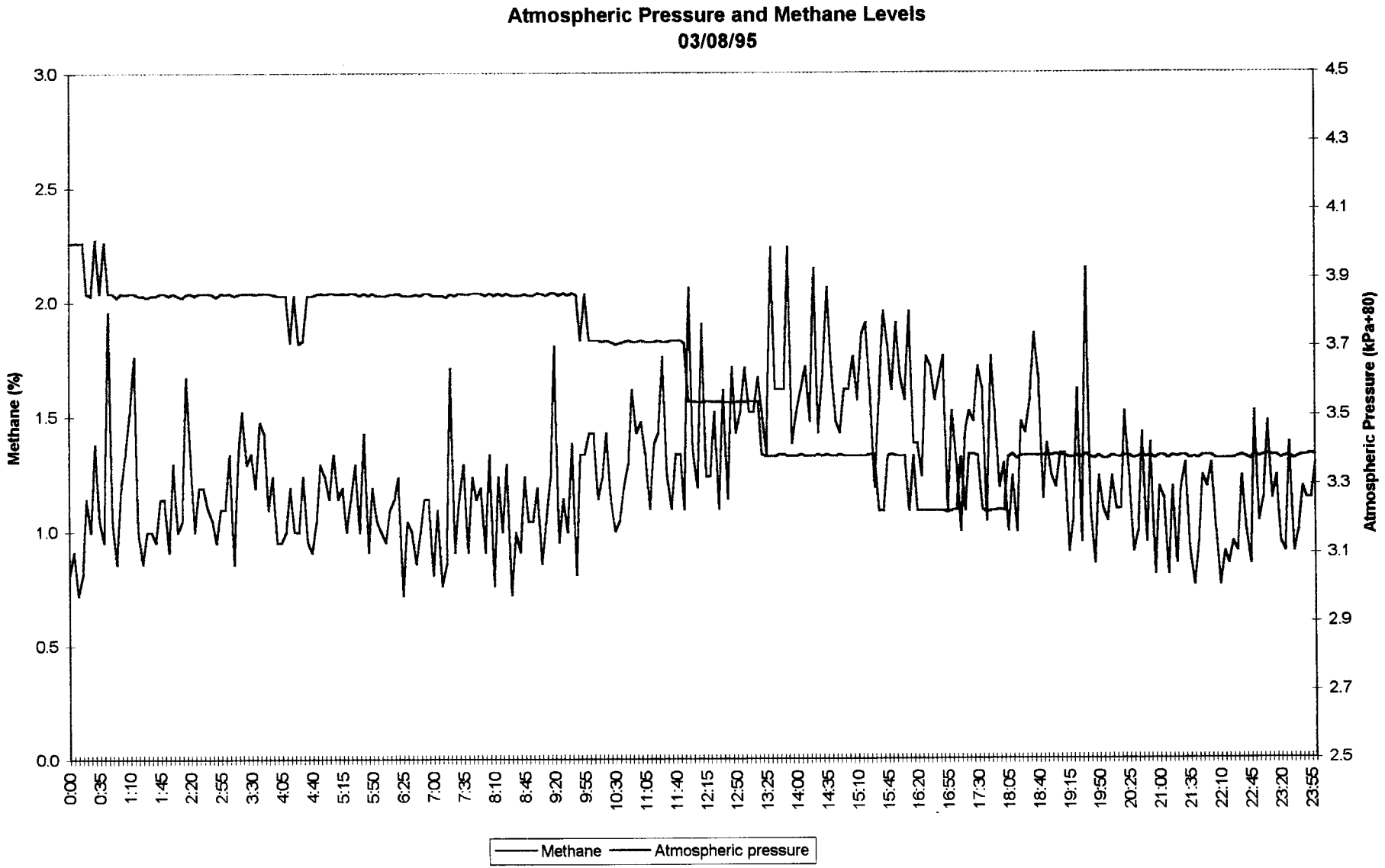
Atmospheric Pressure and Methane Levels
03/08/95
Methane (%)
Atmospheric Pressure (kPa+80)
3.0
2.5
2.0
1.5
1.0
0.5
0.0
4.5
4.3
4.1
3.9
3.7
3.5
3.3
3.1
2.9
2.7
2.5
0:00
0:35
1:10
1:45
2:20
2:55
3:30
4:05
4:40
5:15
5:50
6:25
7:00
7:35
8:10
8:45
9:20
9:55
10:30
11:05
11:40
12:15
12:50
13:25
14:00
14:35
15:10
15:45
16:20
16:55
17:30
18:05
18:40
19:15
19:50
20:25
21:00
21:35
22:10
22:45
23:20
23:55
Methane
Atmospheric pressure

Chart 34

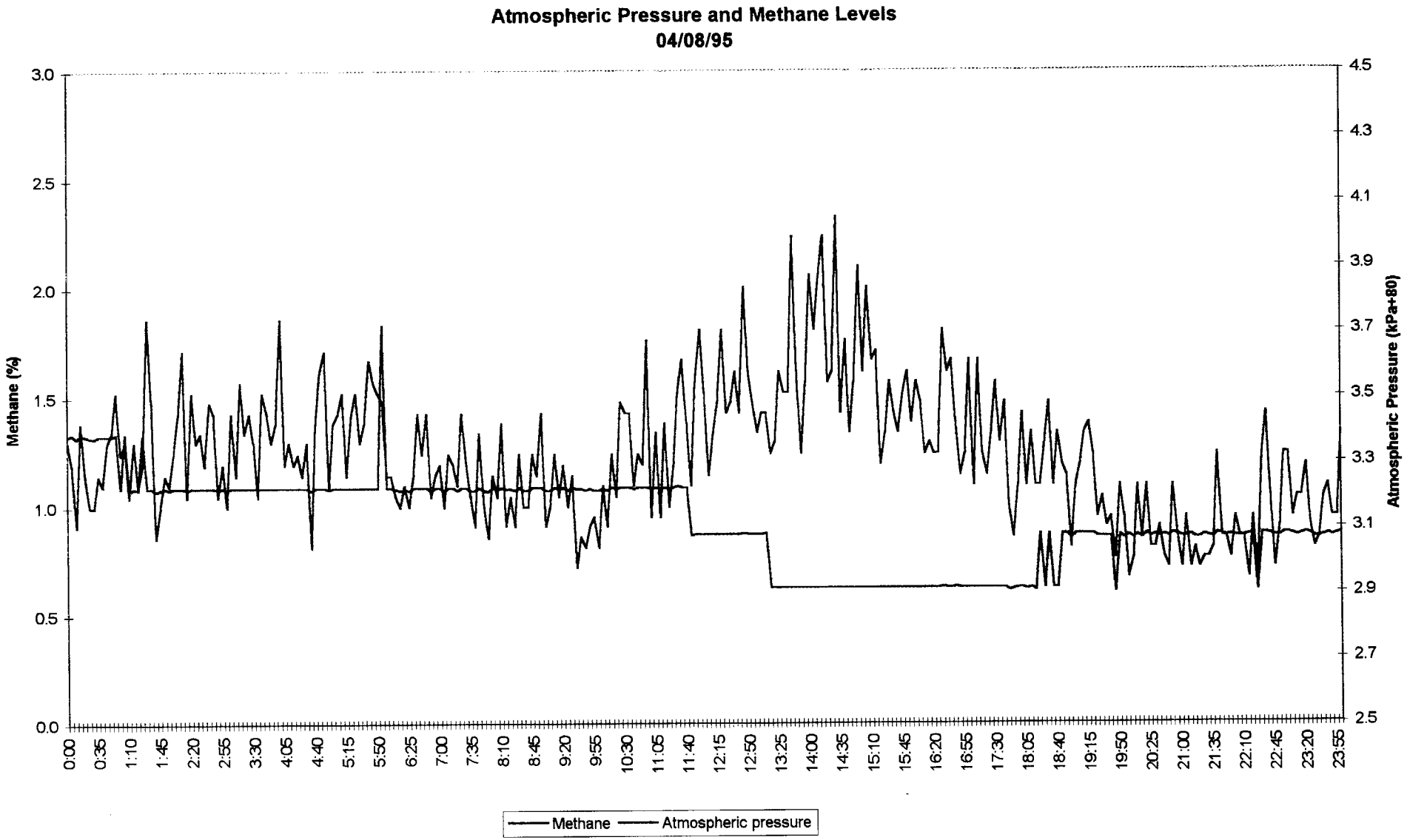
Atmospheric Pressure and Methane Levels
04/08/95
Methane (%)
Atmospheric Pressure (kPa+80)
3.0
2.5
2.0
1.5
1.0
0.5
0.0
4.5
4.3
4.1
3.9
3.7
3.5
3.3
3.1
2.9
2.7
2.5
0:00
0:35
1:10
1:45
2:20
2:55
3:30
4:05
4:40
5:15
5:50
6:25
7:00
7:35
8:10
8:45
9:20
9:55
10:30
11:05
11:40
12:15
12:50
13:25
14:00
14:35
15:10
15:45
16:20
16:55
17:30
18:05
18:40
19:15
19:50
20:25
21:00
21:35
22:10
22:45
23:20
23:55
Methane
Atmospheric pressure

Chart 35

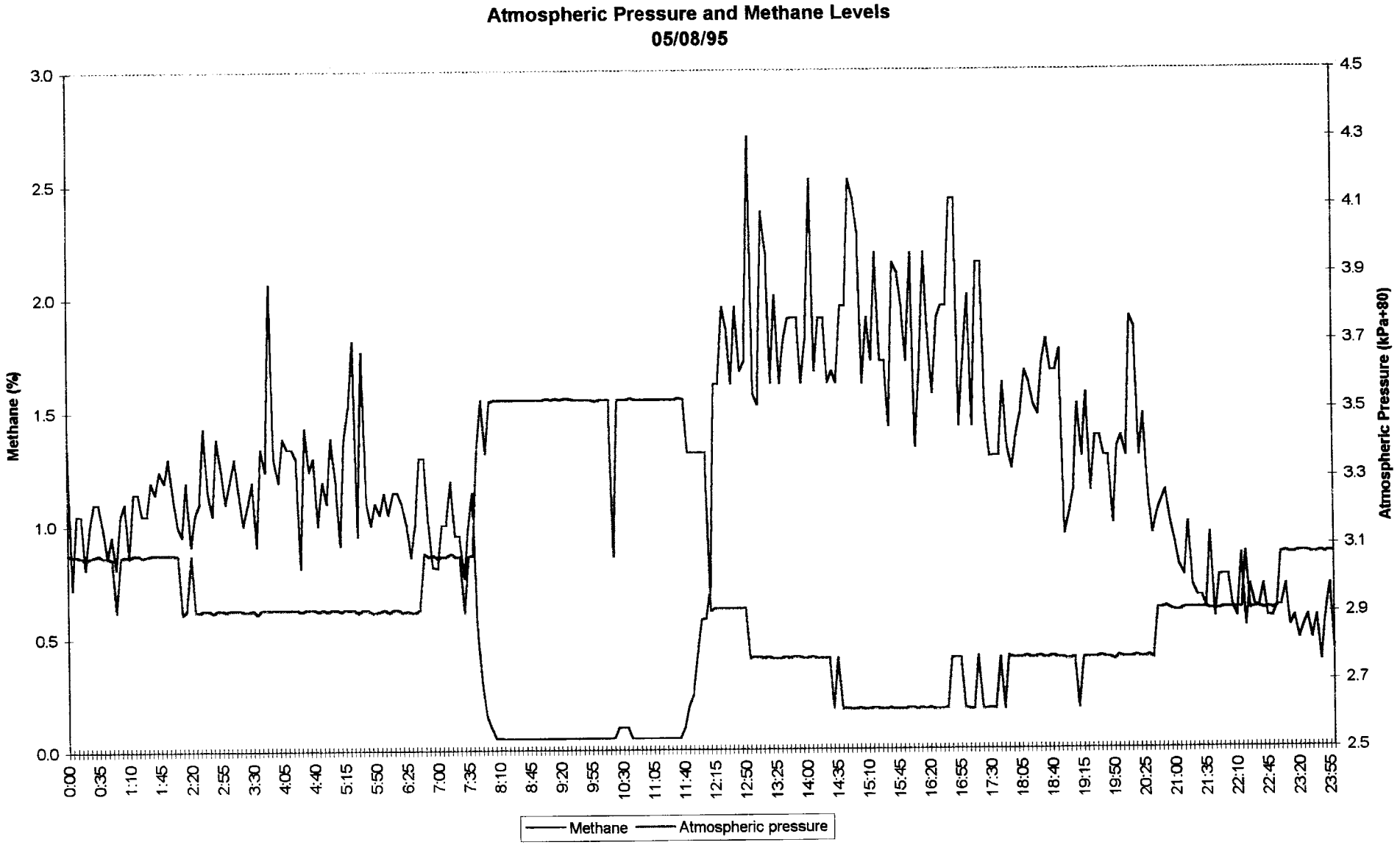
Atmospheric Pressure and Methane Levels
05/08/95
Methane (%)
Atmospheric Pressure (kPa+80)
3.0
2.5
2.0
1.5
1.0
0.5
0.0
4.5
4.3
4.1
3.9
3.7
3.5
3.3
3.1
2.9
2.7
2.5
0:00
0:35
1:10
1:45
2:20
2:55
3:30
4:05
4:40
5:15
5:50
6:25
7:00
7:35
8:10
8:45
9:20
9:55
10:30
11:05
11:40
12:15
12:50
13:25
14:00
14:35
15:10
15:45
16:20
16:55
17:30
18:05
18:40
19:15
19:50
20:25
21:00
21:35
22:10
22:45
23:20
23:55
Methane
Atmospheric pressure

Chart 36

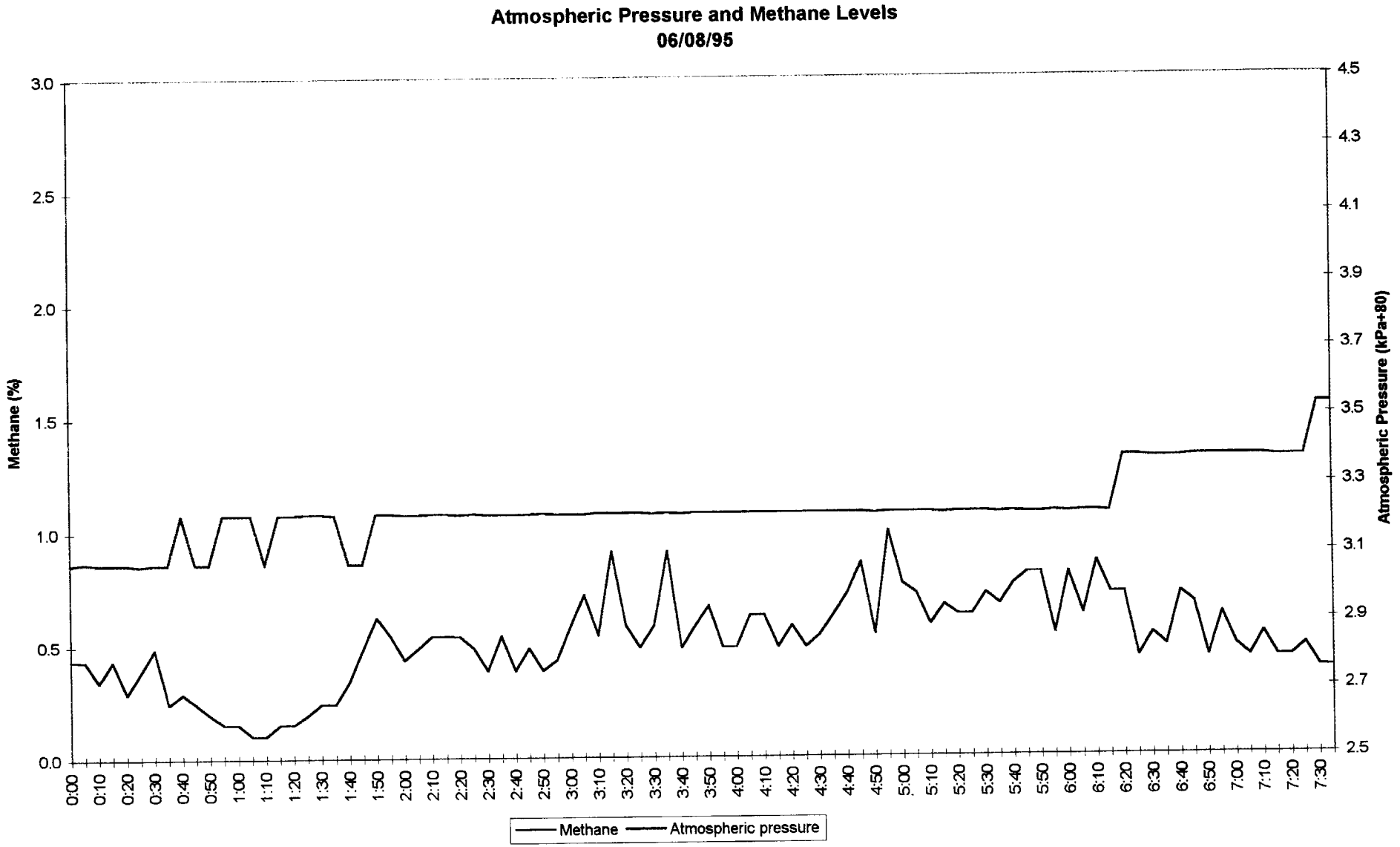
Atmospheric Pressure and Methane Levels
06/08/95
Methane (%)
Atmospheric Pressure (kPa+80)
3.0
2.5
2.0
1.5
1.0
0.5
0.0
4.5
4.3
4.1
3.9
3.7
3.5
3.3
3.1
2.9
2.7
2.5
0:00
0:10
0:20
0:30
0:40
0:50
1:00
1:10
1:20
1:30
1:40
1:50
2:00
2:10
2:20
2:30
2:40
2:50
3:00
3:10
3:20
3:30
3:40
3:50
4:00
4:10
4:20
4:30
4:40
4:50
5:00
5:10
5:20
5:30
5:40
5:50
6:00
6:10
6:20
6:30
6:40
6:50
7:00
7:10
7:20
7:30
Methane
Atmospheric pressure

Chart 37

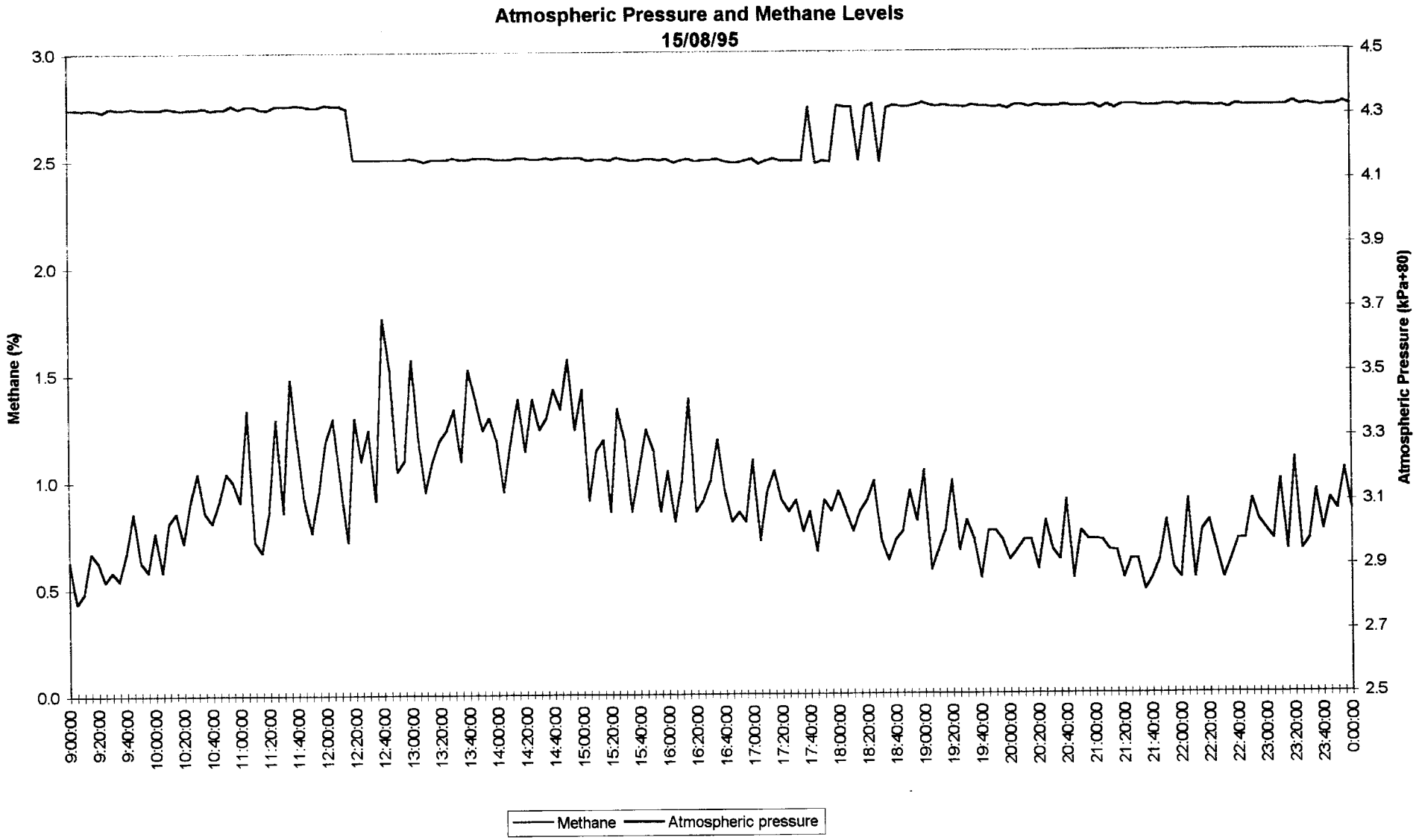
Atmospheric Pressure and Methane Levels
15/08/95
Methane (%)
Atmospheric Pressure (kPa+80)
3.0
2.5
2.0
1.5
1.0
0.5
0.0
4.5
4.3
4.1
3.9
3.7
3.5
3.3
3.1
2.9
2.7
2.5
9:00:00
9:20:00
9:40:00
10:00:00
10:20:00
10:40:00
11:00:00
11:20:00
11:40:00
12:00:00
12:20:00
12:40:00
13:00:00
13:20:00
13:40:00
14:00:00
14:20:00
14:40:00
15:00:00
15:20:00
15:40:00
16:00:00
16:20:00
16:40:00
17:00:00
17:20:00
17:40:00
18:00:00
18:20:00
18:40:00
19:00:00
19:20:00
19:40:00
20:00:00
20:20:00
20:40:00
21:00:00
21:20:00
21:40:00
22:00:00
22:20:00
22:40:00
23:00:00
23:20:00
23:40:00
0:00:00
Methane
Atmospheric pressure

Chart 38

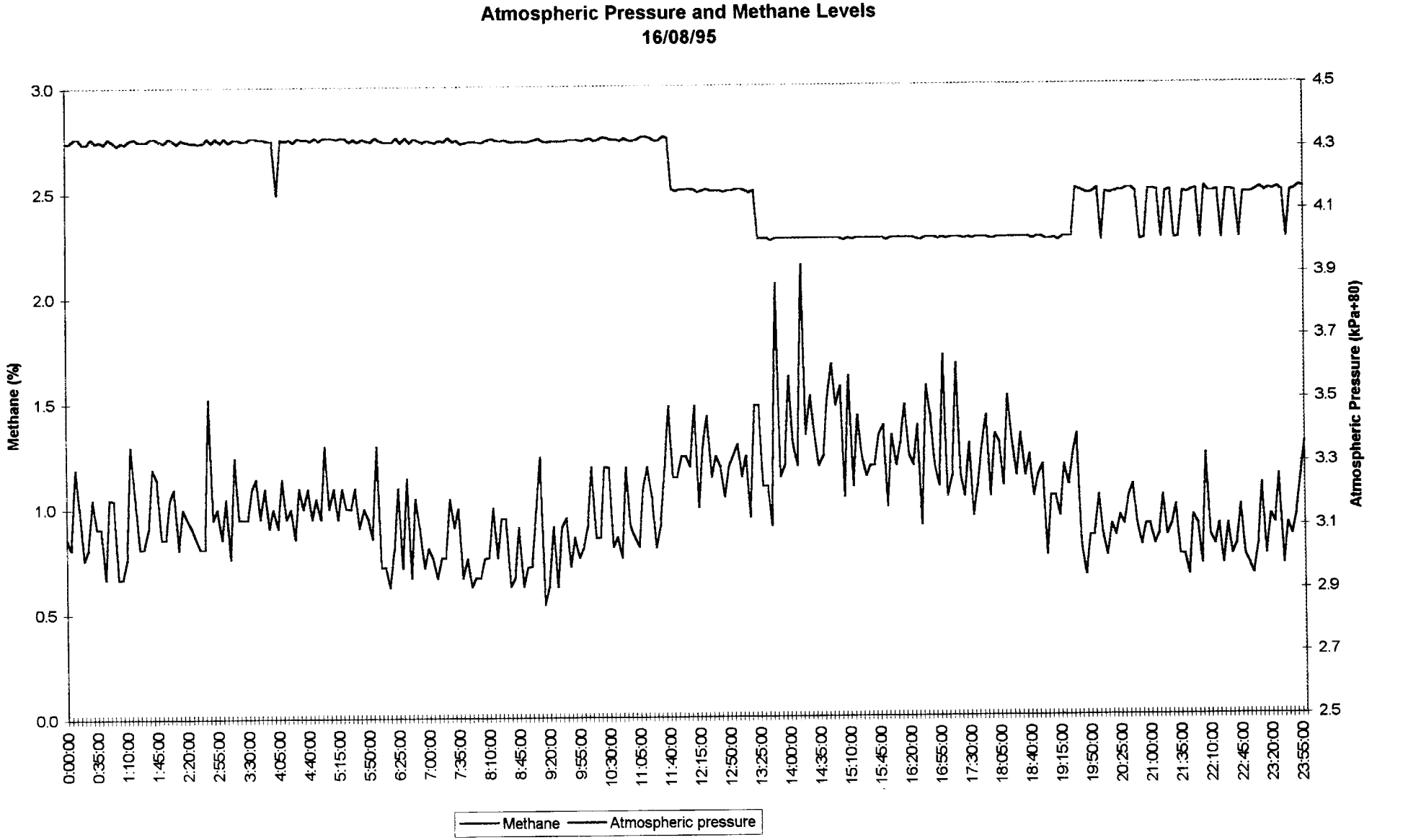
Atmospheric Pressure and Methane Levels
16/08/95
Methane (%)
Atmospheric Pressure (kPa+80)
3.0
2.5
2.0
1.5
1.0
0.5
0.0
4.5
4.3
4.1
3.9
3.7
3.5
3.3
3.1
2.9
2.7
2.5
0:00:00
0:35:00
1:10:00
1:45:00
2:20:00
2:55:00
3:30:00
4:05:00
4:40:00
5:15:00
5:50:00
6:25:00
7:00:00
7:35:00
8:10:00
8:45:00
9:20:00
9:55:00
10:30:00
11:05:00
11:40:00
12:15:00
12:50:00
13:25:00
14:00:00
14:35:00
15:10:00
15:45:00
16:20:00
16:55:00
17:30:00
18:05:00
18:40:00
19:15:00
19:50:00
20:25:00
21:00:00
21:35:00
22:10:00
22:45:00
23:20:00
23:55:00
Methane
Atmospheric pressure

Chart 39

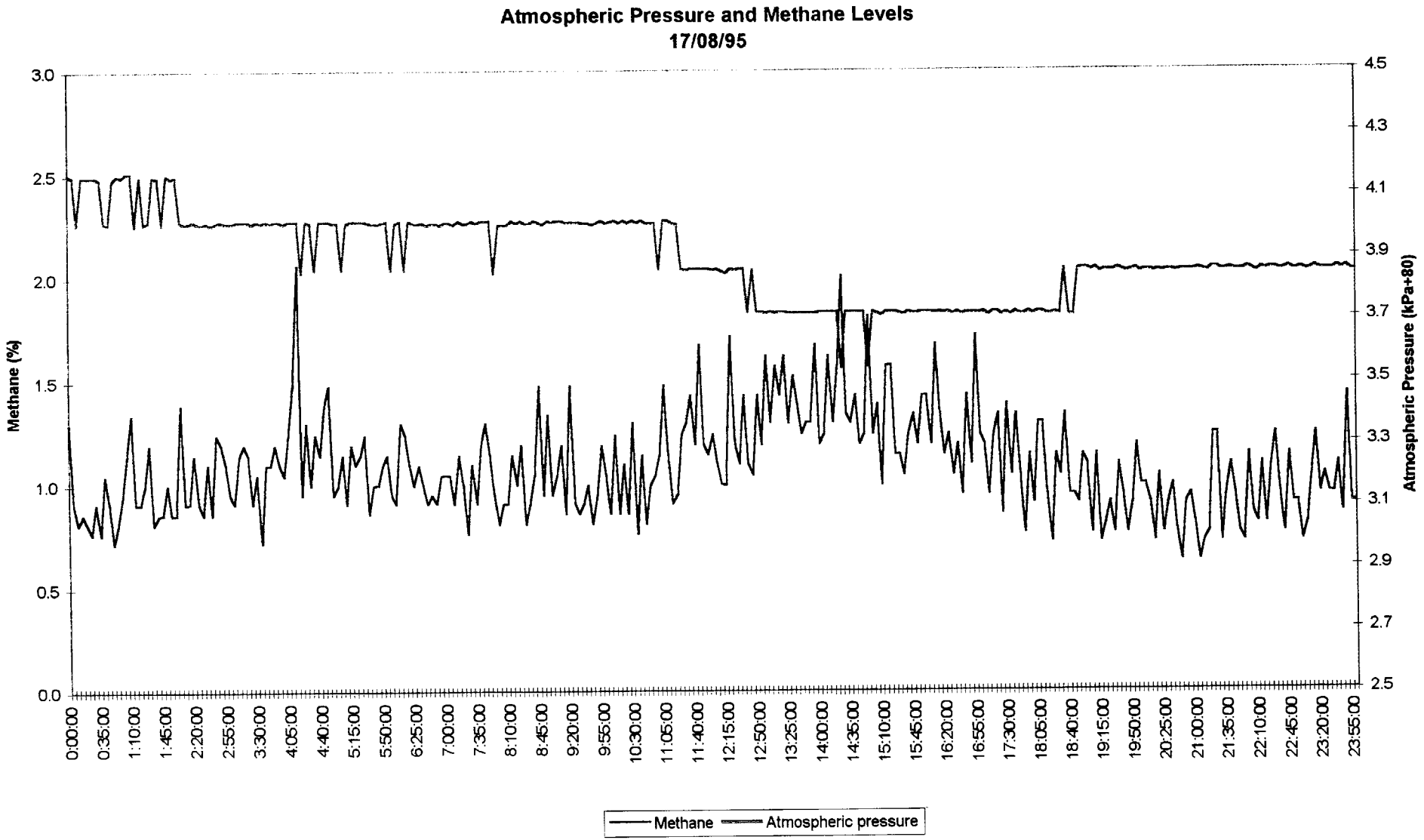
Atmospheric Pressure and Methane Levels
17/08/95
Methane (%)
Atmospheric Pressure (kPa+80)
3.0
2.5
2.0
1.5
1.0
0.5
0.0
4.5
4.3
4.1
3.9
3.7
3.5
3.3
3.1
2.9
2.7
2.5
0:00:00
0:35:00
1:10:00
1:45:00
2:20:00
2:55:00
3:30:00
4:05:00
4:40:00
5:15:00
5:50:00
6:25:00
7:00:00
7:35:00
8:10:00
8:45:00
9:20:00
9:55:00
10:30:00
11:05:00
11:40:00
12:15:00
12:50:00
13:25:00
14:00:00
14:35:00
15:10:00
15:45:00
16:20:00
16:55:00
17:30:00
18:05:00
18:40:00
19:15:00
19:50:00
20:25:00
21:00:00
21:35:00
22:10:00
22:45:00
23:20:00
23:55:00
Methane
Atmospheric pressure

Chart 40

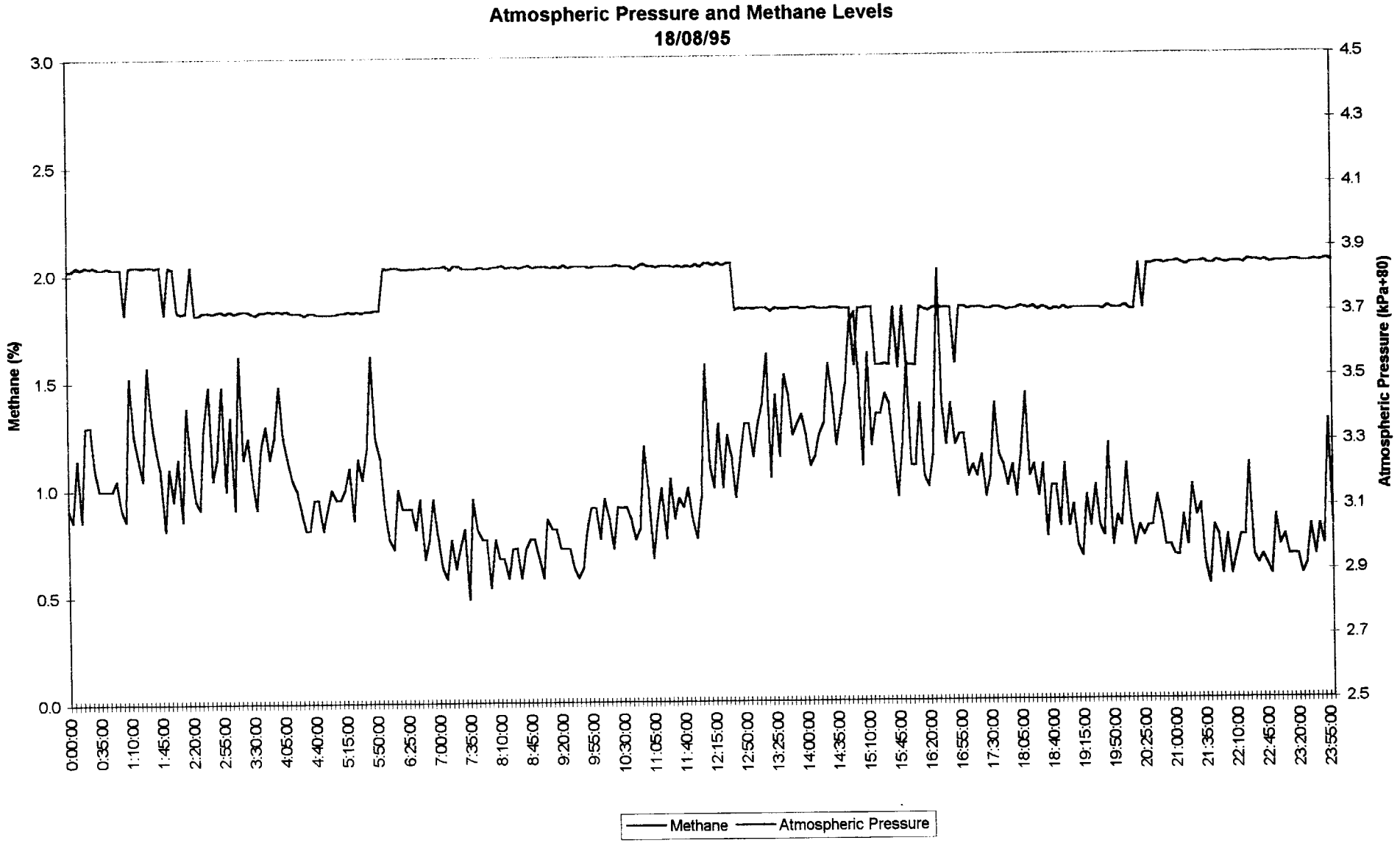
Atmospheric Pressure and Methane Levels
18/08/95
Methane (%)
Atmospheric Pressure (kPa+80)
3.0
2.5
2.0
1.5
1.0
0.5
0.0
4.5
4.3
4.1
3.9
3.7
3.5
3.3
3.1
2.9
2.7
2.5
0:00:00
0:35:00
1:10:00
1:45:00
2:20:00
2:55:00
3:30:00
4:05:00
4:40:00
5:15:00
5:50:00
6:25:00
7:00:00
7:35:00
8:10:00
8:45:00
9:20:00
9:55:00
10:30:00
11:05:00
11:40:00
12:15:00
12:50:00
13:25:00
14:00:00
14:35:00
15:10:00
15:45:00
16:20:00
16:55:00
17:30:00
18:05:00
18:40:00
19:15:00
19:50:00
20:25:00
21:00:00
21:35:00
22:10:00
22:45:00
23:20:00
23:55:00
Methane
Atmospheric Pressure

Chart 41

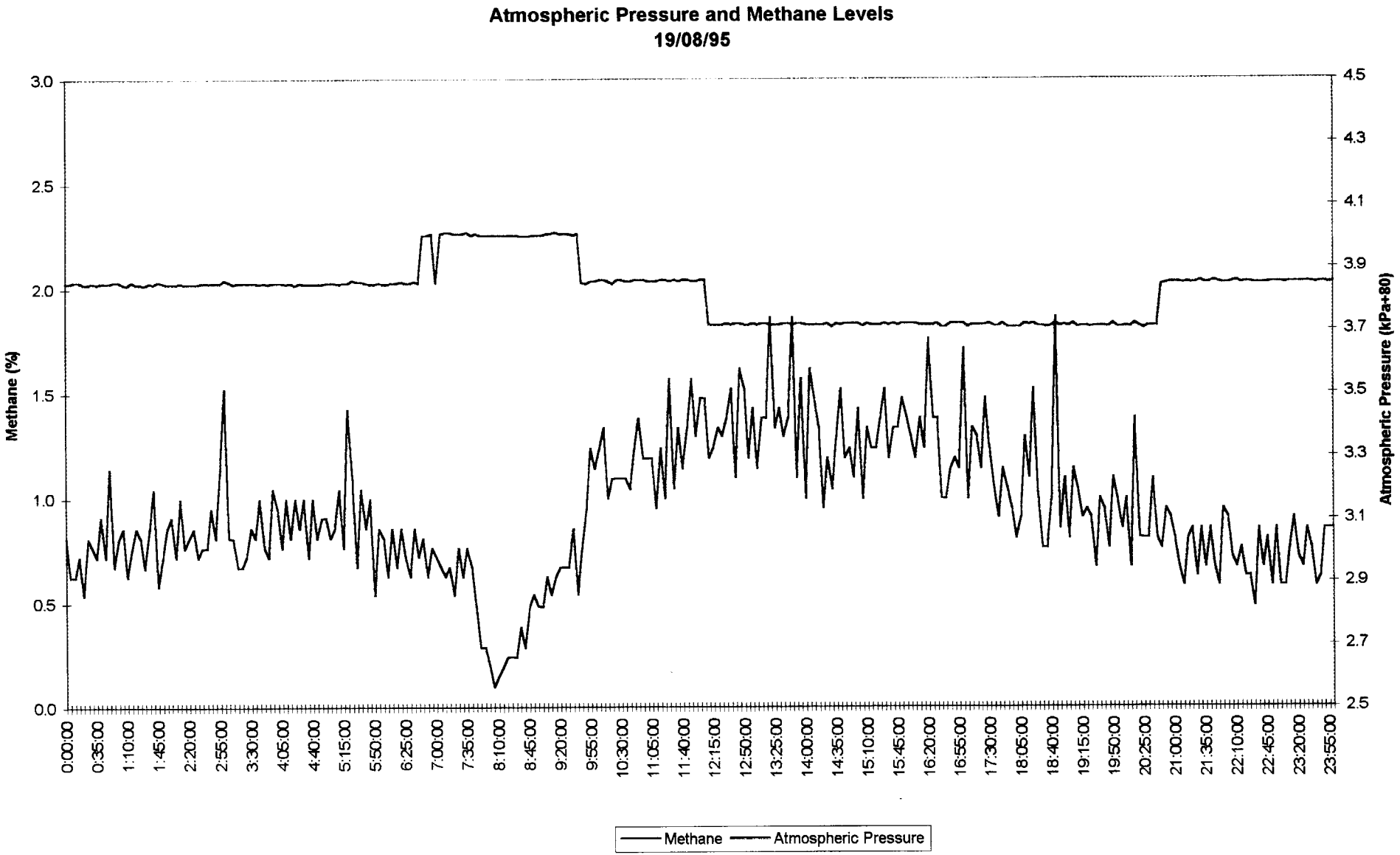
Atmospheric Pressure and Methane Levels
19/08/95
Methane (%)
Atmospheric Pressure (kPa+80)
3.0
2.5
2.0
1.5
1.0
0.5
0.0
4.5
4.3
4.1
3.9
3.7
3.5
3.3
3.1
2.9
2.7
2.5
0:00:00
0:35:00
1:10:00
1:45:00
2:20:00
2:55:00
3:30:00
4:05:00
4:40:00
5:15:00
5:50:00
6:25:00
7:00:00
7:35:00
8:10:00
8:45:00
9:20:00
9:55:00
10:30:00
11:05:00
11:40:00
12:15:00
12:50:00
13:25:00
14:00:00
14:35:00
15:10:00
15:45:00
16:20:00
16:55:00
17:30:00
18:05:00
18:40:00
19:15:00
19:50:00
20:25:00
21:00:00
21:35:00
22:10:00
22:45:00
23:20:00
23:55:00
Methane
Atmospheric Pressure

Chart 42

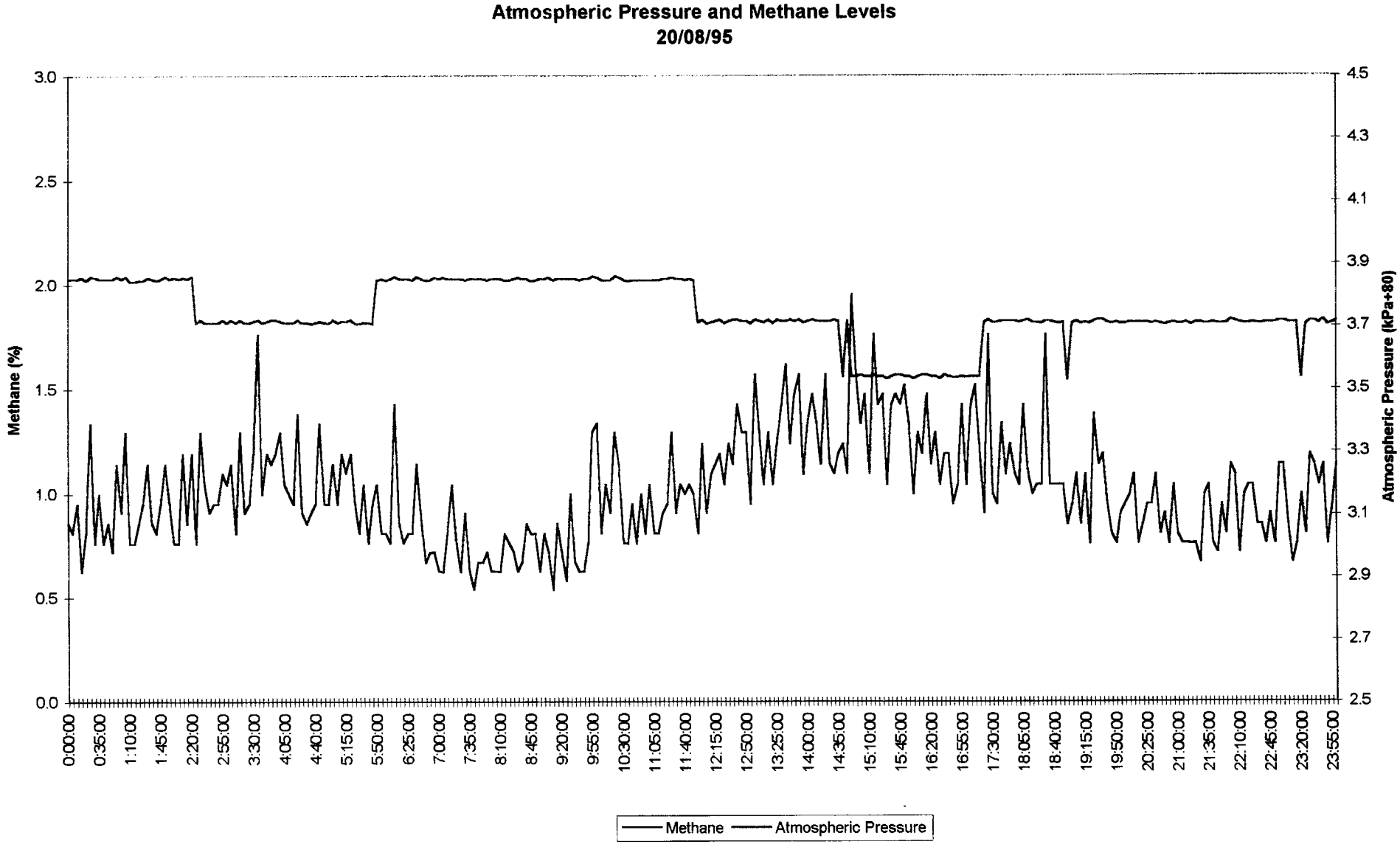
Atmospheric Pressure and Methane Levels
20/08/95
Methane (%)
Atmospheric Pressure (kPa+80)
3.0
2.5
2.0
1.5
1.0
0.5
0.0
4.5
4.3
4.1
3.9
3.7
3.5
3.3
3.1
2.9
2.7
2.5
0:00:00
0:35:00
1:10:00
1:45:00
2:20:00
2:55:00
3:30:00
4:05:00
4:40:00
5:15:00
5:50:00
6:25:00
7:00:00
7:35:00
8:10:00
8:45:00
9:20:00
9:55:00
10:30:00
11:05:00
11:40:00
12:15:00
12:50:00
13:25:00
14:00:00
14:35:00
15:10:00
15:45:00
16:20:00
16:55:00
17:30:00
18:05:00
18:40:00
19:15:00
19:50:00
20:25:00
21:00:00
21:35:00
22:10:00
22:45:00
23:20:00
23:55:00
Methane
Atmospheric Pressure

Chart 43

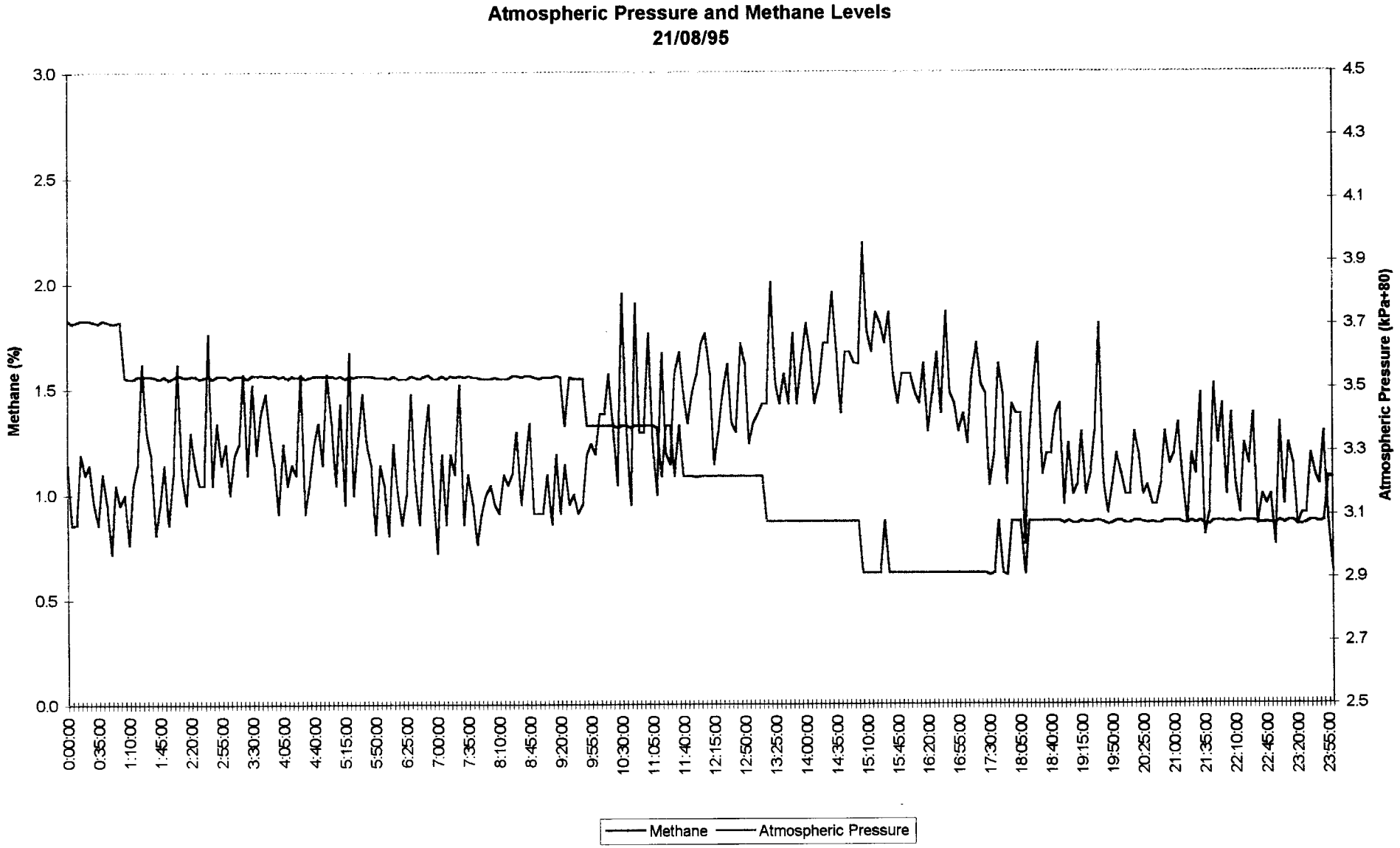
Atmospheric Pressure and Methane Levels
21/08/95
Methane (%)
Atmospheric Pressure (kPa+80)
3.0
2.5
2.0
1.5
1.0
0.5
0.0
4.5
4.3
4.1
3.9
3.7
3.5
3.3
3.1
2.9
2.7
2.5
0:00:00
0:35:00
1:10:00
1:45:00
2:20:00
2:55:00
3:30:00
4:05:00
4:40:00
5:15:00
5:50:00
6:25:00
7:00:00
7:35:00
8:10:00
8:45:00
9:20:00
9:55:00
10:30:00
11:05:00
11:40:00
12:15:00
12:50:00
13:25:00
14:00:00
14:35:00
15:10:00
15:45:00
16:20:00
16:55:00
17:30:00
18:05:00
18:40:00
19:15:00
19:50:00
20:25:00
21:00:00
21:35:00
22:10:00
22:45:00
23:20:00
23:55:00
Methane
Atmospheric Pressure

Chart 44

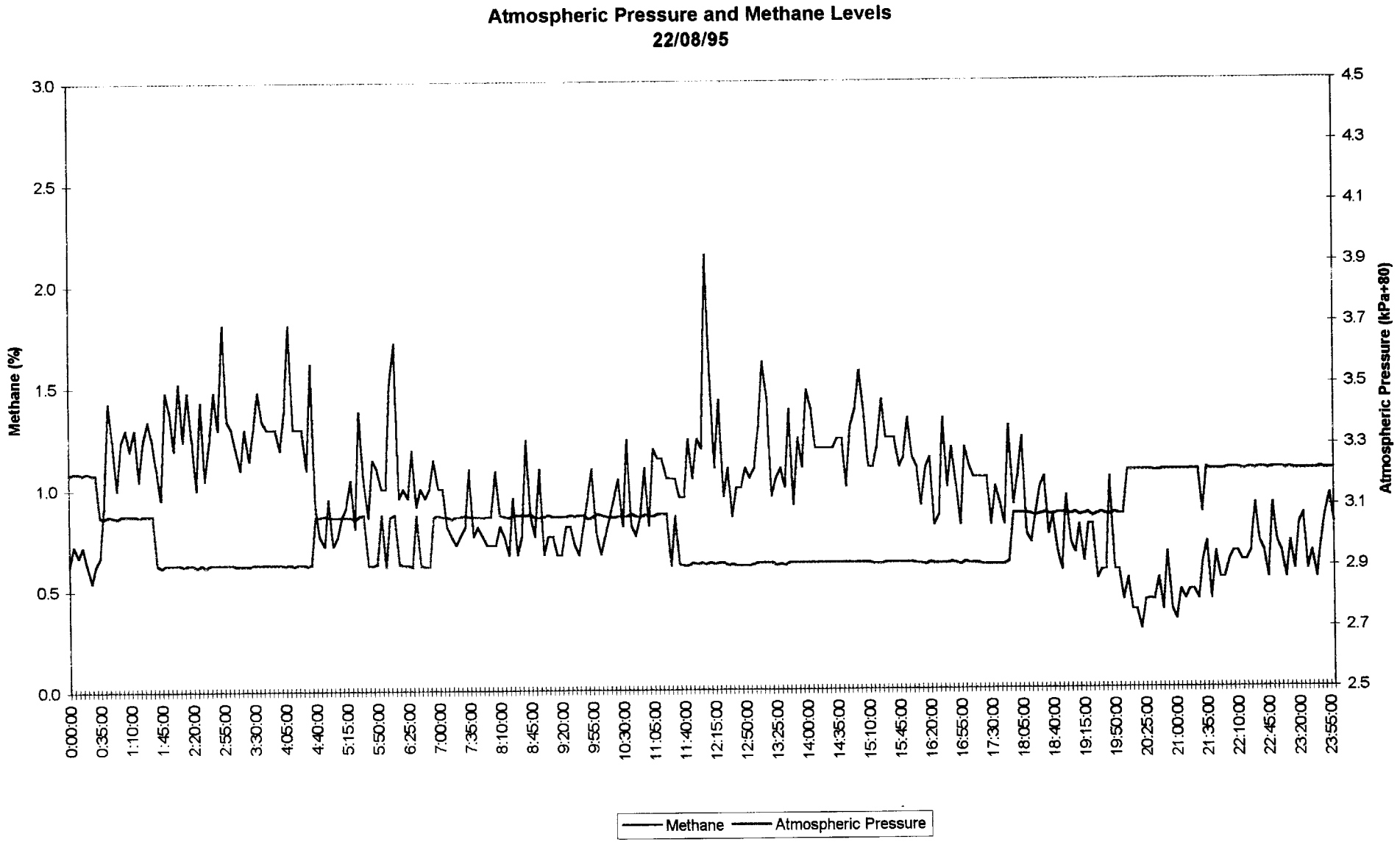
Atmospheric Pressure and Methane Levels
22/08/95
Methane (%)
Atmospheric Pressure (kPa+80)
3.0
2.5
2.0
1.5
1.0
0.5
0.0
4.5
4.3
4.1
3.9
3.7
3.5
3.3
3.1
2.9
2.7
2.5
0:00:00
0:35:00
1:10:00
1:45:00
2:20:00
2:55:00
3:30:00
4:05:00
4:40:00
5:15:00
5:50:00
6:25:00
7:00:00
7:35:00
8:10:00
8:45:00
9:20:00
9:55:00
10:30:00
11:05:00
11:40:00
12:15:00
12:50:00
13:25:00
14:00:00
14:35:00
15:10:00
15:45:00
16:20:00
16:55:00
17:30:00
18:05:00
18:40:00
19:15:00
19:50:00
20:25:00
21:00:00
21:35:00
22:10:00
22:45:00
23:20:00
23:55:00
Methane
Atmospheric Pressure

Chart 45

Atmospheric Pressure and Methane Levels
23/08/95

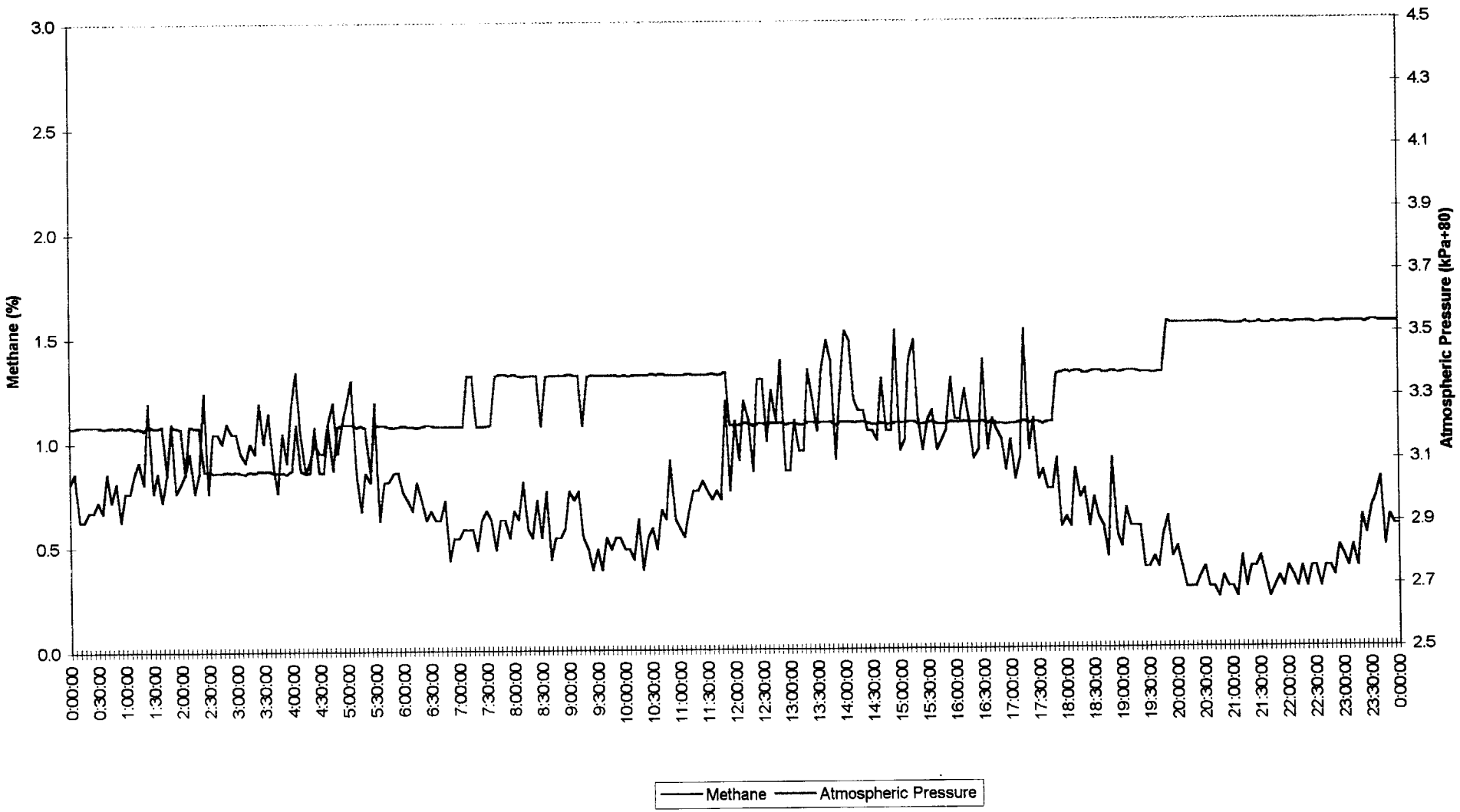

Chart 46

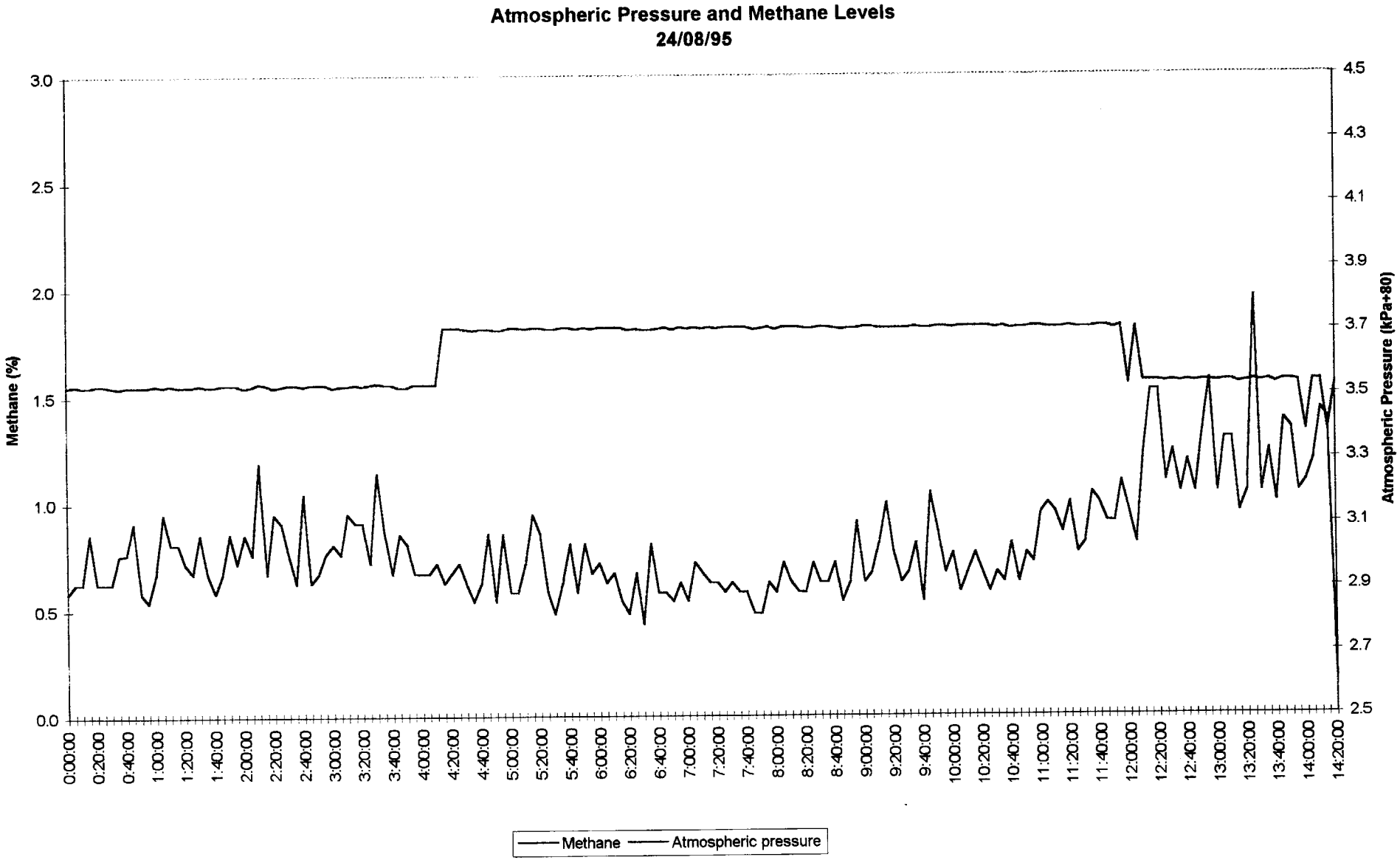
Atmospheric Pressure and Methane Levels
24/08/95
Methane (%)
Atmospheric Pressure (kPa+80)
3.0
2.5
2.0
1.5
1.0
0.5
0.0
4.5
4.3
4.1
3.9
3.7
3.5
3.3
3.1
2.9
2.7
2.5
0:00:00
0:20:00
0:40:00
1:00:00
1:20:00
1:40:00
2:00:00
2:20:00
2:40:00
3:00:00
3:20:00
3:40:00
4:00:00
4:20:00
4:40:00
5:00:00
5:20:00
5:40:00
6:00:00
6:20:00
6:40:00
7:00:00
7:20:00
7:40:00
8:00:00
8:20:00
8:40:00
9:00:00
9:20:00
9:40:00
10:00:00
10:20:00
10:40:00
11:00:00
11:20:00
11:40:00
12:00:00
12:20:00
12:40:00
13:00:00
13:20:00
13:40:00
14:00:00
14:20:00
Methane
Atmospheric pressure

Chart 47

Atmospheric Pressure and Methane Levels
Curve Fitting - 14/6/95

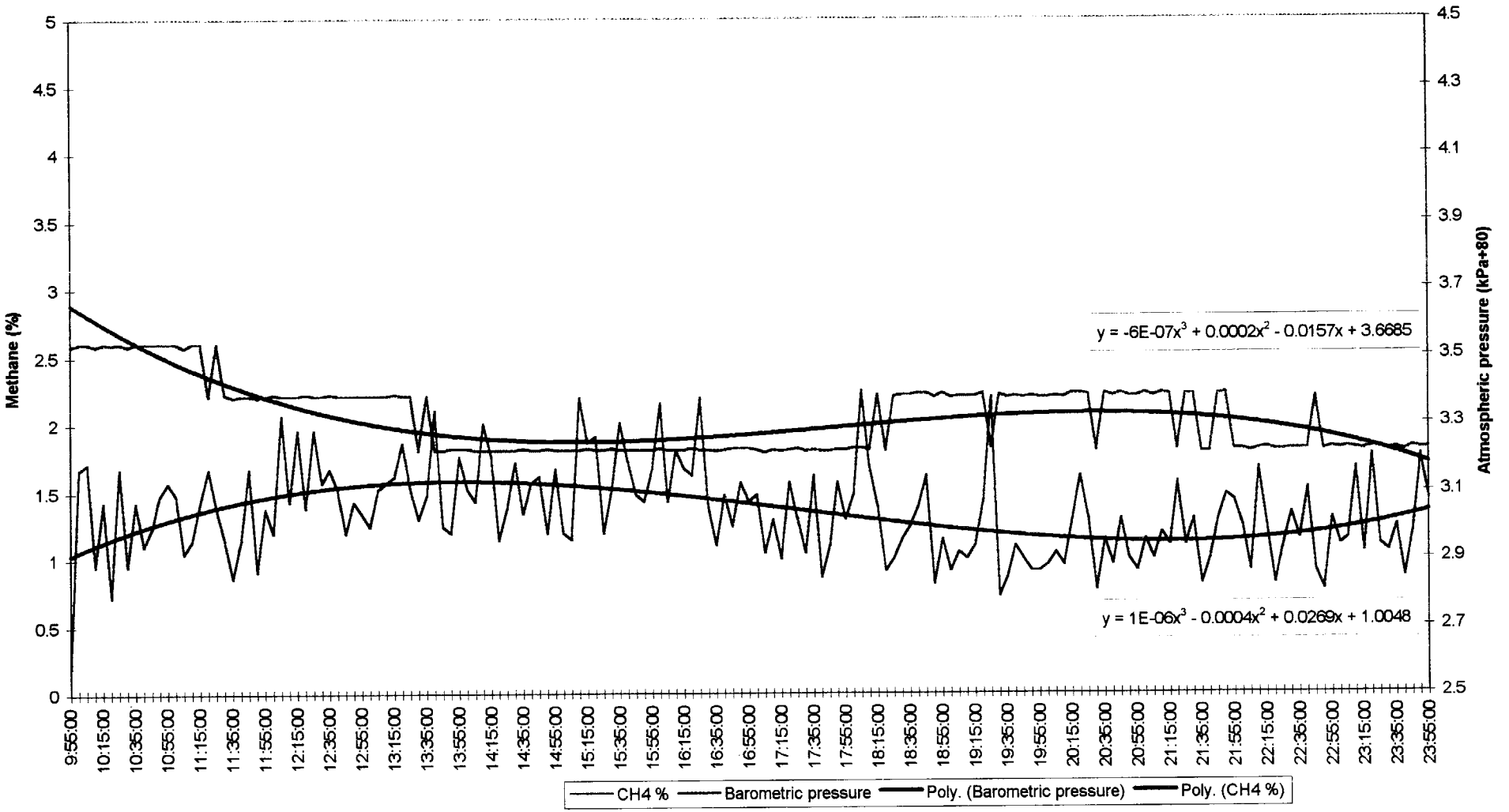

Corr -0.1891923

Chart 48

Atmospheric Pressure and Methane Levels
Curve Fitting - 20/6/95

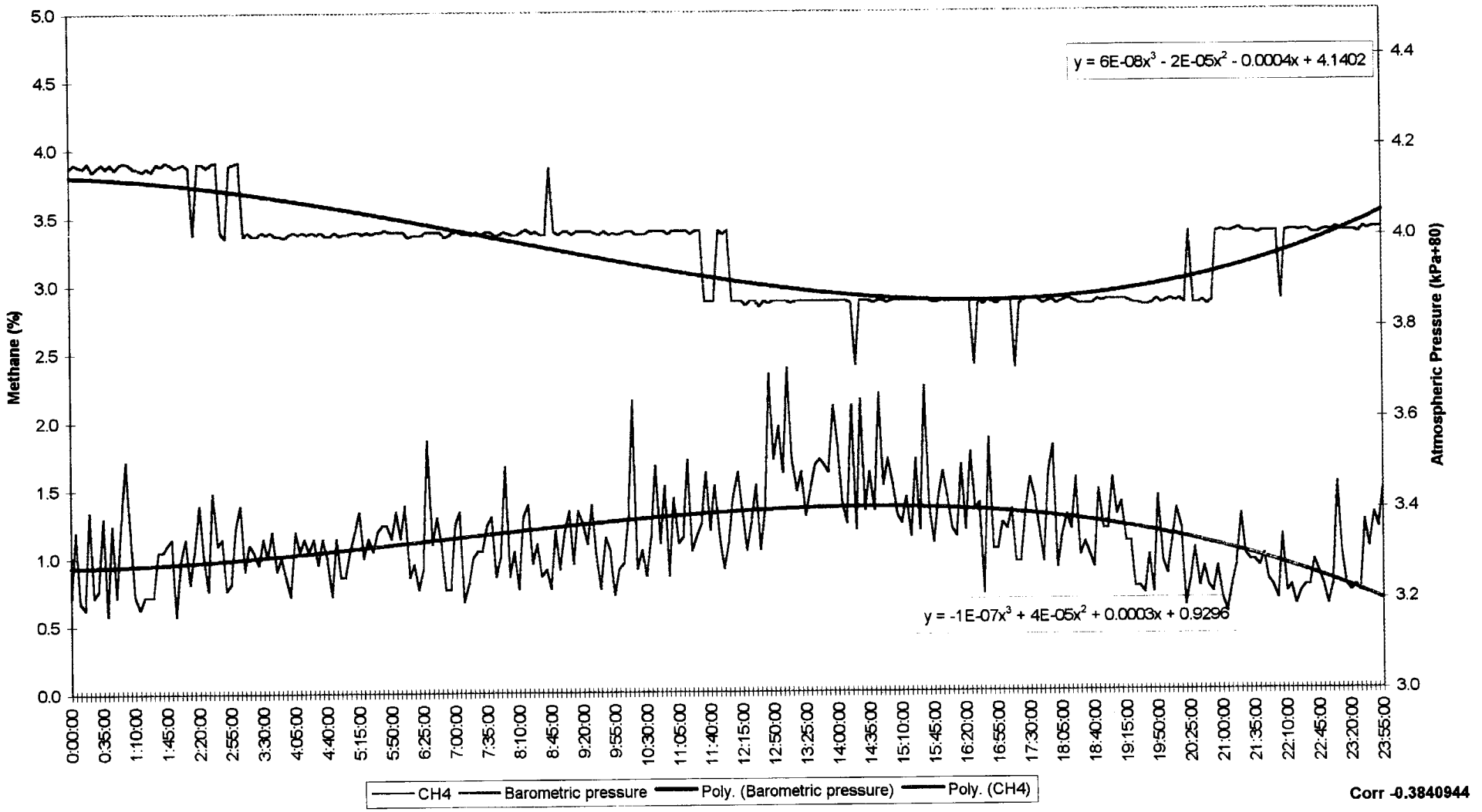

Corr -0.3840944

Chart 49

Atmospheric Pressure and Methane levels
Curve fitting 16/6/95

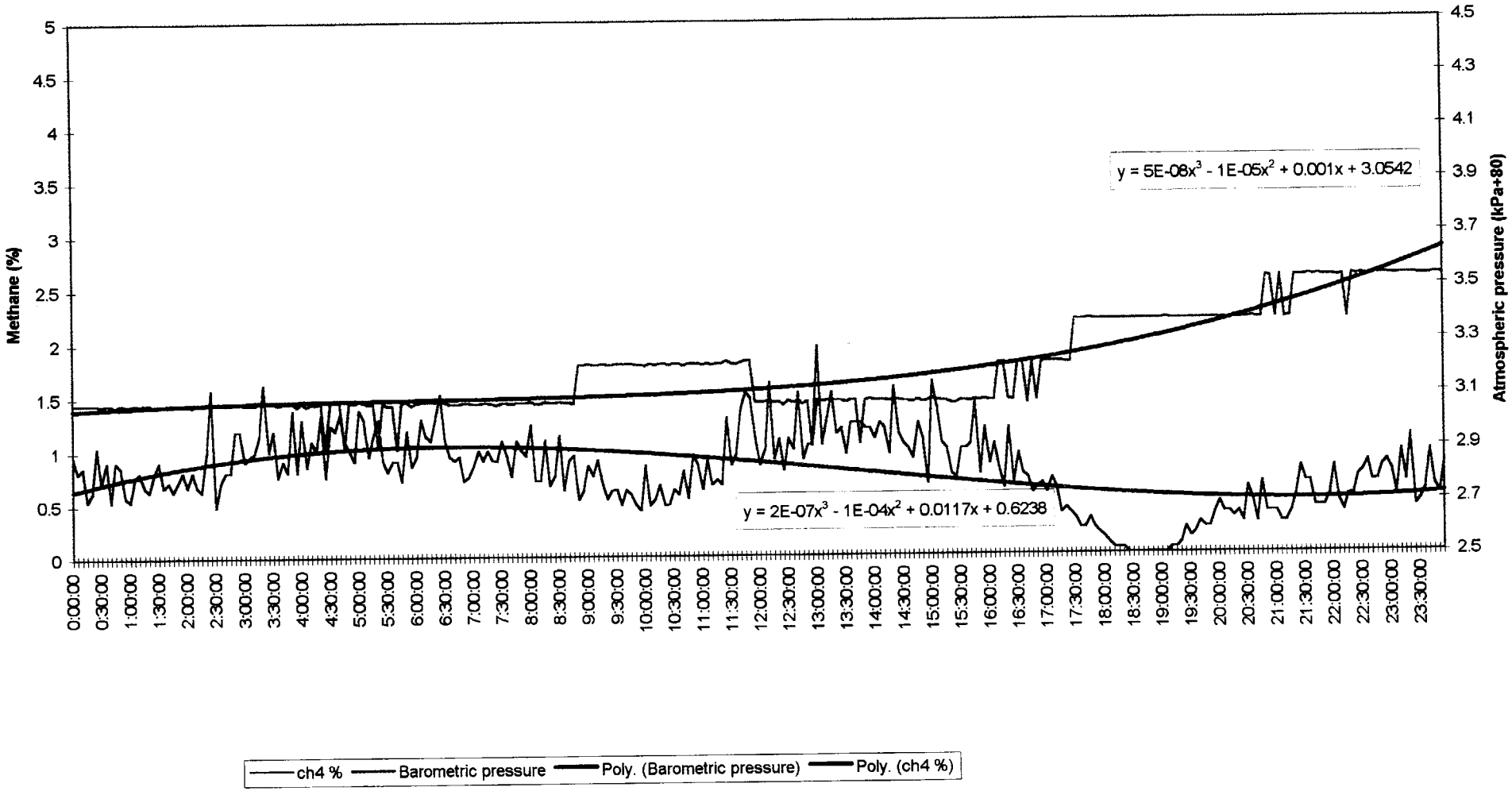

Corr -0.591179

Chart 50

Atmospheric Pressure and Methane Levels on a Two Day Period
Curve Fitting (14-15 JUNE 1995)

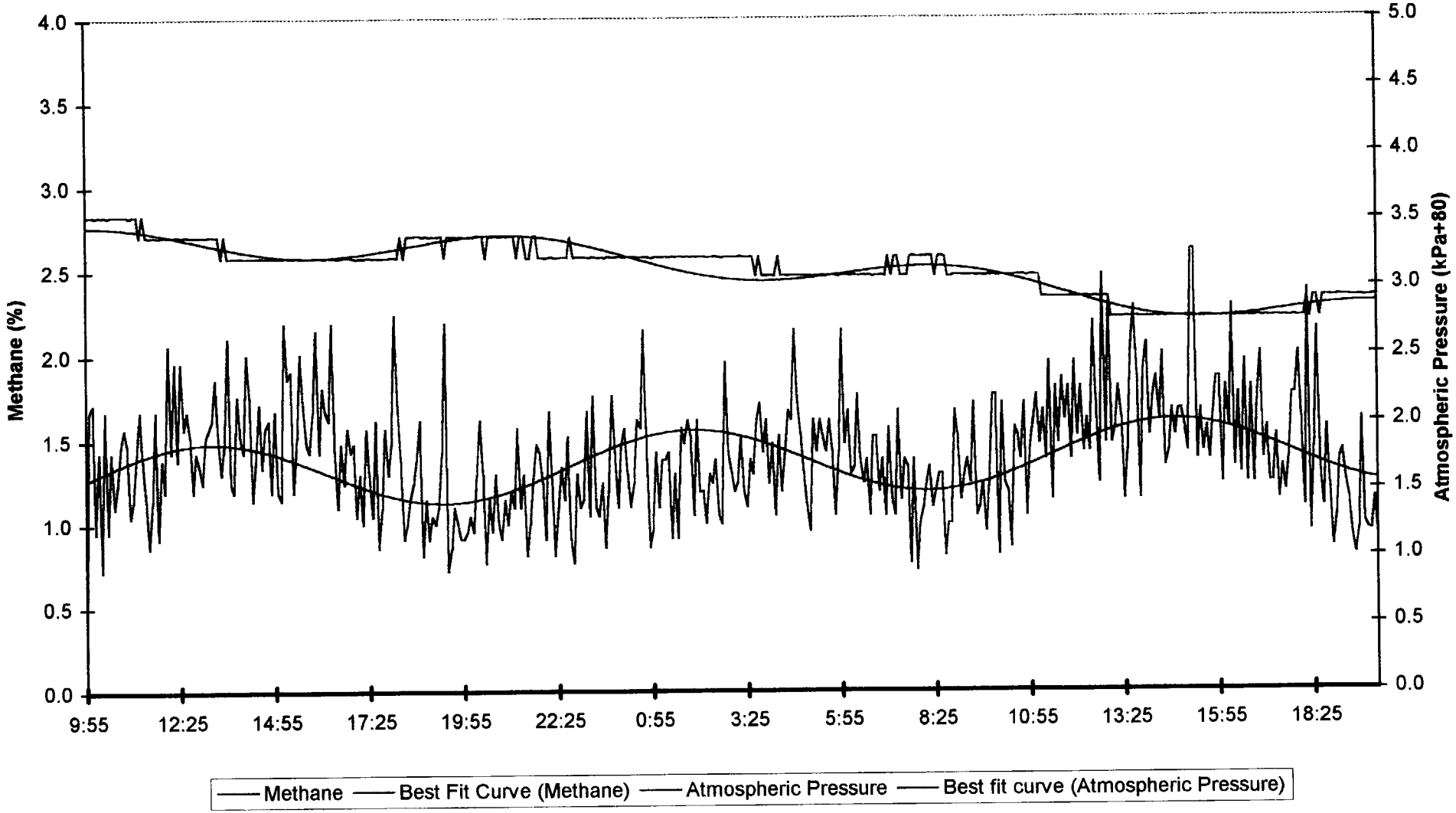

Chart 51

Atmospheric Pressure and Methane Variations - 7/11/94 to 14/11/94
AtmBase1.0 CH4Base 0.2

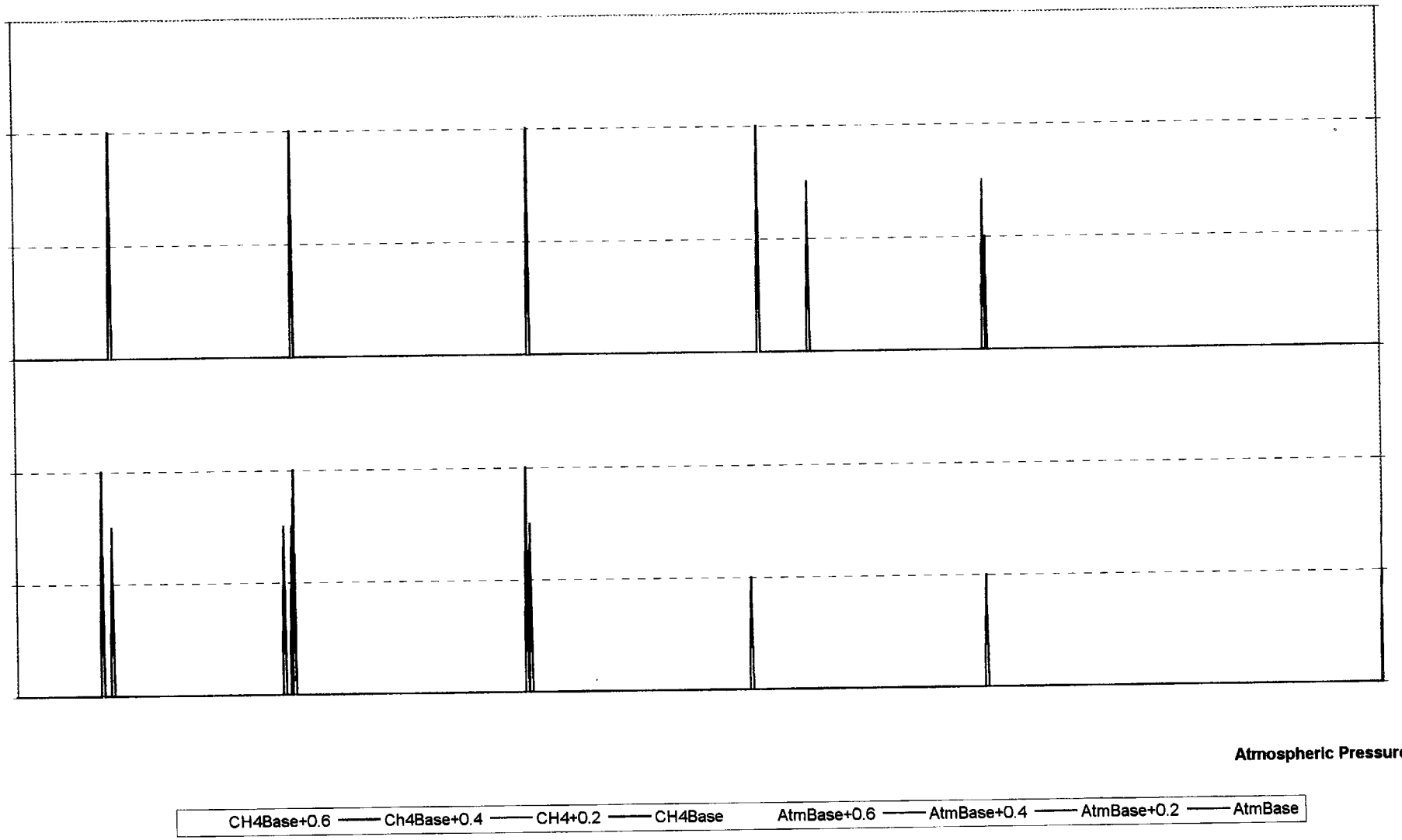

Chart 52

Methane

Atmospheric Pressure and Methane Level Variations 25/07/95 - 06/08/95

AtmBase: 0.2 CH4Base 0.9

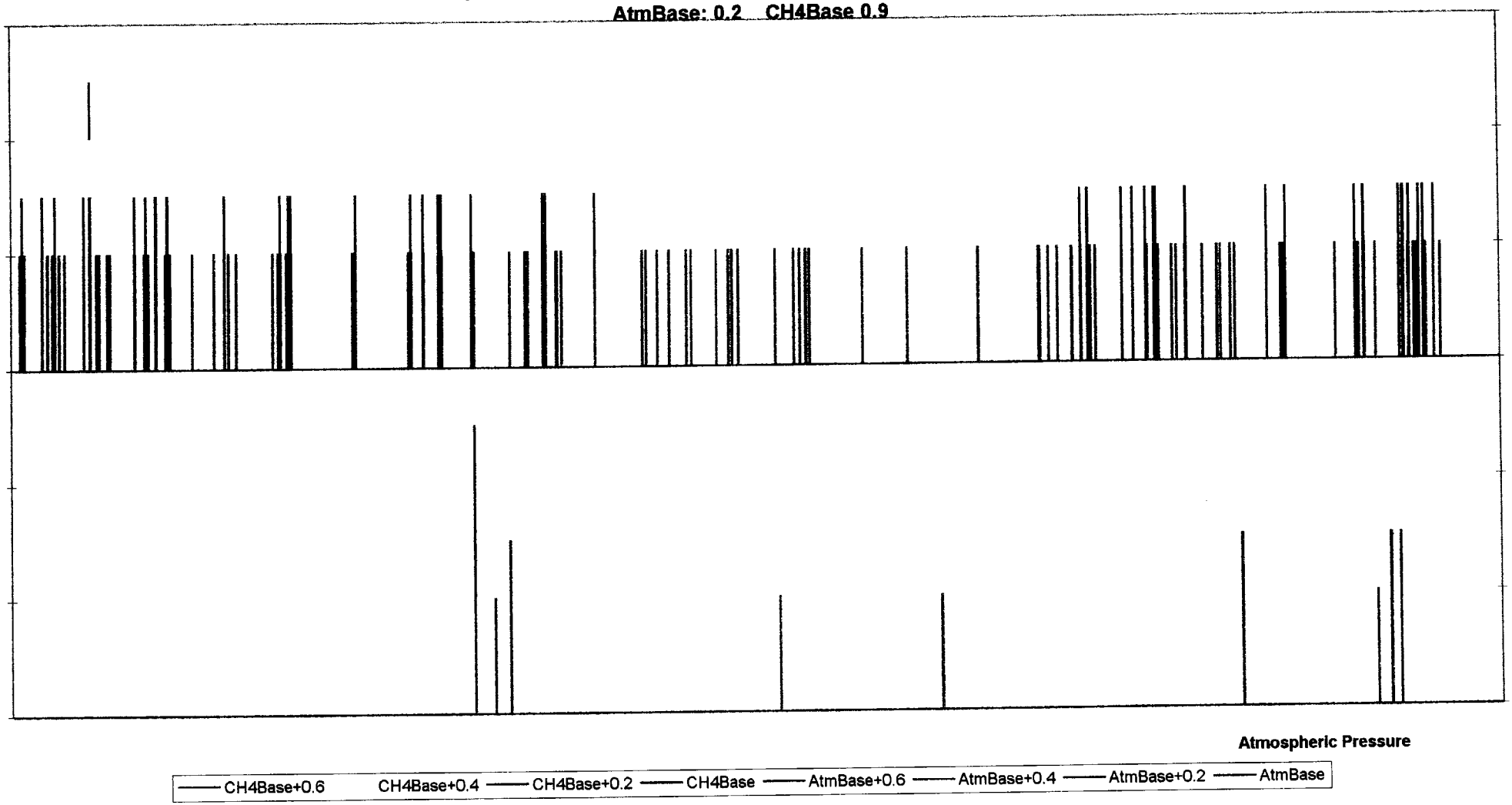

Chart 53

Methane

Atmospheric Pressure and Methane Levels Variation Over 5 minutes 15-24 Aug 95
AtmBase 0.1 CH4Base 0.8

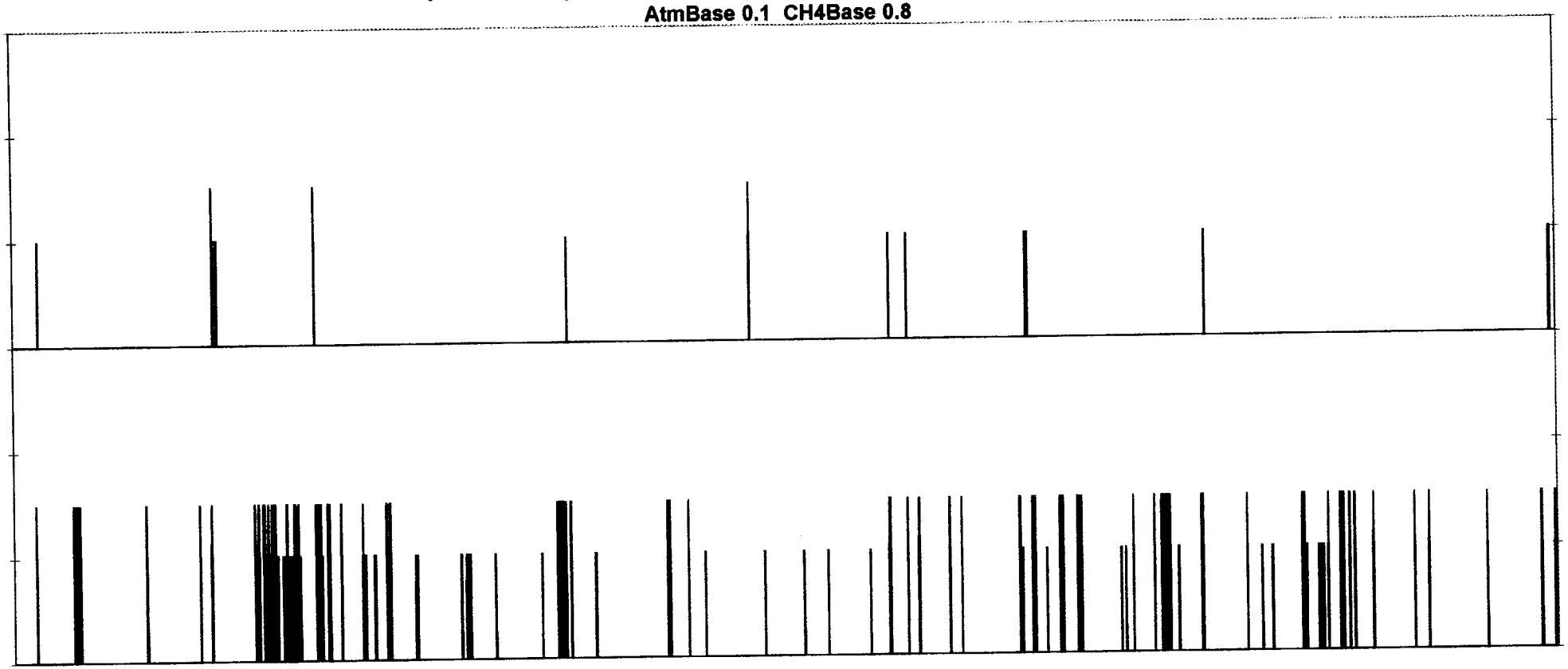

Atmospheric Pressure

CH4BAse+0.6 —— CH4Base+0.4 —— CH4Base+0.2 —— CH4Base AtmBase+0.15 —— AtmBase+0.1 —— AtmBase+0.05 —— AtmBase

APPENDIX E

E1. A.P. Cook, Methane Drainage in South Africa an Overview, Interim Report, August 1995, CSIR Division of Mining Technology.

E2. A.P. Cook, Methane Drainage Systems and Future Requirements for South African Coal Mines, 6th US Ventilation Symposium, January 1993, COMRO Coal Mining Division.

E3. A.P. Cook, A Brief Overview of Coal Bed Methane, Interim Note, March 1993, COMRO Coal Mining Division.

APPENDIX E1

METHANE DRAINÁGE IN SOUTH AFRICA, AN OVERVIEW

A.P. Cook

SIMRAC INTERIM REPORT
COLO3O
AUGUST 1995

METHANE DRAINAGE IN SOUTH AFRICA, AN OVERVIEW

INTRODUCTION

Methane drainage is widely practised worldwide by the coal mining industry, principally to improve safety by reducing seam methane emissions into workings, but also as a related or independent commercial venture. Drainage is generally carried out where seam gas contents or emission rates make standard ventilation techniques inadequate or impractical.; General guidelines for when drainage becomes necessary range from simple application of seam contents to simultaneous application of several different conditions. This report will discuss the drainage carried out in South African collieries, and compare conditions with those of other countries, and consider the necessity for similar guidelines.

METHODS OF DRAINAGE

Methane drainage can be carried out underground or from surface. A great deal of literature is available on both techniques, and from different countries employing different mining methods, so there is no need for a detailed review here. Underground drainage is normally applied for deeper seams, where surface drilling is not economical, or for specific localised areas, and when time is limited. Surface drilling is usually applied over a longer time period, often many years, ahead of mining operations, and covers a much larger area with borehole spacing of hundreds of metres.

In South Africa the application of both methods has been very limited and little information is available on the effectiveness. Some in-seam drainage has been monitored from long horizontal holes, but no figures are available for vertical holes drilled from surface, although some initial work has been considered by several companies. The very limited application of any form of drainage compares with 127, or 42 %, of UK mines at one time practising drainage[1], and 108 (18 %) of mines in China presently draining methane[2].

METHANE CHARACTERISTICS OF SOUTH AFRICAN COAL SEAMS

South African production coal seams are relatively shallow, with correspondingly low methane pressures and contents.

The methane adsorption properties (which control the volume of methane contained) are generally similar to those reported of coals from other countries[3], but the diffusive properties (which control the release rate) are lower[4]. Figure 1 compares methane adsorption curves of coal from Majuba Colliery[5] with those of West Cliff Colliery in Australia[6], and from the Pittsburgh Coalbed in the USA[7]. These have been chosen as examples as all sites have practised methane drainage, and much has been reported on the Australian and USA sites. The Majuba isotherm is very similar to that of West Cliff and higher than that of Pittsburgh.

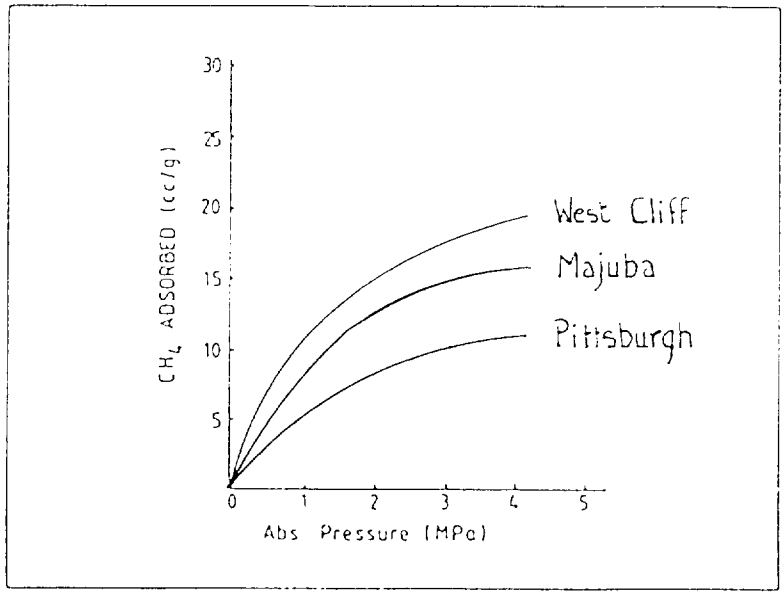

FIGURE 1: Methane Adsorption Isotherms

Seam content from the adsorption isotherms is directly affected by seam gas pressure. Pressure is related to depth so the relatively shallow production seams in South Africa do not have such high gas pressures. Maximum pressures measured in South Africa have been around 1.6 MPa at Majuba at a seam depth of 300 m[8], and this compares to pressures as high as 8.25 MPa reported from China[2], at a seam depth of 729 m.

Seam gas contents in South Africa, determined from adsorption and in seam pressure results, range up to a likely maximum of around 10 m^3/t, but with an "average" being more likely around 4 m^3/t. These values are not dissimilar to figures quoted for other countries working at similar depths, but are very much less than gas contents for deeper coal seams, particularly in Europe where contents can exceed 30 m^3/t [1].

METHANE DRAINAGE VOLUMES

Volume flows from South African drainage sites are relatively low [9]. Volumes from in-seam boreholes at Majuba ranged from 73 to 922 $m^3/m/y$, which compare with 2190 to 8468 $m^3/m/y$ for the Pittsburgh seam[10], 9513 $m^3/m/y$ for West Cliff [6], and 1187 to 2470 $m^3/m/y$ for European mines[11]. These relative flows support the results of the diffusion coefficients, with slower release rates, although very high initial drainage volumes have been reported for another site in South Africa[12], but with no decrease in seam pressure after five months, which suggests the high volume flows were not maintained.

DISCUSSION

Methane drainage has not been widely practised in South Africa, and few *in situ* results are available to make a complete evaluation. Figures that are available show methane drainage rates well below those reported from similar in-seam holes in other countries. More information is available of the methane properties of coals, which show similar adsorption properties to those in other countries but lower diffusion rates. Relatively shallow seams results in lower seam gas pressures and hence lower seam gas contents. All this suggests that methane drainage may not be particularly suitable for South African production coal seams.

This does not mean that methane drainage should be disregarded. The methane prediction model being developed for COL030 includes the effects of drainage, and

will allow the simulation of drainage applied to particular seams or collieries. Also benefits may be obtained on localised applications, rather than industry wide. No actual figures are available for the majority of seams, with diffusion coefficients in the range of 10^{-9} cm^2/s, which should have faster release rates than seen at Majuba. Any drainage practised in South Africa, either surface or underground should be monitored, to compare with both the prediction model, and the methane properties of the coal.

CONCLUSION

Information available on drainage rates, seam pressures and contents, and coal properties suggests that methane drainage may not be as successful in South African coal mines as in other countries. This does not mean it should be disregarded as there may be some localised benefits, and also because no figures are available for long-term surface drainage boreholes. Any drainage that is carried out should be monitored to expand the limited data base presently available.

The methane emission prediction model does include drainage, and will indicate the effects for South African coal seams.

REFERENCES

1. SWIFT, R.A. Methane drainage in Great Britain. Coal Age, February 1970.
2. YONGYAN, W. and EDWARDS, J.S. Coal mine methane drainage in China. The Mining Engineer, November 1993.
3. COOK, A.P. and ERWEE, E.C. Methane properties of South African coals. Part 1: sorption characteristics. COMRO Reference report, May 1991.
4. COOK, A.P. The methane-emission characteristics of South African coals. MASSMIN 92, SAIMM, Johannesburg 1992.
5. BAXTER, L. Laboratory analysis report. ME internal note 07/93, Miningtek 1993.
6. HEBBLEWHITE, B.K., LAMA, R.D. and HARGRAVES, A.J. Gas drainage experiment and practice in Australia. 6th ICCR Conference, London, 1982

7. KISSEL, F.N., McCULLOCH, C.M. and ELDER, C.H. The direct method of determining methane content of coalbeds for ventilation design. USBM report of investigation RI7767, 1973.

8. COOK, A.P. Towards a method of methane prediction for South African collieries. 23rd International conference of safety in mines research institutes, Washington, 1989.

9. COOK, A.P. Methane drainage systems and future requirements in South African collieries. 6th US mine ventilation symposium, Salt Lake City, 1993.

10. TREVITS, M.A. and FINFINGER, G.L. Results given of studies concerning methane extraction from coalbeds. Mining Engineering, August 1986.

11. BOXHO, J, et al. Firedamp drainage. Coal Directorate of the Commission of the European Communities, Essen, 1980.

12. BARNARD, M.C.C. Methane drainage at Indumeni. SA Mining and Engineering Journal, June 1977.

APPENDIX E2

METHANE DRAINAGE SYSTEMS AND FUTURE REQUIREMENTS IN SOUTH AFRICAN COAL MINES

A.P.COOK

Coal Mining division, COMRO
Johannesburg, South Africa

Methane drainage on a mine-wide scale is a relatively new technology to South African coal mines. Shallow seams and apparently low methane contents have been assumed to result in less methane problems than experienced in other countries.
The introduction of deeper mines however, has now resulted in methane drainage taking on a higher priority.

Methane contents in the region of 12 m^3\t have resulted in one colliery introducing drainage as a ventilation support. Although a low seam permeability initially indicated reduced potential for drainage, early borehole flows of 90 m^3\m\year have since increased to 450 m^3\m\year.

Rapid inflow of methane into goafs and sealed areas from seams surrounding the main production seam at another colliery have warranted extensive evaluation of the methane properties of these seams with the projected introduction of predrainage from surface. Methane pressures in excess of 1000 kPa and contents in the region of 10 m^3\t again give methane volumes suitable for drainage.

Coal seam drainage ahead of mining is becoming more significant and is likely to see an increase in the near future.

INTRODUCTION

Methane gas is an everpresent hazard associated with underground coal mining. Safe working levels of methane in the mine atmosphere are normally maintained by ventilation practises, ensuring sufficient dilution of the gas. However in some cases the ventilation must be assisted by methane drainage, either from the mined seam, or from adjacent seams and strata, or from goafed areas.

South African collieries have practised only limited methane drainage until now. Relatively shallow mining depths, and apparently low in-seam methane contents have been assumed to result in fewer problems with methane than are the normal for other countries. This is now being shown to not necessarily be the situation. Work carried out by the Coal Mining division of COMRO (Cook and Erwee, 1991) indicates South African production coal seams have very similar methane retention properties to those of coals in other countries, with seam gas contents of up to 12 m^3/t. This awareness, as well as greater mining depths, and higher degrees of mechanisation, has resulted in higher priority being given to methane emission problems throughout the industry.

Increased levels of safety, as well as possible commercial applications, are the main reasons for the interest now being shown in methane drainage. Not only is there possible applications in the present production coalfields, but South Africa has vast areas of coal reserves which are presently non-mineable, now being seen as possible alternative energy sources.

Limited methane drainage is practised within the industry, but only on collieries that have identified specific methane problems that can be alleviated by drainage. Historically this has been restricted to surface drainage of longwall goafs, reducing emissions onto the faces. More recently, horizontal in-seam holes have been drilled, until now for bord and pillar sections, but the results are being evaluated for later application to shortwall faces. Adjacent seams pose problems at some sites and vertical and cross measure boreholes are now being considered.

IN-SEAM DRAINAGE

As mining depths increase, so does the methane gas hazard. This has been observed at a recently opened colliery, mining at depths in excess of 300 m, compared with a common South African depth of around 100 m. Methane seam pressures approaching 2 MPa have been measured (Cook, 1989), with seam gas contents in the range of 8 - 12 m^3/t.

Provisional methane drainage has been practised at this site for the past three years, to evaluate its effectiveness for future mine wide application. The mine is planned to eventually operate on high advance longwall and shortwall mining methods, and relatively high methane emissions can be anticipated, according to the research results to date, and to the methane emissions encountered in the present bord and pillar workings.

After initial pressure and content evaluations using inflatable borehole packers and a gravimetric sorption apparatus (Cook, 1989), drainage monitoring is carried out of volumetric flow from individual boreholes. This is achieved using a rotameter type flowmeter installed as in Figure 1.

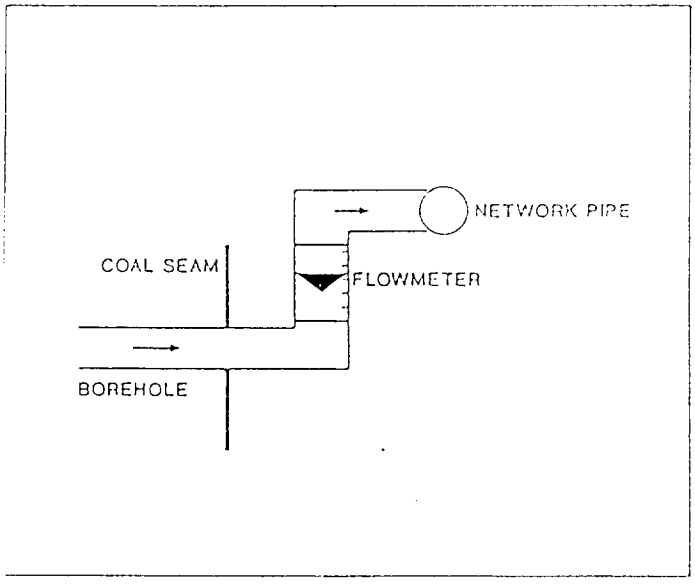

Figure 1. BOREHOLE FLOWRATE MONITORING

Methane draining from the borehole registers on the flowmeter before connecting to the main network pipeline.

The pipe network drains to a vertical column near to the main shaft, where the gas is presently vented to atmosphere. Earlier monitoring using a mass flowmeter installed on this column monitored the flow from the entire network. This was considered inadequate in terms of identifying localised results for individual holes and areas.

Results from the mass monitoring on the vertical column indicated an initial specific volume flowrate of approximately 90 $m^3/m/year$. This is very low, and unlikely to make any sigificant reduction to seam methane content ahead of mining. However, results from the individual boreholes are generally greater than this, as seen in Table 1.

Table 1. SPECIFIC VOLUME FLOWRATES

B/H No	LENGTH (m)	FLOW (m^3/hr)	SPECIFIC FLOWRATE ($m^3/m/y$)
A	137	5	320
B	279	15	471
C	228	10	384
D	564	30	466
E	859	10	102
F	597	5	73
G	285	30	922
H	996	40	352
I	306	30	859

This shows a specific volume flowrate range of 73 $m^3/m/yr$ - 922 $m^3/m/year$, with the average being 439 $m^3/m/year$. Although this is significantly improved on the original value of approximately 90 $m^3/m/year$, it is still not particularly high. For example, boreholes drilled at 50 m centres through a developed shortwall block of 2 m seam height * 60 m * 1000 m, at 10 m^3/t, as in Figure 2, would drain less than 15% of the seam gas if each hole had a drainage term of 6 months.

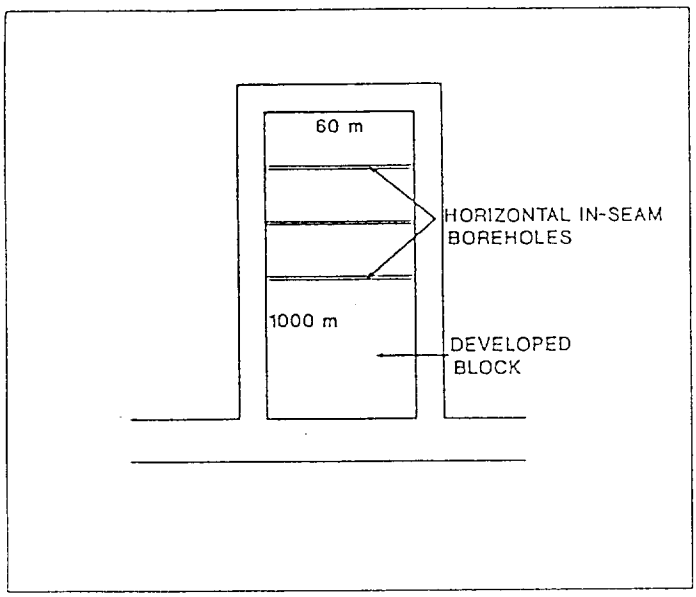

Figure 2. DRAINAGE FOR DEVELOPED BLOCK

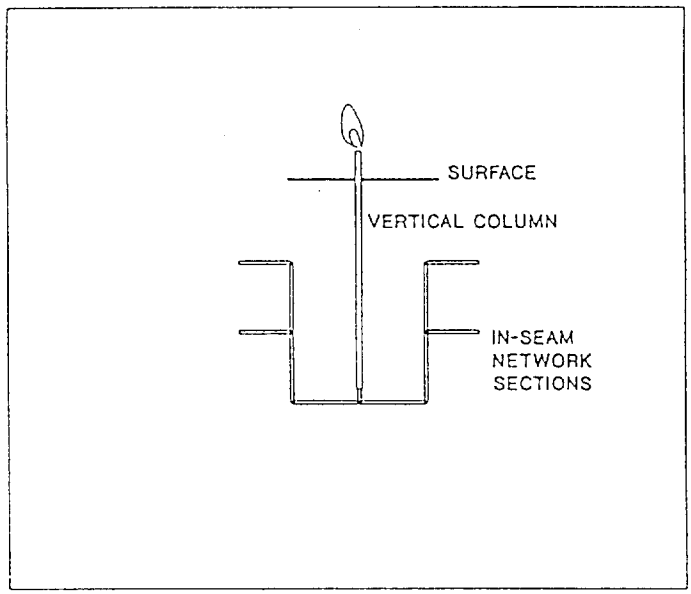

Figure 3. DRAINAGE NETWORK

Therefore, short term (i.e. 6-12 months) methane drainage from horizontal in-seam holes may still not greatly reduce the seam gas content ahead of mining, but there may still be possible alternative energy uses for the gas. The total methane flow from the section would be in the region of 1500 m^3 per day, sufficient to supply an on-site use.

The flowrates from the holes remain fairly constant over the monitoring period of several months. This is due to the relatively low seam permeability (Cook, 1989), and associated slow methane release. This means that a steady gas supply could be delivered, with boreholes with a useful life of several months being continually replaced to maintain the supply.

Due to the relatively low borehole flowrates, a combination of in-seam horizontal holes, and vertical drainage columns seems the most effective drainage technique. Vertical wells from surface into virgin ground would need several years to effectively drain. The intended system is to link several underground networks to centralised vertical columns, see Figure 3.

ADJACENT STRATA DRAINAGE

Surrounding seams and adjacent strata have been identified as methane sources at other sites. Their main influence has been into goafed areas after stooping (Site A) or longwalling (Site B). The relative positions of the seams in question are given in Figure 4 for the stooping section and Figure 5 for the longwall.

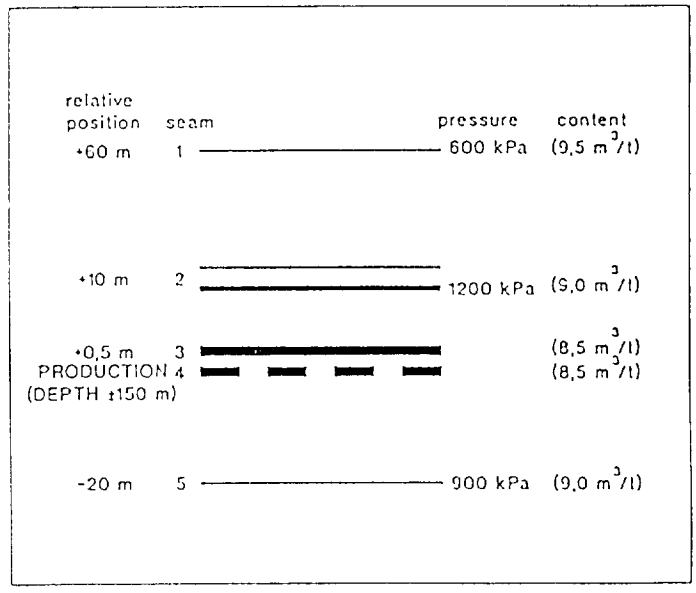

Figure 4. SURROUNDING SEAMS, STOOPING SITE

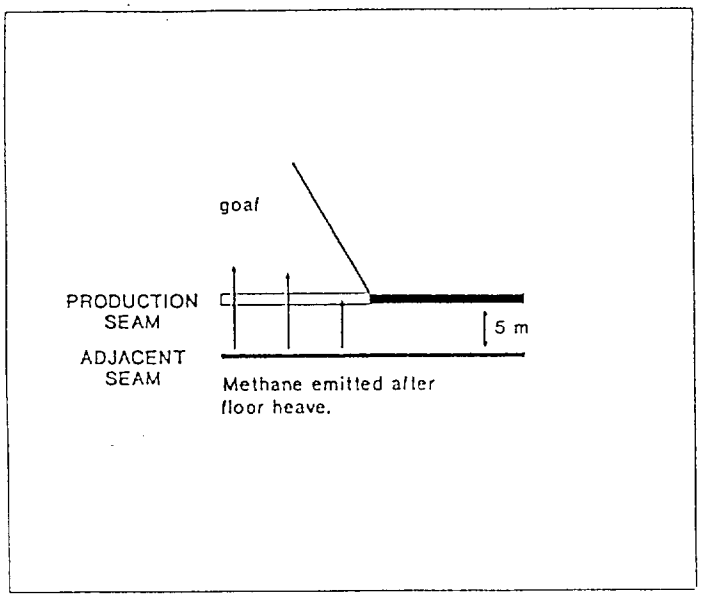

Figure 5. FLOOR SEAM, LONGWALL SITE

Figure 4 also shows the seam gas pressures and seam gas contents of each of the seams. Contents range from 8 - 10 m^3/t at pressures up to 1200 kPa. The influence that these have on the workings varies depending on the degree of extraction of the production seam (4). Methane from the immediate roof seam (3) is deliberately bled into the workings via bleeder holes drilled at the intersections to relieve the pressure. However these short drainage holes have no effect on the higher seams, as seen by the measured gas pressures. When goafing occurs after stooping, methane is then released from seams (1) and (2) into the goaf. Longer drainage holes are presently being evaluated to reduce this effect prior to stooping. No floor heave takes place at this site, so seam (5) makes no significant contribution to the methane make.

For Site B, the longwall, the seam in the immediate floor contributes substantially to methane make in the goaf. Although the colliery practises goaf drainage by vertical holes to surface, methane problems are still encountered on the face. Seam gas contents are in the region of 10 m^3/t and limited predrainage of the lower seam is being evaluated.

Borehole interference tests have been completed, drilling short vertical holes down through the seam, and monitoring flowrates and pressure decays. Borehole spacing was as shown in Figure 6, with each borehole sealed with a standpipe fitted with a pressure gauge. Pressure decays recorded with B/h 1 open and the others sealed are given in Figures 7 and 8.

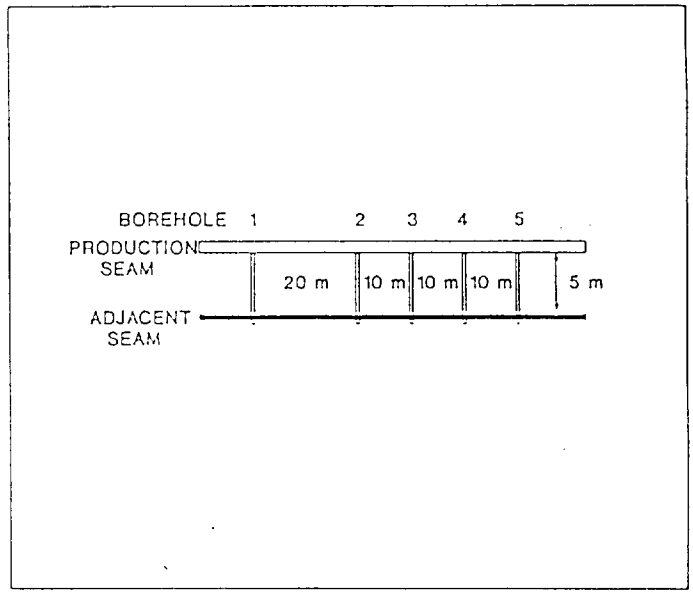

Figure 6. BOREHOLE INTERFERENCE TEST

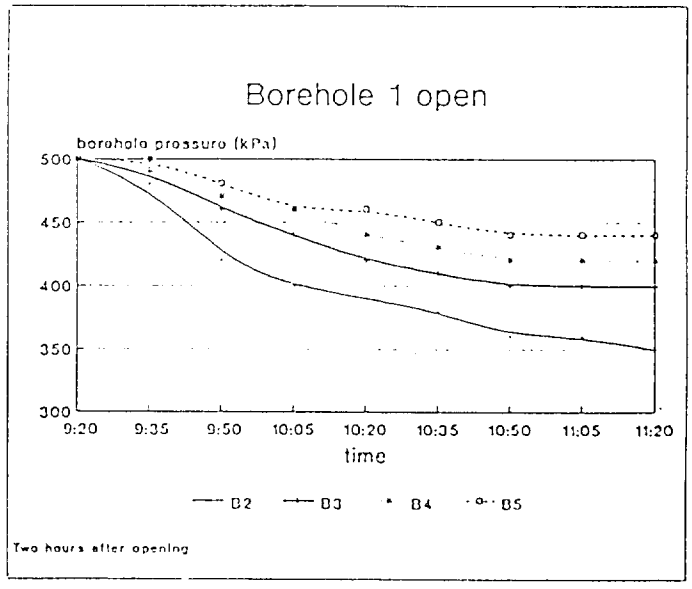

Figure 7. BOREHOLE PRESSURE DECAY, 2 HOURS

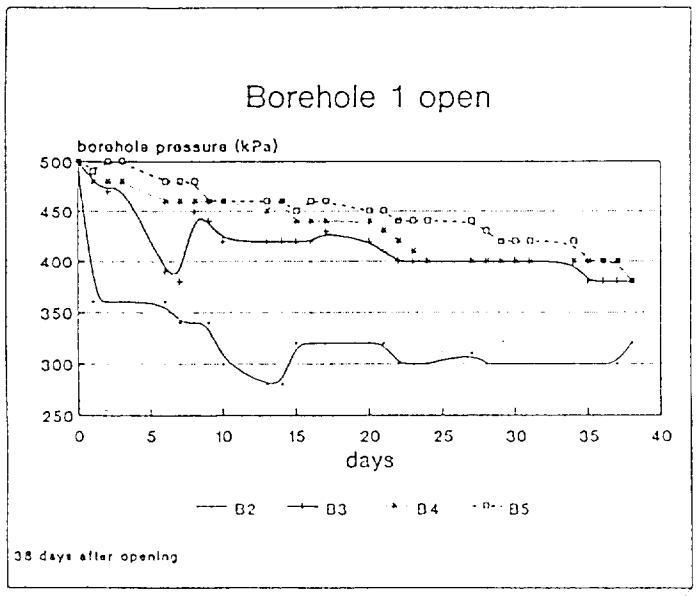

Figure 8. BOREHOLE PRESSURE DECAY, 38 DAYS

The initial rate of pressure decay decreased as the radial distance from B/h 1 increased. Within the first few days rapid pressure drop occurred at a distance of 20 m, before levelling off to a gradual decay. The next most rapid decay was observed at a distance of 30 m, with the boreholes at 40 m and 50 m distances being slowest and similar to each other. So, initially, an effective radius of 30 m drains around the holes. B/h 3 remains at lower pressure than B/h 4 and B/h 5 until approximately 25 days. At this time B/h 4 reaches the same level as B/h 3, and the two pressures continue to drop equally, effectively increasing the drainage radius to 40 m. Approaching 40 days, B/h 5 also reaches the same pressures as B/h 3 and B/h 4. So with time the radius continues to increase. By extrapolating the angle of decay of B/h 2 compared with B/hs 3,4 and 5, it would appear that all four will have drained to the same pressure after approximately 60 days. At this time the seam pressure will have dropped from an initial 500 kpa to below 300 kPa.

Therefore, for effective drainage within 20 days, boreholes at this site must be drilled at 30 m radii, or 60 m centres. If drainage continues for 60 days or more then 100 m centres is sufficient. Longterm effects, and the reduction in goaf methane problems, are presently being evaluated.

GOAF DRAINAGE

This has been the only form of practised methane drainage until recently, and then limited to a few longwall sites. No substantial flows have endured for any significant length of time, and the methane has always been vented to atmosphere with no consideration given to alternative uses. At the present deeper sites, as in Site B in the previous section, this drainage is proving inadequate. Further longwalling, planned for even deeper mines will almost certainly require in-seam or cross measure drainage.

Due to the high incidence of lightning strikes in the region, and the association of these with methane ignitions, some protection is required for exposed goaf holes. This usually takes the form of a water trap to isolate the methane in the vertical columnn from that already emitted to atmosphere.

FUTURE REQUIREMENTS

The South African underground coal mining industry is already beginning with limited approaches to methane drainage. This will be expanded as methane problems increase, and as the potential for on-site methane use is realised.

Mining depths have now extended beyond 300 m, with associated seam gas pressures approaching 2000 kPa, and seam gas contents around 10 m^3/t. This has given problems not only of higher methane emissions into the workings, but also into the goafs, and the pressures in surrounding seams have contibuted to poor roof conditions.

The vast areas of coal reserves presently unmineable are now being closely considered as gas producing areas, to reduce methane contents ahead of future mining, as well as alternative energy sources.

CONCLUSIONS

Methane drainage is relatively new, and not yet widespread, throughout the South African coal mining industry. But seam methane contents of 10 m^3/t and above, at seam pressures of up to 2000 kPa are increasing awareness and interest, and an increase in drainage will be seen in the near future. Several sites are being assessed for commercial use of the gas, although this will most probably be on-site uses.

REFERENCES

COOK, A.P., 1989 "Towards a method of Methane Prediction for South African Collieries," 23rd International Conference of Safety in Mines Research Institutes, Washington, 1989.

COOK, A.P. and ERWEE, E.C., 1991 "Methane Properties of South African Coals. Part 1: Sorption Characteristics." COMRO Reference Report No. 16/91, Johannesburg, 1991.

APPENDIX E3

A BRIEF OVERVIEW OF COAL-BED METHANE

A.P. COOK

INTERIM REPORT

MARCH 1993

BRIEF OVERVIEW OF COALBED METHANE

1 INTRODUCTION

Coalbed methane is the term applied to the drainage of methane from virgin seams or areas for commercial purposes. It is a well established industry in the US, particularly in Alabama, and saw rapid growth during the 1980s. Several other countries have evaluated, or operated, similar systems, but do not appear to have had the same success as the US.

Numerous companies operate within the industry in the US, and many of the other operations around the world are initiated or overseen by these same companies. However it would appear that the technology they apply in the US does not always work as effectively elsewhere.

This is a brief review of the industry and techniques, as well as some possible applications for South Africa.

2 COALBED METHANE

Coalbed methane is generally a high quality natural gas produced from coal seams. The gas can be drained off either to sell commercially, to provide an on-site energy supply, to reduce methane contents ahead of future mining, or a combination of these. As all seams contain gas, and the location of coal seams is generally known, the exploration success rate is high, however this does not guarantee high gas production rates.

The largest producers of coalbed methane are the US, where they can provide up to 5 % of the domestic natural gas requirements. The industry expanded rapidly during the last decade, supported by Federal tax concessions for alternative energy supplies. An existing national gas network provides a virtually guaranteed market for the gas.

Alabama and Colorado/New Mexico have established industries, operating in the Warrior and San Juan Basins. Presently developing and expanding production are Virginia, West Virginia, Pennsylvania and Washington.

One problem that can arise wtih commercial drainage is ownership rights to the gas. This is mostly resolved in the US but is possibly untested in other countries. Rights to the mineral may not guarantee rights to any gas liberated from the mineral or adjacent strata.

3 METHANE PRODUCTION

The favoured method is vertical surface wells into virgin coal, although surface gob holes and underground gob and seam holes are also used.

3.1 Vertical Wells

Typical production wells are 300 m - 1000 m deep, with a producing life of 10 years, peaking between 1 and 3 years. Normally water production precedes gas, lasting for 6 - 24 months before sustantial gas flows are realised. A gas field consists of a grid of wells at ±400 m centres, with the total wells in the Warrior Basin projected at 1200 in the first half of this decade. A typical US production development plan has Year 1 as Feasability and Pilot Installation, Year 2 as Pilot Test and Evaluation and Year 3 onwards as Production Scale Up. The cost of evaluation and pilot studies as charged by a US company is in the region of $ 500 000.

Gob wells involve less capital cost, do not require water pumping or hydrofrac stimulation, but generally have shorter production lives. South African goaf drainage holes usually upcast significant gas volumes for only a few months after being undermined.

3.2 Underground Wells

Underground wells are generally in-seam or gob cross-measure holes. In-seam holes are drilled during development to pre-drain ahead of mining, the cross measures can continue to drain after

mining is complete. Both hole types are generally used in conjunction with retreat longwalling.
Underground holes involve less capital costs than vertical wells, the greatest being for the required pipeline network, this varying with distances. Typical US figures, including vertical holes to surface servicing about 7 underground panels each, are $ 250 000.
The wells do not produce as long as surface wells so are not favoured commercially, but have the advantage of draining specific areas where mining will or has taken place.

4 WELL STIMULATION

Stimulation techniques can be applied to wells to enhance methane flow. The most common is hydrofracturing, pumping water, gel, or similar, down the wells under pressure and into the seam via prepared casing slots. This causes vertical fractures extending out from the slots. These fractures are then prevented from closing again by pumping sand with the water, which is deposited in the fractures keeping them open and retaining a high permeability flow path.
The technique was initially developed for the petroleum industry, and whether it is directly suited to coalbed methane is uncertain due to the different gas release mechanisms involved, particulary that of adsorbed methane, which desorbs into the fissures and microfissures. Unless the hydrofraccing creates more fractures, reducing the diffusing distance, its effectiveness appears limited. However it is widely used and accepted in the US industry.
A reported detrimental effect of hydrofraccing is poor roof conditions during subsequent mining. Field tests indicate that roof damage does not take place, but the results do not appear to be very conclusive.

Horizontal wells are not so easy to stimulate if required. Hydrofraccing techniques have been applied but do not appear to have been successful, possibly due to the relatively long length

of hole. Various other fracturing techniques have been applied, but again not always successfully. Explosive fracturing may produce a compacted zone around the borehole, effectively reducing permeability and sealing off flow. An alternative to explosives is propellants, which rather than detonate, are designed to burn or deflagrate at slower rates. This is called tailored-pulse fracturing and has been shown to produce multiple fractures extending out radially around boreholes.

5 DISCUSSION

Vertical well gas drainage works well in areas of the US, where the seams are generally in excess of 500 m depth, and appear much more permeable than typical SA seams. They also have a ready market in the national gas network, so commercial drainage is a viable proposition. The techniques have not been so successful in Australia, where the coals are more similar to SA coals, but where the main purpose has been safety reasons for pre-drainage, rather than commercial. The volume flowrates are therefore not so important and the methods are still applied there but not on a large scale. The Australians also use in-seam horizontal drainage, and are now evaluating a combination technique with vertical surface holes angled to continue horizontally in the seam. This drilling technique is being introduced to SA but initially for exploration purposes. Coalbed methane has seen a recent revival in Australia after a low period over the last two decades. This may be due to union pressure for increased safety, and the persuasiveness the US companies, rather than any increased success rate.

Other countries where evaluation is being undertaken include China, Poland, Switzerland and Zimbabwe, where the potential market is as a diesel substitute. To date no results are available from Zimbabwe, but this is probably due to the many delays encountered with shortages of equipment and skills, and does not necessarily indicate a lack of success. As SA coals are more similar to Zimbabwean coals than US coals, results from

Zimbabwe should give an indication of the potential for commercial South African applications.

COMRO has an increasing data base on the methane characteristics of SA coals, a great deal of which gives an indication of potentials for commercial drainage. In general SA seams are much shallower than the commercial seams in the US, so the methane contents are less for equivalent coals, however actual contents are still expected in the region of 6-12 m^3/t. Diffusion properties, indicators of methane release rates, are low and this is supported by horizontal in-seam flowrates which, thus far, are considerably less than those quoted for European and US coals.

No field data is yet available for vertical wells in SA, and without this it is difficult to predict expected success rates. Some exploration holes have produced large gas flows, under high pressure, especially in the "Evander gas field". Many other holes have flared methane for years, or sometimes periodically, possibly due to variations in water table. However none of these holes have been properly quantified for methane, or had water pumped out to evaluate any increase in gas flow. There is certainly sufficient evidence to support further evaluation, possibly even of narrow seams not economical from a mining consideration. An example being the Free State goldfields, where several open holes flare methane.
It must be remembered that large scale commercial drainage should not be the only objective. Any reduction in seam methane contents ahead of mining, either by surface or underground methods, reduces the risk of a subsequent incident; and the drainage quantities may well be sufficient to provide a colliery energy source in terms of heating or electricity generation.

So vertical wells may be successful in SA, but only if suffucient time is available ahead of mining (probable minimum 5 years). Underground drilling, with a higher density of shorter duration holes, is also an option which merits further evaluation. As most collieries operate the necessary drill equipment underground,

simple initial evaluation programmes should not be too difficult to carry out. By varying drilling parameters such as borehole lengths, inclinations, directions and diameters, and monitoring flowrates any potential for this method can be seen. Vertical hole evaluation will require water pumping and fracturing.

Further information on coalbed methane and the industry can be obtained from:

The Eastern Region Coalbed Methane Information Centre
School of Mines and Energy Development
The University of Alabama
323 Farrah Hall
Box 870164
Tuscaloosa
Alabama

6 BIBLIOGRAPHY

Baker, E.C., Garcia, F. and Cervik, J., *Cost comparison of gob hole and cross-measure borehole systems to control methane in gobs.* USBM Report of Investigation RI 9151, 1988.

Carter, R.A., *Methane fever flares in USA, Part I and Part II.* Engineering and Mining Journal, Feb, Mar 1991.

Chadwick, J., *Coalbed methane potential.* Mining Magazine, July 1991.

Cuderman, J.F., *Tailored pulse fracturing in cased and perforated boreholes.* Unconventional Gas Technology Symposium, Louisville, Kentucky, 1986.

Diamond, W.P., *Underground observations of mined through stimulation treatments of coalbeds.* Quarterly Review of Methane from Coal Seams Technology, Volume 4, Number 4, June 1987.

Gas Research Institute, *Coalbed methane: from nuisance to new source.* GRID Volume 12, No. 2, 1989.

Oil and Gas Journal, *Coalbed methane.* Special Report, Oil and Gas Journal, Oct. 1989.

Hebblewhite, B.K., Lama, R.D. and Hargraves, A.J., *Gas drainage experiment and practise in Australia.* 6th ICCR Conference, London, 1982.

Hobday, D.K., In-Situ (Australia) *Personal communication.* 1991.

Kavonic, M.F., *Methane gas drainage, utilisation and research in the Australian coal industry.* Rand Mines Internal Report, 1991.
Kelafant, J.R., *The technology of coalbed methane.* ICF Resources Symposium, COMRO, 1989.
Kelafant, J.R., ICF Resources (USA) *Personal communication.* 1989 - 1992.
Klenowski, G., Lynch, P., and Byrnes, R., *Vertical well degasification trial, Central Colliery, German Creek, Queensland.*
Kline R.J., Mokwa, L.P. and Blankenship, P.W., *Island Creek Corporation's experience with methane degasification.* Proceedings of the 1987 Coalbed Methane Symposium, Tuscaloosa, Alabama, Nov. 1987.
Lama, R.D., *Drainage of methane from the solid at Westcliffe Colliery, optimisation of drainage hole parameters.*
Geomechanics of coal mining report No. 18. CSIRO, Victoria, Australia, 1980.
Malone, P. GeoMet (USA) *Personal communication.* 1992.
McHugh, S.J. and Keough, D., *Fracture and permeability enhancement with pulse tailoring.* Unconventional Gas Recovery Symposium, Pittsburgh PA, 1982.
Thakur, P.C., *Methane flow in the Pittsburgh coal seam.*

APPENDIX F

F1. J.N. van der Merwe, Analysis of Methane Gas Occurrences at Secunda Collieries, Report to CSIR Miningtek, October 1993, Sasol Mining (Pty) Ltd Coal Division.

F2. P. Botha, The Origin of Methane Gas in the Secunda Area, Report to CSIR Miningtek, August 1995, Sasol Coal Division.

F3. W.C.A. van Niekerk and P. Broere, The Characterisation of Natural Gases, Analytical Report, June 1994, Atomic Energy Corporation of South Africa.

APPENDIX F1

SASOL MINING (PTY) LTD

COAL DIVISION

ANALYSIS OF METHANE GAS OCCURRENCES AT SECUNDA COLLIERIES

DR J N VAN DER MERWE, Pr. ENG

OCTOBER 1993

TABLE OF CONTENTS

ABSTRACT

While the four underground mines operated by Sasol in the Secunda coal field, collectively known as Secunda Collieries, experienced only intermittent occurrences of methane, the consequences thereof may be disastrous. Analysis of the occurrences indicated that distinct differences existed in the character of the occurrences as described by their times and localities, for different regions in the coal field.

Viewed holistically, the Secunda coal field is characterised by intermittent occurrences of methane, predominantly in the region of dolerite dykes and more frequently in winter. More ignitions occurred in the spring period, and the number of ignitions did not necessarily coincide with the frequency patterns of occurrences in either time or space. The occurrences were not distributed uniformly over the area. Middelbult had a significantly higher frequency than the other mines, while the highest proportion of ignitions occurred at Twistdraai. At three of the mines, 70% or more of the methane occurrences were associated with dolerite dykes, the exception being Bosjesspruit where only 17% of occurrences followed the same pattern.

It is suspected that there may be more than one source of gas, and research will now be directed towards locating the possible sources and determining the contents of the gas mixtures.

PART A

a. BACKGROUND

Methane gas is the one hazard in coal mining which is not accompanied by natural warning signs. Loose roof slabs are visible. Machinery can be seen and heard. Consequently, those hazards can be detected without external means and often without paying special attention.

Methane cannot be smelt, seen or heard. It can only be detected by external tests. Once it is present, there are a number of potential ignition sources, and the gas may be ignited, sometimes with disastrous consequences.

The efforts of the coal mining industry to prevent disasters from occurring focus on three main areas. Firstly, instruments for both periodic and continuous monitoring to detect the presence of the gas have been developed and are used. Once the gas has been detected, procedures to prevent its ignition and to remove it are implemented.

Secondly, sufficient volumes of fresh air are supplied to working places to dilute the gas to below dangerous concentrations and remove it from the mine. These high air volumes are supplied continuously, whether the gas is present or not. Stringent measures to ensure that fresh air in sufficient quantities is supplied to the right places are applied. Old areas of mines, where routine maintenance cannot be carried out, are isolated from the rest of the mine to prevent leakage of methane into the mine.

In the third instance, all machinery and instruments which are used underground are constructed such that it should restrict methane emistions. Again, the assumption is made that methane is always present in all areas of a mine.

Yet, despite these precautions, methane ignitions still occur. If our understanding of methane is correct, the gas can only ignite if more than one of the mutually compensating precautionary measures are absent at the same time.

There are thus two alternative causes of ignitions : either human failure or our understanding of methane gas is lacking. Methane could also be ignited in areas of a mine where normal control procedures cannot be implemented. Preventive action has to be directed at the cause of an accident if it is to be successful. Thus the cause has to be fully understood before preventive actions can be implemented.

Against this background Sasol Coal decided to start afresh and take a new look at the methane issue. The first phase of the investigation was to be aimed at the gas - this is to be followed by a program aimed at the people.

At around the same time SIMRAC awarded a national research

could be obtained by joining forces and hence this collaboration between Sasol Coal and Miningtek.

This report deals with the initial part of Sasol Coal's responsibility in the project : to determine when and where methane occurs and whether there are any fixed trends or marked differences in different areas of the Secunda coal field.

Records of reported instances of methane occurrences were analyzed with regard to the parameters time and space and relationships with geological features were investigated. The report will show that a number of old beliefs and previous conclusions were confirmed, while some new information which can now be followed up in following phases of the project came to light.

b. DESCRIPTION OF DATA

There are four underground mines in the Secunda coal field, shown in Figure 1.

Middelbult is located in the north-western part of the field, Brandspruit in the south-west, Twistdraai in the north-east and Bosjesspruit in the south-east. For the purposes of the investigation the data was grouped according to the mine boundaries.

Selected features of the mines related to this investigation are summarized in Table 1.

TABLE 1

	AVE DEPTH (m)	YEAR STARTED	AVE. MINING ht (m)	% AREA COVERED BY DOLERITE	MIDDLING TO WITS (m)
Brandspruit	130	1977	3,3	98	82
Bosjesspruit	170	1977	2,9	100	100
Twistdraai	130	1981	3,5	90	90
Middelbult	100	1981	3,8	60	70

On each mine a data sheet - shown in Appendix A - was completed by the local Geologist and chief of the environmental department. Use was made of records kept over the period 1985 to 1991. The findings are thus subject to the diligence with which records were kept. However, in the light of the seriousness with which the methane hazard is regarded, deviations from the legal and local mine requirements with regard to methane reporting are estimated to be small. Whatever deviations there are, are also expected to be consistent.

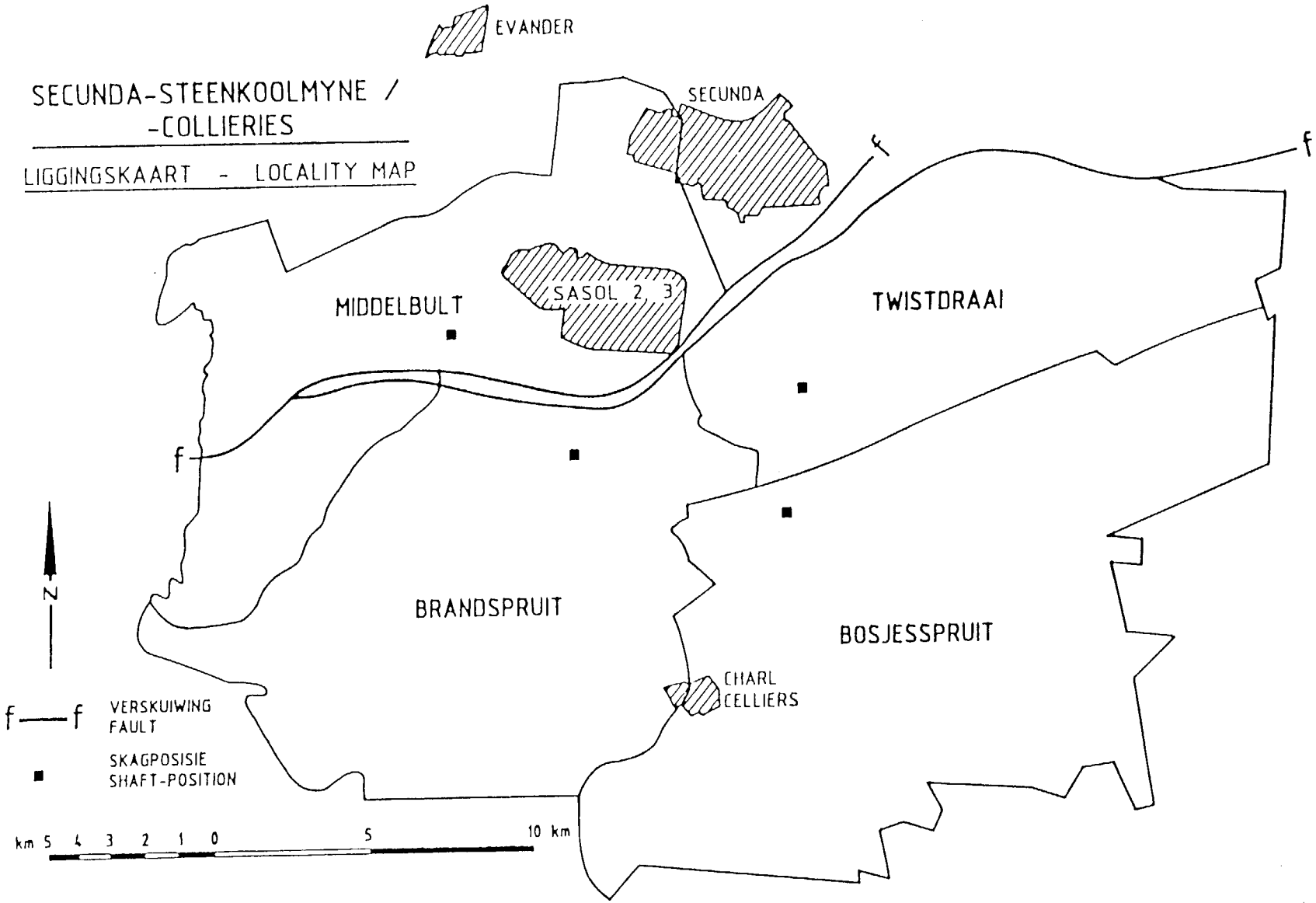
EVANDER
SECUNDA-STEENKOOLMYNE /
-COLLIERIES
LIGGINGSKAART - LOCALITY MAP
SECUNDA
SASOL 2 3
MIDDELBULT
TWISTDRAAI
BRANDSPRUIT
BOSJESSPRUIT
CHARL
CELLIERS
f
N
f—f VERSKUIWING
FAULT
SKAGPOSISIE
SHAFT-POSITION
km 5 4 3 2 1 0 5 10 km

Figure 1

Geologist were asked to express an opinion regarding the relationships between methane occurrences and geological features. This aspect cannot be proven scientifically (especially with regard to historical data) but it was felt that the measure of subjectivity would be minimized by relying on the geologist's opinion rather than anybody else's.

APPENDIX A

* Merk toepaslike kolom

K&P - Kamer en Pilaar
DHV - Delwer Hoofverhaal
S/A - Strookafbou

F - Front
AA - Agterarea
P - Puin

Gevalnommer	Datum	Tyd	Aard van geval *			Geologiese verbintenis *				Eienskappe van versteuring			Mynboumetode *			Plek van voorkoms *			Metaankonsen
			Slegs voorkoms	Ontbranding	Ontploffing	Geen	Steilgang	Plaat	Verskuiwing	Dolerietdikte	Gebrande dikte	Verplasing	K&P	DHV	S/A	F	AA	P	

ANALYSIS OF METHANE OCCURRENCES

PART B

1. TIME OF OCCURRENCE

This section will deal with methane occurrences against the background of the time dimension.

1.1 Trend over 1985 - 1991

Figure 2 shows a weakly developed upward inclination of methane occurrences over the period 1985 to 1991. On average, 16 occurrences were reported annually (standard deviation 8). The occurrences increased at a rate of 0,7 per year. In the light of the scatter of the data, this trend is not considered meaningful, but nonetheless indicates continued awareness of underground personnel. It also follows the trend of continued increase in coal production, and the reate of coal production. It does not take into account the increase in the number of testing apparatus underground.

A slightly disturbing feature is shown by the dotted line indicating the number of ignitions per year. There were sometimes more ignitions in the years with fewer occurrences. If all other factors had remained constant, the number of ignitions should be directly proportional to the number of occurrences.

1.2 Time of Year

A breakdown of the months during the year when occurrences were reported, is shown in Figure 3. June and August displayed more occurrences than the other months, and in general it would appear that the colder months were more prone to methane occurrences than the warmer months. Barometric pressures are usually higher during the colder months, which indicates an unexplained anomaly. Usually more methane is emitted during low pressure periods, when measured over shorter time spans.

Going into slightly more detail, it is seen that the different mines exhibited different patterns. Especially Bosjesspruit, and to some extent Middelbult, displayed the anomalous behaviour. Brandspruit tended to find more methane during summer, while Twistdraai again tended to favour the winter months. This analysis does not indicate a geographical grouping for methane occurrences during certain calender months.

The preference for methane occurrences during the colder months is amplified in Figure 4, which indicates that the quarter from May to July was the most popular, closely followed by August/October. The

Methane occurrences per year

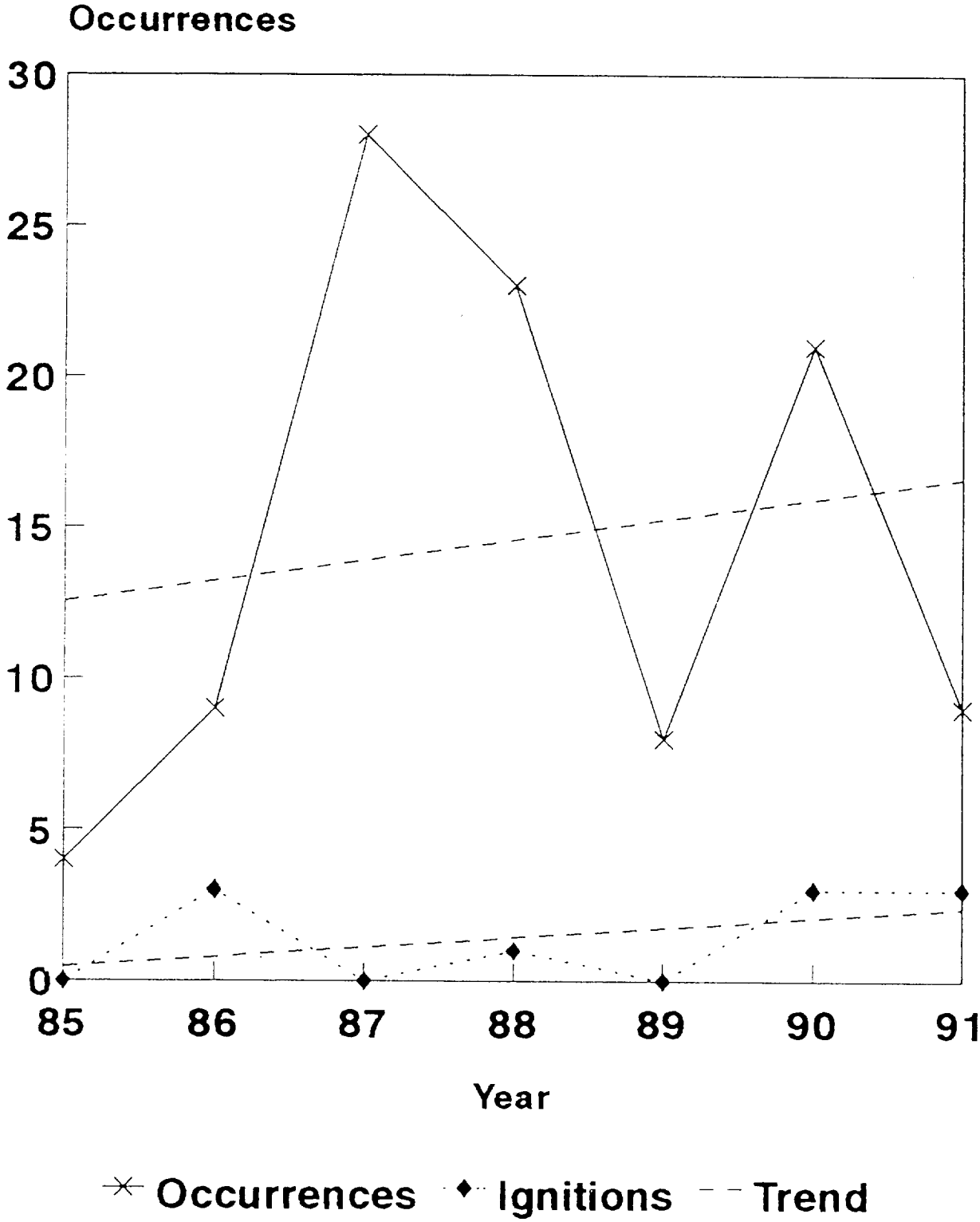

Figure 2

Methane Occurrences
per month

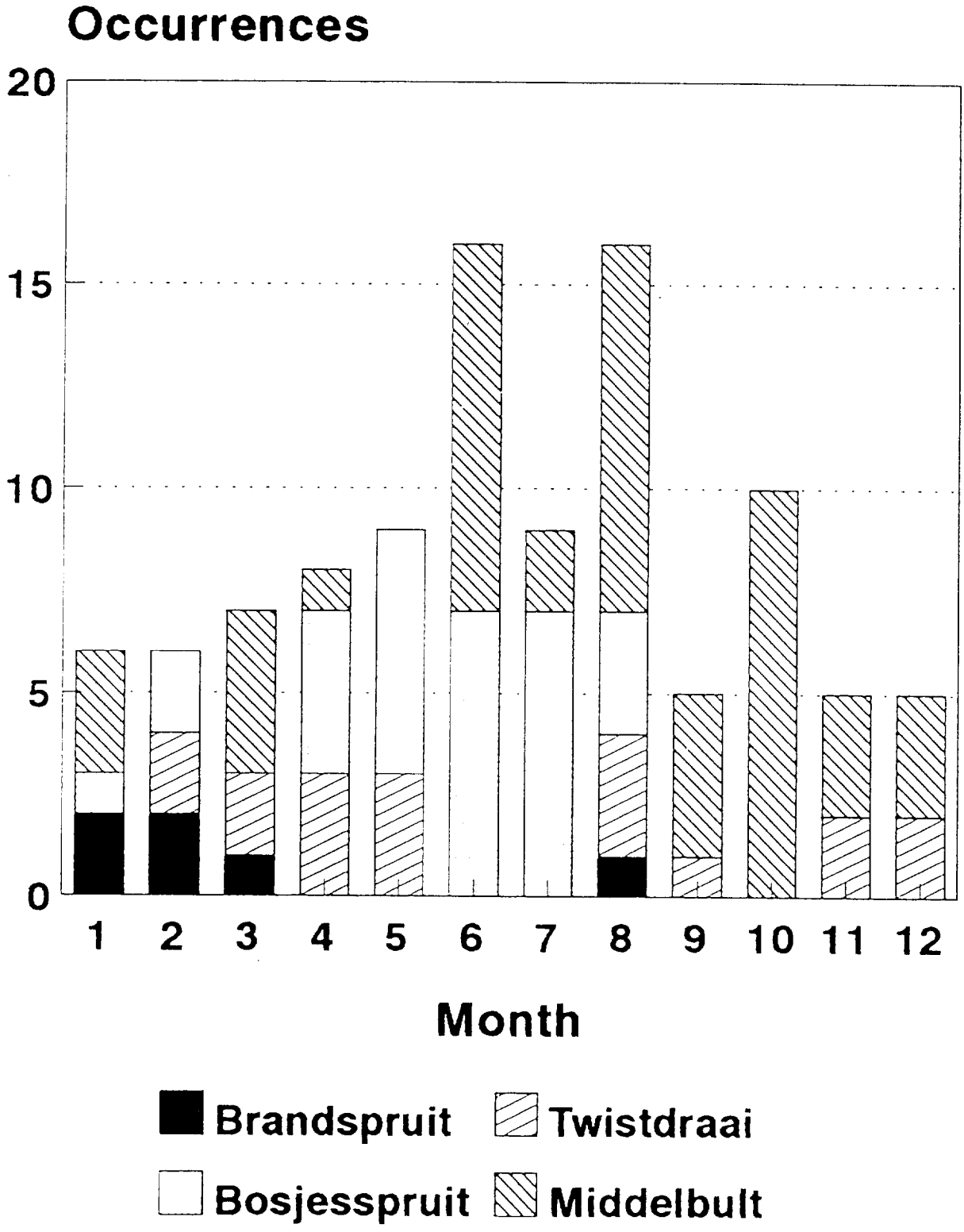

Figure 3.

Methane Occurrences
per quarter

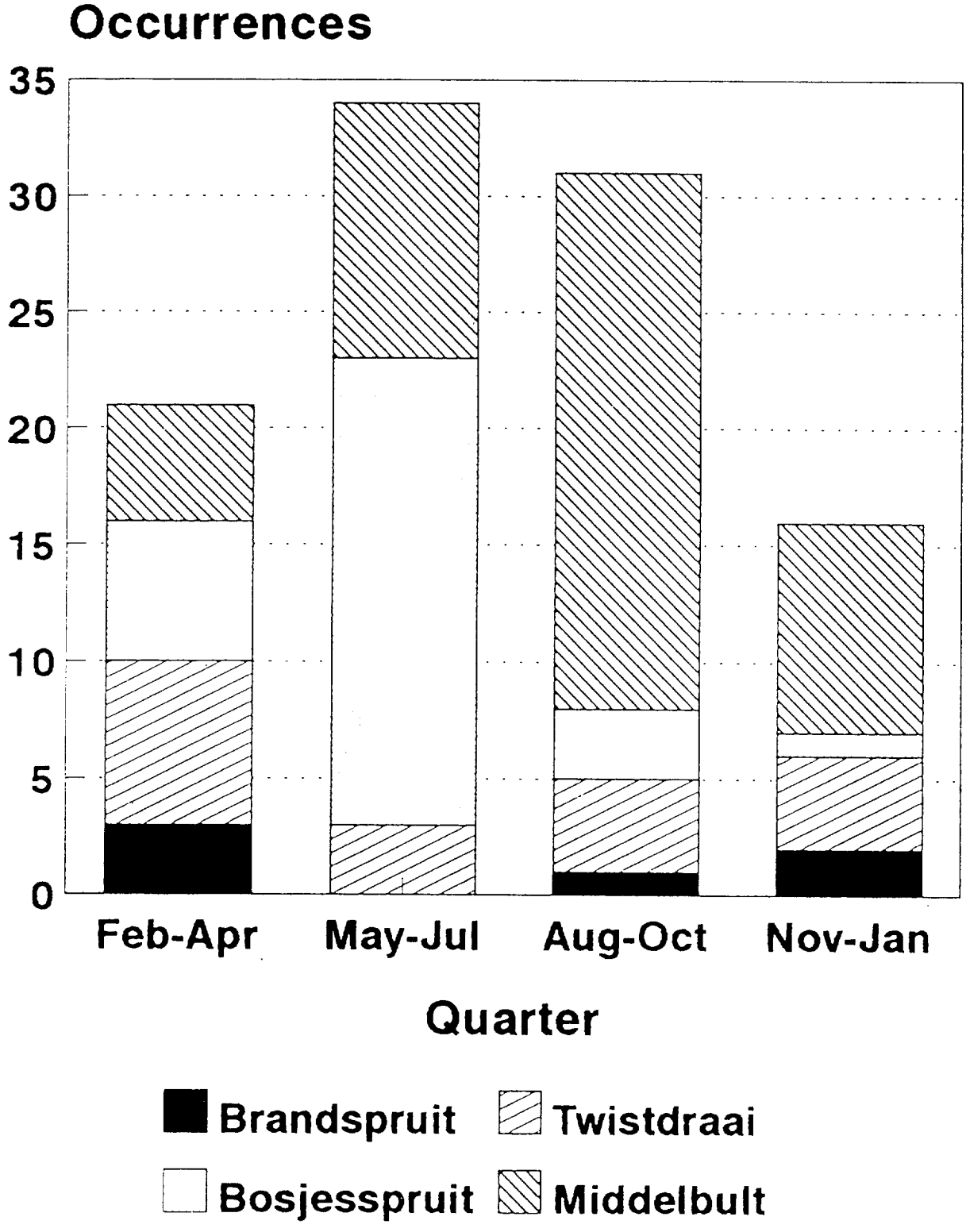

Figure 4

1.3 Shift and Time of day

The vast majority of methane occurrences were reported on day shift, and more specifically at the beginning of the shift, when miners routinely test for methane.

1.4 Time of Ignitions

Figure 5 shows a very strong tendency for ignitions to occur during the period August to October. This coincides with the minor peak occurrences during the same period. However, the peak period for occurrences during May to July, does not exhibit a peak period for ignitions - it is in fact the lowest ignition period.

The latter observation supports the observation made in 1.1, namely that peak ignitions of methane did not necessarily correspond with peak occurrences.

2. SPATIAL DISTRIBUTION

In this section methane occurrences will be viewed against their localities. The area will progress from large to small, i.e. from geographical region to positions in the panels. Only working areas will be covered, the sealed off sections will be excluded from the analysis.

2.1 Occurrences per Mine

The total number of methane occurrences per mine is shown in Figure 6, which indicates that Middelbult had the greatest number, followed by Bosjesspruit, Twistdraai and Brandspruit, in that order.

Figure 6 does not take cognisance of the fact that the mines cover different areas. Figure 7, in which the number of occurrences have been normalized with respect to the areas mined, is thus more reliable.

It is noteworthy that while the relative order of occurrences remain the same, the differences between Middelbult and the other mines are accentuated.

2.2 Ignitions per Mine

The relative number of ignitions, defined as the percentage of occurrences which ignited, are shown in Figure 8. While Middelbult had the greatest number of methane occurrences, the greatest relative number of ignitions were experienced by Twistdraai. This observation is further confirmation that methane ignitions and occurrences are not necessarily linked.

2.3 Geological Association

Ignitions per quarter

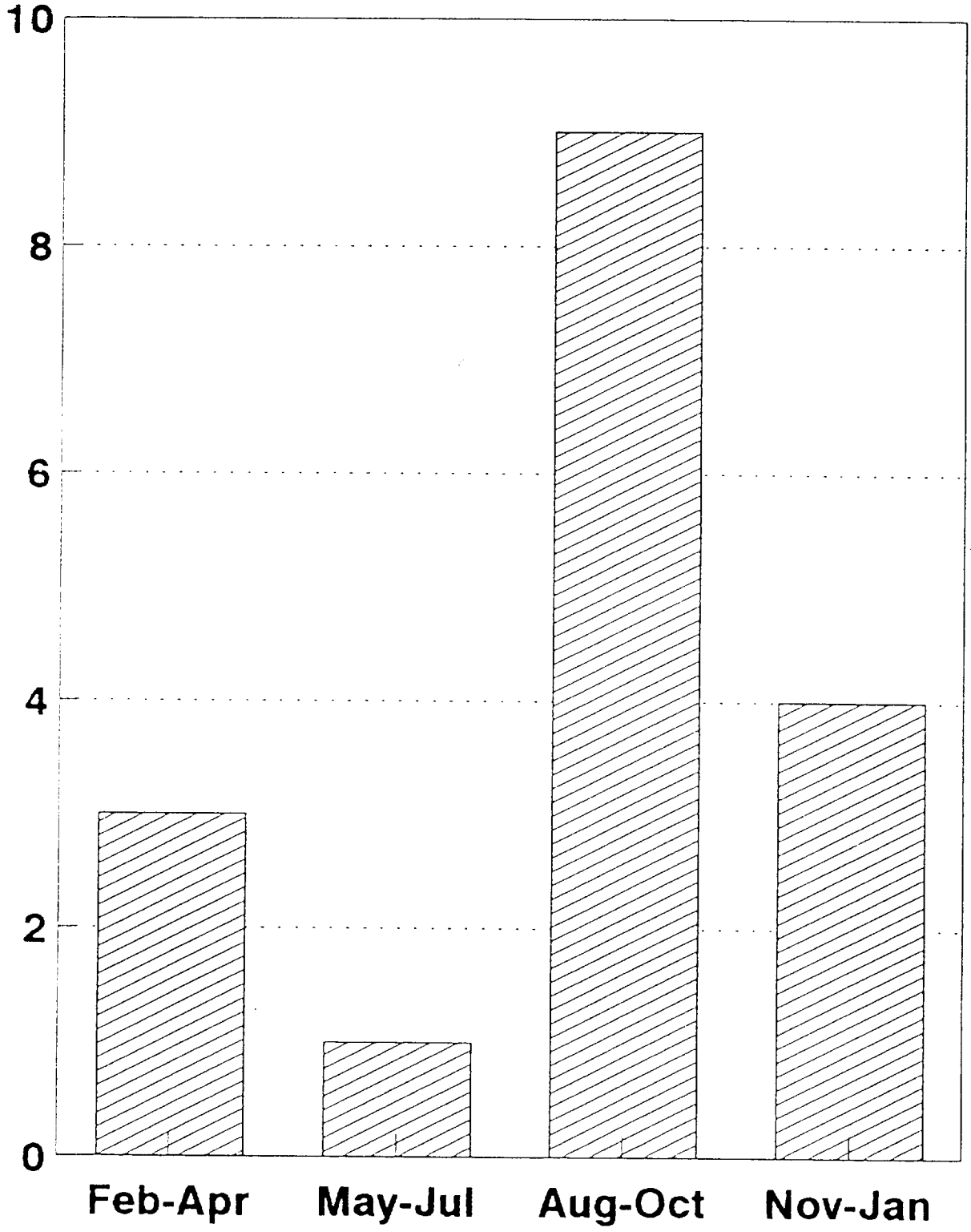

Figure 5

Methane occurrences per mine

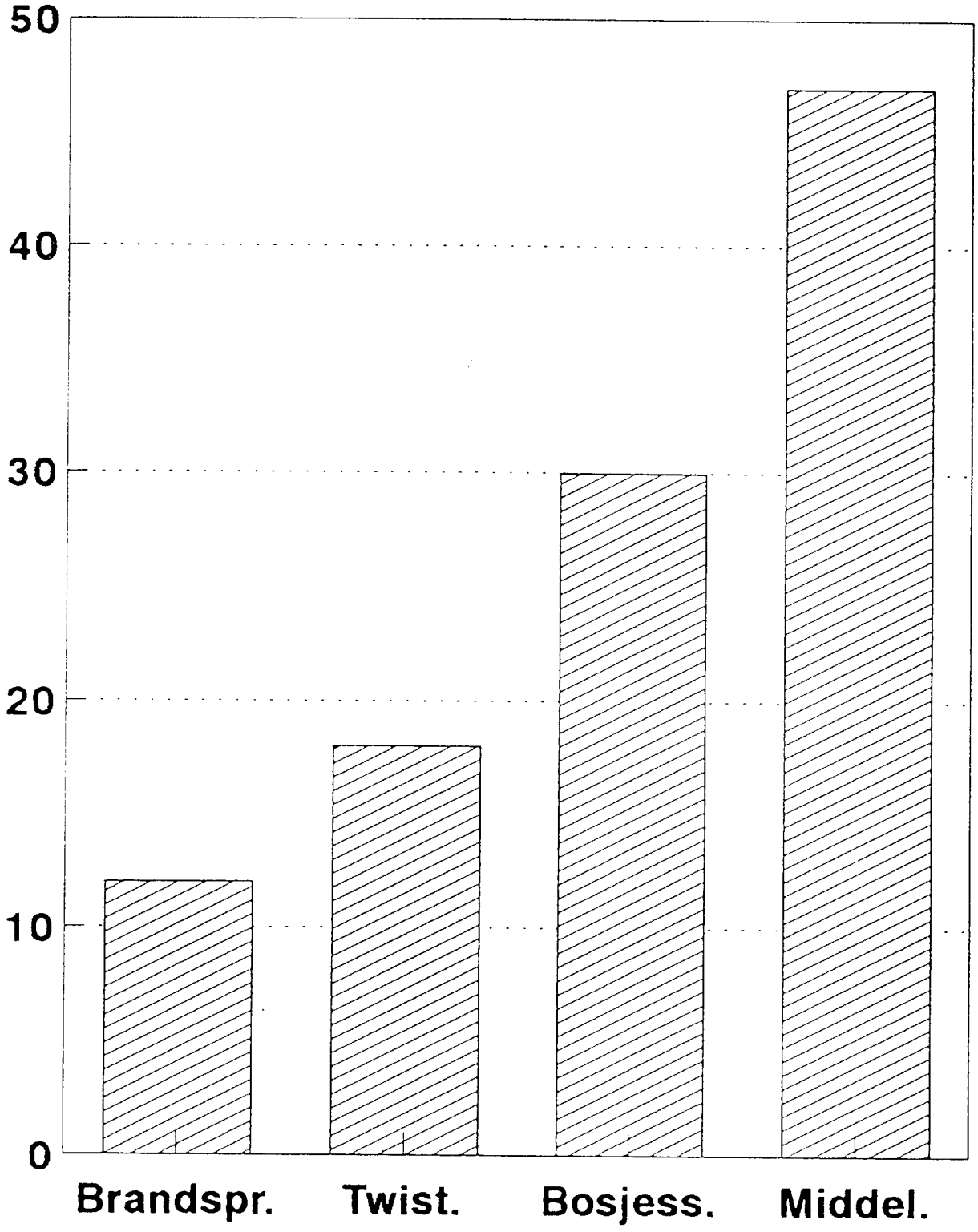

Figure 6

Occurrences per area mined

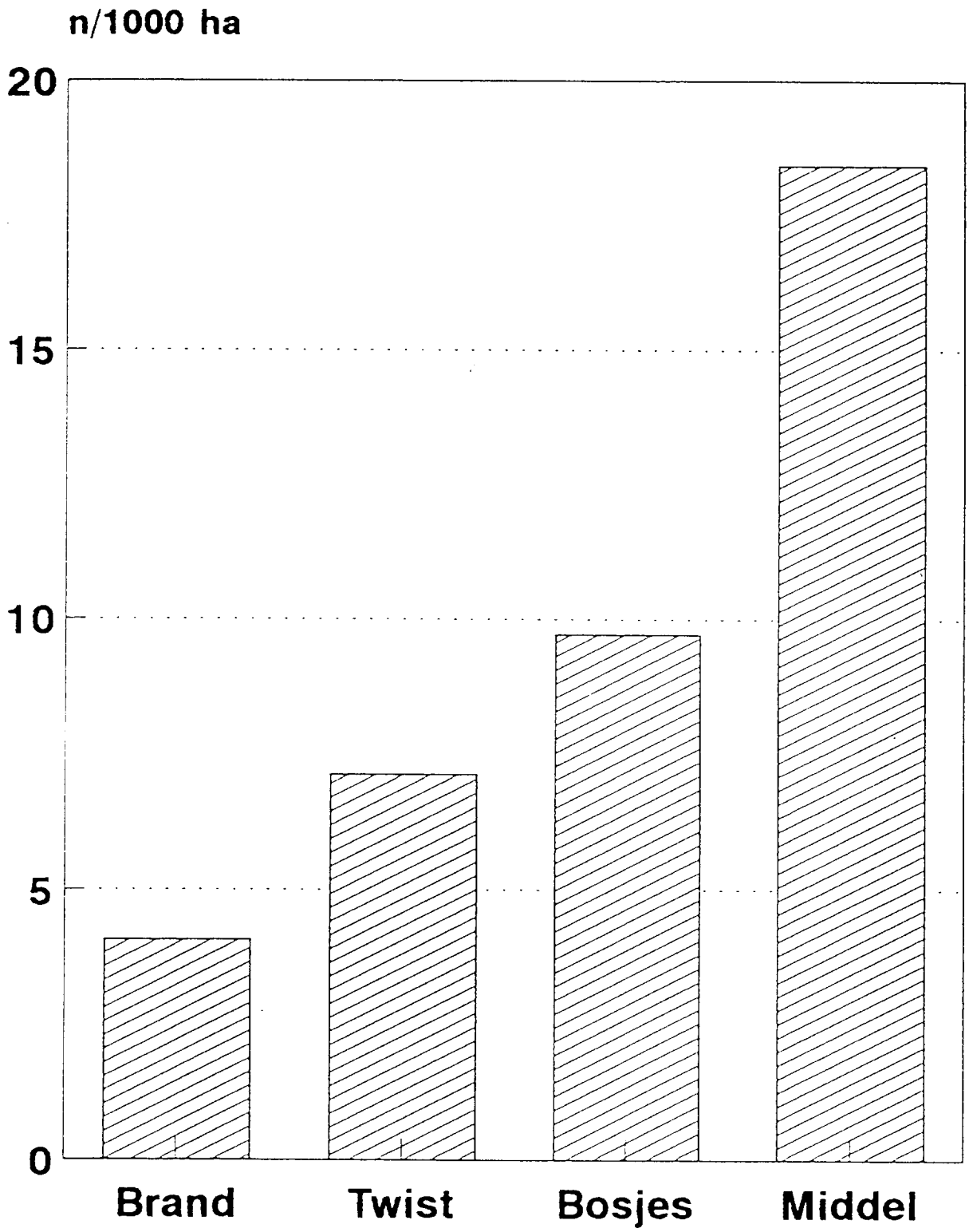

Figure 7

Percentage ignitions

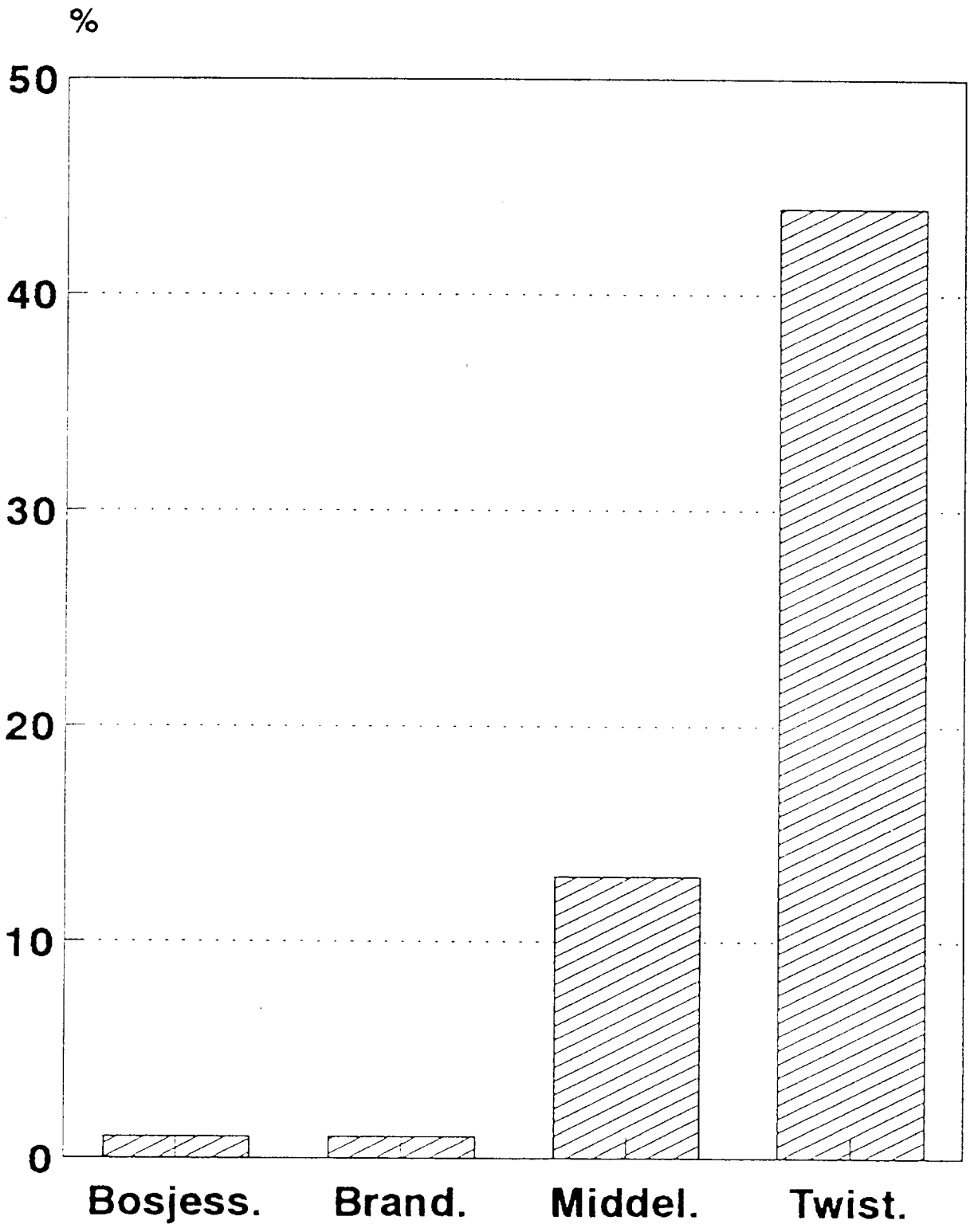

Figure 8

2.3.1 Ratio of Occurrences Associated with Disturbances

More than half, or 63% of all methane ignitions at Secunda Collieries were associated with geological disturbances - see Figure 9. The anomalous mine in this instance was Bosjesspruit, with only 17%. All of Brandspruit's occurrences could be connected to a geological disturbance, while for the remaining two mines around 70% of the methane detections were in the vicinities of disturbances. The term "geological disturbance" implies either a fault or a dolerite dyke. No distinction is made, because the dykes in the area are usually also associated with vertical displacement of the coal seam.

Some light is shed on Bosjesspruit's low disturbance association by the fact that the distribution of disturbances is not uniform throughout the field. Some measure of this is demonstrated in Figure 10, which shows the average areas of coal blocks delineated by disturbances. Bosjesspruit had the largest blocks, indicating that it had fewer (or more widely spaced) disturbances than the other mines.

Of the four mines, it is also the only one still to employ longwalling as a mining method. The smallest intact blocks were found at Middelbult, the only mine of the four where longwalling was never used.

2.3.2 Non-Associated Occurrences

The frequency of methane occurrences which were not associated with geological disturbances ("non-associated occurrences") were normalised with respect to the area mined, as shown in Figure 11. Middelbult had the highest frequency, followed by Bosjesspruit and Twistdraai. Brandspruit had none.

2.3.3 Associated Occurrences

The frequency of methane occurrences which were associated with geological disturbances was normalised with respect to the total length of disturbances which had been exposed by mining (including areas not truly exposed but mined within coal affected by the disturbance) on each mine. This is shown in Figure 12.

The highest frequency is again displayed by Middelbult, indicating that Middelbult does not only have the most associated occurrences because it has the highest frequency of disturbances, it also has a higher frequency of occurrence per unit length of disturbance. By the same token, Bosjesspruit not only has a low frequency of occurrences because of a low frequency of disturbances, but the number of occurrences per unit length of exposed disturbance was also lower.

Geological association

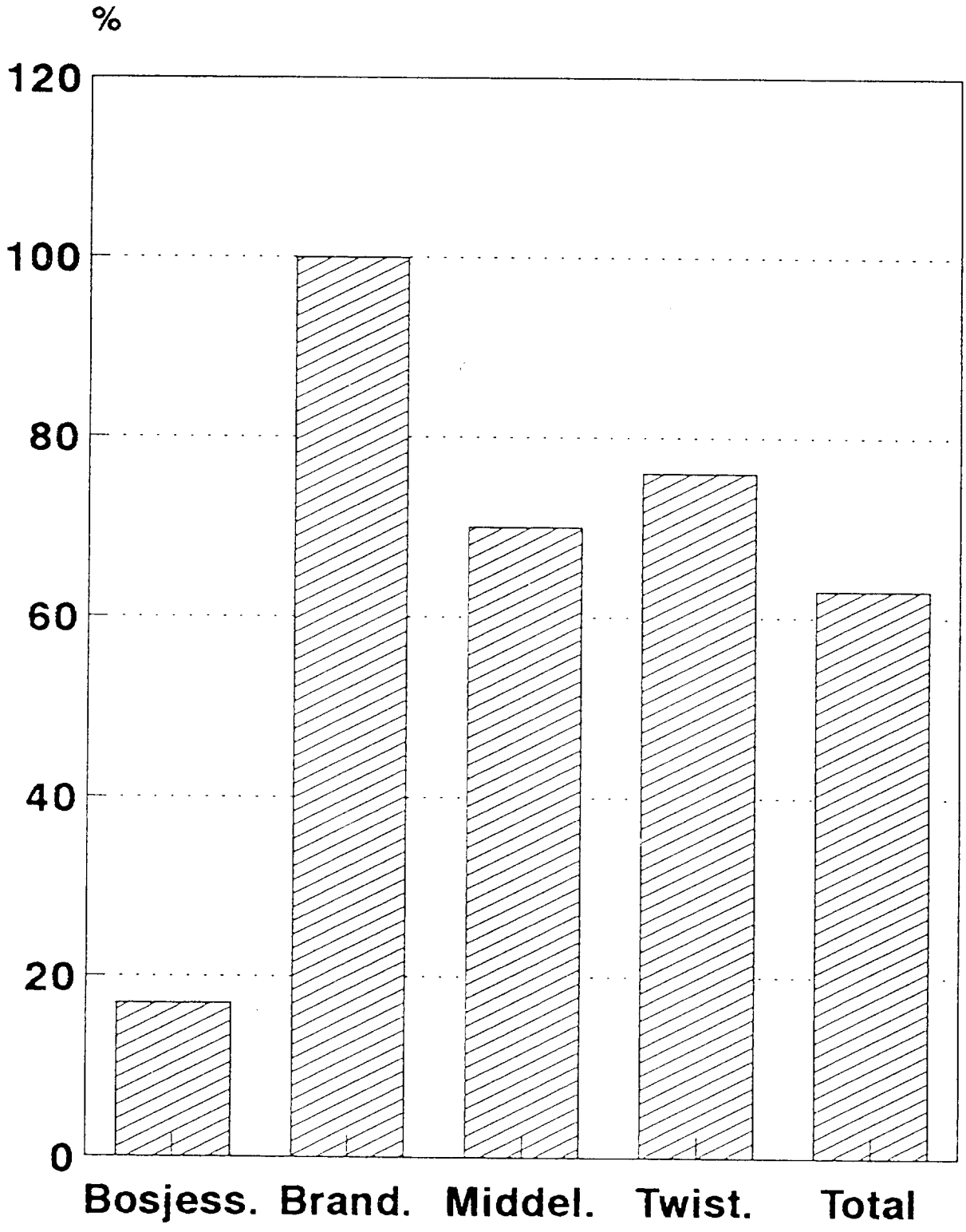

Figure 9

Intact block sizes per mine

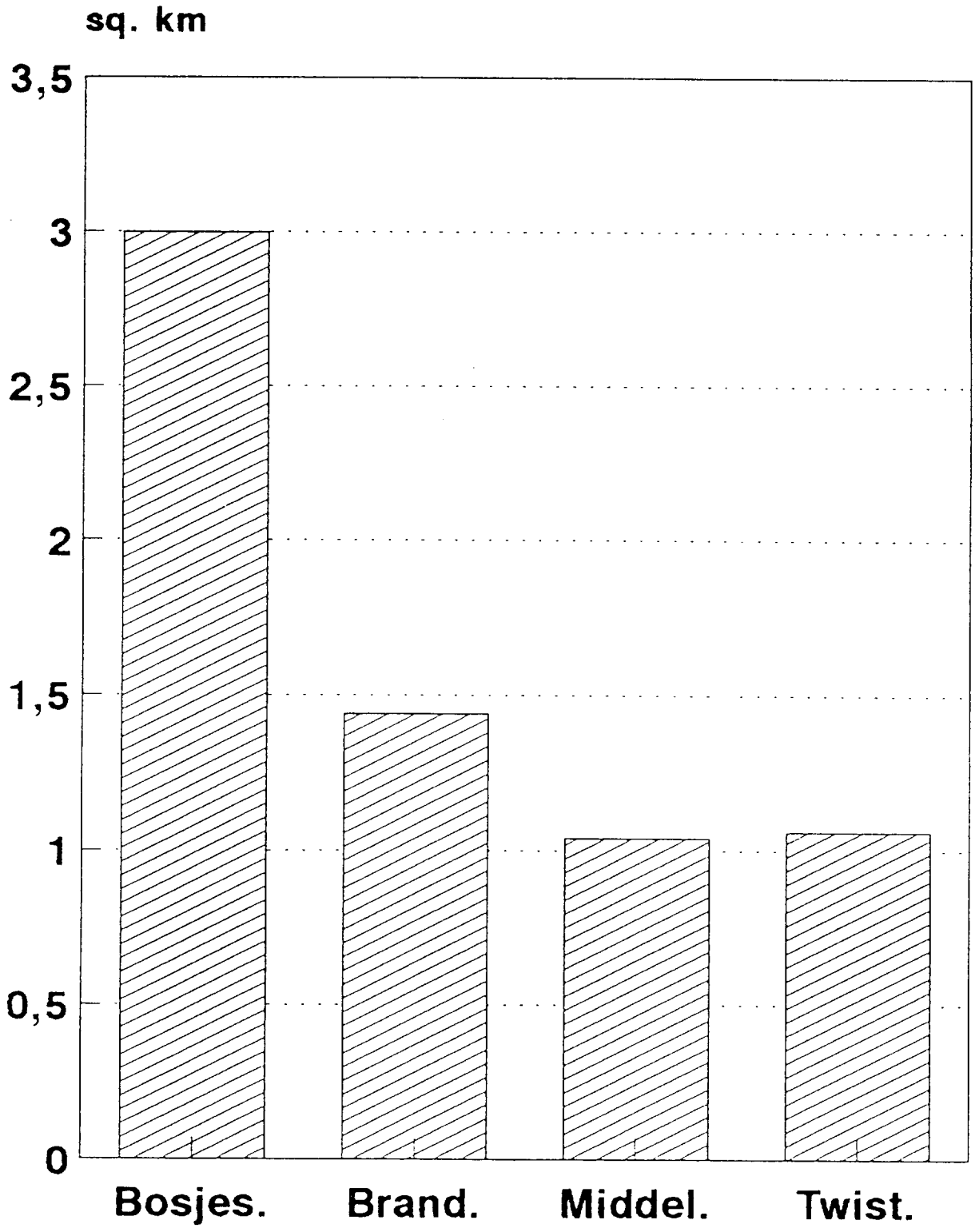

Figure 10

Non-associated occurrences per area mined

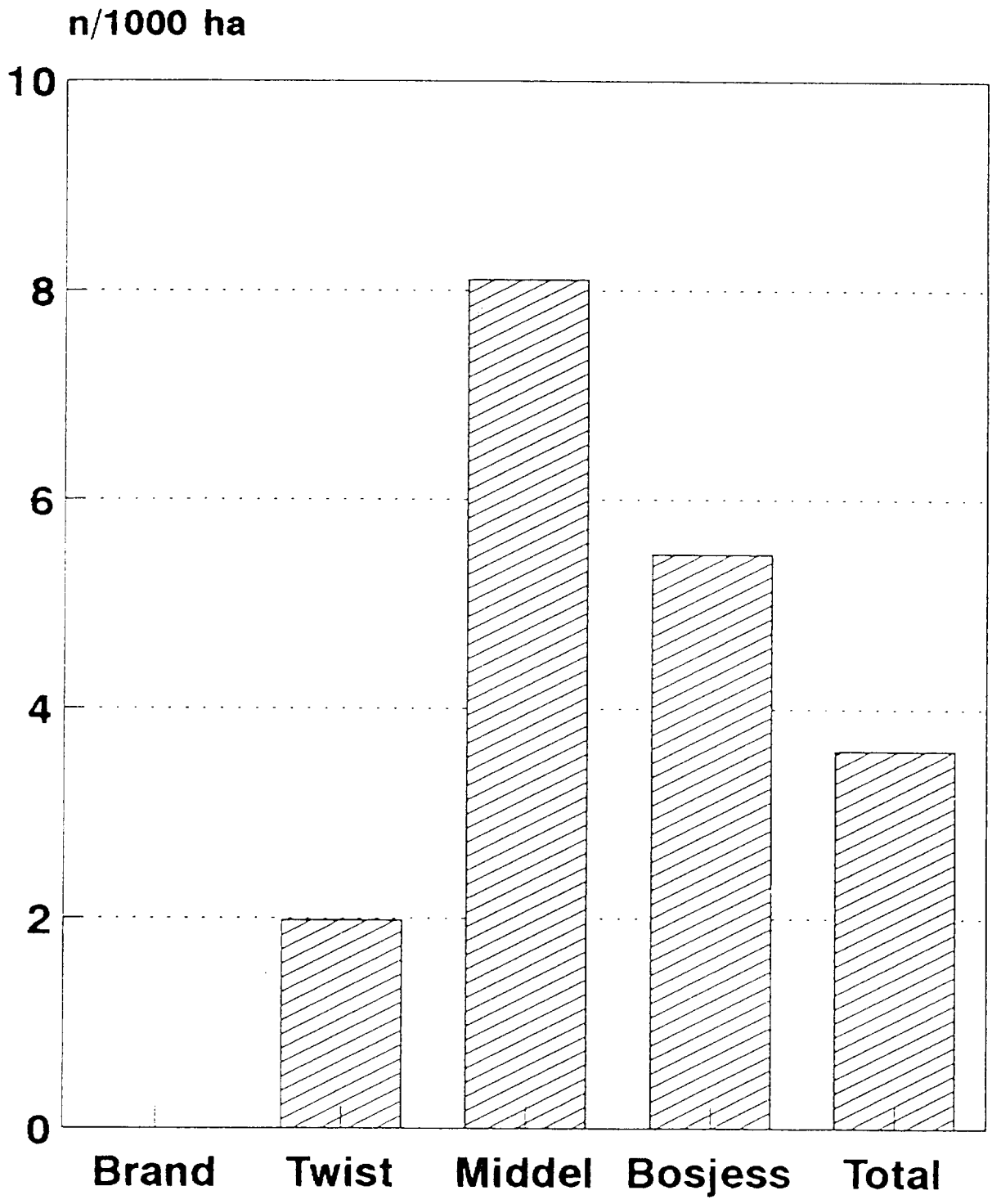

Figure 11

Associated Occurrences per km Disturbance

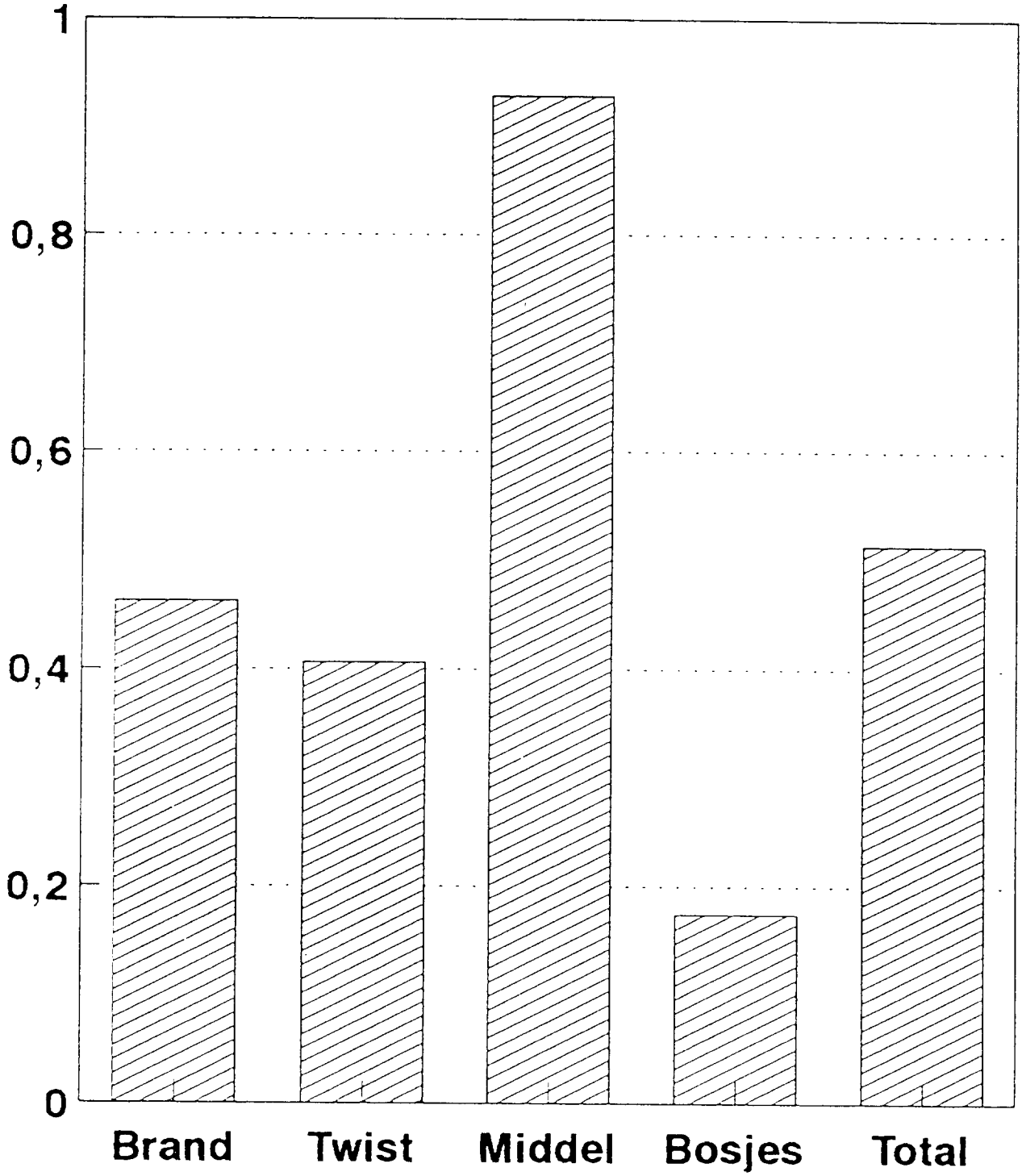

Figure 12

2.4 Occurrences per Mining Method

Figure 13 shows the relative numbers of occurrences per mining method for each of the mines. Not surprisingly, bord and pillar mining heads the list, as it is the primary mining method in all cases and thus the first to intersect methane should it be present. The Bosjesspruit data should be viewed against the background of the dominance of longwalling on that mine, which explains the relatively high proportion of longwall occurrences.

2.5 Position of Occurrence in Panel

The relative distributions of occurrences in different panel localities are shown for each mine in Figure 14. As can be expected, by far the most methane detections occurred on the face with only a few detections in the back areas and goafs. Only "active" goafs and back areas were considered for this analysis, methane build-up in sealed off goaf and bord and pillar areas being excluded.

3. DISCUSSION

3.1 Time Distribution of Methane occurrences

From a broad perspective, the time distribution of methane occurrences yielded somewhat unexpected results. This is especially true for the observation that more occurrences were manifested during the periods of high barometric pressure. Even if the data base is incomplete, there would be no reason for it to be more incomplete during certain periods of the year. Therefore, even if the total number of occurrences is somewhat below the actual, the relative statement should still hold true.

The data also displays the sporadic nature of reportable methane occurrences. On average, only 16 occurrences were reported per year from the four very large mines together. Against the background of the coal production - around 30 Mtpa - this indicates that the presence of methane in reportable quantities is not a frequent occurrence.

This does not diminish the magnitude of the problem in any way. Disasters occur despite the low frequency.

The low frequency of occurrence is at least a partial explanation for the observation that the number of ignitions do not always coincide with periods of high frequency of occurrence. Methane occurrence is only one of two basic pre-requisites for an ignition, the ignition source being the other. At low frequencies of occurrences, the probability of an ignition source being available at the same time and place as an accumulation of methane diminishes. Furthermore the concentrations of methane were not taken into account in the analysis.

Occurrences per mining method

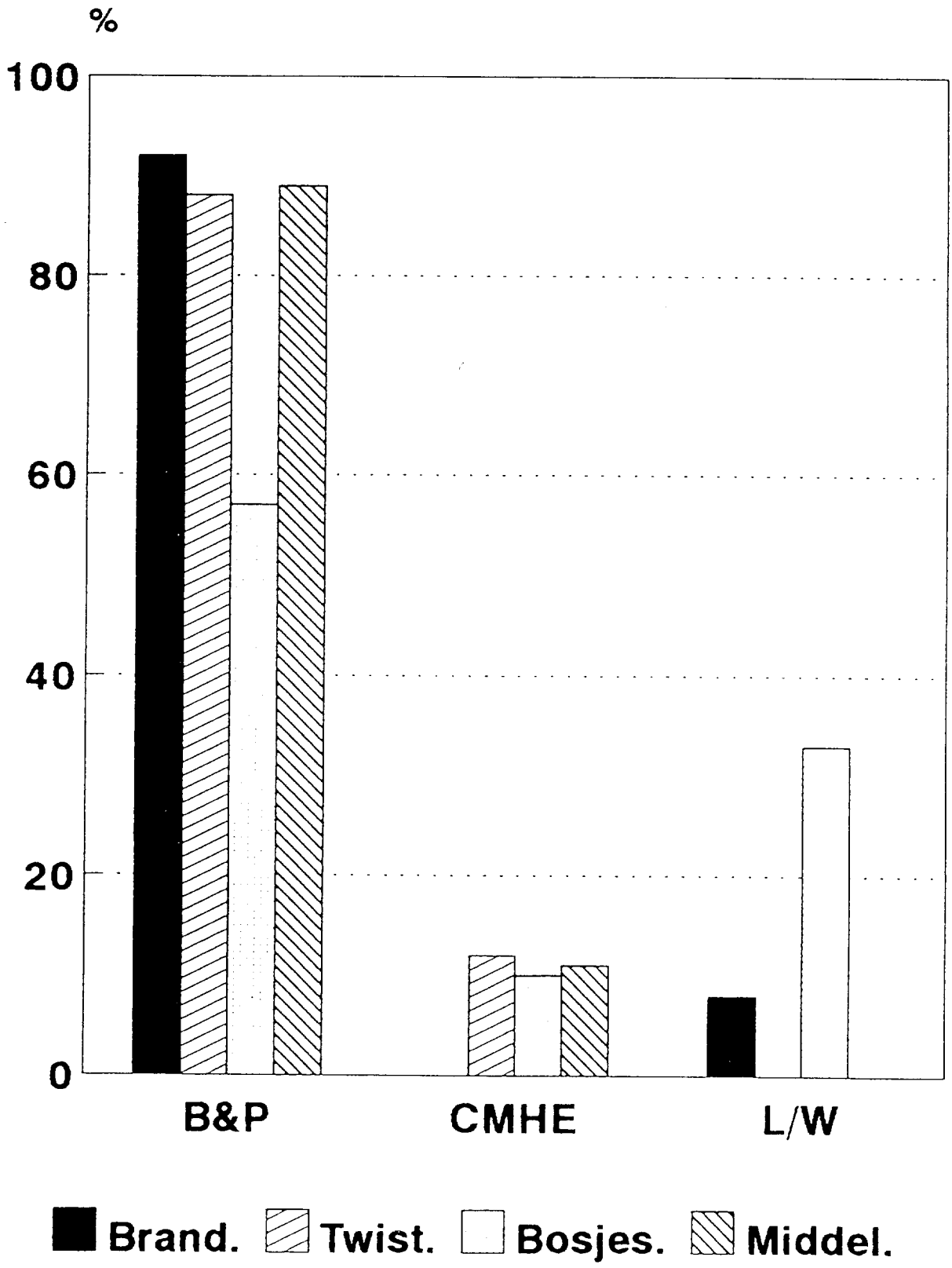

Figure 13

Occurrences vs locality in panel

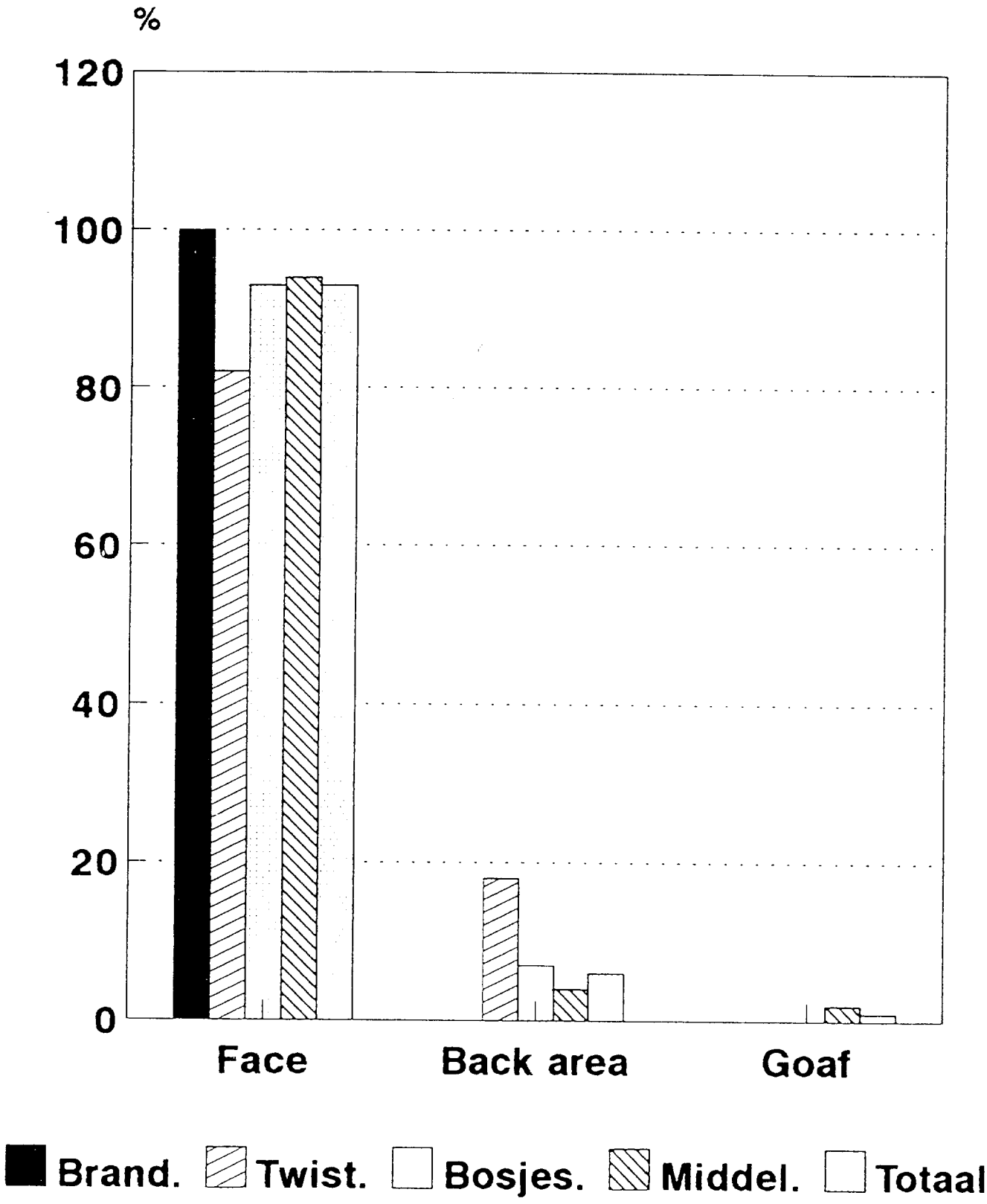

Figure 14

3.2 Spatial Distribution of Methane Occurrences

There were few similarities between the methane occurrences on the different mines, representing the four quadrants of the currently worked Secunda coal field. Each quadrant appears to exhibit unique characteristics.

Middelbult had significantly more methane occurrences than the other mines. The occurrences also differed markedly in nature, the Middelbult, Brandspruit and Twistdraai occurrences being predominantly located in the vicinity of geological disturbances and the Bosjesspruit ones in predominantly undisturbed areas. The differences in the trends are too large to ascribe to different interpretations by different geologists.

Based on preconceived ideas regarding the occurrence of methane and its containment in a certain area, the physical descriptions of the mines at Secunda would lead to the expectation that Middelbult should experience less methane than the other mines at Secunda. It is both shallower and the competent dolerite cover (which could be seen as a seal) is smaller in areal extent. Over geological time, the gas should thus have had more time to escape than at the other mines. While one would not have expected Middelbult to have significantly less methane, as the physical conditions at the Secunda collieries are much the same from a broad perspective, it is rather unexpected that Middelbult should have significantly more.

There must therefore be a different explanation for the higher frequency of methane occurrences at Middelbult. Of the four mines, Middelbult is the only one on the northern side of the Twistdraai fault - refer to Figure 1. If the source of Middelbult's methane is the Evander gas field, and if that field is cut off by the Twistdraai fault, it could be subject to a higher rate of gas recharge than the other mines. The other mines may then obtain methane from a different source (the coal itself) or from more than one source. It is possible that all the mines may receive methane from the coal, with Middelbult being subject to an additional source.

If this is the case, it is also possible that the composition of the gas from the different sources may be different. This, in turn, may explain the differences in the ignition ratios which were found.

Following from this, it is clear that further research should include establishing the source or sources of the gas and the full composition of gas from those sources.

A previous observation that the frequency of ignitions do not necessarily follow the frequency of methane occurrences is supported by the observation that Twistdraai experienced the highest proportion of ignitions while it had only the second highest frequency of occurrence. This non-correlation is thus evident both in time and in space.

In general it may be stated that overall in the Secunda coal field, methane occurrences are more prevalent along geological disturbances. The exception is Bosjesspruit, where only 17% of the occurrences could be associated with disturbances. This observation is only partially explained by the fact that disturbances occur less frequently at Bosjesspruit - even after normalising the data to discount for the frequency of disturbances, Bosjesspruit's occurrences still tended to localize in undisturbed areas.

Each of the four mines, representing different geographical zones of the same coal field, displayed unique methane occurrence characterization. The different characterisations are summarized in Table 2.

In figure 15 the major characteristics are displayed in geographical context. There does not appear to be any clear directional gradient for any of the major parameters, with the possible exception that the percentage ignitions may appear to increase in the north-easterly direction.

4. CONCLUSIONS

4.1 There were significant differences in the nature of methane occurrences in the different geographical areas of the currently mined Secunda coal field.

4.2 The differences could not be satisfactorily explained by geographical or geological features.

4.3 No definite gradients linked to geographical progression could be found (i.e. more frequent methane occurrences from east to west, etc).

4.4 Methane occurred sporadically over the whole field, at relatively low frequencies.

4.5 Over most of the area, methane occurrences tended to cluster around geological disturbances (dolerite dykes), with the significant exception of Bosjesspruit in the south-east.

4.6 There were no well developed relationships between methane ignitions and occurrences, either with regard to time or locality.

TABLE 2

	Time of Most Frequent Occurrences	Time of least Frequent Occurrences	Number of Occurrences per 1000 ha Mined	Preferred position of occurrence	Percentage Ignitions
Middelbult	Spring	Autumn	18	Disturbance (70%)	14%
Brandspruit	Autumn	Winter	4	Disturbance (100%)	<1%
Bosjesspruit	Winter	Summer	9,5	Intact (83%)	<1%
Twistdraai	Summer	Winter	7	Disturbance (75%)	44%
Secunda Collieries	Winter/Autumn	Summer	9,6	Disturbance (63%)	13%

Geographical distribution of selected characteristics

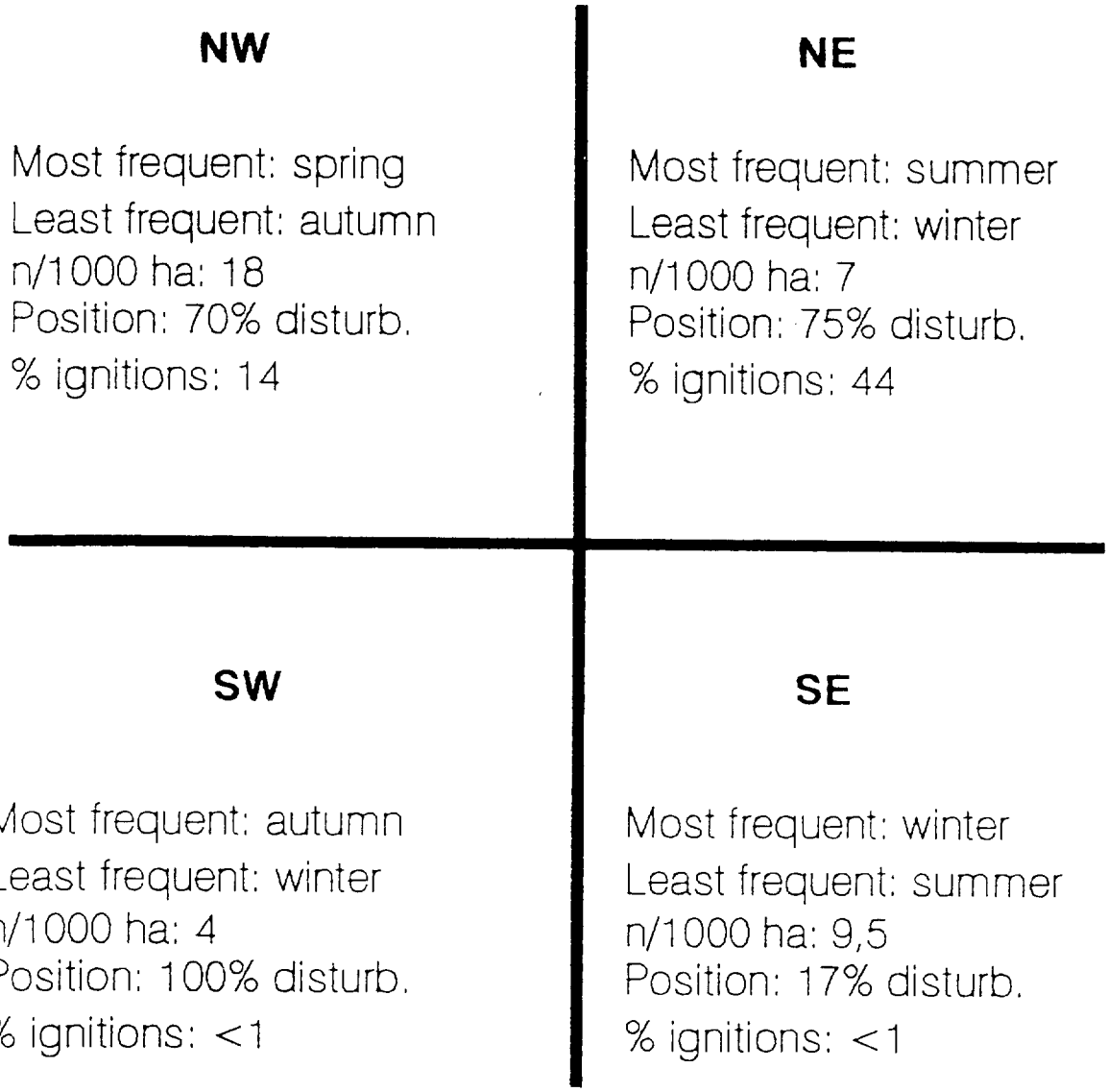

Figure 15

5. INDICATIONS FOR FURTHER RESEARCH

5.1 Sasol Responsibility

The investigation to date did not succeed in characterising the problem area of methane occurrences satisfactorily. Some of the differences which were found may be explained by different sources of methane gas. This is due to be researched by analysing the isotope ratios of carbon and hydrogen of samples collected in spatially distributed areas. The same samples will also be subjected to 100% content analyses. This will be compared with chemical analyses of the coal in the different areas.

Attempts will also be made to determine possible migration routes of methane from the Witwatersrand super group to the coal horizons.

5.2 Miningtek Responsibility

This aspect will be dealt with in more detail in the relevant Miningtek report. Briefly, however, the methane content of coal in the different areas, desorption rates, permeabilities in the different zones and methods of methane detection will be researched and combined with the Sasol results. It is envisaged that fundamental conclusions will be reached in this manner.

6. ACKNOWLEDGEMENTS

The Safety in Mines Research Advisory Committee (SIMRAC) is gratefully acknowledged for partial funding of the work via Miningtek, with whom excellent co-operation in the execution of this project is being experienced.

In Sasol the General Managers of the Middelbult, Brandspruit and Bosjesspruit/Twistdraai Collieries are thanked for their co-operation, as are the Geologists and Environmental Officers of the respective mines.

APPENDIX F2

SASOL COAL DIVISION

THE ORIGIN OF METHANE GAS IN THE SECUNDA AREA

P BOTHA
AUGUST 1995

THE ORIGIN OF METHANE GAS IN THE SECUNDA AREA

1. INTRODUCTION

The origin of natural gas is closely related to the diagenetic and thermal alteration of organic matter. Bacterial processes produce methane during early stages of diagnesis (coalification) whereas increasing thermal maturation of organic matter produces both methane and C_2 through C_5 hydrocarbons.

Likewise, the isotopic composition of both $\delta^{13}C$ (Carbon 13) and D (deuterium) or hydrogen from a methane molecule indicate the source from which the CH_4 has been derived as well as the maturation.

The main object of the study was to determine the origin of the gas and to see if this information can be applied to predict gas occurrences within a mining environment.

Three main origins for the methane gas in the Secunda area have been postulated and are as follows :

- the methane originated in situ by bacterial processes during coalification,

- the methane is mainly the product of thermal alteration of coal during dolerite intrusion,

- the methane migrated from the underlying Witwatersrand Group which is known to have generated large quantities of methane.

2. METHODOLOGY

The samples were taken and analysed by the CSIR and Atomic Energy Corporation. Samples were taken in accordance with the procedures as laid down by the CSIR.

The samples from each borehole were analysed by gas chromatography. The composition of one sample from each borehole was confirmed by mass spectroscopy. Duplicate samples were then analysed for carbon isotopes.

3. RESULTS

The chemical composition of the gas is illustrated in Table 1 and isotopic abundance in Table 2.

Three values are found useful in describing variability in natural gases and deducing their origin and processes involved with their origin : the concentration of C_2 to C_5 hydrocarbons (C_{2+}) relative to C_1 and both the carbon and hydrogen isotopic composition of methane. These properties are defined as follows :

$$C_2+ = \left(1 - \frac{C_1}{\Sigma C_n}\right) \times 100 \text{ in pph or \%.}$$

where :

C_n = the sum of all hydrocarbons C_1 through C_5 and C_1 denote the relative methane content. The carbon and hydrogen isotope concentrations of methane are expressed in the usual δ (delta) notation,

$$\delta = \left(\frac{R_{sample}}{R_{standard}} - 1\right) \times 1000 \text{ in ppt or \%}_0.$$

where

R = the isotope ratio of deuterium versus hydrogen and ^{13}C versus ^{12}C respectively. The $\delta^{13}C$ abundance is normally reported as PDB (Pee Dee Belmnite) and δD (deuterium) as SMOW units (Standard Mean Oceanic Waters)

Interpretation

The concentration of C_2 through to C_5 hydrocarbons (C_{2+}) relative to C_1 all fall in the 99,95 to 100% range and therefor classify the Secunda gas as a "dry" gas formed in situ during coalification.

Three types of natural gases are generally distinguished :

- bacterial (biogenic) gas
- mixed gas
- themogenic gas.

Bacterial gases originate through bacterial degradation of organic material near surface at temperatures less than 80°C. This is the natural window where most of the coals have passed through the ranks from peat to low volatile bituminous coals and therefor represent methane that has typically formed within coal mines. The $\delta^{13}C$ range for these coals are between -75‰ to -60‰ with δD between -200‰ to -180‰

Thermogenic gases, derived from organic matter (coal material) or oil prone algae organic matter have $\delta^{13}C$ values from -50‰ to -20‰ and δD values between -150‰ to -120‰

Isotopic abundances of $\delta^{13}C$ between -60‰ to -50‰ are normally grouped as mixed and therefore contains an element from both the biogenetic and thermogenetic gases.

A plot of the $\delta^{13}C$ ‰ against "dryness" index (C_1/C_2 - C_5) for Secunda gas is illustrated in Figure 1. Most of the samples fall within the biogenic and mixed fields. The three samples known to be associated with dolerite intrusions generally display an enrichment in $\delta^{13}C$ (lower - ‰ values) than those samples not associated with dolerites.

4. CONCLUSION

Methane present in the coal seams within the Secunda mines has mainly derived in situ by biogenic processes during coalification in situ and has been influenced by local dolerite intrusion.

Methane gas will therefore be ubiquitous through the coal with higher concentrations near the dolerite intrusions.

From the results it is unlikely that the methane has migrated from the underlying Witwatersrand Group.

TABLE 1 CHEMICAL COMPOSITION OF THE SECUNDA GAS

SAMPLE	#1	#2	#3	#4	#5	#6	#7	#8
CH_4	18.8	93.0	77.5	91.2	97.3	60.0	18.4	13.6
C_2H_6	0.01	0.01	0.01	0.03	0.02	0.02	<0.01	-
N_2	66.3	4.77	19.0	5.23	0.78	31.0	64.5	69.9
O_2	17.4	-	4.14	0.41	-	7.40	17.1	18.4
CO_2	-	-	-	0.80	0.66	-	-	-
H_e	-	-	-	0.12	-	-	0.76	0.49
TOTAL	102.5	97.8	100.7	97.8	98.8	98.4	100.8	102.4
C_2+	99.95	99.9	99.9	99.9	99.9	99.7	99.9	100%

TABLE 1(a) MORE ANALYSIS

SAMPLE	#1	#2	#3	#4	#5	#6
CH_4	97.1	96.3	40.9	44.2	46.0	51.9
C_2H_6	0.04	0.03	0.01	0.01	0.01	0.01
Air	2.23	2.73	57.7	55.0	54.0	47.3
CO_2	0.12	0.12	0.19	0.20	0.10	0.12
TOTAL	99.6	99.2	98.8	99.4	100.1	99.3
C_2+	99.9	99.9	99.9		99.9	99.9

$$C_2+ = \left(\frac{C_1}{C_2 - C_5}\right) \times 100$$

TABLE 2 ISOTOPIC ABUNDANCES OF ISOTOPES FROM METHANE WITHIN THE SECUNDA MINES

SAMPLE #	CARBON ISOTOPES	HYDROGEN ISOTOPES
	$^{13}C‰$ (PDB)	‰ SMOW
1	-54.1	-172
2	-62.7	-181
3	-65.2	-192
4	-58.6	-199
5	-59.0	-193
6	-57.5	-195
7	-58.1	-180
8	-56.2	-164
9	-56.6	-194
10	-56.7	-200
11	-58.3	-199
12	-58.2	-203
13	-57.6	-203
14	-56.9	-210

SECUNDA METHANE

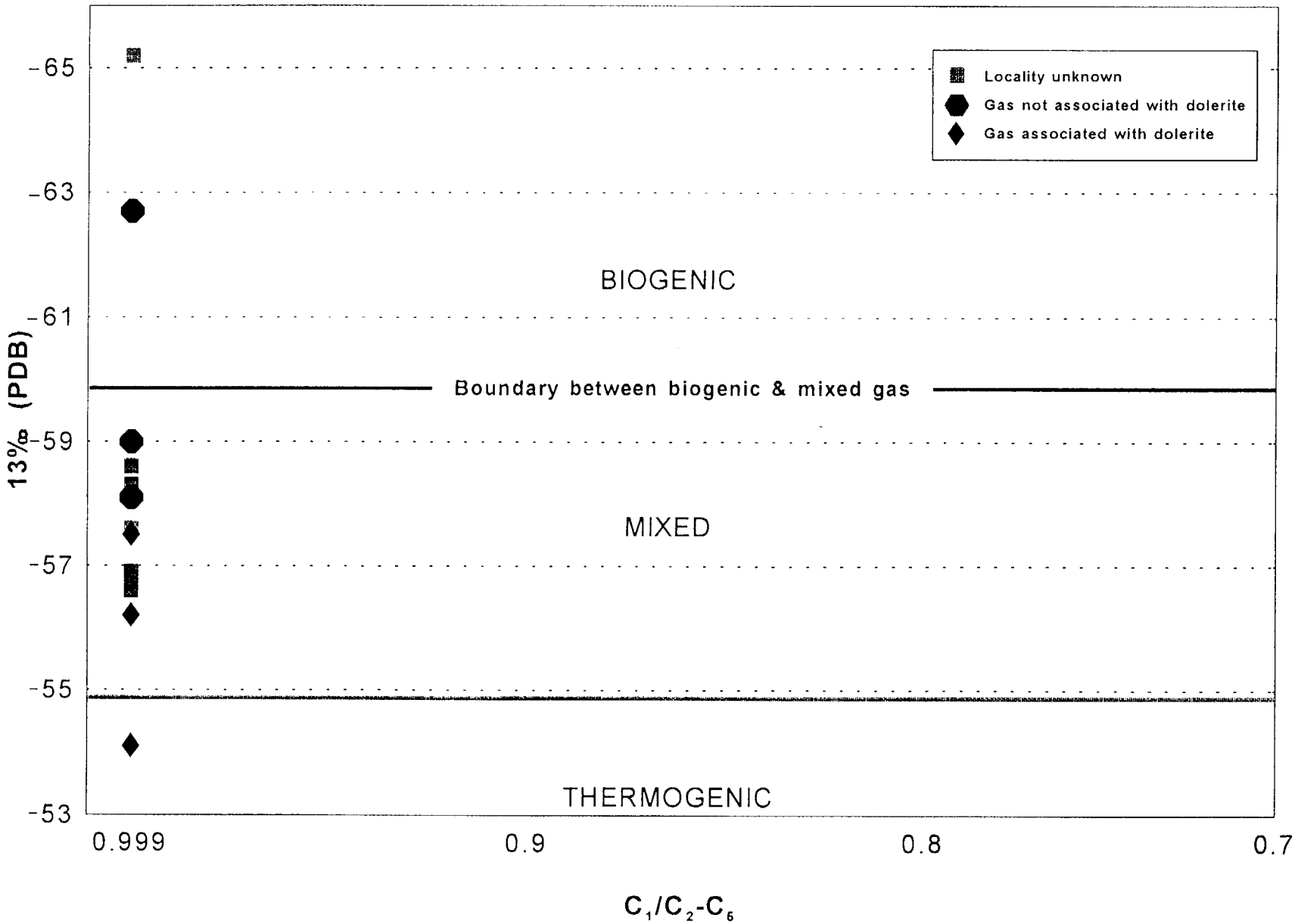

FIGURE 1

PJBAUG11 CH395

APPENDIX F3

1. SAMPLE VESSEL PREPARATION

1.1 MATERIAL

Sample vessels: stainless steel 316L

Valves: stainless steel metal bellows with all-metal sealing surfaces.

1.2 QUALITY ASSESSMENT OF VESSELS

1.2.1 Pressure test

The vessels were pneumatically pressure tested and certified.
These are certified to be used to a maximum working pressure of 500 kPa.

1.2.2 Leak test

All the vessels were helium leak tested with a calibrated leak detector. Vessels were certified as leak tight according to the specification $< 1 \times 10^{-9}$ std cc/sec (1×10^{-9} milli bar l/sec).

1.3 SAMPLE IDENTIFICATION

Sample vessels were numbered with an electrical engraving pen for identification and control purposes. These numbers were:

Sample #	Mine	Date	Borehole	Valve no
1	Middelbult	23/2/1994	B23	4264/5
2			B30	4204/5
3	Brandspruit	23/2/1994	K616/HM69	4198/9
4			K800/HP73	4238/9
5	Twistdraai	24/2/1994	T972	4282/3
6			T941	4276/7
7	Bosjesspruit	24/2/1994	B5504	4192/3
8			FU76F119	4208/9

BAW/0822

AEC-AEK

THE CHARACTERISATION OF NATURAL GASES

ANALYTICAL REPORT

Project Management

W C A van Niekerk

P Broere

Atomic Energy Corporation of South Africa Limited

P O Box 582, PRETORIA 0001, Republic of South Africa

JUNE 1994

F O R E W O R D

The Atomic Energy Corporation of South Africa (AEC) is pleased to submit this analytical report to Secunda Collieries. We trust that the analytical data will provide adequate information for the characterisation of the natural gases. We look forward to further collaboration in this project.

The AEC wishes to acknowledge the assistance of the Council for Scientific and Industrial Research (Mr. S Talma) with the carbon and hydrogen isotope ratio determinations.

W C A Van Niekerk PhD

SENIOR CONSULTING SCIENTIST

Tel: (012) 316 2766

Fax: (012) 316 2945

6 June 1994

CONTENTS

1. SAMPLE VESSEL PREPARATION

1.1 MATERIAL

Sample vessels: stainless steel 316L

Valves: stainless steel metal bellows with all-metal sealing surfaces.

1.2 QUALITY ASSESSMENT OF VESSELS

1.2.1 Pressure test

The vessels were pneumatically pressure tested and certified.
These are certified to be used to a maximum working pressure of 500 kPa.

1.2.2 Leak test

All the vessels were helium leak tested with a calibrated leak detector. Vessels were certified as leak tight according to the specification $< 1 \times 10^{-9}$ std cc/sec (1×10^{-9} milli bar l/sec).

1.3 SAMPLE IDENTIFICATION

Sample vessels were numbered with an electrical engraving pen for identification and control purposes. These numbers were:

Sample #	Mine	Date	Borehole	Valve no
1	Middelbult	23/2/1994	B23	4264/5
2			B30	4204/5
3	Brandspruit	23/2/1994	K616/HM69	4198/9
4			K800/HP73	4238/9
5	Twistdraai	24/2/1994	T972	4282/3
6			T941	4276/7
7	Bosjesspruit	24/2/1994	B5504	4192/3
8			FU76F119	4208/9

1.4 PACKAGING

A special aluminium case with polystyrene support linings were used to transport the vessels.

2. SAMPLING

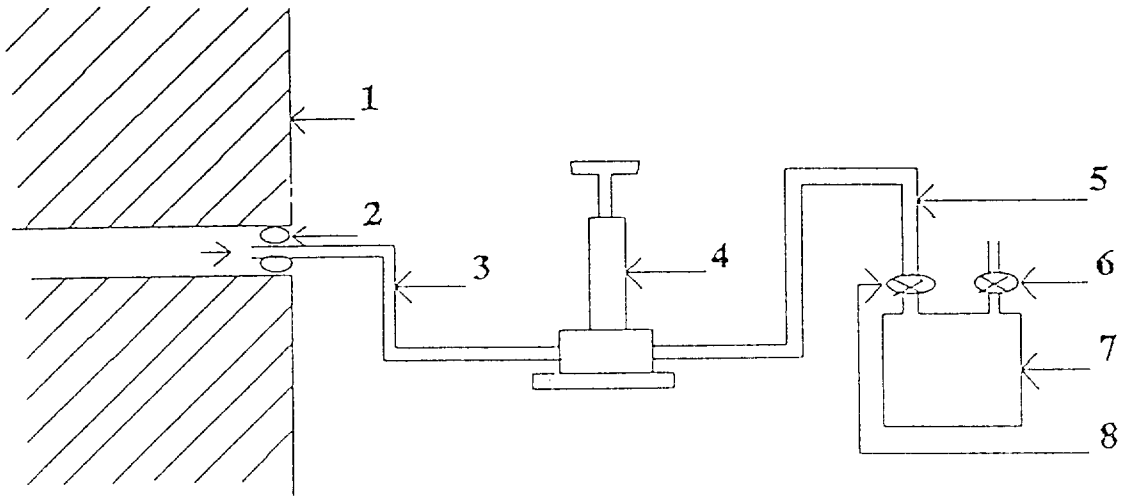

Figure 1
Sampling setup

(1) Mine wall
(2) Stoppers
(3) PTFE tubing
(4) Pump
(5) PTFE tubing
(6) Sample vessel outlet valve
(7) Sample vessel
(8) Sample vessel inlet valve

2.1 The setup for sampling was as shown in Figure 1. A torque wrench was used to close the valves properly and reproducibly at 6Nm.

2.2 The inlet- and outlet valves of a sampling vessel were opened and gas from the borehole was pumped through to condition the inner surfaces of the vessel. A hand pump, supplied by Secunda Collieries, was used.

2.3 After conditioning of the vessel, the outlet valve was closed with the torque wrench. The vessel was then pressurised with gas and the inlet valve closed with the torque wrench.

2.4 The sampling information was fully documented at the sampling point.

3. ANALYTICAL RESULTS

3.1 GASEOUS COMPOUNDS OF C, H, O, N AND S (PERCENTAGE BY VOLUME)

All the samples were analysed by gas chromatography. The external method of calibration was used to calibrate for each of the gases listed below. The composition of each borehole was confirmed by mass spectroscopy. Gas chromatography-mass spectrometry (GC-MS) was used to analyse each sample. It was not possible to analyse for H_2 with the technique that was used.

Gaseous composition (%)								
	Middelbult		Brandspruit		Twistdraai		Bosjesspruit	
Sample #	# 1	# 2	# 3	# 4	# 5	# 6	# 7	# 8
CH_4	18.8	93.0	77.5	91.2	97.3	60.0	18.4	13.6
C_2H_6	0.01	0.01	0.01	0.03	0.02	0.02	<0.01	-
N_2	66.3	4.77	19.0	5.23	0.78	31.0	64.5	69.9
O_2	17.4	-	4.14	0.41	-	7.40	17.1	18.4
CO_2	-	-	-	0.80	0.66	-	-	-
He	-	-	-	0.12	-	-	0.76	0.49
Total	102.5	97.8	100.7	97.8	98.8	98.4	100.8	102.4

3.2 ISOTOPIC ABUNDANCE

Samples were send to the CSIR on 25 March 1994 for analysis.

3.2.1 Carbon Isotopes

Isotopic abundance

	Carbon Isotopes
Sample #	^{13}C °/$_{oo}$(PDB)
1	-54.1
2	-62.7
3	-65.2
4	-58.6
5	-59.0
6	-57.5
7	-58.1
8	-56.2

The reproducibility for the ^{13}C analysis (1δ) is 0,2°/$_{oo}$

3.2.2 Hydrogen Isotopes

Isotopic abundance

	Hydrogen isotopes
Borehole / sample	$^{o}/_{oo}$ SMOW
1	-172
2	-181
3	-192
4	-199
5	-193
6	-195
7	-180
8	-164

The reproducibility for deuterium analysis is $4^{o}/_{oo}$.